

AD-A018 842

FORCE MEASUREMENTS IN SHORT-DURATION HYPERSONIC  
FACILITIES

Leonard Bernstein, et al

Advisory Group for Aerospace Research and Development

Prepared for:

North Atlantic Treaty Organization

November 1975

DISTRIBUTED BY:

**NTIS**

National Technical Information Service  
U. S. DEPARTMENT OF COMMERCE

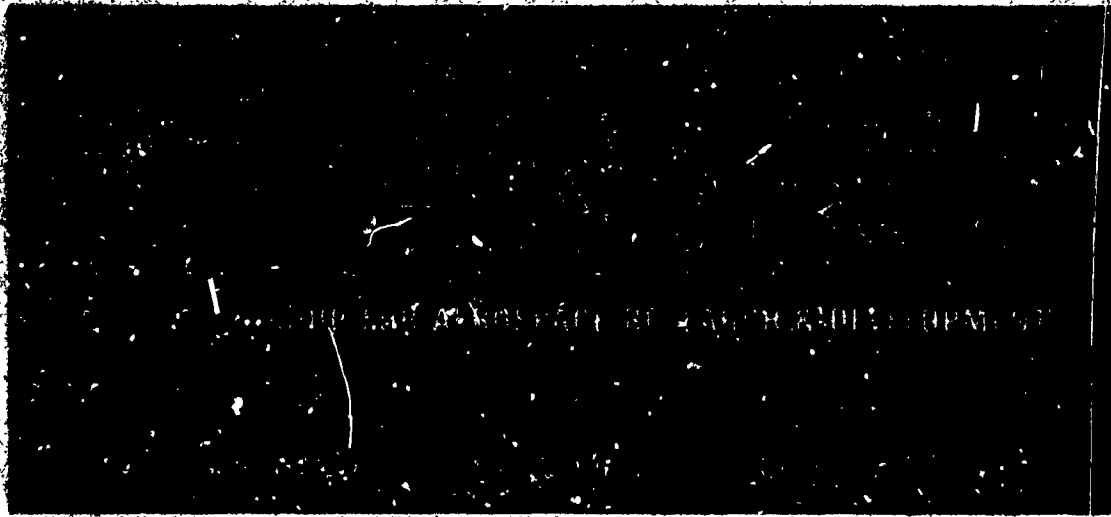
006104



AGARD-AG-214

AGARD-AG-214

ADA018842



AGARDograph No. 214

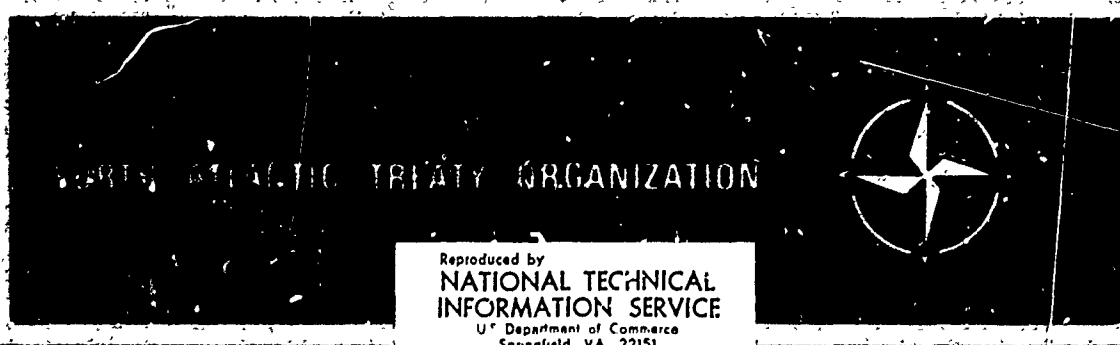
on

# Force Measurements in Short-duration Hypersonic Facilities

by

L. Bernstein

DDC  
RECEIVED  
DEC 30 1975  
R



NORTH ATLANTIC TREATY ORGANIZATION



Reproduced by  
NATIONAL TECHNICAL  
INFORMATION SERVICE  
U. S. Department of Commerce  
Springfield, VA. 22151

DISTRIBUTION AND AVAILABILITY  
ON BACK COVER

**REPORT DOCUMENTATION PAGE**

1. Recipient's Reference	2. Originator's Reference AGARD-AG-214	3. Further Reference	4. Security Classification of Document UNCLASSIFIED
5. Originator		Advisory Group for Aerospace Research and Development North Atlantic Treaty Organization . 7 rue Ancelle, 92200 Neuilly sur Seine, France	
6. Title		Force Measurements in Short-Duration Hypersonic Facilities	
7. Presented at			
8. Author(s)  Leonard Bernstein      Editor: R.C.Pankhurst			9. Date  November 1975
10. Author's Address	Department of Aeronautical Engineering Queen Mary College, University of London, Mile End Road, London E1 4NS.		11. Pages  224
12. Distribution Statement    This document is distributed in accordance with AGARD policies and regulations, which are outlined on the Outside Back Covers of all AGARD publications.			
13. Keywords/Descriptors  Hypervelocity wind tunnels Wind tunnel models Aerodynamic forces		Acceleration physics Supports Strains Transducers	14. UDC  533.6.071:533.6.048.1: 533.6.011.6
15. Abstract  Attention is drawn to the principle whereby the aerodynamic forces on a model in a wind tunnel are determined by measuring the reactions to them. The discussion is based upon a division of such reactions into two basic classes, depending on the restraints imposed. Where no restraints exist, the model flies freely and the forces may be inferred from the accelerations, either measured directly or derived from displacement vs. time data. When the model is supported, the forces are determined from measurements of the mechanical strains induced in suitably designed supports. Hybrid techniques, where these extreme cases of no restraint or nearly complete restraint cannot be assumed, are also discussed.  A detailed discussion of transducer sensing elements and their incorporation into measuring systems is given. Some particular systems are also described.  This AGARDograph was prepared at the request of the Fluid Dynamics Panel.			

NORTH ATLANTIC TREATY ORGANIZATION  
ADVISORY GROUP FOR AEROSPACE RESEARCH AND DEVELOPMENT  
(ORGANISATION DU TRAITE DE L'ATLANTIQUE NORD)

AGARDograph No.214

FORCE MEASUREMENTS IN SHORT-DURATION HYPERSONIC FACILITIES

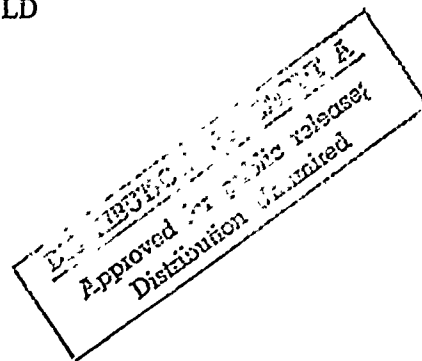
by

Leonard Bernstein

Department of Aeronautical Engineering  
Queen Mary College  
University of London  
Mile End Road, London E1 4NS

Edited by

R.C.Pankhurst  
ADR(AIR)  
Ministry of Defence, Procurement Executive  
St. Giles Court  
1-13 St. Giles High Street  
London WC2 H 8LD



## THE MISSION OF AGARD

The mission of AGARD is to bring together the leading personalities of the NATO nations in the fields of science and technology relating to aerospace for the following purposes:

- Exchanging of scientific and technical information;
- Continuously stimulating advances in the aerospace sciences relevant to strengthening the common defence posture;
- Improving the co-operation among member nations in aerospace research and development;
- Providing scientific and technical advice and assistance to the North Atlantic Military Committee in the field of aerospace research and development;
- Rendering scientific and technical assistance, as requested, to other NATO bodies and to member nations in connection with research and development problems in the aerospace field;
- Providing assistance to member nations for the purpose of increasing their scientific and technical potential;
- Recommending effective ways for the member nations to use their research and development capabilities for the common benefit of the NATO community.

The highest authority within AGARD is the National Delegates Board consisting of officially appointed senior representatives from each member nation. The mission of AGARD is carried out through the Panels which are composed of experts appointed by the National Delegates, the Consultant and Exchange Program and the Aerospace Applications Studies Program. The results of AGARD work are reported to the member nations and the NATO Authorities through the AGARD series of publications of which this is one.

Participation in AGARD activities is by invitation only and is normally limited to citizens of the NATO nations.

The content of this publication has been reproduced directly from material supplied by AGARD or the author.

Published November 1975

Copyright © AGARD 1975

National Technical Information Service is authorized to reproduce and sell this report.

533.6.071:533.6.048.1:

533.6.011.6



### SUMMARY

Attention is drawn to the principle whereby the aerodynamic forces on a model in a wind tunnel are determined by measuring the reactions to them. The discussion is based upon a division of such reactions into two basic classes, depending on the restraints imposed. Where no restraints exist, the model flies freely and the forces may be inferred from the accelerations, either measured directly or derived from displacement vs. time data. When the model is supported, the forces are determined from measurements of the mechanical strains induced in suitably designed supports. Hybrid techniques, where these extreme cases of no restraint or nearly complete restraint cannot be assumed, are also discussed.

A detailed discussion of transducer sensing elements and their incorporation into measuring systems is given. Some particular systems are also described.

#### EDITOR'S PREFACE

This AGARDograph is the second to be commissioned by the Fluid Dynamics Panel to deal with instrumentation techniques used in hypersonic short-duration facilities. The first (by D.L. Schultz and T.V. Jones) was concerned with heat-transfer measurements in these flow conditions; the present volume provides a comprehensive account of the measurement of aerodynamic forces and moments.

Balance methods and free-flight techniques are discussed fully and in separate chapters. These are preceded by a detailed mathematical analysis of unrestrained motion, of reactions in support systems with one or more degrees of freedom, and of partially restrained motion. The author has thus been at pains to cater throughout for the differing needs of the wind-tunnel experimentalist, the balance designer and the data analyst: indeed, the opening chapter provides these respective users with pointers which indicate where in the subsequent chapters their requirements are met.

R. C. PANKHURST

FORCE MEASUREMENTS IN SHORT-DURATION  
HYPERSONIC FACILITIES

by

Leonard Bernstein

CONTENTS

	<u>Page</u>
<u>CHAPTER 1 INTRODUCTION</u>	1
<u>CHAPTER 2 SOME FUNDAMENTAL PRINCIPLES</u>	
2.1 Introduction	7
2.2 Aerodynamic data from the analysis of unrestrained motion	9
2.201 The inertial coordinate system	10
2.202 The laboratory-fixed coordinate system	10
2.203 The body-fixed coordinate system	11
2.204 The body-oriented fixed-plane coordinate system	11
2.205 Wind axes	11
2.206 The relationship between coordinate systems	12
2.21 Some kinematic considerations relevant to the use of accelerometers	13
2.22 The equations of motion	15
2.2201 Planar motion	17
2.2202 Small angular motion	17
2.2203 Bodies with axial symmetry	18
2.221 The aerodynamic forces and moments	18
2.2211 Aeroplane-like bodies	20
2.2212 Axially-symmetric (or equivalent) bodies	21
2.222 The differential equations of motion in dimensionless form	22
2.2221 The linearised equations for aeroplane-like shapes	23
2.2222 The equations for axially-symmetric spinning bodies	24
2.23 The analysis of experimental data	26
2.231 The derivation of position and attitude from photographic records	27
2.232 Position and attitude from an optical telemetry system	28
2.233 The estimation of aerodynamic derivatives	29
2.2331 The drag coefficient	30
2.2332 Static and dynamic longitudinal stability derivatives	32
2.2333 Lift analysis	34
2.2334 Numerical integration of the equations of motion	36
2.3 Aerodynamic data from measurements of the reaction in the supports	37
2.31 Systems with one degree of freedom	37
2.311 Responses to transient force inputs	38
2.312 Base excitation	40
2.32 Systems with more than one degree of freedom	41
2.321 Calculation of the natural frequencies and modes of vibration	43
2.322 Lumped-parameter representations	44
2.323 Calculation of the inertia and stiffness matrices	46
2.4 Hybrid Techniques	47
2.41 Acceleration-compensation methods	48
2.42 Methods using partially-restrained models	49
2.5 Aerodynamic interference from the supports	50

	<u>Page</u>
<u>CHAPTER 3 FORCE BALANCE METHODS</u>	52
3.1 Introduction	52
3.2 Transducer elements	53
3.21 Piezoelectric materials	55
3.211 Some theoretical aspects	55
3.212 Low frequency characteristics	57
3.213 High frequency characteristics	57
3.2131 Compression waves parallel to the axis of polarisation	58
3.2132 Compression waves normal to the axis of polarisation	58
3.2133 Transverse shear waves	58
3.2134 Bending modes	59
3.214 Sensitivity of a selection of transducing modes	59
3.215 Comparison between various configurations	62
3.22 Piezoresistive materials	62
3.221 Some theoretical aspects	64
3.222 Low frequency characteristics	67
3.223 High frequency characteristics	67
3.224 Practical aspects of using piezoresistive strain gauges	68
3.2241 Environmental problems	68
3.2242 Temperature compensation	68
3.2243 Non-linearities	69
3.2244 Choice of strain gauge	70
3.23 Force transducers	70
3.231 Piezoelectric force transducers	71
3.232 Piezoresistive force transducers	76
3.233 Pivots	80
3.24 Accelerometers	81
3.3 General aspects of force-balance design	85
3.31 Force resolution systems	97
3.32 Strength and rigidity of the main supports	89
3.33 Attachments	90
3.34 Dynamic considerations	90
3.341 The model-supporting system	91
3.342 Design of the system and estimation of its dynamic characteristics	92
3.343 Acceleration-compensation	93
3.4 Electrical systems for signal generation and processing	95
3.41 Energy sources and bridge-circuits for resistance strain-gauges	95
3.42 Signal amplification	98
3.5 Data recording	100
3.6 Calibration techniques	102
<u>CHAPTER 4 FREE-FLIGHT TECHNIQUES</u>	104
4.1 Introduction	104
4.2 Design and manufacture of models	105
4.21 Design criteria	105
4.22 Manufacture of models	110
4.221 Uninstrumented models	111
4.222 Instrumented models	112
4.23 Determining the physical properties of the model	113
4.3 Model suspension, launching and capture systems	115
4.31 Suspension and launching systems for unrestrained models	115
4.311 Simple fracturing-thread supports	115
4.312 A magnetic support and retraction system	116
4.313 An explosively-retracted system	116
4.314 Gun-launching systems	116

	<u>Page</u>
4.32 Model capture	118
4.33 Systems providing partial constraint	118
4.331 Weakly-restrained systems	119
4.332 Pivoted systems	121
4.3321 A system with a knife-edge pivot	122
4.3322 A system with a gas-bearing pivot	123
4.4 Measuring techniques	125
4.41 Position and attitude as a function of time	125
4.411 Photographic methods	126
4.4111 The provision of reference frames	126
4.4112 Optical arrangements	127
4.4113 Light sources	128
4.4114 Ciné-photography	129
4.4115 Multiple-exposure of a single plate	130
4.4116 Providing a time-base	131
4.4117 Photographic materials	132
4.4118 Calibration methods	132
4.4119 Reading the photographic record	133
4.412 An optical telemetry system	133
4.413 Light-occluding and similar methods	134
4.42 Velocity measurements	136
4.43 Acceleration measurements	136
REFERENCES	139
NOMENCLATURE	147
TABLES	151
FIGURES	156

#### Acknowledgements

The author would like to take this opportunity of expressing his gratitude to the many individuals and organisations who helped in the preparation of this AGARDograph by making information and material freely available.

Particular thanks are extended to Dr. R.C. Pankhurst, the Editor of this series of monographs, whose encouragement and careful reading of the manuscript were invaluable; to Mrs. Doris Creasey whose patient, good-humoured typing is very much appreciated; to Miss Ann Boswell for preparing the illustrations, and to Mr. Don Husband for his help with the photographs.

## CHAPTER 1

### INTRODUCTION

Experimental aerodynamics has two main functions. It must provide design data for more or less specific projects and it is also used to carry out fundamental research into the behaviour of flowing fluids. Frequently the two functions become inseparable, increasingly so as flight vehicles become more refined. The origins of experimental aerodynamics are not entirely clear, but certainly by the middle of the eighteenth century Benjamin Robins was investigating the drag of cannon balls at speeds greater than that of sound, using the ballistic pendulum which he had invented for the purpose. He also carried out tests using a whirling arm, as did several others including Cayley about a hundred years later. The wind tunnel seems to have been first used by Wenham and Brown in 1866. A few years later Horatio Phillips used an ejector driven stream to carry out systematic tests on aerofoil shapes which demonstrated that the larger part of the lift arises from a fall in pressure on the upper surface. However it was the Wright brothers who first undertook systematic tests in a wind tunnel with the deliberate aim of obtaining data for a specific project; these experiments culminated in their historic flight of 1903 (see Gibbs-Smith, 1970).\*

It has been claimed (Poisson-Quinton, 1968) that design data of the kind sought by the Wrights in preparation for the first powered, manned flight have to be accurate in contrast to measurements for research purposes which need often be only qualitative. This is perhaps to overstate the case, since even when obtaining design data, it is rarely possible to achieve complete aerodynamic simulation in ground test equipment, and the pursuit of extreme precision may be misguided. On the other hand high accuracy in measurement is often needed when testing the predictions of some fundamental theory.

This is not to say that the "global information" needed for design purposes need be no more than qualitative; far from it. But when, for example, the results have to be extrapolated to different Reynolds numbers from those of the tests, one may be forced to accept uncertainties in the extrapolated results, and may not be justified in pursuing very high accuracy in the measurements themselves. Nevertheless one would like to be quite clear how the uncertainties arise, so that when it is necessary remedial action can be taken to reduce them. To do this one must of course have control over the performance of the measuring system, and the extent to which this is possible is governed by its detailed design, and the soundness of the principles upon which this design is based. Simplicity of concept and application are both generally regarded as conducive to high reliability, if only because there are then fewer things to go awry. However it is not always possible to achieve this simplicity throughout a measuring system which often consists of a chain of interconnected devices. Such is the case when one is faced with measuring the aerodynamic loading on a body immersed in a flow which lasts a fraction - often a very small fraction - of a second.

The early force measuring systems in continuously-operated wind-tunnels were simple lever arrangements in which the aerodynamic load was balanced by weights - hence the name "force-balance" -. The later balances of this type were capable of measuring several components of the load, in some cases all six; in other words they were able to resolve the force vector and determine the point through which it acted. Pankhurst & Holder (1952) describe several such balances. These balances are on the whole cumbersome to operate, particularly when large loads are involved; and because of their high inertia, they are unsuitable for other than steady situations. Automatic balancing systems can of course be used, and often are in the interests of efficient use of expensive plant. Even so the response times of these automatic "weighing machines" are very limited. As the aerodynamicist became interested in higher speeds, the need for economy of operation became greater. Some of these high-speed tunnels are of the intermittent type, driven by the release of air stored at high pressure. The characteristic test times of such tunnels may be measured in minutes. They can be operated manually, but automatic or semi-automatic systems, both for operation and data recording, provide a more efficient means of gathering data. For a given quantity of stored energy, the test flow duration reduces with increase of test flow speed. This does not in itself raise any fundamental difficulty, since the storage capacity may always be increased, in principle. However as the flow-speed in the test section becomes higher, condensation,

---

\* An alphabetical list of references is appended.

both of its water vapour content and of some of the constituents of the air, takes place. Driers can be included in the system to remove the moisture, and heaters added to enable the expansion to take place to high supersonic Mach numbers. The test-times in such tunnels are still fairly long and in some cases continuous-operation is possible. Even in these last cases however, the tunnels are so costly to operate that automatic systems become the norm. The aerodynamic forces are derived from measurements of the strain in calibrated "load-links" on which the models are mounted (Rebuffet, 1956), or, when support interference has to be avoided, by flying models freely in the test stream and recording their motion (Dayman, 1966).

When, in the 1950's, experimental aerodynamicists turned their attention to hypersonic flows, the emphasis had changed. Although hypersonic flows can be generated in continuously-operated tunnels, for example by using helium as the test gas (Bogdonoff & Hammit, 1954 and Bogdonoff & Vas, 1959) or by using just sufficient heating to avoid liquefaction without being too concerned about complete simulation, the aerodynamic heating problem itself had become the major interest. The main preoccupation in these early tests was the simulation of the high specific enthalpy of flows typical of those corresponding to the flight of ballistic missiles and of satellite re-entry. Such high enthalpies were readily generated in a shock-tube, a device invented by Vieille (1899), revived by Payman & Shepherd in the 1930's, and then after 1950, when electronic instruments became widespread, widely used for fundamental studies in aerothermodynamics, following the work of Bleakney and his colleagues (see, for example Griffith, 1971).

The shock-tube is basically a very simple device. It consists of a long tube divided into two sections by a diaphragm. On one side of this diaphragm there is the test gas at a low pressure; on the other side the driver gas at a high pressure. When the diaphragm is burst, the expanding driver gas is preceded into the low pressure region by a shock-wave which heats, accelerates and compresses the test gas. The working fluid is the gas between the moving shock-wave and the expanding driver gas. Although the flow Mach number is fairly low (about 3 is the maximum value that can be achieved in air), the temperature may be several thousand kelvin. For studies of heat-transfer-rate in a stagnation region, the Mach number is relatively unimportant, and the shock-tube proved an admirable tool for such measurements. The techniques used are the subject of the first monograph (Schultz & Jones, 1973) in a series, of which this is the second.

The feature which perhaps most distinguishes a shock-tube from the fairly conventional intermittent high-speed tunnel, is the very short duration of the quasi-steady, uniform test region, often only a few microseconds, rarely exceeding a millisecond. The cross-sectional dimensions are also generally fairly small, typically less than 150 mm in diameter, so that only the simplest tests can be conducted. In such flows there seemed little hope of making any significant force measurements. Then several devices were invented to generate hypersonic flows with longer durations in somewhat larger test chambers; almost all these devices stem in one sense from the shock-tube, and have a short test duration, though longer than that of the simple shock tube. For the very high enthalpy tunnels this is both a strength and a weakness; a strength because the tunnel structure is not heated significantly and thereby weakened, a weakness because the measuring techniques become complex.

The basic shock-tube was modified, first by adding an expansion nozzle to its end, so as to increase the flow Mach number from supersonic to hypersonic, and at the same time increase the size of the test section (Hertzberg, 1951). Because the gas had been heated by the passage of the shock-wave, its enthalpy was high enough to avoid liquefaction after expansion. Unfortunately the shock-wave was severely attenuated as it passed along the divergent nozzle, and the duration of quasi-steady flow was severely curtailed below that in the shock-tube itself. Subsequently Hertzberg, Smith, Glick & Squire (1955) allowed the primary shock-wave to reflect from the end wall of the shock-tube, thus creating a region of even hotter, high pressure gas which they used as the reservoir for a convergent-divergent nozzle, rather in the manner of a conventional blow-down tunnel. The effects of the wave interactions and reflections which occur within the shock-tube were delayed by operating the "shock-tunnel" in the "tailored-interface mode", the name given to the condition in which the acoustic impedances of the shock-compressed gas and the expanded driver gas are equal. The starting process within the nozzle was accelerated by using a second diaphragm at the nozzle entrance (which bursts as the shock is reflected from it) and evacuating the nozzle and test section to a very low pressure prior to operation. In this way test flow durations up to about 25 ms can be achieved.

With the emphasis still on simulating high enthalpy flows the "hotshot" tunnel appeared (Perry & MacDermott, 1958). In this device the gas in the reservoir was heated by discharging an electric arc through it. Such tunnels are capable of stagnation temperatures of about 10 000 K, the flow duration depending on the stagnation pressure level and the extent of any cooling provided for the electrodes and nozzle throat. At very low pressures such tunnels can be operated continuously, while at high pressures the test duration may be about 100 ms. Unfortunately the flow in an arc-heated tunnel is usually contaminated with electrode materials, and they are far from ideal for aerodynamic studies.

It was soon realised that for many such studies, complete simulation was not necessary. When the flow chemistry plays a secondary rôle, one can concentrate on obtaining realistic Mach and Reynolds numbers, and relax the requirement on stagnation enthalpy; the stagnation temperature need be only sufficiently high to avoid liquefaction of the test gas as it expands and cools in the nozzle. This led to the development of a number of tunnels in which the reservoir gas is heated and compressed by a free piston - in some a light piston, in others a heavy piston is used. In the light, free-piston tunnel, or gun-tunnel, a piston is placed just downstream of the diaphragm separating the high and low pressure regions of a device otherwise resembling a shock-tube. Upon diaphragm rupture, the piston is driven along the low pressure section containing the test gas, which is thus heated by a sequence of compressions as a shock wave is reflected back and forth between the piston face and the end of the drive tube. High stagnation pressures, and consequently high Reynolds numbers, can be achieved in these gun-tunnels, with stagnation temperatures limited to about 2000 K, their early promise (Cox & Winter, 1957) being somewhat unrealised because of the structural inability of a light piston to withstand the shock loading. At moderate stagnation temperatures, of order 1100 K say, the rate of heat loss from the reservoir gas to the tunnel walls is tolerable and test flow durations are typically in the range 20 ms to 100 ms (Bray, 1962).

Of the many other piston driven tunnels, the "Longshot" tunnel of Perry (1964) is the most important from the present viewpoint. A heavier piston is used than in a gun-tunnel, and to minimise the effects on the reservoir gas of the piston "rebound", a system of one-way check-valves is used to trap the compressed test gas and allow it to expand along the nozzle from a constant-volume region. Because the reservoir is a constant-volume region, the stagnation pressure decreases during a test. This tunnel is now installed at the von Kármán Institute for Fluid Dynamics, Brussels, and reservoir conditions of 2000 K and 2 000 atmospheres pressure have been obtained (Richards & Enkenhus, 1970a) with test flow durations of about 40 ms.

A device of a slightly different kind was proposed by Ludwig (1957). In essence, it is a conventional blow-down supersonic tunnel, but it makes use of an unsteady expansion to accelerate the gas before it enters the convergent-divergent nozzle. In the conventional tunnel, reflected waves within the reservoir lead to severe pressure fluctuations during the tunnel start; in the Ludwig-tube tunnel, the reservoir consists of a very long tube, and the useful flow is terminated when the unsteady rarefaction wave, having been reflected from the far end of this tube, returns to the nozzle entrance. To obtain hypersonic flows without liquefaction, the gas in the reservoir must be heated; an external tube heater is used at the AVA, Göttingen, where test flow durations up to about 500 ms are obtained in the longest of their Ludwig-tube tunnels.\*

An important feature of all these flow generating devices, or impulse tunnels, is the manner in which a test is initiated. Because the duration of the quasi-steady flow used for test purposes is so short, one cannot afford to lose any of it. The release of the gas stored in the reservoir - using this in the wider sense to include the driver chamber of a shock-tunnel for example - must be very rapid. In general, conventional valves are unsuitable, and bursting diaphragms are used. To withstand the high initial pressures across them, these diaphragms are often thick metal discs, which after bursting and

---

\* A variety of other hypersonic impulse tunnels has been proposed and some are being actively developed. They are characterised by very short test times on the whole, typically ten microseconds or so, and there seems little prospect of making force-measurements in such devices using established techniques. We shall not therefore pursue their description here, being merely concerned to set the scene for a discussion of the established methods and those which may be readily foreseen. The interested reader is referred to the recent survey by Lukasiwicz (1973).

"petalling" (they are usually so weakened that they "petal" cleanly, and do not shed fragments) impact the walls of the tunnel. This sends stress waves along the structure as does also the release of the pressure as the diaphragm opens. Forces are likewise transmitted through the structure of the tunnel as the shock waves are reflected from the end wall of the channel. Unless the model upon which the aerodynamic forces are to be measured is isolated from the tunnel structure, it will vibrate, and the measuring system will register these vibrations, spoiling the test record.

Again the nozzle starting process is such that a shock-wave passes along it initially, followed by other waves which all impinge on the model before the onset of the quasi-steady flow. The model thus suffers a transient loading which has a fairly complex waveform. Both the model and the measuring system react to this loading, and are "in motion" before the quasi-steady flow is established around the model. The nature of this motion depends upon how the model is supported. The transient starting process is, hopefully, of shorter duration than the test period, which as we have noted may be in the range from below one millisecond up to perhaps several hundreds of milliseconds, depending on the type of tunnel. However the effects of the motion which it induces will persist during the test period, and some way of accounting for it must be found. The starting process itself must occupy as little time as possible, and the practice of isolating the nozzle and test section from the reservoir by a diaphragm, and evacuating the former, is common. Typically the ambient pressure in the test section prior to initiating a test is of order 0.01 torr, so that the starting waves pass rapidly through it in spite of the severe attenuation they suffer along the divergent section of the nozzle. The designs of the model, its supports and the measuring systems must take account of this vacuum environment. For example transducers which are operated by means of an external electrical energy supply must have an adequate means of dissipating any heat generated, and time must be allowed for the system to equilibrate before the test is conducted.

In most of these impulse tunnels, the "preparation time" is measured in hours, and it culminates in a test which lasts milliseconds. These preparations involve setting up the test model at the required attitude, loading diaphragms into place, evacuating the different sections of the tunnel separated by these diaphragms, and charging them with the appropriate gases to the required pressures. At the same time, the measuring equipment must be made ready. This latter is itself of a somewhat specialist nature. Because of the short test period it must respond quickly and the data produced must be recorded automatically. To achieve adequate time resolution, the "measure and record" command must be given at a time related to the start of the useful test period. This means that it must be provided by some event which occurs during the "firing sequence" of the tunnel. This is not difficult in principle - in fact the modern "transient event recorder" makes it particularly simple as we shall discuss later (see Chapter 3) -. It does however mean that "trigger signals" have to be provided to determine the period during which data are recorded. In some tunnels (hot-shot tunnels and combustion-driven shock-tunnels for example) large electrical discharges initiate the firing sequence, and stray electro-magnetic radiation often interferes with the triggering pulse generators and with the transducer amplifiers. These problems arise with all measurements in such tunnels, not just force measurements, but we draw attention to them merely to point out that the overall system design must take account of a variety of indirect influences upon it.

The measurement of transient forces is an indirect process; one does not measure them by comparison with a standard in the way one measures length. In general we measure the reaction to a transient force. Force of course is a vector quantity, so that its direction as well as its magnitude is important. Moreover its line of action is also important - in other words the couple it produces, another vector quantity, must also be determined. We must therefore measure six independent quantities, in the general case, to determine the aerodynamic load. The six components are often of widely differing magnitudes; even when some are nominally zero, the remainder may differ considerably in magnitude from one another. These differences create a number of problems for the designer of a measuring system.

The magnitudes of the aerodynamic loads vary considerably from one tunnel to another, and even for a particular tunnel can be varied over two or more orders of magnitude by changing the initial pressure and effective nozzle-area ratios. A brief glance at the "Inventory of wind-tunnels in the United States" (Pirrello, Hardin, Heckart & Brown, 1971) for example, shows that in the 2440 mm (96 in) shock-tunnel at Cornell Aeronautical Laboratory (now CALSPAN) the dynamic pressure in the test section may vary in the range 1 - 1000 kN/m<sup>2</sup>, while that in the Boeing 762 mm (30 in) shock tunnel has an even wider range of

operating conditions.

In general, one is clearly not going to be able to use one force measuring system to cover all the conditions which might be met in a single tunnel, let alone expect to be able to transfer the system from one tunnel to another without considerable modification. Although we shall later describe in some detail a few of the force measuring systems which have been successfully used, we shall therefore largely concentrate in this monograph on the more fundamental aspects of system design and the interpretation of the data produced. Particular systems will be described where they illustrate the application of these principles.

Chapter 2, which follows this Introduction, is a discussion of the general kinematic and dynamic (including aerodynamic) principles involved. We have remarked already that the forces are determined by measuring the reactions to them. The discussion is founded on this concept and it is divided into two main parts depending on the nature of these reactions, which in turn depend upon the constraints imposed. When the model is held in the test stream on supports stiff enough to maintain it at the required attitude to the flow, these supports are strained by the loads transmitted from the model. By a suitable choice of supports these strains may be measured and interpreted in terms of the aerodynamic loads on the model. This constitutes the "force-balance technique".

When the model is unconstrained, it accelerates under the action of the forces, and by measuring the accelerations the forces may likewise be determined. This is the "free-flight technique".

In fact the force-balance technique cannot involve a strictly stationary model, because no strains would result. A motion therefore takes place, and because of the restoring forces due to the stiffness of the supports, the model and its mounting oscillate. Part of the reaction to the transient loading is thus inertial, and it may be necessary to compensate the "strain data" for this inertial response. This involves a hybrid technique usually referred to as the "acceleration-compensation" method.

It is general practice among aerodynamicists to express the aerodynamic forces with reference to "wind axes"; thus we use lift and drag and describe their variation with incidence, angle of yaw, etc. During a free flight, the attitude of the model to the flow will, in general, change. We must therefore be quite clear, in describing the measured data, to just what axis system the components of the vector refer. Chapter 2 begins with a description of the more widely used coordinate systems and the relations between them. We then proceed to consider the equations of motion for a model flying freely in a wind-tunnel, and draw attention to the approximations usually made in formulating them, and to the forms they take in special cases of interest. The particular forms in which free-flight data are usually obtained are then related to these equations in a discussion of the analysis of experimental data. Particular attention is paid to the way in which one can relate the aerodynamic data to the flow, assumed known, though the measurements concern the motion of the model relative to the laboratory. Most of these data handling procedures are adaptations of those used in the ballistic range, procedures which have been very fully discussed by Canning, Seiff & James (1970) in AGARDograph 138, to which we shall continually refer.

We then discuss the fundamental aspects of measuring transient forces on a model from the reactions induced in the supports. The emphasis is largely on the design problem of minimising the effects of the induced motion, albeit small. Where these inertial effects cannot be made negligible one must resort to compensation; the principles of such methods are outlined. Analogously, freely-flying models carrying accelerometers may need to be compensated for the weak restraints exerted by the signal leads and any tethering system used to prevent damage to these leads.

Chapter 2 concludes with a brief account of the aerodynamic interference caused by the presence of supports.

Chapters 3 and 4 are concerned with the choice and design of measuring equipment and with the experimental methods themselves. Chapter 3 is devoted to force-balances and includes some account of acceleration compensation and the principles of the design of the accelerometers which are needed to effect it. We treat in some depth the principles of transducer design; in particular the chapter contains a detailed discussion from the phenomenological viewpoint of piezo-electric and piezo-resistive transducer sensing elements. Because large outputs can be obtained for small strains, they are eminently suitable as the sensors of devices with high inherent natural frequency and low deflections. Although

much of the accounts can be found elsewhere, it is hoped that by bringing them together here and keeping in mind a particular application, the tasks of both the balance designer and the user are better served. The design of balances using piezo-resistive sensors - the so-called strain-gauge balances - owes much to conventional strain-gauge balance design. We have not hesitated to draw heavily on this experience. On the other hand, the use of piezo-electric sensors in wind-tunnel force-balances has been pioneered in, and is almost exclusive to, hypersonic impulse tunnels, although a variety of load cells based on piezo-electric quartz is available commercially for general applications, and special transducers have been developed to measure the cutting forces exerted by various machine tools (Kistler Instruments catalogue). On the whole the constraints imposed on a force transducing system for use in a short duration hypersonic wind-tunnel are such that each balance is a separate design, though occasionally scaling can be employed. It is hoped that the account given in Chapter 3 will enable the designer to exercise his wide discretion, and because we have strayed slightly outside conventional applications, perhaps produce some innovative designs.

The sensors themselves are only part of the measuring system. The way they are incorporated is fully discussed also. In the case of piezo-resistive strain-gauge systems, electrical supplies and high sensitivity amplifiers are also needed. On the other hand, piezo-electric devices are self-generating, but they require rather special amplifiers. These electrical systems together with techniques for recording transient data are also outlined in Chapter 3, which ends with a discussion on the calibration of force-balances.

Chapter 4 is an account of free-flight methods, interpreted broadly to include partially-constrained systems in which the number of degrees of freedom is limited. The chapter begins with a discussion of the criteria which govern the design of the model so that full advantage can be taken of the available test time and the size of the test volume. It continues with descriptions of some of the techniques which have been used to make models having appropriate inertial characteristics. The success of the free-flight technique depends, in part, upon being able to "launch" the model at the required attitude with a minimum loss of valuable test-time. The nature of this launch depends upon the particular measuring techniques to be employed. The remainder of Chapter 4 is devoted to both of these topics.

No attempt is made at a critical appraisal of the aerodynamic data obtained by the methods outlined, nor is any attempt made at a summary. At various stages throughout this monograph it is pointed out that each system must be to a large extent unique, and this is the conclusion to be drawn if there is one. The duration of the test period does restrict the choice of the kind of system which can be used in a particular tunnel. Where for example the free-flight technique is chosen together with conventional photographic methods for recording the motion, the test time must be sufficient to produce displacements which can be adequately resolved. When it is not sufficient, the free-flight technique may still be possible, but a different data collection method is necessary, for example accelerometers, or Doppler frequency-shift techniques. This does not always mean that similar systems cannot be used in different tunnels, but merely that to obtain optimum performance, the tunnel and its force-measuring system should be carefully matched.

The present state of the art is such that reasonably reliable measurements can be made, but none of the methods developed so far can claim a very high overall precision. Perhaps it is remarkable enough that a multi-component measuring system should be capable of producing data, accurate within a few per cent, in the small fractions of a second typical of the test duration of most hypersonic impulse tunnels.

CHAPTER 2  
SOME FUNDAMENTAL PRINCIPLES

2.1 Introduction

The measurement of forces and moments acting on a body cannot be carried out directly in the same sense that length can be measured by comparison with a standard. Forces, and we shall use the term hereafter in the generalised sense to include moments, can only be determined by measuring the effects they produce, that is by determining the reactions to them. Either the displacements of the body itself or of its supports, or the time rates of change of the displacements of the body are measured, directly or indirectly.

For the measurement of forces of short duration - transient forces - the difficulties are at once clear. Significantly "large" displacements can only take place when the inertia of the body is relatively small so that the accelerations are also large. When it is not possible to provide a body of sufficiently low inertia one must either be able to measure very small displacements or the accelerations produced by the transient forces must themselves be measured. Fortunately it is possible to detect very small displacements. Using strain gauges, either active or passive, the small strains in the supports produced by the forces transmitted to them can be used to produce substantial electrical changes. With these several possibilities in mind we can examine the relationship between the forces to be measured and the effects they produce. All practical systems are in some degree compliant so that they move under the action of forces. The motion produced by the action of forces on a system is described by the equations of motion for the system. These equations of motion may be formulated in a number of ways, but for our purposes two will be sufficient, the Newtonian and the Lagrangian. A complete discussion of the two approaches may be found in a number of textbooks; here we merely review the results cast in the forms suitable for our purpose.

In the Newtonian approach the force on a particle is essentially defined as the rate of change of that particle's momentum referred to an inertial frame, that is, a frame stationary with respect to the so-called "fixed-stars". The idea is readily extended for the case of a rigid body of finite extent by regarding the body as a collection of "connected" particles, the distances apart of which remain fixed. The equations of motion for the body can then be written in terms of its global properties, the mass  $m$  and the inertia tensor, the latter being a second order symmetric tensor. There are now six equations of motion. Three describe the linear motion of the centre of mass  $C$  of the body; the remainder describe the angular motion of the body. In vector form, these equations are

$$\underline{F} = m\ddot{\underline{R}}_C \quad (2.1)$$

$$\text{and } \underline{L}_A = \dot{\underline{H}}_A + m\dot{\underline{R}}_A \wedge \dot{\underline{R}}_C \quad (2.2)$$

where  $\underline{F}$  is the external force,  $\underline{L}_A$  is the external moment about any general point  $A$  in space,  $\underline{R}_C$  and  $\underline{R}_A$  are respectively the position vectors of  $C$  and  $A$  in an inertial frame,  $\underline{H}_A$  is the vector moment of momentum about  $A$  of the body and the dot notation is used to denote differentiation with respect to time. The vector product of the second term in equation (2.2) vanishes when the points  $A$  and  $C$  coincide (among other cases) and we shall find this choice of moment centre convenient. Equation (2.2) becomes

$$\underline{L}_C = \frac{d\underline{H}_C}{dt} \quad (2.3)$$

and the moment of momentum vector is given by

$$\underline{H}_C = \underline{\omega} \cdot \left[ \underline{I}_C \right] \quad (2.4)$$

where  $\underline{\omega}$  is the angular velocity of the body and  $\left[ \underline{I}_C \right]$  is the inertia tensor referred to the centre of mass  $C$ .

These equations are sufficient in principle to determine the motion of a rigid body, but in practice it is often difficult to decide what constitutes the applied forces and moments. Where the body is in "free-flight", the forces are gravitational and aerodynamic and the moments are merely aerodynamic. Since it is these aerodynamic loads that we seek to determine, a knowledge of the motion and the gravitational forces should suffice. There are however certain complications. For example the data concerning the motion are frequently measured in a reference frame fixed with respect to the laboratory, while it is far more convenient to calculate the components of  $\underline{H}_C$  in a frame fixed in the body. Accordingly we need

equations which provide this coordinate transfer. We shall discuss the analysis of unrestrained motion in more detail in Section 2.2 where some attention is also given to a description of the aerodynamics of a freely-flying model.

Where the body is supported the motion is clearly restricted if not entirely eliminated. The aerodynamic loads are then comparatively well-defined and are reacted by loads in the supports. It is by measuring these reactive loads that one hopes to infer the aerodynamic loads. However such loads are usually derived from measurements of the displacements or strains in calibrated load-links which constitute parts of the support. Of necessity such load-links possess a finite stiffness, so that some accelerations must occur and in consequence inertial forces will contribute to the responses of the load-links. These responses will be of an oscillatory nature because of the spring restraints and the more or less sudden force input typical of an impulse tunnel. The exact nature of the input force is not of course known, if only because no one has yet been able to resolve it precisely. In general terms a typical component has the time history sketched in figure 2.1 with some very rapid transients symptomatic of the passage of shock-waves and rarefactions over the model, followed, hopefully, by a period of quasi-steadiness which constitutes the test time  $\Delta t$ . It can be readily appreciated that to follow the important transients, whichever they are considered to be, a measuring system must have a uniform response over a frequency band extending at the very least to include a value of order  $1/(\Delta t)$ . If static calibration is required this frequency band must extend down to zero. The designer of a force-balance is therefore faced with the problem of ensuring that the resonant frequencies of the measuring system and supporting structure do not compromise its performance.

Two approaches are open to him. In one he aims so to design the measuring system that all the natural frequencies, or rather, since it is fairly easy to filter a single frequency, all but one of them lie outside the critical range. In the other approach, known as the "acceleration-compensation" or "inertia-compensation" technique, the reactive force in the load link and the appropriate component of the inertia force are separately measured and then combined to yield a component of the aerodynamic load. In order to utilise fully either the direct or the acceleration-compensation technique we need a method for estimating the natural frequencies of what is a fairly complicated system of flexible linkages and relatively stiff components. Although these latter parts may be regarded as rigid to a sufficiently good approximation the Newtonian equations of motion for a rigid body are not particularly convenient for this estimation because we need to specify in some manner the internal forces exerted by the flexible linkages. The complication arises because of the increased number of degrees of freedom, and for systems of this kind the formulation of Lagrange is more convenient.

For a system with  $n$  degrees of freedom a set of generalised independent coordinates  $q_i$  ( $i=1,2, \dots, n$ ) is chosen sufficient to describe the configuration of the system. In general the location in space of any part of the system will be a function of all the  $q_i$  and of the time. Making use of d'Alembert's principle and of the principle of virtual work a set of  $n$  equations is obtained having the form

$$\frac{d}{dt} \left( \frac{\partial T}{\partial \dot{q}_i} \right) - \frac{\partial T}{\partial q_i} - Q_i = 0 \quad (2.5)$$

$(i = 1, 2, \dots, n)$

where  $T$  is the total kinetic energy of the system and  $Q_i$  represents a generalised force associated with the coordinate  $q_i$ . In one of the particular variations of these equations of Lagrange  $Q_i$  is written in terms of a potential energy function  $U$

$$Q_i = - \frac{\partial U}{\partial q_i} \quad (2.6)$$

Such a function will exist for a conservative system. For the purpose of estimating the natural frequencies of a model-balance-support system, damping may be ignored and the potential energy function is simply the elastic strain energy in the flexible elements of the system. The  $n$  equations of motion are then derived from

$$\frac{d}{dt} \left( \frac{\partial T}{\partial \dot{q}_i} \right) - \frac{\partial T}{\partial q_i} + \frac{\partial U}{\partial q_i} = 0 \quad (2.7)$$

$(i = 1, 2, \dots, n)$

This set of equations leads to  $n$  natural frequencies for the system. The real physical system is, in essence, continuous and as such will have an infinite number of natural frequencies. The problem is to

represent the real system by one composed of a reasonable number of discrete parts and therefore a manageable number of degrees of freedom in such a way that several of the lowest natural frequencies are given with an accuracy sufficient for design purposes. We shall consider this further in Section 2.3 where the discussion centres on the response of spring-mass systems to transient force inputs.

In the succeeding section, relevant elements of Sections 2.2 and 2.3 are briefly conjoined in a discussion of the fundamentals underlying acceleration-compensation techniques. Finally in this Chapter we shall give some consideration to the aerodynamic interference problems which can arise in making force measurements, in particular those which result from the presence of supports.

## 2.2 Aerodynamic data from the analysis of unrestrained motion

The external forces and moments acting on a freely flying body arise in a number of ways, but for our purposes only those of aerodynamic origin and on occasion the gravitational forces, are significant. Buoyancy forces are negligible as usual in gasdynamics, and the Coriolis forces arising from the non-inertial character of the laboratory-fixed coordinate frame are also negligible, since both the angular velocity of the Earth and the flight velocity of the model relative to the Earth are small. The effects of gravity are also often small enough to be ignored, but when necessary the trajectory coordinates are readily corrected to eliminate the motion associated with the free fall. This is only necessary for flight of extended duration. For example a flight time of ten milliseconds results in a displacement due to gravity of only about 0.5 mm, the corresponding velocity increment being 0.1 m/s by the end of the test. However for a flight time of 100 ms the displacement would be about 50 mm, which clearly needs to be taken into account, and the maximum velocity increment is about 1 m/s which, although small compared with that of the free stream, is of the same order as that attributable to the aerodynamic loads.

It is these aerodynamic loads which give flight mechanics its distinctive character. The pioneering works of Lanchester (1907, 1908) and Bryan (1911) on the flight stability of aeroplanes and that of Fowler and his colleagues (1921, 1922) in ballistic aerodynamics have provided the bases upon which subsequent workers have built an extensive body of knowledge. Initially the two fields of study grew up quite separately, the "engineering requirements" in the two cases being rather different. With the advent of the high speed aeroplane and the possibility of testing models by firing them along an instrumented range in the manner used by ballisticians, the two sciences came together. Charters (1955) made a comparative study which provided among other things a translation between the two widely diverse notations. Since then the ballistic range has become an accepted apparatus for testing aerodynamic models and its technology forms the subject of the recent AGARDograph No. 138 edited by Canning, Seiff and James (1970).

The extraction of aerodynamic data from studies of the motion of freely-flying models is not confined to tests carried out in enclosed, laboratory ranges. Similar methods are used for models flown freely in the atmosphere (see, for example Waterfall, 1972 for a recent summary).

Clearly much of the work in these fields is directly relevant to the present study, and in many cases we shall find it unnecessary to discuss in detail several aspects which are fully described in the AGARDograph mentioned above. There is however, one important respect in which conventional range testing differs from free-flight testing in a wind-tunnel, and that is in the presence of the "counter-flow". Chapter 5 of AGARDograph 138 is concerned with "counter-flow facilities" but the chapter concerned with the analysis of the motion, Chapter 7, makes no allowance for a counter flow. An earlier review by Dayman (1966) of free-flight testing in high-speed tunnels is also of direct interest here, but Dayman's account is by no means so comprehensive as that of AGARDograph 138.

When a model is allowed to fly more or less freely under the action of the aerodynamic and gravitational forces and moments, its motion will in general be fairly complicated. We have noted that measurements of the motion can in principle be used to estimate the aerodynamic loads. Such measurements may be made by any of a variety of techniques, for example,

- (i) on-board accelerometers may be used.
- (ii) the position as a function of time in a laboratory-fixed coordinate frame may be determined using repetitive spark or cine photography of the model together with fixed reference lines within the field of view.

- (iii) an optical system carried aboard the model may be used to transmit light pulses in directions fixed relative to the model. When such signals are recorded as tracks on a stationary film, the position of the model can be determined as a function of time.

If we suppose that some kind of "ideal linear accelerometer" is available, one which responds only to acceleration along its axis, how, we might ask, in the general case should such accelerometers be placed to resolve the motion? It is fairly clear that to measure all six components of the motion, three linear and three angular, will require at least six accelerometers. What is not so obvious is that, except in special cases, we cannot employ just three, say, when only three components of the motion are required. Suppose for example only the linear motion is required. It is not possible to position three accelerometers, with their axes mutually orthogonal to another, all at the centre of mass. In consequence two at least will respond to the angular motion about the centre of mass. To eliminate this component it is necessary to employ a second accelerometer in each case, as we shall see. Moreover it is no straightforward matter to make use of the extra information so obtained to provide the aerodynamic moments also because the proportion of the couple contributed by the gyroscopic components of the acceleration depends upon the inertial properties of the model, which the accelerometers cannot take into account. The accelerometers are of course in a moving coordinate frame, one which is fixed in the body, and one of the objects of this section is to list the relations between quantities expressed as components in such a frame to the same quantities expressed as components in other frames, in particular in the inertial frame which is the primary postulate of Newtonian mechanics.

#### 2.201 The inertial coordinate system

Newtonian mechanics makes reference to the momenta of systems in an inertial framework. This frame is generally taken to coincide with one attached to the "fixed stars", stars which have "no" apparent general motion with respect to the Earth. A coordinate system attached to the surface of the Earth is of course in accelerated motion relative to these fixed stars and so is not strictly inertial. The angular velocity is however small and the resulting Coriolis terms in the equation written in terms of an Earth-bound frame can be neglected in laboratory ballistic studies. For our purposes no distinction need be drawn between the inertial frame and a laboratory-fixed coordinate system.

#### 2.202 The laboratory-fixed coordinate system

In describing the motion of a model in free flight we shall use a laboratory-fixed coordinate system. In most applications this is a right-handed cartesian frame in which the  $\zeta$ -axis is co-directional with the gravity vector (of course, a parallel gravity field is assumed within the laboratory) and the  $\xi$ -axis is downrange. The origin of course is arbitrary, but will usually be taken as the position of the centre of mass of the model at the onset of quasi-steady flow. We note in passing that the model will already be moving by this time as a result of the passage of the starting flow through the test-section.

Occasionally we shall find it convenient to use a cylindrical coordinate system in which case the  $\xi$ -axis coincides with the axis of the test-section and is again positive downrange, and the polar coordinates are  $R, \lambda$  with  $\lambda = 0$  coinciding with the gravity vector. Both frames are illustrated in figure 2.2.

Measurements are made in these coordinate systems of the position of the centre of mass of the model and of the angular attitude of the model using a further set of reference axes fixed in the model. In general the motion of the model is not along the  $\xi$ -axis, so that the centre of mass has velocity components  $U_B, V_B$  and  $W_B$  in the laboratory-fixed coordinate frame - in vector notation we shall use  $\underline{V}_B$ .

In these particular (laboratory-fixed) coordinate frames the flow velocity in the tunnel test-section assumes a relatively simple form, although when it is non-uniform and time-dependent this may be of minimal advantage. In any case it is the relative motion between the fluid and the model which determines the aerodynamic loads and this complicates matters considerably. We shall use  $\underline{V}_\infty$  to denote the velocity vector of the fluid, and  $U_\infty, V_\infty$  and  $W_\infty$  its components in the laboratory-fixed frame  $O\xi\eta\zeta$ . In general,  $\underline{V}_\infty = \underline{V}_\infty(\xi, \eta, \zeta, t)$ , but in a well-designed tunnel it will be sensibly uniform over the test region and constant during the test-time.

### 2.203 The body-fixed coordinate system

We have several times referred to the usefulness of a system of axes fixed in the body. The moment of momentum vector  $H_C$  is conveniently decomposed in this axis system and such a frame is also needed to define the attitude of the body both to laboratory-fixed axes and to the relative wind. The particular advantage of body-fixed axes is that the time derivatives of the inertia tensor components implied by equation 2.3 vanish for such axes. A further advantage is gained by choosing the body-fixed axes to be principal axes through the centre of mass C, so that the inertia tensor has but three non-zero elements.

It is conventional in aerodynamics to use a set of cartesian axes in which Cx is the longitudinal principal axis in the plane of symmetry which almost invariably exists, and is positive tail-to-nose, Cy is to starboard when the model is the right-way-up and Cz is perpendicular to Cxy forming a right-handed system.

We note immediately that when the model is the "right way up" and the Cxy-plane is horizontal, Cz and Oz are co-directional while Cx and Cy are oppositely directed to Oξ and On. In describing the orientation of the axes Cxyz it may be found convenient to use an intermediate set Oξ'n'ζ of laboratory-fixed axes, obtained from Oξηζ by rotation about Oz through 180°.

Because rotations are non-commutative, the order in which they are performed in passing from Oξ'n'ζ to Oxyz must be specified. Of the several conventions we shall adopt the (modified) Eulerian angles defined as follows (see figure 2.3):

- (i) beginning with Oξ'n'ζ rotate (yaw) about Oz through an angle  $\psi$  to a new set of axes Oξ'n'ζ; alternatively we may regard the first rotation as being about Oz through an angle  $\pi + \psi$  beginning with Oξηζ;
- (ii) rotate (pitch) about On' through an angle  $\theta$  to a new set Oxn'ζ;
- (iii) finally rotate (roll) about Ox through an angle  $\phi$  to the final position Oxyz.

The angular velocity components (p, q, r) about the body axes Cx, Cy, Cz respectively, are shown in figure 2.4. The components of linear velocity of the body relative to the laboratory are denoted by (u, v, w) in this frame.

### 2.204 The body-oriented fixed-plane coordinate system

A set of axes which takes advantage of the axial symmetry of a model where it exists is also found convenient. For an axially symmetric body only the principal axis Cx along the axis of symmetry is uniquely defined. Any pair of mutually perpendicular axes in the cross-section normal to the axis of symmetry are principal axes so that a set of axes which do not rotate about Cx with the body remains a set of principal axes and the inertial properties referred to these non-rotating axes remain time invariant.

The Eulerian angles  $\psi$ ,  $\theta$ ,  $\phi$  still describe the orientation of the model relative to laboratory axes Oξ'n'ζ, but the fixed plane axes Cy' and Cz' are not rolled with the body through  $\phi$  about Cx, and Cy' remains in its original plane which is normally horizontal. The fixed-plane, body-oriented axes Cx'y'z' are illustrated in figure 2.5.

### 2.205 Wind axes

It is common practice to specify some of the aerodynamic loads in particular the lift and drag, by reference to the direction of the relative wind vector. For this purpose it is convenient to define a coordinate frame, with origin at the centre of mass C of the body such that the axis Cx<sub>w</sub> is directed along the velocity vector of the body relative to the fluid. The axis Cz<sub>w</sub> then lies in the plane of symmetry for aeroplane-like bodies, and Cy<sub>w</sub> forms a right-handed cartesian system. For bodies with axial symmetry, Cz<sub>w</sub> is arbitrary. The components of angular velocity of this frame relative to the laboratory-fixed frame are denoted by (p<sub>w</sub>, q<sub>w</sub>, r<sub>w</sub>) about the axes Cx<sub>w</sub>, Cy<sub>w</sub> and Cz<sub>w</sub> respectively.

A set of angles ( $\psi_w$ ,  $\theta_w$ ,  $\phi_w$ ) similar to the Eulerian angles of section 2.203 is sometimes used to define the orientation of these wind axes relative to the laboratory-fixed frame. This system is illustrated in figure 2.6;  $\theta_w$  is effectively the angle of climb.

The linear motion of the body in this coordinate frame is described by the magnitude of the relative wind velocity vector V and two angles. These two angles are of fundamental importance to the

aerodynamics and represent the orientation of the body to the wind. If we define a velocity potential  $\phi$  for the flow in the test section, then the components of flow velocity along the body-fixed axes are  $\phi_x$ ,  $\phi_y$  and  $\phi_z$ , where the suffix denotes partial differentiation.

The angle of incidence  $\alpha_x$  is then defined by

$$\tan \alpha_x = \frac{w - \phi_z}{u - \phi_x} \quad (2.8)$$

and the angle of sideslip  $\beta$  by

$$\sin \beta = \frac{v - \phi_y}{V} \quad (2.9)$$

For a wing-like body in some general attitude defined by Eulerian angles  $(\psi, \theta, \phi)$  the effective aerodynamic incidence will vary considerably over the wing surface. In situations like this the concept of a single wing incidence or angle of sideslip has little meaning, and the usefulness of the concept is really confined to situations in which the angle between the relative wind and the plane  $Cxz$  of symmetry is small.

Some care must also be exercised in using this incidence to describe the aerodynamic loads. Zero incidence of the principal axis  $Cx$  does not necessarily coincide with the zero-lift incidence, for example. For this reason we use the suffix  $x$  so that it is quite clear which angle is intended. Of course the aerodynamic incidence only differs from  $\alpha_x$  by a constant.

## 2.206 The relationship between coordinate systems

Frequently it is necessary to represent the components of a vector in more than one coordinate system. For example we have already had occasion to refer to the components of the test section flow velocity vector in both laboratory-fixed and body-fixed coordinate frames. In normal circumstances the test section flow will be known as the result of a tunnel calibration in terms of  $U_\infty$ ,  $V_\infty$ ,  $W_\infty$ , the components in a laboratory-fixed frame. To define the "aerodynamic attitude" we need the components in a body-fixed frame.

The components of any vector in one cartesian frame, 0123 say, are related to those of the same vector in a second cartesian frame 01'2'3' by

$$\begin{Bmatrix} x_1 \\ x_2 \\ x_3 \end{Bmatrix} = \begin{bmatrix} l_{11'} & l_{12'} & l_{13'} \\ l_{21'} & l_{22'} & l_{23'} \\ l_{31'} & l_{32'} & l_{33'} \end{bmatrix} \begin{Bmatrix} x_1' \\ x_2' \\ x_3' \end{Bmatrix} = [L_{ij'}] \{x'\} \quad (2.10)$$

$i = 1, 2, 3$

where  $l_{ij'}$  is the cosine of the angle between  $O_i$  and  $O_i'$ . (Note that  $l_{ij'} \neq l_{j'i'}$  in general). In terms of the Eulerian angles  $\psi, \theta, \phi$  the transformation matrices  $[L_{ij'}]$  of direction cosines between the coordinate systems described above are well known. They will be discussed separately together with some useful approximations. Because  $[L_{ij'}]$  is simply a matrix of direction cosines it has the property that its inverse and its transpose are equal, making it unnecessary to write the equations for both the forward and inverse transformations.

The matrix which accomplishes the transformation between the two laboratory-fixed frames  $O\xi\eta\zeta$  and  $O\xi'\eta'\zeta'$  is very simple:

$$\begin{Bmatrix} \xi' \\ \eta' \\ \zeta' \end{Bmatrix} = \begin{bmatrix} -1 & 0 & 0 \\ 0 & -1 & 0 \\ 0 & 0 & 1 \end{bmatrix} \begin{Bmatrix} \xi \\ \eta \\ \zeta \end{Bmatrix} \quad (2.11)$$

The transformation between laboratory-fixed axes  $O\xi'\eta'\zeta'$  and body-fixed axes  $Oxyz$  is given by

$$\begin{Bmatrix} x \\ y \\ z \end{Bmatrix} = \begin{bmatrix} \cos\psi \cos\theta & \sin\psi \cos\theta & -\sin\theta \\ (\cos\psi \sin\theta \sin\phi - \sin\psi \cos\phi) & (\sin\psi \sin\theta \sin\phi + \cos\psi \cos\phi) & \cos\theta \sin\phi \\ (\cos\psi \sin\theta \cos\phi + \sin\psi \sin\phi) & (\sin\psi \sin\theta \cos\phi - \cos\psi \sin\phi) & \cos\theta \cos\phi \end{bmatrix} \begin{Bmatrix} \xi' \\ \eta' \\ \zeta' \end{Bmatrix} \quad (2.12)$$

while for the transformation from  $O\xi\eta\zeta$  to  $Oxyz$  the transformation matrix of equation (2.12) is post multiplied by that of equation (2.11) which has the effect of replacing  $\psi$  by  $(\pi+\psi)$  in equation (2.12), so changing the sign of any term containing the angle  $\psi$ .

The transformation from laboratory-fixed axes  $O\xi'\eta'\zeta'$  to body-oriented fixed plane axes  $Ox'y'z'$  is effected by omitting the roll through angle  $\phi$ ; that is  $\phi = 0$  is inserted into equation (2.12) giving

$$\begin{bmatrix} x' \\ y' \\ z' \end{bmatrix} = \begin{bmatrix} \cos\psi \cos\theta & \sin\psi \cos\theta & -\sin\theta \\ -\sin\psi & \cos\psi & 0 \\ \cos\psi \sin\theta & \sin\psi \sin\theta & \cos\theta \end{bmatrix} \begin{bmatrix} \xi' \\ \eta' \\ \zeta' \end{bmatrix} \quad (2.13).$$

We are now in a position to write the stream velocity components  $\phi_x$ ,  $\phi_y$  and  $\phi_z$  along body-fixed axes in terms of the components along the laboratory-fixed axes, or more usefully we can transform the components of the relative wind. Thus

$$\begin{bmatrix} u - \phi_x \\ v - \phi_y \\ w - \phi_z \end{bmatrix} = [\underline{L}]_{B/L} \begin{bmatrix} U_\infty - U_B \\ V_\infty - V_B \\ W_B - W_\infty \end{bmatrix} \quad (2.14)$$

where  $[\underline{L}]_{B/L}$  is the transformation matrix of equation (2.12). The resulting expressions for the angles of incidence and of sideslip are somewhat complicated, and we are led to seek suitable approximations. As we have remarked already, the concept of sideslip is really only useful for small angles, and we are led to the "small angle approximation". In the case when  $\psi$ ,  $\theta$  and  $\phi$  are all small the matrix for transformation from laboratory-fixed to body-fixed axes becomes

$$[\underline{L}]_{B/L} = \begin{bmatrix} 1 & \psi & -\theta \\ -\psi & 1 & \phi \\ \theta & -\phi & 1 \end{bmatrix} \quad (2.15)$$

and consistent with this approximation, we find upon expansion of (2.14) that

$$\alpha_x = \tan^{-1} \frac{w - \phi_z}{u - \phi_x} = \theta + \frac{W_B - W_\infty}{U_\infty - U_B} = \theta - \gamma_2 \quad (2.16)$$

and

$$\beta = \tan^{-1} \frac{v - \phi_y}{u - \phi_x} = -\psi + \frac{V_\infty - V_B}{U_\infty - U_B} = -\psi + \gamma_1 \quad (2.17)$$

the angles  $\gamma_1$  and  $\gamma_2$  defining the direction of the relative wind; they are effectively trajectory angles.

The quantities  $(U_B, V_B, W_B)$  and  $(\psi, \theta, \phi)$  as functions of time are those to be obtained experimentally from a freely-flying model in the tunnel gas stream. Together with the physical properties of the stream and the inertial properties of the model, we should be able to determine the aerodynamic forces and moments, which depend in addition upon such quantities as  $\alpha_x$  and  $\beta$ . The aerodynamic loads in the general case are thus changing during the test period, and to determine them, we need the equations of motion in differential form.

Before discussing these equations, we shall digress slightly to consider some kinematics relevant to an instrumented body in unrestrained motion.

## 2.21 Some kinematic considerations relevant to the use of accelerometers

We have remarked earlier that the interpretation of accelerometer records may not always be straightforward. The difficulty arises because not more than one accelerometer can be placed at the centre of mass  $C$  of the body, and so those components of the acceleration which occur when the body has a general angular motion are also sensed. The differential operator  $d/dt$  of equations (2.1) and (2.3) refers to rates of change in an inertial frame. It may be decomposed in the form

$$\frac{d}{dt} \equiv \frac{\partial}{\partial t} + \omega \wedge \quad (2.18)$$

where the partial derivative is taken with respect to the moving axis system which has an angular velocity  $\omega$ . Suppose now we consider an accelerometer located in the body at a position  $A$  for which the position

vector is  $r_A = x_A i + y_A j + z_A k$ , relative to the centre of mass, this latter having a position vector  $R_C$  in an inertial frame. The "absolute" position of the accelerometer is then

$$R_A = R_C + r_A$$

and repeated application of equation (2.18) yields the absolute acceleration as

$$\ddot{R}_A \equiv \frac{d^2 R_A}{dt^2} = \ddot{R}_C + (\dot{\omega} \wedge r_A) + \omega \wedge (\omega \wedge r_A) \quad (2.19)$$

Let us postulate a second accelerometer, its axis aligned with the first, at a position B, such that

$$r_A = -r_B \quad (2.20)$$

Clearly the inertial acceleration of the centre of mass in the direction of the accelerometer axes will then be given by half the sum of the outputs, since

$$\ddot{R}_C = \frac{1}{2} (\ddot{R}_A + \ddot{R}_B) \quad (2.21)$$

and the accelerometers respond to a component of the "absolute" acceleration. The difference in the outputs certainly eliminates the common motion  $\ddot{R}_C$  of the centre of mass, but the angular motion remaining is somewhat complicated. We have

$$\ddot{R}_A - \ddot{R}_B = \dot{\omega} \wedge (r_A - r_B) + (\omega \cdot (r_A - r_B)) \omega - \omega^2 (r_A - r_B) \quad (2.22)$$

and we wish to resolve the common motion by having  $r_A + r_B = 0$ . Suppose then that the two accelerometers are placed with their sensitive axes along the direction Cz in such positions that

$$x_A = x_B = z_A = z_B = 0 ; y_A = -y_B.$$

This commonly-used arrangement is illustrated in figure 2.7.

We then have

$$\ddot{R}_A - \ddot{R}_B = 2y_A ((\omega_x \omega_y - \dot{\omega}_z) i + (\omega_y^2 - \omega^2) j + (\dot{\omega}_x + \omega_y \omega_z) k) \quad (2.23)^*$$

and for "ideal" accelerometers with no cross-axis sensitivity, the difference in outputs will be proportional to  $(\dot{\omega}_x + \omega_y \omega_z)$ . We shall see in the following sub-section that the couple about the Cx-axis which we might expect to be associated with  $\dot{\omega}_x$  and  $\omega_y \omega_z$  is not simply proportional to the sum. Unless therefore we have good reason to believe that at least one of these terms is negligible they must be separately resolved.

One possible way of achieving this is to use a further pair of accelerometers, placed at D and E, as also shown in figure 2.7, with their sensitive axes along the direction Cy. The sum of their outputs now yields the component of the common motion along Cy while the difference in the outputs is proportional to

$$2z_D (\omega_y \omega_z - \dot{\omega}_x)$$

Combination of the two differential outputs gives  $\omega_x$  and  $\omega_y \omega_z$  separately. When some initial value  $\dot{\omega}_x(0)$  is known, the angular acceleration  $\dot{\omega}_x(t)$  may be integrated to give  $\omega_x(t)$ . However at least one further pair of accelerometers is needed to obtain the component of the common acceleration along Cx and such a pair could also produce a differential output proportional to  $(\dot{\omega}_y - \omega_x \omega_z)$  or  $(\omega_x \omega_y - \dot{\omega}_z)$  depending upon whether they are placed on the Cz-axis or the Cy-axis respectively. Although the information yielded by either pair taken with the other two pairs at A, B, D and E, would be sufficient, in principle, completely to determine the motion, the resulting non-linear equations are not easily solved. A further complementary pair, selected to give  $(\dot{\omega}_y + \omega_x \omega_z)$  or  $(\dot{\omega}_z + \omega_x \omega_y)$  makes the analysis easier and also provides redundant information which would be useful for checking the data.

The table below lists the output combinations of pairs of accelerometers placed symmetrically on the axes with their sensitive directions in different alignments. It would appear that the commonly-used arrangement in which the axes of sensitivity are normal to the axis upon which the accelerometer is placed is not the optimum. Three pairs, each placed symmetrically about C on an axis, with their sensitive axes aligned with that axis, would yield outputs proportional to  $(\omega_x^2 + \omega_y^2)$ ,  $(\omega_y^2 + \omega_z^2)$  and  $(\omega_z^2 + \omega_x^2)$  from which  $\omega$  is readily determined.

\* We deliberately refrain from using (p, q, r) as the angular velocity components here to avoid the possible confusion between the last component and  $|r|$ .

Positions of accelerometer pair	Direction of sensitive axes	Sum of outputs proportional to:	Difference of outputs proportional to:
(x, 0, 0) & (-x, 0, 0)	Cx	$\ddot{\xi}_C$	$-2x(\omega_y^2 + \omega_z^2)$
	Cy	$\ddot{\eta}_C$	$2x(\dot{\omega}_z + \omega_x \omega_y)$
	Cz	$\ddot{\zeta}_C$	$-2x(\dot{\omega}_y - \omega_x \omega_z)$
(0, y, 0) & (0, -y, 0)	Cx	$\ddot{\xi}_C$	$-2y(\dot{\omega}_z - \omega_x \omega_y)$
	Cy	$\ddot{\eta}_C$	$-2y(\omega_x^2 + \omega_z^2)$
	Cz	$\ddot{\zeta}_C$	$2y(\dot{\omega}_x + \omega_y \omega_z)$
(0, 0, z) & (0, 0, -z)	Cx	$\ddot{\xi}_C$	$2z(\dot{\omega}_y + \omega_x \omega_z)$
	Cy	$\ddot{\eta}_C$	$-2z(\dot{\omega}_x - \omega_y \omega_z)$
	Cz	$\ddot{\zeta}_C$	$-2z(\omega_x^2 + \omega_y^2)$

Such an arrangement is illustrated in figure 2.8.

In practice the space available is likely to limit the deployment of accelerometers in either manner; usually the space available along the Cz axis is restricted, so that a compromise is necessary. Moreover cross-axis sensitivities may also complicate matters seriously.

There remains the further possibility, which we have not discussed, that angular acceleration can be measured directly using an "angular accelerometer".

## 2.22 The equations of motion

We have already noted the two methods of formulating the equations of motion, the Newtonian and the Lagrangian. The latter possesses certain advantages as regards the equations of angular motion, particularly when approximations are being made to render them tractable.

The equations of Newton for the motion of a rigid body of invariable mass  $m$  are equations (2.1) and (2.3), which we repeat for convenience,

$$\underline{F} = m\underline{\ddot{R}}_C \quad (2.1)$$

$$\underline{L}_C = \underline{\dot{H}}_C \quad (2.3)$$

with the moment of momentum vector  $H_C$  being given by equation (2.4)

$$\underline{H}_C = \underline{\Omega} \cdot [\underline{I}]_C \quad (2.4)$$

The momenta are here referred to an inertial frame, and for a moving frame, the dot notation implies  $\frac{d}{dt}$  which we have pointed out already, may be decomposed into

$$\frac{d}{dt} = \frac{\partial}{\partial t} + \underline{\omega} \cdot \quad (2.18)$$

where  $\underline{\omega}$  is the angular velocity of the moving frame, which is identical with  $\underline{\Omega}$  only for body-fixed axes.

In the Lagrangian equations of motion,

$$\frac{d}{dt} \left( \frac{\partial T}{\partial \dot{q}_i} \right) - \frac{\partial T}{\partial q_i} - Q_i = 0 \quad (2.5)$$

we need an expression for the total kinetic energy  $T$  of the body in free motion. In terms of the angular velocity components ( $p, q, r$ ) about the principal axes  $Cx, Cy, Cz$ , we may write

$$T = \frac{1}{2} m (\dot{\xi}_C^2 + \dot{\eta}_C^2 + \dot{\zeta}_C^2) + \frac{1}{2} I_{xx} p^2 + \frac{1}{2} I_{yy} q^2 + \frac{1}{2} I_{zz} r^2 \quad (2.24)$$

laboratory-fixed axes being equated with inertial axes, the resulting error being negligibly small.

When the body possesses axial symmetry,

$$I_{yy} = I_{zz}$$

and the total kinetic energy is then

$$T = \frac{1}{2} m (\dot{\xi}_C^2 + \dot{\eta}_C^2 + \dot{\zeta}_C^2) + \frac{1}{2} I_{xx} p^2 + \frac{1}{2} I_{yy} (q^2 + r^2) \quad (2.25)$$

Using either equation (2.1) or equations (2.5) with  $\xi_C$ ,  $\eta_C$  and  $\zeta_C$  as the generalised coordinates, we readily obtain the equations describing the linear motion in component form:

$$F_{\xi} = m\ddot{\xi}_C; \quad F_{\eta} = m\ddot{\eta}_C; \quad F_{\zeta} = m\ddot{\zeta}_C + mg \quad (2.26)$$

Referred to the body-fixed axis system, the forces are

$$\begin{aligned} F_x &= X + mg_x = m(\dot{u} + qw - rv) \\ F_y &= Y + mg_y = m(\dot{v} + ru - pw) \\ F_z &= Z + mg_z = m(\dot{w} + pv - qu) \end{aligned} \quad (2.27)$$

where  $(X, Y, Z)$  are the components of the aerodynamic force alone.

In the majority of experimental free-flight techniques (see Chapter 4) the coordinates  $(\xi_C, \eta_C, \zeta_C)$  as functions of time are measured, so that these force components follow directly. Before examining these forces in terms of the aerodynamics we shall consider the equations for the angular motion.

Using equations (2.3), (2.4) and (2.18) we readily find for the moments about the centre of mass of the body

$$\begin{aligned} L &= I_{xx}\dot{p} + I_{zz}r\omega_y - I_{yy}q\omega_z \\ M &= I_{yy}\dot{q} + I_{xx}p\omega_z - I_{zz}r\omega_x \\ N &= I_{zz}\dot{r} + I_{yy}q\omega_x - I_{xx}p\omega_y \end{aligned} \quad (2.28)$$

For an aeroplane-like configuration, body-fixed axes would be used, in which case  $\omega = \Omega = p\mathbf{i} + q\mathbf{j} + r\mathbf{k}$  and equations (2.28) simplify to

$$\begin{aligned} L &= I_{xx}\dot{p} + qr(I_{zz} - I_{yy}) \\ M &= I_{yy}\dot{q} + pr(I_{xx} - I_{zz}) \\ N &= I_{zz}\dot{r} + pq(I_{yy} - I_{xx}) \end{aligned} \quad (2.29)$$

It is these equations that should be compared with the accelerometer responses listed in the table of section 2.21. One can see that in general, the relationship between these responses and the couples are not simple. However if at least one of the angular velocity components remains zero throughout the motion, accelerometer pairs placed as described in section 2.21, (symmetrically about the centre of mass, on a principal axis, with their sensitive axes parallel to one another and normal to that principal axis) provide a direct measure of the moments about the principal axes.

For axially-symmetric shapes, body-oriented fixed-plane axes are suitable. These do not rotate about  $Cx = Cx'$ , so that  $\omega = 0 + q'\mathbf{j}' + r'\mathbf{k}'$  and equations (2.28) reduce for this case to

$$\begin{aligned} L' &= I_{x'x'}\dot{p}' \\ M' &= I_{y'y'}\dot{q}' + I_{x'x'}pr' \\ N' &= I_{y'y'}\dot{r}' - I_{x'x'}pq' \end{aligned} \quad (2.30)$$

Because there is no preferred direction in the plane  $Cyz$  of an axially-symmetric body it is possible to combine the last two of equations (2.30) into a single equation, giving the "combined motion". This is conveniently achieved by introducing the complex variable,  $i$  and writing

$$\vec{Q}' = q' + ir' \quad (2.31)$$

$$\text{and } \vec{M}' = M' + iN' \quad (2.32)$$

in which case equations (2.30) become

$$\begin{aligned} L' &= I_{x'x'}\dot{p}' \\ \vec{M}' &= I_{y'y'}\dot{Q}' - i(I_{x'x'}p)Q' \end{aligned} \quad (2.33)$$

The commonly-used approximations to the equations for the angular motion assume small angular motions of some kind. In order to make such approximations, the equations must first be written in terms of the angles themselves; the angles  $\psi$ ,  $\theta$  and  $\phi$  are suitable in the present case. To carry out this

exercise we first express the angular velocity components ( $p$ ,  $q$ ,  $r$ ) in terms of these Eulerian angles as follows:

$$\begin{aligned} p &= \dot{\phi} - \dot{\psi} \sin \theta \\ q &= \dot{\theta} \cos \phi + \dot{\psi} \cos \theta \sin \phi \\ r &= \dot{\psi} \cos \theta \cos \phi - \dot{\theta} \sin \phi \end{aligned} \quad (2.34)^*$$

These expressions are derived in most textbooks on dynamics; a "geometric derivation" is illustrated in figure 2.9. For body-oriented, fixed-plane axes  $Cx'y'z'$ , suitable for axially-symmetric shapes, the angular velocity components ( $p'$ ,  $q'$ ,  $r'$ ) can be obtained from equations (2.34) simply by putting  $\sin \phi = 0$  and  $\cos \phi = 1$ , since the axes do not roll with the body which still has the component  $\dot{\phi}$ .

Substituting equations (2.34) into the expression (2.24) for the kinetic energy  $T$ , we can then use the Lagrangian equations (2.5) with  $\psi$ ,  $\theta$ ,  $\phi$  as the generalised coordinates to give

$$\begin{aligned} \frac{d}{dt} \{I_{xx}(\dot{\phi} - \dot{\psi} \sin \theta)\} + I_{yy}(\dot{\theta} \cos \phi + \dot{\psi} \cos \theta \sin \phi)\{\dot{\theta} \sin \phi - \dot{\psi} \cos \theta \cos \phi\} \\ + I_{zz}(\dot{\psi} \cos \theta \cos \phi - \dot{\theta} \sin \phi)\{\dot{\theta} \cos \phi + \dot{\psi} \cos \theta \sin \phi\} = Q_{\phi} = L \end{aligned} \quad (2.35a)$$

$$\begin{aligned} \frac{d}{dt} \{I_{yy} \cos \phi (\dot{\theta} \cos \phi + \dot{\psi} \cos \theta \sin \phi) + I_{zz} \sin \phi (\dot{\theta} \sin \phi - \dot{\psi} \cos \theta \cos \phi)\} + I_{xx}(\dot{\phi} - \dot{\psi} \sin \theta) \dot{\psi} \cos \theta \\ + I_{yy}(\dot{\theta} \cos \phi + \dot{\psi} \cos \theta \sin \phi) \dot{\psi} \sin \theta \sin \phi + I_{zz}(\dot{\psi} \cos \theta \cos \phi - \dot{\theta} \sin \phi) \dot{\psi} \sin \theta \cos \phi = Q_{\theta} \\ = M \cos \phi - N \sin \phi \end{aligned} \quad (2.35b)$$

$$\begin{aligned} \frac{d}{dt} \{I_{xx} \sin \theta (\dot{\psi} \sin \theta - \dot{\theta}) + I_{yy} \cos \theta \sin \phi (\dot{\theta} \cos \phi + \dot{\psi} \cos \theta \sin \phi) \\ + I_{zz} \cos \theta \cos \phi (\dot{\psi} \cos \theta \cos \phi - \dot{\theta} \sin \phi)\} = Q_{\psi} = (M \sin \phi + N \cos \phi) \cos \theta \end{aligned} \quad (2.35c)$$

the first of these being identical to the first of equation (2.29).

These general equations for a rigid body are so complicated that little can be done with them in this form. We have drawn attention to them here, merely to make the point that one is unlikely to obtain useful information from an experiment in which a freely flying model so behaves that no approximations to these equations can be justified. In practice some care is taken to ensure that the motion is naturally limited in some way, and we shall next proceed to a discussion of some special cases of interest.

### 2.2201 Planar motion

Motion confined to one plane is conceptually the simplest. For this reason the most frequently performed free-flight experiments are designed to achieve planar motion in the  $O\xi\zeta$ -plane. In this case  $\psi$  is identically zero, and there is no rolling motion;  $\dot{\phi} = 0$ . A single degree of rotational freedom remains, and equation (2.35b) simplifies to

$$I_{yy} \ddot{\theta} = M \quad (2.36)$$

### 2.2202 Small angular motion

If we assume that the angular displacements, velocities and accelerations are all small, the left-hand sides of equations (2.35) become completely uncoupled:

$$\begin{aligned} I_{xx} \ddot{\phi} &= L \\ I_{yy} \ddot{\theta} &= M \\ I_{zz} \ddot{\psi} &= N \end{aligned} \quad (2.37)$$

These linearised equations are the ones most commonly used as a first approximation. The first of these equations does not depend upon  $\phi$  remaining small, and in the absence of an externally applied rolling moment, it may be integrated to give  $\phi$  as a linear function of time. When however this is substituted into equations (2.35b, c) with the other angles and rates small, these remain coupled equations with variable coefficients and are not easily handled.

\* These equations also apply for wind axes; that is, a suffix  $w$  can be added to the angles and angular rates.

2.2203 Bodies with axial symmetry

Bodies with axial symmetry frequently arise in practice; cones, cone-cylinders, hemisphere-cylinders and several standard test models such as AGARD HB-2, are used for comparison purposes when investigating new measuring techniques and new wind-tunnels. The equations of motion for such shapes are therefore of special interest. Unfortunately the mass-geometric constraint does not help to simplify the equations of angular motion in any significant manner, and equations (2.33) with

$$q' = \dot{\theta} \quad (2.38)$$

$$\text{and } r' = \dot{\psi} \cos \theta$$

must be linearised. We then have

$$L' = I_{x'x'} \dot{p} = I_{x'x'} \ddot{\phi} \quad (2.39)$$

$$\text{and } \vec{M}' = I_{y'y'} \ddot{\psi} - i(I_{x'x'} p) \ddot{\psi}$$

where

$$\vec{\psi} = \theta + i\psi \quad (2.40)$$

The force equation in the cross-section plane can likewise be written

$$(Y' + iZ') + m(g_{y'} + ig_{z'}) = m(\dot{v}' + iw' - iu'(q' + ir'))$$

which upon linearisation becomes

$$Y' + iZ' = m((\dot{\beta}' + i\dot{\alpha}') - i(q' + ir')) - m(g_{y'} + ig_{z'}) \quad (2.41)$$

We have seen that to simplify the kinematic aspects of the equations of motion, drastic assumptions are necessary. It remains to consider the other sides of the equations of motion, that is the forces and moments. This we shall now proceed to do; we shall find that similar approximations are needed to represent the aerodynamics in a consistent manner.

2.221 The aerodynamic forces and moments

The aerodynamic forces and moments which act on a body in a free-flight test in a wind-tunnel are basically unsteady. In a static test, the lift on a wing, for example, is a function of the state of the flow and the incidence and sideslip angle of the wing. In the unsteady situation these independent variables are time-dependent, and because the lift on a wing is associated with the circulation around it, which in turn depends on the establishment of particular conditions near the trailing edge, this lift will depend not only on the instantaneous value of incidence, but also on its past history. This functional relation may be written in the form (Etkin, 1972)

$$L(t) = L(\alpha(\tau)), \quad -\infty < \tau < t \quad (2.42)$$

Similar relations may be written for the other independent variables and on the assumption that the effects are simply additive, that is, the system is linear - an exact formulation may be made which results in integro-differential equations of motion. Such equations are not easy to handle, and an alternative approach using transfer functions can be used which results in algebraic equations. However these methods, though exact, are restricted by the assumption of linear aerodynamics, and it is far from clear how they may be developed to include non-linear effects.

The classical approach, initiated by Bryan (1911) is less soundly based, both mathematically and physically, but non-linearities can be included in an approximate fashion. Its chief justification is perhaps that it works in a very wide variety of situations, and because free-flight testing often involves non-linear effects, we shall confine our discussion to this classical approach. The relation between the linearised classical theory and the more exact formulations is well discussed by Etkin (1972), to whom reference may be made for a more complete account of what follows.

The assumption which is at the heart of Bryan's theory is that when  $\alpha(\tau)$  is a well-behaved analytic function in the neighbourhood of  $\tau = t$ , it may be expanded as a Taylor series about this point so that equation (2.42) can be replaced by

$$L(t) = L(\alpha, \dot{\alpha}, \ddot{\alpha}, \dots)$$

the explicit time-dependence being thereby removed. A further series expansion gives the incremental lift as

$$\begin{aligned} \Delta L(t) = & L_{\alpha} \Delta \alpha + \frac{1}{2} L_{\alpha\alpha} (\Delta \alpha)^2 + \dots \\ & + L_{\dot{\alpha}} \Delta \dot{\alpha} + \frac{1}{2} L_{\dot{\alpha}\dot{\alpha}} (\Delta \dot{\alpha})^2 + \dots \\ & + \dots \\ & + L_{\alpha\dot{\alpha}} (\Delta \alpha) (\Delta \dot{\alpha}) + \dots \end{aligned} \quad (2.43)$$

where

$$L_{\alpha} = \left. \frac{\partial L}{\partial \alpha} \right|_{\alpha=0} \text{ etc.} \quad (2.44)$$

are the aerodynamic derivatives which the tests are designed to determine. In the vast majority of cases it has been found sufficient to retain one or two terms only of equation (2.43); thus

$$\Delta L(t) \approx L_{\alpha} \Delta \alpha + L_{\dot{\alpha}} \Delta \dot{\alpha} \quad (2.45)$$

is the main result of Bryan's method, and it is assumed to hold even when  $\alpha(\tau)$  is not an analytic function. Obviously the effects of non-linearities can be taken into account by including more terms of the expansion (2.43) or by regarding the derivatives, such as  $L_{\alpha}$ , as being themselves functions of the differentiation parameter, in this case  $\alpha$ .

In this way an incremental force or moment component is written

$$\Delta F_i = F_{\alpha} \Delta \alpha + F_{\dot{\alpha}} \Delta \dot{\alpha} + F_{\beta} \Delta \beta + F_{\dot{\beta}} \Delta \dot{\beta} + F_V \Delta V + F_p \Delta p + F_q \Delta q + F_r \Delta r + \dots \quad (2.46)$$

in the linear approximation, the term in  $\Delta V$  accounting for changes in the relative wind speed. A number of simplifications are possible consequent upon the symmetry which usually exists for aerodynamic models. For aeroplane-like shapes, the  $C_xz$ -plane is usually a plane of symmetry, asymmetric control configuration being handled by the addition of a term  $\Delta F_c$  to the right-hand side of equation (2.46). In symmetric flight, the lateral force and moment components ( $Y$ ,  $L$ ,  $N$ ) are identically zero when the plane of symmetry is vertical, in which case  $\beta$ ,  $p$  and  $r$  are all zero. The derivatives of these lateral components with respect to the longitudinal variables,  $V$ ,  $\alpha$ ,  $\dot{\alpha}$  and  $q$  are therefore zero. In addition the derivatives of the longitudinal components ( $X$ ,  $Z$ ,  $M$ ) with respect to the asymmetric motion are usually negligibly small, as are all those derivatives with respect to  $\dot{\alpha}$  and  $\dot{\beta}$  except  $Z_{\dot{\alpha}}$  and  $M_{\dot{\alpha}}$ . The derivative  $X_q$  is also usually neglected.

With axially-symmetric or equivalent shapes\* a number of further simplifications are possible because the  $C_y$  and  $C_z$  directions are indistinguishable. Thus  $M_{\alpha}$  and  $N_{\beta}$  are of equal magnitude, but opposite sign.

Consistent with linearisation, the increments in the state variables which appear on the right-hand side of equation (2.46) must be treated as small perturbations about some equilibrium value. For all the state variables except incidence  $\alpha$  and the relative wind speed  $V$ , this equilibrium value is zero, so the symbol  $\Delta$  is not needed.

Although the use of dimensional rather than dimensionless quantities is becoming more common, aerodynamic data, derivatives included are conveniently expressed in dimensionless form. Expressions such as equation (2.46) can be readily written in dimensionless form using  $\frac{1}{2} \rho V^2 S$  as the unit force,  $\frac{1}{2} \rho V^2 S \bar{c}$  or  $\frac{1}{2} \rho V^2 S b$  as the unit couple<sup>†</sup> and  $V/\bar{c}$  or  $V/b$  for the angular rates, but the question naturally arises as to which velocity  $V$  should be used. The quantity of aerodynamic significance is the magnitude of the relative velocity vector, but in free-flight testing in wind-tunnels this varies throughout the test. We have noted that this variation can arise not only as a result of the motion of the model but also from non-uniformities in the test stream consequent upon the use of a conical nozzle. In this connection two remarks are in order. In the first place, the useful motion of the model is confined to the viewing area which is not likely to exceed say 0.5 m in diameter. If we suppose the model to traverse this in a test

\* Bodies with trigonal symmetry together with mirror symmetry may be regarded as axially-symmetric so far as linear aerodynamics is concerned (Maple & Synge, 1949).

† For aeroplane-like shapes the mean chord  $\bar{c}$  is used with the pitching components  $M$ ,  $q$ ,  $\dot{\alpha}$  and the wing span  $b$  with the lateral components  $L$ ,  $l$ ,  $\dot{\beta}$ ,  $p$ ,  $r$ . For axially symmetric bodies it is more convenient to use a single reference length.

period of about 10 ms, starting from rest, it reaches a speed of about 100 m/s which is a few per cent of the typical stream velocity in a hypersonic impulse tunnel. To regard the magnitude of the relative wind velocity as constant in spite of this is not likely to result in serious errors. On the other hand the presence of non-uniformities in the test stream, particularly "conicity" of the flow, is less easily dismissed. To achieve as realistic a Reynolds number simulation as possible models would normally occupy as large a fraction of the test section as is consistent with avoiding tunnel interference effects. Defining the relative wind velocity, even for a stationary model, is difficult when the flow is source-like. When the model moves off-axis sideways, spurious lateral loads will arise on winged or wing-like bodies, which although they might be "calculable", have little relevance to the measurement of aerodynamic derivatives. It would seem therefore desirable either that free-flight testing be confined to streams with minimal non-uniformity, or that only the simplest of such tests, such as drag measurement, be conducted in conical flows.

We shall therefore suppose that the free-stream in the test-section is given by

$$(U_\infty, V_\infty, W_\infty) = (U_\infty, 0, 0) \quad (2.47)$$

that is, it is parallel to the tunnel axis. The velocity potential introduced in Section 2.203 is then simply

$$\phi = U_\infty \xi \quad (2.48)$$

and equations (2.16) and (2.17) for the angles of incidence and sideslip become

$$\alpha_x = \theta + \frac{W_B}{U_\infty - U_B} = \theta + \gamma_2 \quad (2.49)$$

and

$$\beta = -\psi - \frac{V_B}{U_\infty - U_B} = -\psi - \gamma_1 \quad (2.50)$$

where the trajectory angles  $\gamma_1$  and  $\gamma_2$  are clearly very small. It should be noted that  $\gamma_1$  and  $\gamma_2$  define the trajectory relative to the stream and not that in a laboratory-fixed frame which is the trajectory usually measured. The incidence  $\alpha_x$  differs from the aerodynamic incidence only by a constant.

The results of this linearised approach to the aerodynamics are conveniently summarised separately for aeroplane-like shapes and axially symmetric shapes. We shall include expansions for the lift and drag coefficients (these forces being referred to wind axes) as well as expressions for the components referred to body-axes. As usual the drag  $D$  is defined as the component of force along the direction of the relative wind vector. The lift  $L$  is normal both to this wind and the body axis  $Cy$  for aeroplane-like configurations, but for axially-symmetric shapes it is so defined that the side force is zero.

Conventionally the symbol  $L$  is used for both lift and rolling moment, but the context always make clear which is intended. In coefficient form,  $C_L$  is used for the lift coefficient and  $C_2$  for the rolling moment coefficient, consistent with the use of lower case subscripts for moment coefficients.

The derivatives with respect to velocity have been omitted since they are usually small. They can become significant in transonic flows, but this is of no concern in a hypersonic impulse-tunnel test. Where ambiguity might arise we distinguish dimensionless quantities from dimensional quantities by the use of a circumflex  $\hat{\phantom{x}}$  over the former, though we do not pursue this notation into the suffices indicating partial differentiation. We therefore define, for example,

$$C_{m_q} = \frac{\partial C_m}{\partial \hat{q}} \quad (2.51)$$

### 2.221 Aeroplane-like bodies

For bodies with mirror symmetry about the plane  $Cxz$ , the expressions for aerodynamic force and moment coefficients, referred to body-axes, assume the form

$$\begin{aligned}
C_X &= C_{X_0} + C_{X_\alpha} \Delta\alpha + \{C_{X_\alpha} \hat{\alpha} + C_{X_q} \hat{q}\} \\
C_Y &= C_{Y_\beta} \beta + C_{Y_p} \hat{p} + C_{Y_r} \hat{r} + \{C_{Y_\beta} \hat{\beta} + \Delta C_{Y_c}\} \\
C_Z &= C_{Z_0} + C_{Z_\alpha} \Delta\alpha + C_{Z_\alpha} \hat{\alpha} + C_{Z_q} \hat{q} \\
C_L &= C_{L_\beta} \beta + C_{L_p} \hat{p} + C_{L_r} \hat{r} + \{C_{L_\beta} \hat{\beta} + \Delta C_{L_c}\} \\
C_m &= C_{m_0} + C_{m_\alpha} \Delta\alpha + C_{m_\alpha} \hat{\alpha} + C_{m_q} \hat{q} \\
C_n &= C_{n_\beta} \beta + C_{n_p} \hat{p} + C_{n_r} \hat{r} + \{C_{n_\beta} \hat{\beta} + \Delta C_{n_c}\}
\end{aligned} \tag{2.52}$$

The quantities in brackets are normally negligible, but may be included where necessary. In this connection we have included the components, such as  $\Delta C_{n_c}$ , which arise from an activation of control surfaces in the lateral force and moment coefficients only, since for free-flight tests in an impulse tunnel these control surfaces will be pre-set and their contributions to the longitudinal components may be included in the "trim" values  $C_{X_0}$ ,  $C_{Z_0}$  and  $C_{m_0}$ .

The lift and drag coefficients are written in terms of their own expansions as

$$C_L = C_{L_0} + C_{L_\alpha} \Delta\alpha + C_{L_\alpha} \hat{\alpha} + C_{L_q} \hat{q} \tag{2.53}$$

and

$$C_D = C_{D_0} + C_{D_\alpha} \Delta\alpha + \{C_{D_\alpha} \hat{\alpha} + C_{D_q} \hat{q}\}$$

to the same order. Note that we have not adopted the practice of some writers in which the X and Z components of force are pre-fixed by a negative sign so as to accord with the "known" physical situation. Thus at small incidence  $C_X = -C_D$  and  $C_Z = -C_L$ .

#### 2.2212 Axially-symmetric (or equivalent) bodies

With axially symmetric bodies the spin rate  $p$  can be large; indeed spin is often used to stabilise a body along a particular flight trajectory. In such circumstances the Magnus forces and moments may be significant. These Magnus effects arise when the body possesses a component of spin about an axis normal to the relative wind. Since the spin axis  $C_x$  is usually at a small angle  $\alpha_R$  to the relative wind, where

$$\tan^2 \alpha_R = \tan^2 \alpha + \tan^2 \beta \tag{2.54}$$

the effects are of quadratic form in the state variables. However the magnitude of the spin rate  $p$  may make these terms comparable with the linear, first order terms. We shall therefore include the Magnus terms for completeness, though to the present writer's knowledge no tests on a deliberately spun model have yet been conducted in a hypersonic impulse tunnel.

For bodies with axial symmetry then, the force and moment coefficients are (Charters, 1955)

$$\begin{aligned}
C_X &= C_{X_0} + C_{X_{p^2}} \hat{p}^2 \\
C_Y &= C_{Z_\alpha} \beta + C_{L_\alpha} \hat{\beta} - C_{Z_q} \hat{r} - C_{Z_{\beta p}} (\alpha \hat{p}) - C_{Z_{\beta p}} (\hat{\beta} \hat{p}) + C_{Z_{rp}} (\hat{q} \hat{p}) + \Delta C_{Y_c} \\
C_Z &= C_{Z_\alpha} \alpha + C_{Z_\alpha} \hat{\alpha} + C_{Z_q} \hat{q} + C_{Z_{\beta p}} (\beta \hat{p}) + C_{Z_{\beta p}} (\hat{\beta} \hat{p}) + C_{Z_{rp}} (\hat{r} \hat{p}) + \Delta C_{Z_c} \\
C_L &= C_{L_p} \hat{p} + \Delta C_{L_c} \\
C_m &= C_{m_\alpha} \alpha + C_{m_\alpha} \hat{\alpha} + C_{m_q} \hat{q} + C_{m_{\beta p}} (\beta \hat{p}) + C_{m_{\beta p}} (\hat{\beta} \hat{p}) + C_{m_{rp}} (\hat{r} \hat{p}) + \Delta C_{m_c} \\
C_n &= -C_{m_\alpha} \beta - C_{m_\alpha} \hat{\beta} + C_{m_q} \hat{r} + C_{m_{\beta p}} (\alpha \hat{p}) + C_{m_{\beta p}} (\hat{\beta} \hat{p}) - C_{m_{rp}} (\hat{q} \hat{p}) + \Delta C_{n_c}
\end{aligned} \tag{2.55}$$

Again terms such as  $\Delta C_{Y_c}$  represent the effects of pre-set controls.

It will be noticed that advantage has been taken of the axial symmetry to replace the Y and N derivatives by the equivalent Z and M derivatives (Charters, 1955). This is justifiable in the dimensionless form of the equations only if the same reference length is used to reduce both the longitudinal and lateral components (see footnote on page 19). It is immaterial whether the axial length or a diameter of the body is used provided consistency is maintained, but any data published should make it clear which convention has been adopted.

As one might expect the symmetry also allows the replacement of the force components Y and Z by a single component normal to the axis of symmetry. Introducing the complex number  $i = \sqrt{-1}$ , we write upon rotation to fixed-plane coordinates:

$$\begin{aligned} C_{Y'} + iC_{Z'} = & (C_{Z_\alpha} + iC_{Z_{\beta p}} \hat{\beta})(\beta' + i\alpha') + (C_{Z_{rp}} \hat{\beta} + iC_{Z_q})(\hat{q}' + i\hat{r}') \\ & + (C_{Z_{\hat{\alpha}}} + iC_{Z_{\hat{\beta p}}} \hat{\beta})(\hat{\beta}' + i\hat{\alpha}') + \Delta(C_{Y'_c} + iC_{Z'_c}) \end{aligned} \quad (2.56).$$

Since for axially-symmetric bodies the lift is defined as the force component normal to the relative wind such that no side force exists, equation (2.56) gives the lift coefficient to first order, directly. Again to first order, the drag coefficient is given by

$$C_D = C_{D_0} + C_{D_{p^2}}(\hat{\beta})^2 \quad (2.57).$$

The last pair of equations (2.55) may also be combined and written in terms of the complex variables  $(\beta' + i\alpha')$  and  $(\hat{q}' + i\hat{r}')$  as follows:

$$\begin{aligned} (C_{n'} - iC_{m'}) = & -i(C_{n'} + iC_{m'}) = -(C_{m_\alpha} + iC_{m_{\beta p}} \hat{\beta})(\beta' + i\alpha') - (C_{m_{rp}} \hat{\beta} + iC_{m_q})(\hat{q}' + i\hat{r}') \\ & - (C_{m_{\hat{\alpha}}} + iC_{m_{\hat{\beta p}}} \hat{\beta})(\hat{\beta}' + i\hat{\alpha}') + \Delta(C_{n'_c} - iC_{m'_c}) \end{aligned} \quad (2.58).$$

Note that with Magnus forces present the resultant force component in the plane normal to the axis of symmetry does not lie in the plane containing the effective incidence  $\vec{\alpha}_R$ , which in this small angle approximation is simply

$$\vec{\alpha}_R = \beta' + i\alpha' \quad (2.59).$$

so that

$$\alpha_R^2 = \alpha'^2 + \beta'^2$$

### 2.222 The differential equations of motion in dimensionless form

We are now in a position to complete the differential equations of motion. However we have expressed the aerodynamic loads in the form of dimensionless coefficients and the state variables  $(\alpha, \beta, \hat{\alpha}, \hat{\beta}, \hat{p}, \hat{q}, \hat{r})$  are also in dimensionless form. The dynamic terms which appear in equations (2.27) and (2.28) or any of the subsequent equivalent forms or approximations to them must first also be put into a consistent form. There is no especial difficulty about this, but it is necessary to choose the unit of time  $\hat{t}$  which appears in the differential operator  $\frac{d}{d\hat{t}}$ . Strictly of course we have units of time already defined, used to render the angular rates dimensionless. Unfortunately we have two units of time for aeroplane-like bodies,  $\bar{c}/V$  and  $b/V$ , and although the small-disturbance approximation uncouples the lateral and longitudinal motions so that it is perfectly legitimate to have separate time scales for the two, in free flight tests this is not particularly convenient. We shall therefore choose a single time scale, and define, for aeroplane-like bodies

$$\hat{t} = tV/\bar{c} \quad (2.60)$$

so that the aspect ratio  $R$  will appear in some equations. No ambiguities arise for axially-symmetric shapes, since we use a single length scale.

We also define

$$\mu = \frac{2m}{\rho S \bar{c}} \quad (2.61)$$

and

$$\hat{I}_{\hat{t}\hat{t}} = \frac{2I_{\hat{t}\hat{t}}}{\rho S \bar{c} b^2}$$

for all three principal moments of inertia. Equations (2.27) then become

$$\begin{aligned} C_X - C_W \sin\theta &= \mu(D\hat{u} + \hat{q}\hat{w} - (\hat{r}\hat{v}/AR)) \\ C_Y + C_W \cos\theta \sin\phi &= \mu(D\hat{v} + (\hat{r}\hat{u} - \hat{p}\hat{w})/AR) \\ C_Z + C_W \cos\theta \cos\phi &= \mu(D\hat{w} + (\hat{p}\hat{v})/AR - \hat{q}\hat{u}) \end{aligned} \quad (2.62)$$

where

$$C_W = \frac{2mg}{\rho V^2 S} \quad (2.63)$$

and the operator  $D \equiv d/d\hat{t}$ .

A similar set of equations may also be written for the lift, drag and side force coefficients using velocity components referred to the wind axes. The latter however are not so directly available from the measured data. Accordingly it would seem appropriate to utilise the relations

$$\begin{bmatrix} C_X \\ C_Y \\ C_Z \end{bmatrix} = \begin{bmatrix} \cos\alpha_X \cos\beta & -\cos\alpha_X \sin\beta & -\sin\alpha_X \\ \sin\beta & \cos\beta & 0 \\ \sin\alpha_X \cos\beta & -\sin\alpha_X \sin\beta & \cos\alpha_X \end{bmatrix} \begin{bmatrix} -C_D \\ -C_S \\ -C_L \end{bmatrix} \quad (2.64)$$

to rewrite equations (2.62) as a set of simultaneous equations in  $C_D$ ,  $C_L$  and  $C_S$ . In principle  $C_W$  is known and all the other quantities are measured functions of time,  $\alpha_X$  and  $\beta$  being determined using their definitions, equations (2.8) and (2.9).

Thus we can find  $C_L(t)$ ,  $C_D(t)$ ,  $C_S(t)$  corresponding to the particular combination of state parameters  $\{\alpha(t), \beta(t), p(t), q(t), r(t)\}$  which happen to arise in each free-flight test. Such information is not especially useful. What we should like to determine is how each of the coefficients varies when only one state variable changes; in other words we seek aerodynamic derivatives such as  $C_{L_\alpha}$  and  $C_{L_q}$ .

Before considering this problem we must complete the set of dimensionless equations with the three describing the angular motion. A little care must be exercised over the inertia terms involving the rates of change of angular velocity, since the dimensionless forms of  $(p, q, r)$  include the velocity  $V$  in their definition, and in the general case  $V$  is a variable. Thus

$$\begin{aligned} \dot{p} &= \frac{dp}{d\hat{t}} = \frac{V}{c} \frac{d}{d\hat{t}} \left( \frac{\hat{p}V}{b} \right) = \frac{V^2}{b\bar{c}} \left\{ D\hat{p} + \hat{p} \frac{D\hat{V}}{\hat{V}} \right\} \\ \dot{r} &= \frac{V^2}{b\bar{c}} \left\{ D\hat{r} + \hat{r} \frac{D\hat{V}}{\hat{V}} \right\} \\ \dot{q} &= \frac{V^2}{b\bar{c}} \left\{ D\hat{q} + \hat{q} \frac{D\hat{V}}{\hat{V}} \right\} \end{aligned}$$

and equations (2.29) take the form

$$\begin{aligned} C_x &= \hat{I}_{xx} \left\{ D\hat{p} + \hat{p} \frac{D\hat{V}}{\hat{V}} \right\} + (\hat{I}_{zz} - \hat{I}_{yy}) \hat{q} \hat{r} \\ C_m &= \hat{I}_{yy} \{AR^2\} \left\{ D\hat{q} + \hat{q} \frac{D\hat{V}}{\hat{V}} \right\} + (\hat{I}_{xx} - \hat{I}_{zz}) \hat{p} \hat{r} \\ C_n &= \hat{I}_{zz} \left\{ D\hat{r} + \hat{r} \frac{D\hat{V}}{\hat{V}} \right\} + (\hat{I}_{yy} - \hat{I}_{xx}) \hat{p} \hat{q} \end{aligned} \quad (2.65).$$

Similar remarks may be made about these equations as were made about those for the force coefficients.

The difficulties are resolved by linearisation. The aerodynamic coefficients then appear in terms of the required derivatives and the state variables. Together with the kinematic relations, equations (2.16), (2.17) and (2.34), linearised and cast into dimensionless form, we then have a set of simultaneous differential equations in which the aerodynamic derivatives appear as coefficients. Again it is convenient to list the results for aeroplane-like and axially symmetric configurations separately.

#### 2.2221 The linearised equations for aeroplane-like shapes

Upon linearisation the six equations of motion fall naturally into two groups of three, one group defining the longitudinal or symmetric motion, the other the lateral motion. In matrix form, we have for

the longitudinal motion

$$\begin{bmatrix} D\hat{u} \\ D\alpha \\ \hat{I}_{yy} AR^2 D\hat{q} \\ D\theta \end{bmatrix} + \begin{bmatrix} 0 & \frac{1}{\mu}(C_{D_\alpha} - C_{L_0}) & 0 & \frac{C_W}{\mu} \\ 0 & \frac{C_{L_\alpha}}{C_{L_\alpha} + \mu} & \frac{C_{L_q} - \mu}{C_{L_\alpha} + \mu} & 0 \\ 0 & \left( \frac{C_{m_\alpha} C_{L_\alpha}}{C_{L_\alpha} + \mu} - C_{m_\alpha} \right) & \left( \frac{C_{m_\alpha} (C_{L_q} - \mu)}{C_{L_\alpha} + \mu} - C_{m_q} \right) & 0 \\ 0 & 0 & -1 & 0 \end{bmatrix} \begin{bmatrix} \hat{u} \\ \alpha \\ \hat{q} \\ \theta \end{bmatrix} = \begin{bmatrix} -\frac{C_{D_0}}{\mu} \\ \frac{C_W - C_{L_0}}{C_{L_\alpha} + \mu} \\ \left( C_{m_0} + \frac{C_{m_\alpha} (C_W - C_{L_0})}{C_{L_\alpha} + \mu} \right) \\ 0 \end{bmatrix} \quad (2.66)$$

where the expansion of the aerodynamic coefficients has been taken about  $\alpha_x = 0$ , so that we can write  $\alpha_x = \Delta\alpha = \alpha$ , and the values  $C_{L_0}$ ,  $C_{D_0}$ , and  $C_{m_0}$  and all the derivatives are evaluated at  $\alpha_x = 0$ .

The quantity  $\mu$  is of the order of the ratio of density of the model to density of the gas stream. Consequently both  $C_{L_\alpha}$  and  $C_{L_q}$  are negligible in comparison with it, and these equations can be simplified considerably in practical cases. Thus

$$\begin{bmatrix} D\hat{u} \\ D\alpha \\ D\hat{q} \\ D\theta \end{bmatrix} + \begin{bmatrix} 0 & \frac{1}{\mu}(C_{D_\alpha} - C_{L_0}) & 0 & \frac{C_W}{\mu} \\ 0 & \frac{C_{L_\alpha}}{\mu} & -1 & 0 \\ 0 & -\frac{C_{m_\alpha}}{\hat{I}_{yy} AR^2} & \frac{-1}{\hat{I}_{yy} AR^2} (C_{m_\alpha} + C_{m_q}) & 0 \\ 0 & 0 & -1 & 0 \end{bmatrix} \begin{bmatrix} \hat{u} \\ \alpha \\ \hat{q} \\ \theta \end{bmatrix} = \begin{bmatrix} -\frac{C_{D_0}}{\mu} \\ \frac{C_W - C_{L_0}}{\mu} \\ \frac{C_{m_0}}{\hat{I}_{yy} AR^2} \\ 0 \end{bmatrix} \quad (2.66a).$$

The equations for the lateral motion are

$$\begin{bmatrix} D\hat{\beta} \\ D\hat{p} \\ D\hat{r} \\ D\hat{\phi} \end{bmatrix} = \begin{bmatrix} \frac{C_{Y_\beta}}{\mu} & \frac{C_{Y_p}}{\mu} & \left( \frac{C_{Y_r}}{\mu} - \frac{1}{AR} \right) & \frac{C_W}{\mu} \\ \frac{C_{\ell_\beta}}{\hat{I}_{xx}} & \frac{C_{\ell_p}}{\hat{I}_{xx}} & \frac{C_{\ell_r}}{\hat{I}_{xx}} & 0 \\ \frac{C_{n_\beta}}{\hat{I}_{zz}} & \frac{C_{n_p}}{\hat{I}_{zz}} & \frac{C_{n_r}}{\hat{I}_{zz}} & 0 \\ 0 & \frac{1}{AR} & 0 & 0 \end{bmatrix} \begin{bmatrix} \hat{\beta} \\ \hat{p} \\ \hat{r} \\ \hat{\phi} \end{bmatrix} + \begin{bmatrix} \frac{\Delta C_{Y_c}}{\mu} \\ \frac{\Delta C_{\ell_c}}{\hat{I}_{xx}} \\ \frac{\Delta C_{n_c}}{\hat{I}_{zz}} \\ 0 \end{bmatrix} \quad (2.67).$$

### 2.2222 The equations for axially-symmetric spinning bodies

For axially-symmetric bodies the equations are conveniently grouped into a pair which describe the motion along and about the axis  $Cx'$  of symmetry and a second complex pair which specify the motion "in" the cross-section plane  $Cy'z'$  which does not rotate with body. As we have seen, it is possible to define two complex state variables

$$\hat{\alpha}_R = \beta' + i\alpha' \quad (2.59)$$

$$\text{and } \hat{Q}' = \hat{q}' + i\hat{r}' \quad (2.68)$$

when the disturbances are all small, the latter being the dimensionless form of equation (2.31). In terms of these the equations are

$$D\hat{u} = \frac{1}{\mu} \{C_{X_0} + C_{X_p} \hat{p}^2 - C_{W\theta}\} \quad (2.69)$$

$$D\hat{p} = \frac{1}{\hat{I}_{x'x'}} \{C_{L_p} \hat{p} + \Delta C_{L_c}\} \quad (2.70)$$

and

$$\begin{bmatrix} D\hat{\alpha}_R \\ D\hat{Q}' \end{bmatrix} = \begin{bmatrix} a_{11} & a_{12} \\ a_{21} & a_{22} \end{bmatrix} \begin{bmatrix} \hat{\alpha}_R \\ \hat{Q}' \end{bmatrix} + \begin{bmatrix} b_1 \\ b_2 \end{bmatrix} \quad (2.71)$$

where

$$a_{11} = \frac{C_{Z_\alpha} + i C_{Z_{\beta p}} \hat{p}}{(\mu - C_{Z_\alpha} - i C_{Z_{\beta p}} \hat{p})}$$

$$a_{12} = \frac{C_{Z_{rp}} \hat{p} + i(\mu + C_{Z_q})}{(\mu - C_{Z_\alpha} - i C_{Z_{\beta p}} \hat{p})}$$

$$a_{21} = \frac{1}{\hat{I}_{y'y'}} \{ (C_{m_{\beta p}} \hat{p} - i C_{m_\alpha}) + \frac{(C_{m_{\beta p}} \hat{p} - i C_{m_\alpha})(C_{Z_\alpha} + i C_{Z_{\beta p}} \hat{p})}{(\mu - C_{Z_\alpha} - i C_{Z_{\beta p}} \hat{p})} \} \quad (2.72)$$

$$a_{22} = \frac{1}{\hat{I}_{y'y'}} \{ a_{12}(C_{m_{\beta p}} \hat{p} - i C_{m_\alpha}) + (C_{m_q} - i C_{m_{rp}} \hat{p}) + i \hat{I}_{x'x'} p \}$$

$$b_1 = \frac{\Delta C_{Y_c} + i(\Delta C_{Z_c} + C_W)}{(\mu - C_{Z_\alpha} - i C_{Z_{\beta p}} \hat{p})}$$

$$b_2 = \frac{1}{\hat{I}_{y'y'}} \{ (C_{m_{\beta p}} \hat{p} - i C_{m_\alpha}) b_1 + \Delta C_{m_c} + i C_{n_c} \}$$

It is important to note that the control forces and moments,  $C_{K_c}$  (where  $K = Y, Z, m, n$ ) are referred to fixed-plane axes in these equations. In other words, for controls attached to the body, the control forces spin at the rate  $p$  relative to the frame  $Cy'z'$ . They may be written

$$(\Delta C_{Y_c} + i \Delta C_{Z_c}) = (\Delta C_{Y_c} + i \Delta C_{Z_c}) e^{i\hat{p}\hat{t}} \quad (2.73)$$

and

$$(\Delta C_{m_c} + i \Delta C_{n_c}) = (\Delta C_{m_c} + i \Delta C_{n_c}) e^{i\hat{p}\hat{t}}$$

where the complex amplitudes on the right-hand sides are constant and will of course normally be small if the conditions of axial symmetry are to be maintained. Again advantage can be taken of the fact that  $\mu$  is large in comparison with the terms with which it is bracketed.

Equations (2.66), (2.67) and (2.69) to (2.72) are rather forbidding in appearance in spite of the approximations which have been made in deriving them. We feel however that by including as many terms as we can at this stage, we shall be better able to see just what assumptions are being made when free-flight data are analysed. Free-flight experiments are normally designed so that the simplest possible motion consistent with the required derivatives ensues. Frequently the motion departs to some extent from that intended. For example an experiment to measure the position of the centre of pressure of a model requires the model to be so balanced that it fly at constant incidence. This will normally require several individual tests in which the position of the centre of mass is adjusted from test to test (Pennelegion, Cash & Shilling, 1967). Questions naturally arise as to whether any useful aerodynamic data can be obtained from the preliminary, "abortive," tests in which the incidence varies, and if so how these data

are to be extracted from the measurements. This is among the problems we shall consider briefly in the following section.

### 2.23 The analysis of experimental data

Free-flight testing has always been a major component of ballistics research and during the last thirty years or so the techniques have become very sophisticated. Extraordinarily detailed information has been obtained by launching models from light-gas guns along instrumented ranges in which, in many cases, the pressure may be adjusted from sub-atmospheric to super-atmospheric. The motion of the model along the range is usually determined by timing and photographing its passage of a number of carefully spaced measuring stations. In this way the trajectory coordinates and model attitude are found as functions of time, and from these data a great deal of aerodynamic knowledge has been gained. The whole technology has been recently reviewed in AGARDograph 138 (Canning, Seiff & James, 1970). One might expect much of this to be fairly directly applicable to flight-testing in wind-tunnels and so of course it is. The experimental procedures, particularly the ways in which measurements are made, are largely common to both - but there are essential differences.

The 'counterflow' present in the wind-tunnel considerably modifies the motion referred to a laboratory-fixed coordinate system. It has also some bearing on the way the equations of motion are formulated, as we have already seen. The results of these differences are twofold. In the first place, whereas in the range data are collected at a number of discrete stations, from which the changes in the motion must be inferred, in the tunnel all the data are obtained at a single station, and it is the changes in the trajectory relative to the stream that are measured. The different primary data and the slightly different equations of motion mean that the analytic methods developed for handling ballistic range data must be modified to some extent when dealing with other than the simplest motions.

Because so little experience has been reported it is difficult to discuss the adaptation of any of these analytic methods in detail, since the 'efficiency' of modified methods using the different measurements will remain uncertain until they have been tried. In these circumstances it is felt that in many cases little more can be done than draw attention to some of the methods that might be adapted and some of the principles underlying them.

One of the difficulties often encountered in the free flight testing of models in wind-tunnels, is the relative paucity of data, a particularly acute problem in short duration experiments where in some cases measurements can be made at perhaps only ten or so 'instants' - this would correspond to ten measuring stations along the ranges. Such measurements give both the angular and linear positions at each instant, but the forces and moments are related to the accelerations. The double differentiation needed to derive the accelerations can introduce large errors and the transformation to a more convenient coordinate frame than the laboratory-fixed one can also introduce further errors since the measured angles must be used. One obvious way of diminishing these errors is to 'smooth' the primary data by a curve-fitting procedure and then carry out the differentiation and coordinate transformation using the fitted curves. However the aim is to determine the aerodynamic coefficients relevant to the test, and a somewhat different approach, practical since the advent of the high speed digital computer, has been found more sensitive. From the test one first gauges which state parameters are important and the equations of motion are written in terms of these. Values of the relevant aerodynamic coefficients are then assumed and the equations of motion are integrated numerically to obtain position data equivalent to those actually measured. The aerodynamic coefficients are then adjusted until a good fit to the measurements is obtained. It is not obvious that this method will provide a unique solution to the problem in the general case when the motion is complicated, particularly as the measurements are few. However in many cases restrictions are effectively placed on the method because only the equations corresponding to small disturbances can be easily integrated.

Some remarks have already been made concerning the interpretation of accelerometer records. In this section we discuss only the handling of position vs. time data. The experimental techniques are discussed in Chapter 4. The discussion is essentially in two parts. In the first we summarise briefly how the raw information - usually in the form of photographs - is converted into position coordinates as a function of time. In the second part, methods of estimating aerodynamic derivatives are reviewed.

In principle the experimental records must provide sufficient information to enable six coordinates to be determined as functions of time, the coordinates  $(\xi_C, \eta_C, \zeta_C)$  of the centre of mass of the model

and the Eulerian angles ( $\psi$ ,  $\theta$ ,  $\phi$ ). In many cases of course experiments may be so designed that some of these should remain unchanged during the test; for example a truly axially symmetric model should not roll or translate normal to its plane of incidence so long as there is no initial spin. However it may be necessary to provide experimental checks that assumptions of this nature are justified.

Where standard shadowgraph methods are used two photographs from different angles must be taken at each instant in the general case; usually orthogonal views are most convenient, one vertical and one horizontal, but other stereoscopic systems are possible. An alternative, optical telemetry, system has been described by Requardt & Kabelitz (1971). Although the information is recorded photographically in this case also, we consider it separately in sub-section 2.232. First we look briefly at conventional shadowgraph methods.

### 2.231 The derivation of position and attitude from photographic records

Photographic recording of a model in free flight is a standard measuring technique of ballistic range technology. As such it has been excellently reviewed by James and his colleagues (1970) at NASA-Ames in AGARDograph 138 (Chapter 6). We shall not attempt a summary of their article here, but content ourselves with an account of the factors which it may be necessary to record. The potential user of this method is recommended to their article for further details.

Obtaining the position of the model at any instant necessarily implies the existence of a reference frame. Where cinephotography is used, indexing from one frame to another is necessary and this is conveniently provided by including reference lines in the field of view. For flows of relatively long duration, a large number of frames can be obtained with modern high speed cameras, but the images are necessarily small. Timing marks must also be provided since the framing rate is rarely reliably constant. In shock-tunnels, where the flow duration is frequently less than 10 ms, multiple spark-exposures of a single photographic plate showing successive images of the model overlaid, are more practical. Here the relative position from one instant to another can be obtained more directly, but some reference is needed to specify the vertical and the downrange directions. Such references are readily provided by plumb lines and tautly stretched wires, positioned outside the flow, or by appropriately aligned straight edges within the field of view. Single references in each direction are sufficient when each light beam is a well-collimated, parallel beam exactly normal to the flow direction. The uncertainty can be reduced by providing pairs of wires in each direction on both the near and far sides of the flow. They must of course be staggered so that one pair does not occult the other. The known relative positions of these wires and their images in the plane of the photographic plate not only provide evidence on how well the light beam is aligned and collimated but also give the optical magnification of the system. The uniformity of this optical magnification which may be affected by spherical aberrations of the mirrors or off-axis light sources can be tested by photographing a grid spanning the test section prior to flight tests.

Errors may also arise because of refraction of the light beam when it is not perpendicular to the windows - in fact where the walls of the test-section are divergent to allow for boundary layer growth, systematic errors due to refraction must be taken into account.

Occasionally conical projection systems are used instead of parallel beams. Such systems produce apparent distortions of the shape of the model and of course the Eulerian angles cannot be obtained quite so directly as they can with the carefully aligned collimated system.

Depending upon the shape of the model the roll attitude may or may not be deducible from the orthogonal views implied above. When the model is axially symmetric some reference marks must be attached to the model if the roll attitude is to be determined. Pins projecting from the base are commonly used. Frequently however such positive reference lines in the model are needed merely to define its position coordinates and the pitch and yaw angles ( $\theta$ ,  $\psi$ ). The axis of an axially-symmetric model is clearly defined in a shadowgraph and models with sharply-pointed noses and cylindrical portions present few problems. Some shapes however will clearly present difficulties (see Seiff & Wilkins, 1961 for a good example) and a base-pin defining the longitudinal principal axis can be of great assistance. When this is possible the same reference point or points should be used in making measurements pertinent to a single flight. Not only are systematic distortions due to refraction and diffraction compensated automatically; the computations needed to obtain ( $\xi_C$ ,  $\eta_C$ ,  $\zeta_C$ ,  $\psi$ ,  $\theta$ ,  $\phi$ ) are then standardised and more readily programmed for a digital computer.

Details of the working formulae needed for any particular optical system are simply obtained from the geometry of that system. Relations for collimated and conical projection systems are given by James and others (1970) in the review mentioned above.

### 2.232 Position and attitude from an optical telemetry system

Requardt & Kabelitz (1971) have described an optical telemetry system for use in free flight tests in the piston driven gun tunnel at DFVLR, Porz-Wahn. Further practical details of the system are given in Chapter 4. Here it is sufficient to say that a single flashing light source carried in the model produces three focussed beams in a cross-section plane (parallel to the  $Cyz$ -plane) which are spaced  $120^\circ$  apart about the roll axis, see figure 2.10. A photographic film is wrapped around the test section forming a circularly cylindrical surface coaxial with the test section. With the model in flight and the light flashing at a known frequency, three tracks of light spots are recorded on the film. So long as the corresponding spots on each track can be identified, the six coordinates, two for each spot on the developed film, are sufficient to determine the six coordinates  $(\xi_C, \eta_C, \zeta_C, \psi, \theta, \phi)$  defining the position and attitude of the model.

Suppose that two lines are marked on the film, one along a generator ( $\lambda = 0, R = a$ ) the other along the circle ( $\xi = 0, R = a$ ). When the cylindrical film is unwrapped these lines form a set of Cartesian axes and the position of any light spot image is given by its coordinates  $(\xi, a\lambda)$ . The cartesian coordinates in  $(\xi, \eta, \zeta)$  space follow immediately since (see figure 2.11)

$$\begin{aligned}\xi &= \xi \\ \eta &= -a \sin \lambda \\ \zeta &= a \cos \lambda\end{aligned}\quad (2.74)$$

Having identified the three corresponding images formed by the same flash, we seek that point  $S$  which lies in the plane of the three images and at which the angle subtended by any two of the images is  $2\pi/3$ . We first define unit vectors  $(\underline{i}'' , \underline{j}'' , \underline{k}'')$  in the laboratory fixed frame  $O\xi\eta\zeta$ , and label each image by a suffix  $1, 2$  or  $3$ . Then the condition that  $S$  and the images  $J_1, J_2$  and  $J_3$  lie in the same plane is

$$\begin{aligned}\vec{S}J_1 \cdot (\vec{J}_1J_2 \wedge \vec{J}_1J_3) &= 0 \\ \text{or} \quad (\xi_S - \xi_1)A_1 + (\eta_S - \eta_1)A_2 + (\zeta_S - \zeta_1)A_3 &= 0\end{aligned}\quad (2.75)$$

where

$$\begin{aligned}A_1 &= (\eta_2 - \eta_1)(\zeta_3 - \zeta_1) - (\zeta_2 - \zeta_1)(\eta_3 - \eta_1) \\ A_2 &= (\zeta_2 - \zeta_1)(\xi_3 - \xi_1) - (\xi_2 - \xi_1)(\zeta_3 - \zeta_1) \\ A_3 &= (\xi_2 - \xi_1)(\eta_3 - \eta_1) - (\eta_2 - \eta_1)(\xi_3 - \xi_1)\end{aligned}\quad (2.76)$$

We note that the direction of the longitudinal axis  $Cx$  of the model, which is normal to the plane  $J_1J_2J_3$ , is given by

$$\frac{A_1 \underline{i}'' + A_2 \underline{j}'' + A_3 \underline{k}''}{(A_1^2 + A_2^2 + A_3^2)^{\frac{1}{2}}}\quad (2.77)$$

In addition we have

$$\cos \frac{2\pi}{3} = -\frac{1}{2} = \frac{(\vec{S}J_1) \cdot (\vec{S}J_2)}{(\vec{S}J_1)(\vec{S}J_2)} = \frac{(\vec{S}J_1) \cdot (\vec{S}J_3)}{(\vec{S}J_1)(\vec{S}J_3)} = \frac{(\vec{S}J_2) \cdot (\vec{S}J_3)}{(\vec{S}J_2)(\vec{S}J_3)}\quad (2.78)$$

and

$$\vec{S}J_p = (\xi_p - \xi_S)\underline{i}'' + (\eta_p - \eta_S)\underline{j}'' + (\zeta_p - \zeta_S)\underline{k}''\quad (2.79)$$

where  $p = 1, 2, 3$ .

though one of equations (2.78) is redundant if (2.75) is used. Since equation (2.75) is linear in the unknowns  $\xi_S, \eta_S$  and  $\zeta_S$  while equations (2.78) are not, the solution is somewhat simplified by using it. We thus have

$$\begin{aligned}
 (\xi_S - \xi_1)A_1 + (\eta_S - \eta_1)A_2 + (\zeta_S - \zeta_1)A_3 &= 0 \\
 \frac{(\xi_1 - \xi_S)(\xi_2 - \xi_S) + (\eta_1 - \eta_S)(\eta_2 - \eta_S) + (\zeta_1 - \zeta_S)(\zeta_2 - \zeta_S)}{\sqrt{((\xi_1 - \xi_S)^2 + (\eta_1 - \eta_S)^2 + (\zeta_1 - \zeta_S)^2)((\xi_2 - \xi_S)^2 + (\eta_2 - \eta_S)^2 + (\zeta_2 - \zeta_S)^2)}} &= -\frac{1}{2} \quad (2.80). \\
 \frac{(\xi_1 - \xi_S)(\xi_3 - \xi_S) + (\eta_1 - \eta_S)(\eta_3 - \eta_S) + (\zeta_1 - \zeta_S)(\zeta_3 - \zeta_S)}{\sqrt{((\xi_1 - \xi_S)^2 + (\eta_1 - \eta_S)^2 + (\zeta_1 - \zeta_S)^2)((\xi_3 - \xi_S)^2 + (\eta_3 - \eta_S)^2 + (\zeta_3 - \zeta_S)^2)}} &= -\frac{1}{2}
 \end{aligned}$$

No analytic solution of equations (2.80) is available, so that a numerical procedure is necessary. Since the point  $(\xi_S, \eta_S, \zeta_S)$  is known approximately from the solution involving the preceding set of three images, an iterative procedure would be suitable.

The Eulerian angles may also be obtained as follows. Since the expression (2.77) gives the direction of Cx, and the pitch angle  $\theta$  is the angle Cx makes with the horizontal, we have

$$\theta = \cos^{-1} \left[ \frac{A_1^2 + A_2^2}{A_1^2 + A_2^2 + A_3^2} \right]^{\frac{1}{2}} \quad (2.81).$$

Similarly, the angle  $\psi$  of yaw, which is the angle between the horizontal projection of Cx and the unit vector  $-i''$ , is given by

$$\psi = \cos^{-1} \left[ \frac{A_1^2}{A_1^2 + A_2^2} \right]^{\frac{1}{2}} \quad (2.82).$$

The roll angle  $\phi$  is a little more difficult to determine. The horizontal line in the plane normal to Cx is given by

$$\frac{-A_2 i'' + A_1 j''}{\sqrt{A_1^2 + A_2^2}} \quad (2.83).$$

If we assume then that the initial position of the Cz axis is vertical,

$$\phi = \cos^{-1} \left\{ \frac{A_2(\xi_1 - \xi_S) - A_1(\eta_1 - \eta_S)}{\sqrt{(A_1^2 + A_2^2)((\xi_1 - \xi_S)^2 + (\eta_1 - \eta_S)^2 + (\zeta_1 - \zeta_S)^2)}} \right\} \quad (2.84).$$

The centre of mass C of the model then follows from the known geometry of the model relating the position of the light-source S to that of C. Usually S will lie on the Cx-axis of the model and application of the transformation equations (2.11) and (2.12) is considerably simplified. The matrices in both these equations are simply matrices of direction cosines, so that the inverses which are needed are obtained by transposing rows and columns.

The complications of an iterative solution to equations (2.80) could be avoided by a slightly different geometrical arrangement for the light beams. If instead of  $2\pi/3$  each pair of beams  $\vec{S}\vec{J}_1$ ,  $\vec{S}\vec{J}_2$  and  $\vec{S}\vec{J}_1$ ,  $\vec{S}\vec{J}_3$  subtend an angle  $\pi/2$  at the source, the right-hand sides of the last two of equations (2.80) are also zero. Removing the radical in each case and subtracting one equation from the other we obtain a second linear equation (expressing the fact that  $\vec{J}_2\vec{J}_3$  is normal to  $\vec{S}\vec{J}_1$ ). An explicit algebraic solution for  $(\xi_S, \eta_S, \zeta_S)$  can then be found. There are however certain practical disadvantages. The arrangement of the optical components is not symmetrical and, for an axially-symmetric model, the effect would be to move the centre of mass off-axis. Where additional mass can be tolerated, ballast could be used. A better arrangement, if space is available, is to accommodate a fourth beam providing redundant information, so that uncertainties could be reduced.

### 2.233 The estimation of aerodynamic derivatives

Our discussion so far has taken account of any general motion that a model may execute. However we saw when examining the equations of motion and when trying to formulate expressions for the aerodynamic forces and moments that small motions only are amenable to analytic treatment. The experimenter usually goes one stage further in limiting the motion. Where possible he tries to arrange that as many of the state variables remain unchanged during the motion as is consistent with the measurements to be made. Thus in measuring the drag coefficient he would try to ensure that only motion along the direction of the

relative wind vector takes place. Since drag cannot be eliminated an unrestrained model will always have some motion along that direction, so that experiments designed to determine any other aerodynamic coefficient or derivative must take account of it. An alternative method would be to provide positive restraints for some degrees of freedom only, but such techniques are rather special, and are best discussed separately (see section 2.4).

The equations of motion in conventional dimensionless form have as independent variable the non-dimensional time  $\hat{t}$ . We discussed earlier the advantages of a single unit of time for both the longitudinal and lateral motions, but there remains a fundamental difficulty. We have defined

$$\hat{t} = \frac{tV}{\bar{c}} \quad (2.60)$$

for aeroplane-like shapes, while for axially-symmetrical configurations  $\bar{c}$  is replaced by some other representative length. The inherent difficulty centres upon the presence of the relative speed  $V$  in the definition. This is given by

$$V = \{(U_\infty - U_B)^2 + V_B^2 + W_B^2\}^{\frac{1}{2}} = U_\infty - U_B$$

and so varies throughout the test. The dimensionless time  $\hat{t}$  is therefore not a particularly convenient variable for analysing free-flight data. A change of variable to

$$\xi^* = U_\infty t - \xi = \bar{c} \hat{\xi}^* \quad (2.85)$$

removes the difficulty, since both  $\xi$  and  $t$  are measured fairly directly. Thus

$$\frac{d}{d\hat{t}} = \frac{d}{d\xi^*} \cdot \frac{d\xi^*}{d\hat{t}} = V \frac{d}{d\xi^*}$$

and

$$\frac{d^2}{d\hat{t}^2} = \frac{d}{d\hat{t}} \left\{ (U_\infty - U_B) \frac{d}{d\xi^*} \right\} = V^2 \frac{d^2}{d\xi^{*2}} - \frac{dU_B}{d\hat{t}} \frac{d}{d\xi^*}$$

In dimensionless form

$$D \equiv \frac{d}{d\hat{t}} = \frac{\bar{c}}{V} \frac{d}{d\hat{\xi}^*} = \frac{d}{d\hat{\xi}^*}$$

and

$$D^2 \equiv \frac{d^2}{d\hat{t}^2} = \frac{d^2}{d\xi^{*2}} - \frac{C_D}{u} \frac{d}{d\xi^*} \quad (2.86)$$

where we have used

$$m \frac{dU_B}{d\hat{t}} = C_D \frac{1}{2} \rho V^2 S$$

It is convenient to review the ways in which aerodynamic information can be obtained from free-flight test data by treating each item separately; accordingly we begin with the simplest, the drag coefficient.

### 2.2331 The drag coefficient

We suppose, to begin with, that a model possessing mirror symmetry has been released with zero initial motion at its no-lift incidence and with zero yaw. The motion which then ensues is along the direction of the wind vector, which we assume is parallel to  $O\xi$ . However the period of steady test flow does not begin immediately and the model begins its motion under the influence of the tunnel starting process. The displacement and velocity of the model at the end of this starting process are of course unknown, and the drag analysis must take account of this.

The basic equation of motion is

$$D_0 = \frac{1}{2} \rho S C_{D_0} (U_\infty - U_B)^2 = m \frac{d^2 \xi}{dt^2} = m \frac{dU_B}{dt} \quad (2.87)$$

and as a first approximation, we might assume that  $U_B \ll U_\infty$ . In this case the drag force and the consequent acceleration are constant, and equation (2.87) may be integrated to give

$$\xi = \xi_0 + U_{B_0} (t - t_0) + \frac{\rho S C_{D_0} U_\infty^2}{4m} (t - t_0)^2 \quad (2.88)$$

where  $\xi_0$  and  $U_{B_0}$  are respectively the displacement and velocity at time  $t$  when the quasi-steady period begins. A least-squares fit of the experimental data to equation (2.88) yields first approximations to  $C_{D_0}$  and  $U_{B_0}$ . This method has been used by Pennelegion, Cash & Shilling (1967). A difficulty present in all methods of drag estimation is the strong dependence of  $C_{D_0}$  on the dynamic pressure of the stream, which in hypersonic impulse tunnels is rarely known with great accuracy. Pennelegion and his colleagues at the National Physical Laboratory avoided this problem by flying a calibration sphere, the drag coefficient of which was assumed known.

Using the variable  $(\xi - U_\infty t)$  which represents the distance travelled relative to the gas, equation (2.87) may be integrated exactly, subject to the assumption that  $C_{D_0}$  remains constant (in addition of course to  $\rho$ ,  $S$  and  $m$ ). Of the several possible forms of the results, we draw attention first to the reformulated differential equation

$$C_{D_0} = \frac{2m}{\rho S} \cdot \frac{d\{\ln(1 - U_B/U_\infty)\}}{d(U_\infty t - \xi)} = \mu \frac{d\{\ln(1 - U_B/U_\infty)\}}{d\xi^*} \quad (2.89)$$

which might in principle be used directly as suggested by Prislín (1966) and Dayman (1966). Plotting  $\ln\{1 - U_B/U_\infty\}$  vs  $(U_\infty t - \xi)/\bar{c}$  using measured data and taking the slope gives a value for  $C_{D_0}$ . A double differentiation is involved, the first being necessary to determine  $U_B$ , so that the procedure is unlikely to yield very accurate results.

Integration of equation (2.89) twice results in an equation relating  $\xi$  and  $t$  as follows

$$t = t_0 + \frac{\{\exp[-K C_{D_0} \{(\xi - U_\infty t) - (\xi_0 - U_\infty t_0)\}] - 1\}}{K C_{D_0} (U_\infty - U_{B_0})} \quad (2.90)$$

where  $K = \rho S/2m$  and  $t_0$ ,  $U_{B_0}$  and  $\xi_0$  have the same meanings as in equation (2.88). Equation (2.90) can be used as the basis for a "more accurate" estimation of  $C_{D_0}$  even though it is not given explicitly. The problem is basically to determine that value of  $C_{D_0}$  which provides a "best fit" to the measurements  $\xi = \xi(t)$ , and the details of the procedure depend upon how this "best fit" is defined. One might choose to minimise either the sum of the squares of the residuals of the measured and calculated times at a given value of  $\xi$ , or those of the measured and calculated positions at a given time  $t$ . Equation (2.90) is readily inverted for the latter approach which appears less complicated:

$$\xi = \xi_0 + U_\infty (t - t_0) - \frac{1}{K C_{D_0}} \ln\{1 + K C_{D_0} (t - t_0)(U_\infty - U_{B_0})\} \quad (2.91)$$

A standard optimisation procedure might then be used. For example, with the value of  $C_{D_0}$  obtained from equation (2.88) one obtains values of  $U_{B_0}$  and  $\xi_0$  by fitting equation (2.91) to the measurements using a least-squares approach. The sum of the squares of the  $\xi$ -residuals is computed, the drag coefficient is changed and the process repeated. If the sum of the residuals decreases,  $C_{D_0}$  is changed further in the same direction; if it increases it is changed in the opposite sense and the calculation of residuals repeated. So long as the sum diminishes, one continues to change  $C_{D_0}$  in the direction which reduces the sum of the squares of the residuals. When this sum increases  $C_{D_0}$  is changed by a smaller amount in the opposite sense, the calculation continuing until the increments are less than some specified value.

The preceding analysis is based upon the assumption that only a drag force acts upon the model. It may however be applied directly to other cases in which  $C_D$  remains constant. In such cases the flight trajectory will not be parallel to  $O\xi$ , since in general a lift force may also act when the model is at incidence. Since the drag force is defined as the component of force along the direction of the relative wind, we should replace equation (2.87) by

$$D = -m \frac{d^2 x_w}{dt^2}$$

where  $x_w$  is measured opposite to the relative wind as in section (2.205). The trajectory angle  $\gamma_2$  relative to the wind is normally very small (at most a few degrees), and since

$$d\xi = - dx_w \cos \gamma_2 \quad (2.93)$$

little error is involved in taking  $\cos \gamma_2 = 1$  and using the  $\xi$ -coordinates in the analysis.

Additional complications arise when the drag coefficient cannot be regarded as constant during the flight. The drag coefficient is usually a function of incidence, so that one implication of the paragraph above is that the incidence remains constant throughout the test. In so far as the velocity components ( $U_B, W_B$ ) of the model are functions of time, this can never be strictly true unless  $W_B$  remains zero, or the pitch angle  $\theta$  changes so as to compensate exactly the change in  $W_B$ . The latter circumstance is somewhat unlikely, but as we have already noted  $\gamma_2$  remains small, so that the effect on the incidence, see equation (2.16), is also small. It may nevertheless be necessary to take it into account, in particular when  $C_D$  is a fairly strong function of incidence.

Changes of incidence will also occur when the model is not statically balanced; that is, when the centres of mass and of pressure do not coincide. If the position of the centre of pressure depends upon incidence, then it will move as  $W_B$  changes, so that for such a model, static balance cannot be exactly maintained throughout the flight, and the model will pitch.

Seiff & Wilkins (1961) have indicated how these variations may be accommodated. They suppose that the drag coefficient is a quadratic function of resultant incidence  $\alpha_R$ ,

$$C_D = C_{D_0} + C_{D_2} \alpha_R^2 \quad (2.94)$$

the effective incidence  $\alpha_R = (\alpha^2 + \beta^2)^{1/2}$  being appropriate for axially symmetric or equivalent shapes. This form is fairly common in practice, the second term being the drag-due-to-lift, but the method may be generalised to other powers than 2, and even to polynomials when sufficient data exist.

Equation (2.94) is then substituted into (2.89) which is then integrated to yield

$$(C_{D_0} (\hat{\xi}_2^* - \hat{\xi}_1^*) + C_{D_2} \int_{\hat{\xi}_1^*}^{\hat{\xi}_2^*} \alpha_R^2 d\hat{\xi}^*) = \mu \ln \left( \frac{U_\infty - U_{B_2}}{U_\infty - U_{B_1}} \right) \quad (2.95)$$

Had  $C_D$  been assumed constant, the quantity in curly brackets on the left-hand side of (2.95) would have been  $C_D (\hat{\xi}_2^* - \hat{\xi}_1^*)$ , so that it may be regarded as the product of an effective drag coefficient  $C_{D_{eff}}$  and the 'distance'  $(\hat{\xi}_2^* - \hat{\xi}_1^*)$ . In other words

$$C_{D_{eff}} = C_{D_0} + C_{D_2} \bar{\alpha}_R^2 \quad (2.96)$$

where

$$\bar{\alpha}_R^2 = \frac{1}{(\hat{\xi}_2^* - \hat{\xi}_1^*)} \int_{\hat{\xi}_1^*}^{\hat{\xi}_2^*} \alpha_R^2 d\hat{\xi}^* \quad (2.97)$$

is the mean-square incidence over the interval. Note that, in defining  $C_{D_{eff}}$  using equation (2.95), only the end point velocities  $U_{B_1}$  and  $U_{B_2}$  are needed. When sufficiently good data exist, these equations may be used over several intervals of a single flight trajectory to yield an element of the  $C_{D_{eff}}$  vs.  $\sqrt{\alpha_R^2}$  curve, rather than a single point.

### 2.2332 Static and dynamic longitudinal stability derivatives

We suppose that the model is designed so that its centre of mass is forward of its centre of pressure. A nose-down pitching moment will then act to reduce the incidence of the model, which will tend to oscillate. We restrict attention to simple planar motions. Such motions will occur when the model possesses a plane of mass-geometric symmetry and is launched or released with this plane aligned with the oncoming stream. The equations of motion are then equations (2.66a) for aeroplane-like shapes and equations (2.71), suitably simplified to take account of zero spin rate  $p$  and large  $\mu$ , for axially-symmetric models. As before we change the independent variable from  $\hat{t}$  to  $\hat{\xi}^*$  in accordance with equations (2.86), and using a dash ('') to denote differentiation with respect to  $\hat{\xi}^*$ , we obtain

$$\alpha'' + B_1 \alpha' + B_2 \alpha = B_3 \quad (2.98)$$

upon eliminating  $\theta$  and  $\hat{q}$ . The coefficients  $B_k$  are given by

$$\begin{aligned}
 B_1 &= \frac{1}{\mu} (C_{L_\alpha} - C_D) - \frac{1}{\hat{I}_{yy} R^2} (C_{m_\alpha} + C_{m_q}) \\
 B_2 &= - \frac{C_{m_\alpha}}{(\hat{I}_{yy} R^2)} \\
 B_3 &= \frac{C_{m_0}}{(\hat{I}_{yy} R^2)}
 \end{aligned} \tag{2.99}$$

where terms involving products of aerodynamic coefficients have been neglected. The quantity  $B_1$  is a measure of the dynamic stability. These equations apply to the small amplitude motions of any shape possessing a plane of mirror symmetry; for axially-symmetric shapes the choice of a single reference length necessitates the replacement of  $(\hat{I}_{yy} R^2)$  by  $\hat{I}_{yy}$  and  $C_{m_0}$  is zero.

The solution of equation (2.98) is the well-known decaying harmonic motion, which may be written in the form

$$\left( \alpha + \frac{C_{m_0}}{C_{m_\alpha}} \right) = A_0 e^{-\frac{1}{2} B_1 \xi^*} \cos 2\pi \left( \frac{\xi^* - \xi_0^*}{\lambda} \right) \tag{2.100}$$

where the wavelength  $\lambda$  is given by

$$\begin{aligned}
 2\pi/\lambda &= \sqrt{B_2 - (\frac{1}{2} B_1)^2} \\
 &= \sqrt{B_2}
 \end{aligned} \tag{2.101}$$

since in most practical cases the aerodynamic damping is small and  $B_2 \gg \frac{1}{4} B_1^2$ . The constants of integration  $A_0$  and  $\xi_0^*$  are determinable only from the initial conditions of the motion.

For small amplitude motions then, the wavelength  $\lambda$  is constant, and the static stability is given by

$$C_{m_\alpha} = - \frac{4\pi^2}{\lambda^2} (\hat{I}_{yy} R^2) \tag{2.102}$$

The dynamic stability parameter follows from the decay rate of the motion. Assuming that two peak values  $(\alpha_1 + \alpha_0)$  and  $(\alpha_2 + \alpha_0)$  one wavelength  $\lambda$  apart are known, it follows from equation (2.100) that

$$B_1 = \frac{2}{\lambda} \ln \left( \frac{\alpha_1 + \alpha_0}{\alpha_2 + \alpha_0} \right) \tag{2.103}$$

the inclusion of  $\alpha_0 = C_{m_0}/C_{m_\alpha}$  taking account of the possibility that the oscillation is about some mean incidence different from zero.

The above method is suitable when a sufficient number of oscillations occur to define adequately at least two peaks of the same sign. Another procedure is described by Chapman, Kirk and Malcolm (1970) which can be used when a single peak only is well-defined, but the data have to be accurate enough for the second derivatives  $\alpha_1''$  and  $\alpha_2''$  at two values of  $\hat{\xi}^*$  to be estimated. Making use of the fact that the static moment coefficients  $(C_m)_s$  are identical at two points, either side of the peak, which have the same incidence, they show that

$$B_1 = - \frac{\alpha_1'' - \alpha_2''}{\alpha_1' - \alpha_2'} \tag{2.104}$$

and

$$\frac{(C_m)_s}{\hat{I}_{yy} R^2} = \frac{\alpha_2'' \alpha_1' - \alpha_1'' \alpha_2'}{\alpha_1' - \alpha_2'}$$

which reduces to

$$\frac{(C_m)_s}{\hat{I}_{yy} R^2} = \alpha_1'' = \alpha_2''$$

when the damping is negligibly small. In these equations  $(C_m)_s$  corresponds to the term  $(C_{m\alpha}) (\hat{I}_{yy} AR^2)^{-1} = B_2 \alpha$  of equation (2.98). In determining the static and dynamic stability using either of these methods, but particularly with the second, the effects of scatter in the experimental data are removed by using a "best-fit" polynomial. A standard least-squares procedure would be suitable, and different polynomials may be used either side of the single peak.

The analysis above is restricted to cases of linear aerodynamics, that is situations in which the static pitching moment is a linear function of incidence. When the incidence remains small this assumption is justified, but it is unlikely to be so at large incidence. One effect of non-linearities in the pitching moment incidence characteristic is that the wavelength varies with the amplitude of the oscillation. Because aerodynamic damping is generally small, the amplitude does not change greatly during a single flight, so that non-linearities are really only detectable using data obtained from a series of flights of a particular model, each flight having a different peak incidence. Chapman and his colleagues (loc. cit.) discuss several non-linear relations  $M = M(\alpha)$  of the polynomial type and Jaffe (1964) has examined in some detail a relation having the form  $M = M_p \sin(r\alpha)$ , where  $r$  is a constant. According to Jaffe (1964) a relationship of this kind is fairly representative of the results of Newtonian theory for a number of axially-symmetric shapes at incidences up to and even beyond  $\pi/2$ . Jaffe's analysis is rather complicated and we shall not attempt a summary here.

A body for which the surface geometry is axially-symmetric may nevertheless have its centre of mass off-axis by a small amount. In such cases there will be lateral aerodynamic moments about the centre of mass and the resulting motion will be non-planar. Although the equations developed in section 2.222 are not strictly applicable, the products of inertia are likely to be negligibly small for a small offset of the centre of mass. Again an imperfect release or launching of the model may result in a precessional motion about the mean flight path and even perhaps a rolling motion. Nicolaidis (1953) has described a method - the so-called tricyclic method - which can be used in such circumstances, but it is formulated in terms of so many "unknowns" that a fairly large quantity of high quality data is probably needed to utilise it properly. The method is based on the assumption of linear aerodynamics so far as the static pitching moment vs. incidence is concerned; it is well summarised in AGARDograph 138, and it was once the most widely-used means for analysing free-flight data in order to obtain aerodynamic coefficients. It depends however on having a closed-form analytic solution for the equations of motion, a need which can be circumvented by using modern, very high speed, automatic digital computers to produce numerical solutions. We shall refer to these numerical techniques in section 2.2334 after a brief discussion of the lift derivatives.

### 2.2333 Lift analysis

The equations describing the linear motion in the vertical plane, of the centre of mass are equations (2.26):

$$\begin{aligned} F_\zeta &= m \frac{d^2\zeta}{dt^2} + mg \\ F_\xi &= m \frac{d^2\xi}{dt^2} \end{aligned} \quad (2.26).$$

When the motion is confined to this plane, the lift  $L$  is given by

$$L = -F_\zeta \cos \gamma_2 - F_\xi \sin \gamma_2 \quad (2.105)$$

where the trajectory angle  $\gamma_2$  is

$$\gamma_2 = \tan^{-1} \left( \frac{-W_B}{U_\infty - U_B} \right) = \tan^{-1} \left( \frac{d\zeta/dt}{U_\infty - d\xi/dt} \right) \quad (2.106).$$

Thus measurements of the trajectory  $\xi(t)$  and  $\zeta(t)$  directly yield the lift  $L(t)$ . In general circumstances this is of little direct use, since with incidence changing as a result of both pitch and heave, the aerodynamic lift derivatives are not easily separated.

As a first approach then we postulate a series of flights each at a constant but different incidence. According to equation (2.16)

$$\alpha_x = \theta - \gamma_2 \quad (2.16)$$

so that in practice this means a zero pitching rate and a negligible change in  $\gamma_2$  during each flight, since it is unlikely that  $\dot{\theta}$  could be so matched that it cancelled exactly the effects of changes in the vertical velocity component  $W_B$ . In typical cases however  $\gamma_2$  rarely exceeds a couple of degrees, so that as a first approximation we write

$$m \frac{d^2 z}{dt^2} + mg = - C_L \frac{1}{2} \rho V^2 S \quad (2.107)$$

and treat  $C_L$  as a constant, taking the value estimated as appropriate to the mean incidence during the flight.

Of course flight in this mode implies that the model is statically balanced; that is, the centres of mass and of pressure coincide. The achievement of such a state is generally the result of a set of trial flights in which the centre of mass of the model is adjusted from one to another. We have seen in the previous section how a pitching motion may be analysed, and if we imagine a pair of tests conducted with different positions  $x_{C_1}$  and  $x_{C_2}$  for the centre of mass, then since only  $C_{m_\alpha}$  changes, it follows from

$$C_{m_\alpha} = C_{z_\alpha} \frac{(x_C - x_{C.p})}{\bar{c}} \quad (2.108)$$

that both the location  $x_{C.p}$  of the centre of pressure and the normal force derivative  $C_{z_\alpha}$  can be determined. For small angles we have

$$- C_{z_\alpha} = C_{L_\alpha} + C_D \quad (2.109)$$

so that the static lift derivative  $C_{L_\alpha}$  follows when  $C_D$  has been found as described in section 2.2331.

A method analogous to that mentioned in the previous section for utilising the variations either side of a peak incidence can also be used to estimate both the static and dynamic lift derivatives. If the vertical motion  $z(t)$  is known, the true coordinates can be corrected to eliminate the effects of gravity, since the vertical displacement due to gravity is simply  $\frac{1}{2}gt^2$ . Equation (2.107) is then re-written in the approximate form

$$z''_{\text{corr}} = - \frac{1}{\mu} C_L = - \frac{1}{\mu} [(C_L)_s + (C_L)_d] \quad (2.110)$$

the term  $(C_D \gamma_2 / \mu)$  having been neglected after changing the independent variables from time to  $\xi^*$ . Using a least-square polynomial fit to the experimental data in the form  $\alpha(\xi^*)$  and  $z_{\text{corr}}(\xi^*)$ , two values are chosen at the same incidence  $\alpha$  either side of the peak. The corresponding values of  $z''_{\text{corr}}$  and  $\alpha'$  are estimated. Then because the static lift coefficient  $(C_L)_s$  depends only upon the instantaneous incidence, so that it is the same at both points, we have at that incidence

$$- (C_L)_s = \frac{1}{2} \mu [z''_1 + z''_2]_{\text{corr}} + \frac{1}{2} [(C_L)_{d_1} + (C_L)_{d_2}].$$

Approximating the dynamic lift coefficients by

$$\begin{aligned} (C_L)_d &= (C_{L_\alpha} + C_{L_q}) \alpha' && \text{gives} \\ - (C_L)_s &= \frac{1}{2} \mu [z''_1 + z''_2]_{\text{corr}} + \frac{1}{2} [C_{L_\alpha} + C_{L_q}] [\alpha'_1 + \alpha'_2] \end{aligned} \quad (2.111)$$

and

$$(C_{L_\alpha} + C_{L_q}) = - \mu \frac{[z''_1 - z''_2]_{\text{corr}}}{\alpha'_1 - \alpha'_2}$$

The contribution to the lift of the dynamic term is generally very small, so that it is unlikely that it can be estimated accurately using a method which depends upon a double differentiation of experimental data, albeit smoothed.

When the motion is non-planar, the tricyclic method of Nicolaides (1953) can be used, but as we have noted in the discussion on stability derivatives, the restrictions inherent in the method can be avoided by utilising numerical integration instead of analytic integration of an approximating function for  $\alpha_R = \alpha_R(\phi)$ .

## 2.2334 Numerical integration of the equations of motion

Obtaining trajectory data from photographic records is a time-consuming and therefore costly procedure. Add to this the fact that impulse tunnels can rarely be operated more than a few times a day, and it becomes clear that methods must be sought for extracting as much information from each test as possible. Thus fairly complicated numerical schemes, using high-speed digital computers to integrate the (coupled) equations of motion are justified. Such procedures have been developed, for much the same reasons, to handle data obtained from ballistic ranges, and the methods can presumably be adapted for use with free-flight tests in wind tunnels. What remains in doubt to some extent, at least until the methods have been successfully used, is whether the quantity and quality of data obtainable in very short test times are sufficient. A typical ballistic range used for aerodynamic stability measurements may have 30 or more measuring stations, though fewer are sometimes used (Canning & Seiff, 1970). In the range of course these measuring stations are spatially separated, and the photographic records obtained are distinct. Although the impulse tunnel avoids the problem of knowing accurately the relative positions of several measuring stations, it introduces a more serious difficulty, that of separating the successive records. The quality of very high speed "ciné-photographs" may prove inadequate, while the multiple exposure of a single, large photographic plate (see Chapter 4) may not yield sufficient information. In these respects the optical telemetry system developed by Requardt & Kabelitz (1971) looks the most promising. It may be pertinent to remark that in a recent report (McAlister, Stewart & Petersen 1971) from N.A.S.A. Ames, where the more sophisticated of these numerical techniques have been developed, two sets of free-flight tests with a particular model series were described. For one set, conducted in the pressurised range, a fairly detailed analytic procedure based on the tricyclic equation (Malcolm & Chapman, 1968) is specifically mentioned as used for the data reduction. No such specific mention is made concerning the data obtained in the 42-inch shock tunnel which were measured from ciné-photographs taken at 500 frame/s during a nominal test period of 20 ms.

In contrast Richards & Enkenhus (1970) have used a modified framing camera together with a repetitive spark as a light source operating at up to 8000 /s, to obtain photographs in the V.K.I. free-piston "Longshot" tunnel, which has a test flow duration of about 20-25 ms. They were able to obtain information of sufficient quality to define accurately about 4 cycles of oscillation in pitch of a 30° half-angle cone (in only one test was the model in free flight; in the others the model was restrained on a knife-edge mounting, so that it had only a single degree of freedom).

In order to determine the aerodynamic derivatives appropriate to the motion, they integrated the differential equations using a Runge-Kutta scheme with assumed values for the coefficients. They were able to account for temporal variations in the stagnation conditions by choosing as the "initial condition" for the integration the measured time at which the pitching rate first passed through zero, thereby also ignoring the initial phase of the motion which results largely from the tunnel starting transients. The predicted motion is then compared with that measured, and the aerodynamic derivatives are adjusted until agreement is reached. It would appear from their account that these adjustments are made by a trial and error method, and the agreement or otherwise is judged by visual comparison of the plotted results.

Two other schemes have been used with ballistic range data which provide a more systematic comparison of the measured motion with that predicted by integration of the equations of motion. In the simpler scheme (Boissevain & Intrieri, 1961) the coupled equations are written as four second order, ordinary differential equations in which  $\xi$ ,  $\hat{\eta}$ ,  $\alpha$ ,  $\beta$  appear as the dependent variables with  $\hat{\xi}^*$  as the independent variable. They are then integrated twice, term by term, treating the coefficients which are algebraic functions of the aerodynamic derivatives as constants. All the terms which then appear, apart from the coefficients just mentioned, can be computed from the measured data once integration limits are chosen.

A number  $N$  of upper limits  $\hat{\xi}^*$  for integration is then chosen, and all the "known" quantities calculated using smoothed curves fitted to the measurements. For each value of the upper limit, four equations are obtained in which the unknown coefficients containing the aerodynamics appear linearly. The number  $4N$  is made larger than the number of unknowns so that a redundant set of equations is obtained. These are then "solved" for the aerodynamic coefficients using a straightforward least-squares procedure. Although this method is simple and does not require a very large computer, it has the disadvantage that there is no way of optimising the results except by trial and error. Only the value of  $N$  and the

particular integration limits chosen can be altered, and there does not appear to be a systematic way of doing this.

The second method is a very much more sophisticated iteration scheme, which is designed to choose those aerodynamic coefficients which when used with the equations of motion provide a "best-fit" to the measurements (Chapman & Kirk, 1969, 1970). The scheme begins with a "starting solution", which may be obtained using any of the earlier methods, including the approximate one just outlined. "Differential corrections" to the unknowns are then calculated, using the method of parametric differentiation to calculate the necessary partial derivatives of the dependent variables with respect to the coefficients and initial conditions. The coefficients and initial conditions are then corrected, and the procedure repeated until a prescribed degree of convergence has been achieved. The method is too elaborate to be described in more detail here, and it requires a fairly large, high speed digital computer because of the number of differential equations involved. It is however a very powerful method which can not only handle "non-linear aerodynamics" and known streamwise density variations but it can even use simultaneously, data from several flights of the same model configuration to find a "best fit" for that shape. The latter may be of particular advantage with very short duration impulse tunnels wherein only a very limited number of good quality "records" can be obtained for any one flight.

Both of these numerical schemes are described in more detail in AGARDograph 138, where the results of applications in particular cases are also given.

### 2.3 Aerodynamic data from measurements of the reaction in the supports

We turn our attention next to the supported system, one in which the aerodynamic loads on the model are reacted by loads in the supports. These aerodynamic loads are relatively well-defined, since the model remains at a fixed attitude during the test. Since however the principle of this force-measuring system depends upon measurable strains occurring in the supports, these supports must have flexibility. The combination of inertia and flexibility means that the system is liable to oscillate, particularly when the loading is transient in nature, as it is in an impulse tunnel. In order to infer the aerodynamic loading on the model we need to understand the relationship between this loading and the strains or displacements undergone by the supports. Having ascertained the desirable qualities of a "force-balance" we shall then review briefly how the pertinent properties of a real system may be estimated so that the designer can exercise some control over its performance and the user can better interpret his records.

In this connection it is useful to begin with a discussion of the simplest system - one possessing a single degree of freedom. We shall then generalise our results to systems more representative of those met in practice.

#### 2.31 Systems with one degree of freedom

The single degree of freedom system is not especially representative of any that might be used to measure aerodynamic forces, though in principle it could be used to describe some aspects of the behaviour of a drag-balance, drag being the only component of aerodynamic load that can arise in isolation. Nevertheless it provides a good deal of insight into the behaviour of vibratory systems and its main features are worth reiteration. Detailed treatments will be found in many standard textbooks, see for example Thomson (1966) or Jacobson & Ayre (1958). Here we shall be concerned with those features relevant to the present applications.

The equation of motion for a system such as that shown in figure 2.12, consisting of a body of mass  $m$ , a linear spring of stiffness  $k$ , and a viscous damper of coefficient  $c$  is

$$m\ddot{x} + c\dot{x} + kx = F(t) \quad (2.112).$$

We have included the damper since a few remarks are in order on the feasibility of using artificial mechanical damping. The problem essentially revolves on the determination of the force input  $F(t)$  from the measured reaction of the system. The force transducer measures the strain in the elastic member; in essence then the relative displacement  $x(t)$  of the two ends of the spring constitutes the reaction, or response. The general solution of equation (2.112) is well known. It may be derived in several ways; for example the method of Laplace transforms or the convolution integral is particularly suitable for

transient functions  $\varphi(t)$ . To proceed further we need to be a little more specific about the input force  $F(t)$  that we are trying to resolve.

### 2.311 Response to transient force inputs

We have remarked earlier that the precise form of  $F(t)$  in practical cases is not known, but in general terms it is represented by the sketch in figure 2.1. Idealisations of this curve are possible and we shall consider these in more detail later. To begin we shall discuss the response  $x(t)$  to a step input, defined by

$$\begin{aligned} F(t) &= 0 \quad \text{for } t < 0 \\ F(t) &= F_0 \quad \text{for } t > 0 \end{aligned} \quad (2.113).$$

Such an input function might be regarded as the leading-edge of an ideal input since it represents a zero time for both the tunnel starting process and the establishment of flow about the model. Strictly we should use a 'rectangular pulse' so as to represent the finite duration of the test flow, but for the present we are concerned with the onset of flow only. In any case the end of the rectangular pulse is merely a negative step, and but for the fact that the system is already in motion it may be handled by the same procedures as the positive step.

The responses of the system illustrated in figure 2.12 to a step are shown in figure 2.13 for various values of the damping ratio  $\zeta = c/(2\sqrt{mk})$ . One notices immediately that in no case does the response exactly follow the input. Those cases in which the damping is sub-critical,  $0 < \zeta < 1$ , always exhibit an overshoot, the first peak value  $x_p$ , being the largest. It can readily be shown that

$$x_p = \frac{F_0}{k} \left[ 1 + \exp \left[ \frac{-\pi\zeta}{\sqrt{1-\zeta^2}} \right] \right] \quad (2.114)$$

and that this peak value occurs at a time  $t_p$  given by

$$t_p = \frac{\pi}{\omega_n \sqrt{1-\zeta^2}} \quad (2.115)$$

where  $\omega_n^2 = k/m$ . Clearly as  $\zeta \rightarrow 1$  the overshoot is diminished but the time-to-peak-amplitude, and correspondingly the "rise-time", increases. Although some compromise is called for ( $\zeta = 0.7$  is often regarded as an optimum value), some damping would appear to be desirable. If we argue that the response should settle within say 2% of the steady value  $F_0/k$ , then the settling time, after which  $|x(t) - F_0/k| < 0.02$ , is about  $4/(\zeta\omega_n)$ . This time must be somewhat less than the duration  $\Delta t$  of the rectangular pulse which is an idealisation of the input force resulting from a flow of duration  $\Delta t$ .

A few sample calculations show that for the longer duration flows - say about 0.1 s - , a mechanical damper using a high viscosity silicone oil and occupying a volume of order 1 cm<sup>3</sup>, could provide the required viscous damping. Unfortunately a practical system with sufficient lateral rigidity is not easily conceived, even for a simple, drag-only balance. For a multi-component system, the difficulties are compounded, and since structural damping is generally small, we shall ignore damping in the remaining discussion of mechanical systems.

For the case  $\zeta = 0$  then, the step-function response is simply  $(F_0/k)(1 - \cos \omega_n t)$ , an oscillation at the natural frequency  $\omega_n$  about the steady state value  $F_0/k$ , the amplitude of this oscillation also being  $F_0/k$ . To "recover" the input in this special case is relatively simple; we merely take the mean value. This is not necessarily justifiable for other input functions however. Returning to the basic equation, we have for zero damping

$$\ddot{x} + \omega_n^2 x = F(t)/m \quad (2.116)$$

or

$$\frac{\ddot{x}}{\omega_n^2} + x = \frac{F(t)}{k}$$

Three approaches suggest themselves

- (i) The system is designed so that  $\omega_n$  is very small. In the limiting case,  $\omega_n \rightarrow 0$ , we have  $F(t) = m\ddot{x}$  which of course is the free-flight case discussed already in section 2.2.

- (ii) The natural frequency is made very large, so that  $\omega_n^2 x \gg \ddot{x}$ . We then have

$$F(t) \approx kx.$$

This case, sometimes referred to as "acceleration-control", is the principle we seek to employ for force-balance design.

- (iii) When  $\omega_n^2 x$  and  $\ddot{x}$  are of comparable magnitude, both displacement and acceleration need to be measured and combined in suitable proportions to yield  $F(t)$ . This case is commonly referred to as "acceleration-compensation" and we defer a discussion of it until section 2.4.

For the present we shall concentrate on case (ii). The outstanding question we have to answer is how large  $\omega_n$  has to be for  $kx(t)$  to be approximately representative of  $F(t)$ , and in the light of what we have noted about the step-response quite what is meant by the question. So far as the step-response is concerned, its nature appears to be independent of  $\omega_n$ , so that to recover  $F_0$  we would need to use the acceleration-compensation method to eliminate the oscillatory component. The important feature of the step input is that it is composed of the series of odd harmonics extending to infinite frequency:

$$F_0 = \frac{4 F_0}{\pi} \left( \sin \frac{\pi t}{\tau} + \sin \frac{3\pi t}{\tau} + \sin \frac{5\pi t}{\tau} + \dots \right) \quad *$$

for  $0 < t < \tau$ .

It is in relation to the frequency content of the input function  $F(t)$  that  $\omega_n$  has to be large. The infinitely fast rise at the leading edge of the step necessitates the infinite frequency. If we moderate this to a somewhat more realistic rise-time, say a linear ramp of duration  $t_1$  followed by a constant level  $F_0$ , we now have as input

$$F(t) = F_0 \frac{t}{t_1} \quad \text{for } 0 < t < t_1$$

$$\text{and } F(t) = F_0 \quad \text{for } t > t_1 \quad (2.117)$$

The response to this input is

$$x(t) = \frac{F_0}{k} \left( \frac{t}{t_1} - \frac{\sin \omega_n t}{\omega_n t_1} \right) \quad \text{for } 0 < t < t_1$$

$$\text{and } x(t) = \frac{F_0}{k} \left( 1 - \frac{\sin \omega_n t}{\omega_n t_1} + \frac{\sin \omega_n (t-t_1)}{\omega_n t_1} \right) \quad \text{for } t > t_1 \quad (2.118)$$

and it is clear that as  $(\omega_n t_1)$  becomes large,  $x(t) \rightarrow F_0/k$  for  $t > t_1$ . Figure 2.14 shows the shapes of these responses for several values of  $(\omega_n t_1)$ . The designer of a balance has no control over the rise-time  $t_1$  but the requirements on  $\omega_n$  in relation to  $t_1$  are clear. The characteristic time  $(1/\omega_n)$  for the system must be short compared with the rise-time of the forcing function if the undamped oscillations are not to be too obtrusive. This aspect is well illustrated by the maximax response spectra (Jacobsen & Ayre, 1958). The single degree of freedom, second order system in general responds to a transient excitation with an oscillatory motion, so that more than one maximum value in the mathematical sense may occur. However the largest excursion, the maximum absolute value of say, the displacement, gives the "maximax displacement" and this is a function of the ratio of the characteristic time of the forcing function to the characteristic time of the system. Figure 2.15 shows the maximax displacement spectrum for the "ramp-rise-step" defined by equation (2.117).

Although the details of their maximax response spectra differ, one may draw similar conclusions regarding  $\omega_n$  for "step" inputs with differently-shaped but monotonic fronts. A number of examples are given by Jacobsen & Ayre (1958) and are reproduced by Ayre (1960). Our earlier question is now partly answered; we need to ensure that  $(\omega_n t_1)$  is large.

A comparison of figure 2.1 with the step-like input functions we have so far considered, suggests that the effects of an overshoot in  $F(t)$  ought to be investigated. One possible idealisation which may be used for this is illustrated in figure 2.16. It consists of a ramp rise as before, but on this occasion one which overshoots the final steady value to reach a peak value  $F_1$  before settling exponentially to the steady value  $F_0$ . Mathematically, we represent the input by

\* Strictly this defines a rectangular pulse of duration  $\tau$ .

$$F(t) = F_1 \frac{t}{t_1} \text{ for } 0 < t < t_1 \quad (2.119)$$

$$\text{and } F(t) = F_0 + (F_1 - F_0) e^{-(t-t_1)/t_2} \text{ for } t > t_1$$

The response is readily calculated as

$$x(t) = \frac{F_1}{k} \left[ \frac{t}{t_1} - \frac{\sin \omega_n t}{\omega_n t_1} \right] \text{ for } 0 < t < t_1$$

$$\text{and } x(t) = \frac{F_1}{k} \left[ 1 - \frac{\sin \omega_n t}{\omega_n t_1} + \frac{\sin \omega_n (t-t_1)}{\omega_n t_1} \right] - \frac{(F_1-F_0)}{k} \left[ 1 - \cos \omega_n (t-t_1) \right]$$

$$+ \frac{(F_1-F_0)}{k \left( 1 + \frac{1}{(\omega_n t_2)^2} \right)} \left[ e^{-(t-t_1)/t_2} - \cos \omega_n (t-t_1) + \frac{1}{\omega_n t_2} \sin \omega_n (t-t_1) \right] \text{ for } t \geq t_1 \quad (2.120).$$

This response, equation (2.120), contains three terms which may be interpreted in the following way. The first term is identical to equation (2.118) and represents the ramp rise to a level  $F_1$  in time  $t_1$ . The second term is the response to a negative step of magnitude  $(F_1-F_0)$  at time  $t_1$  and the final term results from the exponential input  $(F_1-F_0)e^{-(t-t_1)/t_2}$  which also occurs at time  $t_1$  (see figure 2.10). A second characteristic time for the input function must now be considered; the decay constant  $t_2$ . When  $t_2 \rightarrow \infty$ , equation (2.120) becomes identical to equation (2.118) as we expect. However when  $(\omega_n t_2)$  is small, the contribution of the third term of equation (2.120) to the response is also small, but the second term shows that an oscillation at the natural frequency  $\omega_n$  with amplitude equal to the overshoot remains. Of course as  $t_2 \rightarrow 0$ , the exponential decay becomes a negative step, so we might expect this result.

We conclude that in the absence of damping,  $\omega_n$  should in general be large compared with the reciprocal of any characteristic time associated with the input, if oscillations are not to be of an obtrusive amplitude. Looked at in another way, the natural frequency of the system should be so high that the input appears "slow", and its frequency content is such as not to excite the natural oscillation of the system. In the context of the impulse tunnel, this requirement can rarely be met, as we shall see later, but there are other points that must be considered first.

### 2.312 Base excitation

So far we have taken it for granted that one end of the flexible element is anchored to a point which remains stationary. In practice the "earth-side" of the spring element of a force transducer may also have some motion of its own. For example the test model and balance may be connected to the internal structure of the tunnel in order to avoid the sealing problems which arise when supports independent of the tunnel are used. An impulse-tunnel is characterised by very rapid starting. Whether this is achieved by the bursting of a diaphragm, by the discharge of electrical energy or by some other method of quickly releasing stored energy, the result is that stress waves are transmitted through the tunnel structure, and because the velocity of such waves is high, the model-support system is excited before or during the test period. Even when the model is mounted independently of the tunnel, motion may arise as a result of vibrations of the laboratory floor which can be excited by pumps or other machinery or by passing traffic some distance from the building. The effects of this base excitation must be eliminated.

Figure 2.17(a) represents a system in which the base undergoes a displacement represented by

$$x = \sum_i x_{0i} \sin \omega_i t \quad (2.121)$$

The general response is

$$x(t) = x(0) \cos \omega_n t + \frac{\dot{x}(0) \sin \omega_n t}{\omega_n} + \sum_i \frac{x_{0i} \sin \omega_i t}{(1 - (\omega_i/\omega_n)^2)} \quad (2.122)$$

the final term representing the motion arising as a result of the base motion. A force transducer in the present context measures the relative displacement of the two ends of the spring - it may be, for example, a strain gauge bonded to the spring, or a piezoelectric element which itself constitutes the flexible element. The output then is proportional to  $(x - \chi)$ . Assuming that the natural frequency is not excited, we have

$$(x(t) - \chi(t)) = \sum_1 \frac{\omega_1^2 x_{01} \sin \omega_1 t}{\omega_n^2 - \omega_1^2} \quad (2.123)$$

so that vibrations of the support can be rendered unimportant by ensuring that  $\omega_1 < \omega_n$ . This implies a "soft mounting" of the system, which can be achieved using either a body of very large mass, or very flexible springs to connect the balance supports to the tunnel or laboratory floor, or a combination of the two. We now have a system with more than one degree of freedom, and some care is needed in making generalisations from the behaviour of a system having a single degree of freedom to the more complex systems typical of practical situations.

### 2.32 Systems with more than one degree of freedom

A real physical system is not separable into elements which have inertia but no flexibility together with flexible, inertia-less components. However in all but the simplest cases, continuous systems are not amenable to analysis. Even if one resorts to numerical methods of solution, formulation of the governing equations is not always easy. Accordingly it is common practice to represent a real system having distributed mass and flexibility by one in which these are replaced by discrete "lumps". In this way the infinite number of degrees of freedom of the continuous system is replaced by the finite number of the lumped-parameter system. Thus for a system of  $N$  rigid bodies, there may be up to  $6N$  degrees of freedom, when rotations and translations of each body are taken into account.

In many cases however the representations used are based on further simplifications. Often a "one-dimensional" configuration is adequate, each body having only a single degree of freedom. Such a system, shown in figure 2.17, may be used to represent the one-component force-balance, flexibly-mounted to the structure of the tunnel which is regarded as fixed for the present. Thus  $m_1$  is the mass of the model,  $k_1$  the stiffness of the force-sensor,  $m_2$  the mass of the supporting structure and  $k_2$  is the stiffness of the springs between this structure and the main tunnel. In terms of the absolute displacements  $x_1$  and  $x_2$ , the equations of motion are

$$\begin{aligned} m_1 \ddot{x}_1 + k_1(x_1 - x_2) &= F_1(t) \\ m_2 \ddot{x}_2 + (k_1 + k_2)x_2 - k_1 x_1 &= F_2(t) \end{aligned} \quad (2.124)$$

where  $F_1$  and  $F_2$  are the externally applied loads. These equations are "coordinate-coupled" and must be solved simultaneously. They may be written in matrix notation as

$$\begin{bmatrix} m_1 & 0 \\ 0 & m_2 \end{bmatrix} \begin{bmatrix} \ddot{x}_1 \\ \ddot{x}_2 \end{bmatrix} + \begin{bmatrix} k_1 & -k_1 \\ -k_1 & (k_1 + k_2) \end{bmatrix} \begin{bmatrix} x_1 \\ x_2 \end{bmatrix} = \begin{bmatrix} F_1(t) \\ F_2(t) \end{bmatrix} \quad (2.125)$$

or

$$[\underline{M}](\ddot{\underline{x}}) + [\underline{K}](\underline{x}) = \{\underline{F}(t)\} \quad (2.126)$$

The second form, equation (2.126) applies to the more general lumped parameter system, the order of the inertia matrix  $[\underline{M}]$  and of the stiffness matrix  $[\underline{K}]$ , both of which are square and symmetrical, being that of the number of degrees of freedom.

To find the natural frequencies of the system, we put the right hand side  $\{\underline{F}(t)\}$  equal to zero, and assume that harmonic oscillations take place of the form

$$x_i = \tilde{x}_i e^{i\omega t} \quad (2.127)$$

where the 'tilde' is used to denote amplitude.

(Note that we assume that all parts of the system oscillate with the same frequency.) The natural frequencies are then solutions of the characteristic equation

$$|[\underline{K}] - \omega^2[\underline{M}]| = 0 \quad (2.128)$$

which is the condition that the equations be satisfied for arbitrary values of the amplitudes  $\tilde{x}_i$ .

In the particular case described by equation (2.125) the off-diagonal terms of  $[\underline{M}]$  are zero, while those of the stiffness matrix are non-zero. Such a system is said to be statically-coupled. A different set of coordinates might lead to the off-diagonal terms of  $[\underline{M}]$  being non-zero, while those of  $[\underline{K}]$  are zero. The system is then dynamically-coupled. In general a system will be both statically and dynamically coupled.

However it is always possible to find a set of coordinates  $q_i^*$ , called principal coordinates, for which both the stiffness and inertia matrices are diagonalised, and those coordinates are uncoupled. The equations of motion for free oscillation now take the form

$$\begin{bmatrix} m_{11}^* & 0 & 0 & \dots & 0 \\ 0 & m_{22}^* & 0 & \dots & 0 \\ 0 & 0 & m_{33}^* & \dots & 0 \\ \vdots & \vdots & \vdots & \ddots & \vdots \\ 0 & 0 & 0 & \dots & m_{NN}^* \end{bmatrix} \begin{bmatrix} \ddot{q}_1^* \\ \ddot{q}_2^* \\ \ddot{q}_3^* \\ \vdots \\ \ddot{q}_N^* \end{bmatrix} + \begin{bmatrix} k_{11}^* & 0 & 0 & \dots & 0 \\ 0 & k_{22}^* & 0 & \dots & 0 \\ 0 & 0 & k_{33}^* & \dots & 0 \\ \vdots & \vdots & \vdots & \ddots & \vdots \\ 0 & 0 & 0 & \dots & k_{NN}^* \end{bmatrix} \begin{bmatrix} q_1^* \\ q_2^* \\ q_3^* \\ \vdots \\ q_N^* \end{bmatrix} = 0 \quad (2.129)$$

$$\text{and } \omega_{n_i}^2 = k_{ii}^*/m_{ii}^* \quad (2.130)$$

there being one natural frequency calculable for each independent coordinate, that is, for each degree of freedom. In practice computer programmes usually exist as library sub-routines for extracting the natural frequencies (or eigenvalues) directly from the determinantal characteristic equation (2.128) or its equivalent. However the notion of principal coordinates gives us some insight into the requirements for a well-designed multi-component balance, as we shall see. The general linear transformations between the coordinates  $x_i$  and  $q_i^*$  are of the form

$$x_i = \sum_j r_{ij} q_j^* \quad (2.131)$$

or in matrix notation

$$\{x\} = [R] \{q^*\} \\ \text{and } \{q^*\} = [R]^{-1} \{x\}$$

If then we substitute for  $\{x\}$  in the general equation (2.126) for forced motion, we find

$$[M] [R] \{\ddot{q}^*\} + [c] [R] \{\dot{q}^*\} = \{F\} \quad (2.132)$$

and premultiplying by the transpose of  $[R]$  we have

$$[M^*] \{\ddot{q}^*\} + [K^*] \{\dot{q}^*\} = \{Q^*\} \quad (2.133)$$

where

$$[M^*] = [R]^T [M] [R] \quad (2.134)$$

and

$$[K^*] = [R]^T [K] [R]$$

are diagonal matrices, and

$$\{Q^*\} = [R]^T \{F\} \quad (2.135)$$

is a set of generalised forces associated with the principal coordinates  $\{q^*\}$ . The left-hand side of equation (2.133) is of course identical with that of equation (2.129) so that, writing equation (2.130) in the matrix form

$$[M^*]^{-1} [K^*] = [\Omega^2] \quad (2.130)$$

equation (2.133) becomes

$$\{\ddot{q}^*\} + [\Omega^2] \{q^*\} = [M^*]^{-1} \{Q^*\} \quad (2.136)$$

or written out in long-hand

$$\ddot{q}_i^* + \omega_{n_i}^2 q_i^* = \frac{1}{m_{ii}^*} Q_i^*(t) \quad , \quad (i = 1, 2, \dots, N) \quad (2.137)$$

The behaviour of each of the principal coordinates is independent of the others; each behaves as though it were an isolated single degree of freedom system, and the transient response is readily found so long as the input on the right-hand side of equation (2.136) is known. Because  $[M^*]$  is a diagonal matrix, its inverse is also diagonal, each element on the diagonal being simply the reciprocal of the corresponding

element in  $[M]^*$ . The problem reduces to finding the matrix  $[R]$  which diagonalises  $[M]$  and  $[K]$  according to equations (2.134). This mathematical problem defines the approach used as the basis of some iterative numerical techniques for finding the natural frequencies and modes of vibration for multi-degree of freedom systems, but in other methods the transformation matrix or its inverse is one of the products of the solution. Once  $[R]$  is known, the generalised force  $\{Q\}$  can be found, and the transient response of the system determined as a linear combination of the "normal mode" response.

However the independence principle suggests that a measuring system should employ a set of transducers each of which is sensitive only along one principal coordinate, since then each transducer is decoupled from all inputs but its own. We can infer that a system designed to measure 6 (generalised) forces on a model will require at least 6 transducers, but only when proper decoupling of this kind exists are 3 say, sufficient for a three-component balance. Thus if the force transducers can be so positioned, that not only are they decoupled from one another, but are also such that the generalised forces are those sought, then both the measurements and data analysis are considerably simplified.

Such an ideal is not easily achieved. Indeed it is usual to use a pair of parallel transducers to resolve the force component along their sensitive axis and the moment about the axis normal to the plane containing them. An arrangement such as that illustrated in figure 2.18 gives the normal force and pitching moment as linear combinations of the transducer outputs.

The question of the natural frequencies of the resulting system is of course still an important one, and these need to be calculated. If any of the natural frequencies lies inside the "critical range", the corresponding mode will be excited, and unless the transducers can be totally decoupled from this motion, the performance of the balance will be compromised. To employ "acceleration-control" therefore requires all these frequencies (or perhaps all but one) to be outside the "critical range". As we have seen, this "critical range" corresponds at its upper end to the inverse of the fastest transient requiring resolution, and at the lower end either to the inverse of the total test time, or to zero if static calibration is desired.

### 2.321 Calculation of the natural frequencies and modes of vibration

The natural frequencies of a system with several degrees of freedom are given by the values of  $\omega^2$  which satisfy the equation

$$[\omega^2 [M] - [K]] \{\tilde{x}\} = 0 \quad (2.138)$$

only the positive root of  $\omega$  having physical meaning. Clearly for a system with  $N$  degrees of freedom, the characteristic equation (2.128) is a polynomial of order  $N$  (in  $\omega^2$ ). In practice only the lowest few natural frequencies are of interest. In any case the physical model of the real system is rarely sufficiently adequate to justify much confidence in the higher modes predicted. To obtain the lowest, or fundamental frequency  $\omega_{n1}$ , a simple, rapidly converging\* iterative scheme is available (see, for example, Anderson, 1967).

Equation (2.138) is written in the form

$$\frac{1}{\omega^2} \{\tilde{x}\} = [K]^{-1} [M] \{\tilde{x}\} \quad (2.139).$$

In fact the equation usually arises in the way, the elements of the flexibility matrix  $[K]^{-1}$  - commonly referred to as influence coefficients - being more readily calculable than those of the stiffness matrix.

A trial eigenvector  $\{\tilde{x}\}^{(0)}$  is assumed, arbitrarily normalised with say,  $\tilde{x}_N^{(0)} = 1$ . Substitution into the right-hand side of equation (2.139) leads to a new eigenvector

$$\{\tilde{z}\}^{(1)} = [K]^{-1} [M] \{\tilde{x}\}^{(0)}$$

which can be normalised by factoring out  $\tilde{z}_N^{(1)}$ . Comparison with equation (2.139) shows that the next approximation to  $\{\tilde{x}\}$  is

\* Special procedures may be needed when the system has two frequencies which are very close together, or which coincide.

$$\{\tilde{x}\}^{(1)} = \begin{Bmatrix} z_1/z_N \\ z_2/z_N \\ \vdots \\ \vdots \\ 1 \end{Bmatrix}^{(1)} \quad (2.140)$$

and

$$\left(\frac{1}{\omega^2}\right)^{(1)} = z_N^{(1)} \quad (2.141)$$

This process is repeated to find  $\{z\}^{(2)} = [K]^{-1} [M] \{\tilde{x}\}^{(1)}$  and continued until successive eigenvectors differ by amounts less than some specified value. The fundamental natural frequency then follows from

$$\left(\frac{1}{\omega^2}\right)^{(r)} = z_N^{(r)} \quad (2.142)$$

where  $z_N^{(r)}$  results from the final iteration. Provided the matrices are not "too large", the calculation is readily carried out using a desk machine, particularly since  $[M]$  is often in diagonal form.

In the event that the fundamental mode is of higher frequency than the critical range, no further calculations may be needed. Such circumstances are likely to be rare, because models are usually sting-mounted, and the fundamental mode of a cantilever system is of comparatively low frequency. It may conceivably even be lower than that corresponding to the test time, and therefore below the critical range. It is then necessary to determine the second and perhaps higher modes. A number of methods are available which provide iterative schemes that converge on successively higher modes as the lower ones become known (Anderson, 1967; Fox, 1964). Most digital computers nowadays have standard subroutines which calculate the eigenvalues and eigenvectors of a (square) matrix.

There remains the problem of calculating the elements of the inertia and flexibility (or stiffness) matrices. Essentially we require a formal procedure for writing equations which describe the motion of the system. Such is Lagrange's method, based upon equation (2.5). Before we can use this we need some guide as to how a real, continuous system might be represented by a lumped-parameter system which has some physical significance, yet is sufficiently simple to have a manageable number of degrees of freedom.

### 2.322 Lumped-parameter representations

In general circumstances the representation of a physical system by a model involving discrete elements is a task which often depends for meaningful results as much upon experience as on any other factor. To some extent the complexity of the representation devolves upon the nature of the information required. For example a simple cantilever can, for some purposes, be replaced by a concentrated "mass-point" together with an inertialess "beam" of appropriate flexibility. Such a model is clearly useless for determining the natural frequency of any but the fundamental mode. The limitations of any particular representation must therefore always be borne in mind. The task of modelling his system is made a little easier for the balance designer by the specific requirements of his problem. It is in the force transducers that the strains are largest. Consequently it is these and their linkages which constitute the important elements of the flexibility matrix. The relatively more rigid parts, such as the aerodynamic model and perhaps the balance body, contribute significant elements in the inertia matrix. However difficulties are encountered when it comes to representation of the structure which supports the model in the test flow. To minimise aerodynamic interference, the model is usually mounted on a fairly slender "sting", itself attached to a support which may incorporate a means for changing the attitude of the model to the oncoming flow. This support in turn may be connected to the tunnel, or via appropriate seals, to the laboratory floor; in both cases further springs may be used. In some of these components the distinction between the inertial and flexible parts is less clear. In particular, the sting itself behaves somewhat like a cantilever with a body attached to its free end. In representing this part of the system by lumped-parameters, we must recognise that the higher modes calculated for the whole system are affected by how many 'lumps' we use. As a general rule of thumb, modes should not be excluded that have natural frequencies of an order similar to those which are included.

The particular example of a uniform, slender cantilever is instructive, enabling us to obtain some idea of the order of the errors involved in lumped-parameter representation. The exact solution for this case is well-known. The natural frequencies  $\omega_n$  are solutions of the characteristic equation

$$\cos \beta L \cosh \beta L = 1$$

$$\text{where } \beta^4 = \frac{m\omega_n^2}{EI} \quad (2.143)$$

$m$  being the total mass,  $L$  the length and  $EI$  the flexural stiffness of the cantilever.

As an approximation the uniform beam might be divided into  $N$  equal elements as shown in figure 2.19. Each element, of mass  $m/N$ , is replaced by a mass particle at the mid-point of the element it represents. Using  $v$  to denote the transverse displacement, it is readily shown using simple beam theory, that a unit load distant  $z_j$  from the built-in end produces a static deflection  $v_j$  at a point  $z_i < z_j$  given by

$$\frac{EI}{L} v_j = \frac{1}{2} \left( \frac{z_j}{L} \right)^3 \left\{ \frac{3z_i}{z_j} - 1 \right\} = a_{ji}' \quad (2.144)$$

and by Maxwell's reciprocal law,  $a_{ji}' = a_{ij}'$ . Using these flexibility influence coefficients, the natural frequencies are given by

$$\begin{bmatrix} \tilde{v}_1 \\ \tilde{v}_2 \\ \tilde{v}_3 \\ \vdots \\ \tilde{v}_N \end{bmatrix} = \frac{\omega_n^2 L^4}{24N^4 (EI)} \begin{bmatrix} a_{11} & a_{12} & \dots & a_{1N} \\ a_{21} & a_{22} & & a_{2N} \\ a_{31} & & & a_{3N} \\ \vdots & & & \vdots \\ a_{N1} & & & a_{NN} \end{bmatrix} \begin{bmatrix} \tilde{v}_1 \\ \tilde{v}_2 \\ \tilde{v}_3 \\ \vdots \\ \tilde{v}_N \end{bmatrix} \quad (2.145)$$

where

$$a_{ij} = \frac{(2j-1)^3}{2} \left[ \frac{3(2i-1)}{(2j-1)} - 1 \right] \quad \text{for } i > j$$

$$i, j = 1, 2, \dots, N$$

and

$$a_{ij} = a_{ji}$$

Here  $\rho$  is the density of the material of the beam, and  $A$  its cross-sectional area. Solutions of equation (2.145) are presented in the table below for several values of  $N$ . Included in the table are the exact values for the first 7 natural frequencies. It can be seen that to obtain a value within say 10% for the frequency of the  $N^{\text{th}}$  mode, one needs to use  $(N+1)$  discrete elements to represent the beam, though to get within 5% requires  $(N+2)$  elements.

Natural frequencies  $\omega_{n_i} L^2 \sqrt{\frac{\rho A}{EI}}$  of a uniform  
cantilever as represented by  $N$  lumped-masses.

$i =$ $N =$	1	2	3	4	5	6	7
2	3.730	31.04	-	-	-	-	-
3	3.608	24.17	77.69	-	-	-	-
4	3.567	23.18	66.32	141.0	-	-	-
5	3.549	22.76	64.83	126.1	221.3	-	-
7	3.528	22.39	63.31	124.9	205.2	292.0	434.4
$\infty$	3.516	22.04	61.70	120.9	199.2	298.6	417.0

However it is probably less important to obtain an accurate estimate of the frequencies, than it is to provide an adequate representation. Provided therefore that one does not lose sight of the fact that this method often overestimates the frequency, replacing a continuous system by just sufficient elements to enable calculation of the requisite number of modal frequencies may be sufficient. One can then ascertain how many of the natural frequencies are in the critical range, or rather one can determine whether a particular system is likely to be suitable for measuring the forces within the available test-time.

It is frequently the case that the natural frequency of some elements of the system, in isolation, are far higher than those of the parts in combination, and consequently approximations are justified.

Thus the effect of the mass  $m_s$  of the spring itself in the single degree of freedom system of figure 2.14 may be taken into account by adding  $(1/3)m_s$  to the mass  $m$  of the rigid body attached to its end. Another useful result, also obtained using Rayleigh's energy method, enables us to take account of the mass  $m_b$  of a cantilever which has a rigid body of mass  $m$  at its end. Here the effective mass  $(m + 0.23 m_b)$  gives the frequency of the fundamental mode with surprising accuracy. Such results may be used to facilitate lumped-parameter representations.

On this basis the three-component balance shown schematically in figure 2.20(a) with a model attached, might be simulated so far as the pitch-plane motion is concerned, by the system of springs and rigid bodies sketched in figure 2.20(b). The sting is represented by the lumped components  $k_3$  and  $m_3$ , and its support by  $k_4$  and  $m_4$ . Usually the incidence-arc and platforms are made sufficiently massive and their supporting springs so flexible, that the mode associated essentially with these is effectively decoupled from the remainder and may be treated in isolation. The axial motion may also be regarded as decoupled from the transverse motion and treated separately, because the influence coefficients relating transverse loads and axial deflections (or vice versa) are zero. The axial motion can then be described by that of the system discussed earlier, see figure 2.17, consisting of a pair of springs and bodies.

With a suitable representation of the system we can proceed to a discussion of how the inertia and flexibility (or stiffness) matrices are derived.

### 2.323 Calculation of the inertia and stiffness matrices

The inertia and stiffness matrices are of course merely coefficients in the equations of motion for the system and so in principle we need to write these. We have already noted that Lagrange's method is more convenient than Newton's for multi-degree of freedom systems and therefore we begin with expressions for the kinetic energy  $T$  and potential energy  $U$  of the system, which is assumed to be conservative.

In a formal sense, in terms of the generalised coordinates  $q_i$  we have

$$T = \frac{1}{2} \sum_i \sum_j m_{ij} \dot{q}_i \dot{q}_j = \frac{1}{2} (\dot{q})^T [M] (\dot{q}) \quad (2.146)$$

$$\text{and } U = \frac{1}{2} \sum_i \sum_j k_{ij} q_i q_j = \frac{1}{2} (q)^T [K] (q) \quad (2.147)$$

so that because the kinetic energy does not depend upon the coordinates  $q_i$ , Lagrange's equations reduce to

$$\frac{d}{dt} \left( \frac{\partial T}{\partial \dot{q}_i} \right) + \frac{\partial U}{\partial q_i} = 0, \quad i = 1, 2, \dots, N \quad (2.148)$$

Our first task then is to choose suitable coordinates, which must be sufficient in number to describe the configuration of the system. Again by way of illustration, we can conveniently refer to the representation for the pitch-plane motion of the three-component balance of figure 2.20(b), choosing the coordinates  $x_i$  shown. Note that two coordinates are used to describe the position of the body of mass  $m_1$ . Then for this example

$$\begin{aligned} T &= \frac{1}{2} m_1 \left[ \dot{x}_1 + \frac{L_1}{L_1+L_2} (\dot{x}_{1r} - \dot{x}_{1f}) \right]^2 + \frac{1}{2} I_1 \left[ \frac{\dot{x}_{1f} - \dot{x}_{1r}}{L_1+L_2} \right]^2 + \frac{1}{2} m_2 \dot{x}_2^2 + \frac{1}{2} m_3 \dot{x}_3^2 + \frac{1}{2} m_4 \dot{x}_4^2 \\ &= \frac{1}{2} \dot{x}_{1f}^2 \left[ m_1 \left( \frac{L_2}{L_1+L_2} \right)^2 + I_1 \left( \frac{1}{L_1+L_2} \right)^2 \right] + \dot{x}_{1f} \dot{x}_{1r} \left[ m_1 \frac{L_1 L_2}{(L_1+L_2)^2} - I_1 \frac{1}{(L_1+L_2)^2} \right] \\ &\quad + \dot{x}_{1r}^2 \left[ m_1 \left( \frac{L_1}{L_1+L_2} \right)^2 + I_1 \left( \frac{1}{L_1+L_2} \right)^2 \right] + \frac{1}{2} \dot{x}_2^2 m_2 + \frac{1}{2} \dot{x}_3^2 m_3 + \frac{1}{2} \dot{x}_4^2 m_4 \end{aligned} \quad (2.149)$$

and

$$\begin{aligned}
 U &= \frac{1}{2} k_{1f} (x_{1f} - x_2)^2 + \frac{1}{2} k_{1r} (x_{1r} - x_3)^2 + \frac{1}{2} k_2 (x_2 - x_3)^2 + \frac{1}{2} k_3 (x_3 - x_4)^2 + \frac{1}{2} k_4 x_4^2 \\
 &= \frac{1}{2} x_{1f}^2 k_{1f} + \frac{1}{2} x_{1r}^2 k_{1r} + \frac{1}{2} x_2^2 (k_{1f} + k_2) + \frac{1}{2} x_3^2 (k_{1r} + k_2 + k_3) \\
 &\quad + \frac{1}{2} x_4^2 k_4 - x_{1f} x_2 k_{1f} - x_{1r} x_3 k_{1r} - x_2 x_3 k_2 - x_3 x_4 k_3
 \end{aligned} \tag{2.150}$$

The equations of motion may then be obtained by substitution in equation (2.148) but it is not necessary to do this for our purpose.

The inertia and stiffness matrices follow directly from a comparison of equations (2.149) and (2.150) with the expanded forms of the formal matrix expressions (2.146) and (2.147), identifying the coordinates  $x_{1f}$ ,  $x_{1r}$ ,  $x_2$ ,  $x_3$ ,  $x_4$  with  $q_1$ ,  $q_2$ ,  $q_3$ ,  $q_4$ ,  $q_5$  respectively.

Thus, for this example

$$\underline{[M]} = \begin{bmatrix} \frac{\{m_1 L_2^2 + I_1\}}{(L_1 + L_2)^2} & \frac{\{m_1 L_1 L_2 - I_1\}}{(L_1 + L_2)^2} & 0 & 0 & 0 \\ \frac{\{m_1 L_1 L_2 - I_1\}}{(L_1 + L_2)^2} & \frac{m_1 L_1^2 + I_1}{(L_1 + L_2)^2} & 0 & 0 & 0 \\ 0 & 0 & m_2 & 0 & 0 \\ 0 & 0 & 0 & m_3 & 0 \\ 0 & 0 & 0 & 0 & m_4 \end{bmatrix}$$

and

$$\underline{[K]} = \begin{bmatrix} k_{1f} & 0 & -k_{1f} & 0 & 0 \\ 0 & k_{1r} & 0 & -k_{1r} & 0 \\ -k_{1f} & 0 & (k_{1f} + k_2) & -k_2 & 0 \\ 0 & -k_{1r} & -k_2 & (-k_{1r} + k_2 + k_3) & -k_3 \\ 0 & 0 & 0 & -k_3 & k_4 \end{bmatrix}$$

and these would be used with equation (2.139) to estimate the natural frequencies of the three-component balance.

#### 2.4 Hybrid techniques

It is often not possible to meet the stringent requirements we have set out for force balances regarding the elimination of its natural frequencies from the critical range. This is particularly so with impulse tunnels having test flow durations of order 10 ms or less. In these circumstances the aerodynamic forces and moments are not entirely reacted by quasi-static loads in the supports and the inertia terms must be taken into account. The "acceleration-compensation" is generally provided by separately measuring the accelerations and summing appropriate combinations of the accelerometer and force transducer output signals.

Precisely the same situation arises in situations where the model is deliberately mounted so as to be partly free and partly restrained. Typically the model is supported so that it has a single degree of freedom only. For example pitch, roll or axial motion may be unrestrained and the simple motions which result are measured. In some cases a weak restraint may be applied even to the nominally free coordinate. In this case the inertia term is dominant, but the measurements of acceleration must be compensated by the inclusion of a term representing the reaction in the support.

We discuss the two methods separately.

#### 2.41 Acceleration-compensation methods

The design of a sting upon which to mount a model in the test section of a wind-tunnel is a compromise between minimising its aerodynamic interference and trying to ensure that its natural frequencies are outside the critical range. The former requires a long slender sting which is not compatible with a high fundamental natural frequency. In practice it is rare that the fundamental frequency of a sting is more than perhaps several hundred hertz, so that in many impulse tunnels motion of the model associated with transverse oscillations of the sting are potentially troublesome. When only a single frequency of the system falls within the critical band, it may be removed by electronic filtering of the output signal from the force transducer. This becomes more difficult with two and virtually impossible when more than two lie within the critical range. Some method of "compensation" is therefore required, though "digital filtering" may be possible when the data exist in suitable form. As we have noted the simplest form of compensation, conceptually at least, involves separate measurement of the accelerations, suitable proportions of which can be used to cancel the oscillatory component in the output of the force transducer. Difficulties arise because the force transducer and its associated accelerometer cannot occupy the same position. It is moreover sometimes necessary to place the accelerometers at the extremities of the model to achieve an adequate signal level. As a result the accelerometer and force transducer signals may not be in phase. In the absence of damping, of course, the phase difference must be either zero or  $180^\circ$ , and even with small damping similar phase shifts occur except at frequencies close to the natural frequency. At first sight it appears that no difficulty exists: either one adds or subtracts the scaled accelerometer signal in order to provide compensation. Unfortunately the phase difference in the motion of different points of the system depends upon the mode.

This point is well illustrated by the uniform cantilever considered in section 2.322. The modal shapes for this system are well-known - the first few are sketched in figure 2.21. The addition of the model and the transducers only alters the picture in details which do not affect our argument. Suppose that a force transducer is attached to a point  $z_f$  and an accelerometer is placed at  $z_a$  as shown in figure 2.21. Clearly if the acceleration at  $z_a$  is in phase with the force at  $z_f$  for the first mode, then the acceleration associated with the second and fourth modes will be in antiphase with the force at  $z_f$ , while the acceleration for the third mode will not be sensed because  $z_a$  corresponds with a node for this mode. Only some acceleration components can therefore be cancelled, while some may actually be enhanced by subtracting a proportion of the signal appropriate to say, the fundamental mode, which generally has the largest amplitude. It is in fact the lowest modes which require compensation; the higher modes are often outside the critical range and can be removed by a low-pass electronic filter. Some modes will always remain uncompensated because the accelerometers do not detect the motion associated chiefly with the model itself or with the force transducer vibrations. The corresponding frequencies should therefore be kept high; in particular the model should be very stiff and of low mass so that it behaves as a rigid body.

Although the "exact" conditions for compensation are impossible to fulfil for a real system, it is only the lower modes with natural frequencies in the critical range that are of practical concern, and a linear combination of the responses from a few accelerometers should provide adequate compensation. In practice a system designed to measure all six components of the aerodynamic load would probably require at least six accelerometers, so that one could use the outputs from all of them to compensate each force component. The positions of these accelerometers must be chosen so that accelerations associated with each of the modes that require cancellation are sensed by at least one, and preferably not more than one. When the force transducers themselves are properly decoupled, compensation should be considerably simplified because they will only sense a single inertia component; that directed along their axis of sensitivity. It should be borne in mind however that the accelerometers may also have "cross-axis" sensitivities, so that although one oscillatory component is removed it may be at the cost of introducing another, albeit smaller component.

The general problem of "inertia-compensation" may be formulated in the following way. In a simple one degree of freedom system, the external force  $Q_i$  to be determined is given by

$$Q_i = kq_i + m\ddot{q}_i \quad (2.151)$$

in the absence of damping. By using a force transducer to produce a voltage proportional to  $kq_j$  and an accelerometer to produce a voltage proportional to  $\ddot{q}_j$ , the input force  $Q_j$  may be recovered by suitable scaling and adding. This idea can be extended to multi-degree of freedom systems in which the force transducer axes and accelerometer axes do not coincide, and neither is coincident with the reference axes of the model.

For the six aerodynamic components, we have for coincident axis systems

$$\begin{bmatrix} X \\ Y \\ Z \\ L \\ M \\ N \end{bmatrix} = \begin{bmatrix} F_X \\ F_Y \\ F_Z \\ F_L \\ F_M \\ F_N \end{bmatrix} + m \begin{bmatrix} \ddot{q}_X \\ \ddot{q}_Y \\ \ddot{q}_Z \\ \ddot{q}_L \\ \ddot{q}_M \\ \ddot{q}_N \end{bmatrix} \quad (2.152)$$

where  $F_j$  represents the spring force and  $m$  is the mass of the model. Suppose there are six force transducers and six accelerometers generally disposed so as to be non-redundant, but whose axes do not in general coincide with the axis system of the model to which  $\{X, Y, Z, L, M, N\}$  are referred. Then assuming perfect, linear instruments, the resolved components  $F_j$  and  $\ddot{q}_j$  ( $j = X, Y, Z, L, M, N$ ) are, in general, linear combinations of the force transducer outputs  $f_j$  and the accelerometer outputs  $\gamma_j$  ( $j = 1, 2 \dots 6$ ) respectively; for example

$$F_X = \alpha_{X1} f_1 + \alpha_{X2} f_2 + \dots + \alpha_{X6} f_6 \quad (2.153)$$

and

$$\ddot{q}_X = \beta_{X1} \gamma_1 + \beta_{X2} \gamma_2 + \dots + \beta_{X6} \gamma_6$$

The equations for the generalised aerodynamic force can now be written in matrix form

$$\{A\} = [\underline{\alpha}]\{f\} + m[\underline{\beta}]\{\gamma\} \quad (2.154)$$

where  $[\underline{\alpha}]$  and  $[\underline{\beta}]$  are  $6 \times 6$  matrices and  $\{A\}$ ,  $\{f\}$  and  $\{\gamma\}$  are 6 component "vectors", or column matrices.

Inertia-compensation and axis transfer then require the determination of the 72 coefficients which make up the  $[\underline{\alpha}]$  and  $[\underline{\beta}]$  matrices.

A well-designed system will however have the off-diagonal terms of  $[\underline{\alpha}]$ , the force-transducer interaction coefficients, small compared to those in the leading diagonal, so that as a good approximation, each of the aerodynamic forces and moments involves a combination of seven terms; for example

$$\begin{aligned} Z &= \alpha_{Z3} f_3 + m \sum_j^6 \beta_{Zj} \gamma_j \\ &= F_Z + m \sum_j^6 \beta_{Zj} \gamma_j \end{aligned} \quad (2.155)$$

In practice, a force resolution system may be employed in which two parallel load-cells, spaced apart, are used to react both a force component and the moment in the plane containing their axes. In this case one may either include the extra term on the right-hand side of the appropriate equation corresponding to equation (2.155), or carry out the "axis-transfer" on the left-hand sides to obtain the aerodynamic forces referred to conventional model-fixed axes.

In application the proportion of each signal which is added algebraically to each force transducer output would need to be adjusted empirically to minimise the undesirable oscillatory components.

A discussion of some practical systems and the way they are adjusted is deferred until Chapter 3.

## 2.42 Methods using partially restrained models

By deliberately limiting the motion which can take place a certain amount of restricted information can be obtained. By allowing only a single degree of freedom, the motion is conceptually simple and the equations describing it readily formulated. The chief uncertainty is an unknown reaction associated with the nominally free coordinate, which can arise as a result of friction in the bearings which support the

model, or because of some other imperfection in the pivots. The problem can usually be overcome by introducing a weak, known restraint and repeating the tests. The two sets of results can then be used to eliminate the unknown reaction. The chief difficulties associated with methods of this type are practical ones and we shall discuss these in Chapter 4, treating them under the broad heading of "free-flight techniques".

### 2.5 Aerodynamic interference from the supports.

We have already drawn attention to the particular advantage that the free-flight technique has over force-balance methods, namely the absence of aerodynamic interference arising from the presence of supports. This interference, as is well known, is more than just the obvious change in the geometric configuration immersed in the test stream. Even when thin wires are used to support the model the effects can be serious, since such wires can modify considerably the structure of the boundary layer on the model. This is in fact the crux of the interference problem, because the likelihood or extent of the interference is far from obvious. A detailed discussion of the problem is beyond the scope of this account. Because, however, it introduces constraints on the design of a force-balance system, we must draw attention to some of the more important aspects, and at least try to provide some guide-lines for balance design.

The sting support which is commonly used is itself an attempt at a design which introduces a minimum of interference, and in a supersonic flow it takes full advantage of the limited upstream influence which exists. However boundary layers and wakes have subsonic regions, so that there is always some upstream influence. This can vary from a relatively unimportant small modification in the "base drag" to a serious breakdown in the flow resulting from premature separation of the boundary layer on the model. Between these extremes the skin-friction drag may be affected by premature transition to turbulence.

By its very nature the extent of the interference will depend upon the shape and attitude of the model. Even where particular, simple shapes are concerned however, systematic tests are few, and most of these have been conducted in subsonic, transonic and supersonic flows rather than in hypersonic streams. One might expect nevertheless that the differing situations have some common elements.

The problem is perhaps best understood by reference to a simple example, such as that of a slender, axially-symmetric body in a supersonic stream. In the interference-free case, the flow would separate at the base, and the supersonic flow would expand through a conical rarefaction wave towards the centre-line. This would form a "cavity", in the near-wake region, of slowly-moving fluid, terminated by a recompression region as sketched in figure 2.22. The details of this near-wake region, and in particular the base pressure, are likely to depend fairly critically on the state of the boundary layer at separation. The presence of a supporting sting in this base region is clearly going to affect the wake. There are basically two effects to be considered. The presence of a sting of any size is going to modify the flow, and this is generally referred to as the "sting-diameter effect". There is evidence that such effects exist at both low Reynolds number (Kavanau, 1954) and at very high Reynolds number (Sivier & Bogdonoff, 1955) and probably the measured axial force would require some correction in all cases. The second effect concerns the length of the sting. It is common practice to provide aerodynamic shielding of the supports so that the loads on them do not contribute to the force-balance readings. The shroud is necessarily somewhat larger than the sting, so that the effective length between the base of the model and this shroud will also influence the flow. It is apparent that the support in the wake region should be as long and as slender as possible, but this conflicts with the requirement for high natural frequencies in a system designed to measure transient loads. The problem is essentially to decide just how large a diameter and how short a sting one can tolerate from the aerodynamic viewpoint, and how closely aerodynamic shielding of the sting can be brought to the base of the model. Similar considerations apply to stiffening of the sting by tapering in order to raise the natural frequency of transverse oscillations.

Over the last twenty years or so it has become established practice for standard models to be tested so that comparisons can be made between different wind-tunnels and measuring techniques. AGARD committees have drawn up specifications for a number of such calibration models, and one of these, Model B, was subjected to systematic tests by Schueler (1960) who varied the sting configuration by moving the windshield to leave different lengths of sting exposed. Model B is a wing-body combination. Tests were carried out in supersonic flows at Mach numbers of approximately 2, 3 and 4 and over a Reynolds number range of  $3.5 \times 10^6$  to  $13.5 \times 10^6$ , based on body length. Both the base pressure and the static pressure just

forward of the base region were measured.

Schueler concluded that for a sting-to-base diameter ratio of 0.296, the static pressure just upstream of the base was hardly affected by the length of sting so long as this was greater than 1.12 model base diameters. The base pressure however was affected by sting lengths up to a little more than twice this value, though the tests at a Mach number of 4 were thought to be at Reynolds numbers where the sting diameter itself is influential.

In all Schueler's tests the boundary layer on the body had undergone transition forward of the base. He points out that the critical sting length - that is, the shortest sting for which the base pressure remains unaltered by sting length - is very dependent on the state of the boundary layer approaching the base, and he quotes some results of Kavanau (1953) on a cone-cylinder model at a Mach number of 2.84 in which this boundary layer was laminar. Schueler's results, those of Kavanau and some other data are summarised in figure 2.23. A laminar wake is very sensitive to the length of sting as one might expect.

The results illustrated in figure 2.23 were obtained on slender shapes in supersonic streams, and for such conditions are probably fairly representative of the effect of windshield position.

Tests on a sting-mounted bluff body in a hypersonic flow of Mach number 20 in the Langley Hotshot tunnel are reported by Miller (1965). A hemi-sphere cylinder having a length-to-diameter ratio of one was mounted in turn on one of several stings ranging in diameter from 0.25 to 0.625 times the diameter of the model. Two movable shrouds were tested, both of diameter 0.834 times the model diameter; one had a semi-apex angle of  $30^\circ$ , the other of  $90^\circ$ . Like Schueler, Miller found little effect on the after-body pressure just forward of the base. The base pressure however was affected by sting lengths less than about 2 model base diameters for the  $30^\circ$  shroud, while interference occurred with the  $90^\circ$  shroud for sting lengths less than about 3 model base diameters. No effects of sting diameter were found over the range tested. The Reynolds numbers/metre of Miller's tests were in the range  $10^6$  to  $1.55 \times 10^6$ , and the length of the model was 76.2 mm, so that the highly-cooled boundary layer on the model was probably entirely laminar.

We have noted already that the state of the boundary layer as it separates in the base region plays an important role in determining the base pressure. It will likewise be important in determining the extent of any interference due to sting length. The interference arising from the proximity of the windshield is governed by the position of this shield in relation to the "throat" of the wake, see figure 2.22. Whitfield (1959) points out that the "transitional" wake may well require longer sting lengths than the 3 or so body diameters needed with the fully turbulent wake, and he suggests that the wind-shield should be 1 to 1.5 model base diameters downstream of the wake "throat", see figure 2.24. On the whole it is probably wise to treat all these "rules-of-thumb" with reservation, since so many factors can influence the flow, particularly when separation upstream of the base is involved as it may be when the rear of the body is tapered.

Finally we must point out that the transient nature of the flow in an impulse tunnel also poses some unresolved problems related to the time any flow takes to become established. The point we wish to draw attention to is not the possible inadequacy of an impulse tunnel as regards establishing a steady flow about certain shapes of test model, even in ideal circumstances, but rather the possibility that the support and its aerodynamic shield may affect this flow establishment time adversely. In the absence of experimental data, the designer of a force-balance must proceed with caution, noting that, on the whole, separated flows are likely to take longer to establish than attached flows, and that the former will also result in more extensive upstream influence.

CHAPTER 3  
FORCE BALANCE TECHNIQUES

### 3.1 Introduction

The design of a force balance for transient measurements must take into account both its static and its dynamic performance. As always primary consideration must be given to ensuring that the design meets its specification in so far as it is capable of doing its job. However, ease of operation is of fundamental importance also, since a device which is complicated in use is likely to lead to frustration on the part of the operator, to mistakes and to time-consuming expense. For these reasons among others, it is important that specifications be set realistically, not only in regard to resolution and accuracy, but also range of operating conditions. In the present context for example, a balance designed for use in a specific wind-tunnel to measure say, the three components lift, drag and pitching moment, is likely to perform better in that tunnel than a six-component balance designed to cope with conditions appropriate to two dissimilar wind-tunnels.

The first decision to be made therefore is how many force components are to be measured simultaneously, for the force-resolution system depends upon this. A design with a superfluity of linkages will usually lead to errors arising from inadequate decoupling of the components, errors which may be avoidable by reducing the number of linkages to that which is essential.

We may at the outset dismiss from consideration the old-fashioned beam-balance in which the aerodynamic forces were balanced by a direct comparison with known weights. Necessarily most of the balance in such cases is situated outside the tunnel, and even with a servo-system measurements would not be possible in the test-times with which we are concerned. A number of other disadvantages, such as the large tare weight of the model support system, the fact that the support struts must be shielded from the flow and the need for pressure sealing, have already militated against such balances, even in general practice, in favour of the "sting-balance" employing force-transducers. In these cases the "balance" (the name has persisted) is situated either within a single axial strut (or "sting") supporting the model, or within the model itself, the "earth-side" in the latter case being connected rigidly to the support. Although minimising the aerodynamic interference the sting may seriously affect the flow by causing premature boundary layer separation.

A balance designed to measure  $n$  (generalised) static force-components\* will require a minimum of  $n$  force-transducers. For example when only the static longitudinal behaviour of a model is of concern, as in a symmetrical configuration, a balance having three force-transducers arranged as shown schematically in figure 3.1 is necessary and sufficient to determine the normal force, axial force and the pitching moment. In an ideal situation the axial force gives rise to an output from  $F_2$  only, while the normal force and pitching moment are respectively proportional to the sum and difference of the outputs from  $F_1$  and  $F_3$ . When the "hinges" are imperfect, and in the general case they need to be "universal joints" with zero backlash and zero friction, an axial output at  $F_2$  may arise from the presence of normal force-components or arbitrary moments. The hinges or pivots then are an important feature of the force-measuring elements. The complete force-transducer generally consists of two basic parts; a suitably-pivoted element which undergoes strain and a strain-sensitive device which produces an output, invariably electrical, which is, ideally, proportional to the force to be measured. We discuss this "gauging" problem separately, in Section 3.2, since the design of the complete force-balance or of individual force-transducers depends upon the level of strain that can satisfactorily be measured. At this stage we merely note that the performance constraints imposed by dynamic rather than static considerations essentially limit the strain sensors to solid state devices.

In the succeeding Section 3.3, we examine the design of balances as a whole. Although the desirable qualities of a balance are readily set forth and most of the pitfalls are well known, the designer has a wide discretion. We shall find that, having set out some of the basic design principles, we can do little better than learn from the examples of our predecessors. Accordingly continual reference

---

\* "Generalised forces" are deemed to include "moments". In conjunction with "generalised displacements" they are such that;  $\text{work-done} = \int F_i \cdot dx_i$ .

will be made to designs reported in the literature.

The performance of a force-balance in a flow of short duration depends critically on the resonant frequencies of the system as a whole - that is upon the combination of model, balance and supporting structure. In essence either all these resonances must be outside a frequency range equivalent to the flow duration, or at worst one such critical frequency may be removed by electrical filtering of the outputs from the transducers. With two critical frequencies, filtering is difficult without losses in accuracy, and more than two are virtually impossible to remove by filtering. Resort must then be had to acceleration-compensation. In Section 3.3 we discuss also the design of a balance and its support from a dynamic viewpoint.

The transient nature of the system necessitates some method of automatic recording of the data. With the output in the form of an electrical signal we may take advantage of a number of modern devices to amplify and filter the signal either before or after recording. We discuss the relative merits of several systems in Sections 3.4 and 3.5.

A measuring system requires calibration. In the case of a multi-component force-balance, calibration may be a complex procedure, which by its very nature does to some extent evaluate the performance of the balance. This is particularly true where the interactions between components are concerned. Although the balance is required to measure transient loads, calibration is much more easily carried out under static conditions. It is desirable therefore that the balance be capable of measuring static as well as transient loads. However it is also essential that dynamic testing be carried out by way of calibration to ascertain the relevance of static calibrations to the dynamic situation. In these circumstances it would be unrealistic to restrict the design of a balance by requiring that it be capable of static calibration. Instead methods of dynamic calibration must be sought. The final section of this Chapter examines such methods.

### 3.2 Transducer elements

In this section we shall review the properties of those solid-state materials which are useful as electromechanical transducers in force balances having a sufficiently good high-frequency performance for use in short duration hypersonic wind-tunnels. We shall also discuss the way in which these materials may be employed. As a general rule any transducer element in which a significant displacement is required before a useful electrical output signal is generated is thereby inhibited from having a good high frequency performance. Thus such devices as variable reluctance and variable capacitance transducers have not found wide application, though a commercial vibration pick-up based upon the principle of mutual inductance with a frequency range up to 20 kHz is available.\*

Materials most obviously suitable for transducer elements in the present application are those with piezoelectric or piezoresistive properties.\*\*

---

\* Tel Instrument Electronics Corporation, Model 501.

\*\* Whether photosensitive devices could also be used as strain sensors is an interesting point on which a designer might exercise ingenuity. Used in conjunction with a light-occluding system, the basic principle of one possible device is clear. However the high frequency response requirements precludes significant displacements of say knife edges or shutters. A further possibility which springs to mind is the use of fine, parallel gratings from which pulses, and consequently digital measuring techniques might result. An obvious difficulty is knowing the sign of the strain which is taking place at any instant.

A somewhat different approach was adopted by Bratt & Wight (1944) in their proposal for an automatic balance to measure varying forces. They suggested a light-occluding system which was to be used in conjunction with a photo-cell to control the current in a coil suspended in a magnetic field. The current needed to balance the displacement produced by the load is a measure of the load. They suggest that such a system should be capable of operation at up to 20 Hz which is perhaps pessimistic.

Piezoelectric devices have perhaps received rather less attention than their potentiality warrants. The property known as piezoelectricity, whereby certain materials develop an apparent\* electrical charge when under mechanical strain is fairly well understood (see, for example, the classic treatise by Cady, 1946 & 1964). However Cady's work is not easily assimilated and few efforts have been made to 'translate' it into engineering terms, though the work of Mason (1947, 1950) and his colleagues at the Bell Laboratories are notable exceptions. The reciprocal effect, applying an electrical potential to generate mechanical strain, has received a good deal of attention, quartz oscillators being widely used as frequency standards. The stability of quartz crystals and the phenomenal range over which they are linear as far as the piezoelectric effect is concerned make them eminently suitable as transducer elements, and in recent years pressure transducers and load cells using quartz have become commercially available.

Other piezoelectric materials have also been developed commercially over the last twenty years or so, materials which are more sensitive than quartz, and which can be machined to a variety of shapes, though they are less stable, less linear and pyroelectric. These are far from fully exploited but some idea of their potential can be gauged from a recent discussion of their application to transient pressure measurement (Goodchild & Bernstein, 1972). In the following section, 3.21, we shall discuss piezoelectric devices in some detail, since for the most part it is only the "bare" piezoelectric element which is available commercially. It is up to the balance designer to incorporate such elements into force transducers.

The property known as piezoresistivity whereby materials undergo a change in their electrical resistance with applied mechanical strain is well-known to engineers. Wire and metal foil strain gauges are familiar devices in experimental stress analysis. More recently, semiconductor strain gauges offering much higher sensitivities have become available, but because they possess certain disadvantages which complicate their use, they have perhaps yet to be fully exploited.

The literature on bonded strain gauges is fairly voluminous and gives details not only on their construction, but also on how they should be bonded to the region where the strain is to be measured and on suitable electrical circuits which make maximum use of their properties. To some extent therefore a detailed account here is superfluous, with the works of Neubert (1967) and Dean & Douglas (1962) for example widely available in addition to comprehensive data produced by the manufacturers.

Several reasons may be put forward however for including rather more than just references. The most obvious is to make this work more "self-contained". From the balance-designer's and user's point of view, this is clearly an advantage. It does moreover enable us to extract just those features of particular relevance to the problem in hand. Again, an appreciation of the more fundamental characteristics of the devices he is using should enable the user to interpret his results the more readily. From the designer's point of view the "inhibiting effect" of what is commercially available may be diminished so that novel applications are born in attempts to meet the stringent requirements of high sensitivity and fast response.

We therefore discuss piezoresistivity from a phenomenological point of view in a fairly full manner, in Section 3.22. The resistance strain gauge of course is only an element in the measuring chain. Their lack of strength means that they cannot usually be used to react the total load component as piezoelectric devices can. They need support, and it is the surface strain in these supports to which they respond. The force transducers, which incorporate not only the "strain cell" and "strain sensor" but also a mechanism for decoupling it from "off-axis" loads are clearly a very important part of the design, and strain cell and sensor each play a part in selection of the other. It is however more convenient to consider them separately for the obvious reason that much of the discussion on force transducers and decoupling pivots is applicable to other strain sensing devices.

Accordingly the remainder of Section 3.2 will be devoted to discussing strain sensors only.

---

\* The word "apparent" is used deliberately since on open-circuit there can be no net free charge on the conducting surfaces of the dielectric, though a potential difference between them is generated by the mechanical strain. The confusion arises from the analogy with the theory of a capacitor. The "apparent charge" is that charge whose opposite would, on being applied, reduce the potential difference to zero. The point is more fully discussed by Goodchild (1968).

### 3.21 Piezoelectric materials

A piezoelectric material is one in which a change in the electrical polarisation takes place when it undergoes a mechanical strain. When parts of the surface of the material are plated with a conducting material, this change manifests itself as a potential difference across the plated parts. A typical material may well produce 1 volt on open-circuit when subjected to a mechanical strain of order  $10^{-7}$ . Thus large electrical signals may be produced with only moderate stress levels. The converse effect also occurs; an electrical potential applied across a piezoelectric material produces a change in dimensions, so that an alternating voltage will induce a vibration.

There are two basic classes of piezoelectric material which have found application in measuring instruments, though many others are known. Some naturally occurring crystals such as quartz and Rochelle salt and some synthetic crystals such as lithium sulphate and ammonium dihydrogen phosphate (ADP) are piezoelectric. In addition there are the synthetic polarised ferroelectric ceramics such as the barium titanates, lead zirconate titanates (PZT)\*, and lead metaniobate which behave in a similar way.

Of the crystals Rochelle salt, although somewhat more sensitive than quartz, is considerably more affected by temperature and humidity and has a highly non-linear response characteristic, all features which are undesirable in a transducer sensing element. Lithium sulphate monohydrate and tourmaline have both been used to measure stress, but artificially-grown quartz has found by far the widest application, alpha-quartz being the piezoelectrically active variety. Transducer sensing elements are cut from single crystals, the "cuts" being designated by referring the major faces of the cut element to the crystal axes together with the orientation of the remaining axes where these are important. Thus a  $45^\circ$ -X-cut crystal has its thickness in the X-direction and the length of the plate is at  $45^\circ$  to the Y- and Z-axes. Such a cut is illustrated in figure 3.2. The major faces normal to the X-axis of the crystal are plated or are in contact with conducting material and it is across these surfaces that the potential difference appears. In other applications a quartz plate is Y-cut with its thickness in the Y-direction; it is then used in a shear mode, that is a potential difference appears when a shear load is applied. Clearly the potential difference depends in general upon the orientation of the "cut" relative to the crystal axes as well as on the manner of loading and the location of the electrodes.

In the ferroelectric ceramics, the relation between the applied stress and the change in polarisation depends upon the magnitude and direction of the induced polarisation. The barium titanate ceramics are made by compressing barium titanate powder into the desired shape and sintering it at high temperature. Various additives may be used to improve some of its properties. The fired ceramic may also be machined to shape. A permanent polarisation is given to the ceramic by applying a strong electric field across it while it is raised above its Curie temperature, and then allowing it to cool slowly in the electric field. The strength of the field and the cooling time for complete polarisation depend upon the particular additives (see Anderson, 1964 for further details).

The relative ease of manufacture to almost any desired shape, their lower cost and the fact that they have far higher sensitivities than quartz, make the ceramics particularly useful at low force levels. However they suffer to some extent from aging and are more sensitive to temperature changes than quartz, though the addition of small amounts of calcium and lead titanate not only reduces the temperature sensitivity but improves the piezoelectric performance of the ceramics. Extreme conditions of high stress and temperature can also lead to depolarisation. Quartz on the other hand is extremely stable and can be used over a very wide range of stress level ( $1:10^6$ ) remaining essentially linear. Thus it is suitable for use as the transducer element in a "primary" standard.

#### 3.211 Some theoretical aspects

In order to discuss in detail the relative merits of different materials and element configurations it is necessary to examine the equations which describe the behaviour of piezoelectric materials. The important parameters are the mechanical stress tensor  $[\sigma]$ , the strain tensor  $[\epsilon]$ , the electric displacement vector  $\underline{D}$  and the electric field strength vector  $\underline{E}$ . Any pair consisting of one mechanical and one electrical quantity may be regarded as the independent variables and the others written as functions of these two. Any of the resulting four pairs of equations may be used. For the present purpose it is

\* Copyright trade name of ceramic manufactured by Brush Clevite Co.

convenient to use  $[g]$  and  $E$  as the independent parameters. Assuming a linear relationship between the electric displacement and the mechanical stress which causes it, we may combine this "piezoelectric property equation" with that for a dielectric relating  $D$  to  $E$  to give

$$D_i = d_{ijk} \sigma_{jk} + \epsilon_{ij}^{\sigma} E_j \quad (3.1)$$

where the superscript  $\sigma$  denotes that the dielectric permittivity  $\epsilon_{ij}$  is to be evaluated at constant stress. The quantities  $d_{ijk}$  are the piezoelectric constants of the material and we use here the suffix notation for cartesian tensors, the summation convention being implied by repeated suffices appearing in any product of terms.

For a material which obeys the generalised Hooke's Law, it may be shown that inclusion of the effect of the electric field on the strain leads to

$$S_{ij} = s_{ijkl}^E \sigma_{kl} + d_{kij} E_k \quad (3.2)$$

where the fourth order tensor  $s_{ijkl}^E$  is the elastic compliance which is to be evaluated at constant electric field. These equations are given in full together with the other three pairs of equations in a classic paper by Mason (1947). It is perhaps pertinent to point out at this stage that these other equations involve  $\epsilon_{ij}^S$  and  $s_{ijkl}^D$  among other quantities. Which values are used in any given situation depends upon the boundary conditions. However Mason (1947) gives values which show that for quartz the differences are small though for Rochelle salt they approach 50% for some components. For the ceramics the differences between some elastic compliance components is of order 10% so that the electrical boundary conditions strictly affect the strain corresponding to an applied stress system. Likewise some of the components of the dielectric permittivity differ by about 20% for ceramics, so that the mechanical boundary conditions govern the solution of the electrical problem to some extent. However for transducer design these difficulties can be ignored, since ultimately the transducer performance depends upon other factors as well, and needs to be determined by calibration.

Assuming weak electro-mechanical coupling then, and neglecting the electric field external to the piezoelectric material, it is possible to show that the voltage generated is

$$V = Q/C_0 = -\frac{1}{C_0} \int_B (d_{ijk} \sigma_{jk}^0 E_i) dB \quad (3.3)$$

where  $C_0$  is the static capacitance,  $Q$  the apparent charge,  $\sigma_{jk}^0$  the stress distribution in the electrically-free element and  $E_i$  is the field produced by unit applied voltage to the mechanically-free element, the integral being taken over the volume  $B$  of the element. Thus  $\sigma_{jk}^0$  and  $E_i$  are solutions of a purely elastic and purely electrical problem respectively.

In the majority of transducer applications the piezoelectric sensing element is essentially a thin plate, that is the thickness  $t$ , in the direction 03 say, normal to the conducting surface is small. In this case  $E_i = \bar{E}_3 = 1/t$  so that equation 3.3 becomes

$$V \left\{ \frac{\epsilon_{33}^{\sigma} A}{t} \right\} = -\frac{1}{t} \int_B (d_{3jk} \sigma_{jk}^0) dB \quad (3.4)$$

where  $A$  is the area of a plated surface.

Because it closely approximates most cases of interest and also because it affords a considerable simplification we shall use equation (3.4) throughout most of the remaining discussion. In essence the procedure adopted is to insert  $\sigma_{jk}^0$  as the solution of a purely elastic problem in order to determine the potential difference  $V$  or the apparent charge  $Q$ . These solutions of the elastic problem are usually approximations themselves since isotropy is commonly assumed though piezoelectric materials are essentially non-isotropic. In addition it is common practice to ignore either some of the stress components or the compatibility of strains in determining the solution of the purely elastic problem. Thus several approximations are involved in determining the sensitivity of a transducer sensing element, but for design purposes where we seek to compare different configurations, these are not serious.

Before examining different configurations, we may note that the sensitivity depends directly upon the magnitude of the piezoelectric coefficients  $d_{ijk}$ . Other properties however are also of importance. Thus account must be taken of (i) the relative permittivity, and specific resistivity which have a direct bearing on the low frequency characteristics since they determine the natural time constant of the sensing

element, (ii) the elastic constants and the mass density which determine the natural frequencies of the element, and (iii) the changes in the behaviour of the material which occur with change of temperature. Because piezoelectric materials are not isotropic, the properties must be referred to a specific set of axes which avoid ambiguity. These may be crystallographic or polarisation axes and some care is necessary regarding the relation between these axes and those used in the stress analysis. We shall employ "transducer axes" which simplify the stress analysis; these do not necessarily coincide with the crystallographic or polarisation axes and where they do not the equations for the transformation of tensor components must be used in order to substitute the appropriate coefficients into equation (3.4), for example.

It is very common to find, particularly in the commercial literature, that a "restricted tensor notation" is used. This restricted notation is possible because of various symmetries which exist; for example there are only 6 independent strain components making up the strain tensor. The relationship between the two notations is given by Mason (1947) and by Nye (1957). In this restricted notation, equation (3.4) becomes

$$V \left\{ \frac{\epsilon_{33}^{\sigma} A}{t} \right\} = Q = - \frac{1}{t} \int_B (d_{3n} \sigma_n) dB \quad (3.5)$$

n = 1, 2, ..., 6

where  $O_3$  is normal to the plated surfaces.

The properties of some selected piezoelectric materials are listed in Table 3.1. Table 3.1(a) sets out the components in a matrix form which clearly brings out the symmetries; for example the ceramics are symmetrical about the polarisation axis  $O_3$ . Table 3.1(b) gives some typical numerical values which may be used for initial transducer design, but because constant improvements are being made in the production of the ceramics, the designer should refer to the manufacturer's latest literature. Many piezoelectric materials are also pyroelectric, that is a potential difference is produced as a result of thermal strain. Moreover the properties depend to some extent on temperature, that is the piezoelectric coefficients themselves are temperature dependent. Much of the effort involved in selecting quartz crystal "cuts" has been expended in trying to find one with a near-zero temperature sensitivity. In ceramic production, additives have been sought which reduce the deficiencies arising from temperature-dependence. In this respect the lead-zirconate titanates are a considerable improvement over the barium titanates.

### 3.212 Low frequency characteristics

The low frequency characteristics depend upon the natural time constant of the material. For the simple configuration of thickness  $t$  and plated area  $A$  we may write

$$R_0 = \frac{\rho_{33} t}{A} \quad \text{and} \quad C_0 = \frac{\epsilon_{33}^{\sigma} A}{t} \quad (3.6)$$

so that the natural time constant

$$\tau = R_0 C_0 = \rho_{33} \epsilon_{33}^{\sigma} \quad (3.7).$$

Here  $\rho_{33}$  is the specific resistivity between the conducting surfaces<sup>†</sup> and  $R_0$  is the resistive impedance. Orders of magnitude for  $\rho$  and  $\tau$  are included in Table 3.1 from which it can be inferred that quartz has a somewhat longer time constant than the ceramics and therefore a superior low frequency performance. As we shall see later (Section 3.6) this eases the problem of transducer calibration.

### 3.213 High frequency characteristics

The transient response of a measuring system depends chiefly on its natural frequencies. With force balances the natural frequencies which cause most concern are usually those of the larger parts of the system as a whole, particularly where the model upon which the aerodynamic forces are being measured is sting-mounted. The reason is that these natural frequencies are usually lower than those of the transducer element, and it is not easy to eliminate these lower frequency components without cutting off the higher frequencies also. However for some force components, drag for example, a well-designed balance may have only a single prominent vibration mode to which the force-sensing element responds and when this

† see Section 3.22

response to vibration is "eliminated" using acceleration-compensation, the vibration of the transducer itself may become significant. Although the construction and design of the transducer as an entity governs its lowest natural frequency, with some designs the natural frequency of the transducer sensing element itself may assume importance. The same is true of accelerometers.

Accordingly some discussion of the natural frequencies of piezoelectric sensing elements vibrating in various modes is justified. We shall consider here the natural frequency  $f_0$  of the sensing element alone. Later we shall draw attention to the way in which loading of the element affects the vibration characteristics. The modes of interest involve longitudinal compression waves, transverse shear waves and bending vibrations. The longitudinal compression waves may be parallel or normal to the axis of polarisation and these are discussed separately.

### 3.2131 Compression waves parallel to the axis of polarisation

A convenient way of describing the transient response of an element is to outline its behaviour for a particular input function; in the present case a step input is appropriate. The response to such an input will depend upon the transit time  $\tau_t$  of the wave through the element and upon the way in which this wave is reflected from the back face. When the back face is "free" the reflected wave is of opposite sense to the incident wave; that is, an incident, plane compression is reflected as a rarefaction, or extensional, wave. In this case the element returns to its initial state after a time  $2\tau_t$  and the corresponding value of frequency is that usually quoted by the manufacturer of the piezoelectric element since he usually has in mind the common application as an electrical oscillator when mechanical loading is kept to a minimum.

However for a "rigid" backing, a wave of like sense, equal in magnitude to the incident wave, is reflected. The corresponding period before the element returns to its initial state is  $4\tau_t$ . When the backing material is "matched", that is, it has the same acoustic impedance, no wave is reflected at all, but when the input wave form is sinusoidal, the full output is first reached after one-quarter of a cycle. This suggests that for the applications we have in mind, a natural frequency for the element corresponding to  $4\tau_t$  should be used. The appropriate velocity  $v$  of wave propagation is shown by Redwood (1961 a) to be identical to that for a non-piezoelectric material. This is given by

$$v^2 = c_{33}^D / \rho \quad (3.8)$$

where  $\rho$  is the density of the material and the elastic constant  $c$  is evaluated at constant electric displacement, the axis of polarisation being  $O_3$ .

### 3.2132 Compression waves normal to the axis of polarisation

In this case the transit time depends upon the velocity of waves in a direction perpendicular to the axis  $O_3$  of polarisation. Redwood (1961 b) shows that in this case the appropriate elastic constant is to be evaluated at constant electric field, so that

$$v^2 = c_{11}^E / \rho \quad (3.9)$$

Again on physical grounds it may be argued that a natural frequency corresponding to four times the wave transit time (in the  $O_1$  direction) is appropriate. Although this mode is rarely used directly because the sensitivity is poor, it may be necessary to consider it when taking account of the "cross-axis sensitivity" of a transducer.

### 3.2133 Transverse shear waves

Whereas with plane compression waves the displacement of a particle takes place in the same direction as the wave motion, with shear waves the particle displacement is in a direction normal to the wave motion. For a system with axial symmetry only one type of wave travelling parallel to the axis of polarisation is possible. For waves moving in directions normal to this axis, two types are possible: one in which the particle displacement is normal to the axis of polarisation and one in which it is parallel to it. The wave speeds appropriate to these three cases are respectively  $(c_{44}/\rho)^{1/2}$ ,  $(c_{66}/\rho)^{1/2}$  and  $(c_{44}/\rho)^{1/2}$ , the external circumstances determining whether these should be evaluated at constant electric field or constant electric displacement. However in practice a shear element can only be loaded by a force transmitting device of some kind. This may take the form of an "anvil" which is kept in contact

with the piezoelectric element by preloading to such a degree that friction suffices to transmit the force. The mechanical loading due to the additional mass of the anvil has a considerable effect on the natural frequency of the transducer, so that differences between  $c^E$  and  $c^D$  are of minor importance. Indeed the natural frequencies given by the above wave speeds may only be taken as a fairly crude guide to those of transducers which make use of the shear mode.

### 3.2134 Bending modes

Lewis (1961) has shown that to a first approximation, the natural frequencies in bending of a beam of piezoelectric material are the same as those for non-piezoelectric material with identical elastic properties. Unfortunately however the readily available solutions for the frequencies in bending all assume that the beam is of a material which has isotropic elastic properties. To make use of these simple solutions we must decide which of the elastic properties of the non-isotropic piezoelectric material are best likely to describe its behaviour in bending. The commonest element configuration used in transducers employing the bending modes are thin plates or beams polarised across the thickness direction  $O_3$ . The restoring forces then arise as a result of the tensile and compressive stresses along a direction normal to  $O_3$ . For a material with axially-symmetric properties about the axis of polarisation, the appropriate elastic constant would be  $c_{11}$ . Comparison of this case with that in which compressive waves are propagated normal to the axis of polarisation would suggest that this should be evaluated at constant electric field, so that the appropriate wave velocity is given by

$$v^2 = c_{11}^E / \rho \quad (3.10).$$

### 3.214 Sensitivity of a selection of transducing modes

We next examine a variety of sensing element configurations, in particular those illustrated in figure 3.4. We assume that the axis of polarisation lies along  $O_3$  and we shall consider the sensitivity to a uniformly distributed pressure  $p$  or to a point load  $F$  as appropriate. With some configurations one is more easily achieved than the other. The static capacitance  $C_0$  also has to be considered as this has some bearing on the design of the associated electronic amplifier.

We shall illustrate the application of equation (3.5) by reference to the configuration of figure 3.4(a) in which a thin plate of thickness  $t$  is subject to a load  $F$  in the  $O_3$ -direction, uniformly distributed over the surface area  $A$ . To a first approximation the stress field is given by

$$\sigma_n = 0 \text{ for } n \neq 3; \quad \sigma_3 = F/A \quad (3.11)$$

where we neglect any constraints arising from the way in which the sensing element is fixed in the transducer.

Substituting this stress field into equation (3.5), only one term arises, giving

$$Q = -\frac{1}{t} \int_B (d_{33} \sigma_3) dB = -d_{33} F \quad (3.12).$$

Defining a sensitivity to force by  $Q_F = Q/F$  we find that for this configuration

$$Q_F = -d_{33} \quad (3.13)$$

so that in this direct compressive mode, the sensitivity to force depends only upon the piezoelectric constant  $d_{33}$  of the material\*.

The static capacitance  $C_0$  is given by

$$C_0 = \epsilon_{33}^{\sigma} A/t \quad (3.14)$$

---

\* Care must be taken when substituting numerical values for  $d_{33}$ . For piezoelectric ceramic elements it is usual to choose  $O_3$  as the direction of polarisation so that  $d_{33}$  is also the symbol for polarisation axes. For quartz on the other hand, X-cut crystals are usually used for the direct compressive mode, and the appropriate piezoelectric constant is usually designated  $d_{11}$ , the crystallographic  $Ox$ -axis coinciding with the transducer  $O_3$ -axis.

so that the voltage sensitivity to force, defined by  $V_F = V/F$ , is

$$V_F = \frac{td_{33}}{A\epsilon_{33}^{\sigma}} \quad (3.15).$$

It would appear that by increasing the thickness  $t$  of the sensing plate, an increase in voltage sensitivity to force may be obtained. However we shall see later that the charge sensitivity  $Q_F$  is somewhat more important than  $V_F$  and in addition increasing  $t$  increases the wave transit time through the element thereby reducing the natural frequency which for this mode is given by

$$f_0 = \frac{1}{4t} \sqrt{\frac{C_{33}^D}{\rho}} \quad (3.16).$$

There is however a useful method of increasing the sensitivity of the normal compressive mode. This consists of building a "stack" of sensing elements with their polarisation axes co-directional, these elements being connected electrically in parallel, as illustrated in figure 3.5(a). Using equation (3.12) we see that for a stack of  $N$  identical plates

$$Q_F = -Nd_{33} \quad (3.17).$$

The natural frequency however is inversely proportional to  $N$ , so that the product  $Q_F f_0$  is independent of the number of plates in the stack. This suggests that the product of charge sensitivity and natural frequency is a useful measure of the performance of a mode. It is analogous to the product of gain and bandwidth as a performance figure for some classes of electronic amplifying systems. The product  $Q_F f_0$  must however be used with some caution by the designer seeking a suitable transducer mode. It is not simply a question of choosing the configuration with the largest value, since that configuration may not meet the sensitivity requirements, for example. For the stack of elements in normal compression, one could choose an overall thickness  $Nt$  consistent with the required natural frequency, and then make up this thickness by choosing  $N$  as large as is practicable to increase the sensitivity. In a similar way one may determine the sensitivity to force, the natural frequency and the static capacitance of the other configurations illustrated in figure 3.4. The results are summarised in Table 3.2.

The plate undergoing transverse compression is essentially similar to that in direct compression, but for ceramics the piezoelectric constant  $d_{31}$  replaces  $d_{33}$ , thereby reducing the sensitivity by a factor of two or three. Consequently this mode has found little application though a configuration which consists of a thin-walled ceramic cylinder polarised radially could prove useful. For X-cut quartz the appropriate constant, referred to crystallographic axes, is  $d_{12}$  which is equal to  $-d_{11}$ , and this mode has some advantages.

For ceramics the shear mode arises as a result of the non-zero piezoelectric coefficient  $d_{15}$ , a shear stress  $\sigma_5$  producing an electric field in the  $O_1$ -direction. For quartz the relevant non-zero coefficients referred to crystallographic axes are  $d_{14}$ ,  $d_{25}$  and  $d_{26}$ , the electric fields arising from the application of shear stresses  $\sigma_4$ ,  $\sigma_5$  and  $\sigma_6$  respectively. A shear stress  $\sigma_4$  would need to be applied to the Y- or Z-cut faces of the quartz element, but  $\sigma_5$  and  $\sigma_6$  can be applied to the X-cut faces. Since the piezoelectric coefficient  $d_{26}$  is some six times  $d_{25} = -d_{14}$  the Y-cut has the advantage so far as shear sensitivity is concerned.

However  $d_{26} = -2d_{11}$  for quartz and for ceramics  $d_{15}$  is somewhat larger than  $d_{33}$ , so that the shear mode is potentially more sensitive than the direct compressive mode. A disadvantage of a practical kind arises because some kind of pre-loading or cementing is necessary in order to apply the load.

Again with ceramics a thin-walled cylinder is a useful variant; the load may be applied tangentially to the inner face, say, the outer face being held fixed, see figure 3.4(c). Provided the wall is thin, the analysis for a flat plate is valid to a good approximation and  $Q_F$  depends only upon  $d_{15}$  and not upon the dimensions of the cylinder.

The sensitivity of the shear mode configuration may also be improved by "stacking" a series of plates as shown in figure 3.5(b). The effect is analogous to that in the direct compressive mode case; the sensitivity  $Q_F$  is proportional to the number of plates in the stack, but the product  $Q_F f_0$  remains constant.

The bending modes essentially make use of the transverse compression effect, and the sensing elements must be of bimorph or sandwich construction. That is, two similar plates, with conducting plating on their upper and lower surfaces, are connected electrically and mechanically at their common surface. They are polarised in the thickness ( $O_3$ ) direction. Applying equation (3.5) to the case of a beam in simple two-dimensional bending, we find

$$V = \frac{-1}{\epsilon_{33} \sigma} \iint_{\text{area}} \left\{ \int_{-t/2}^0 (d_{31} \sigma_1) dx_3 + \int_0^{t/2} (d_{31} \sigma_1) dx_3 \right\} dx_1 dx_2 \quad (3.18).$$

Since the simple theory gives

$$\sigma_1(x_1, x_2, x_3) = -\sigma_1(x_1, x_2, -x_3) \quad (3.19)$$

the voltage generated is zero, because the potential difference across the upper half is equal but opposite in sign to that across the lower half, so that the upper and lower surfaces are at equal potentials. By using a bimorph construction with appropriate electrical connections however, or by using bimorph plates polarised in opposite directions (thereby changing the sign of  $d_{31}$  in one of the integrals of equation (3.18)) an output may be obtained across the outer faces, see figure 3.4(e). The two configurations are known as parallel- and series-connected. Clearly the series connection, which is the more practical, has twice the voltage sensitivity to force, half the charge sensitivity and a quarter the static capacitance of the parallel connection.

The simple theory of bending relates the stress  $\sigma_1$  at a distance  $x_3$  from the neutral axis to the bending moment  $M_2$  and second moment of area  $I_{22}$  of the cross section by

$$\sigma_1 = \frac{M_2 x_3}{I_{22}} \quad (3.20).$$

Applied to the beam of length  $l$  and rectangular cross-section, this equation together with equation (3.5) yields for the series connection

$$Q = \frac{3d_{31}}{t^2} \int_0^l M_2(x_1) dx_1 \quad (3.21).$$

This integral is proportional to the difference in slopes between the two ends of the beam (see any standard text on the bending of beams). Thus the end fixings should be such as to make this difference a maximum; a beam built-in at both ends would have zero sensitivity.

A similar approach may be applied to the bimorph disc configuration which may in principle either be loaded uniformly or by a point load as shown in figure 3.4(f). The results listed in Table 3.2 for this configuration were calculated by Goodchild (1968) using the values for the circumferential and radial stresses given by Roark (1954).

A configuration which responds directly to torsional loading also makes use of the bimorph beam construction. In this case it is the shear mode which is involved (see figure 3.4(g)). The bimorph is polarised across the beam, in the plane of the sandwich. For the series connection, the two parts are polarised in opposite directions along the  $O_3$  axes. A torque produces a shear stress  $\sigma_4$  when the  $O_2$  axis is along the beam. A field is then produced in the  $O_1$  direction, across the sandwich. Assuming that the approximate distribution of shear stress is given by

$$\sigma_4 = \frac{-6 M_2}{at^3} x_1 \quad (3.22)$$

where  $a$  is the width of the beam subjected to a torque  $M_2$ , and that  $t \ll a$ , we find

$$Q = -\frac{2}{t} \int_{-a/2}^{a/2} \int_0^l \int_0^{t/2} \left( -\frac{6M_2 d_{14}}{at^3} x_1 \right) dx_1 dx_2 dx_3$$

where  $l$  is the length of the beam.

Hence

$$Q = \frac{3M_2 d_{14} l}{2t^2} \quad (3.23)$$

for the series connection. (By interchange of the  $O_1, O_2$  axes, the shear stress  $\sigma_5$  is induced, and  $d_{25}$  is the appropriate piezoelectric coefficient.) The piezoelectric constants  $d_{14}$  and  $(-d_{25})$  are equal for quartz and are non-zero. For ceramics they are zero.

### 3.215 Comparison between various configurations

In order to provide a more direct comparison between the modes and give some idea of the magnitude of the output which may be expected, values of the properties of a typical ceramic, PZT-5A have been used with the expressions in Table 3.2a to give Table 3.2b. The dimensions of the elements have been retained as variables but this is not a serious obstacle to making comparisons.

For typical sizes, the compressive modes produce the highest natural frequencies and have a moderate sensitivity, and the thickness shear mode is fairly similar. The bending modes however have a greater sensitivity but a considerably lower resonant frequency. In practice a good deal depends upon the ingenuity of the designer, who has to ensure that the load is transmitted uniformly, that the same proportion of the total load is always reacted by the sensing element and that loads of both signs can be measured. We shall return to these topics in sections 3.23 and 3.24 where force transducers and accelerometers are discussed in more detail, but they clearly have considerable bearing on the ease with which any particular transducing mode can be utilised.

Other factors also are important, the most significant perhaps being the "cross-axis" sensitivity and the thermal sensitivity. Short term thermal response can be minimised by good design, the sensing element being kept well insulated from the surroundings, but any long-time drift in the characteristics which affects the calibration is best avoided by careful selection of the sensing element material. Quartz is probably the best from this point of view but frequently its sensitivity is inadequate. Lead metaniobate appears to be the least thermally sensitive of the ceramics, but its piezoelectric coefficients are only some 15% of the best of the lead zirconate titanates commercially available at present.

Cross-axis sensitivity can be controlled to some extent by the designer. Apart from choosing sensing modes which have small inherent transverse sensitivity, careful attention to detail can minimise the amount of any transverse loading that is reacted by the piezoelectric element itself.

The thickness shear mode of the ceramics has some advantage as regards cross-axis sensitivity. Polarised along the direction  $O_3$  and placed on the surfaces normal to  $O_1$ , the thickness shear mode makes use of the piezoelectric effect associated with the coefficient  $d_{15}$ . No other loading on the element produces an electric field along  $O_1$ , so that any cross-axis sensitivity which does occur will be due to imperfections of some kind. One disadvantage of the shear mode is the difficulty of providing reliable load transmission. Cemented joints have not been found entirely satisfactory (Goodchild & Bernstein, 1972) but a bolted design has been successfully devised for a commercially-available accelerometer.\*

### 3.22 Piezoresistive materials

All solid materials possess electrical resistance - that is, when an electrical potential is applied across two points, the current which flows is finite. The magnitude of this electrical resistance varies widely from one material to another. Moreover for some materials, the resistance depends upon the direction of the potential gradient in relation to the internal structure of the material. In general, single crystals will exhibit non-isotropic conduction of this kind, and the formal relation between the electric field vector  $\underline{E}$ , and the current density vector  $\underline{j}$ , shows that the resistivity must be a tensor quantity of rank two. The materials of particular interest as transducer elements are some metals, some metallic alloys and two semi-conductors, one based on germanium, one on silicon. The metals and alloys are essentially in polycrystalline form and are more or less isotropic conductors in the unstressed state, so that  $\underline{E}$  and  $\underline{j}$  are co-directional. Single crystals of germanium and silicon have a cubic structure and they too are isotropic conductors when unstressed. In the pure state they have a high resistivity, and might then be regarded as "insulators" rather than "conductors". The addition of small amounts of impurities however, lowers their resistivity considerably; hence the term "semi-conductor" is applied to these crystalline materials when they are "doped" with certain specific impurities which act as extra electrical charge carriers.

---

\* Gulton Industries, Inc.

The resistivity of a semi-conductor is inversely proportional to the number of such charge carriers and their average mobility. Thus the specific resistivity can be controlled by adjustment of the impurity level. The effect of a mechanical strain is to alter the effective mobility of the charge carriers, and consequently the resistance. The strain in general distorts the structure of the crystal and so the mobility is not altered isotropically. In addition the dimensions of the specimen are also changed, and the resistivity changes on both counts. For the polycrystalline metals, the effect of the dimensional changes is always important and usually dominant. For semi-conductors a few per cent only of the change in resistivity arises from this source. Of particular importance is that the sense of this change in resistivity may be either positive or negative depending on the specific impurity used. This enables the construction of compound gauges which offer some advantages as we shall note later.

Changes in temperature also induce dimensional changes and affect the mobility of the charge carriers. Consequently the resistivity changes with temperature, more markedly for semi-conductors than for the metals. Temperature changes therefore give rise to an "apparent strain" which can be misinterpreted when these materials are used as strain transducers. The effects must be minimised and allowances of some kind made for them if necessary.

The important features of a strain transducer are its sensitivity, the linearity of its characteristic defining curve and the extent to which these are altered by environmental changes and by aging. The sensitivity is usually expressed as a "gauge factor"  $G$ , giving the ratio of the fractional resistance change of the strain gauge to the mechanical strain producing it. For metallic gauges this gauge factor is between 2 and about 12, though commercially available gauges generally have  $G \approx 2$ . The gauge factor of a semi-conductor strain transducer depends upon which mode is used, as we shall see in the next section, but it may be as high as 170. Gauges with such high sensitivity are however somewhat temperature dependent. By increasing the concentration of charge carriers to something of order  $10^{20}/\text{cm}^3$  the gauge factor becomes more or less independent of temperature but is somewhat lower in magnitude, perhaps 50 to 60. It is also less strain dependent; that is, linearity is improved by perhaps an order of magnitude, so that the reduction in gauge factor is worth tolerating. The impurity level also affects the temperature coefficient of resistance which may therefore be controlled. In the majority of applications the strain sensor is bonded to a load-carrying member and it is the surface strain of the latter which is sensed. Tailoring the temperature coefficient of resistance to that of the material forming the load-link has clear advantages, and gauges are available, matched to commonly used materials. On the whole the ratio of temperature sensitivity to mechanical strain sensitivity is about the same for silicon gauges with  $G \approx 50$  as it is for metallic gauges with  $G \approx 2$ , so that semi-conductor gauges have clear advantages where signal levels are marginal, or when it is necessary to keep the strains in the force-linkages to a minimum to improve the overall performance of a multi-component force-transducer.

Because of its mono-crystalline nature, silicon, which has largely superseded germanium on account of its greater stability, is virtually free of hysteresis and creep, though creep may arise from stresses in the bonding material. The fatigue life of silicon gauges is somewhat better than that of metal wire gauges, but not so good as that of metal foil. Repeated strain may also change the sensitivity to some extent and produce a zero drift. Rohrbach & Czaika (1961, R.A.E. translation) found that  $10^6$  cycles of  $\pm 2 \times 10^{-3}$  strain produced a change in the gauge factor of less than 2% and a zero change of order  $10^{-5}$  strain in a silicon gauge bonded with Baldwin EPY-150 cement. Changes of this magnitude can be handled by periodic calibration.

Strain-gauges are available commercially in a variety of shapes and sizes, and in most cases the balance designer will find some of these suitable for his purpose. Moreover the manufacturers' literature is generally helpful as regards such topics as cementing the gauges in position, and in the use of electrical circuit arrangements to minimise non-linearities and compensate temperature changes. Modern manufacturing processes involving surface diffusion techniques enable single crystals to be produced, only parts of which are effectively piezoresistive (Pfann & Thurston, 1961). This has already led to the commercial production of "integrated" pressure transducers, in which a silicon diaphragm has diffused impurities which enables its deflection to be sensed. Although unsupported semi-conductors, acting as complete load cells in the sense that they react the total load as well as detect it, are difficult to envisage because of their relative brittleness, very small integrated accelerometers would appear feasible. We shall therefore digress slightly at this point to consider piezoresistivity from the phenomenological

viewpoint in a manner analogous to that of section 3.211 in which we considered piezoelectricity. To some extent the discussion which follows is an oversimplification, because we assume a linear relation between the change in resistivity and the stress (or strain) producing it. The characteristics of semi-conductor strain gauges are in fact non-linear, but this does not affect the general features of such devices, to which we now turn.

### 3.221 Some theoretical aspects

For a general, non-isotropic electrical conductor, the equation linking the potential gradient  $E$  and the current density  $i$  is written in the form of a generalised Ohm's law

$$E_i = \rho_{ij} i_j \quad i, j = 1, 2, 3 \quad (3.24)$$

the Cartesian summation convention being implied, and the suffices referring to orthogonal crystal axes. Only when  $\rho_{ij} = 0$  for  $i \neq j$  and  $\rho_{11} = \rho_{22} = \rho_{33} = \rho_0$  is there isotropic conduction. Such is the case for polycrystalline metals and crystals having a cubic structure in the unstressed state. The resistivity coefficients  $\rho_{ij}$  are dependent upon both temperature and stress, probably for all materials, but particularly for semiconductors. We are concerned here primarily with the stress dependence, which we assume to be linear. Following Geyling & Forst (1960) we write

$$E_i = (\rho_{ij} + \pi_{ijk\ell} \sigma_{k\ell}) i_j \quad (3.25)$$

$$i, j, k, \ell = 1, 2, 3$$

where  $\sigma_{k\ell}$  are the components of the stress tensor and  $\pi_{ijk\ell}$  are those of a fourth rank tensor known as the piezoresistive tensor. As with the piezoelectric properties a number of symmetries exist, and certain of the piezoresistive coefficients vanish when referred to crystal axes. For materials which are isotropic conductors in the unstressed state, further simplifications are possible, and taking advantage of the "reduced tensor" notation of Voigt (c.f. Mason, 1947) yet again, we can define a new set of coefficients  $\pi_{st}$  by

$$\rho_0 \pi_{11} = \pi_{1111} ; \rho_0 \pi_{12} = \pi_{1122} ; \rho_0 \pi_{44} = 2\pi_{2323} \quad (3.26)$$

etc., both  $s$  and  $t$  taking the values 1 to 6. The factor 2 in the shear stress coefficients arises because each term appears twice in the formal relation (3.25). Written in full, and taking advantage of the symmetry, equations (3.25) take the simple form

$$\frac{E_1}{\rho_0} = i_1 \{1 + \pi_{11}\sigma_1 + \pi_{12}(\sigma_2 + \sigma_3)\} + i_2 \pi_{44}\sigma_6 + i_3 \pi_{44}\sigma_5 \quad (3.27)$$

$$\frac{E_2}{\rho_0} = i_1 \pi_{44}\sigma_6 + i_2 \{1 + \pi_{11}\sigma_2 + \pi_{12}(\sigma_1 + \sigma_3)\} + i_3 \pi_{44}\sigma_4 \quad (3.28)$$

$$\frac{E_3}{\rho_0} = i_1 \pi_{44}\sigma_5 + i_2 \pi_{44}\sigma_4 + i_3 \{1 + \pi_{11}\sigma_3 + \pi_{12}(\sigma_1 + \sigma_2)\} \quad (3.29)$$

where  $\sigma_1 = \sigma_{11}$ ,  $\sigma_2 = \sigma_{22}$  and  $\sigma_3 = \sigma_{33}$  are the direct stresses and  $\sigma_4 = \sigma_{23}$ ,  $\sigma_5 = \sigma_{13}$  and  $\sigma_6 = \sigma_{12}$  are the shear stresses.

The terms  $(\pi_{11}\sigma_1 i_1)$ ,  $(\pi_{11}\sigma_2 i_2)$  and  $(\pi_{11}\sigma_3 i_3)$  are those which arise ordinarily with metal strain gauges, where the potential field gradient, current flow and stress are codirectional. The remaining terms represent the cross-coupling arising from the more complicated behaviour of a stressed crystal lattice.

In conventional applications a slender cylinder is subjected to a load along its axis, the potential gradient also being applied between the ends. This uniaxial system, with  $E'_1$ ,  $i'_1$  and  $\sigma'_1$  directed along axis  $O_1'$ , is not necessarily such that  $O_1'$  is a crystal axis. In fact the piezoresistive effect can be maximised by suitable orientation of  $O_1'$  in relation to the axes of the crystal  $O123$ , that is by suitably cutting the filaments from the crystalline blank. Writing

$$E'_1 = \rho_0 i'_1 \{1 + \pi'_x \sigma'_1\} \quad (3.30)$$

to define the "longitudinal piezoresistance coefficient"  $\pi'_x$  it can be shown that (Mason & Thurston, 1957)

$$\pi_{\ell} = \pi_{11'} = \pi_{11} + 2\{\pi_{44} + \pi_{12} - \pi_{11}\}\{\ell_{11}^2, \ell_{21}^2, + \ell_{21}^2, \ell_{31}^2, + \ell_{31}^2, \ell_{11}^2, \}$$
 (3.31)

where  $\ell_{ij}$  represent the direction cosines between axes  $O_i$  and  $O_i'$ . Clearly the magnitude of  $\pi_{\ell}$  depends upon the relative orientation of the axes. Mason & Thurston (1957) show further that  $\pi_{\ell}$  has an extremum along lines specified by

$$\ell_{11'} = \ell_{21'} = \ell_{31'} = \pm \sqrt{\frac{1}{3}}$$
 (3.32)

the [111]-axes\*, provided either

$$\pi_{11} \text{ and } \{\pi_{44} + \pi_{12} - \pi_{11}\} \text{ have the same sign,}$$
 (3.33)

$$\text{or, } 2|\pi_{44} + \pi_{12} - \pi_{11}| > 3\pi_{11}$$

Otherwise the extremum value occurs along a crystal axis, that is [100]-axes.

The magnitudes of the coefficients  $\pi_{11}$ ,  $\pi_{12}$  and  $\pi_{44}$  depend upon the base material, the impurity and the impurity level, the latter being particularly important for semi-conductors. Some typical values are listed in Table 3.3 for doped germanium and silicon. It may be noted that n-type silicon does not satisfy the inequalities (3.33) so that the gauge factor  $G_1'$  has its largest value, which is negative, along [100] crystal axes. The well-known expression for the gauge factor  $G$  is

$$G = \frac{\delta R/R}{S_1'} = 1 + 2\nu_1' + \frac{\delta \rho}{\rho_0 S_1'} = 1 + 2\nu_1' + G_1'$$
 (3.34)

where  $S_1'$  is the mechanical strain along  $O_1'$ ,  $\nu_1'$  is Poisson's ratio and  $\delta R/R$  is the fractional change in gauge resistance. For semi-conductors the term  $G_1'$  is clearly dominant, since comparison of equations (3.30) and (3.34) shows that

$$G_1' = \frac{\delta \rho}{\rho_0 S_1'} = \pi_{\ell} \frac{\sigma_1'}{S_1'} = \pi_{\ell} Y_1' = m_{\ell}$$
 (3.35)

where  $Y_1'$  represents Young's modulus appropriate to this uniaxial stress system\*\*. Values of  $m_{\ell} = G_1'$  are included in Table 3.3.

So far we have only considered the longitudinal effect, in which  $\sigma_1'$ ,  $E_1'$  and  $i_1'$  are co-linear. Both the transverse and the shear effects can also be utilised, and several possible devices have been described by Pfann & Thurston (1961). For cubic crystals such as germanium and silicon, the piezo-resistive coefficients referred to crystallographic axes can be written as a 6 x 6 matrix, many elements of which are zero, and only three are numerically distinct:

\* These are the "Miller indices" used to define planes and directions within a crystal lattice, see for example, Moffatt, Pearsall & Wulff, (1964).

\*\* Since the gauges are used as strain rather than stress tensors, it is perhaps more logical to define an "elastoresistivity" tensor  $[m]$  in place of  $[\pi]$ . The two are of course related, through the stiffness tensor  $[c]$ , by the doubly-contracted tensor product  $[m] = [\pi] : [c]$ . Again many of the coefficients  $m_{ijkl}$  are zero and only three independent quantities exist for cubic and polycrystalline structures so that the analogous equations to (3.27-29) take the form

$$\frac{E_1}{\rho_0} = i_1 \{1 + m_{11} S_1 + m_{12} (S_2 + S_3)\} + i_2 m_{44} S_6 + i_3 m_{44} S_5 \quad \text{etc.}$$

$$\text{with } m_{11} = m_{22} = m_{33} = \pi_{11} c_{11} + 2\pi_{12} c_{12},$$

$$m_{12} = m_{21} = m_{13} = m_{31} = m_{23} = m_{32} = \pi_{11} c_{12} + \pi_{12} (c_{11} + c_{12})$$

$$m_{44} = m_{55} = m_{66} = \pi_{44} c_{44}$$

The longitudinal elastoresistance coefficient  $m_{\ell}$  is found in a manner analogous to  $\pi_{\ell}$ .

$$[\pi] = \begin{bmatrix} \pi_{11} & \pi_{12} & \pi_{12} & 0 & 0 & 0 \\ \pi_{12} & \pi_{11} & \pi_{12} & 0 & 0 & 0 \\ \pi_{12} & \pi_{12} & \pi_{11} & 0 & 0 & 0 \\ 0 & 0 & 0 & \pi_{44} & 0 & 0 \\ 0 & 0 & 0 & 0 & \pi_{44} & 0 \\ 0 & 0 & 0 & 0 & 0 & \pi_{44} \end{bmatrix} \quad (3.36).$$

However when referred to arbitrary axes, all 36 may be non-zero and any one can be made quite large for highly anisotropic materials like doped Ge and Si by a suitable choice of axis system. The matrix now has a typical element  $\pi_{s't'}$ , ( $s', t' = 1', 2', \dots 6'$ ). The transverse piezoresistance coefficients are those which give the relative change in resistivity resulting from a simple direct stress which is normal to the current density vector, namely  $\pi_{1'2'} = \pi_{2'1'}$ ;  $\pi_{2'3'} = \pi_{3'2'}$ , and  $\pi_{1'3'} = \pi_{3'1'}$ . These coefficients are related to those of equation (3.36) by equations of the form

$$\pi_{1'2'} = \pi_{2'1'} = \pi_{12} + (\pi_{11} - \pi_{12} - \pi_{44})\{\ell_{11}^2, \ell_{21}^2, + \ell_{12}^2, \ell_{22}^2, + \ell_{13}^2, \ell_{23}^2\} \quad (3.37)$$

where  $\ell_{ij}$ , again represents the direction cosine between  $O_i$  and  $O_i'$ . Two types of shear coefficient may be distinguished. In one the electric field and current are in the same direction, in the other they are normal to each other. Thus, suppose the electric field and current are along  $O_1'$ . A shear stress  $\sigma_6'$  then produces a resistance change when the coefficient  $\pi_{1'6'}$ , is non-zero. The same shear stress  $\sigma_6'$  may also alter the ratio of  $E_1'$  to the current density  $i_2'$  along  $O_2'$  via the coefficient  $\pi_{6'6'}$ . Shear effects of the first kind, in which the electric field and current are co-linear, will have the first subscript (on  $\pi$ )  $1', 2'$  or  $3'$ ; effects of the second kind are described by piezoresistive coefficients having both subscripts greater than  $3'$ . For a general orientation

$$\pi_{1'6'} = 2\pi_{6'1'} = 2(\pi_{11} - \pi_{12} - \pi_{44})\{\ell_{11}^3, \ell_{21}^3, + \ell_{12}^3, \ell_{22}^3, + \ell_{13}^3, \ell_{23}^3\} \quad (3.38)$$

and

$$\pi_{6'6'} = \pi_{44} + 2(\pi_{11} - \pi_{12} - \pi_{44})\{\ell_{11}^2, \ell_{21}^2, + \ell_{12}^2, \ell_{22}^2, + \ell_{13}^2, \ell_{23}^2\} \quad (3.39)$$

with analogous relations for the other coefficients (Pfann & Thurston, 1961). Either one may choose orientations to produce a maximum effect, or one might choose to use an element in such a way that secondary effects are minimised. For example the quantity in curly brackets which appears in equations (3.37) and (3.39) varies between 0 and  $\frac{1}{2}$ . Thus  $\pi_{1'2'}$ , or its analogues can be made to vanish if

$$0 \leq -\pi_{12}/(\pi_{11} - \pi_{12} - \pi_{44}) \leq \frac{1}{2} \quad (3.40).$$

Using the values quoted in Table 3.3 we see that this is possible for p-Ge, n-Ge and n-Si but not for p-Si. Gauges of the first three materials may therefore be designed with zero sensitivity to transverse direct stress, although the longitudinal sensitivity will be less than the maximum possible for the material. Pfann & Thurston (1961) describe a number of possible arrangements containing multiple gauges already connected to form two (active) arms or even all four (active) arms of a Wheatstone bridge. Among the advantages claimed for the latter are enhanced sensitivity; automatic compensation for thermal effects, whether produced by changes in gauge resistance with temperature or by differential expansion between the gauge and backing material, and simplicity since no external bridge resistors are needed. Moreover, hydrostatic pressure and contraction of the bonding material affect all arms of the bridge equally and so do not alter its balance.

The examples are too numerous to be described here in detail, but especially noteworthy are the suggestions for torque transducers and for a cantilever of high resistivity material the upper and lower surfaces of which have diffused impurities to increase the conductivity where the strain due to bending is greatest. Such beam elements are commercially available and might well be used, as Pfann & Thurston (1961) suggest, as the heart of an accelerometer. Most of their suggestions do not seem to have been adopted yet by the manufacturers of strain gauges. This is particularly unfortunate in the case of the complete bridge consisting of two p-type and two n-type gauges in a square formation.

### 3.222 Low frequency characteristics

Piezoresistance devices respond to static loading and so the question of their low frequency behaviour does not really arise. In this respect they have a considerable advantage over piezoelectric devices. Static calibration of piezoresistive transducers can be readily carried out, but it may be necessary when doing so to take account of a number of factors, such as zero drift and thermal sensitivity which need not affect their performance as dynamic devices.

### 3.223 High frequency characteristics

The application of resistance strain gauges to the measurement of forces and accelerations in impulse tunnels necessarily involves a discussion of their response to transients. We have noted already in connection with piezoelectric sensors that the natural frequencies of the transducers are likely to be somewhat higher than those of other elements of the system, though on occasion they may also assume importance. However the question arises here in a different connection, in that one might well enquire as to the relevance of a static calibration to the response of a transducer to a transient input. Put in another way, we may ask how the gauge factor  $G$  is affected by the strain-rate.

Experimental investigations on metallic strain gauges have been conducted by Cunningham & Goldsmith (1959), Nisbett, Brennan & Tarpley (1960) and by Koshiro Oi (1965).

Cunningham and Goldsmith examined the response of strain gauges mounted on both steel and aluminium bars when these were subjected to the impact of a steel ball. They concluded that the response time  $\tau_r$  was less than  $7 \mu\text{s}$  for the steel-mounted gauge and less than  $10 \mu\text{s}$  for that mounted on the aluminium bar. By measuring also the impulsive force using a piezoelectric device they concluded that the gauge factor remained constant for  $\tau_r > 7 \mu\text{s}$ .

Nisbett and his colleagues vibrated a steel bar in the longitudinal mode, and using an independent optical method for measuring the strain, concluded that the strain gauges mounted on the bar had the same gauge factor up to a frequency of 23 kHz.

Koshiro Oi subjected bars to step-like strain pulses by loading them slowly in tension until brittle fracture occurred at a notch. The strain pulse was detected by two pairs of strain gauges along the bar. Because the gauges are of finite length  $L$ , the idealised response to the step would be a ramp of duration  $L/v$  where  $v$  is the speed of sound along the bar, figure 3.6(b). In practice the response would be somewhat as shown in figure 3.6(c). When the overshoot is small it is more practical to specify the rise-time (actually, the strain falls in this case)  $\tau_r$  as that between the 10% and 90% amplitude levels. For the idealised response this would give  $\tau_r = 0.8 L/v$ .

Koshiro Oi's measured rise times for wire gauges of length  $L = 3 \text{ mm}$  and foil gauges of length  $L = 1 \text{ mm}$  mounted on steel were somewhat longer than is indicated by this relation, being about  $1.6 \mu\text{s}$  and  $1.0 \mu\text{s}$  respectively. This was explained as due to the finite time of crack propagation leading to a somewhat "rounded-step" strain pulse. However he concluded that for bonded metal strain-gauges

$$\tau_r < 0.5 \mu\text{s} + 0.8 L/v.$$

From static and dynamic measurements of the gauge factor he found differences of the same order, 3-5%, as that between gauges from the same batch.

Using the relation  $\tau_r f_c = 0.35$  to define the frequency  $f_c$  at which the ratio of output/input is  $1/\sqrt{2}$ , we find for gauges mounted on steel ( $v = 5.1 \text{ mm}/\mu\text{s}$ )

L/mm	1	3	10
$f_c/\text{kHz}$	530	360	170

Of course the gauges cannot be used at this frequency without large corrections; for the gauge factor to be within 1% of the static value, the frequency must be limited to about  $f_c/6$ . It is probable that a frequency of 30 kHz will be higher than other resonances in the measuring system as a whole, so that in practice the usable frequency range will be cut-off below this.

Thus for force measurements in impulse tunnels the response time of bonded strain gauges is not likely to be a serious limitation on the frequency response of the measuring system as a whole.

Although no measurements relating to bonded semi-conductor gauges are known to the writer, the discussion above is expected to apply to these also, since the inherent response time is extremely rapid.

For unbonded gauges in which the sensitive regions are simply areas of diffused impurity on the surface of a crystal, the response times may be calculated in a similar way to those of piezoelectric elements, (section 3.213).

### 3.224 Practical aspects of using piezoresistive strain gauges

The essential difference between piezoelectrical and piezoresistive devices resides in the fact that the former are active and the latter passive in the sense that piezoresistive devices require an independent supply of energy. To this extent the associated electrical circuitry is more complicated for resistance strain gauges, but they do have the great advantage that they can be calibrated statically. Signal levels are lower than with piezoelectric sensors, which is occasionally a serious problem even for dynamic measurements, but their low impedance is an advantage when it comes to amplification. The main difficulty in utilising them lies in providing a suitable load bearing link upon which they can be mounted, because they are not generally suitable for reacting the total load as piezoelectric devices are.

Since bonded metal strain gauges first became available more than thirty years ago a voluminous literature has appeared, which reflects the collective experience concerning their application. In addition the manufacturers issue pamphlets containing sound advice on how to obtain the best results from strain gauges. It is not our purpose to summarise this literature here - indeed it is often attention to detail that ensures good results, and such detail is inevitably omitted from a summary. Rather do we draw attention to some of the more important points which arise in the present application, and recommend both the designer and the user to the early monographs of Perry & Lissner (1955) and of Murray & Stein (1958), the collection of articles edited by Dean (1962), the work of Dorsey (1964), the review by Higson (1964) and Neubert's (1967) fairly recent monograph.

#### 3.2241 Environmental problems

The electrical energy supplied to the strain gauges is of course dissipated as heat. In operation the circuits are usually switched on some time before a test and the system is allowed time to reach equilibrium. Calibration is ordinarily carried out under atmospheric conditions whereas in operation an impulse tunnel is evacuated, so that the temperatures in the two cases may be different. Where the gauge factors are strongly temperature dependent it will be necessary to take account of this. The vacuum environment may also affect the cement used to attach the gauges to the load link. Organic cements are potentially subject to evaporation, sublimation or even decomposition at low pressures and should be avoided. The evidence is fairly scanty, but Henny (1965) reports that in tests carried out at ultra high vacuum, epoxy resin based cements are generally satisfactory, though some care is necessary in mounting the gauges, so that air bubbles are not included. Such inclusions may well expand as the pressure in the tunnel is reduced and the effective calibration may be altered. Careful attention to detail will probably obviate most of these problems.

#### 3.2242 Temperature compensation

Although it is common to dismiss thermal effects as comparatively unimportant in dynamic measurements, they can assume serious proportions during calibration. For multi-component balances, where a multitude of interactions have to be investigated, such calibrations can occupy several hours, and if zero drifts also have to be monitored continually, this time can be doubled. Where space is available on a load link, further gauges can be used not only to provide temperature compensation, but also to reduce the effects of non-linearities. Most of the methods devised for use with metal strain gauges can also be used with semi-conductor gauges. Indeed one of the best known is somewhat more readily applied with semi-conductor gauges than with metal gauges. It relies on having a second gauge which undergoes the same temperature changes but is not subject to the same strain. Several variations are possible with metallic gauges. The second gauge may be mounted as a dummy on a block which remains unstressed; it may be so mounted on the specimen as to suffer a much smaller strain, for example close to the main sensor but at right angles

to it; or when the strain field is suitable the two gauges can be subjected to equal and opposite strain. By suitable connections in the bridge circuit, the thermal effects cancel; the strain signal in the last case will be doubled.

The last method is considerably easier to use with semi-conductors since gauges with positive and negative gauge factors are available and the strain field does not have to be of a special type. Matched pairs of gauges made from n-type and p-type material mounted on the same backing, are in some manufacturers' catalogues; usually they are so arranged as to minimise the zero drift arising from the differential thermal expansion between the silicon gauges and a particular force link material such as steel. Two such pairs connected to form a four-arm fully-active Wheatstone bridge could also be suitable, as we shall see in section 3.41, for reducing non-linearities in the system.

To the extent that the gauge factor is a function of temperature, the sensitivity will change with temperature. The elastic moduli of transducer materials such as steel and aluminium alloy also vary a little with temperature, and semi-conductor materials are available commercially, in which the temperature coefficient of the gauge factor is just sufficient to compensate this change, so that the output signal is proportional to stress rather than strain.

### 3.2243 Non-linearities

Non-linearities in the system can arise from three sources, since the strain-gauge transducer, or load-cell, is really a chain of three transducers. Initially the load gives rise to a strain, the strain is converted by the elastoresistive device to a change in resistance, and by means of an electrical energy supply this is converted into a change of voltage. Any or all of these conversion processes may be non-linear; here we are concerned with the second and third.

Metallic strain-gauges are linear over a very wide strain range, but some semi-conductor gauges are markedly non-linear even over fairly small ranges of strain. Mason, Forst and Tornillo (1962) suggest an equation of the form

$$\frac{\delta R}{R_0} = G_1 S + G_2 S^2 + G_3 S^3 \quad (3.41)$$

to describe the behaviour of silicon, the coefficients  $G_1$ ,  $G_2$  and  $G_3$  being inverse functions of temperature as well as dependent upon the doping level. For a typical strain-gauge material Dorsey (1964) has shown that the cubic term contributes only about 1% to the relative resistance change at a strain of  $10^{-2}$ , so that this term is negligible for practical purposes. He finds as fairly typical, that (at 298K)

$$\frac{\delta R}{R_0} = 120 S + 4000 S^2 \quad (3.42)$$

for p-type silicon

and

$$\frac{\delta R}{R_0} = -110 S + 10\,000 S^2 \quad (3.43)$$

for n-type silicon

so that non-linear effects are serious even at fairly low strains, and should be taken into account. It is not possible to eliminate entirely this non-linearity, but the effects can be minimised (i) by careful matching of the gauge pairs in the Wheatstone bridge circuit arrangements which are normally used, (ii) by the use of special circuit arrangements in which the non-linearities are of opposite sense to those of equations (3.42) and (3.43), (iii) by restricting the strains to very low levels, a maximum of  $10^{-4}$  say, and (iv) by using low resistivity gauges which are more nearly linear, but which have lower gauge factors.

The third method, which can of course be used in addition to the first two, has much to recommend it. The signal levels will be correspondingly smaller, thus reducing non-linearities within other parts of the electrical system, and the deflections associated with such small strains are also advantageously small. The high sensitivity of semi-conductor gauges enables one to resolve such small strains accurately and relatively easily.

Strain-gauges of low resistivity materials are also available in which the non-linearity is very small,  $\pm 0.02\%$  or less over a strain range of  $\pm 10^{-3}$ . These gauges are of p-type silicon, and have a gauge factor of order 50 rather than the 100+ or so of the more common types. Such gauges are necessarily of the low resistance type, 60-120  $\Omega$ , and the signal is therefore limited for a given power dissipation,

since the bridge voltage is restricted. However because greater strains are allowable, the balance of advantage for transducer applications probably lies with gauges of this type. We describe some of the circuit arrangements which may be used in section 3.41.

### 3.2244 Choice of strain gauges

For balance applications it is important that interactions between components should be minimised, and this generally means keeping the deflection of each load-link, or force transducer, to a minimum. The implication is that strains should be small, so a high conversion factor from strain to output voltage is required. High sensitivity gauges are therefore an advantage provided other disadvantages are not thereby introduced. In comparison with metal wire and foil gauges, semi-conductor devices are more than an order of magnitude more sensitive, but are more temperature dependent and the relation between resistivity and strain is non-linear for the majority of such gauges. For dynamic measurements temperature effects are not usually serious, but where calibration takes a long time, temperature compensation may be necessary. The restriction to low strain levels also minimises the problems which arise from non-linearities, but where a reduced sensitivity is acceptable highly linear gauges are available some 25 times as sensitive as metallic gauges.

Where space is available for only a single gauge, a p-type gauge of moderate gauge factor should be used, since this type of gauge is less non-linear than a gauge made from n-type material. If it is known in advance that the strain will be predominantly of one sign, advantage can also be taken of the fact that p-type gauges are more nearly linear for positive than negative strains, the reverse being true for n-type gauges. P-type materials on the other hand magnify the effects of temperature changes; the positive gauge factor produces a signal proportional to the differential expansion between the semi-conductor and the load link which has the same sign as that due to the change in resistance with temperature. A negative gauge factor will of course reduce this zero drift, but in the laboratory applications of present concern, the environmental temperature is relatively constant and the maintenance of linearity probably of greater importance.

The choice of a strain gauge is therefore governed by a number of factors and it cannot be made independently of other decisions. As we have implied earlier, it is the performance of the balance as a whole that is important, and it is of little use insisting say, on metallic strain gauges because of their better linearity, if in order to achieve a reasonable signal level the deflections within the load-cells become non-linear functions of the load. Some procedure must be adopted which optimises the overall design. In general it is probably wisest to favour low deflections because interactions as well as non-linearities are thus minimised, so that the more sensitive semi-conductor gauges are preferable to the metallic gauges. Even though the usable linear strain range of some of these gauges is less than half that of metallic gauges, the gauge factor is so much higher that for a given noise level in the system, semi-conductor gauges offer much better resolution.

Thus if one assumes as typical, a resolution of 50  $\mu\text{V}$  (see section 3.42) and a bridge supply of 3.6 V giving 30 mA for a 120  $\Omega$  bridge, the resolution in terms of strain is about  $0.14 \times 10^{-6}$  for a four active-arm bridge (section 3.41) using semi-conductor gauges and about  $7 \times 10^{-6}$  for a bridge using 120  $\Omega$  metallic gauges. With maximum strains limited, very conservatively to say,  $\pm 10^{-4}$  for the former and  $\pm 10^{-3}$  for the latter so as to keep within the linear range, the working range is some 700:1 for semi-conductors and only 140:1 for metallic gauges. In fact semi-conductor gauges linear over the same strain range,  $\pm 10^{-3}$ , are available with a gauge factor of about 50 compared with the 2 for metallic gauges. For the same noise signal, the operating range will be 25 times as large for the silicon gauges, that is 3500:1. One should in fairness point out however that metallic gauges of higher resistance could be used with a correspondingly higher bridge voltage to increase the signal level and hence the working range.

### 3.23 Force transducers

The force transducers or load-cells are of course the vital elements of a balance, and it is largely upon their performance that the accuracy and ease of operation of the system depend. They must satisfy a number of conditions which in many cases conflict with each other so that the overall design must be a compromise.

In the first place they must fit the available space. This particular requirement has led to the wide adoption of the "single-piece" balance, in which each of the force transducers is strictly an integral part of a single piece of metal, which is so machined that the force components are more or less uncoupled from one another. Although any particular force-transducer is materially contiguous with the other parts of the model support, the links are highly compliant in all but one degree of freedom. To this extent we may regard each force transducer separately whether it be part of a single-piece balance or literally a separate element which is incorporated into the system.

The prime purpose of a force-transducer is that it produce some kind of output, usually electrical, for a load input, and ideally this output should be a linear function of only one load component, that along its "axis of sensitivity". In other words the cross-axis sensitivities, or interactions, should be minimal. Hysteresis should be absent and the performance should be repeatable and independent of environmental changes such as variations in temperature, pressure and humidity.

Additionally, ruggedness and ease of construction are great advantages, the latter particularly making it more likely that the characteristics are controllable, so that more than one example having a given nominal performance can be built.

Necessarily some deflections must occur within the system under the action of the aerodynamic loads; indeed it is some of these deflections which are measured by the sensors. These deflections must remain small, since large deflections are not consistent with measurements on the given configuration which is changed when such movements occur. As it happens, small deflections are consistent with low interactions and non-linearities are also minimised by keeping the deflections small. Signal levels however are correspondingly reduced making the sensitivity to other changes more important.

The number of possible transducer configurations is virtually unlimited, and it is in this part of the design that most ingenuity can be exercised. Some particular types have been widely used with considerable success in continuously operating wind-tunnels, and there is no a priori reason why many of these should not be suitable for transient measurements in impulse tunnels. Piezoelectric sensors however do not seem to have been used in steady flows, and because transducers incorporating such devices are rather different in kind from those employing piezoresistive sensors we shall consider the two separately. They do however have some general features in common, the most important of which is the way in which the load is transmitted to the transducer as a whole. As we have noted each transducer should be sensitive to a single load component, and this means decoupling it from the others. This is accomplished in one of two ways: either pivots are provided which are stiff in the load sensing direction only, or each sensor is so positioned that the strain it senses results from a single component of the load only. Essentially the two methods are identical, but in the former positive steps are taken to increase the stiffness presented along the sensing axis to all but one of the load components. These pivots are vital parts of the complete measuring system, but are conveniently considered as parts of the load cells. We shall however defer a discussion of the pivots until section 3.233.

In the discussion which follows we give brief descriptions of some of the force transducers that have proved successful. We also make one or two general suggestions that we hope will be found sufficiently stimulating to make the prospective designer reach for pencil and paper.

### 3.231 Piezoelectric force-transducers

The design of a transducer is governed to a large extent by the output signal level that may be conveniently resolved. We shall see later that so far as piezoelectric transducers are concerned, the charge amplifier has some advantages over the voltage amplifier, and that such amplifiers are readily available with sensitivities up to 100 mV/pC. Assuming a fairly realistic noise level of 100  $\mu$ V - lower values can be achieved by careful design and selected components - an output signal of 0.1 pC may be resolved to within 1%. It is this value of 0.1 pC then that largely decides the transducer configuration and the force sensor material. Smaller signals can of course be handled, but probably only with lower resolution on a routine basis.

The materials most suitable for use as piezoelectric sensors are quartz and the ceramics. Quartz, despite its relatively low sensitivity, is in many ways preeminent. Its charge sensitivity to force, expressed by the piezoelectric coefficients ( $d_{im}$ ), is constant over a very large stress range - of order

$10^6$ . The dependence on temperature is small;  $d_{11}$  varies by between  $-0.05\%/K$  and  $0.02\%/K$  over the temperature range  $-200^\circ C$  to  $200^\circ C$ . Its single crystalline form means that hysteresis is negligible and its characteristics are readily repeatable from one specimen to another, the crystals being grown artificially under carefully controlled conditions. It may be used at temperatures up to  $500^\circ C$  and at stress levels up to about  $4 \times 10^9 \text{ N/m}^2$  (Spescha & Volle, 1971). It is very stiff, having elastic moduli of order  $10^{11} \text{ N/m}^2$  and so deflections are negligible. The insulation resistance is of order  $10^{14} \text{ ohm}$  for a typically-sized element, so that long time constants - in excess of  $10^3 \text{ s}$  in practice - make static calibration of quartz transducers possible. Apart from its low sensitivity the main limitations arise from the need to utilise particular cuts from a single crystal. Even so some ingenious transducers have been produced which circumvent this restriction. The sensitive modes of quartz are the parallel and transverse direct stress modes, expressed respectively by the coefficients  $d_{11}$  and  $d_{12}$ , and the shear modes corresponding to the coefficients  $d_{14} = -d_{25}$  and  $d_{26}$ . As may be seen from Tables 3.1,  $d_{12} = -d_{11}$  and  $d_{26} = -2d_{11}$  (see Spescha, 1971 for a simple theoretical explanation of this) which is numerically some six times greater than  $d_{14}$ , so that the Y-cut crystal, plated on the faces normal to a Y-axis, is suitable as a sensor to the thickness shear stress  $\sigma_6$ .

The sensitivity to a direct stress may, as we have noted, be enhanced by stacking several discs electrically-connected in parallel. Although preloading is necessary to ensure a response to tensile forces, there is a tendency for such stacks to come apart under such loads, and this can result in non-uniform loading and a lack of repeatability which in a dynamic situation may appear to be hysteresis. The transverse mode has definite advantages so far as quartz is concerned. The charge sensitivity to force  $Q_F$  of a stack of  $N$  X-cut discs is simply

$$Q_F = Nd_{11} \quad (3.44)$$

On the other hand, a rectangular bar used in the transverse mode as shown in figure 3.4(b) has a force sensitivity

$$Q_F = d_{12}(b/a) = -d_{11}(b/a) \quad (3.45)$$

so that the force sensitivities of the bar and the stack may be made comparable. The natural frequency of the bar and the stack will be much the same if  $b = Nt$ , and the problem of elements coming apart does not arise. Kistler Instruments AG have successfully used the transverse effect in pressure transducers (Spescha & Volle, 1971) but they do not appear to use it in load cells.

Kistler do market a range of load cells and three-component force-platforms, some of which might be incorporated directly into an aerodynamic force-balance, though many are either too large or of unsuitable shape. These load cells are based either on quartz rings as shown in figure 3.7 or on discs connected mechanically and electrically in parallel as illustrated in figure 3.8. Two Kistler type 901A load washers, the smallest in their current range, with an axial load capacity of 15 kN have been used together with the somewhat larger type 903A in a three-component balance at Douglas Aerophysics Laboratory (Griffiths\*). Although this larger load cell has a capacity of 60 kN, its resolution, 0.01 N and its sensitivity, 4 pC/N are claimed to be the same as those of the smaller 901A, which is 8 mm thick and 14 mm in diameter, excluding the microdot coaxial connector. Some care needs to be exercised in applying the load and a series of special adaptor washers is available. According to equation (3.13) the charge sensitivity to force does not depend on the dimensions of the sensing element in this parallel mode, and it is moreover independent of the point of application of the load. However so as not to exceed the maximum working stress level anywhere in the crystal, the quartz is sandwiched between accurately ground steel plates, and it is probably wise, for the same reason, to apply the load fairly uniformly. The central hole enables the cell to be precompressed during installation using a simple bolt; tensile forces can then be measured.

Kistler also market a transducer, type 9251, which resolves a general force input into three perpendicular components. It is small, 10 mm thick by 24 mm square (excluding the three microdot connectors) and uses three pairs of quartz rings, one pair in the parallel mode and two pairs in the shear mode, as shown in figure 3.9. (The use of pairs in a symmetrical arrangement is a good general principle since second order effects are thereby cancelled.) A more useful load-resolving platform for wind-tunnel

\* private communication

applications would perhaps replace the compressive rings by an "in-plane" torque sensor, though the small size makes the multiple disc arrangement of figure 3.8 somewhat difficult. A "sectored" array, figure 3.10, might be easier to construct, and has in fact been used with a piezoelectric ceramic (Duryea & Martin, 1966).

The crystal axes of a quartz specimen may be accurately determined with the aid of an X-ray goniometer - a task performed by the manufacturer of the cut quartz elements. Accurately-cut quartz shear elements are not sensitive to loads in any other direction, so that additional mechanical decoupling of such loads is not necessary. However in order to transfer the shear load to the quartz, one must use either a cemented construction, or rely on friction, in which case preloading is necessary. Spescha (1971) suggests a friction coefficient of 0.15, so that the quartz must be precompressed by a load nearly seven times the design load capacity of the transducer. Such preloading is easily applied if the transducer has a central bolt-hole, as in the Kistler designs. If however the general external load on the measuring system involves a tensile force in the preloading bolt as well as the shear component to be measured, the maximum load measuring capacity will be reduced even though the sensitivity to shear load remains unaltered. This point needs to be borne in mind during design, and where troubles are envisaged, mechanical decoupling in the form of pivots can be provided.

Thermal problems are not usually serious in dynamic situations. Provided the sensors are well insulated from the hot-flow environment of the hypersonic impulse tunnel, no difficulties should arise in most test situations. Quartz is not pyroelectric and the piezoelectric coefficients are insensitive to temperature. However in any multiply-connected structure, stresses can arise as a result of differential thermal expansion of the parts, and such stresses will appear as a charge output indistinguishable from that due to a true external load. Such charges can be eliminated by "grounding" the output terminal of the transducer immediately prior to a test. This procedure should be standard in wind-tunnel tests involving piezoelectric devices, and could also be used during calibration, incremental values being always measured. Although such a method is perfectly sound, and indeed has much to recommend it since a force change of one newton in the presence of a load of one meganewton can be measured by this technique, it is probably wise to design transducers with some compensation for differential thermal expansion. Such compensation is easily provided by interposing washers between the quartz and the loading platens, of a material having a suitable thermal expansion coefficient; in this way the maximum load capability of the transducer can be more directly related to the maximum stress level in the quartz.

The piezoelectric ceramics are considerably more sensitive than quartz, and have the particular advantage that they may be machined, or otherwise formed, to any desired shape. Machining is probably best carried out before polarisation, but this is not always convenient, and with care it can be done afterwards. Tool forces should be kept low since high stress levels lead to partial or even total depolarisation. Where the effects of machining are localised within the ceramic element, the performance of the transducer is likely to be very sensitive to minor constructional variations. A lack of repeatability between nominally identical transducers will then arise even though the sensors are cut from the same piece of bulk material. On the whole piezoelectric ceramics are more temperature sensitive than quartz. The effects arise in two ways - the ceramics are usually pyroelectric, and the piezoelectric coefficients are functions of temperature. Some data for two lead zirconate titanate ceramics, Glennite G-1278 and G-1500\*, and a lead metaniobate ceramic Glennite G-2000\* are reproduced in figure 3.3. The most promising of these materials appears to be G-2000 [only data for the transverse coefficient  $d_{31}$  are given by the manufacturer, but the behaviour of the other coefficients,  $d_{33}$  and  $d_{15}$  is presumably similar]. Although the magnitudes of the piezoelectric coefficients of G-2000 are somewhat lower than those of the others, its Curie temperature is higher, and this may be an advantage where an interference fit is used in assembling the transducer, as is suggested later. New materials are however constantly being introduced, and reference should be made to current catalogues before a material is finally selected.

The piezoelectric coefficients of ceramics are not entirely independent of stress-level; that is the ceramics are non-linear as force-transducers. Over a moderate range of stress however, the coefficients are sensibly constant, and transducers should be designed with this limitation in mind. To increase the load capacity, the size of the sensing element should be increased to keep the stress within the linear

\* Trade-names for products manufactured by Gulton Indust. Inc., U.S.

range. Information on the extent of this linear range is not usually given in manufacturers' catalogues and may not always be known, which makes the designer's task difficult. Martin, Duryea & Stevenson (1962) in describing their force balance mention the range  $(-10 \pm 2) \text{ MN/m}^2$  for the preloaded PZT discs they employed, but they give no source for this information.

Ceramic discs, rings, plates and sectors of discs can be used in much the same way as quartz, the appropriate coefficients being  $d_{33}$  and  $d_{31}$  for direct stresses, which produce an electric field parallel to the axis of polarisation, and  $d_{15}$  for the shear stress  $\sigma_5$  which produces an electric field  $E_1$ . For ceramic  $|d_{31}|$  is somewhat smaller than  $|d_{33}|$ , so that the transverse mode is not quite so useful. However other shapes are also possible. As with quartz, the shear mode is most attractive, since mechanical decoupling is unnecessary. A thin-walled tube, polarised axially and plated subsequently on the cylindrical surfaces which form the electrodes, see figure 3.4(c), has some constructional advantages because of the axial symmetry, but if it has to rely on cemented joints to transfer the load it may not be possible to make full use of this configuration (Goodchild & Bernstein, 1972). The possibilities of using interference fits should be investigated, but the assembly temperatures must be limited to values well below the Curie temperature, since polarisation cannot be carried out afterwards in this case. Electrical isolation of one part of the system from the others may also be troublesome with this configuration but it should be possible to apply a thin insulating layer of epoxy resin say, over both plated surfaces before assembly. This would have two advantages. The electrical lead wire, welded or soldered to the plated surfaces, could be embedded in the resin, and the surfaces could be machined to closer tolerances than the  $\pm 0.125 \text{ mm}$  typically specified by the manufacturers of the ceramic tubes. A more uniform interference fit could then be obtained, but of course no compensation for differential thermal expansion can be provided, though this is not serious. But for the preloading due to the interference fits, one has virtually reproduced the cemented joint construction, the epoxy being the cement; it should be possible however to remove any surplus prior to assembly in this case.

Because of their theoretically zero cross-axis sensitivity, shear elements can be built directly into a multi-component force-balance without further decoupling, and such a balance - the K-balance - has been constructed at Cornell Aeronautical Laboratory - see section 3.31. To make full use of the inherent decoupling of shear mode transducers, alignments are fairly critical, particularly during the manufacture of the sensors. The silver electrodes must be deposited on faces normal to the 01-axis after polarisation along the 03-direction. Duryea & Martin (1966), describing the experience at Cornell, suggest that some care is required in ensuring a uniform polarising field, strictly parallel to the faces to be silvered, and they lap the surfaces of their PZT ceramic elements to ensure parallelism within  $0.013 \text{ mm}$ . Electrodes are formed by vacuum deposition on the lapped surfaces; a smooth electrode is thus obtained. This method was deliberately chosen because it avoided heating the ceramic. Even so they found a much lower sensitivity than expected which they could only ascribe to partial depolarisation resulting from radiant heating of the ceramic by the boat containing the silver in the vacuum deposition plant. They devised a radiation shield for subsequent cases, but give no clue as to its success.

Compressive elements using either the direct or the transverse mode, require mechanical decoupling of some kind since direct stresses both parallel and normal to the axis of polarisation produce an electric field  $E_3$ . It should be possible to accomplish this decoupling simply by ensuring that the element is unrestrained in directions perpendicular to 03, and this principle is behind the design of the Cornell Aeronautical Laboratory's K-balance. In their other balances (Martin, Duryea & Stevenson, 1962) and in a similar balance at the Technischen Hochschule, Aachen (Schaguhn, 1970) several "conventional" force-links with decoupling pivots have been used to make a six-component balance. These force-links are basically ceramic discs - or rather, rings - clamped, and thus pre-loaded, between pressure plates as illustrated in figure 3.11. These pressure plates are slotted in such a way that only axial loads are transmitted efficiently. The ceramic sensing element of a typical load cell in the Cornell Aeronautical Laboratory balances, is a PZT disc of diameter  $15 \text{ mm}$  and thickness  $2.5 \text{ mm}$ , having a central hole to accommodate the preloading screw. The ceramic is prestressed to about  $-10 \text{ MN/m}^2$ , the preloading screw being locked in position by a transverse set screw, and the linear working range is given as  $\pm 2 \text{ MN/m}^2$ , equivalent to a load of about  $\pm 350 \text{ N}$ . Electrical leads are soldered to the edges of metal plates adjacent to the silvered faces of the disc and mylar (melinex) spacers are used to insulate the element from the plattens, and thereby from the remainder of the system. Further spacers are used to make up the overall length of

the capsule to that required for the assembled balance. A number of similar capsules, the size varying with load capacity requirements to keep the stress within the linear range, are used to make up the complete balance (see section 3.3). In their later paper, Duryea & Martin (1966) report that some unexplained interactions in the Cornell Aeronautical Laboratory's balances using these force capsules were alleviated by removing the silver plating from the ceramic, lapping the surfaces and resilvering by vacuum deposition so as to obtain smooth electrode surfaces. By implication they recommend this procedure in general circumstances, and employed it, as we have noted, in the construction of their K-balance.

The bimorph bending-modes have been used successfully in high-sensitivity pressure transducers (Macdonald & Cole, 1963; Goodchild & Bernstein, 1972) but not, so far as the writer is aware, as part of a force-link. They offer very high sensitivity, albeit at reduced natural frequency, but (more important) at the expense of increased deflections. Moreover their capacity for withstanding overload is not so good as that of the other modes, so that stops would probably be necessary to limit the deflection. Nevertheless in very low density flows where the high sensitivity required makes all other modes unsuitable it may be possible to make use of one of the bimorph configurations. One schematic arrangement using a bimorph disc is illustrated in figure 3.12(a). The disc is supported on a post which passes through a central hole and is clamped on both sides, so that loads can be transmitted in both directions. The edge fixing must approximate the pinned condition, and to achieve this the central electrode extends beyond the ceramic, forming a kind of diaphragm. Although the centre post must not make electrical contact with this central electrode so that the transducer terminals are the upper and lower attachment points, this is not convenient, because the load cell would need to be electrically isolated from the balance structure. Separate wire connections should be used together with insulation in the most convenient places, such as under the nuts on the centre post. Clearly a number of practical constructional difficulties need to be overcome but the promise of sensitivities of order  $10^4$  pC/N means that such devices merit serious consideration.

More easily assembled arrangements using a bimorph beam can also be envisaged, but do not possess the advantages of axial symmetry. Such beam elements can be used as the basis of a sensitive accelerometer and we shall illustrate this application in section 3.24. Again in very low level force situations one may conceive a balance in which the connection between the model and the support is via a system of cantilever beams which are themselves piezoelectric bimorphs. Such an arrangement for a three component system is illustrated schematically in figure 3.12(b). The success of such an arrangement would depend to some extent on whether it were sufficiently robust to handle as well as on any of its more obviously necessary requirements. It would also be relatively difficult to seal a balance of this kind, in order that its performance remain unaffected by environmental changes. Humidity and dust in particular can have serious effects on the low frequency performance of transducers having a high impedance.

Piezoelectric materials are dielectrics of very high specific resistivity. Any charge separation which appears as a result of mechanical strain will leak away at a rate which depends upon the effective time constant of the transducer in combination with the associated electronic circuit. The time constant can be made relatively independent of the capacitance of the transducer and its connecting cable by using a "charge amplifier". It may be further controlled, within limits, by components within the amplifier feedback network, so long as the resistive impedance of the transducer is very high. The specific resistivity of quartz and of the ceramics is large at room temperature, though it falls very rapidly with rising temperature, see Table 3.1(b) and figure 3.3. To maintain the insulation resistance of a transducer at correspondingly high levels requires careful design and special precautions during assembly. The design should be such that the sensing element is hermetically sealed, since surface moisture will lower the electrical resistance drastically. A perfect seal is necessary, since an inefficient seal is worse than none at all. A leaky seal will allow moist air to enter, but provides a poor escape for any condensate. Baking is not recommended for most piezoelectric transducers, not only because of possible depolarisation of the ceramics, but also because low-melting point solders are often necessarily used in their construction.

In some cases the simplest method of sealing is to encase the clean, dry piezoelectric element in an insulating shroud, though epoxy resins may not always be suitable because they have a tendency towards electrical instability under load, (Neubert, 1963, p.337). Moisture can also affect other parts of the electrical circuit within the transducer, which is often small, and a sealed overall construction is to

be preferred where this is possible. Assembly is best carried out in a "laminar-flow" cabinet, in which the atmosphere can be maintained dry and dust-free.

Again to realise the full potential of piezoelectric transducers operational cleanliness is also necessary, a frequent cause of poor performance being dirty connections at such points as the small "microdot" coaxial connectors.

### 3.232 Piezoresistive force-transducers

Although unbonded wire strain-gauges have been used in some pressure transducers, they are not really suitable for use in force transducers since the number of wires needed to react a typical load component would make construction impractical. The semi-conductor materials are rather brittle in bulk form and, except in very special circumstances, they are also unsuitable in situations where they need to react the total load. Strain-gauges are therefore used to sense the surface strain on a load-bearing link of some kind, and the design of a piezoresistive force transducer is largely concerned with the design of such links. In comparison with the minute strains needed in piezoelectric materials to generate a measurable signal, piezoresistive transducers are relatively deflective. However to ensure that the strain gauges remain within their linear range, it is necessary to restrict the strain levels. Typical maxima are  $10^{-3}$  for metallic gauges and  $0.5 \times 10^{-3}$  for semi-conductor gauges though there are advantages in having a lower maximum for the latter. In most circumstances the deflections associated with such strains are acceptable, but it is important to appreciate that it is the overall deflections of the balance system which are relevant, not just those at the gauge positions.

Two approaches are open to the designer of a force-balance. He can use individually-designed load cells, a number of which are assembled to measure as many of the six components as are required, or he can devise a "single-piece" balance in which, as the name implies, a single block of metal is so machined that the surface strain at particular places results, ideally at least, from only one load component. In practice, there are usually interactions between components, and the designer aims to keep these to a minimum. In many cases this can be achieved by an application of the principle of symmetry, whereby the first order interactions are cancelled using two suitably-positioned sensors, the outputs of which are added or subtracted, depending upon the particular configuration and the load to be measured.

The simplest load transducer is the tension/compression link in which a prismatic bar has a pair of strain gauges, one affixed to each of two opposite faces as illustrated in figure 3.13(a). Pivots are provided at each end of the link to decouple other than axial loads, but with the gauges connected in opposite arms of a Wheatstone bridge circuit, for example, (see section 3.41) the strains due to bending are theoretically cancelled. The effects of temperature changes are not however cancelled by this simple arrangement, though the addition of a second pair at right angles to the first, as in figure 3.13(b) will provide compensation for temperature changes and slightly enhance the sensitivity. As an alternative, matched pairs of p- and n-type silicon gauges can be used in a four active-arm bridge as described in section 3.2242.

This simple load link has many advantages so far as measurements in impulse tunnels are concerned. It is compact, fairly robust, easily constructed and above all it has a high inherent natural frequency. Such links often constitute parts of a single-piece balance. It does however possess disadvantages. The need to dissipate the electrical energy supplied to the gauges sets a minimum to the volume of the tension-link. The length of the link is determined by the need to fix the gauges, which incidentally should occupy as much of the available space as possible so that secondary variations in the strain-field are averaged. The cross-sectional dimensions must be such that buckling does not occur under the expected compressive loads. Although a buckled link will normally return to its original state when the load is removed, the gauge itself may be damaged or its bonding affected. Particular attention should therefore be paid to handling loads, when very slender links are proposed.

So that reasonable signal levels are obtained the strain gauges must be operated at reasonably high strains consistent with them remaining within their linear range. For a link of given length and material, the load capacity then determines the cross-sectional area. A sample calculation shows that the simple prismatic bar would be suitable as a load-link of moderate capacity. For example a link of capacity  $\pm 500$  N made from aluminium alloy would have to have a cross-sectional area of  $7.5 \text{ mm}^2$  to attain a strain level of  $\pm 10^{-3}$  at maximum load. With such a strain, metallic strain-gauges could be used, but such a

small cross-section is impractical for a prismatic bar in compression and little can be gained by using other shapes such as the H-cross-section which is sometimes employed. By using the more sensitive semi-conductor strain gauges, the cross-sectional area can be increased and lower strain levels tolerated. Dual-element semi-conductor gauges, having the same temperature coefficient of resistance and gauge factors of opposite sign are available, designed to compensate for the effects of differential thermal expansion when mounted on steel (expansion coefficient =  $11 \times 10^{-6} \text{ K}^{-1}$ ) and when connected in adjacent arms of a Wheatstone bridge circuit. The overall dimensions of a typical such pair are 10 mm x 4 mm, and the gauge factor about 120. With two such pairs in a four active-arm bridge (section 3.41) on a steel link of cross-section 5 mm x 5 mm, a load of 500 N would produce a signal of about 12 mV/V at a strain of  $10^{-4}$ .<sup>\*</sup> Assuming a 3.5 V supply, corresponding to 0.1 W dissipation for gauges of 120  $\Omega$  resistance,<sup>\*\*</sup> and an electrical noise level of 20  $\mu\text{V}$ , the resolution of such a link would be about 1 N or 0.2% of full-scale. The corresponding strain,  $0.2 \times 10^{-6}$  may be equivalent to a temperature change of only one or two kelvin, even for the compensated gauges, so great care would have to be exercised during a lengthy calibration procedure to achieve this resolution, though no difficulty should arise while making dynamic measurements. With such low strains, deflections of the transducer are negligibly small, a very desirable attribute. A tension link of lower capacity, about 70 N or so, could be devised by using aluminium alloy in place of steel and a rather smaller cross-sectional area of T-shape, but such links are not ideal for smaller loads, either because the strains are too low, or because of the manufacturing difficulties of machining thin sections from the solid. Links fabricated by bolting together several parts are likely to introduce hysteresis into the system, and so should be avoided.

The dependence of strain on load alone can be avoided by arranging that the force to be measured exerts a couple on the section occupied by the transducer. The strain in the gauged section can then be increased, independently of the force itself, simply by increasing the moment arm. An obvious modification of the simple tension link is to arrange for the load to be applied eccentrically, figure 3.14. The gauges are then connected to measure the strains due to bending only, the axial strain being cancelled by the Wheatstone bridge circuit arrangement, again using four active arms. The sensitivity to load of this arrangement is a factor  $6e/h$  times greater than the simple axially-loaded bar, where  $e/h$  is the eccentricity ratio,  $h$  being the thickness of the bar in the plane of bending. The eccentrically loaded link is of course more deflective, the total deflection  $\delta$  being given by

$$\delta = 2S_b L \left\{ \frac{e}{h} + \frac{1}{12e/h} \right\} \quad (3.46)$$

where  $S_b$  is the surface strain due to bending only and  $L$  is the effective length of the prismatic bar.

The maximum strain experienced by a gauge is a combination of the bending and axial strains. It may be shown that this is  $\left[1 + \frac{1}{6e/h}\right]S_b$ , and it is this value which must not exceed that specified to ensure the strain gauges remain within their linear range. With this constraint, the minimum deflection occurs for  $e/h = 1/6$ , corresponding to a "useful" strain  $S_b$  of only half the allowable maximum. However by adopting an eccentricity ratio  $e/h \approx 2$  say, and accepting the larger deflection, the "useful" strain becomes 12/13 of the allowable maximum. The parasitic strain, that is the strain due directly to the axial loading which is cancelled by the electrical circuit arrangement, is only 1/13 of the allowable maximum, so that the load capacity is diminished by a factor of 13. Returning to the earlier example of a prismatic steel bar of cross-section 5 mm square, a strain of  $10^{-4}$  is now achieved with a load of about 40 N, which can be resolved to 0.2%. However the strain field is now anti-symmetric, so that (nearly) equal and opposite changes in resistance can be produced by using only p-type silicon gauges. These gauges can be carefully selected and closely matched, and the linear range may be extended by utilising a four active-arm bridge arrangement as described in section 3.41. The allowable maximum strain can be raised to  $10^{-3}$ . Buckling is now unimportant, since it no longer provides an operational limit to the compressive load capacity. The cross-sectional dimensions may therefore be reduced, so that the column

\* For these dual-element gauges, the range of strain over which the fractional resistance change is nearly linear with strain is very limited, because the second order coefficients of the p-type and n-type materials cannot be adjusted independently of the first order coefficient.

\*\* We use this merely as an example. In general circumstances there are clear advantages in using gauges of high resistance, since for a given dissipation the bridge voltage is higher and so therefore is the output signal. In favourable circumstances the resolution may be equivalent to a strain of  $10^{-8}$ .

has the same load capacity but a greatly improved resolution. The "gammaform" link described by Rebuffet (1956) and illustrated in figure 3.15 is one variant of the simple eccentrically-loaded column.

Lateral loads, arising from inadequate decoupling, will also produce bending of the column. In order to minimize such interactions from other force components it is good practice where space permits, to split the eccentric column into two equal parts, one each side of the loading axis. The various loading rings, figure 3.16, which are widely used as load cells are really extensions of this idea. Such rings tend to occupy a great deal of space, are rather deflective, and are perhaps not really suitable for use in very short duration flows, except maybe for measuring small axial loads. Where such rings are used, the rectangular variety with flat surfaces are better for gauge mounting than those with curved surfaces.

The measurement of pitching and yawing moment may be accomplished by measuring the normal and side-force components at a pair of stations spaced a suitable distance apart along the longitudinal axis of the model. One may therefore use force links of the kind we have discussed. The rolling moment is however more efficiently measured using a torque-tube - a thin-walled tube of circular cross-section in which the shear strain is determined using a pair of strain-gauges at an angle of  $\pi/4$  to the generators, as shown in figure 3.17. Usually two such pairs of gauges are used in a four active-arm bridge.

Approaches of this kind, utilising an assembly of individually-designed transducers, are not uncommon - indeed a wide range of such six-component wind-tunnel balances is available commercially.\* However the instrumented cantilever sting-balance is better suited for high frequency applications, since it can be made more compact. The well-known basic principle is illustrated by the instrumented beam of figure 3.18. Suitable combinations of the strain-gauges in Wheatstone bridge circuits each provide an output proportional to only one force component in an axis system aligned with that of the beam. The effects of the other components are decoupled, to first order at least, by the electrical circuit arrangement. Thus the summing and differencing circuits (see section 3.41) for gauges 1, 2, 3 and 4 provide the z-component of force and the moment M about the y-axis, as shown. For dynamic measurements switching from one circuit arrangement to the other is impractical, and the gauges are duplicated.

The simple bar is not really suitable for torque measurements and a specially machined section, such as one of those shown in figure 3.19 is generally provided. The same idea is extended in practice to improve the sensitivity to the other components of force. A number of instrumented, cantilever sting-balances have been built and successfully operated in continuous flow tunnels, notably in France (Rebuffet, 1956). Some examples of machined cantilevers designed to measure five force-components (axial force is excluded) are illustrated in figure 3.20. The chief problem with such balances in general, is to achieve sufficient resolution to measure the axial force without introducing interactions from the other, frequently much larger force components. In hypersonic flows, where lift/drag is of order unity, this may not be so serious a problem, but the difficulty remains of providing a decoupled, sufficiently sensitive transducer to measure the axial force, while at the same time ensuring that the model is adequately supported at the required attitude to the flow. The decoupling for the other force components is essentially provided electrically by the bridge circuits, and the strain levels are made relatively large by appropriately choosing the moment arm. This is less easy to accomplish with the axial force, since space is very limited in lateral directions.

In "static" balances for continuous-flow wind-tunnels, the axial-force measuring system can be moved aft using some kind of kinematic linkage, but this is not suitable for unsteady measurements, because friction and backlash in the bearings remain uncertain, and because of the low resonant frequencies associated with such linkages. One would like, moreover, to house the complete balance system within the model, so as to avoid the complication of shielding the balance from aerodynamic loads on the sting and supporting structure.

Figure 3.21 shows a three-component balance employing metal strain gauges which is used in the gun-tunnel at Braunschweig. It makes excellent use of the limited space available.

The most promising solution to these problems, assuming that resistance strain-gauges are to be used, is to combine the advantages of the single-piece balance with those of individually-designed

---

\* Task Corporation, Anaheim, California, U.S.

transducers. The complete force-balance is then machined from a single-piece of metal, but conceptually it consists of individual force transducers (which may be tension links, load-rings, cantilevers or any other suitable shape) and decoupling pivots. Some early attempts at such a balance have been described by Opatowski (1966, 1971). Both the balances he describes were three-component balances, external to the model itself, and were designed for use in a gun-tunnel where the flow duration is typically 25-45 ms. In the first balance, illustrated in figure 3.22, the force links are cantilevers. The rearmost cantilever measures drag and the other pair were designed to provide both lift and pitching moment. In the event they proved insufficiently accurate to measure the latter and a moment sensing beam was later incorporated in the incidence coarse-adjustment gear at the forward-end of the balance. This sub-assembly was pivoted in a phosphor-bronze bush, the rear end of the assembly being restrained by a pin which was free to slide fore and aft in a slot in the main beam of the balance. Silicon semi-conductor gauges were used for the moment sensor, metal foil gauges for the cantilever links. An interesting feature of this balance is the provision of an hydraulic damper, the natural frequency of the system being deemed too low for electronic filtering. In practice the damper, which used a high viscosity silicone oil (viscosity, 1000 stokes), reduced the amplitude of the oscillations, but also tended to couple the lift and drag.

In the second balance, figure 3.23, a far more compact arrangement was adopted. Lift and drag were now sensed using tension links only 0.25 mm thick; to obviate buckling these were made very short. The pitching moment was measured conventionally at the forward end of the sting. Semi-conductor strain gauges were used throughout, and the lowest natural frequency was 350 Hz with no model attached. In its original form, with light side-covers to the balance, there was considerable interaction between lift and drag, but this was reduced by using 3 mm gauge-plate. The balance was also sensitive to loads on its exterior, and a separate wind-shield had to be added.

The lessons are clear. Those parts of the balance which do not play an active rôle in measurement, either by pivoting to provide decoupling or by undergoing strain to produce an output from the gauges, must be as stiff as possible. For the single-piece balance only the minimum amount of material should be removed to form these pivots and force-links and to allow access to affix the strain gauges.

A brief remark is in order here about suitable materials for force linkages and balance systems. The general requirement that the system has high natural frequencies implies that the material must have a high specific stiffness. Although beryllium is some six times better than steel and aluminium alloy in this respect, its toxicity makes very special machining facilities necessary, so that in most circumstances the more common and less expensive materials are employed. Both the aluminium alloys and the steels remain in their linear elastic regions at the gauged sections, for the strain levels envisaged, but the elastic pivots used for decoupling extraneous loads, as described in the next section, may suffer somewhat larger deflections. In order to provide for these, and for overloads, the material chosen should possess a very high yield strength, and experience indicates that although the aluminium alloys can often be used, a generally suitable material is 17-4 PH stainless steel. Precipitation-hardened materials of this kind do not require quench-hardening, but can be hardened by suitable heat-treatment after machining. Since quenching is a common cause of distortion, it is a process to be avoided where thin sections are involved. Conventional machining processes can also give rise to residual stresses which are released by the subsequent heat treatment and the modern technique of spark-erosion machining provides an excellent alternative. Very small holes and slots of complex shape can be cut using this technique, so that it is eminently suited for the manufacture of single-piece, multi-component balances. A good, smooth surface is produced directly so that "finishing" is not normally required - it would be difficult in any case in the confined spaces to do any other machining. It may however be necessary to roughen the surface so that the gauges can be effectively bonded (see gauge manufacturer's literature).

A successful force transducer is clearly the result of some compromise. By way of summary we list here some of the important points that should be borne in mind during design and construction.

- (i) The piezoresistive transducer should be designed for maximum surface strains of  $10^{-3}$  where metal foil and moderately sensitive semi-conductor strain gauges are envisaged and for half this value when high sensitivity semi-conductor gauges are to be used. When "full" compensation for non-linearity is not possible, for example when using a dual-element p- and n-type pair, the strain should be limited to about  $10^{-4}$ .

- (ii) Mounting on very thin surfaces should be avoided; a minimum thickness of 0.5 mm is suggested.
- (iii) High-resistance gauges can be used when necessary to enhance output; the gauges should be as large as the space permits.
- (iv) Where possible, bridge circuits with four fully-active gauges should be used. These should be positioned fairly close to one another so that temperature changes affect them all equally.
- (v) The gauges should be located on flat surfaces.
- (vi) The gauges should be on surfaces unstrained by extraneous loads.
- (vii) The mounting of gauges should be carried out in accordance with the manufacturers' instructions. Extreme cleanliness and care in handling are usually well rewarded. The resistance of each of the gauges (both forward and reverse for semi-conductors) should be checked at every stage. At any sign of a marked change the gauge should be replaced immediately - with matched gauges it may be necessary to replace more than one.

### 3.233 Pivots

In an ideal balance each transducer would respond to only the one force component it was designed to measure. Decoupling from the other components may be achieved in several ways as we have seen. Here we are concerned principally with mechanically-decoupled balance systems, though in practice they are best used in combination with electrical-circuit decoupling when this is possible. How closely a mechanically-decoupled balance approaches the ideal depends in very large part on the pivots or hinges which allow the "unwanted" force components to by-pass the transducer. The pivots are not required to rotate through a large angle, the relative lateral displacement of the ends of a transducer-pivot system being determined by the axial\* displacement of another transducer. This is shown diagrammatically in figure 3.24 in which only the force component  $F_1$  is supposed to act. The main restraint is provided by the transducer  $T_1$ , which undergoes an axial displacement. In consequence the transducer  $T_2$  suffers a lateral displacement, and its pivots must be laterally very compliant so that  $T_2$  does not respond to the force  $F_1$ . The pivots must also be axially stiff, and of course without backlash or hysteresis. Compactness is a desirable asset. These very stringent requirements are most nearly met by integrally-constructed, elastic flexures. The basic concept of the elastic flexure is illustrated in figure 3.25 where the necessary two lateral degrees of freedom are provided by a pair of thin strips, in tandem, at right-angles to one another. Two such flexure pairs must be provided for each force-link, one either side of the transducer sensing element. The outer ends are connected, one to the model experiencing the load, the other to the support.

The chief disadvantage of the elastic flexure is that it does not possess some lateral stiffness, and to this extent the balance becomes an indeterminate structure. In effect some of the load to be measured by a particular transducer in a multi-component system is reacted in part by the others as a consequence of their finite lateral stiffness, and is "lost". There is thus a small reduction in sensitivity, but more important, interactions occur. Provided the lateral compliances are large however, the flexures closely approximate perfect pivots and the structure is very nearly statically determinate. A crude analysis of the flat strip flexure shows that the fraction of the axial load that is "lost" is proportional to  $(t/H)^2$ , where  $t$  is the thickness of the strip in bending and  $H$  is the distance between coplanar strips. Thus to achieve good decoupling, the thickness of the flexures should be small compared with the distance separating them.

In practice the double flat-strip flexure of figure 3.25 is rather space-consuming, and for this reason is not often used. A more compact arrangement is the "circular arc" flexure, several examples of which are illustrated in figure 3.26. Here each flexure consists of the material remaining between a pair of parallel holes drilled normal to the axis of the element, one either side and parallel to a plane containing this axis. Elongated flat-strip flexures may be formed in a similar manner by milling slots instead of drilling holes. Such flexures may be accurately manufactured, and all the machining completed before the final saw-cuts are made to free the flexures.

Elastic pivots of this type are required to operate under both compressive and tensile loading. As the axial force changes, three important effects occur:-

---

\* The terms "axial" and "lateral" are used here in reference to the axis of the transducer

- (a) the angular or lateral stiffness alters. The existence of angular stiffness leads to an interaction; when the stiffness is load dependent, these interactions will be non-linear;
- (b) the position of the effective centre of rotation changes; and
- (c) the allowable angular deflection corresponding to a maximum stress level in the flexure, varies.

The extent of these changes is different for circular-arc and flat-strip flexures. In general the angular stiffness and position of the centre of rotation change less with axial load for circular-arc pivots, but the allowable angular deflection is greater for the flat-strip pivot. Because the thickness of the circular-arc flexure varies along its length, the lateral stiffness is somewhat higher than that of a flat-strip flexure of the same "length". To achieve the same lateral compliance therefore, the circular-arc flexure must occupy more space axially than would a flat-strip flexure. The axial deflection which takes place is therefore also larger for the circular-arc flexure. On the whole however, its advantages outweigh these deficiencies. Tracy (1961) suggests (as suitable design values) that the ratio of arc diameter to minimum thickness ( $d/t$ ), should lie between 3 and 8. The equivalent length/thickness range for flat-strip flexures having the same bending stiffness is about 1.5 to 2.5. Values of ( $d/t$ ) less than 3 lead to excessive bending stresses and a lack of compliance; values greater than 8 exhibit little gain in compliance and are over-deflective, a feature which is generally undesirable.

The aim should be very thin, widely-spaced flexures, that is ( $t/H$ ) small, with a value of ( $d/t$ )=3. If the stresses due to bending are found to be excessive, the arc diameter  $d$  should first be increased, and the thickness  $t$  increased only if the overall stress is still too large. As a final resort the flexure may be elongated, but according to Tracy (1961) this should rarely be necessary.

### 3.24 Accelerometers

The principle of the accelerometer is based upon the behaviour of the single-degree-of-freedom system discussed in section 2.31. A body of inertial mass  $m$  is connected via a spring of stiffness  $k$  to the object whose acceleration is to be measured. Although the inclusion of a viscous damper is not always possible in a practical accelerometer, the damped instrument has advantages, and in any case the effects of any damping must be understood by the user. We shall therefore include such a damper, of coefficient  $c$ , and examine the system represented in figure 3.27.

Writing as  $x(t)$  the displacement of the body, and as  $\chi(t)$  that of the base to which the spring is attached, the equation of motion for the body is

$$m\ddot{x} = -k(x-\chi) - c(\dot{x}-\dot{\chi}) \quad (3.47).$$

A sensing device attached to the spring - indeed the spring stiffness may be that of the sensor itself - measures the relative displacement  $(x-\chi) = z$ , say. Rewriting equation (3.47) accordingly, we have

$$\ddot{z} + 2\zeta\omega_n\dot{z} + \omega_n^2 z = -\ddot{\chi}(t) \quad (3.48)$$

where  $k = m\omega_n^2$  and  $c = 2\zeta\sqrt{km}$  as before.

Now suppose we consider an harmonic oscillation  $\chi = x_0 e^{i\omega t}$  of the base. With this input function, the complete solution of equation (3.48) is, for  $\zeta < 1$

$$z(t) = Z e^{-\zeta\omega_n t} \sin(\sqrt{1-\zeta^2} \omega_n t + \phi) - \frac{\left(\frac{\omega}{\omega_n}\right)^2 x_0 e^{i\omega t}}{\left(1 - \left(\frac{\omega}{\omega_n}\right)^2 + 2i\zeta\frac{\omega}{\omega_n}\right)} \quad (3.49).$$

Now the first part of this solution, the complementary function, represents a damped oscillation at the frequency  $\omega_n \sqrt{1-\zeta^2}$ , which is a characteristic parameter of the system. We must suppose, either that the damping  $c$  attenuates the transient oscillations at this frequency so that they are unimportant in comparison with the base-excited motion after a short time, or that the transducer output signal can be processed to reduce this oscillatory component to negligible proportions during the test-time. Such filtering should be possible as long as  $\omega < \omega_n$ , that is so long as we do not wish to use the transducer near its resonant frequency (we are concerned here with the undamped or lightly damped instrument). This point has perhaps to be made more forcibly than usual, since we are interested in measuring acceleration transients.

The acceleration of the base is  $\ddot{x} = -\omega^2 x_0 e^{i\omega t}$ , so that equation (3.49) now reduces to

$$\frac{z}{\ddot{x}} = \frac{1/\omega_n^2}{\left[1 - \left(\frac{\omega}{\omega_n}\right)^2 + 2i\zeta \frac{\omega}{\omega_n}\right]} \quad (3.50).$$

We see that when  $\zeta \neq 0$ , there is a phase difference  $\phi$  say, between the relative displacement  $z$  and the acceleration of the base, given by

$$\tan \phi = \frac{-2\zeta \frac{\omega}{\omega_n}}{1 - \left(\frac{\omega}{\omega_n}\right)^2} \quad (3.51)$$

and that the ratio of the absolute magnitudes is given by

$$\left|\frac{z}{\ddot{x}}\right| = \frac{(1/\omega_n)^2}{\sqrt{\left[1 - \left(\frac{\omega}{\omega_n}\right)^2\right]^2 + \left[2\zeta \frac{\omega}{\omega_n}\right]^2}} \quad (3.52).$$

The phase angle  $\phi$  and the "gain factor"  $\left\{\left[1 - \left(\frac{\omega}{\omega_n}\right)^2\right]^2 + \left[2\zeta \frac{\omega}{\omega_n}\right]^2\right\}^{-\frac{1}{2}}$  are both functions of the excitation frequency  $\omega$ . They are plotted against the frequency ratio  $(\omega/\omega_n)$  for several values of the damping ratio  $\zeta$  in figures 3.28 and 3.29.

For an undamped system, there is no phase shift, but the gain factor remains within about 10% of unity up to a frequency ratio of about 0.3, and within 5% of unity only up to about  $\frac{\omega}{\omega_n} \approx 0.2$ .

The inclusion of damping, when it is possible, clearly has advantages so far as the constancy of the gain factor is concerned. The optimum value of  $\zeta = 0.65$  results in a maximum variation in the gain factor of only 1.25% over the frequency range  $0 < \omega \lesssim 0.6 \omega_n$ . There is however a phase shift, but as one can see from figure 3.29 this is very nearly linear with  $\omega$  at  $\zeta = 0.65$ .

In general circumstances the base excitation will not be harmonic. When it is periodic, it may be expressed as a Fourier series of harmonic terms, and by extension a finite pulse can be regarded as one cycle of some periodic behaviour, and therefore expressed likewise. (More general situations can be represented by a continuous Fourier spectrum.) The base excitation is now written

$$x(t) = \sum_j x_{0j} e^{i\omega_j t} \quad (3.53)$$

for  $0 < t < \tau_p$

where  $\tau_p$  is the pulse duration, and we find for the particular integral

$$z(t) = \sum_j \frac{\left(\frac{\omega_j}{\omega_n}\right)^2 x_{0j} \exp[i(\omega_j t - \phi_j)]}{\sqrt{\left[1 - \left(\frac{\omega_j}{\omega_n}\right)^2\right]^2 + \left[2\zeta \frac{\omega_j}{\omega_n}\right]^2}} \quad (3.54).$$

For the case  $\zeta = 0.65$ , the gain factor is nearly unity for  $0 < \omega_j \lesssim 0.6 \omega_n$ . Moreover since  $\phi$  is nearly linear with  $\omega$ , we have

$$\frac{\phi_j}{\omega_j} = \text{constant} = t_0 \text{ say}$$

and equation (3.54) becomes

$$z(t) = \sum_j \left(\frac{\omega_j}{\omega_n}\right)^2 x_{0j} \exp[i\omega_j(t - t_0)] \quad (3.55)$$

so that all the harmonic components are shifted in time by the same amount  $t_0$ , and the acceleration function is reproduced without phase distortion.

We thus have two cases for possible practical application:

- (i) very small damping,  $\zeta \rightarrow 0$ , and  $0 < \omega < 0.3 \omega_n$ ,
- (ii) a specific value of damping corresponding to  $\zeta = 0.65$  and  $0 < \omega \lesssim 0.6 \omega_n$ .

The majority of accelerometers are in the first category, particularly those having a high resonant frequency  $\omega_n$ , and any measurements made with such transducers must be interpreted in the light of the foregoing remarks.

Some response calculations for idealised pulse shapes have been carried out by Levy & Kroll (1950) for various values of damping ratio and of the ratio  $\tau_n/\tau_p$  where  $\tau_n = (2\pi/\omega_n)$  is the characteristic period of the transducer and  $\tau_p$  the duration of the pulse. Some of their results are sketched in figures 3.30. The advantages of a damping ratio  $\zeta$  of about 0.7 are clearly seen, but since practical transducers have  $\zeta < 0.1$ , it is imperative that they be used in situations where  $\tau_n/\tau_p$  is small if the response is to bear an easily interpretable relationship to the input.

The low-frequency response is also of some importance. As an illustration of the general requirement it is sufficient to consider the response to a rectangular acceleration pulse of duration  $\tau_p$ , and assume that the resonant frequency  $\omega_n$  is very high, and is not excited. The output of the measuring system is a sharp rise corresponding to the leading edge of the pulse, followed by an exponential decay which lasts for a time  $\tau_p$ ; a similar, but inverted response then occurs, the decay towards zero output taking an infinite time. If we identify the rectangular pulse with the test-time, the fractional "droop" is  $(1 - e^{-\tau_p/\tau_c}) = \tau_p/\tau_c$  when  $\tau_c$ , the decay time constant, is long. This time constant is generally that of the transducer in combination with the following electronic amplifier and it should be some 50 to 100 times larger than  $\tau_p$ . In situations where accelerometers are likely to be used, say flow durations of less than 10 ms, the low frequency time constant should be about 1 second.

In our discussion so far we have concentrated only upon that part of the "sensitivity factor" which varies with frequency  $\omega$ . Equations (3.50) and (3.55) show that the mechanical transfer function also contains the factor  $1/\omega_n^2$ , which of course is a constant for any particular transducer. However the presence of such a factor indicates that in transducers having a very high resonant frequency, the relative displacement  $z$  for a given acceleration\* is likely to be small. The sensor must therefore be sensitive to these small displacements, and as one might expect piezoelectric, and to a smaller extent piezoresistive, devices have found wide application.

In the piezoresistive accelerometers the spring element is generally in the form of a beam. Strain gauges are mounted on the surfaces of the beam to sense the strains due to transverse bending which occur as a result of the inertia loading due to the motion of the body of mass  $m$  attached to it. Some of the configurations possible are shown schematically in figure 3.31. The resonant frequency of this type of instrument is relatively low even when, to effect miniaturisation, the beam itself is of silicon with diffused areas of impurity on the surfaces to sense the strain. This design does however lend itself more readily than most others to the provision of damping, since the vibrating parts can be immersed in a silicone oil of suitable viscosity. The motion is often limited by stops. Accelerometers of this kind are available commercially, but only those with very low resonant frequency and high sensitivity appear to incorporate damping. Beaussier (1966) describes a cantilever-type accelerometer with strain-gauges arranged in pairs so as to sense accelerations along two axes normal to that of the cantilever. Damping is provided using silicone oil, and Beaussier gives the natural frequency as about 1.6 kHz, the dimensions of the transducer being length, 16 mm and diameter, 5 mm.

High resonant frequencies are much more easily achieved using piezoelectric sensors. The piezoelectric material serves as both the spring element and as the sensor and the compressive, shear and bending modes can all be used. Much of our discussion on force transducers applies directly here, since the accelerometer is merely a device which senses the inertia force. We shall therefore restrict the present discussion to those aspects of particular relevance to accelerometer design and use, and refer the reader to section 3.23 for the more general topics.

Thus shear-mode elements are likely to have an inherently low "cross-axis", "lateral" or "transverse" sensitivity, all three terms being used to describe the sensitivity to accelerations in the plane normal to the main axis of the transducer. Again, some of the advantages of this mode may not be realised when reliance has to be placed on cemented joints. The shear-plate can be used in a bolted construction such

\* It is common practice to specify the sensitivity of a linear accelerometer in terms of its output "per g", where  $g = g_n \approx 9.80665 \text{ m/s}^2$  is implied. In a less Earth-centred world, the numbers will be a factor 9.80665 smaller!

such as that illustrated in figure 3.32(a), the transmission of the load relying on friction; the shear-tube, figure 3.32(b), must rely on cemented joints. Both methods have been used in commercially available accelerometers with a piezoelectric ceramic as the sensor.

The compressive mode is more widely used, because transducer construction is somewhat easier. Electrical isolation of the piezoelectrical material from the transducer housing is conveniently achieved by utilising a pair of discs or rings, suitably polarised, with the common central electrode used as the output terminal. Some typical constructions are shown in figure 3.33. The inertial body is attached somewhat differently in each case and this has an effect on their response to extraneous events. The peripheral mounting of figure 3.33(a) gives a high sensitivity and a high resonant frequency, but because the inertial body is maintained in contact with the piezoelectric sensors by a stiff spring connected to the outer casing, the accelerometer is sensitive to high intensity sound and to temperature variations. In addition strains in the base can be troublesome, and transducers of this type must be mounted with care, at points where no surface distortions of consequence occur, since these may give rise to spurious signals. The centre-mounting design of figure 3.33(b) overcomes many of these deficiencies, the assembly being on a central post with the outer casing only providing general protection. The reduced sensitivity to strains in the base arises from its greater thickness. Almost complete isolation from base strain can be accomplished by the inverted arrangement of figure 3.33(c), but because vibrations in the casing are readily transmitted to the sensor, the resonant frequency of this arrangement is somewhat lower than the others, perhaps 60% or so for the same nominal sensitivity.

At the expense of bandwidth, one can obtain higher sensitivity for a given overall mass by using bimorph elements in a bending mode. The construction is schematically similar to those of the piezo-resistive-gauged beams of figure 3.31, but except when very high sensitivities are required, bending types have no special advantages.

Several factors determine the extent to which the performance potential indicated by the idealised results described above can be realised. In the analysis we considered a single degree-of-freedom system, and assumed a response to the acceleration along only one axis, 03 say. With such an ideal transducer, the directional sensitivity follows a cosine law, the sensitivity locus having the familiar figure-of-eight shape illustrated in figure 3.34. The transverse sensitivity in the plane normal to 03 is zero for the ideal accelerometer. In practice this cannot be realised. Imperfect alignments and poor seatings resulting from manufacturing tolerances can give rise to finite transverse sensitivity. For example, where the axis of maximum sensitivity is not perpendicular to the base of the transducer which serves as a mounting reference, there will be an apparent transverse sensitivity proportional to the sine of the misalignment angle. Deviations of the polarisation axis of the piezoelectric element from the intended direction can give rise to such misalignments in certain transducer configurations. On the whole, axially-symmetric transducer designs probably have lower transverse sensitivity than other configurations.

The range of linear accelerometers available commercially is now very large, extending from sub-miniature piezoelectric transducers having a total mass, including the housing, of less than 0.5 gram with a resonant frequency of 75 kHz and a sensitivity of about  $0.7 \text{ pC/g}_n$ , to much larger transducers having correspondingly lower resonant frequency and higher sensitivity. Triaxial accelerometers consisting of three similar transducers mounted on a common base are also marketed. These commercial accelerometers generally have a fairly small transverse sensitivity. Many are available with a maximum cross-axis sensitivity of less than 5% of that along the main axis, and the direction of minimum transverse sensitivity is frequently indicated with a line or a dot marked by the manufacturer. This information can often be employed to good advantage when the accelerometer is mounted.

The mounting in fact plays a very important rôle in the behaviour of the transducer. The majority are attached by means of a threaded stud. The flat base of the accelerometer must be in firm contact with the object whose acceleration is to be measured, but excessive torque used trying to improve this contact can at best distort the transducer, changing its axial and transverse sensitivities, and at worst it can damage the interior beyond repair. Some manufacturers recommend the mounting torque which should be used, others specify a maximum. In the former case it is possible that the transducer is "torque-sensitive" in which circumstances the same mounting procedure must always be followed carefully if reproducible results are to be obtained. A poor mechanical contact will affect the high frequency performance and the

surface upon which the accelerometer is mounted should be smooth and flat, with the axis of the threaded hole for the stud carefully aligned perpendicular to this surface. To avoid "earth-loops" which are a potential source of electrical noise in the measuring system, an insulating stud and washer can be used.

The tiniest accelerometers available commercially have no space for studs and must be cemented in place. Waxes, epoxy resins and impact adhesives can all be used, depending on the level of acceleration expected, but the cementing must be done with extreme care. Because of the delicacy of these sub-miniature transducers, the pressures which can be applied during mounting are limited. To ensure uniform contact and correct alignment, special jigs and tools should be used; often these are supplied with the accelerometer.

The output cable, which should be of the low-noise variety (see section 3.42) can also present difficulties. Since vibration of the cable can produce spurious signals, it should be anchored in such a way as to prevent "whip". The side-entry position to the accelerometer is usually better than the top entry from this point of view. Manufacturers often give very complete and explicit instructions regarding the mounting procedures to be followed in order to make best use of their transducers.

### 3.3 General aspects of force-balance design

Most engineering design is to some extent a compromise. The design of a transducer, and a multi-component force-measuring system is merely a very complex transducer, is no exception. A number of desirable qualities that any force-balance should possess may be listed and to these may be added those peculiar to the present problem, that is those which arise from the short duration of the high-enthalpy flow. In effect this separates the static performance requirements of the system from its dynamic behaviour. Of course this is not strictly possible. We have seen earlier in this chapter that sensitivity and frequency response are not independent. Indeed for a given configuration, using this term in a very wide sense, their product remains substantially constant. The implication is that there is a limit to the range of conditions in which a force-balance may be used; force-balances employing our present knowledge are unlikely to be suitable for low-force levels of very short duration. The actual limit however depends upon the ingenuity of the designer and probably also on the patience of the user.

Tracy (1961) gives a very good summary of wind-tunnel, sting-balance design. He was, however, concerned only with steady forces, so that the dynamic performance of a balance was given no consideration. What follows is closely patterned on his account, but it is supplemented where necessary so as to include those features peculiar to the measurement of transients.

At the outset the designer is faced with a basic specification setting out the number of force-components to be measured, the maximum values of these components\* and the resolution required, and the general nature of the flow in which measurements are to be made. This latter will include the dimensions of the test section as well as the duration and general state of the flow. In order to meet these special requirements in a satisfactory manner the designer would aim to produce a balance in which each output depends upon only one force-component, one in which the relationship between output and force-component is linear† one that is free of hysteresis and backlash and also a balance that can be readily calibrated. This calibration should be stable and unaffected by the environment to any significant extent. Nor should the balance produce spurious output signals, due for example to a thermal response. To approach this ideal performance, the balance designer must have regard to the following:

- (i) the force-resolution system; this depends upon the number of components to be measured and to some extent upon their relative magnitude,
- (ii) the strength of the component parts in relation to the maximum expected loads,
- (iii) the attachments, both to the model and to the support; these may be critical,
- (iv) the sensing element/transducer design; this has an important effect on the dynamic behaviour of the system,
- (v) the force-transducer pivots; these are critical elements in the design, since upon these depends the extent of the decoupling and the linearity,

---

\* A force-component corresponding to a moment may be specified by dividing the moment by the largest balance dimension in the plane of the moment.

---

† Linearity is not an essential requirement, but is highly desirable from a practical point of view.

- (vi) ease of calibration and operation; these should be borne in mind during the design stages,
- (vii) the dynamic behaviour of the whole system; this needs to be such that at most one resonant frequency only lies within the "critical range", otherwise acceleration-compensation is necessary,
- (viii) thermal sensitivity; this may also lead to undesirable behaviour particularly when interactions between components are not insignificant. Temperature changes may affect the performance of a balance in several ways so that it is usually necessary to consider their effects in conjunction with the other factors listed. In fact they are less important when only transient measurements are to be made, since the thermal response will often be an order of magnitude or more slower. Nevertheless static calibration can be seriously compromised by drift due to thermal sensitivity.

The successful development of the electrical resistance strain-gauge makes possible the measurement of the average surface strain in a fairly small region on a structural member. The total pattern of strain in a structure is uniquely related to the external loading on the structure so that a sufficient number of strain measurements may be used, in principle at least, to determine the external loading. What constitutes a sufficient number depends on the redundancy of the structure. The simplest single-piece balance is little more than an elastic cantilever with strain sensitive devices bonded to its surface. As we have noted a steel beam of square cross-section carrying electrical resistance strain gauges as shown in figure 3.35 might be used, in principle, to measure the axial force, both normal forces, and the pitching and yawing moments, providing the gauges were suitably connected. Rolling moment would require additional strain-gauges. Such an arrangement is not of course particularly suitable for the simultaneous measurement of transients, since in the usual configuration the summing and differencing are carried out automatically by appropriate switching of the connections in Wheatstone bridge circuits. It would be possible to avoid this difficulty by using additional gauges but in practice the arrangement would be very insensitive.

In completely general circumstances, each of the six output signals depends upon all six of the applied (generalised) force-components. If a linear dependence only is assumed, then

$$(\text{Output})_n = \sum_{i=1}^6 k_{in} F_i \quad (3.56)$$

so that there would be an array of 36 coefficients to be determined.

Although not impossible to handle, a balance with such characteristics would be tedious to operate and to calibrate unless  $k_{ii} \gg k_{ij}$  ( $i \neq j$ ). In words, the designer must aim to produce a system in which each output depends predominantly on only one force-component. One may note also that the same problem arises in a balance designed to measure fewer than six components; the transducers must be insensitive to the force-components not measured, for obvious reasons. Second order effects, in which the output signals depend upon the squares and double products of the force-components, may also complicate the situation to some extent, but these may be minimised by careful design.

In many respects the simple cantilever of figure 3.35 does just this. However it does possess disadvantages, the most important of which stems from the fact that in practice not all the force-components are of similar magnitude. Thus to increase the sensitivity to the axial force sensors, for example, the local cross-sectional area of the cantilever beam might be reduced. This would result in a lower limit being imposed on the magnitude of the remaining force-components that could be handled, and it is likely also that the larger strains implied by such an arrangement would lead to increased coupling between components. This deficiency may be overcome by making separate provision for the measurement of the weaker axial force, using an axial force-transducer isolated from the remaining stronger force-components by flexures or pivots.

Because of the excellent decoupling such an arrangement provides, the logical extension of the simple cantilever is so to machine the "single-piece" balance as to provide optimum sensitivity for each force-component transducer, while at the same time decoupling it from the other components. Figure 3.36 illustrates balances of this kind, designed for use in the R.A.E. shock tunnel. Much of the machining was accomplished by spark-erosion.

In essence the machined section provides several parallel paths along which the externally applied loads are reacted, and this is just the function performed by the so-called "floating-frame" balance.

This consists of a cantilever which supports a frame or sleeve via an array of pivoted force-transducer links. The aerodynamic model is carried rigidly on the frame. The array of force-transducers constitutes a statically determinate system, assuming that the pivots are ideal, and each transducer reacts only one component of load.

The most common and in some ways most suitable general arrangement for the transducers is illustrated in figure 3.37. Such an arrangement provides the usual resolution of the external loading into forces along and moments about a set of Cartesian axes with one axis aligned with that of the balance. It also fits reasonably well into a circularly cylindrical sleeve which is convenient for attaching a model.

Two pairs of transducers are placed such that each pair lies in a plane containing the longitudinal axis of the balance, the two planes being perpendicular to one another. The members of each pair are spaced apart longitudinally. In this way the sum of their outputs gives the normal force component and the difference provides the moment, in their plane. A fifth force-transducer provides the axial component and the rolling moment about the axis of the balance is generally resolved by a torque-tube placed concentrically. Each transducer element is so pivoted that it is sensitive, ideally, to one force-component only. The pivots are clearly a critical feature of the system.

It should be apparent that the distinction sometimes drawn between the floating-frame balance and the single-piece balance is often largely one of convenience in manufacture. The floating-frame balance is fabricated from a number of carefully machined parts over which a good deal of control may be exercised. Manufacturing tolerances however must be very small to ensure accurate alignments and thus also, distortion-free assembly. The modern single-piece balance may be made using spark-erosion machining to achieve slender, stress-free flexures, but the configuration corresponds to that of the floating-frame balance. Accurate positioning of the strain-gauges in the confined spaces available is not easy however, but the single-piece construction should possess advantages over the bolted- and dowelled-joint construction in regard to hysteresis and repeatability and also as regards its high frequency performance, an important consideration when transient measurements in flows of short-duration are to be made.

With these points in mind we can proceed to a more detailed discussion of those factors, listed earlier, which have a significant influence on the design and performance of a balance.

### 3.31 Force resolution systems

The choice of a force resolution system, though in principle completely open, is restricted in two ways. The balance can occupy a limited space only, dictated largely by the particular shape of model to be tested. An axially-symmetric model, or even a conventionally-shaped aircraft consisting of a fuselage and thin wings, requires the balance to fit within a circularly-cylindrical package. A rather thicker lifting-body configuration could accommodate a package of rectangular cross-section as illustrated in figure 3.38. The second restriction is somewhat arbitrary, and arises because it is usual to specify the loading by reference to a Cartesian set of axes. It is therefore convenient to arrange the force-resolution system so that components are measured more or less directly along these axes. It may be remarked here that these "balance axes" do not usually coincide with the "wind-axes" to which aerodynamic forces are referred, but the subsequent transformation is straightforward using equations 2.64.

One arrangement which fits into a slender cylindrical sleeve has already been mentioned, see figure 3.37. One pair of elements is aligned along vertical diameters to sense normal force and pitching moment. A second pair placed symmetrically, along horizontal diameters senses side force and yawing moment. The axial force is reacted by a transducer placed axially and rolling moment is carried by a torque tube, usually placed around the axial element. The resulting structure is multiply-connected, and it is well-known that temperature gradients in multiply-connected bodies can give rise to stresses. In this instance, a radial gradient of temperature produces an axial force\* which in some circumstances may be of a magnitude comparable with the axial-force capacity of the balance. Such temperature gradients are unlikely to occur in many short-duration facilities during the flow-time, but it is possible that such thermal effects could be significant in "hot-shot" tunnels where the very high-enthalpy flow may last for

---

\* This is a true force and is not to be confused with "apparent forces" arising from temperature-induced resistance changes in strain gauges, for example.

100 ms. Radial temperature gradients might also arise during the test chamber evacuation period immediately prior to a test, and this would manifest itself as a zero-drift. For transient measurements, this slow zero-drift is most easily overcome by a.c. coupling in the amplifier system, provided that such a zero-drift does not introduce other side effects. For example where electrical resistance strain-gauges are used in a Wheatstone bridge circuit arrangement, the normal practice with transient measurements is to measure the "out-of-balance" signal. The range over which this out-of-balance signal is linearly related to the strain is limited, as we have seen in Section 3.2243, so that zero-drift, when it occurs after the bridge has been balanced and the amplifiers switched to a.c. coupling, may result in non-linearities.

Again temperature drift is frequently a problem during static calibration of the balance, a procedure which can occupy several hours when interactions between components exist. For these reasons, it is probably wise to incorporate temperature compensation even in a balance designed only for transient measurements, provided that it can be accomplished without over-complication.

Thermal stress effects due to radial temperature gradients have been overcome in a simple but ingenious way in a range of wind-tunnel balances produced by the Task Corporation, of Anaheim, California.\* In the absence of the axial constraint introduced by the presence of the axial-force and rolling-moment transducers, the thermal force is "centred" at a point on this axis mid-way between the forward and aft normal and side force sensors. At this point there is no relative movement between the outer frame and the inner cantilever rod of the balance. To avoid responding to the thermal force the axial-force sensor must be placed at this point. In practice this is done by using a pair of sensors placed on the axis symmetrically about this point, the common centre being attached to the outer frame and the other ends to the inner rod. Two rolling-moment sensors are likewise placed, one around each of the axial-force transducers. Such an arrangement not only cancels the effects of radial temperature gradients. It also reduces or eliminates several second order effects, in particular those represented by terms involving the axial-force and rolling-moment in products with the other components. The arrangement is shown in figure 3.39.

Such a scheme is particularly suitable when electrical resistance strain gauges are used as sensors. With piezoelectric strain sensors, temperature compensation can be avoided by grounding the inputs immediately prior to a test. In this way any build-up of charge is removed, and only the transient charges corresponding to the unsteady forces are detected, provided of course the time constant for thermal conduction within the balance is much longer than the test-time.

An example of a different force resolution system, using piezoelectric sensors, is provided by the Cornell Aeronautical Laboratory's type H balance (Martin, Duryea & Stevenson, 1962). This balance, illustrated in figure 3.40, is of relatively large external diameter, and was designed for measurements on bluff bodies - it is correspondingly short in the axial direction. The axial elements  $A_1$ ,  $A_2$  and  $A_3$  are used to measure the axial force-component, the pitching moment about a "horizontal" axis\*\* in the plane containing the "vertical" elements and the yawing moment about a "vertical" axis through the side force element S. The vertical elements  $L_1$  and  $L_2$  provide the normal force and together with the element S, the rolling moment about the axis of the sting. (In practice the natural frequencies of this system, model, balance and sting, were found to be in the critical range as regards the available test-time of the Cornell Aeronautical Laboratory's shock-tunnel. Acceleration-compensation was therefore necessary, but we shall defer a discussion of this until Section 3.343) A similar arrangement has been used at the Technischen Hochschule, Aachen, (Finke & Grönig, 1971).

A third possible arrangement, which could fit a package of rectangular cross-section suitable for lifting-body shapes, is shown in figure 3.41.

The force-resolution systems outlined so far are intended for measuring all six components of the external loading on a model. Frequently fewer components are needed. For example three-component balances are very common. Essentially identical with only the appropriate parts of one of the systems already described, they rely on the assumption that the interaction effects from the unmeasured components are negligible. Three-component balances are normally used to measure normal-force, axial-force and

\* Tracy (1961) attributes the idea to one Robert Davie, but no further reference is given.

\*\* The terms "horizontal" and "vertical" are used for descriptive purposes here; they are accurate for only one particular orientation of the balance.

pitching moment, and for the usual aerodynamic configurations at small angles of yaw, the assumption is reasonable for a well-designed balance. Side-force, yawing moment and rolling moment are rarely measured in isolation. In most cases they are lower in magnitude than the longitudinal components so that even small interactions are likely to introduce significant errors unless they are accounted for - for example, when the ratio of normal to side force-component is say 10:1, a one-per-cent interaction would lead to a 10% error in side-force were it neglected.

The concept of a force-resolution system is not quite so obviously applicable to those single-piece balances which consist of a suitably machined cantilever with appropriately positioned strain sensors. However, strain gauges placed upon the upper and lower surfaces of the beam, perhaps on suitably thinned sections, can with proper electrical connections in a Wheatstone bridge circuit give an output signal proportional to the applied bending moment. By measuring moments about two parallel axes normal to the axis of the cantilever one can infer the normal force and moment referred to an arbitrary axis parallel to the axes of measurement. An appropriate "force-resolution" system for a six-component balance based upon this principle is sketched in figure 3.42.

In each of these systems, the spacing of the measuring sections relative to one another usually depends partly on the space available and partly on the load capacity requirements in relation to the force-transducer sensitivity. The positions of the measuring sections can also have a marked effect on the accuracy. A typical case arises with systems such as that of figure 3.20(b) in which summing and differencing circuits are used to derive the moment and normal-force component from the strains at two essentially similar stations along the beam axis. Effectively the moment and normal-force "transducers" are interactive. There is one point along the axis of the beam, called the moment centre, where the application of a force produces no output from the moment measuring system. If the centre of pressure on a model is far from this moment centre, then the output from the moment (summing) bridge will be large, even for moderate forces. The normal force on the other hand is measured by a differencing bridge, and the signal will depend on the difference between two similar quantities, with a consequent diminution in accuracy. For this reason the balance and model to be tested should be carefully matched. In addition the overall size and mass distribution affect the natural frequencies of the system and this aspect should be borne in mind during design.

A particularly ingenious force-resolution system which makes use of the directional properties of piezoelectric ceramics has been devised for a balance of very compact dimensions, by workers at Cornell Aeronautical Laboratory (see for example, Bogdan, 1967). The aerodynamic force is transmitted to the sting via a coaxial stack of piezoelectric discs as shown in figure 3.43. Some of the discs in this stack are split as shown. The electrode faces are all normal to the axis of the stack and each element is isolated from its neighbours by insulating washers, a central hole through the stack being provided for electrical leads from accelerometers mounted within the model. The stack is held in compression by four screws, so that shear loads can be transmitted. The axes of polarisation of the discs, or disc segments, are so chosen that the pitching moment, yawing moment and axial-force use the parallel or direct sensing mode, while the normal and side-forces and the rolling moment make use of the shear mode. The diameter of the stack of ceramics was about 24 mm (0.96 in) in the prototype 'K' balance, and Bogdan (1967) reports that this balance exhibited good linearity for all components, with linear interactions which were "well-behaved and generally small in magnitude".

### 3.32 Strength and rigidity of the main supports

In conventional wind-tunnels designed for continuous operation it has sometimes been the practice to shield the model and force-balance from overload during the tunnel starting process. In the very short duration flows with which we are concerned this of course is not practicable, and the balance must be built to withstand the starting and stopping loads, which have been reported as being perhaps 5 to 10 times the quasi-steady load in a shock-tunnel (Martin, Duryea & Stevenson, 1962). By "withstand" we imply that significant deflections should not take place, an interpretation which should ensure that the elastic limit is nowhere exceeded in addition to the obvious geometrical constraints which are necessary.

Determining the strength and rigidity of the main support members, the cantilever and the floating frame where one is employed, is a straightforward, if somewhat approximate, stress analysis exercise. The outer frame should occupy a minimum of space, but it must provide adequate attachment points for the

model and the force-transducers as well as being able to transmit the loads from the model without becoming too distorted. It is usually the cantilever or inner rod of the floating frame balance which is the limiting member as far as the load-carrying capacity of the balance is concerned. For this reason, and also to achieve the highest possible rigidity, the inner rod must occupy all the space possible. Since it must be machined to allow room for the transducers and their seatings, the sizes of the force-transducer elements are governed to some extent by the rigidity requirements of this member. Interpreted broadly this applies equally to single-piece balances.

Some means must also be provided for rigidly attaching the cantilever-rod to the main supporting sting. Usually a tapered, keyed joint is used. Although not a critical area as regards balance performance, it is not uncommon for systems to fail at this junction as we explain in the next sub-section.

### 3.33 Attachments

Poor attachments between the component parts of a balance, between the balance and the model and between the balance and the supporting sting can lead to serious deficiencies in the performance of the system as a whole, affecting both the strength and the accuracy. In each case the attachments serve to transmit load. That between the model and the balance for example must be a very close one, whether the attachment is to a floating frame or merely to an extension of the cantilever. Both the latter are structural members which could undergo serious distortions unless they fit closely within the model cavity, and such distortions could result in unwanted interactions between components. A simple, close, push-fit is not of course sufficient to transmit the axial and roll components of the load. In the case of the floating-frame balance, these loads may be transmitted by tightly fitting dowels; a tapered, keyed joint would also be suitable for the simple, cantilever-extension type of fitting. Hysteresis and non-repeatability are the likely results of a poor fit between the model and the balance, or between the balance and the attachment which replaces the model for calibration purposes (see Section 3.6.).

The particular advantages of the balance in which individually constructed force-transducers are assembled are twofold. Firstly closer manufacturing tolerances are usually possible in simple components and rejection is less costly. Secondly, adjustments may be carried out after assembly so as to minimise some of the interactions between components. It is necessary therefore to provide clearances at the points of attachment of the normal and side force elements to the outer frame so that such adjustments can be made.

Hardened steel dowels pressed into burnished holes would be suitable at the other points of attachment, a pair of such pins being necessary at each joint to prevent rotation.

The total load on the model is carried in a relatively small volume at the connection between the balance and the sting-support. This tapered joint reacts bending and shear in two perpendicular planes in addition to the axial and rolling moment loads which are carried by dowels or keys. Tracy (1961) points out that it is at this joint that the limitations arise as regards the lateral force and moment carrying capacity of a balance. Failure may occur in a number of ways. Apart from a straightforward fracture, there may be a bearing failure at the base of the sting, or "bell-mouthing" or cracking at the lip of the socket. Having selected the maximum diameter of the sting on aerodynamic grounds, the only course remaining is to alter the length of the tapered joint. Some compromise has been found necessary since lengthening the joint accentuates the galling of the mating surfaces which results from the inevitable relative motion which takes place under the action of the bending load.

### 3.34 Dynamic considerations

The transient nature of the phenomena being investigated make it essential to consider the dynamic behaviour of the measuring system. We have seen in Chapter 2 that the finite inertia and stiffness imply a set of oscillatory responses to a general transient input at natural frequencies which, for a continuous system, are infinite in number. In practical systems, however, there is always an upper cut-off frequency beyond which the response will be negligibly small, and this cut-off frequency should be above that corresponding to the fastest transient to be resolved. This frequency would also be below the lowest natural frequency of the ideal balance-cum-support system. Unfortunately it is not always possible to approach this ideal closely when designing a multi-component force-balance for use in an impulse tunnel, and one or more of the natural frequencies usually lie in the critical range. In particular, transverse

vibrations of the sting are usually critical. Two basic problems must therefore be faced. How does one design the system so that as few as possible of the characteristic frequencies lie in the critical range, and how does one deal with those remaining few?

The lowest frequency of interest so far as dynamic measurements are concerned, is that associated with the duration  $\Delta t$ , of quasi-steady flow in the tunnel. Where resonant frequencies of the same order occur in the system, they may be manifest as a drift in the mean signal level which is not only difficult to determine, but also may be difficult to recognise for what it is. When resonances with frequencies of order  $(\Delta t)^{-1}$  occur some kind of automatic compensation is essential.

The excitation of the natural modes of the system can occur directly as a result of the onset of the aerodynamic loads to be measured, or indirectly via the supporting system. So far as the former are concerned, the input to the model must be tolerated and the system must be designed to cope. Excitation via the supporting structure can be prevented in most cases by careful design. We shall discuss these topics separately under three headings; design of the supporting system, estimation of the dynamic characteristics of a projected measuring system, and inertia-compensation.

### 3.341 The model-supporting system

The distinguishing feature of an impulse tunnel is the very rapid energy release which precedes the test period. This gives rise to stress waves which are transmitted through the structure of the tunnel and the laboratory floor, and which must be prevented from exciting resonances in the measuring system, at least until the end of the test period. At the same time the measuring system must be isolated from general "mechanical noise", which can emanate from machinery in the laboratory or in adjacent areas, or even from passing traffic.

In essence the support is required to remain stationary during the test period, so that the displacement transmissibility from the tunnel structure and ground to the model must be small. We are concerned in the main with isolating the model from moderately high frequency disturbances, and it is well known that a simple system with a low natural frequency does not transmit such disturbances to any great extent. Although the combined measuring/support system is by no means simple, any mode which has a characteristic frequency widely different from the others can be treated, with a high degree of accuracy, as though it existed in isolation. Thus the design of the supports is a fairly straightforward matter. To obtain a low resonant frequency, a massive support connected via very flexible springs to the tunnel itself or to the ground is needed. Connection to the tunnel has the advantage that the whole of the supporting structure can be housed within the vacuum chamber, and sealing is consequently somewhat easier. However the flexibility of the springs means that adjustments to the mass distribution or the spring tensions may be necessary to set the model at the required attitude, and these must be carried out before sealing and pump-down. Connection to the laboratory floor implies the use of flexible seals - metal bellows are generally used - between the tunnel and the supports, but unless the floor is free of vibration, a double isolation system will be required. Usually vacuum pumps and perhaps other machinery associated with the tunnel are situated nearby, and though they are commonly mounted on vibration isolators for general comfort, the decoupling may not be good enough to allow a rigid connection between the model support and the floor. Pennelegion, Cash and Bedder (1967) have described a system in which the support is firmly connected to the floor of the laboratory, using metal bellows to effect the sealing. A photograph of their system designed for use in a shock-tunnel is reproduced in figure 3.44. An example of a system with flexible connections between the tunnel structure and incidence-arc platforms is shown in figure 3.45 (after Goodchild, 1968).

The response of the "massive support" may be treated separately so long as the natural frequencies of the modes associated with it are widely different from any others. The other coupling terms in the inertia and flexibility matrices are small compared with those associated directly with the massive support, so that they can be neglected, and this group of equations solved separately. To ensure this the constituent parts, which may include the incidence-changing mechanism, must be firmly attached to one another so that they behave as a rigid assembly. It is usually possible to arrange this for all components between the base of the sting and the flexible coupling to the tunnel or ground.

For a step-force input  $F_0$ , which is fairly representative of the starting process in the tunnel, the response of an undamped single degree of freedom system is

$$x(t) = \frac{F_0}{k} [1 - \cos \sqrt{\frac{k}{m}} t] \quad (3.57)$$

so that the displacement  $x(t)$  will remain small as long as  $\sqrt{\frac{k}{m}} t$  is small. The real system will have more than a single degree of freedom, but this equation gives the order of magnitude of the natural frequency that must be achieved. Expanding the cosine term as a power series, we have, using the highest order term only

$$x(t) \approx \frac{F_0}{2m} t^2 \quad (3.58)$$

so that for flows of short duration a large mass  $m$  ensures very little motion during the test period. It is usually necessary to provide stops to limit the total motion, which of course continues after the breakdown of flow.

With longer testing times, say 100 ms or so, the provision of supercritical damping (damping ratio  $\zeta > 1$ ) should be considered. The response to a step force input for such a system is

$$x(t) = \frac{F_0}{k} \left\{ 1 - \frac{e^{-\zeta \omega_n t}}{\sqrt{\zeta^2 - 1}} \cosh [\sqrt{\zeta^2 - 1} \omega_n t + \phi] \right\} \quad (3.59)$$

$$\text{where } \cosh \phi = \zeta \text{ and } \omega_n^2 = k/m.$$

For large damping, say  $\zeta > 3$ , this may be approximated by

$$x(t) = \frac{F_0}{k} \left\{ 1 - e^{-\frac{\omega_n t}{2\zeta}} \left[ 1 + \frac{1}{4\zeta^2} e^{-\frac{(4\zeta^2 - 1)}{2\zeta} \omega_n t} \right] \right\} \quad (3.60)$$

so that for a test time  $\Delta t$ , we require

$$\frac{\omega_n \Delta t}{2\zeta} = \frac{k}{c} \Delta t < 0.01 \quad (3.61)$$

if the displacement of the system during the test is to remain less than 1% of the final equilibrium value for a force  $F_0$ .

### 3.342 Design of the system and estimation of its dynamic characteristics

We have discussed this topic at some length in Chapter 2, and noted that an adequate description of the dynamic behaviour of the system for engineering purposes is provided by a list of those normal mode frequencies which fall within the critical range. Although without a knowledge of the disturbance we are unable to specify to what extent each mode will be excited, this is immaterial, since the pulse-like nature of the input force is such that excitation of any of them is liable to occur and compromise the response of the measuring system unless some kind of "compensation" can be provided. In many cases such compensation is most easily arranged electrically, but this is not always possible. To borrow the terminology of linear control theory, a sub-system is required having a transfer function such that when the input consists of the oscillatory force transducer output, its own output is simply proportional to the force input to be measured. Clearly to design such a sub-system the transfer function of the balance system must be known, and this of course is merely another way of saying that its natural frequencies, and damping constants if there are any, must be known. Unfortunately it is far from easy to design electronic systems which will cope with more than one resonant frequency unless they are very widely spaced, or they all occur in an unwanted band. Occasionally it is possible to filter - for that is what is implied - more than one frequency in the critical band, using "notch" filters, but mutual interference of the filter circuits is often a problem. On the whole the designer should aim to have no more than one resonance in the critical range; those outside the range can be removed by high-pass or low-pass filters as necessary.

In order to estimate the resonant frequencies, the system must first be represented by a manageable number of inertial and flexibility elements as outlined in Chapter 2 (section 2.323). Because the axial motions are generally of much higher frequencies, it is reasonable to treat them as uncoupled from the pitch-plane motions. Having a lumped-parameter representation for each set of motions of the system,

the natural frequencies may be calculated, and in principle adjustments to the system can be made to effect appropriate alterations in the eigenvalues. Any single adjustment of either an inertial element or a stiffness affects all the characteristic frequencies to some extent, and the range of adjustments possible is in most cases very limited.

The major requirements are clear. The balance itself must be very stiff and the model light and "rigid". Since the mass of the model is proportional to its volume, while the aerodynamic forces are proportional to area, small models are something of an advantage, provided aerodynamic sealing is not seriously affected. On the other hand a large model can accommodate a sting of greater cross-section, and this could well be the over-riding criterion, because the most troublesome mode is usually the lowest of those associated with transverse vibration of the sting, behaving as a cantilever with a body attached to its free end. Typically in the range 100 Hz - 500 Hz it is doubtful whether much can be done, within the other constraints on the system, to shift the natural frequency for this mode out of the critical range should it fall within it. Beryllium with a specific stiffness ( $E/\rho$ ) some six times that of steel might be used, thereby raising the natural frequency by a factor of two-and-a-half, but its toxicity makes it necessary to carry out machining under specially-controlled conditions. It is therefore expensive to use, but the additional cost may be offset by the less complicated signal-processing system needed if its use avoids the need for inertia-compensation.

When this resonance cannot be moved out-of-range it must be "tolerated" and efforts concentrated on moving the other resonant frequencies, so that filtering of the single frequency, using a notch filter, can be employed. Even so such a technique is not likely to be successful unless at least several cycles of the remaining frequency occur within the test period. If this is not the case, or when several critical modes exist, one must attempt "acceleration-compensation."

### 3.343 Acceleration-compensation

In principle only those motions having critical frequencies require compensation; any outside the critical range can generally be removed by electronic, low-pass filters. Moreover if, as is usually the case, the transverse vibrations of the sting are critical, then both the pitch-plane and yaw-plane motions will need to be compensated, but so long as interactions are negligible, the axial and roll motions will not, at least on this account. When interactions are not negligible, either those between the force transducers or those between the accelerometers, then full compensation may be necessary. As we saw in Chapter 2, the worst case requires at least a six-component accelerometer-balance, suitable proportions of each accelerometer signal being needed to provide the inertial compensation, and where six force-components are to be measured, a total of 36 coefficients must be determined. In addition, when the force transducer axes and the model reference axes do not coincide, a further 36 coefficients are needed to effect axis transfer, or what amounts to the same thing, to account for the static interactions.

Although it is possible to compensate for the inertia effects, take account of the force interactions and carry out the axis-transfer within one analogue computing system, the setting-up procedure becomes very complex and tedious. It is often more practical to use an analogue computer to provide automatic acceleration-compensation and to carry out the remaining operations as part of the data reduction. An exception to this rule is afforded by those systems in which moments are derived from resistive strain gauges suitably connected in bridge circuits which behave as summing or differencing networks.

The inertia-compensation network can be simplified by a judicious choice of positions for the accelerometers. They should be so placed as to sense only the mode they are to cancel. The best position for each accelerometer, given adequate sensitivity, is close to the force-transducer whose output it is to compensate. In this way the off-diagonal elements of the compensation matrix,  $[g]$  of equation (2.154), should be near zero. With many of the commonly used force resolution arrangements, this argument must be interpreted broadly. For example the pitching moment  $M$  is frequently derived from the responses of two normal force transducers, so that an accelerometer, close to and aligned with one, is likely to respond to the same modes as that near the other. Typical of this arrangement is the three-component, inertia-compensated balance described by Edenfield & Ledford (1962) and illustrated in figure 3.46. The accelerometers are strain-gauged cantilevers having a natural frequency of about 850 Hz; oscillations at 30 - 50 Hz for the normal-force components and at 100 Hz for the axial component were

present in the uncompensated responses. Some typical output signals, taken with models of different mass, are reproduced in figure 3.47, and it can be seen that the compensation has smoothed the responses considerably. However an oscillatory component at about 200 Hz on the normal-force channels remains uncompensated, perhaps because the corresponding mode at the accelerometer positions is in antiphase with the lower modes. A very similar balance utilising piezoelectric force transducer and accelerometers is described by Berry & Hoarau (1964).

Circumstances are often such that an accelerometer has insufficient sensitivity for this optimum position, and it has to be placed at the extremities of the model in order to provide adequate signal-to-noise ratio. In such a position it may respond to other critical modes as well, and these responses must then be cancelled by the introduction of further accelerometer signals. The cross-axis sensitivities of accelerometers, when they are appreciable, must be handled in a similar way. This is the general case referred to already.

An earlier system described by Martin, Duryea & Stevenson (1962), used a system of accelerometers disposed within the model in order to enhance the sensitivity of the system. Their arrangement, reproduced in figure 3.48, is reported to have worked quite well, but as drawn it appears to be misconceived. For example the accelerometer  $a_1$  is claimed to be the only one excited by a rotation about the axis A; however all others except  $a_6$  have centripetal accelerations for such a rotation. It is probable that the upper plane containing the centres of the majority of the accelerometers and the lower plane depicting a typical model planform, are in practice close together, so that such components of acceleration are very small in comparison with the circumferential components used for setting up the compensation summing-networks.

Another inertially-compensated system has been described by Beaussier (1966). This makes use of five of the viscously-damped, bi-axial accelerometers, briefly described in section 3.24, arranged as illustrated in figure 3.49. The component accelerations were obtained by adding or subtracting appropriate outputs as indicated in the figure. A number of other laboratories in the United States are reported to have used inertia-compensated systems, among them Lockheed-Georgia, Douglas Aerophysics Laboratory and Martin-Marietta, Denver, but none has been described in the open-literature to the writer's knowledge.

Determining the proportions and phasing of the compensating signals is an empirical, iterative process, almost impossible to carry out without some kind of automatic computing-aid, usually an analogue-machine. Summing, differencing and scaling units are required at the very least, but in many cases the force-transducers and accelerometers will employ sensors of different kinds, so that impedance-matching circuits will also be necessary. Where amplification of the primary signals is needed, the amplifiers (see section 3.4) will also act as impedance-matching devices, normally providing a voltage output from a low impedance source which is ideal for connection to the input of an analogue computer. So long as there is little damping in the mechanical parts of the measuring system, all signals will be either in phase or in anti-phase, so that summing and differencing units are sufficient; where damping is present, phase-shifting circuits may be needed. Phase-shifting will also occur within the electronic circuits, particularly in filter circuits, and one must ensure that such phase shifts are not serious for frequencies within the critical range, or compensation will be incomplete.

The iterative setting-up procedure is carried out with the aid of a vibration-table or shaker, see, for example, Martin, Duryea & Stevenson (1962), Berry & Hoarau (1964) and Beaussier (1966). The balance is mounted on the table so that excitation occurs along a single axis only. The frequency of this excitation is much lower than any resonances in the measuring system, being of order 10 Hz for most fairly large shakers. As each accelerometer is excited, the proportion of its signal added (algebraically) to each of the force transducer outputs is adjusted to give a minimum output for the combination. The balance is then rotated, and the procedure repeated for each accelerometer in turn. It is usually necessary to go through the cycle several times, and the final settings should automatically take account of any cross-axis sensitivities that the accelerometers possess.

A final check on the efficacy of the system should be made by subjecting the model to step changes in load as described in section 3.6 on Calibration.

### 3.4 Electrical systems for signal generation and processing

It is rare that the output signal produced by a transducer can be fed directly into a recording system; usually some amplification at least is required, and often filtering of noise and unwanted oscillatory components is also necessary before the signal is easily interpreted. It is because such processing is so readily carried out by electronic systems that transducers are used which convert the (mechanical) response under investigation into an electrical analogue. With "active" transducer elements such as piezoelectric devices, no independent energy supply is needed; however impedance matching between the transducer and the following stages, be it amplifier or recorder, is an essential part of the measuring system. On the other hand, "passive" transducers such as piezoresistive strain gauges require an energy source to activate them, and the interaction between the transducer and its energy source may play an important part in the behaviour of the system.

The design of electronic systems is a very sophisticated process, eased somewhat since the replacement of valves and transistors as the basic active elements by the integrated circuit amplifier. It is not our purpose however to enter into the details of the electrical systems which form a vital part of the measuring chain. Rather we hope to bring out the fundamental ideas underlying their use, so that potential sources of error may be avoided or taken into account in the analysis of the results.

Because the characteristics of the different transducers are so dissimilar, so also are the electronic circuits. Resistance strain gauges are essentially low impedance devices, typically 100  $\Omega$  to 1000  $\Omega$  with a negligible reactive component. Piezoelectric gauges, on the other hand, have resistive impedances some ten or so orders of magnitude greater, and their capacitance plays a vital part in their behaviour as we have seen in section 3.21. Again the resistance strain gauge is a d.c. device and is therefore capable of measuring static as well as dynamic displacements; piezoelectric devices can be operated as d.c. devices - or rather at very low frequencies - only if very special precautions are taken. The characteristics of the associated amplifiers thus differ somewhat, and we shall treat them separately.

Because there is almost always an unwanted oscillatory component which forms part of the transient response of the system to the more or less suddenly applied load in an impulse-tunnel, filtering is usually necessary. Such filtering may be fairly straightforward, but when the frequency of the signal to be eliminated lies within the range of interest, some care must be exercised. To some extent alternative techniques are now available in so far as digital recording allows subsequent processing of the data, so that information does not have to be "thrown away" too early. We shall discuss this again in section 3.5.

We have seen that interactions between the force-components are difficult to eliminate entirely. In addition some force-balance techniques involve acceleration-compensation. Some experimenters (Martin, Duryea & Stevenson, 1962) have used an analogue computer to carry out this compensation process. We consider this briefly in section 3.43.

We begin here with a brief discussion of energy sources for resistance strain gauges and the bridge-circuits usually used with them. These have been fully discussed elsewhere (see, for example, Dean & Douglas, 1962, Neubert, 1967, manufacturers' promotional literature) but this review would be somewhat incomplete without some account of these aspects, if only because the requirements for dynamic measurements alleviate to some extent several problems associated with strain-gauge operation in static situations.

#### 3.41 Energy sources and bridge-circuits for resistance strain-gauges

The prime function of the electrical system is to convert the change in resistance of the gauge element or elements into an electrical signal. The simplest way of achieving this is to supply the gauge with an electric current, so that as the resistance changes so also does the potential drop across the gauge. For the change in voltage to be a linear function of resistance change, the current must remain constant, and a simple, but rather wasteful way of meeting this requirement is to use a comparatively large, ballast resistance in series with the gauge, figure 3.50(a). The disadvantage of such an arrangement is that the supply voltage must be much larger than that which appears across the gauge. Constant current sources, in which the current delivered is almost independent of the load, are however available, and these provide a more efficient solution, figure 3.50(b). With this arrangement the change in voltage to be measured appears across the gauge in the presence of the standing voltage. While this is no disadvantage for dynamic measurements, since a.c. coupling can be used, it does make static

calibration more difficult, and static calibration constitutes the chief advantage of the resistance strain gauge. An elegant solution is provided by the circuit of figure 3.50(c), suggested by Frank (1962), though two constant-current sources are required. One of these controls the sensitivity, since the output depends on the current as well as on the change in resistance; the second constant-current source is used to provide an initial balance, so that there is no potential across AB with no strain.

Although a single strain gauge can be used for dynamic measurements in some circumstances, we have noted in our discussion on piezoresistive force transducers that interactions between force components can be eliminated, to first order, in many cases by employing two or four active gauges, and summing or differencing the signals appropriately. Frank (1962) also suggests how these constant-current sources may be used in such circumstances. With two active gauges the dummy resistance position of figure 3.50(c) is occupied by the second gauge, which must change its resistance in the opposite sense to the first. With four active gauges, the circuit of figure 3.50(d) may be used, with adjacent gauges undergoing like changes in resistance, unlike the Wheatstone bridge arrangement. However a system with four active gauges can be used with a single, and less expensive, constant-voltage supply in the usual Wheatstone bridge arrangement, in which case an initially-balanced bridge gives zero output for zero strain. For such a bridge, the open-circuit voltage  $\Delta V$ , appearing at the output terminals is (see figure 3.51)

$$\frac{\Delta V}{V} = \frac{R_2 R_4 - R_1 R_3}{(R_1 + R_4)(R_2 + R_3)} \quad (3.62)$$

assuming that the supply voltage  $V$  remains constant. So long as the measuring circuit connected across the output terminals has a much higher input impedance than the impedance of the bridge, it will measure  $\Delta V$  with little distortion. In the balanced condition,  $\Delta V = 0$  and we shall assume that this is achieved by having all the bridge arms of equal resistance  $R$ . In the unbalanced state, writing  $R_i = R + \delta R_i = R(1+r_i)$  we find

$$\frac{\Delta V}{V} = \frac{(r_2 + r_4) - (r_1 + r_3) + r_2 r_4 - r_1 r_3}{4 + 2(r_1 + r_2 + r_3 + r_4) + (r_1 + r_4)(r_2 + r_3)} \quad (3.63)$$

This equation may be used for a bridge with a single active arm, in which case  $r_2 = r_3 = r_4 = 0$  and

$$\left| \frac{\Delta V}{V} \right| = \frac{1}{4} \frac{\delta R_1}{R} \left[ 1 + \frac{\delta R_1}{2R} \right]^{-1} \quad (3.64)$$

For a semi-conductor gauge with  $G \approx 100$  and the strain limited to a maximum of  $5 \times 10^{-4}$ , non-linearities up to 2½% can arise from the electrical circuit behaviour.

With two arms active, and assuming more or less equal resistance changes, we find for the case  $r_1 = r_3$  and  $r_2 = r_4 = 0$ ,

$$\left| \frac{\Delta V}{V} \right| = \frac{1}{2} \frac{\delta R}{R} \left[ 1 + \frac{\delta R}{2R} \right]^{-1} \quad (3.65)$$

In other words, with opposite arms undergoing the same resistance change we have double the output, with the same non-linearity. On the other hand if a two-active-arm bridge has adjacent arms which change by equal and opposite amounts, say  $r_1 + r_2 = 0$  and  $r_3 = r_4 = 0$ , then

$$\left| \frac{\Delta V}{V} \right| = \frac{1}{2} \frac{\delta R}{R} \left[ 1 + \left( \frac{\delta R}{2R} \right)^2 \right]^{-1} \quad (3.66)$$

and the non-linearity is of second order, so that this arrangement is to be preferred where it is possible.

The four-active-arm bridge, with changes of equal magnitude in all arms, but opposite in sign in adjacent arms, gives

$$\left| \frac{\Delta V}{V} \right| = \frac{\delta R}{R} \quad (3.67)$$

and all non-linearities arising from the circuit arrangements are eliminated, so that this appears to be the best scheme of all. However we have to some extent oversimplified the situation. In our discussion on transducers we pointed out that one of the chief attributes of the four-gauge system was the cancellation of interactions. Thus any one gauge of the four undergoes a strain arising from two sources, that directly due to the load being measured together with a strain from the other components. For one pair of gauges the strains are additive, for the other they are subtractive, so that adjacent arms of the

bridge do not suffer equal and opposite changes in resistance unless they have gauge factors of opposite sign and undergo the same strain. Unless the interactions are large however the non-linearities introduced are unlikely to be serious.

Again equation (3.67) for the four-active-arm bridge cannot be applied to the arrangement of figure 3.20(c) for the normal-force-component bridge, since the gauges at different positions along the cantilever do not experience the same strain. However a simple check shows that the arrangement illustrated eliminates circuit non-linearities also, since the conditions necessary, from equation (3.63),

$$\begin{aligned} r_2 r_4 &= r_1 r_3 \\ r_1 r_4 &= 0 \\ r_2 r_3 &= 0 \end{aligned} \quad (3.68)$$

are all satisfied. So long as the gauges operate within their linear range, the remaining term  $\frac{1}{4}(r_2+r_4-r_1-r_3)$  is proportional to the product of the normal force and the distance between the gauge sections. In fact this particular type of arrangement, in which an anti-symmetrical strain field is utilised, will also lead to a reduction in the non-linearity arising from the resistance-strain relationship of the gauges (equations 3.42, 3.43). This is because all gauges can be of the same (say p-type) material, and the non-linear (Strain)<sup>2</sup> terms tend to cancel in the algebraic sum  $(r_2+r_4-r_1-r_3)$ . Gauges should therefore be chosen from the same batch for any one particular bridge, and the mounting procedures etc., should be as nearly identical as possible. The addition of fixed resistances, either small series resistors or large shunts, in order to provide an initial balance will slightly reduce the effective gauge factors, so that the overall sensitivity and remaining non-linearities must be determined by calibration.

Because the non-linearities of n-type and p-type silicon are of different magnitudes, cancellation is less complete when using a bridge composed of such pairs in a uniform strain field, such as occurs on a simple tension/compression link. In this case the unequal arm bridge suggested by Sanchez & Wright (1962) is superficially attractive. They point out that the non-linearity of the Wheatstone bridge circuit is of opposite sense to that of silicon strain gauges, so that one should be able to improve the linearity by a judicious choice of circuit components. For the single active-gauge in the unequal-arm bridge of figure 3.52(a), the open-circuit output is given by

$$\frac{\Delta V}{V} = \frac{k}{(1+k)^2} \cdot \frac{\delta R}{R} \left[ 1 + \frac{\delta R/R}{(1+k)} \right]^{-1} \quad (3.69)$$

Using equation (3.41), we find

$$\frac{\Delta V}{V} = \frac{k G_1 S}{(1+k)^2} \left\{ 1 + \left( \frac{G_2}{G_1} - \frac{G_1}{(1+k)} \right) S + \dots \right\} \quad (3.70)$$

so that the non-linearity is reduced to second order for  $(1+k) = G_2^2/G_1$ , which is possible when  $G_2 < G_1^2$ . On a tension link the single gauge can of course only be used when the mechanical decoupling of extraneous loads is good. However the interaction due to a bending moment on the link can be reduced by using a pair of identical gauges mounted on opposite faces of the link, but connected in series with one another to form the active arm of a bridge, figure 3.52(b). The fractional change in resistance for the active arm is then

$$\frac{\delta R}{R} = G_1 S + G_2 (S^2 + S_b^2) \quad (3.71)$$

where  $S$  is the strain due to the primary load as before, and  $S_b$  if the strain due to bending. Provided  $S_b^2 \ll S^2$  one may choose  $k$  as for a single gauge. The main disadvantage of these arrangements is that the bridge supply voltage has to be higher, for a given output, by the factor  $(1+k)^2/k$ . Temperature compensation can be provided, if necessary, by using dummy gauges, either unstrained or mounted to take advantage of the Poisson's ratio effect, in the adjacent arm of the bridge. In practice of course the properties of the gauges can only be determined after they have been mounted and aged, so that  $k$  is chosen empirically. In these circumstances one would optimise to give as nearly a linear relation as possible between the input load and the output being recorded, so including the effects of all elements of the measuring chain.

In a multi-component measuring system, several bridge circuits need energising. Financial constraints lead one to investigate the possibility of using a single high-capacity supply for all the

strain gauge bridges. Several problems arise of which the most important are the avoidance of mutual interference via the common supply, the greater difficulty of keeping noise in the power supply within bounds, and (most critical of all) the problem of circuit isolation. If a common power supply is used, both sides of each bridge must be isolated, and in practice this means using differential rather than single-ended input amplifiers. The net saving in cost may be negative! On the whole a separate energy supply should be used for each bridge (Bynum, Ledford & Smotherman, 1970), this having the added advantage that each may be adjusted to a convenient level so that the output can be interpreted in "mechanical units".

### 3.42 Signal amplification

The resolution of a measuring system is largely dependent on the extent to which a signal can be amplified without noise becoming obtrusive. A major factor therefore is the noise level of the system referred to the amplifier input, since analogue signals of the same amplitude as the noise cannot be resolved. As a typical working figure, the resolution may be taken as three times the noise level, and part of the specification of a system is the required signal-to-noise ratio. At the output terminals of any amplifier or impedance matching circuit, the requirements are governed by the data recording system to be adopted, which for transient measurements are fairly restricted in kind. For the longer flow durations, say 10 to 100 ms, galvanometer recorders can be used, though they are by no means ideal. The deflections of such electro-mechanical devices are fairly limited even at moderately high frequencies, and typically a few centimetres deflection requires a driving current of order tens of milliamperes. High quality magnetic tape recorders typically require about one volt maximum. For the faster transients, cathode ray oscilloscopes are very widely used, and instruments are available with sensitivities as high as 1 mm deflection per  $\mu\text{V}$  input, though a figure of 10 mm/mV is more common. As a measuring instrument, the C.R.O. is likely to be superseded by the "transient recorder" which stores information in digital form and requires a minimum signal of amplitude 10 - 50 mV to give "full-scale deflection".

With low impedance devices such as resistance strain gauges no special problems arise in the operational mode. A fairly conventional a.c. coupled voltage amplifier with an input impedance of 100 k $\Omega$  or greater is suitable for use with a C.R.O. or a transient recorder. For bridge circuits in which neither output terminal is grounded, a differential amplifier is needed; alternatively one of these output terminals may be earthed and the bridge supply left floating. Special "transducer amplifiers" are commercially available as "plug-in" units for one range of C.R.O.'s. They have a sensitivity of 10  $\mu\text{V}/\text{div}$  and a noise level of less than 12  $\mu\text{V}$  at the full bandwidth of d.c. to 1 MHz. This noise level can be reduced by limiting the bandwidth. They incorporate a d.c. power supply for energising the transducers, with voltage stabilised to 1%. The differential amplifier provides a common-mode rejection ratio of  $10^5$ , so that power supply ripple which appears at the output terminals of the bridge is largely eliminated. Other general purpose differential amplifiers with similar sensitivities and noise levels are also readily available, so that a realistic resolution, limited by noise, may be taken as about 50  $\mu\text{V}$ , the value assumed in section 3.2244.

For the rather less sensitive vertical-deflection amplifiers of many C.R.O.s, and for the transient recorders, a preamplifier would be necessary. This would of course need to have similar characteristics to those listed above: noise less than about 15  $\mu\text{V}$  - 20  $\mu\text{V}$ , a bandwidth commensurate with the test-time or the fastest transients of interest, a stable gain of up to 100, and a differential input. Again d.c.-coupled amplifiers with such a specification are available; the gain can be fixed and reliance placed on the sensitivity control of the following C.R.O. or transient recorder.

So far we have ignored the requirements of static calibration. The special transducer amplifier mentioned earlier can handle directly-coupled signals, the d.c. drift being less than 10  $\mu\text{V}/\text{h}$  or 0.1 divisions of deflection (whichever is greater) after allowing 1 hour warm-up. Low drift rates are fairly difficult to achieve, and the cost of d.c. amplifiers with this sort of performance is relatively high. Without d.c. amplifiers of course, a static calibration cannot be carried out. We shall discuss the subject of calibration further in section 3.6, but we can note here another approach to the amplification of low-level d.c. signals which avoids the problem of drift. This is to use a carrier-wave amplifier in which the bridge is fed with an alternating current, and the bridge output is used to modulate the amplitude of the carrier-wave. The modulated wave is amplified by a high-gain a.c. amplifier, and then demodulated to produce a voltage proportional to the bridge output which can be used to deflect the C.R.O.

beam or to drive some other suitable recording device. The chief disadvantage of the carrier wave amplifier for transient measurements is its limited bandwidth; the upper frequency is limited to about one-fifth of the carrier-wave frequency. Commercially available systems have carrier-wave frequencies up to about 25 kHz; higher values lead to difficulties which arise from the reactive unbalance of the bridge due to stray capacitance and inductance. Systems using carrier-wave amplifiers of this kind are only likely to be useful where the transients have rise-times somewhat longer than 70  $\mu$ s (for the 25 kHz carrier-wave instrument). Even in these circumstances they may be regarded as more or less obsolete, having been overtaken by the successful development of highly stable d.c. amplifiers which are much simpler to operate.

Piezoelectric transducers have completely different requirements. In order to measure the charge separation which occurs when the piezoelectric material is mechanically strained a measuring circuit must be connected to it. This measuring circuit inevitably draws some current, so that the charge  $Q$ , leaks away. To minimise this leakage the input impedance of the measuring circuit must be made very large. Early approaches to this problem involved the use of special "electrometer valves" in what were referred to as "valve voltmeters". The input impedance of such valves is very high so that negligible current is drawn - less than  $10^{-12}$ A - but they have certain disadvantages. They tend to be sensitive to light and sound and the useful portion of the grid characteristic is fairly small. Used in a simple voltage amplification circuit, figure 3.53, the output signal  $V_{out}$  is a function of the cable capacitance  $C_c$ , and any stray capacitance  $C_s$ , between the input and ground as well as on the range setting capacitance  $C_i$ . Thus

$$V_{out} = \frac{-mQ}{(C_0 + C_c + C_s + C_i)} \quad (3.72)$$

and the cable capacitance  $C_c$ , about 75 pF/m for coaxial cable, has a significant effect on the sensitivity, particularly with quartz transducers for which  $C_0$  is perhaps between 5 pF and 50 pF.

This strong dependence on cable and stray capacitance is circumvented by using the somewhat inaptly named "charge-amplifier". This is effectively an operational amplifier, in which the high input impedance is retained, but strong negative capacitive feedback is employed as illustrated in figure 3.54. Although electrometer-valves can be used, and were in the early versions, modern charge-amplifiers employ high input impedance field effect transistors (FETs) in the input stage; the input impedance is of order  $10^{14}$   $\Omega$ . For such an arrangement it can be shown that the output voltage  $V_{out}$  is given by

$$V_{out} = \frac{-Q}{C_F(1 + \frac{1}{m}) + \frac{C_{in}}{m}} \quad (3.73)$$

where  $C_{in}$  is the total capacitance at the input, including the transducer, cable and any stray capacitance in the wiring, and  $C_F$  is the feedback capacitance, which is assumed to be highly insulating. If the open-loop gain  $-m$ , of the amplifier is very large (in practice  $m > 5 \times 10^4$ ), equation 3.73 reduces to

$$V_{out} = -\frac{Q}{C_F} \quad (3.74)$$

so that a voltage output proportional to the charge  $Q$  is produced. The sensitivity of the amplifier is governed by the magnitude of  $C_F$ , and a number of switchable capacitors are provided in practical circuits (10, 100, ...,  $10^4$  pF). The arrangement gives excellent linearity and is highly stable, with few aging symptoms, unlike the "simple" electrometer-amplifier. The performance is independent of the open-loop gain  $-m$ , so long as it remains very large.

The noise level in commercially available charge-amplifiers is equivalent to less than 0.02 pC at the input, even at maximum sensitivity for which  $C_F = 10$  pF, provided low-noise cables are used. With low signal levels, charge separation within the coaxial cable can be troublesome, since it is indistinguishable from the transducer output. It arises as a result of friction and separation between the inner conductor and its insulator in a coaxial cable. Dynamic loading of the cables occurs very readily in an impulse tunnel and low-noise cables should therefore always be employed. They are sufficiently flexible for most purposes, having an outer diameter of about 2.5 mm, but a rather higher capacitance, up to about 140 pF/m. As we have seen this is unimportant if a charge amplifier is used.

Because the open-loop gain of the amplifier is not infinite a small voltage  $V_{in}$ , exists across the input, so that the charge on the input capacitance  $C_{in}$  tends to leak away through the input resistor  $R_{in}$ , figure 3.55. Because of the feedback loop, the output voltage  $-mV_{in}$  also falls towards zero through  $R_{in}$ , so that the input time constant is approximately  $R_{in}(C_{in} + mC_F)$ . So long as  $R_{in}$  is very large, say  $10^{12}\Omega^*$ , this time constant will be very long, about  $5 \times 10^5$ s for  $m = 50\ 000$  and  $C_F = 10$ pF. However a second time constant also exists; that of the feedback loop itself,  $R_F C_F$ . With good quality capacitors  $R_F > 10^{14}\Omega$ , so that when  $C_F = 10$ pF, this time constant is about 1000 s minimum - it will tend to be larger, since low capacitances have better insulation resistance.

With time constants of this order, "static" measurements are possible, provided drift is not serious - commercially available instruments have drift rates equivalent to 0.03 pC/s. In practical amplifiers, several resistances  $R_F$  having values of perhaps  $10^9$ ,  $10^{11}$  and  $10^{14}$  are provided in parallel with the feedback capacitances. These give control over the time constant and consequently of the lower frequency limit, so that for dynamic measurements, drift presents no problems. In addition a subsequent amplifier stage with potentiometric feedback, giving a continuously variable gain from 1 to 10, is also very useful, and is a feature of some commercial instruments. It enables one to make efficient use of the full-scale span of the data recorder, with a consequent improvement in the reading accuracy.

The discussion so far has been concerned with amplifiers producing a voltage output, so that the following stage, the data recorder, must have a relatively high input impedance. Where galvanometer-recorders are to be used, a driving current is required and in this case a power output stage must be added.

### 3.5 Data recording

A variety of methods has been adopted to record transient data which already exist in electrical analogue form; among the more common are the galvanometer-recorder, the cathode-ray oscilloscope equipped with a camera and the magnetic tape recorder. A magnetic drum-store, as used in digital computers, has also been employed, and in principle magnetic discs and cards might also be utilised. More recently the transient-recorder has become commercially available, and has decided advantages over the other methods, as we shall describe.

The galvanometer-recorder is fundamentally a mirror-galvanometer in combination with a photographic system which records the deflections of the mirror. The galvanometer coil and mirror assembly is suspended in a silicone-oil bath to provide damping. A light beam is focussed, via the mirror, onto a sheet of sensitive paper which is translated in a direction at right angles to that of the beam deflection. Ultra-violet light is used, and the record is developed by exposure to daylight. To obtain a fast response, relatively large input currents are needed, and the paper speed must also be high. The maximum deflection is rarely more than a few centimetres for the faster-responding systems, so that the resolution is very limited. Compared with that of an electronic amplifier and cathode ray oscilloscope, the transfer function of this electro-mechanical system is ill defined, and its effects on the input signal are to this extent uncertain. Although multi-channel systems are available, using several galvanometers recording on a single wide chart, calibration is difficult. Calibration traces can only be recorded sequentially, that is on a length of the paper chart different from that containing the main signal. Since paper is not the most stable of materials, being humidity sensitive and subject to stretching, reading errors are potentially large. The fastest systems have a bandwidth of about 10 kHz and so are only suitable for the longer flow durations. The single-shot nature of an impulse tunnel means that recording has to be initiated by a trigger signal of some kind, derived from an event in the tunnel. The very-high paper speeds,  $\sim 300$  cm/s, needed to provide good time resolution, make it necessary to trigger the drive early, sufficiently early that is, for the paper to attain uniform speed by the time the data signal arrives. A good deal of paper is thereby wasted.

Although probably the cheapest in terms of initial capital cost, galvanometer-recorders are far from ideal for investigating the relatively fast events which occur in most impulse tunnels, and the tedious nature of the subsequent data reduction militates against them.

---

\* For quartz it may be as high as  $10^{13}\Omega$ , for the ceramics a little lower. The importance of cleanliness and the exclusion of moisture should now be clear.

Magnetic tape systems have also been used. Like the galvanometer-recorder the recording medium is in rapid motion; in this case however the recording-head is stationary. Standard high-speed systems are available with facilities for recording simultaneously 7 or 14 channels. The signal-to-noise ratios obtainable with direct analogue recording are usually inadequate, so that frequency-modulated systems are employed. They give excellent signal-to-noise ratios, but the bandwidth is limited to one-fifth of the carrier-wave frequency, which makes them less than ideal for shock-tunnels. The best systems, in which great care is taken to maintain constancy of tape-speed and uniform tension of the tape, are very costly. In order to recover the data, playback is necessary, and this can be done at a speed slower than that of the recording, with a consequent decrease in circuit complexity and saving in cost. Moreover only 2 playback heads are needed, each signal being read in turn together with a single reference signal, say a timing marker. The seven-channel system provides space for six force-components together with such a reference, and the fourteen channel system would be sufficient to include acceleration-compensation signals. However the problem of reading the magnetically-recorded data is not straightforward, a further "transducer-system" being necessary. The obvious methods are to use a cathode-ray or other oscillograph to provide an analogue display or to use an analogue-to-digital converter to provide the record in digital form. Although these read-out devices need not have a bandwidth as large as similar instruments used directly for data recording, and are consequently less costly, they do add further expense to an already costly system. The problems of initiating the record and of providing a calibration signal are similar to those of the galvanometer-recorder.

The direct-display cathode-ray-oscilloscope is a much simpler system, one beam being required for each signal. Either storage oscilloscopes may be used or the transient can be recorded by photographing the display using a stationary film with the C.R.O. operated in the single-shot mode - this is most conveniently done using Polaroid film developed within the camera. With modern wide-band C.R.O.s no problems exist regarding the frequency response, and since calibration signals can be recorded on the same film as the record itself, uncertainties in the gain of the vertical deflection amplifiers, typically 3%, are less important. The horizontal sweep rates are sufficiently accurate in most cases not to require separate timing signals, but these are readily provided if necessary. Triggering the display is accomplished using a prior event in the tunnel, and many instruments have facilities for varying the time between the trigger pulse and the initiation of the sweep. The Polaroid print, roughly full-size, provides an image about 8 cm vertically by 10 cm horizontally. Subsequent data analysis, aided a little by including in the photograph an image of an illuminated graticule which is on, or just in front of the C.R.O. screen, is somewhat tedious. Accuracy is limited by the thickness of the photographed trace, the resulting error being at least 2% from this source alone, and greater when full use is not made of the 8 cm deflection.

To a large extent, all the instruments described so far have been superseded by the introduction of the "transient recorder". This consists in essence of a high-speed analogue-to-digital converter (ADC) backed by a digital store. The incoming data are sampled at a rate that depends upon the size of the store and the setting of the "sweep-time", that is the duration of the record. Typically a 1024-word store is used, but the sweep-time is related to the first 1000 of these words. Thus for a test run of duration  $t$  milliseconds, data are sampled and stored every  $t$  microseconds. Each word commonly has 8 bits, giving a resolution of one part in  $2^8$ , or 0.4%. The input controls are essentially identical to those of a cathode ray oscilloscope. As with the tape-recorder, "playback" can be at any speed, and several output facilities are provided. A digital-to-analogue converter enables the contents of the store to be viewed on a C.R.O. or plotted by an automatic graph-plotter. Digital output is also available for punching tape or cards or for feeding directly to a computer for processing. An internal crystal-controlled oscillator provides the time-base, but where more than one recorder is used, they may all be operated using a single oscillator. In some instruments the store, usually 2024 words in this case, can be shared between two input channels which are sampled alternately, and again the "writing-rate" can be changed part way through the record using pre-adjustable controls. One unique and very useful feature of the transient recorder is its ability to record information received prior to the arrival of the triggering pulse. This somewhat surprising ability is obtained by having the instrument set in the "continuous record" mode. In this mode each time the "end" of the store is reached, it returns to the "beginning" and writes the store anew, erasing as it proceeds. On receiving the trigger signal it

continues to write only for a preset time after the trigger, this time being adjustable from zero up to the sweep-time. In single-shot devices such as impulse-tunnels, this facility has obvious advantages, it no longer being necessary to have prior knowledge of the sequence and precise timing of events in the tunnel in order to set up all the recording instruments.

The other singular advantage of systems having variable playback rate arises from the possibilities afforded for filtering. With galvanometer-recorders and with C.R.O.s, signals must be filtered before recording, if they are to be filtered by any method other than "fairing the trace" by hand. With the transient recorder, and with magnetic tape systems, the signal is stored in such a form that it can be subsequently passed through a filter. It can be "viewed" on a C.R.O. after passing through any one of several filters, or more efficiently through a variable pass-band filter. But another and cheaper approach is also possible. A single filter of well-known characteristics can be used and the playback rate through it can be varied. An analogue C.R.O. display of the filtered signal can be used to optimise the playback rate, in effect obtaining the optimum filter setting.

Although presently costing between  $1\frac{1}{2}$  and perhaps 5 times\* as much per channel as does a C.R.O. plus camera, the gain in accuracy, the ease of operation and subsequent data analysis, and the versatility of the transient recorder as a measuring instrument are advantages well worth the extra cost.

In situations where the flow conditions of interest are known to be relatively steady, and the outputs from the transducers are correspondingly constant, fewer samplings of the data may be adequate. It should be possible to devise switching circuits which would enable up to six signals to be fed alternately into a single transient recorder, and this may provide a less expensive solution to the problem. Although the digital information is handled by a computer no less easily in this case, providing analogue signals for display on a C.R.O. would also require special circuits, and the saving in cost would therefore be reduced.

### 3.6 Calibration techniques

A measuring system can clearly be no more accurate than its calibration allows. Moreover a well-designed and carefully executed calibration procedure can throw up anomalies and deficiencies in the system before it is put into operation, and for this reason some parts at least of these calibration checks should also be carried out at intervals during service.

The general features of any calibration process are well-known and will not be reiterated here. Rather shall we concentrate on those which may be regarded as special to the current problem. The prime function of a calibration is of course to determine the sensitivity of the measuring system as a whole - that is, the relation between the input forces and the output signals which are recorded over the working range of the system. However because our present concern is with transient forces, the dynamic response of the system must also be investigated. There are basically two approaches to dynamic calibration, namely frequency-domain and time-domain calibration. In the former, periodic inputs of known amplitude - usually sinusoidal - are applied to the system, and the responses are recorded as functions of frequency. In the time-domain method, a step or similar transient input is used and the response is recorded in real time. Either or both methods can be employed, but the frequency domain technique is not easily used at high frequencies, except with small systems such as accelerometers. In any case the frequency domain characteristics can be obtained from those in the time domain using Fourier transform techniques, either digital (Bowersox & Carlson, 1957) or analogue (Broome, 1961). The frequency domain characteristics are of most interest when phase-shifts occur between the input and output. On the other hand the time-domain calibration is closely representative of the actual conditions in an impulse tunnel, and for this reason is to be preferred.

In general terms a static calibration, or a quasi-static calibration in the case of piezoelectric devices, is usually regarded as easier to perform and as yielding higher accuracy than a dynamic calibration. The reasons are partly psychological, though until recently static calibrations were

---

\* This wide range is accounted for by different standards of comparison. The lower figure compares a single channel transient recorder with a C.R.O. of similar bandwidth, the higher figure with one of much lower, but generally adequate bandwidth. However for multi-channel systems a single control unit can be used with several storage modules, and the cost ratio is then nearer  $1\frac{1}{2}$  to 2.

inherently more accurate than dynamic, chiefly because meters for measuring a steady voltage output are more precise than the galvanometer-recorders and cathode ray oscilloscopes which were used for measuring transients. With the advent of fast analogue-to-digital converters of high accuracy backed by compact digital stores, this no longer applies, and since it is necessary to calibrate the transient recorder as part of the measuring chain, the dynamic calibration procedure is only slightly more complicated than the static. This is more especially true in an era where the tendency is towards the automatic recording of data. The main extra complication arises in providing known transient loads rather than static loads.

The loading harness must be such that these loads can be applied at known positions in relation to the balance/model geometry, these positions corresponding to those of the aerodynamic loads. At the same time provision must be made for monitoring the output of all the measuring chains simultaneously so that the interactions between components can be determined. There is nothing especially difficult about this. A special loading-sleeve which can be attached to the balance in exactly the same manner as the model would be, is desirable. Transient changes in load are most easily provided by the rapid "unloading" of known weights using a "fused-link" which is burned by discharging a capacitor through it (Martin, Duryea & Stevenson, 1962).

In order to accommodate different amplifiers or for that matter different gain-control settings on the amplifier or recording instrument, the calibration should be in terms of load versus transducer output. This is readily achieved by injecting a known electrical signal into the system in place of the transducer output immediately before or after the calibration load. A comparison of the records then yields the transfer characteristics of the transducer. If the same procedure is adopted with the balance in operation, the effects of drift in the gain of the electrical system can be minimised. The electrical calibrating signal, preferably a step or a square-wave, should be of such amplitude that no controls need be altered in the amplifier/recorder chain, except perhaps to switch the input from "measure" to "calibrate". With piezoelectric transducers a calibrating charge is used with the same capacitance to ground as in the measuring situation - no different or additional cable capacitance need be introduced (Goodchild & Bernstein, 1973). With resistance strain-gauges a voltage from a low-impedance source should be used.

At least one complete calibration should be carried out in the wind-tunnel so that the effectiveness of the sting-support-isolation system can be thoroughly investigated. Resistance strain-gauge systems must be allowed to reach an equilibrium temperature before the calibration sequence is begun, and because calibration is a lengthy procedure, the ambient temperature should be monitored for constancy. Moreover since it is usual to evacuate the impulse tunnel test chamber to facilitate the nozzle starting-process, the effective cooling in the test situation may differ from that during calibration. Where the difference is appreciable in the sense that the calibration change with temperature is important, corrections need to be made, or means provided to calibrate at a raised ambient temperature. A thermo-couple junction could be included within the balance housing as a check on conditions.

The calibration of accelerometers does not strictly arise in the context of force-balance calibration. Where inertia-compensation is found to be necessary, the gain of each accelerometer channel is adjusted empirically as part of the setting-up procedure outlined in section 3.343. The accelerometer-balance per se belongs properly to the chapter on free-flight techniques which follows, and is further discussed there.

CHAPTER 4  
FREE-FLIGHT TECHNIQUES

#### 4.1 Introduction

In this chapter we shall be concerned with methods of acquiring force data based on studies of the motion of models "flying" under laboratory conditions. Although in the present case data are essentially collected at one station while in the ballistic range several measuring stations are used, the method clearly has something in common with those techniques used in ranges. Thus much which is pertinent regarding the acquisition of data may be learned from Ballistic Range Technology (Canning, Seiff & James, 1970). We shall interpret the term "freely flying" fairly liberally so as to include circumstances in which some weak restraint is present. However the essential feature is that some significant motion of the model takes place, and it is from an analysis of this motion that the forces are inferred. With this interpretation we may, with some logic, include in this chapter techniques in which models are pivoted in order to study oscillatory motions.

The main attractions of the free-flight technique lie in its apparent simplicity of conception and the closeness with which the "real geometry" is simulated. In particular the model is potentially free of all extraneous influences from supports, and in consequence premature boundary layer separation and inaccurate representation of the base region are avoided in addition to those problems arising from vibration of the supports.

However to achieve this ideal some penalties have to be paid. To obtain measurable motion, the models must be of low inertia, and yet sufficiently rigid to avoid aeroelastic effects. If the models are expensive to produce, or carry complicated instruments, some means of recovery without damage is necessary. Moreover, unless the general motion which results from a time-dependent force acting on the model is acceptable for analysis, some degree of aerodynamic balancing is needed, and since this balancing relies upon data which the tests themselves are designed to provide, the balancing process is empirical and somewhat tedious.

The initial support and release mechanism is of some importance. It is required to support the model at a specific initial attitude, so that some fine adjustment is desirable. Model release should be rapid, and after release a minimum of aerodynamic and mechanical interference should be present. The process of release should not introduce unknown forces of significance. For example a multiple-thread suspension should be such that all detach at the same "instant" - otherwise rotations of the model may occur during release. When accelerometers are incorporated into the model and cables are used to transmit the output signals to the data recording system, these cables will exert some mechanical constraint. This constraint must be made small. They will also interfere aerodynamically, and to maintain consistency, the cables might be enclosed in a narrow sting, itself supported by very weak springs which limit the total motion and provide a "capture mechanism". Some of the advantages of the free-flight technique are compromised by the method used to collect data in this case.

To a large extent free-flight techniques may be separated into two fairly distinct classes, depending on the nature of the data being collected. Position and attitude versus time are usually collected by a photographic method; frequently straightforward ciné-photography is used. In such cases the models are generally unencumbered by instrumentation, though in at least one laboratory, flashing lamps within the model are used to provide data on a stationary photographic film surrounding the test section (Requardt & Wyborny, 1973).

Acceleration data are obtained directly from accelerometers mounted within the model, and data transmission is usually by cable, though in principle radio telemetry might be used. The basic requirements are rather different so far as the models are concerned and it is convenient to treat the two classes separately. The discussion which follows is organised with this classification in mind, though there is some overlap. Section 4.2 contains an outline of the criteria which govern the overall characteristics, and in particular the inertial characteristics of a model intended for free or partially constrained flight. This is followed by an account of some of the techniques which have been used in the construction of models; inevitably the emphasis is on models of low mass. Included in this section is a brief resumé of methods for determining the inertial properties of the models and adjusting them

to suit particular requirements.

The following section contains brief accounts of systems which have been used to suspend, launch and capture the models.

Section 4.4 is devoted to measuring techniques suitable for use with freely-flying models. The emphasis is on photographic methods of recording the position and attitude of the model as a function of time, though other methods are discussed. Acceleration data depend upon suitable accelerometers being available, and where these cannot be obtained commercially it may be possible to design special instruments in accordance with the principles outlined in Chapter 3.

#### 4.2 Design and manufacture of models

The design of a model depends both on the nature of the tests to be carried out and upon the capabilities of the impulse tunnel and its measuring systems. Specifying the Mach number and the Reynolds number of the tests closely limits the size of the model which may be used in a given tunnel, and the resolution and nature of the measuring system constrains the inertial properties, so limiting the choice of both construction materials and construction methods. Maintaining constant test conditions and achieving measurable motion are conflicting requirements, so that some compromise is necessary. The accuracy of the aerodynamic forces deduced from the measured motion is directly dependent upon an accurate knowledge of the inertial properties, and in many cases these must be adjusted in order to carry out the desired tests. For example to achieve flight at a constant attitude, the centres of mass and of pressure must coincide, but since one object of the tests is to determine the position of the centre of pressure, the centre of mass must be adjustable from test to test in a known way.

In this section we shall attempt to define some of the design parameters and indicate how particular requirements might be met.

##### 4.21 Design criteria

The detailed requirements are slightly different depending upon whether displacements or accelerations are to be measured, but basically the total mass of a freely-flying model should be

- (i) sufficiently low that measurable motion occurs, and
- (ii) large enough for the model to remain within the useful "field of view" during the whole of the available test period.

Just what constitutes a measurable motion depends upon the resolution of the measuring system to be used. However, in general, for any measuring system the larger the quantity to be measured the more accurately can it be determined. In essence this makes the second criterion potentially the more important except in those cases where the forces are so small that it is difficult to achieve models of sufficiently low mass to take full advantage of the useful "field of view".

When photographic recording of the motion is being used this "field of view" may be synonymous with the cross-section of the optical system. However we shall employ the term in a more general sense so that it implies also the extent of the uniform (or near-uniform) flow region. For example when motion of the model takes place in a direction normal to that of the main flow, the diameter of the core of uniform flow may be a more critical dimension than the effective diameter of the optical system. With the optical telemetry system mentioned above (Requardt & Hyborny, 1973) and described in more detail in Section 4.4.12, the "field of view" is limited by the size of the photographic film. When on-board accelerometers are being used the mass of the model may be limited also by the maximum acceleration to which the accelerometers and signal transmission system may be subjected without serious electrical overload or damage occurring.

Making the simplifying assumption for design purposes that under the action of an aerodynamic load  $F$  the acceleration  $\ddot{x}$  of the model of mass  $m$  remains constant during the flow duration  $\Delta t$ , we may write

$$F = m\ddot{x} = \frac{2m\Delta x}{(\Delta t)^2} \quad (4.1)$$

where  $\Delta x$  is the displacement which takes place in time  $\Delta t$ . Writing the aerodynamic force in terms of a force coefficient  $C_F$  based upon a suitable representative area  $S$ , we have

$$\frac{m}{C_F S} = \frac{1}{2} \frac{(q_\infty \Delta t)}{(\Delta r / \Delta t)} \quad (4.2)$$

where  $q_\infty = \frac{1}{2} \rho V^2$  is the dynamic pressure of the relative free stream, which is here assumed to remain constant. The quantity  $m/(C_F S)$  is a ballistic parameter depending upon the properties of the model, while the right hand side of equation (4.2) is a function of the wind tunnel performance, the displacement  $\Delta r$  being interpreted as that appropriate to the "field of view" discussed earlier.

To take full advantage of the performance of any particular wind tunnel the range of values of the right hand side of equation (4.2) which may be achieved in that tunnel should first be computed (ignoring of course any variations in  $q_\infty$  due to the motion of the model). Then with an expected value for the force coefficient, the optimum value of  $m/S$  may be found. The model should then be constructed with a value as close to this as is practicable. Too high a value will result in the displacement being less than the optimum, too low a value implies that the whole of the test time is not used. Some care is needed in interpreting this criterion for design purposes. For example in attempting to measure a lift coefficient  $C_L$  it is of little use ensuring that the model does not fly out of the field of view in the vertical direction if it does so in the horizontal direction during the test time  $\Delta t$ . Thus it is politic to regard  $C_F$  as the total aerodynamic force coefficient - the effect of gravity is small for test durations below about 30 ms and may readily be taken into account for longer times.

We have also tacitly assumed that the model is released without an initial velocity being imparted to it. It is of course possible to launch the model upstream so that it traverses the field of view once in each direction. This technique is suitable for tunnels with relatively long flow durations. The design criteria are slightly more complicated in this case, and we shall defer our discussion of them until Section 4.314.

As we have seen in Chapter 1, short duration hypersonic wind tunnels vary over a very wide range in their performance, both as regards steady flow duration and dynamic pressure level. Taking representative sizes for models the range of forces likely to be encountered in such facilities extends from below 1 N up to perhaps 10 000 N while flow durations are generally in the range below 100 ms though 500 ms are possible in a Ludwieg-tube tunnel. Making the assumption that for reasonably accurate position versus time data the displacement of the model during the test flow duration should be about 10 cm, figure 4.1 has been prepared using equation 4.2. (With other displacements a simple scaling is all that is necessary, since the mass of the model is inversely proportional to the displacement required.) This figure enables one to see at a glance that models of widely different mass are necessary to meet the requirements of different tunnels; some tunnels can accommodate models with masses of order 1 kg while others require very light models with a mass of order tens of grams.

Figure 4.1 also suggests at first sight that the free flight technique is not really suitable for use with tunnels having flow durations less than about 1 millisecond, since the low mass models necessary would be subject to very high accelerations.\* However it must be borne in mind that the chart is drawn for a fixed, fairly large displacement, suitable for collecting displacement data as a function of time. Limiting the displacement by up to two orders of magnitude (to 1 mm) enables a corresponding increase in the mass of the model, though data must now come via accelerometers. Figure 4.1 may be regarded from a different point of view; one in which the force scale is replaced by acceleration such that the ordinate represents displacement. It is re-presented as figure 4.2. The smallest mass that a model may have is governed to some extent by the number and mass of the on-board accelerometers. This is not a serious limitation since accelerometers having a mass of a few grams only are available commercially or may be constructed. The range of accelerations which may be measured is also very wide, extending to values in excess of 10 000 m/s<sup>2</sup>. More important is the method by which data are transmitted to the recording system. Telemetry systems are somewhat complex, particularly multi-component systems. Damage to transmission cables must be avoided, so that the maximum acceleration may be limited on this account. Capture mechanisms are necessary also. A simple net may suffice, but when cables are used it will be necessary to limit the displacement of the model. With a particular limit chosen and the test duration known, the acceleration follows from figure 4.2 and thus for given tunnel operating conditions and model

\* Note that because the chart of figure 4.1 is drawn for constant displacement  $\Delta r$ , lines of constant  $\Delta t$  imply constant acceleration.

configuration the optimum mass may be found. Extreme cases of very small accelerations, corresponding to large mass and in particular to very small displacements are of course equivalent to the force-balance systems discussed in Chapter 3. However one may note that the measurement of small accelerations is associated with instruments of high sensitivity and correspondingly limited frequency response. Relatively long test times are implied. To achieve good measurements at low force levels (of order 1 N, say) in very short duration flows, say of order 1 ms, requires models of low mass (< 0.1 kg) with very weak restraint from cables or supports if such are used. Such models are possible, provided too much is not expected of them. For example, a model intended to measure only three force components (axial force, normal force and pitching moment) is likely to tax the ingenuity of the designer.

It has been implicit in the above discussion that the model is statically stable during its flight; that is, it maintains effectively constant attitude to the oncoming stream so that the force coefficient remains constant. Several factors may affect the static stability in a practical case. A component of velocity normal to that of the oncoming tunnel stream is equivalent to a change of attitude of the model. If the static margin for the configuration under test is a critical function of incidence, the model will not remain at constant attitude. A similar effect can arise as a result of non-uniform stream conditions. Frequently, for example, conical rather than properly contoured nozzles are used to generate the hypersonic flow. Provided the effects are small, they may be taken into account during data analysis, but the effects should be borne in mind during design to ensure they remain acceptably small.

Confining attention to planar motion we may consider the likely magnitudes of what are essentially changes in the test conditions arising as a result of the motion of the model. For this purpose we shall assume the conditions illustrated in figure 4.3 in which the model is shown at an initial incidence  $\alpha_0$  with its centre of mass at  $C_0$ ; at time  $t$  the centre of mass is at  $C_t$ . Axes  $C_0\xi\zeta$  are fixed in the laboratory and the velocity components  $U_B(t)$  and  $W_B(t)$  are respectively parallel to  $C_0\xi$  and  $C_0\zeta$ . The angle  $\epsilon$  represents the local flow direction relative to the laboratory axis  $C_0\xi$  and thus is clearly a function of position  $(\xi, \zeta)$  at least. The incidence  $\alpha(t)$  of the model is given by

$$\alpha(t) = \alpha_0 + \int_0^t \dot{\alpha} dt + \tan^{-1} \left[ \frac{V \sin \epsilon + W_B}{V \cos \epsilon - U_B} \right] \quad (4.3)$$

where  $\dot{\alpha}$  is the pitching rate about an axis normal to the plane  $C_0\xi\zeta$  and the stream velocity  $V$  is a function of position  $(\xi, \zeta)$  and, if the reservoir conditions for the nozzle are changing with time, a function of time also.

The flow conicity will usually be small so that equation (4.3) may be approximated by

$$\alpha(t) = \alpha_0 + \int_0^t \dot{\alpha} dt + \epsilon + \frac{W_B(t)}{V(\xi, \zeta, t)} \quad (4.4)$$

For the derivation of static quantities therefore, the "best" that may be achieved is flight at constant incidence  $\alpha_0$ . Such an achievement however is likely to arise only as a result of a fortuitous cancellation of terms on the right hand side of equation (4.4). For example in a parallel, steady stream, the effect of the pitching might just cancel that due to the vertical velocity  $W_B(t)$ . In practice it is wiser to ensure that each term remains acceptably small, though the fact that the terms  $\epsilon$  and  $W_B/V$  are always of opposite sign does help.

The variations in  $(\epsilon + W_B/V)$  experienced by a model during the test time  $\Delta t$  will depend upon the displacement which takes place and upon the acceleration  $\ddot{z}$ . Thus it is a function of the mass of the model, and so far as  $\epsilon$  is concerned, the characteristics of the wind tunnel.

One may obtain estimates of the possible magnitudes of the terms of equation 4.4. The stream velocity in the test section of a hypersonic tunnel depends largely on the specific stagnation enthalpy  $h_0$ , the specific static enthalpy  $h$  being negligible in comparison. Thus

$$V = \sqrt{2(h_0 - h)} = \sqrt{2h_0} \quad (4.5)$$

For the present estimate it is sufficiently accurate to assume that the test gas is perfect, in which case

$$V = \sqrt{\frac{2\gamma R T_0}{\gamma - 1}} \quad (4.5a)$$

where  $T_0$  is the stagnation temperature,  $R$  is the specific ideal-gas constant and  $\gamma$  the ratio of the principal specific heat-capacities. It is the lower values of  $V$  which are likely to prove critical, so taking  $T_0 = 1400$  K say, and  $\gamma = 1.4$ , we obtain  $V = 1700$  m/s. Again, assuming that the acceleration of the model is constant, the maximum value of the velocity  $W_B$  is given by

$$W_{Bmax} = 2 \frac{\Delta \zeta}{\Delta t}$$

where  $\Delta \zeta$  is the displacement. Using  $\Delta \zeta = 0.20$  m in a time  $\Delta t = 10$  ms, we find

$$\frac{W_{Bmax}}{V} = 1.4^\circ \text{ which is acceptably small, but not perhaps negligible.}$$

A typical conical (uncontoured) nozzle may well have a semi-angle of  $10^\circ$ . The change in flow direction  $\epsilon$  experienced by a model will in practice be somewhat less than the maximum of  $20^\circ$  for such a nozzle, partly because the whole flow is rarely traversed, but also because viscous effects on the nozzle walls considerably reduce the conicity. Nevertheless the change is serious and needs to be taken into account when analysing the results. At the same time the spatial and temporal variations of  $V$  and  $W_B$  may be included in the analysis, but it is clear that conical nozzles are far from ideal for the free-flight technique.

There remains the pitching term  $\int \dot{\theta} dt$  of equation (4.4).

To ensure a low value of pitch during a test, the model should possess a large moment of inertia  $I_{yy}$  about the pitching axis. On the other hand, during the initial tests to determine the position of the centre of mass for static stability, a measurable pitch is required, so that  $I_{yy}$  should not be too large. Since the geometry of the model is determined, and the volume fixed, by aerodynamic considerations such as Reynolds number simulation and tunnel interference, the moment of inertia may only be adjusted by judicious distribution of the already-determined optimum mass. A practical approach in this case might be to use heavy rods as inserts for adjusting the position of the centre of mass during the exploratory tests, subsequently replacing the rod by a hollow cylinder of the same mass and centre of mass position, so increasing the moment of inertia without altering any other parameters.

A large moment of inertia implies of course a small angular acceleration as well as a low angular velocity. In our discussion concerning the derivation of force coefficients we have, so far, made the tacit assumption that quasi-static conditions prevail, and in such cases the largest possible moments of inertia consistent with the geometry and optimum mass should be the design target.

When dynamic derivatives are to be determined, the requirements are somewhat different. The general motion of a freely flying model may be quite complicated, as we saw in Chapter 2. Even when the motion is restricted to one plane, the governing parameters are many. However, if we consider small amplitude motions, we may as a first approximation to the stability of the longitudinal motion of an aircraft or missile-like shape, separate the short period oscillation from the phugoid (see, for example, Milne-Thomson, 1958). The short period motion is then described by

$$I_{yy} \ddot{\theta} = M_\alpha \theta + (M_q + M_\alpha) \dot{\theta} \quad (4.6)$$

In many experiments designed to measure dynamic derivatives the model is pivoted so that it is free to rotate but not translate. This equation may then be modified slightly to take account of spring restraint  $k_\theta$ , and viscous damping  $c$  at the pivot:

$$I_{yy} \ddot{\theta} - (M_q + M_\alpha - c) \dot{\theta} - (M_\alpha - k_\theta) \theta = 0 \quad (4.7)$$

A statically-stable configuration will have  $M_\alpha < 0$ , so that this equation represents an oscillation which is either damped or growing depending upon the sign of the coefficient of  $\dot{\theta}$ , so long as the coefficients are constant. The aerodynamic terms are not constant in general, but to a first approximation we may treat them so. Assuming that the damping is small, the frequency of the oscillations is given approximately by

$$\omega = \sqrt{\frac{k_\theta - M_\alpha}{I_{yy}}} \quad (4.8)$$

so that if a particular number of oscillatory cycles is needed for an accurate analysis, there is an upper

limit on the moment of inertia  $I_{yy}$  for any configuration in a given tunnel.

Thus dynamic stability tests of freely flying or pivoted models require small moments of inertia, while measurements of static coefficients on the other hand need small angular motions and correspondingly high moments of inertia. The experimenter must expect to use different models to carry out the two kinds of test.

It is less easy to be specific about the range of magnitudes of the moment of inertia of a model intended for say, pitching derivative measurements, because the oscillatory motion depends on aerodynamic characteristics which are less "well-behaved" than the aerodynamic forces. Moreover, given the mass, volume and shape of the model, the moment of inertia may in practice be varied only over a small range, since the distribution of mass within the model is controlled partly by the requirement for rigidity and maybe also by the need to mount instruments inside it.

For the unrestrained model, the frequency of pitching oscillations is approximately

$$\omega = \sqrt{\frac{-M'_\alpha}{I_{yy}}} = \left[ \frac{-C_{m_\alpha} q_\infty S \bar{c}}{m \kappa_{yy}^2} \right]^{\frac{1}{2}} \quad (4.9)$$

where  $\bar{c}$  is the moment reference length and  $\kappa_{yy}$  is the radius of gyration about the pitching axis  $C_y$ .

For the model to execute  $n$  oscillations during the test time  $\Delta t$ , we have

$$\Delta t = \frac{2\pi n}{\omega}$$

and if we assume constant linear acceleration and utilise equation (4.2), we obtain

$$\frac{\kappa_{yy}}{\bar{c}} = \frac{0.1125}{n} \sqrt{\frac{-C_{m_\alpha}}{C_F} \frac{\Delta r}{\bar{c}}} \quad (4.10)$$

where  $\Delta r$  is the displacement which occurs.

Even to obtain  $1\frac{1}{2}$  cycles - the minimum number necessary for a "definition" of the oscillation when perhaps only 10 or so data points can be obtained - is difficult. Small, light-weight models, with the mass concentrated well-forward but consistent with them remaining within the field of view, are suggested by equation (4.10). Richards & Enkenhus (1970b) report the use of lead spheres and mercury-filled ping-pong balls embedded in light plastic cones to meet this requirement, but because this condition is difficult to meet, positive restraint in the form of a pivot is often used to prevent translation when rotary derivatives are to be measured.

Once such a pivot is introduced into the configuration it becomes possible to optimise the design, as pointed out by Richards & Clemens (1971). The moment of inertia  $I'_{yy}$ , and the aerodynamic moments of concern, are now those about the pivot. Richards & Clemens consider the case of a pivot which introduces negligible mechanical stiffness and damping (see section 4.322) and note that the number of oscillations\* which take place in a given test time  $\Delta t$  can be increased by increasing  $(-C_{m_\alpha})$  and reducing the moment of inertia  $I'_{yy}$ . The minimum value of  $I'_{yy}$  occurs with the pivot at the centre of mass of the model while  $(-C_{m_\alpha})$  is increased by moving the pivot well forward towards the nose. The optimum position for the pivot as specified by the maximum frequency of oscillation will depend on the external geometry and also on such practical considerations as minimum wall thickness for the model, and the need to distribute within the model the aerodynamic load reacted at the pivot. Clearly also, dynamic stability tests are more easily carried out in tunnels capable of producing high dynamic pressure.

The aerodynamic damping is also of fundamental interest and provides a further design criterion. The fractional damping which occurs during a time  $\Delta t$  is given by

$$\delta = 1 - \exp \left\{ \frac{(M'_\alpha + M'_q) \Delta t}{2 I'_{yy}} \right\} \quad (4.11)$$

\* Although the frequency of oscillations can be increased by introducing a spring restraint, this also introduces mechanical damping. The aerodynamic damping is often very small at hypersonic speeds, so that it is easily obscured by that in the pivot, and becomes difficult to measure (see section 4.322).

so that the damping can also be increased by keeping  $I_{yy}^1$  small and making the aerodynamic damping moments large. An optimum pivot position can also be found for a given model shape, based upon maximising the fractional damping to be measured; in general this position will be different from that based on the frequency criterion.

However Richards & Clemens (1971) show that for cones at least, after making some more or less arbitrary decisions to meet the practical requirements mentioned above, the optimum positions are not critical, in the sense that neither the frequency of oscillation nor the fractional damping varies rapidly with pivot position. For their optimisation study, Newtonian theory was used to give estimates of the aerodynamic derivatives, but when a more accurate theory is available this could of course be used. For some shapes other than simple cones, the concept of an "equivalent cone" might be used to obtain estimates for a design feasibility study. To this extent, their optimisation charts, calculated for cones made of expanded polystyrene, reinforced with aluminium (alloy?), see figure 4.4, may be of more general utility. Although calculated for the particular test conditions of the Longshot tunnel (see Richards & Enkenhus, 1970 a), namely  $\Delta t = 15$  ms, pitot pressure  $p_t = 1$  atm, and free stream velocity  $V = 2200$  m/s, they have been redrawn as figures 4.5(a) and (b) with the scales generalised for other test conditions as suggested by Richards & Enkenhus (1970 b).

It should be emphasised however that in all the discussion so far we have assumed linear aerodynamics, and non-linearities can have a very marked influence on the oscillatory characteristics. Equations such as (4.9) and (4.11) although useful for the design of experiments, may not be adequate for the analysis of the results.

Finally in this section, before we discuss the manufacture of models, it is perhaps pertinent to recall some practical requirements of a rather different kind. When photographic methods are used to determine the displacements, the result is usually a silhouette. To obtain accurate data some reference points or lines are needed on this silhouette. The edges of many shapes are adequate for defining the position of the centre of mass, and in most cases also the incidence in the plane normal to the line-of-sight. There are however some configurations where ambiguity arises - an example is given in Chapter 6 of AGARDograph 138 - and a base pin is then needed to define the axis of the model. Yaw can often be gauged from the apparent profile of the base of the model; for example a circular base will appear semi-elliptic in profile when the model has yawed, and fitting an ellipse yields the angle of yaw. At best this method is approximate, but it can be used to check the occurrence of yaw. An orthogonal viewing system should be used where possible for measurements of yaw, since the resolution is greater by a factor equal to the ratio of model length to base diameter. The roll angle is usually the most difficult to determine, particularly with axially-symmetric shapes. A pair of pins of different length, eccentrically placed in the base of such models, is one simple solution to this problem.

#### 4.22 Manufacture of models

It has been pointed out that the characteristics of the tunnel in which the model is to be flown play a very large part in the determination of the "disposable characteristics" of the model. The manufacturing process must however meet certain needs other than enabling me to control the inertial properties and the location of the centre of mass. For example, in cases in which each model is regarded as disposable, ease and low cost of manufacture are highly desirable. By implication, it must be possible to make several models identical in their external geometry (unless the effectiveness of control surfaces is being measured, when particular changes of shape are desired) in which the position of the centre of mass may be easily adjusted. Accurate reproduction of the surface finish, generally required to be smooth, is also necessary, so that differences in the behaviour of nominally identical models should not occur as a result of uncontrolled changes in the behaviour of the boundary layer. Models must also be rigid and able to withstand the accelerations imposed on them, not only by the quasi-steady test flow, but also by the tunnel starting transients. Accurately calculating the stress distribution in a model subject to transient loading even when its geometry is relatively simple, is far from easy. In practice, one proceeds intuitively. First the potentially weak areas are identified and estimates of the stresses in such regions may be made by fairly crude approximations. For example, one might assume that all the material forward of this region is subject to the acceleration, thereby imposing an inertia load which is reacted by the stress. Stress concentrations at abrupt changes of shape, such as internal holes and

corners, should of course be avoided where possible. When the models are easy and inexpensive to produce, it is feasible to "prove" them by environmental testing.

#### 4.221 Uninstrumented models

For the very light-weight models needed in some tunnels the choice of materials with a sufficiently high strength/mass is very limited. In some early work Geiger (1962) reports the use of balsa wood. He found it far from satisfactory in a number of respects. It is not possible to make balsa wood models having sharply pointed noses nor models with sharp, straight leading edges and the shapes of these edges were not easily maintained, the material being sensitive to temperature and humidity. The difficulties of precise shaping of the model led to non-uniformities which resulted in asymmetric loading in flight and consequently in asymmetric motion of an unpredictable nature. In addition balsa wood proved to be insufficiently rigid and the deflections of the leading edges of a delta wing under aerodynamic loading were thought to have contributed to the asymmetric motion.

Geiger (1962) also used light-weight models made from Isofoam<sup>†</sup> PE-2, a foamed polyurethane plastic of low density. Initially a master model was made from a suitable metal and the female mould was then cast in a room-temperature-curing silicone rubber. The Isofoam is a two-constituent material and provided one of these and the mould are suitably heated, no release agent is required and a tough smooth-surfaced model results. No further details are given by Geiger, but a similar technique is reported by Pennelegion, Cash and Shilling (1967) and their procedure has been followed by workers at the von Kármán Institute, Brussels (see, for example, Enkenhus, Culotta & Krogmann, 1970). The latter used sharp-nosed cones in their tests, the sharp noses being obtained by using aluminium tips. These metallic parts are placed in the female mould, for which an epoxy resin or low-melting-point alloy was used, before the polyurethane is cast. When the plastic has cooled the casting is withdrawn, and the metal tip cemented in place.

Both the team at N.P.L. and that at V.K.I. use Cloce<sup>1\*</sup> GP-2 a foamed polyurethane similar to Isofoam. The foamed plastic has a structure made up of closed cells, so that a smooth outer surface conforming to the shape and surface finish of the mould is obtained. The mould must be insulated so that the heat generated during the foaming action is retained; in some circumstances it may be necessary to heat the mould. Adequate ventilation should also be ensured during the foaming process and the suppliers recommend that this be planned before setting up the foaming operation. The density of the foamed polyurethane is about 30 kg/m<sup>3</sup> (see Table 4.1) and when the mass of the model is reduced by hollowing the casting from the rear a typical model has an unballasted mass of about 15-20 g. The centre of mass is adjusted to the desired position by the addition of small metal or epoxy resin inserts. For proper aerodynamic simulation of the base region, this is closed by a thin sheet of plastic film; polythene or Melinex (Mylar) is suitable. Because the test section of a hypersonic tunnel is evacuated prior to a test, and the plastic film is cemented in place under atmospheric conditions, a small hole in the film is necessary so that the interior of the hollow model may be evacuated. Otherwise the model may burst, since its yield strength is fairly low (see Table 4.1).

Somewhat similar weight models may be made using expanded polystyrene. As supplied by the manufacturer in the form of small beads a fairly dense model is produced. The density may be reduced by pre-expanding the beads. This is done by heating them to about 80°C, the expansion which takes place depending upon how long they are maintained at this temperature. Five minutes is a typical time. The beads are then graded by sieving, and the expanded beads, now of a fairly uniform size, are used to cast the model. A mould, again either of epoxy resin or metal, is filled with the beads and the whole is simply immersed in boiling water for about 15 minutes. Sharp nose-cones or leading-edges are again obtained using metallic pieces cemented to the casting, the correct shapes being ensured by placing them in the mould prior to casting. No releasing agent is required. Again the mass may be reduced by hollowing and the centre of mass position adjusted by the addition of suitable ballast.

<sup>†</sup> Isocyanate Products Inc., 900 Wilmington Road, New Castle, Del., U.S.A.

\* Baxenden Chemical Co.Ltd., Baxenden, Nr. Accrington, Lancs., U.K.

Heavier models may be made from a variety of materials. Simple shapes which are easily and cheaply reproduced by standard methods in the workshop may be of PVC\*, nylon, PTFE (Teflon) or of metals ranging in density from that of magnesium† to that of brass. Somewhat more costly materials such as platinum might also be used. The properties of these and other materials are included in Table 4.1.

In many circumstances the shape of the model may be so intricate that machining from the solid is too costly for several examples to be produced. Often such shapes may be fabricated from small easily-machined components. Some care is needed in fitting the parts together, since poor joins may affect the behaviour of the boundary layer differently in successive examples. An alternative procedure is to use the slip-casting technique as described for the light-weight models, but with an epoxy resin such as Araldite as the casting material. A variety of fillers may be used from powdered aluminium to powdered tungsten to vary the mean density. Alternatively heavy inserts may be used as ballast in a relatively light material. In this way the desired mass, centre of mass position and moments of inertia may be achieved together.

The moments of inertia of a model need to be maximised when angular motion is to be minimised. In such cases the material should be concentrated away from the centre of mass of the model. With very light-weight models, little more can be done than to use hollow models. When the outer geometry necessitates casting techniques, the inserts which are used as ballast to achieve the required total mass should preferably be in the form of hollow cylinders of dense material such as tungsten or brass rather than in the form of rods or homogeneous spheres.

The converse is of course true when large angular motions are required. The mass should be concentrated and the outer shell defining the aerodynamic shape should be of a low-density, rigid material.

#### 4.222 Instrumented Models

The important difference between instrumented and uninstrumented models lies in the provision of good anchorages for the instruments. These instruments may be accelerometers or the components of a telemetry system. In the former case, the accelerometers are usually built onto a rigid sub-frame - an "accelerometer-balance" - which is encased by a model shell of appropriate external geometry and inertial characteristics. The attachments must be rigid so that the accelerometers respond to the motion of the model system as a whole. When accelerometers are placed at the extremities of a model, as they may be to improve the resolution, it is necessary to ensure that the model is very rigid. Otherwise the primary component of an accelerometer's response may prove to be due to flexural vibrations of the model loaded by the mass of the accelerometer! In this connection, Vidal (1956) suggested that a model shell of low-density plastic material may have advantages over a metallic shell, because the internal damping of the material will cause such vibrations to die away more rapidly. The accelerometers must of course be very firmly anchored, so that they respond to the motion of the point to which they are attached.

The disposition of accelerometers is chosen in much the same manner as a force-resolution system (see Chapter 3), except that where large angular velocities are involved, one must exercise particular care (see section 2.21). Thus the early, three-component, accelerometer-balance built at Cornell Aeronautical Laboratory very much resembles a three-component force-balance (see figure 4.11), with one important difference. Where the force-transducers are essentially linkages between the model and its support, the accelerometers are attached only to the model; any supports which are used must be such as not to restrain the motion of the model during the test period. We shall discuss this very important

\* PVC - polyvinylchloride - may be cast, injection-moulded and machined. Depending on the plasticiser used it may be flexible or rigid, though in the rigid form it is fairly brittle. It may also be foamed, and if the mould is first sprayed with PVC a smooth-skinned foam is produced. Unfoamed the relative density is approximately 1.0.

† The surface finish of some metals deteriorates with time due to oxidation. Magnesium is an example of a useful material which does so. In this case oxidation may be prevented by "chromating", that is, soaking for about 90 minutes at room temperature in a solution of sodium dichromate 10%, manganese sulphite 5% and magnesium sulphite 5% by mass in water. The magnesium model should of course be thoroughly clean and free of grease beforehand.

aspect of the design in more detail in section 4.331, but it does have a direct bearing on the design of the "balance" and the surrounding model shell. In the normal operation of an impulse-tunnel, the test chamber is evacuated to a pressure somewhat lower than any pressure which arises during a test, in order to facilitate the tunnel starting-process. If the model is hollow and not sealed, test-time will be lost while the interior is filled. To avoid this loss the model should be sealed, but this seal must be very compliant if it connects the model to a sting-support, and it must also allow access for signal transmission cables from the accelerometers.

Both these signal leads and the supporting harness exert some restraint on the motion. The actual restraining forces will increase with the displacement of the model, so that the relationship between the inertial properties of the model and the stiffness of the restraints must be such that the restraining forces remain a small fraction of the aerodynamic loads. Since the displacements, and hence the restraining forces, are proportional to the square of the time, systems are not readily transferable from one tunnel to another with a longer test period.

Within the overall inertia limits, one must accommodate the accelerometers and the rigid platform to which they and the model shell are attached. The geometry of the latter is fixed by the nature of the tests, and an accelerometer platform for axially-symmetric bodies may be different from one for wing-like shapes in much the same way as the force-balance packages differ from each other. The total volume available for the balance will depend on the size on the test-section, though not so critically as in the case of the completely unrestrained model which traverses the test-section. These factors affect the choice of accelerometers, both as regards their physical size and their sensitivity. The natural frequency requirements, or rather, the usable frequency range, which as we saw in section 3.24 is up to about  $0.3 f_n$  for an undamped instrument, is fixed by the available test time. A realistic requirement is that the maximum usable frequency should be at least ten times the reciprocal of the test time ( $0.3 f_n > 10/\Delta t$ ), and since accelerometer-balance techniques are best suited to short duration flows as we shall see, this calls for transducers with high resonant frequency.

When there is still some choice available within the limits imposed by these global criteria, the designer of an accelerometer-balance may be able to take advantage of other features, such as minimal cross-axis sensitivity or particular internal construction and cable connections as discussed in section 3.24.

In another approach an instrumented model is used to telemeter information to a stationary receiver, thereby avoiding the need for cables and thus of tethers to prevent damage to cables. Although radio FM telemetry has been used to transmit data from pressure and heat transfer sensors on models flown in a wind-tunnel (McDevitt, Harrison & Lockman, 1964) the method has not been used for acceleration data. (Waterfall (1973) mentions such an application for free-flight testing in the atmosphere.) We have referred already to an optical telemetry method developed at D.F.V.L.R., Porz-Wahn, and we shall describe it in more detail in section 4.412. It is only necessary to point out at this stage that the instrument package must comply with the inertial requirements and that the materials from which the outer shell of the model can be made may be determined by the nature of the energy source for the transmission system. For the Porz-Wahn system, an external R.F.-excitation source was used, so that the model shell had to be non-metallic to avoid shielding.

The inertial properties of an instrumented model may be adjusted, when necessary, in the same manner as those of an uninstrumented one, but of course one has a little less control over them because of the presence of the instrument package. In this regard, Requardt & Kabelitz (1971) report that small metallic inserts can be used as ballast for adjustments of the position of the centre of mass, without serious effects on the efficiency of the R.F. energy transfer.

#### 4.23 Determining the physical properties of the model

The physical properties of the model have a very direct bearing on the forces inferred from measurements made during its free flight. Consequently they must be accurately known. The geometric properties can be determined adequately by conventional methods involving micrometers, height gauges etc., but the surface finish is a little more difficult to measure without causing damage. Even very light pressure from a mechanical profile sensor can scratch a highly-polished surface, and an optical technique is preferable where this is regarded as serious. Two such methods are described by Wilkins & Darsow (1959),

but we shall not pursue this aspect any further.

Of rather more direct concern are the mass and the moments and products of inertia, all of which can be determined by fairly conventional methods to within a fraction of one per cent, and the position of the centre of mass which cannot be easily located to better than about 0.02 mm.

Precision balances are widely available which enable the mass of an object to be determined to better than one part in  $10^5$ , which is more than adequate.

The moments of inertia can be found by utilising the principle of the torsional pendulum. The period of oscillation  $\tau$  of such a pendulum is given by

$$\tau = 2\pi \sqrt{\frac{I_{ii} + I_{ii_0}}{k_\theta}} \quad (4.12)$$

where  $k_\theta$  is the torsional stiffness of the suspension,  $I_{ii_0}$  is the moment of inertia of the system without the model, and  $I_{ii}$  is that of the model, both about the torsional axis. The period  $\tau$  may be measured very accurately using a modern electronic chronometer in conjunction with a fixed light source, a photodiode and a reflecting surface on the pendulum platform. To avoid the need for centring the oscillation, the chronometer can be started and stopped by alternate pulses from the photodiode, so that  $\tau$  is indicated directly. To maintain accuracy  $I_{ii_0}$  should be small compared with the moments of inertia of the model, and both  $I_{ii}$  and  $k_\theta$  can be found by timing the periods when accurately-machined, uniform, right circular cylinders or rectangular parallelipeds are placed on the platform.

Often the platform is superfluous. Duryea & Sheeran (1969) describe a simple method in which the model is suspended by three vertical wires, each of length  $\ell$ , which intersect a circle of radius  $R$  with its centre at the centre of mass of the model. The period  $\tau_R$  of small rotational oscillations and the period  $\tau_p$  of small pendulous oscillations are then measured. Since

$$\tau_p = 2\pi \sqrt{\frac{\ell}{g}} \quad \text{and} \quad \tau_R = 2\pi \sqrt{\frac{\ell I_{ii}}{mgR^2}}$$

the moment of inertia  $I_{ii}$  about a vertical axis through the centre of mass can be found from

$$I_{ii} = m \left\{ \frac{\tau_R}{\tau_p} R \right\}^2$$

without having to measure the length  $\ell$  of the wires. Duryea & Sheeran report that a length of 1 m giving a period of about 2 seconds has proved workable.

When the principal axes of inertia of the model are not obvious, it will be necessary to mount the model on the pendulum platform at several angles to the torsion axis in order to determine all six independent elements of the inertia tensor.

The centre of mass of a model may be found with the aid of a modified, equal-arm, laboratory balance (DeRose & Intrieri, 1970). One of the scale-pans is replaced by a plate attached to the balance beam as sketched in figure 4.6(a) at a known distance  $x_1$  from the fulcrum. Bodies of known mass  $m_{\text{tare}}$  are added to the remaining scale-pan to balance the beam. The model is then attached to the plate and the new mass  $m_{\text{tot}}$  needed to effect balance is found. The distance  $x_{\text{c.m.}}$  of the centre of mass of the model from the plate is then given by

$$x_{\text{c.m.}} = x_2 \left\{ \frac{m_{\text{tot}} - m_{\text{tare}}}{m} \right\} - x_1 \quad (4.13)$$

where  $m$  is the mass of the model and  $x_2$  is the distance from the scale-pan to the fulcrum. Again  $x_1$  and  $x_2$  can be found by "calibration", using accurately machined cylinders with known properties. DeRose & Intrieri quote a possible error of 0.025 mm for the method, which although small, may represent a significant fraction of the static margin of a model.

An alternative method is described by Grauer-Carstensen (1971), though he gives the possible error for the system as 0.1 mm. The principle of his method is illustrated in figure 4.6(b). The effective length  $L$  and a calibration of the balance are found using cylinders of known properties as before. The reduced accuracy is probably a consequence of this not being a null-reading device as is the system described earlier.

#### 4.3 Model suspension, launching and capture systems

To make full use of the advantages of the free-flight technique, the model should be completely unencumbered during the test period. The ideal suspension or launching system is therefore one which does not disturb the flow field about the model in any way during the test, and if some initial supporting mechanism has to be withdrawn, it should be done sufficiently rapidly as not to curtail the test time. Moreover the releasing of the model must not result in forces or moments being applied which alter the flight attitude from that desired. By implication it should also be possible to set the initial attitude accurately. A variety of devices has been used ranging from the elaborate to the very simple, and we shall describe some of these in the following paragraphs.

When the models are costly to produce, or carry instruments, it is desirable to recover them without damage. Even with easily reproduced, cheap models it may be necessary to provide a capture mechanism in order to prevent damage to the tunnel and its auxiliary equipment, such as valves, pumps and pressure gauges. We shall consider this problem in a separate sub-section. Where however only partial freedom is allowed the model, so that signal leads, for example, are not severed, the supporting and "capture" mechanism are essentially integral, and so we shall discuss these partially-constrained systems as single entities in section 4.33.

##### 4.31 Suspension and launching systems for unrestrained models

A number of different methods for supporting the model and releasing it at or just prior to the start of the test period have been mentioned in the literature, but few have been described in any detail. The general principle of each is in fact quite simple, and in practice the way in which it is adapted must depend on the detailed construction of the impulse tunnel and its characteristics. Thus for a shock-tunnel with its relatively short test duration, say of order 10 ms or less, the emphasis must be on very rapid release, while for gun-tunnels and "hot-shot" tunnels, where the test times are rather longer, systems which involve a retraction of the support are feasible. For the very much longer quasi-steady flow in a Ludwig-tube tunnel, conditions are not so critical, but where the support has to be retracted, a trigger signal is necessary to initiate the process. This retraction occupies a time of order 10 ms, so that this trigger signal must be derived from an earlier event in the tunnel than the onset of the test flow, in order to avoid losing some of it.

##### 4.311 Simple fracturing-thread supports

The simplest support system, and the one which effects the most rapid release was first described by Geiger\* (1962) and consists of just two nylon threads. When the flow starts, the aerodynamic forces are sufficient to break the threads and sweep them very rapidly away from the model. To ensure success, the multi-stranded threads are first weakened by severing all strands but one, just where they meet the model; in this way no excrescences are left on the surface of the model (see, for example, Pennelegion, Cash & Shilling, 1966).

To avoid a gravitational moment on the model if one thread breaks before the other, the suspension can sometimes be arranged as a single loop which passes inside the model. However so long as the threads break within about one millisecond or so of each other, the rotation of the model will be negligible - a simple order of magnitude calculation suggests less than  $0.01^\circ$ . The initial incidence of the model can be adjusted using a simple lever mechanism as illustrated in figure 4.7. Yaw can be arranged by swivelling the bar to which the threads are attached.

This technique is suitable for use with models of low average density, the weakened threads being sufficiently strong to support the model initially, but not strong enough to withstand the aerodynamic loads, which are proportional to the dynamic pressure and the surface area. Where models of higher

\* He attributes the basic idea to the Naval Ordnance Laboratory, Silver Spring, Md., U.S.A.

average density are necessary to keep the motion within the field of view, one may use fine metallic wires in place of nylon threads. Such wires may be severed or weakened just prior to the onset of flow by pulsing them with a large electric current. An initiating signal from an earlier event in the tunnel is necessary, and because the release is fairly rapid, the method can be used even in shock-tunnels (Stollenwerk, 1966). One possible deficiency is that the heated wires may not elongate equally before breaking. A looped wire, with the fusing link inside the model may overcome the disadvantages in this case, provided of course one has access to the interior of the model.

#### 4.312 A magnetic support and retraction system

A rather more elaborate system is described by Requardt & Kabelitz (1971, 1972). This uses an electro-magnetic support at the end of a long piston, the latter passing through the coil of a second, long-pull, electro-magnet, see figure 4.8. Upon receipt of the trigger signal, the supporting magnet is de-energised and the long-pull magnet is energised. The support is thus withdrawn a distance of 50 mm in a time of about 13 ms. In this case of course, at least a part of the model must be of ferromagnetic material; a thin-walled tube can be used to maintain axial symmetry. The system described by Requardt & Kabelitz was used in conjunction with an optical-telemetry system in which energy for the flash lamp carried within the model was supplied by a radio frequency (RF) oscillator. The steel ring in their system had to be split to avoid complete shielding and the consequent poor coupling between the transmission coil and the secondary, pick-up coil carried within the model (see section 4.412).

#### 4.313 An explosively-retracted system

Although few details appear to have been published, the explosively-retracted platform used with the shock-tunnel at N.A.S.A.-Ames deserves a mention because of its unique feature. Several models could be mounted on the platform and flown simultaneously. To avoid interference, these models were mounted 30 mm or two model lengths apart, whichever was the greater (Kussoy, Stewart & Horstman, 1972). The table was retracted explosively, 2 ms before the start of flow, travelling 160 mm downwards. No time is given for the actual retraction, but the models are said to remain "motionless" until the flow starts; they would fall a distance of about 0.02 mm in 2 ms. The duration of quasi-steady flow in the Ames shock-tunnel is about 20 ms.

#### 4.314 Gun-launching systems

By using some sort of gun, the model may be launched with an initial velocity in the upstream direction. There are two possible reasons for doing this. The most obvious is to achieve a higher relative velocity between the model and the fluid and in this case the velocity at launch will be of fairly large magnitude if it is to be worthwhile. Under these conditions the model will need to be protected by a sabot so that it can be accelerated along the firing tube, and but for the "counter-flow" the technique is basically that of the ballistic range. As such it has been very well described by Carros & DeRose (1970) in AGARDograph 138, and need not concern us here.

The second reason is that one may thereby take advantage of a "very long" test flow duration, and allow the model to traverse the test section twice, once "against" the stream, and once "with" it - we use quotation marks, because of course, the model travels against the stream throughout the test. This method is particularly suitable for use with a Ludwig-tube tunnel in which the quasi-steady flow period may last as long as 500 ms and in many practical tunnels exceeds 100 ms. The models are launched upstream at low velocity, up to perhaps 10 m/s, so that no sabot is needed. The incidence may be adjusted simply by altering the direction in which the model is fired. The actual launch velocity is fairly critical, and must be adjusted according to the dynamic pressure of the test stream and the size and mass of the model, so that maximum use can be made of the available test time without the model passing out of the test region. This test region is synonymous with the aperture of the optical system if one is used to record data.

By way of an example, suppose the initial velocity of the model to be directly upstream, and of magnitude  $U_{B_0}$  relative to the laboratory. Assuming that the aerodynamic drag  $D$  remains constant, we have, following Grauer-Carstensen (1971),

$$U_{B_0}^2 = 2\ddot{\xi} \cdot \Delta\xi = 2 \frac{D}{m} \Delta\xi \quad (4.14)$$

where  $\Delta\xi$  is the horizontal distance travelled in each direction. This must be less than or equal to the effective size of the test area.

The allowable values of the ratio drag/mass are limited by the test time  $\Delta t$  according to

$$\frac{D}{m} = \frac{8\Delta\xi}{(\Delta t)^2} \quad (4.15)$$

while the test time itself must be less than or equal to the value  $(\Delta t)_{\max}$  fixed by the vertical motion arising from lifting and gravitational effects. Thus

$$\begin{aligned} (\Delta t)_{\max}^2 &= \frac{2 \cdot \Delta\xi}{\ddot{\xi}} = \frac{2\Delta\xi}{|g - \frac{L}{m}|} \\ &= \frac{2\Delta\xi}{g \left| 1 - \frac{D}{m} \frac{C_L}{C_D} \right|} \end{aligned} \quad (4.16)$$

Combining these, we find for the limiting case when  $\Delta t = (\Delta t)_{\max}$

$$\frac{D}{mg} = \frac{\pm 4 \cdot \frac{\Delta\xi}{\Delta\xi}}{\left\{ 4 \frac{C_L}{C_D} \frac{\Delta\xi}{\Delta\xi} \pm 1 \right\}} \quad (4.17)$$

where the positive sign is taken if  $mg > L$   
and the negative sign if  $mg < L$ .

In a typical case, the model might be axially-symmetric, so that the average lift is very small. Since for most tunnels  $\Delta\xi = \Delta\xi$ , we find  $D/mg \approx 4$ .

For a test flow duration of 100 ms say, a displacement of about 50 mm x 50 mm would need to be viewed and the initial launch velocity would have to be 2.0 m/s. The size of the viewing windows would in practice need to be somewhat larger to accommodate the finite size of the model. A doubling of the test flow duration results in a doubling of the launch velocity and a quadrupling of the displacement of the same model.

Of course in deriving these values using equation (4.17) we have taken the limiting case  $\Delta t = (\Delta t)_{\max}$ , so that the vertical and horizontal displacements are equal. In many tests this would be unrealistic, and the condition  $\Delta t < (\Delta t)_{\max}$  should be used. If we write  $\Delta t = \lambda(\Delta t)_{\max}$  where  $\lambda < 1$ , equation (4.17) is replaced by

$$\frac{D}{mg} = \frac{\pm \frac{4}{\lambda^2} \frac{\Delta\xi}{\Delta\xi}}{\left\{ \frac{4}{\lambda^2} \frac{C_L}{C_D} \frac{\Delta\xi}{\Delta\xi} \pm 1 \right\}} \quad (4.18)$$

the effect being of course to reduce the vertical displacement  $\Delta\xi$  by the factor  $\lambda^2$ .

The drag  $D$  for any given model is proportional to the dynamic pressure of the stream, so that the mass of the model must be tailored to the tunnel conditions. If the launch velocity is too high, the model will pass out of view upstream, in mid-test, so that vital information is lost; if the launch velocity is too low, the model will pass out of view in the downstream direction before the available test period is over, and the useful displacement will be less than the optimum.

Several practical difficulties arise in attempting to achieve the launch velocity with sufficient accuracy. As we have seen, this velocity is usually low, and might in principle be obtained with the aid of a spring-loaded device. Because the launch takes place into a supersonic stream, any disturbances which arise from the subsequent oscillatory motion of the device should not affect the test stream, but it is possible that the wake behind the model would be affected. The method chosen at D.F.V.L.R.(A.V.A.) - Göttingen (Grauer-Carstensen, 1971) involved a compressed-air gun. A piston is held back by pawls until the flow starts. When the pawls are retracted, the compressed-air drives the piston forward, see figure 4.9. The model is mounted fairly loosely on the face of the piston, which is brought to a stop by an obstruction in the guide tube. The model continues to move forward, but because of friction in releasing the model from its mounting, the launching velocity is not quite equal to the highest velocity

attained by the piston. This latter velocity cannot itself be easily predicted because of friction between the guide tube walls and the piston. The frictional forces between the model and the axial pin upon which it is loosely fitted can be minimised by ensuring that there are no significant lateral loads on the pin. Such loads may be caused when the model enters the supersonic flow. To avoid this possibility, the guide tube can be extended forward so that the model is "released" before it enters the flow. In this case however, it has to pass through the shock-wave which stands ahead of the launch tube, and this introduces a further uncertainty. In addition there is a greater likelihood that the wake behind the model will be disturbed because the launching device is closer to the test area.

Any compromise will depend inevitably on the particular configuration of the tunnel, and the pressures needed in the gun to obtain a particular velocity for the model as it enters the test area will need to be obtained empirically.

#### 4.32 Model capture

In the majority of cases the models are simple, easily reproduced and expendable, so that the emphasis is on the prevention of damage to the tunnel and its auxiliary equipment. For this purpose it is sufficient to deflect the model using a tensioned net, for example a tennis racquet, onto thick foam cushions on the floor of the test section or the dump tank, which absorb its remaining kinetic energy. In some cases the deflection net is unnecessary, the natural trajectory intersecting the foam lining of the tunnel.

Where the model is instrumented, a little more care is needed if the instruments are to be recovered undamaged. The only instrumented, unrestrained model reported so far is the optical-telemetry system of Requardt & Kabelitz (1971, 1972). In the D.F.V.L.R. gun tunnel at Porz-Wahn, the model trajectory intersects the floor of the test-section upon which an "impact cushion" is placed. This cushion absorbs most of the model's kinetic energy; it is then allowed to bounce into a net stretched across the dump tank, though in the latest reports (Requardt & Wyborny (1973) and Wyborny & Requardt (1974)) the net appears to have been replaced by cushions. According to Wyborny (1975)\* this recovery procedure works satisfactorily, and models have been re-used several times.

#### 4.33 Systems providing partial constraint

In some impulse tunnels, usually shock-tunnels, the available test time under certain operating conditions is so short, and the forces are so small, that even with models of very low mass the displacements are too small to be resolved easily with any great accuracy. Nevertheless the imposed accelerations may be significant, so that it is feasible to determine the forces by a direct measurement of these accelerations. The use of accelerometers implies a need for signal transmission and although FM telemetry is feasible, the simpler approach employs cables. To avoid damage to these cables, the total motion of the model, which of course continues after the breakdown of the quasi-steady test flow, must be restricted. Some support and restraint system is therefore necessary, but it must not exert significant forces on the model, or the "accelerometer balance" will give erroneous information, unless the readings are corrected. This of course is "force-compensation", which is the direct analogue of the "acceleration-compensation" discussed in Chapter 3.

In the limiting case that the restraints are vanishingly small, we recover the freely-flying model conditions, so there is some logic in including accelerometer-balance techniques in this Chapter. We shall however, as pointed out earlier, also include a brief reference to partially-restrained models of a different kind. What we have in mind are cases in which the number of degrees of freedom is limited. The reason for employing positive restraints is the incompatibility between the needs for a model with a low moment of inertia but a large mass, so that a useful number of oscillatory cycles can be completed during the test period, but without the model flying out of the "field of view". A typical case, which is very common in wind-tunnel testing at all speeds, is that in which only freedom in pitch is allowed. The pivots which permit the motion may introduce some rotational stiffness and damping, and these will add to the aerodynamic stiffness and damping which are the objects of the measurements. We shall point out methods of minimising and making allowances for these effects in section 4.332.

---

\* private communication

4.331 Weakly-restrained systems

The term "weakly-restrained" is intended to imply that the forces restraining motion are negligibly small, so that the model is essentially in free-flight during the test period. In order to utilise this concept in a particular case, we must be more specific; that is, we must quantify the restraints for that case.

We shall assume that the model is rigid, with accelerometers firmly attached to it, and that it is supported in the tunnel by a system of weak springs. We assume further that these supports can be approximated by idealised, lumped-parameter, linear-spring elements, and that the damping within the supporting system is negligibly small. For a general, lumped-parameter system containing inertia and stiffness elements, we have the equations of motion in the form (see Chapter 2):

$$[M]\{\ddot{x}\} + [K]\{x\} = \{F(t)\} \quad (4.19)$$

where  $\{F(t)\}$  is a column matrix of the aerodynamic forces to be measured. The principle of the accelerometer balance is that  $\{F(t)\}$  can be determined by measuring  $\{\ddot{x}\}$  only and since we assume the model to behave as a single rigid body, so that  $[M]$  is a diagonal matrix, the aerodynamic forces are easily derived if the restraint term  $[K]\{x\}$  is negligibly small in comparison with the other terms of equation (4.19). This can be achieved by making all the elements of  $[K]$  small and, since some will be non-zero, also ensuring that the displacements  $\{x\}$  remain small during the test period. It is because these displacements increase with time, that the accelerometer-balance is only suitable for short-duration flows.

It is relatively easy to ensure, in most cases, that the majority of the static coupling terms - the off-diagonal elements  $k_{ij}$  ( $i \neq j$ ) of  $[K]$  - are near zero, but if some support is to be provided for the model, then the diagonal elements  $k_{ii}$ , will be non-zero. Some contribution to the stiffness will also come from the signal-transmission cables attached to the accelerometers. The question arises: how small must they be in a typical case so that ignoring them is justified?

As such a typical case we shall consider a model having a plane of symmetry  $Cxz$ , set without yaw in a stream so that the only aerodynamic forces acting are in this plane of symmetry. We shall postulate the supporting system illustrated in figure 4.10, the pair of springs of stiffnesses  $k_2$  and  $k_3$  being necessary so that the model may be set at incidence (a torsional spring might be used in place of one of them). For simplicity we shall assume that the line of action of the force in the axial spring, of stiffness  $k_1$ , passes through the centre of mass  $C$ , of the model (which comprises all the moving parts). Conceptually this three-component accelerometer balance is very similar to a three-component force balance. In this case however, the spring elements are not intended to react the load; this is done by the rigid body itself and its acceleration is measured.

The equations of motion for this system, which has three degrees of freedom, are given in a body-fixed coordinate system by Vidal (1956):

$$\begin{aligned} m\ddot{x} + k_1x &= X(t) \\ m\ddot{z} + (k_2 + k_3)z + (a_3k_3 - a_2k_2)\theta &= Z(t) \\ I_{yy}\ddot{\theta} + (a_2^2k_2 + a_3^2k_3)\theta + (a_3k_3 - a_2k_2)z &= M(t) = eZ(t) \end{aligned} \quad (4.20)$$

Here  $X(t)$  is the axial force and  $Z(t)$  is the normal force which acts a distance  $e$  aft of the centre of mass  $C$ . It has also been assumed that the springs exert negligible lateral restraints.

Vidal solves these equations for  $x$ ,  $z$  and  $\theta$ , assuming that  $e$  is constant, in terms of integral functions of the aerodynamic forces  $X(t)$  and  $Z(t)$ . Then making use of the fact that the solution is required for small values of the time only, he differentiates the displacement functions twice to obtain the accelerations as

$$\begin{aligned} \ddot{x} &= \frac{X(t)}{m} - \frac{k_1}{m^2} \int_0^t X(\tau) \cdot (t - \tau) d\tau \\ \ddot{z} &= \frac{Z(t)}{m} - \frac{1}{m} \left\{ \frac{k_2 + k_3}{m} + \frac{e}{I_{yy}} (a_3k_3 - a_2k_2) \right\} \int_0^t Z(\tau) \cdot (t - \tau) d\tau \\ \text{and } \ddot{\theta} &= \frac{eZ(t)}{I_{yy}} - \frac{e}{I_{yy}} \left\{ \frac{a_3k_3 - a_2k_2}{me} + \frac{a_2^2k_2 + a_3^2k_3}{I_{yy}} \right\} \int_0^t Z(\tau) \cdot (t - \tau) d\tau \end{aligned} \quad (4.21)$$

where  $\tau$  is a dummy variable.

Clearly the second term in each of equations (4.21) represents a "correction" accounting for the spring restraints. Because of the integrals it is difficult to determine the forces from measurements of the accelerations. However, the relative magnitudes of the terms can be found by examining, as representative, the case when the forces are constant.

Thus for  $X(t) = X_0$  and  $Z(t) = Z_0$ , we obtain the accelerations as

$$\begin{aligned}\ddot{x} &= \frac{X_0}{m} \left\{ 1 - \frac{k_1}{2m} t^2 \right\} \\ \ddot{z} &= \frac{Z_0}{m} \left\{ 1 - \left[ \frac{k_2 + k_3}{m} + \frac{(a_3 k_3 - a_2 k_2)e}{I_{yy}} \right] \frac{1}{2} t^2 \right\} \\ \text{and } \ddot{\theta} &= \frac{eZ_0}{I_{yy}} \left\{ 1 - \left[ \frac{a_3 k_3 - a_2 k_2}{me} + \frac{a_2^2 k_2 + a_3^2 k_3}{I_{yy}} \right] \frac{1}{2} t^2 \right\}\end{aligned}\quad (4.22).$$

The relative errors are proportional to (time)<sup>2</sup>, so that a system of this nature is best suited to facilities with very short flow duration such as shock-tunnels, where comparatively "stiff" springs might be used. Even so, to keep the relative errors small, the "frequencies"  $\sqrt{k_1/m}$ ,  $\sqrt{(k_2 + k_3)/m}$  etc. should be kept small. At first sight it would seem possible to choose  $a_2$ ,  $a_3$ ,  $k_2$  and  $k_3$  so that the quantities in square brackets are zero. However when this is attempted, we find that the requirement reduces to

$$a_2 = -a_3 = I_{yy}/(me)$$

(with  $k_2$  and  $k_3$  arbitrary); both springs are required to occupy the same position, so that their effects are additive. Clearly this is not a very practical solution, because the incidence is uncontrollable. An alternative approach would appear to be to choose  $(a_3/a_2)$ ,  $(k_3/k_2)$  and  $(ma_2e/I_{yy})$  so that both the error terms in the second and third of equations (4.22) remain small, if non-zero. However within the workable ranges of these ratios, say 0.5 to 2.0, the fractional errors  $(\Delta Z/Z_0)$  and  $(\Delta e/e)$  cannot be reduced significantly together, both being of order  $(k_2 t^2/m)$ . These fractional errors are defined as the ratios of the errors incurred by neglecting the spring restraints to the "true" values. Thus for the case of constant aerodynamic forces, we find

$$\begin{aligned}\frac{\Delta X}{X_0} &= \frac{k_1 t^2}{2m} \\ \frac{\Delta Z}{Z_0} &= \frac{1}{2} t^2 \left\{ \frac{k_2 + k_3}{m} + \frac{(a_3 k_3 - a_2 k_2)e}{I_{yy}} \right\} \\ \text{and} \\ \frac{\Delta e}{e} &= \frac{1}{2} t^2 \left\{ \frac{a_3 k_3 - a_2 k_2}{me} + \frac{a_2^2 k_2 + a_3^2 k_3}{I_{yy}} \right\} - \frac{\Delta Z}{Z_0}\end{aligned}\quad (4.23).$$

The practical case for which  $a_2 k_2 = a_3 k_3$  enables us to estimate some numerical values. Taking as representative a test duration of one millisecond, one would require the frequencies  $\sqrt{k_1/m}$  and  $\sqrt{(k_2 + k_3)/m}$  to be less than about 150 rad/s for the errors to be less than 1%, though because of the presence of the term  $\Delta Z/Z_0$  in the expression for  $\Delta e/e$ , the decoupled pitching frequency  $\sqrt{(a_2 k_2)(a_2 + a_3)/I_{yy}}$ , can be about 200 rad/s for the same fractional error in  $e$ .

For a model of mass 100 g, each of the springs would need a stiffness of order 1N/mm, and  $a_2$  and  $a_3$  should be of the same order as the radius of gyration of the model about the axis  $C_y$ , to keep the errors within 1% during a test of one millisecond duration. This value of the stiffness must of course include the restraining effect of the signal transmission cables.

Accelerometer balance techniques seem to have been initiated and developed at Cornell Aeronautical Laboratory (now Calspan) and several balances have been described in a series of their reports: Vidal (1956); Wittliff & Rudinger (1958); Sheeran & Duryea (1969) and Duryea & Sheeran (1969).

Their first balance (Vidal, 1956) was suspended from the sting-support by sponge-rubber springs of annular shape as shown in figure 4.11. The axial restraint was provided by shearing of the rubber, the normal-motion restraint by tension and compression. For low deflections, rubber behaves approximately as

a weak linear spring; for large deflections, the effective stiffness increases. In this way, it was hoped to obtain negligible restoring forces during a test, but that after the flow breaks down, the rubber would act as a "stop", preventing the model from striking the support. The effective stiffnesses for small displacements were measured and found to be in the range  $1\frac{1}{2}$  to 3 N/mm, which with their model, gave estimated errors of 1 or 2% for a test flow duration of one millisecond.

This balance was never fully tested for several reasons. The initial tests in a shock-tunnel showed that the natural frequencies of the accelerometers were excited by the impact loading, and electronic filtering had to be introduced. While these developments were taking place, the shock-tunnel was modified, giving a test-time of several milliseconds. The errors for the longer test-time would have been unacceptable so that the balance had to be redesigned. It was also realised that the sponge-rubber would allow gas to leak into the evacuated model cavity during the test, a process that would take a time similar to the flow duration.

The redesigned balance, for cone rather than cone-cylinder models is shown in figure 4.12. Advantage was taken of the somewhat larger test chamber of the modified shock-tunnel, as well as the sponge-rubber being replaced by thin (0.125 mm) rubber membranes. The sheet at the rear formed a seal, and both membranes were attached to the hollow, steel sting slightly off-centre to allow for the deflection caused by the weight of the model. The attachment position for the best alignment was found by trial and error. The effective spring constants of the assembled system, which includes the accelerometer signal leads, were given by Wittliff & Rudinger (1958) as:

$$k_1 < 0.7 \text{ N/mm}$$

$$k_2 < 1.8 \text{ N/mm}$$

$$k_3 < 0.9 \text{ N/mm}$$

(using the notation of figure 4.10) and the estimated errors were expected to be less than 5% for the test-time, which proved to be somewhat shorter than the expected 5 ms. The mass of the model was about 200 g.

The thin surgical rubber sheet could not be expected to stop the motion at the end of the test without suffering damage, so separate, hard rubber stops were incorporated into the design. Stops were also provided to prevent rotation, as can be seen in figure 4.12 but these were subsequently removed, because they were suspected of transmitting vibrations of the tunnel structure excited by the bursting of the main diaphragm of the shock-tube.

In some later work at Cornell Aeronautical Laboratory an external support system was adopted (Sheeran & Duryea, 1969). The model, with the accelerometers attached internally was suspended within the test stream by vertical, thin wires, the upper ends of these wires being connected to the tunnel by very compliant, vertical springs. Aerodynamic shielding was provided for these springs, see figure 4.13. The model was virtually unrestrained in the horizontal plane, so that it could accelerate axially, sideways and in yaw. The compliant vertical springs provided very little restraint on the vertical motion, so that the model could pitch, roll and translate vertically, though of course the actual displacements which take place during the test period are small. A separate tether system, which does not make contact until the test period is over, was provided to prevent damage to the signal transmission leads.

#### 4.332 Pivoted systems

Pivoted systems are used essentially to measure dynamic stability derivatives. The measurement of these aerodynamic derivatives was comprehensively reviewed fairly recently by Schueler, Ward & Hodapp (1967) and they included examples of systems used in impulse tunnels. A detailed account here would therefore be superfluous. The following paragraphs are a very brief summary of their review as it pertains to tests in hypersonic impulse tunnels, and the interested reader is referred to their paper for further details.

Partially-restrained systems employing pivots are used to measure the rotary derivatives in pitch, roll or yaw, the unwanted motions being restrained. In particular, translation of the low inertia models must be prevented to keep them within the test volume. In principle one may measure either the applied moments needed to sustain an oscillation at particular frequencies and amplitudes (forced oscillation), or one may follow the motion which occurs following a disturbance.

Whichever of these techniques is used, the pivots and the supports are important parts of the system, while in the second method - the free oscillation technique - some mechanism for introducing a disturbance is also required.

The aerodynamic damping can be fairly small for some kinds of model under hypersonic conditions, and if it is to be measured with any reasonable accuracy the "tare damping" within the balance must be kept small, or alternatively it must be possible to measure it very accurately. Of the available pivot systems, - ball-bearings, elastic flexures, gas-bearings and knife-edges or cones, - the first two types are not generally suitable for use in hypersonic impulse tunnels.

Ball-bearings are capable of supporting large loads, and the amplitude of oscillations is unlimited, both desirable features. However they not only introduce "parasite" inertia into the moving parts of the system, a disadvantage when the flow duration is short, but also the frictional damping is high and somewhat unrepeatably, and "free play" in the bearings is always a potential problem.

Elastic flexures have many advantages. They are rugged, easily manufactured, do not introduce hysteresis or backlash and require no lubrication. Nor do they wear. However the amplitude of any rotational oscillations must be kept small if excessive stresses are to be avoided. The damping in flexural pivot systems is predominantly structural, and though considerably smaller than occurs with ball-bearing pivots, it may nevertheless exceed the aerodynamic damping for some models at hypersonic speeds. An example, reproduced as figure 4.14, of the relative contributions to the damping is given by Schueler, Ward & Hodapp (1967).

The gas-bearing, which uses a thin film of gas at high pressure as a lubricant, has most of the features desirable in a pivot. It is capable of supporting large loads, the amplitude of oscillations is unlimited, and the damping is very low indeed, see figure 4.11. It is however rather more complicated to manufacture and to operate.

Knife-edge pivots, or their three-dimensional equivalents, cone pivots, can also be used. They are conceptually very simple, and almost frictionless, but they must be adjusted carefully and the knife-edge and its seating must be held in contact in some way.

Supporting a pivoted model in the test stream also presents some problems, particularly for cases in which it is desirable to be able to vary the position of the pivotal axis. Two-dimensional configurations are usually supported at the side-walls of the test section (or false side-walls are introduced), only the pitching motion being of interest in these circumstances. Likewise three-dimensional half-models can be mounted on one side-wall, but in both cases wall-interference effects may be serious. Three-dimensional full-span models and axially-symmetric shapes are usually sting-mounted, but the amplitude of oscillation is then limited by kinematic interference between the sting and the base of the model. For large-amplitude oscillations a transverse rod (or strut) has been used by Welsh, Ledford, Ward & Rhudy (1959) in continuous and intermittent supersonic tunnels and they also investigated the interference effects of such a support. Their results suggest that aerodynamic interference is not serious provided that the boundary layer on the model is already turbulent ahead of the support and that the supporting rod is small compared with the model.

We shall conclude this brief discussion by drawing attention to two systems developed since the review by Schueler, Ward & Hodapp (1967) appeared. One uses a knife-edge pivot and the other a gas-bearing pivot.

#### 4.332] A system with a knife-edge pivot

We have already referred in some detail to the work at the von Kármán Institute in Brussels by Richards & Clemens (1971) on the optimum design of cone-shaped models for use in oscillatory tests. Some associated experimental work was also carried out and is more fully reported by Richards & Enkenhus (1970 b).

The cone models were moulded using expanded polystyrene, the tips of the cones being of aluminium alloy, as described in section 4.22. The seating for the knife edge was formed by machining a 90° notch along a steel spindle of diameter 3 mm. This spindle was cemented to an aluminium alloy disc, of thickness 1 mm, which in turn was glued into the partly hollow cone, figure 4.15(a). This metal disc serves to distribute the aerodynamic load through the plastic - without it the load would be concentrated at the contact between the steel spindle and the plastic model - . The contact, between the horizontal knife-

edge provided at the end of a sting support and its seating, was maintained during a test simply by the aerodynamic drag force. The model was held in position at an initial incidence, prior to the test, by a nylon thread attached to the edge of the base and to a support above and behind the model as shown in figure 4.15(b). When the flow starts, the nylon thread breaks and the model is free to perform pitching oscillations about the axis defined by the knife-edge.

The peak amplitudes in the tests reported were about  $14^\circ$ ,  $12^\circ$  and  $8^\circ$  for cones of  $30^\circ$ ,  $15^\circ$  and  $9^\circ$  half-angle respectively, these being possible because of the large cavity in the base of the model. It is not clear what effect this cavity might have on the measurements; Richards and his colleagues do not comment upon it. Certainly the large opening at the rear may be expected to allow the cavity to fill rapidly as the tunnel starts, so that test-time is not lost.

#### 4.3322 A system with a gas-bearing pivot

Ghosh (1973) has described a system using gas-bearing pivots designed for use in the gun tunnel at the University of Southampton. This tunnel has a flow duration typically in the range 25 ms to 35 ms. The model to be tested, either two- or three-dimensional, was mounted between false side-walls in the open jet issuing from a conical nozzle into a large vacuum chamber. A typical model, with its support, is shown in figure 4.16. A spanwise support behind the model passed through the side walls and was linked to a streamwise arm on each side. Both the spanwise and the streamwise parts of the linkage were designed to withstand the aerodynamic loads expected, but because they contributed to the inertia of the moving parts, they were lightened by drilling holes. The spanwise link had to react a torsional load as well as a bending load, so that it had to be made very stiff in torsion to avoid oscillations in this mode which appear as a "pitching motion" to the measuring apparatus. Static balancing was achieved by extensions to the streamwise parts of the linkage. Aerodynamic shielding was provided for the supports.

This model shown in figure 4.16 is itself of some interest. Usually when thin delta wings or similar shapes are to be oscillated about a mean non-zero incidence, a half-model is mounted on a side-wall with a spring restraint to provide trim, which introduces damping which is greater than the aerodynamic damping under hypersonic conditions, as we have already noted. In addition, aerodynamic interference effects arise both from the boundary layer on the side and the inevitable gap between the half-wing and the wall. These effects can be severe at supersonic speeds.

Ghosh (1973) used the double model illustrated in figure 4.16, the upper and lower wings being mirror images of each other. The interference effects present with wall-mounted half-models were avoided, and because the leeward surface of a slender delta wing at incidence in a hypersonic stream is at a very low pressure, the major aerodynamic effects coming from the pressure on the windward side, the two wings did not interfere with each other. Each wing could be at incidence, though the double model was at zero incidence, and no spring was needed to provide longitudinal trim. Moreover the aerodynamic moments were four times those of the half-wing model having the same chord. There is however one serious disadvantage; the moment of inertia about a pitching axis is also considerably larger because of the support linkage needed with the double model. In Ghosh's (1973) model the two wings were linked by thin vertical struts in the low pressure region, and the supporting linkage was attached to these struts.

Although the position of the model and its support was fixed in relation to the side-walls, the chordwise pivot position could be adjusted by translation of the bearings in the streamwise direction, on a track to which the bearing housing was attached.

The two bearings, one either side of the model outside the side-walls, were each designed to carry a transverse load of 12.5 N applied 75 mm from the nearest bearing surface.

The first design, illustrated schematically in figure 4.17(a) was unsuccessful for two reasons, both of which stem from the vacuum environment in which it had to work. The flow of gas from the bearing into the test chamber had to be kept small in order not to upset the test conditions during a tunnel run. Most of this gas supporting the rotor was led from the annular space through a pipe which passed through the wall of the test chamber into the laboratory. However the axial position of the rotor was maintained by radial gas flows from the space (which was more or less at atmospheric pressure) between the journal and the rotor, into the vacuum chamber, through gaps at the thrust faces (see figure 4.17(a)). These flows were of course choked, and an axial instability arose because of the over-expansion. In addition

the rotor tended to spin because the radial clearance was too large. Ghosh attributes this latter deficiency to the use of aluminium alloy for the rotor, which could not be machined to a tolerance sufficiently close to provide the design radial clearance of 0.013 mm. The instability was rectified by increasing the clearance at the thrust faces, thereby increasing the gas flow rate into the vacuum chamber. As a result the pressure in the chamber rose from 2 torr to 12 torr during a tunnel run, and an apparent drift in the model motion was traced to a variable bearing torque arising directly from this transient pressure rise.

In the second design, see figure 4.17(b), Ghosh overcame these difficulties. The "turbine torque", being dependent on the rate of gas flow through the bearing, was reduced by decreasing the radial clearance. The transient nature of this torque was attributed to the fact that the thrust faces were exposed to a changing environment. The rotor of his second system was machined from titanium alloy, lapped and then anodised, using a stainless steel cathode to deposit a thin protective layer which prevented galling of the surface. The radial clearance was 0.009 mm, between the rotor and the bronze journal. Two thrust bearings were shrink-fitted to the rotor in such positions that the thrust faces, which were subsequently lapped, were inside the bearing casing. The Allen screws securing the bronze journals to the casing also served for adjusting the clearance at the thrust faces. The rotor was drilled axially and then plugged with brass inserts, which were drilled and tapped for various attachments, such as the model mounting. Radial holes were also provided to lead the gas from the bearing to atmosphere.

The outer casing, of stainless steel, was a cylindrical shell of bore 28 mm diameter and wall thickness 8.5 mm. A hole, of diameter 3 mm, was drilled in the shell, parallel to the axis, and the ends plugged. Two radial holes through the casing connected this longitudinal passage to the annular spaces used to supply the bearing surfaces with gas through holes of diameter 0.1 mm. One of the radial holes in the casing was plugged, the other was used for the gas feed. A third radial hole was drilled to vent the exhaust gas to atmosphere through the pipe which passed through the wall of the test chamber. Very little gas escaped from the ends of the bearing through the small gap; with the gas supply to the bearings running at its maximum flow rate, the vacuum pumps kept the test chamber at 3 torr, adequate for efficient starting of the hypersonic nozzle.

Stops were provided limiting the incidence to  $\pm 1^\circ$ ; the aerodynamic loads at greater incidences could damage the system. These peak values were measured using a travelling microscope before the system was installed in the tunnel. The initial incidence of the model - the "disturbance" needed in the free-oscillation technique - was adjustable within this maximum range by a very simple device. A thread, attached to a piece of Melinex (Mylar) at one end, was wound on a screw at the other end. The Melinex 'flag' was stuck to the rear of a model simply by pressing it to the surface by hand. The static balance was adjusted so that a very small out-of-balance kept the thread in tension. Winding or unwinding the thread on the screw served to set the initial incidence. When the flow in the tunnel started, the Melinex and thread were swept away, leaving the model free to oscillate in pitch.

The complete assembly is illustrated in figure 4.18, the main bearing housing being a steel casting. The two holes in the brass bushes into which the bearings were fitted, were drilled and lapped in the same operations to ensure good alignment. Filters, having a mesh size of 0.005 mm, were provided in both the gas supply and the exhaust lines. The latter was necessary in case of reverse flow when the bearing was in the vacuum chamber environment but was unpressurised.

At the design gas supply pressure of  $0.55 \text{ MN/m}^2$ , each bearing withstood an axial load of 24.5 N and a transverse load of 14.7 N applied 40 mm beyond the nearest bearing surface. The turbine torque was of order  $10^{-5} \text{ N m}$ , extremely small compared with the aerodynamic moments, the r.m.s. values of which were of order  $0.1 \text{ N m}$  in Ghosh's experiments. The damping in the gas-bearing pivots was measured by suspending a bar pendulum from an attachment at one end of the rotor of one bearing, the other end being connected to the rotor of the second bearing by a rigid bar. The damping proved to be very small and somewhat difficult to measure. However all the measured values gave a damping coefficient in the range  $2\text{-}7 \mu\text{N m s}$ , a few per cent of the expected aerodynamic damping.

Unfortunately fluctuations in the flow direction of the stream issuing from the gun tunnel nozzle, of order  $0.1^\circ$ , made damping measurements impossible, so that the apparatus was not completely proven. The system however showed great promise, and the work is continuing.

#### 4.4 Measuring techniques

Two basic data-gathering processes have been used with freely-flying or weakly-restrained models, the immediate objectives being slightly different in each case. Indeed as we have noted already, it is these objectives which lead to the presence or absence of the weak restraints. In general, the freely-flying model is associated with techniques in which the position and attitude are measured as functions of time, while with the softly-mounted system the accelerations are measured directly by appropriate on-board transducers. In the intermediate, rather special case of the partially-restrained, pivoted system, it is common to measure the displacement along the "free coordinates" as functions of time. The ultimate objective is a determination of the aerodynamic forces and moments on the model.

As we have seen, so long as the restraints exercised by the supports can be kept small, these forces follow directly from the accelerations, but because the accelerometers are fixed in the model, they are referred to body-fixed axes. If the lift and drag are desired, then the relative orientation of the model and the stream are needed. In principle this can be obtained by a double integration of the acceleration data, or by a supplementary measuring system. In either case an accurate time-base is necessary.

When the primary data are in the form of position versus time, the derivation of the forces implies a double-differential. This is not usually a very accurate procedure, though some improvement in the effective accuracy is possible if the form of the governing equations of motion is known (see Section 2.2334). On the whole, the overall errors for both methods are about the same, instrument errors, interactions between the accelerometer outputs and the greater number of discrete elements in the measuring chain being equivalent to the reading errors and the effective double-differentiation processes.

The singular advantage of the free-flight technique, that the simulation is uncompromised by the presence of supports, is further enhanced by the use of optical methods for collecting data. These methods are generally photographic in nature. The relative simplicity of the data recording is paid for by the tedium of the data extraction process. This is often done manually; though semi-automatic systems can be used, complete automation of the film-reading process is likely to be very costly, and not always reliable, because the film reader may not distinguish an image of the model from a smudge or a fingermark! It is somewhat surprising perhaps that more effort has not gone into the development of other methods of data collection and recording. North (1971) has speculated on the possibilities of using digital recording methods, but apart from a pilot study by Clemens (1971), all the free-flight measurements made of displacements in wind-tunnels seem to be based on the exposure of a photographic plate or film. Most of the remainder of this discussion will be concerned therefore with photographic techniques. Clemens's (1971) method, which has a close affinity with those which are readily used with pivoted models, is discussed at the end of section 4.41, together with some of the ideas put forward by North (1971). North also mentions a possible method of measuring velocities directly. His suggestion is described briefly in section 4.42.

The use of an accelerometer balance poses completely different problems, problems which resemble those experienced with force balances. The final section of this Chapter is devoted to accelerometer-balance methods.

##### 4.41 Position and attitude as a function of time.

Specifying the position and attitude of a body implies that we have two frames of reference, one fixed in the body, the other fixed in the laboratory. To derive the forces acting on the body we need to determine the relative positions and orientations of these frames to one another as functions of time, so that a clock is also needed. The most obvious method of obtaining this information is to record photographically the position of the model, at several, known, discrete instants, against a background on which the laboratory-fixed frame is represented. Such a photographic record may be obtained either by a ciné-camera having an appropriate framing rate, or by repeated exposure of a single photographic plate. The latter method requires a light-source of a particular kind, and both techniques are best utilised with special optical arrangements. Each photographic record contains a good deal of information - in some circumstances the planar record can be made to yield fully three-dimensional information regarding the position and orientation of the model. Some of the coordinates however may not be obtainable in this way with a high degree of accuracy, and stereoscopic or, better, orthogonal views may be necessary. We shall consider each of these topics separately in the following sections.

A rather different approach employs a flashing light-source carried aboard the model. The position of the model and its orientation are then inferred from the pattern of dots on an exposed film wrapped around the test section. This optical telemetry system is described in section 4.412.

When the motion is fairly restricted, as it certainly will be in oscillatory tests on pivoted models, it is possible to use a light-occluding system. This potentially accurate method, we shall discuss in section 4.413, together with some of the suggestions of North (1971).

#### 4.411 Photographic methods

The high-speed photographic techniques used to record transient phenomena have a very comprehensive literature. Several textbooks and reviews have been published in the past 25 years or so, and for the most part they cover adequately the procedures needed to obtain position and attitude versus time data for a freely-flying model with a limited range. The best general sources of information are perhaps Chesterman (1951), Jones (1952), Courtney-Pratt (1957), Holder & North (1963) and chapters 6 and 8 of Ballistic Range Technology by Canning, Seiff & James (1970). Holder & North have a very extensive bibliography on photography of the Schlieren image, which is directly relevant to the current problem as we shall see. We shall assume a large part of this literature as "common knowledge" and not go into general detail on such matters as the quality of the windows and of the optical components that is needed to obtain good results. We shall concentrate on those features which are in some sense special to our problem and outline the ways in which data have been successfully acquired.

##### 4.4111 The provision of reference frames

There is nothing especially difficult about the provision of reference frames. We have already discussed the possible need to provide datum lines on the model in section 4.221 on model manufacture; often the silhouetted edge is sufficient. The laboratory-fixed frame should define the vertical direction at least and the direction of flow where this is known. Reading a film record is much easier if both vertical and horizontal reference lines are included within the field. Optical systems commonly involve some magnification, and often some distortion, and the provision of pairs of vertical and of horizontal lines, known distances apart, can be used to measure the magnification and provide a check on distortions. As we shall note later, shadowgraph methods involving back lighting have advantages. The collimated light beam against which the model is silhouetted should be set normal to the plane of the photographic plate, normal to the centre-line of the test-section and also to the test-section windows (though in some circumstances this latter is not possible because the windows are systematically divergent to allow for boundary layer growth on the tunnel walls). Again the provision of pairs of lines, one line of each pair on either side of the test-section, can provide a check on the correct alignment of the optical system.

Although in principle the optical components can always be aligned with more than sufficient accuracy, it is often not convenient to check the alignment immediately before each test. Indeed vibrations of the tunnel arising from the operation of vacuum pumps etc., may make it impractical, since carrying out checks between shutting down the pumps and operating the impulse tunnel may take too long. It is better, in general, to build into the reference system, self-checking devices as mentioned. The various corrections, among which we may list those for imperfect collimation of the light beam, poor alignment of the beam and of the photographic plate, and lack of parallelism of the window surfaces, are obtained simply from the laws of geometric optics (see, for example, Sammonds, 1970).

The fiducial lines themselves may be fine wires or threads stretched across the field of view or hung as plumb lines in the case of vertical references, outside the flow. Alternatively, they may be lines scribed on the windows; in fact a complete square grid may be scribed on a window or otherwise transparent insert in the optical path (Enkenhus, Culotta & Krogmann, 1970). One of these possible arrangements is illustrated in figure 4.19. When front-lit ciné-photography is used, the model may be photographed against a background grid, figure 4.20, such as is used at N.A.S.A.-Ames (Kussoy, Stewart & Horstman, 1972).

One final point should perhaps be made. When the typical impulse tunnel is "fired", the structure vibrates, albeit at low frequency. If the reference markings are attached to the tunnel, they will move during the test. For very short duration tests, this movement is probably insignificant, but it may not be in all cases. Some recording techniques will detect this motion of the reference system, others will not.

#### 4.4112 Optical arrangements

The basic idea of the photographic methods is to obtain a series of images of the model against a reference frame, each exposure of the film being at a known time. In principle all that is required is sufficient light to illuminate either the model or the background so that there is contrast between them. Thus the simple arrangement of figure 4.21 in which a point source provides a conical beam of light against which the model is silhouetted is a cheap, but rather inconvenient method of meeting this basic requirement. The size of the shadow cast by the model on the photographic plate depends on the relative distances of the model and plate from the light source, and so also does the shape of the shadow. A pair of shadows, preferably from orthogonal systems, is necessary to give unambiguous information on the position and orientation of the model. Conical light beams are therefore far from ideal, and only when multiple systems are necessary, such as in a ballistic range, is the saving in total cost appreciable.

The majority of tunnels with which we are concerned are likely to be equipped with a schlieren apparatus for flow visualisation studies, or at least to be in a laboratory where such equipment is available. In these circumstances the best optical arrangement by far is the direct or the focussed shadowgraph. In these well-known arrangements (see, for example, Ladenburg, 1955 or Holder & North, 1963) the light source is situated at the focus of a collimating mirror or lens. For large field optics, a parabolic concave, front-silvered mirror is somewhat cheaper than a lens, because only one surface has to be figured on the former. The parallel beam of light is then arranged to pass through the test-section in a direction perpendicular to the latter's centre line.

In the direct shadowgraph, figure 4.22(a), the film is simply placed perpendicular to the collimated beam. The sharpness of the shadow depends upon how well-collimated the beam is, which in turn depends on the size of the light source. This should be a point source; however the sharpness is limited by diffraction effects at the edges of the model. In the focussed shadowgraph arrangement, figure 4.22(b), a second parabolic mirror (or lens) brings the collimated beam to a focus in the plane K, which would be occupied by a knife edge in the Toepler schlieren system. The image at K may then be focussed onto the film by a lens L. Because of the depth of focus and the refraction which takes place in the non-uniform flow field, particularly in the boundary layer on the model and in the vicinity of curved shock-waves, the focussed system produces an image which is less sharp generally than that of the direct shadowgraph. However the direct system has a fixed magnification of unity, while the focussed system can be designed to accommodate a convenient film size.

Moreover in high-enthalpy, hypersonic flows, there are often self-luminous regions. The photographic plate in the direct shadowgraph is directly exposed to the flow field, and will therefore be fogged; stray light will have a similar effect. In the focussed system, an aperture plate can be introduced at the focal plane K to exclude almost all the stray light while allowing the wanted beam to pass unhindered. Apart from its properties as a selective attenuator, the focussed system also enables one to control the sensitivity. The shadowgraph sensitivity is ideally zero when the object plane which is focussed on the film coincides with the flight path of the model. If the film is moved either towards or away from the focussing optic, the sensitivity is increased. In regions of high density gradient, such as near the nose of a bluff body, severe optical distortion of the flow field can occur, and the edges of the model become blurred. To obtain results from which the position of the model is to be measured, the system should be adjusted for minimum sensitivity. When the flight path of the model deviates considerably from a plane normal to the collimated beam, changes in sensitivity may cause interpretive difficulties.

Unless the motion is confined to a known plane, a pair of optical systems is needed to define completely the motion of the model. Two separate arrangements can be used, but the timing of the exposures must be synchronised in some way. It is however also possible to employ a single light source and mirrors so arranged, see figure 4.23 for one example, that two images are formed on the same exposure of a single film, each from a different viewpoint. Such an arrangement has been used in a ballistic range, where each film undergoes a single exposure only. It could probably be used with a high-speed ciné camera, in spite of the small frame size; and the multiple-exposure, single plate technique may be easily adapted if one is prepared to use a larger plate to maintain the advantage of a large image.

Finally, one may note that even when ciné-photography is used there are obvious advantages in using the focussed shadowgraph apparatus with its collimated light beam. The alternative front-lit photographs are more difficult to interpret because of parallax, though this can be diminished by using a narrow angle, long-focus lens, provided the field of view is sufficient.

#### 4.4113 Light sources

The light source must provide sufficient illumination to expose the film and be of short enough effective duration that the image of the model is not blurred in the film because of the relative motion between them. In some cases the duration of the exposure is controlled by a shutter with either a continuous source of light or with one of extended duration; in other circumstances the film is exposed by a series of discrete light pulses. In free-flight testing in impulse tunnels, the model does not move at the very high speeds typical of those in a ballistic range, and so the problem of "stopping the motion" is comparatively simple. Typical model speeds in a wind tunnel will be less than 100 m/s, with the critical cases occurring at the highest speeds near the end of a test. If we suppose that the minimum test time for which the free-flight technique is useful is about 5 ms, then an exposure of effective duration 2.5  $\mu$ s (that is 0.05% of the total test time) would enable the position near the end of a test, where the speed is about twice the mean value, to be resolved to within 0.1% of the total path travelled. Since light sources of sub-microsecond duration are available with intensities adequate for exposing fairly ordinary photographic emulsions, these requirements are not difficult to meet. We have of course assumed that the film is stationary. Fast ciné cameras, in which the film transport speed is high, impose more extreme conditions; these are sometimes met, at least in part, by compensating mechanisms within the camera.

The light source must satisfy additional requirements, the nature of which depends on the particular photographic recording technique to be used. With general ciné photography the model and the background reference frame are lit from the front, so that a source of fairly general illumination is required. If the camera is fitted with a suitable high-speed shutter, the light source may be continuous, or of a duration spanning the total test time. The particular advantage of a flash of extended duration is that it can be of higher intensity than a continuous source without the need for cooling. With front lighting, maximum contrast is achieved by using a dark, non-reflective background and a reflective model. The edges of curved reflective models are sometimes not well-defined in this method, but markings on the model can be used to define its attitude. Of course when the background is dark and non-reflective, the reference markings defining the spatial coordinate system must be reflective.

When the shadowgraph arrangement is used, the source size must be small and its position determinate (Holder & North, 1963). The shadowgraph method can be used both with multiple-frame ciné photography and with multiple exposures of a single photographic plate. These techniques will be considered separately in the following sections; here we shall merely note that in the second method the number of exposures of the plate is limited to about ten or so. The need in this case, then, is for ten or so flashes, each of short duration, and spaced at controllable intervals of time.

High-intensity sparks are suitable light sources in this case. A number of such light sources is described in the voluminous literature (see, for example, Holder & North, 1963; Carrus, 1970), though these are designed for single-shot operation. The particular difficulty usually encountered is caused by the conflicting requirements of high intensity and short duration. The former is achieved by storing a large amount of electrical energy in a capacitor, which is then discharged across the gap between a pair of electrodes. The stored energy,  $\frac{1}{2}CV^2$ , can be increased by increasing the capacitance  $C$ , and the voltage  $V$ . However, large capacitance and the ability to withstand high potentials are both achieved by increasing the physical size of the capacitor. This results in a corresponding increase in the dimensions of the inductance loop formed by the discharge circuit, and thus in the characteristic discharge time of the circuit.

When a repetitive spark is required, it is necessary that the last spark (the weakest) be sufficiently intense to expose the film and the stored energy be released in discrete, roughly equal quantities. A system is commercially available (from Ernest Turner Electrical Instruments Ltd., High Wycombe, England) which in conjunction with a suitable spark gap provides a series of 100 flashes at rates

between 10 kHz and 20 kHz. North (1970) reports that the flashes are intense enough to expose fully a schlieren image 25 mm in diameter at 18 kHz, so that the system can be used with a high speed ciné camera, the firing rate being modified if necessary, and synchronised with the framing rate. The same manufacturers also produce a control unit (North, 1970) which provides for up to 11 firings of a single spark gap. Each firing of the argon-jet, spark light-source (Holder & North, 1963) is of duration 0.2  $\mu$ s (time above half amplitude), and these firings can be arbitrarily spaced at preset times so that the images are roughly equally spaced on the photographic record. Although the use of a laminar flow of argon from one electrode to the other results in a flash of slightly longer duration than can be obtained with a simple air gap, the argon-jet performs the very useful function of stabilising the position of the spark discharge at the focus of the collimating mirror.

The light-source in both cases is controlled by a hydrogen thyratron operated with 10 kV on its anode. The large storage capacitor (20  $\mu$ F) runs down only about 15% for a series of 100 firings, and can be charged slowly between tunnel runs.

An alternative approach would be to use 10 or so different sources, with auxiliary optical systems focussing an image of each onto a single aperture. This is not only rather complicated and space-consuming, but can be less reliable in triggering, because the spark gaps may fire in sympathy as a result of photo-ionisation.

The laser as a light source has some unparalleled attributes. As a monochromatic source it can be used with an appropriate filter to exclude unwanted light such as arises from flow luminosity. As a coherent beam it may be used in such a way that three-dimensional pictures can be reconstructed from the negatives produced. The light from a pulsed laser can also be of very short duration, of order 10 ns. Unfortunately the "pumping action" must be started several hundred microseconds before the peak light is required, and the actual exposure must be controlled by a supplementary shutter - usually a Kerr cell is used. The transmission factor of a Kerr cell is low, about 20 - 30% depending on the wavelength of the light. For the repetitive light flashes needed in the current application, a continuous laser (or one of extended duration) would need to be used with a shutter. The high initial cost, additional safety precautions and the need to maintain exceptionally clean optical surfaces for high quality results, militate against using them except in special circumstances. It is also not clear how multiple exposures of a single plate would affect the images.

#### 4.4114 Ciné-photography

The ability to cover a large angular field and the relative familiarity of the equipment are the two chief advantages of ciné photography. With the short duration flows typical of an impulse tunnel, these advantages are less important, the first because the field of view to be covered is relatively restricted and the second because the high speed camera needed is generally less familiar than the domestic variety.

They also have important disadvantages. The sharpness of the image is affected by the motion of the film as well as of the model, an important consideration when the position of the image is to be measured. The camera has to be accelerated to full speed rapidly, triggered by an event in the sequence of operations which initiate an impulse tunnel run. Any malfunction in other sequencing or recording equipment associated with the tunnel, which holds up the firing procedure, can lead to much film being wasted.

However, suitable high-speed framing cameras are widely available commercially and little development work is needed to make use of them. If they are used with a synchronised, short-duration, flash light-source, in place of a shutter and continuous source, the blurring of the image can be much reduced. For relatively long duration tests, say greater than 10 ms, the large number of frames obtained compensates to some extent for the small frame size of the very high-speed cameras, typically 16 mm for framing rates in excess of 5 kHz. Where possible the larger, 35 mm, format should be chosen. In some cases, the highest speeds available with the 35 mm camera result in pictures of half-frame or even quarter-frame height. When the motion of the model is "known" approximately, the camera can be arranged so that the full width of the film is used.

The major deficiencies of the ciné technique result from the need to "set zeros" on the film reader for each frame. This leads to random indexing errors. In addition the frequency of the repetitive light source, or the framing rate of a shutter-controlled camera, cannot be relied upon for accuracy so that timing marks have to be placed on the edges of the film. The time of exposure of each frame is arrived at by interpolation between these timing marks, and again errors may be incurred due to non-uniform motion of the film, or non-uniform stretching of the base material during filming or processing.

Ciné-photography has been very successfully used for studying the motion of freely-flying models in conventional high-speed tunnels (Dayman, 1966) with cameras having framing rates up to 5 kHz. These techniques, with the addition of proper sequencing to start the camera so that it attains full speed at the start of the test period, can be adapted directly for use in impulse tunnels in which the flow duration exceeds about 5 ms. Horstman & Kussoy (1967) have reported data obtained in the shock tunnel at S.A.-Ames using two standard, 16 mm high-speed ciné cameras operating at only 500 frames per second, the test duration implied by their results being about 24 ms. One camera was used simply to monitor the extent to which the models yawed, the other was used to film the motion in the longitudinal plane. The models were flown in the longitudinally trimmed condition, the angle of trim being obtained in a series of exploratory tests, so that only linear displacements needed to be measured. The dozen or so data points were sufficient to determine the ratio lift/drag to within  $\pm 5\%$ . Higher framing rates than 5 kHz are desirable when the motion must be more closely defined, such as near the amplitude peaks of an oscillatory motion. Richards & Enkenhus (1970 b) have used a repetitive spark system, operable at up to 8 kHz, with a shadowgraph optical arrangement and a high-speed, 16 mm ciné camera from which the rotating prism had been removed. This was done because the maximum framing rate of the camera was too low at 1600 Hz. The short-duration sparks ( $< 1 \mu\text{s}$ ) were so spaced as to separate the frames, the picture height being of course smaller, the higher the flash rate. Figure 4.24 shows a strip of film obtained for a cone, supported on a horizontal knife edge, oscillating in pitch in the Longshot tunnel at the von Kármán Institute in Brussels (Richards & Clemens, 1971). The restricted picture height was unimportant in this case, because the motion of the model was partially constrained. In these tests the spark repetition rate was 5 kHz and the flow duration 15 - 20 ms (Enkenhus, Richards & Culotta, 1971). Measurements of the pitch angle  $\theta$  were made from enlargements of each frame; the results of one test are illustrated in figure 4.25. The theoretical curve which appears in this figure was obtained by integrating the relevant equation of motion using assumed values of the aerodynamic derivatives. These derivatives were adjusted until a good fit to the measured data was obtained, the fit being gauged subjectively.

#### 4.4115 Multiple-exposure of a single plate

The typically small format of the ciné-film frame leads to poor spatial resolution, and further errors are introduced in indexing from frame to frame. Both can be avoided by recording the motion of the model on a single, large-format, photographic plate or film, exposed several times during the test. The need to synchronise a camera is also avoided, and the exposures need no longer be made at equally spaced intervals of time.

In principle a reflective model can be lit from the front, so that with a dark, non-reflecting background, only an image of the model is exposed with each flash, and the number of exposures is limited only because stray light produces fogging of the film. This method was employed by Kinslow & Potter (1963) in a continuous tunnel, more than thirty images being recorded. The light from a continuous 1 kW projector lamp was modulated by a "shutter" consisting of a disc with holes drilled near its periphery. The disc was rotated at high speed to give flash rates up to 1 kHz. To achieve success, a wide aperture lens is necessary to collect the limited amount of light reflected from the model. Attempts to use this method in the high enthalpy flow of a typical impulse tunnel have been unsuccessful (Richards & Clemens, 1971) because the flow luminosity quickly overexposes the film. Appropriately coloured light - perhaps from a laser - together with a suitable filter may overcome this difficulty.

It may also be overcome by using back-lighting in a shadowgraph arrangement. The aperture in a focussed shadowgraph system need be no larger than the image of the light source, so that general light from the flow field causes little exposure of the film. In the direct shadowgraph, the effects of flow luminosity can be much diminished by increasing the distance between the test section and the photographic plate; the intensity of the collimated beam is little affected, but that of the unwanted

light falls inversely as the square of the distance from the source. (As the distance between the model and the film is increased, however, so also are errors due to the finite size of the light source.)

On the other hand, the number of exposures is strictly limited when back-lighting is employed. At each exposure, only that part of the film in the shadow of the model is unaffected, so that after a certain number of exposures the film becomes saturated. Suppose that  $N$  exposures are made during a test. If, during the test, the model has not occulted a part of the field, then the corresponding region of the film will be the most fully exposed. A region occulted during only one exposure will be exposed  $(N-1)$  times and if an overlapping of the images occurs, some regions will be even less exposed. However, each region will be adjacent to another which has suffered either one fewer or one more exposure. The contrast between adjacent areas therefore remains fairly uniform, and the number of recognizable images depends on the latitude of the film emulsion. Experience suggests that this number is about 10, though it might be more if a densitometer were used to read the photograph.

Although relatively few data are obtained by this method in comparison with cine photography, their excellent quality largely compensates for this. Figure 4.26 shows a multiply-exposed photograph obtained by Pennelegion, Cash & Shilling (1967) in the shock tunnel at N.P.I. The sparks were fired at a uniform rate, so that the model underwent unequal displacements between successive exposures; the spatial resolution is therefore non-uniform. The timing of the sparks can be measured accurately in a number of ways as discussed in the next section.

The rapid energy release characteristic of the impulse tunnel generally causes the tunnel structure to vibrate. If the reference frame is attached to the tunnel, a grid marked on the windows for example, then any motion of the tunnel during a test will be detected by this method, but not by ciné-photography. The relatively low frequency associated with massive structures means that this problem is only likely to be troublesome for tests of extended duration.

#### 4.4116 Providing a time-base

The operating procedure of an impulse tunnel is characterised by a long preparation time culminating in a final command to "fire". The sequence of events which follows this final command varies from one type of impulse tunnel to another, but in all of them the important processes occur in a fraction of a second, only a part of which constitutes the actual test period. One of the difficulties inherent in these tunnels is that some of the events occupy a time which differs from one tunnel run to another. Typical of these are diaphragm opening times. The data recording procedures must therefore be activated by an event that is more reliable in the temporal sense than the command to fire. It is also usual in such tunnels to monitor the test duration in some way. Accurate sequencing and timing of the events are clearly a necessary feature of impulse tunnel operation, so that the provision of a time-base presents no extra difficulties. Digital electronic chronometers having a resolution of  $1 \mu\text{s}$ , or even  $0.1 \mu\text{s}$ , are commonly used to time the passage of shock waves in a shock-tube, for example. Such chronometers can also be used to time the intervals between firings of the spark-gap light-sources when data are recorded by multiply-exposing a single photographic plate. To time ten sparks requires nine chronometers, which is somewhat costly, although some economy can be achieved by utilising a system having a single power supply serving all nine counters, a master crystal oscillator providing the pulses to be counted, and also by restricting the maximum time which each chronometer can measure. Commercially available instruments all seem to count up to one second, irrespective of their resolution. In impulse tunnel applications, four decades are usually sufficient ( $999.9 \mu\text{s} \pm 0.1 \mu\text{s}$  or  $9999 \mu\text{s} \pm 1 \mu\text{s}$  as the maxima), so that the total number of components can be roughly halved. One may go even further by having a single output display, each counter being switched manually to the display circuits at the end of a test, since it stores its count until it is reset. Certainly there is plenty of time between runs for a fairly leisurely reading of stored data.

An alternative scheme, used in the VKF ballistic range to time events, employs two counter chronometers and a core-store. While the primary counter is dumping its record into the core-store, a process which occupies  $50 \mu\text{s}$ , the secondary chronometer continues the count (Clemens, 1968). Clearly the transfer time means that the events being timed must be at least  $50 \mu\text{s}$  apart.

An extended time-base, with relatively finely divided time intervals, can also be obtained using a cathode ray oscilloscope. An ordinary C.R.O. used in the "raster-mode", in which the spot sweeps back and forth across the screen (brightness not being suppressed for the return, which takes the same time as the forward journey) while at the same time it also moves more slowly down the screen, in effect generates a very long time-base. Timing marks from a calibrated oscillator can be superimposed on this time-base, see figure 4.27, and signals derived from the firings of the sparks can also be fed either to the vertical deflection plates or the brightness control grid. The minor disadvantage of "time lost" as the direction of sweep is reversed can be avoided by using a spiral time-base. In this case the most convenient arrangement utilises a special C.R.O. tube equipped with a central electrode, so that radial deflections can be generated for both timing and event markers (Bernstein, 1963).

#### 4.4117 Photographic materials

The choice of photographic material is governed by the speed of the emulsion, its latitude and the dimensional stability of the base material. In general terms one can achieve high contrasts with fast emulsions, some improvement in both contrast and speed being obtained by increasing the development time and using an energetic developer. However this gain is at the expense of grain size, and when the images are small and require considerable enlargement, it is not obvious which choice provides the optimum spatial resolution. According to Holder & North (1963), the large image with a fast emulsion provides better resolution for schlieren photography, but clearly one should aim for an emulsion with as fine a grain as possible consistent with the available illumination.

As we have seen, the requirement in the case of a multiply-exposed single photograph using back-lighting, is for an emulsion with a wide latitude, since one must be able to distinguish as many shades as possible. Experience in the Aerodynamics Division of the National Physical Laboratory (now transferred to R.A.E.) shows that fast blue-sensitive plates, such as Ilford LN and XK, or Kodak Flash recording plates, are very suitable.

In these plates, the base material is glass, which is very stable; its thermal expansion coefficient is less than  $10^{-5}/K$ . It is therefore very suitable indeed for accurate coordinate determination. The choice of a glass base is not of course available for cine photography, but sufficiently fast orthochromatic films are marketed by the same manufacturers. These films are either acetate- or polyester- based. Both materials are sensitive to temperature and humidity, the acetate-based materials being a factor of about two less stable than the polyester materials. Neither however is so unstable as to make its use unduly difficult. Indeed if one adopts as standard procedure the inclusion of a reference grid as a background to every photograph, dimensional changes can be closely monitored.

#### 4.4118 Calibration methods

We have already discussed the provision of a spatial reference system and of a time base. To be of value the recorded data must be interpreted in terms of the "absolute" displacements of the model as functions of standard time. Account must therefore be taken of distortions and magnifications within the optical system, and strictly the time-base should be checked occasionally even though it is derived from a thermostatically-controlled crystal oscillator. Such oscillators are highly-stable devices, and annual checks are probably adequate, unless a fault is suspected. Some broadcasting stations transmit a standard frequency against which the crystal oscillator may be checked. C.R.O. time-bases are rarely accurate to within 3% or so, and require continual checking. The provision of time-markers from a crystal oscillator constitutes such a check.

Spatial calibration is readily carried out by taking a still photograph of an object (perhaps the model itself) of known size, shape and position against the background reference grid of known spacing. By adjusting the position of the object by known amounts, using a micrometer screw for example, errors due to such effects as parallax can be determined directly.

Finally one may mention here, though it is not strictly within the context of this section, another calibration procedure commonly adopted with the free-flight technique. The aerodynamic data are usually presented in terms of aerodynamic coefficients. To calculate these coefficients one needs the dynamic pressure of the relative stream, which in many tunnels is difficult to determine accurately. The direct measurement is avoided by flying a standard object - a sphere - as well as the model in each

test. In this way the ratio of the force coefficients of the model to the drag coefficient of the sphere can be found. If the latter is known for the conditions of the test, and it is not very sensitive to small errors in the Reynolds and Mach numbers, then the required force coefficients for the model follow. Moreover, if more reliable data for the sphere become available later, the data may be corrected.

#### 4.4119 Reading the photographic record

Obtaining information from measurements of a photographic record is a feature common to ballistic range technology and free flight testing in conventional high-speed wind tunnels. As such it has been discussed by Wilkins (1970) in AGARDograph 138, and by Dayman (1966). A detailed account here would therefore be superfluous, since there are no respects in which the present problem differs significantly from those. Dayman (1966) points out that greater consistency and overall accuracy can be obtained by using a template cut to the size of the photographic image (or its projection on the film reading screen). This template averages the errors resulting from the inevitably blurred edges of the image of the model which arise both from diffraction effects and the relative motion of the model and the film. A line drawing of the edge on a transparency, with the centre of mass marked, would appear to have advantages over a solid template. In the absence of such a template, mounted on a carriage which can be traversed in two perpendicular directions and rotated known amounts, one would need to measure the coordinates of several points of the image, using cursors, in order to determine the position of the centre of mass and the orientation of the model. If the model yaws during a test, a template cannot be used.

The large quantity of data on a ciné film (or two films if orthogonal systems have been necessary) makes film reading a tedious procedure, and therefore it is liable to human error. In some cases it is not necessary to measure every frame, although with oscillatory motions the angular attitude near peak values should be measured on every frame if the motion is to be well enough defined to give the aerodynamic damping. A semi-automatic film reader, either of the type which projects a large image onto a screen, or one in which the image is viewed through a travelling microscope, is more than a convenience.

Although such equipment, when it is available, can be used to great advantage on the multiply-exposed single plate, it is possible in this case to obtain position data manually to within  $\pm 0.2$  mm approximately. The large format photograph, which may be an enlargement of the negative or the negative itself, can be overlaid by a transparent grid which is aligned with the reference lines on the photograph. The coordinates of critical points on the edges of the image are then read using a magnifier, and from these the position of the centre of mass can be computed. Angles may be obtained either from these coordinates also, or by using a protractor.

#### 4.412 An optical telemetry system

The major disadvantages of both ciné-photography and the single-plate, multiple exposure technique using shadowgraph optics have been by-passed in a novel system designed and developed for use in the gun-tunnel at D.F.V.L.R., Porz-Wahn by Requardt & Kabelitz (1971, 1972). Further developments have been reported by Requardt & Wyborny (1973) and Wyborny & Requardt (1974).

In this system a flashing light is carried aboard the freely-flying model, three focussed beams producing rows of exposed dots on a single sheet of film wrapped around the test section. Energy for the light-source is provided by a radio-frequency (R.F.) generator having a continuous-wave power output of up to 1 kW. To inhibit R.F.-excitation of the low density gas in the test chamber, which would fog the film, the primary coil and its leads were surrounded, in the prototype version, by an air-filled plastic tube. In later versions a casting resin is used to insulate all the high voltage components within the low-pressure environment, the casing of the primary coil acting as a "flow-positioning device" downstream of the nozzle exit, see figure 4.28. The transformation ratio has also been carefully chosen to minimise the likelihood of R.F. glowing. Using a primary coil of 8 turns having a diameter of 220 mm and a length of 120 mm, an energy transmission of 50% was achieved into the secondary coil of 13 turns having a diameter of 28 mm (in the prototype versions) and a length of 13 mm. This secondary coil is housed within the model, together with appropriate tuning capacitors. Also carried within the model are a rectifier circuit, the flash lamp and the transmission optics. The miniature flash lamp is operable at frequencies up to 1 kHz, the half-amplitude duration being less than 2  $\mu$ s. The lamp requires 600 V (d.c.) to operate, with a trigger level of 1200 V; to obtain these high voltages from the rectifier circuit, a

number of specially-selected diodes are arranged in cascade. The R.F. source is pulse-amplitude-modulated and triggering of the lamp is accomplished by means of a thyristor and miniature trigger transformer. Details of the 1974-version are illustrated in figure 4.29 where both the circuit and the physical arrangement of the components are shown. The electronic components have been "potted" in polyvinyl chloride (PVC) compound to form a convenient cylindrical package for housing within axially-symmetrically shaped models. In the latest version, (Wyborny, 1975), the electronic-optical instrument package has a mass of 41.5 g, a diameter of 25 mm and an overall length of 53 mm.

The components are arranged as shown in figure 4.30, (see also, figure 2.10) and depending on the position and orientation of the model the exposed spots on the film have a diameter between 3 mm and 8 mm; figure 4.31 shows a typical record. From each triplet\* it is estimated that the position of the model can be determined (see Section 2.232) to within  $\pm 0.2$  mm, and the angular position to within  $\pm 0.2^\circ$ , so long as the images do not overlap. Such overlap can occur when the model moves slowly (or rotates rapidly); in this case data can still be obtained, but the uncertainties are greater. These uncertainties, of course, depend directly on the position of the photographic recording material, which is held in a special cylindrical cassette inside the primary coil. The effective length of the flight path is limited by the size of this film holder, which is 120 mm long.

#### 4.413 Light-occluding and similar methods

Taking measurements from a photographic record can be a very laborious process, although semi-automatic equipment reduces a good deal of the tedium. It is not unnatural therefore that other methods should be sought to determine the displacements of the model as a function of time. The principle of one such system is fairly obvious. A beam of light, projected across the test-section is interrupted - occluded - by the model, and the extent to which it is cut off is monitored by a light-sensitive device, such as a photo-cell. The output from this device is then a measure of the displacement of the model.

A simple system of this kind has been described by Clemens (1971). In his system, a beam of light, rectangular in cross-section is partially cut off by the flat base of a model as shown in figure 4.32. The uninterrupted portion of the beam falls on a spherical mirror (part of the single-pass schlieren system of the tunnel) which focusses it at the plane of a disc. This balanced disc has 100 teeth cut around its edge, and it is rotated at about 3000 rev/min so as to provide a "chopped" frequency of about 5 kHz. The chopped beam falls onto the photocathode of a photomultiplier the output from which can be a.c.-coupled into the cathode ray oscilloscope upon which it is displayed; any other suitable recording device might be used. In this way the problems of drift are avoided, and the effects of flow luminosity are rendered negligible.

The system is readily calibrated statically by replacing the model with a card mounted on a micrometer screw, though Clemens noted that differences in calibration arose, from a slight discharging of the battery supplying the light source, between calibrations before and after a tunnel run. Dynamic calibration can also be carried out by allowing a plate to fall through the beam under gravity, the optical system being rotated through  $90^\circ$ . Such dynamic calibrations give very repeatable results, the value of the local specific gravitational force agreeing to within 1% with the accepted value.

Clearly if the model pitches or yaws, the results are ambiguous. Clemens evaluates the sensitivity of the system and the pitch and yaw interactions. For a rectangular cross-section light beam of height  $h$ , see figure 4.32, the output voltage  $\Delta V$ , produced by a displacement  $\Delta \xi$ , is given by

$$\Delta V = K_c h \Delta \xi \quad (4.24)$$

where  $K_c$  is a calibration factor, which is constant if the photomultiplier characteristic is linear. Thus there are advantages in making  $h$  large, but if the model moves vertically also, not so large that the rear corners enter the beam.

The pitch-interaction  $\Delta V_\theta$ , is also proportional to  $h$ , see figure 4.33. For a small pitching angle  $\theta$ ,

$$\Delta V_\theta \approx \frac{1}{2} K_c h (h_1 - h_2) \theta \approx \frac{1}{2} K_c h x_b \theta^2 \quad (4.25)$$

\* Corresponding points are identified with the aid of a special control unit in the R.F. transmission circuit, which suppresses every ninth flash.

where  $x_b$  is the distance between the base and the centre of mass of the model. The ratio of pitch sensitivity to axial displacement sensitivity is therefore independent of  $h$ . The yaw interaction  $\Delta V_\psi$ , on the other hand, depends upon the size of the base. For a base dimension  $D$  along the path of the light beam, it can be shown that, for small angles of yaw

$$\Delta V_\psi \approx \frac{1}{2} K_c \psi D \quad (4.26)$$

so that this interaction is potentially troublesome.

The technique, even if several channels are installed primarily to resolve motions in different directions, will be difficult to use, because of these interactions, for completely freely-flying models. Clemens (1971) only demonstrated its utility for a model subject to drag and gravity (though pure lift would have caused no problems). However for pivoted models the method is ideal.

East (1962) has used the principle to measure the pitching motion of models supported on a horizontal pivot. The oscillating models were carried on side-walls which moved with the model. An aperture was cut in one of these side walls, and light from a 48 W tungsten filament lamp was focussed on this aperture. Subsequently it passed over a cut-off attached to the fixed walls of the mounting, and then to the photo-detector. The shape of the effective slit was so arranged that the output from the photocell was linear with pitch angle. Ghosh (1974) used the same technique in his experiments.

North (1971) has put forward several ideas which would reduce considerably the labour of data acquisition and processing, if they can be successfully put into practice, although they may not result in any overall improvement in accuracy. His first suggestion is that the single light beam of Clemens (1971) be replaced by linear arrays of sources - essentially light screens - and photo-detectors. As the model intercepts a light screen, the time would be recorded. A system of ten light screens in each of three linear arrays would be needed to obtain the same amount of information as is contained in a single photograph using the multiple exposure technique of section 4.4115. The diameter of each light beam might be of order 0.1 mm, which gives about the same resolution as photographic methods. In a variation of this method, suitable for cases in which the model does not move far, a light beam is focussed onto a fine-pitch grid mounted on the model, beyond which it falls on a photo-detector. With a grid pitch of 0.2 mm and the beam focussed to a diameter of 0.1 mm (a laser is suggested), 50 periods would require a length of 10 mm. The same size is probably desirable along the grid lines, so that considerable aerodynamic interference would arise, unless the model were very much larger. North also points out that a system of virtual grids - in fact a series of interference fringes generated from a laser light source by splitting and then recombining the beams at a small angle - might be projected near the model upon which pins are mounted to occult the fringes as the model moves. There would be less aerodynamic interference in this case, but the pins would need to be sufficiently stiff to remain a "rigid" part of the model. The photo-detectors would also have to be more sensitive than would be necessary with a real grid.

The notion of interference fringes led North (1971) naturally to consider the possibility of using interferometer methods. He notes that displacements are readily measured using a Michelson interferometer and that the laser provides a very suitable, coherent light source. Such an interferometer, see figure 4.34, operates by splitting the incident beam into two; one passes to the object whose displacement is to be measured, the other - the reference beam - to a mirror. Both beams are reflected into the photo-detector. Displacements of the object along the beam direction lead to alternate cancellation and reinforcement of the light intensity at the photo-detector. Because of the double passage of the beam, each fringe represents a displacement of half a wavelength. The practical difficulty of applying this technique arises from the need to reflect the incident beam back into the photo-detector from a model having an "arbitrary" motion, arbitrary in the sense that it is not in general confined to translation along the beam direction. "Retroreflectors" are possible, as North suggests (see figure 4.34), but they are costly to produce and perhaps not the kind of equipment carried by an essentially expendable model.

One should note also that fringes will appear at the photo-detector as a result of the movement of any other part of the optical system, and precautions must be taken to minimise such sources of error by employing suitable anti-vibration mountings.

#### 4.42 Velocity measurements

The existence of a highly coherent radiation source as convenient as the laser makes it possible to measure the velocity of the model using the principle of the Doppler shift in frequency. One possible optical arrangement is proposed by North (1971), see figure 4.35. It is not very different from that of figure 4.34, but the retroreflectors are replaced by diffuse reflecting surfaces on the model and the incident beam is focussed on to these areas by means of a lens. In this system, the reflected signal is at a frequency different from the transmitted signal because of the motion of the reflector, the difference in frequency being proportional to the relative velocity along the beam. If the transmitted and reflected signals are made to "beat", the frequency difference, or Doppler frequency  $f_d$ , can be extracted. The amplitude of the signal depends on the effective scattering area on the model as well as on the intensity of the incident beam, so that noise will arise both from the laser source and from textural variations in the surface of the diffuse reflector. This may make a Doppler-lidar system difficult to operate, as North (1971) points out. The Doppler frequency is given by

$$f_d = \frac{2V_B}{\lambda} \quad (4.27)$$

where  $V_B$  is the velocity of the target along the beam and  $\lambda$  is the wavelength of the light being used. For the commonly-used He-Ne laser,  $\lambda = 632.8$  nm, so that the Doppler frequencies  $f_d$  are rather high, even for velocities of a few metres/second, when they are of order 10 MHz. Assuming that the available recording techniques can handle this, there are some advantages in using a heavy model and so restricting not only its velocity but also its total displacement. The model will thus remain in a confined region of the test-section, so that spatial non-uniformities in the flow field are less serious, and also there is a greater likelihood that the beams reflected from the model will pass back into the photo-detectors. At first sight it would appear that by using the Doppler method, accuracy can be improved, because only one differentiation is then needed to obtain the accelerations and hence the forces. This is not so, however, because as the system is normally used, one is in essence counting the displacement increments when one measures the frequency by counting the number of cycles in a given time interval. This performs the first differentiation. In addition, the derived forces have to be related to the orientation of the model with respect to the stream and to obtain this, the velocity data must be integrated with respect to time, though this does not usually result in serious errors.

North (1971) goes on to point out that with a Doppler frequency as high as 10 MHz, it might be possible to measure the frequency to within 1% in a period as short as 10  $\mu$ s. A succession of such measurements might be stored in digital form for subsequent processing. The stored numbers give directly the average velocity of the model, along the beam, over each 10  $\mu$ s interval. It should be pointed out however that the velocity of the model varies from zero at the beginning of a test up to a few metres/second at the end, and the 10 MHz signal represents the final velocity. To achieve the same accuracy throughout the flight, the interval over which the count is made would need to be greater than 10  $\mu$ s. Perhaps the optimum system is one in which the time interval is measured for a fixed number of waves, since times can be very accurately measured with an electronic counter chronometer.

#### 4.43 Acceleration measurements

As we have already discussed at some length in both Chapter 2 and in this Chapter, the aerodynamic forces and moments can be obtained by measuring the reactions to them of the model, which is assumed to behave as a free, rigid body, the mass and moments of inertia of which are known. The conditions under which this assumption can be justified in practical circumstances were considered in section 4.3.31, and the principle of the accelerometer, upon which the method is based, was outlined in section 3.24. In addition, section 3.343 (on the inertia-compensation of force-balances) is directly relevant to "accelerometer-balance" techniques.

The design of an accelerometer-balance closely parallels that of a force-balance - which accounts for the word "balance" in its title. One begins by deciding upon an acceleration-resolution system, analogous to those discussed in section 3.31, but bearing in mind the comments made in section 2.21. In many applications, probably the majority, the centripetal components of the acceleration will be small, because in the short test-times, the angular velocities do not become large. An arrangement such as that

of figure 3.48 would then be suitable in spite of the reservations expressed in section 3.343. Some other balances, also produced at Cornell Aeronautical Laboratory (now CALSPAN), which has been almost alone in developing the technique, are described by Vidal (1956) and by Wittliff & Rudinger (1958). They are illustrated in figures 4.11 and 4.12. A five-component accelerometer-balance is also described by Sheeran & Duryea (1969) of the same Laboratory. This balance is designed to yield all the aerodynamic forces and moments except the rolling moment. An interesting feature of their arrangement, see figure 4.36, is the inclusion of redundant accelerometers, but these were to be used only if a failure occurred in one of those of the main set.

The most suitable types of accelerometer for the present application are, as we have noted in Chapter 3, piezoelectric types, because of their very high resonant frequency. Used with charge amplifiers, any one of a number of recording techniques can be used. The primary difficulty arises in setting up and calibrating the system in such a way that the results are easily interpreted.

In the first place the accelerometer-balance and the model must be effectively one rigid body. The main frame of the balance must therefore be very stiff, but since it reacts to the aerodynamic loads, it must also be light enough to produce an adequate sensitivity. Beryllium and aluminium alloy would appear to be suitable materials, so long as the special facilities needed to machine the former are available. The accelerometers must be precisely located on this frame, and very firmly attached if their high frequency performance is not to be compromised. The manufacturer generally provides comprehensive instructions on how accelerometers should be fixed. The low-noise, coaxial cables which should be used with piezoelectric devices, should also be clamped, since movement can lead to spurious charge being generated. The model-shell which transmits the aerodynamic load to the accelerometer-balance assembly, must also be "rigidly" attached to the frame, and it must itself not introduce vibrations. Vidal (1956) noted that a thin metallic shell was not ideal because the internal damping in metals is relatively small, and any stress waves do not die away sufficiently in the typically short test time of a few milliseconds for which the technique is suitable. Although low-pass filters can be used in some circumstances, Vidal suggests that the model shell be made from one of the foamed-in-place plastics discussed in section 4.22.

Secondly there are likely to be interactions between components, which must be taken into account. Such interactions may arise either because the accelerometers have an inherent cross-axis sensitivity, or because they are mounted imperfectly on the balance frame. Such cross-axis sensitivities may be only 2% - 3% of that along the main axis, but when the acceleration components to be measured may differ by a factor of 10, such values can lead to serious errors unless some account is taken of them. The initial setting-up procedure is designed to eliminate these interactions.

In principle the output corresponding to that of an ideal accelerometer, positioned to respond to one component of linear acceleration of interest, can be reconstructed from those of all the accelerometers in the balance. Thus for a six-component system, there would be 36 coefficients if all the responses are linear. The setting-up procedure involves exciting an acceleration along each primary axis of the resolution system in turn and adjusting the proportions in which the output signals are summed in an analogue computer, so as to nullify the outputs on all channels except that intended to respond to the particular excitation. In general circumstances this setting-up procedure is iterative, and somewhat tedious. Duryea & Sheeran (1969) describe, in some detail, a procedure for setting-up their five-component system, which is somewhat simplified because the normal and side component transducers are located at the same axial positions. An interesting feature is that, to avoid the difficulties of adjusting to a null in the presence of noise, they make use of Lissajous figures displayed on a cathode ray oscilloscope.

The measuring system with the model attached is set up initially so that it rotates about the centre of mass of the model. A yawing motion should then produce no net output from a proper combination of the outputs from the "side-force" accelerometers, one forward and one aft, figure 4.36. The properly combined output constitutes the side-force channel, and this is connected to the vertical axis input of an oscilloscope. One of the side-force accelerometers is connected to the horizontal axis of the oscilloscope as a reference. With each accelerometer output there are associated potentiometers which determine what proportions of its output are "mixed" with those of the other accelerometers to effect the compensation. The potentiometer on the least sensitive side-force accelerometer is set to full scale

(1000 divisions on a ten-turn helical, precision potentiometer) and that associated with the other side-accelerometer is adjusted to level the sloping Lissajous figure which results from an oscillation in yaw. The side-force channel is then insensitive to yaw.

The model is then rotated continuously about the pitching axis  $C_y$  at about 3 Hz using a special mandrel mounted on air-bearings. In this way the axial-and normal-force accelerometers, and both the normal and axial cross-axis sensitivities of each side-force accelerometer, are excited over the range  $\pm 1g$ . An output from the side-force channel indicates an interaction. This output is again connected to the vertical axis of the oscilloscope, but this time the axial accelerometer output is used as a reference on the horizontal axis. In continuous rotation about  $C_y$ , the harmonic axial and normal accelerations of the model are  $90^\circ$  out of phase. The axial cross-axis sensitivity of the side-accelerometers produces a signal which is in phase with the horizontal reference, and the corresponding trace appears as a sloping line on the oscilloscope. The potentiometer governing the proportion of the axial accelerometer output added to the side-force channel is adjusted to level the trace, thereby eliminating the axial sensitivity.

The normal component of the cross-axis sensitivity is in quadrature with the axial reference signal, so that an elliptical Lissajous figure appears on the oscilloscope. This ellipse can be nulled by adjusting either of the normal-force accelerometer contributions to the side-force channel, or a combination of both. The correct adjustments can be obtained in two ways, one of which is rather special, because the normal- and side-force accelerometers are positioned in pairs at the same axial location. In this case one can assume that the forward side-accelerometer can be compensated for its normal cross-axis sensitivity by the forward normal-force accelerometer output alone. By suppressing the output from the rear side-accelerometer altogether, the remaining ellipse is nulled by adjusting the contribution to the side-force channel from the forward normal-accelerometer. The rear side-accelerometer output is then reconnected and the compensation of the side-force channel is completed by adjusting the contribution from the aft normal-accelerometer.\*

The other channels are set up in an analogous manner.

The measuring system can be calibrated either as a whole or by individually calibrating the transducers which make up the system and determining their positions relative to the centre of mass. In the latter method one also needs to determine the inertial properties of the model (see section 4.23). The calibration of accelerometers has been critically discussed by Kistler (1966). The procedures adopted by Duryea & Stevenson (1969) are as follows.

The system is mounted on the mandrel, which is supported in air-bearings to minimise the noise due to vibration (which occurred when ball-bearings were used). By adjusting the angular position of the axis of rotation with respect to gravity, the sensitive axis of each accelerometer can be subjected to an harmonically varying acceleration of amplitude up to  $1g$ , at a frequency of about 3 Hz. The output is displayed on an oscilloscope together with a standard voltage calibration signal. In addition a commercial vibration table is used to compare the accelerometer with a "standard" instrument over the frequency range 10 - 200 Hz. The low frequency response is checked by turning the accelerometer over rapidly in the gravitational field, and measuring the rate of decay of the output signal.

As a final check the system is calibrated as a whole. The model and accelerometer-balance, supported as it would be during a tunnel test, is subjected to step changes in load by rapidly unloading weights using a fused link. The compensated outputs from all channels are recorded. In principle, as Duryea & Sheeran point out, this method could be used to calibrate the system. They report however that the practical difficulties of accurately locating the weight hanger make the method somewhat less accurate than that involving individual calibrations of the accelerometers together with a determination of their precise location, for which they also describe an empirical technique.

---

\* Duryea & Sheeran (1969) also describe a more general iterative procedure which can be used when the normal and side accelerometers are not placed in pairs at the same axial location. The interested reader is referred to their paper for further details.

## REFERENCES

- Anderson, J.C. (1964) Dielectrics, Chapman & Hall, London.
- Anderson, R.A. (1967) Fundamentals of Vibrations, Macmillan Co., N.Y.
- Ayre, R.S. (1961) Transient Response to step and impulse functions, Shock & Vibration Handbook, (Edited by Harris, C.M. & Crede, C.E.), Vol. I., Chapter 8, McGraw-Hill.
- Beams, J.W. (1954) Shadow and schlieren methods. High speed aerodynamics and jet propulsion, Vol.IX, Section A2, Part 1, Princeton Univ. Press 1954, also O.U.P. 1955.
- Beaussier, J. (1966) A six-component balance equipped with semi-conductor strain-gauges and inertia-compensated for hot-shot wind-tunnels, O.N.E.R.A. T.P.No.377, 2nd ICIAF, Stanford, Aug.1966.
- Bernstein, L. (1963) Some measurements of shock-wave attenuation in channels of various cross-sections, A.R.C. R & M.3321.
- Berry, J. & Hoarau, R. (1964) Mesure des efforts dans une soufflerie à arc par une balance piézoélectrique à trois composantes compensée en inertie, O.N.E.R.A. T.P.159, also Proc. 1st ICIAF, Paris, Sept.1964.
- Bogdan, L. (1967) Instrumentation techniques for short-duration test facilities, CAL. Rep. No. WTH-030.
- Bogdonoff, S.M. & Hammitt, A.G. (1954) The Princeton helium hypersonic tunnel and preliminary results above  $M = 11$ , Princeton Univ. James Forrestal Centre, Rep. No. 260.
- Bogdonoff, S.M. & Vas, I.E. (1959) Operational experience in the Mach number 10 - 20 range in the Princeton University helium hypersonic wind-tunnel, Princeton Univ. Rep. 465.
- Boissevain, A.G. & Intrieri, P.F. (1961) Determination of stability derivatives from Ballistic range tests of rolling aircraft models, NASA TM X-339.
- Bowersox, R.B. & Carlson, J. (1957) Digital Computer calculations of transducer frequency response from its response to a step function, J.P.L. Progress Rep. 20-331. Jet Propulsion Laboratory, Pasadena, California.
- Bratt, J.B. & Wight, K.C. (1944) An automatic electric balance: proposed development for measurements in derivative research, Phil. Mag. 35, p.588.
- Bray, K.N.C. (1962) Evaluation of the hypersonic gun tunnel, Hypersonic flow research, Edit. by F.R. Riddell, Acad. Press N.Y.
- Broome, P.W. (1961) Fourier analysis on analog computers, General Dynamics/Astronautics Rep.
- Bryan, G.H. (1911) Stability in Aviation, MacMillan & Co.
- Bynum, D.S., Ledford, R.L. & Smotherman, W.E. (1970) Wind-tunnel pressure measuring techniques, AGARDograph No. 145.
- Lady, W.G. Piezoelectricity, McGraw Hill, 1946, Dover 1964.
- Canning, T.N. & Seiff, A. (1970) Modern Ballistic Ranges and their uses, Ch.1 of AGARDograph 138 "Ballistic-Range Technology", Edit. by Canning, T.N., Seiff, A. & James, C.S.
- Canning, T.N., Seiff, A. & James, C.S. (1970) Ballistic-Range Technology, AGARDograph 138.
- Carros, R.J. (1970) Light sources, Section 6.4 of AGARDograph 138 "Ballistic-Range Technology", Edit. by Canning, Seiff & James.
- Carros, R.J. & DeRose, C.E. (1970) Counterflow facilities, Ch.5 of AGARDograph 138 "Ballistic-Range Technology", Edit. by Canning, Seiff & James.
- Chapman, D.R. (1951) An analysis of base pressure at supersonic velocities and comparison with experiment, NACA TR 1051.
- Chapman, G.T. & Kirk, D.B. (1969) A (new) method for extracting aerodynamic coefficients from free-flight data, AIAA Paper 69-174. See also AIAA J. 8, (4), 1970.
- Chapman, G.T. & Kirk, D.B. (1970) A method for extracting aerodynamic coefficients from free-flight data, AIAA J. 8 (4) p.753. See also Comment by Murphy, C.H., AIAA J. 8 (11), p.2109 and author's reply.

- Chapman, G.T., Kirk, D.A. & Malcolm, G.N. (1970) Aerodynamics of bodies from motion analysis. AGARDograph 138, Ch.7. (Edit. by Canning, Seiff & James).
- Charters, A.C. (1955) The linearised equations of motion underlying the dynamic stability of aircraft, spinning projectiles and symmetrical missiles. NACA TN 3350.
- Chesterman, W.D. (1951) The photographic study of rapid events, Oxford University Press.
- Clemens, P.L. (1968) Private communication with C.S. James; referenced in Chapter 6 of AGARDograph 138 (Ballistic Range Technology, Edit. by Canning, Seiff & James, 1970).
- Clemens, P.L. (1971) Trajectory readout by progressive eclipsing of a photoelectric screen to obtain aerodynamic force data from free flight wind tunnel models, VKI TN 72.
- Courtney-Pratt, J.S. (1957) A review of the methods of high-speed photography, Reports on Progress in Physics 20, p.379.
- Cox, R.N. & Winter, D.F.T. (1957) The Light Gas Hypersonic Gun Tunnel at A.R.D.E. Fort Halstead, Kent. AGARD Rep. 139.
- Cunningham, D.M. & Goldsmith, W. (1959) Short-time impulses produced by longitudinal impact. S.E.S.A. Proc. XVI p.153.
- Dayman, B. (1966) Free Flight Testing in High-speed Wind Tunnels, AGARDograph 113.
- Dean, M. & Douglas, R.D. (Editors) (1962) Semiconductor and conventional strain gauges, Acad. Press. N.Y.
- DeRose, C.E., & Intrieri, .F. (1970) Model and sabot design and launching techniques, Chapter 3 of AGARDograph 138 (Ballistic Range Technology, Edit. by Canning, Seiff & James).
- Dorsey, J. (1964) Semi-conductor strain-gauge Handbook, Baldwin-Lima-Hamilton Corpn., Waltham, Mass. U.S.A.
- Duryea, G.R. & Martin, J.R. (1966) An improved piezoelectric balance for aerodynamic force measurements in the hypersonic shock tunnel, 2nd IEEE Int. Congress on Instrumentation in Aerospace Simulation Facilities (ICIASF) Stanford University. Also in IEEE Trans. on Aerospace & Elect. systems, Vol AES-4(3), 5/1968.
- Duryea, G.R. & Sheeran, W.J. (1969) Accelerometer Force Balance Techniques, 3rd IEEE Int. Congress on Instrumentation in Aerospace Simulation Facilities (3rd ICIASF), Brooklyn.
- East, R.A. (1962) A theoretical and experimental study of oscillating wedge shaped aerofoils in hypersonic flows, Univ. of Southampton, A.A.S.U.Rep.No.228
- East, R.A. (1964) Oscillatory experiments in short duration hypersonic testing facilities, Proc. 1st ICIASF.
- Eckstrom, D.J. (1968) The Influence of Mass and Momentum Transfer on the Static Stability and Drag of a Slender Cone - An Experimental Correlation, LMSC/DO 51269
- Edenfield, E.E. & Ledford, R.L. (1962) Compensation of dynamic sting effects in Hotshot force measurements, AEDC TDR 62-122.
- Enkenhus, K.R., Culotta, S. & Krogmann, P. (1970) Free flight static stability measurements of cones in hypersonic flow, VKI TN 66.
- Enkenhus, K.R., Richards, B.E. & Culotta, S. (1971) Free Flight stability measurements in the Longshot Tunnel, Proc. 8th Int. Shock Tube Symposium, Chapman & Hall, London.
- Etkin, B. (1972) Dynamics of Atmospheric flight, J. Wiley & Sons Ltd.
- Finke, K. & Grönig, H. (1971) Experimental Determination of the Aerodynamic heating of space vehicles in the hypersonic regime with force and pressure measurements, Institut für Allgemeine Mechanik der Technischen Hochschule, Aachen, BMBW-FB W 71-08.
- Fowler, R.H., Gallop, E.G., Lock, C.N.H. & Richmond, H.W. (1921) The aerodynamics of a spinning shell, (Part 1) Phil. Trans. Roy. Soc.A. 221, p.295.
- Fowler, R.H. & Lock, C.N.H. (1922) The aerodynamics of a spinning shell, (Part 2) Phil. Trans. Roy. Soc.A. 222, p.227-47.
- Fox, L. (1964) Introduction to numerical linear algebra, Oxford Univ. Press.

- Frank, E. (1952) Strain indicator for semiconductor gauges, in Semiconductor & Conventional Strain gauges, Edit. by Dean & Douglas, Acad. Press.
- Geiger, R.E. (1962) Experimental Lift and Drag of a Series of Glide Configurations at Mach numbers 12.6 and 17.5, *J. Ae/Sp. Sci.* 29, (4) 410.
- Geyling, F.T. & Forst, J.J. (1960) Semi-conductor strain transducers, *Bell Sys. Tech. J.* 39, p.705
- Ghosh, K. (1973) Ph.D. Thesis, University of Southampton.
- Gibbs-Smith, C.H. (1970) Aviation, H.M.S.O.
- Goodchild, R.O. (1968) An investigation into force and pressure measurement in a hypersonic shock-tunnel, Ph.D. Thesis, London Univ.
- Goodchild, R.O. & Bernstein, L. (1972) The design of high sensitivity pressure transducers for use in shock-tunnels, A.R.C. Current Paper 1219.
- Goodchild, R.O. & Bernstein, L. (1973) On the calibration of pressure transducers for use in shock-tunnels, A.R.C. Current Paper C.P.1240.
- Grauer-Carstenen, H. (1971) Free-flight testing in a Ludwieg-tube at high supersonic speeds, ICIA SF Record (Rhode-St-Génése).
- Griffith, W.C. (1971) Research with the shock-tube: a case history of science relevant to the needs of society, The Paul Vieille Memorial Lecture Proc. VIIIth Int. Shock Tube Symposium: Shock-Tube Research; Edited by Stollery, J.L. Gaydon, A.G. & Owen, P.R. - Chapman & Hall.
- Harris, C.M. & Crede, C.E. (1961) Shock & Vibration Handbook (3 vols.) 1. Basic Theory and Measurements Ch. 1-20, 2. Data Analysis, Testing & Methods of Control Ch.21-37, 3. Engineering Design and Environmental Conditions Ch.38-50. McGraw-Hill Book Co.
- Henny, R.W. (1965) The effects of ultra-high vacuum on the response characteristics of strain gauges, *Proc. 2nd Int. Congr. on Exp. Mech.* Washington, D.C.
- Hertzberg, A. (1951) A Shock Tube Method of Generating Hypersonic Flows, *J. Aero. Sc.* 18, 803.
- Hertzberg, A., Smith, W.E., Glick, H.S. & Squire, W. (1955) Modifications of the Shock-Tube for Generation of Hypersonic Flow, Cornell Aeronautical Laboratory, Report No. AD-789-A-2.
- Higson, G.R. (1964) Recent advances in strain gauges, *J.Sc.Instr.* 41, p.405.
- Holder, D.W. & North, R.J. (1963) Schlieren Methods, Notes on Applied Science No. 31, National Physical Laboratory, H.M.S.O.
- Horstman, C.C. & Kussoy, M.I. (1967) Free flight measurements of Aerodynamic viscous effects on lifting re-entry bodies, *J. Sp. & Rockets* 4, p.1064-9.
- Jacobsen, L.S. & Ayrr., R.S. (1958) Engineering Vibrations, McGraw-Hill Book Co.
- Jaffe, P. (1964) Obtaining Free-Flight Dynamic Damping of an Axially-Symmetric Body (at all angles of attack) in a Conventional Wind Tunnel, Jet Propulsion Laboratory Tech. Rep. No. 31-544.
- James, C.S., Carros, R.J., Boissevain, A.G., Sammonds, R.I. & Wilkins, M.E. (1970) Systems for measurement of model position, attitude and velocity, AGARDograph 138, Ch.6., (Edit. by Canning, Seiff & James).
- Jones, G. (1952) High speed photography, Chapman & Hall.
- Kavanau, L.L. (1953) Results of some base pressure experiments at intermediate Reynolds numbers with  $M = 2.84$ , Univ. of Calif. Inst. of Eng. Research, Report HE-150-117.
- Kavanau, L.L. (1954) Base pressure studies in rarefied supersonic flow, Univ. of Calif. Inst. of Eng. Research, Rep. HE-150-125.
- Kinslow, M. & Potter, J.L. (1963) Drag of spheres in rarefied hypervelocity flow, *AIAA J.* 1, p.2467-73.
- Kistler, W.P. (1966) Precision Calibration of accelerometers for shock and vibration, *Test Engineering & Management*. See also: "New precision calibration techniques for vibration transducers". *Shock & Vibration Bulletin*, No.35 part 4, U.S. Naval Res. Lab. Washington, D.C.
- Kussoy, M.I., Stewart, D.A. & Horstman, C.C. (1972) Hypersonic rarefied flow over sharp slender cones, NASA TN D-6689.

- Ladenburg, R.W. (Editor) Physical measurements in gas dynamics and combustion., High speed aerodynamics and jet propulsion, Vol. IX, Part 1, Oxford Univ. Press, 1955. (Also Princeton Univ. Press 1954)
- Lanchester, F.W. (1907) Aerial Flight. Vol.1. Aerodynamics, Vol.2. Aerodnetics, Constable & Co. Ltd., London.
- Levy, S. & Kroll, W.D. (1950) Response of accelerometers to transient accelerations, J. Res. Nat. Bur. Standards (RP 2138) Vol.45, No.4., p.303.
- Lewis, J.A. (1961) The effect of driving electrode shape on the electrical properties of piezoelectric crystals, Bell.Sys.Tech.J. 40, p.1259-80.
- Love, E.S. (1954) A summary of information on support interference at transonic and supersonic speeds. NACA RM L53K12.
- Ludwig, H. (1957) Tube-Wind Tunnel - A Special Type of Blowdown Tunnel, AGARD Rep.143.
- Lukasiewicz, J. (1973) Experimental methods of hypersonics, Marcel Dekker, N.Y.
- Macdonald, W.R. & Cole, P.W. (1963) New piezoelectric pressure transducers for aerodynamic research, R.A.E. Tech.Note IR 23. A.R.C.25056.
- Malcolm, G.N. & Chapman, G.T. (1968) A computer programme for systematically analysing free-flight data to determine the aerodynamics of axisymmetric bodies, NASA TN D-4766.
- Maple, C.G. & Synge, J.L. (1949) Aerodynamic symmetry of projectiles, Qu.App.Maths VI (4).
- Martin, J.F., Duryea, G.R. & Stevenson, L.M. (1962) Instrumentation for force and pressure measurements in a hypersonic shock tunnel, Cornell Aeronautical Laboratory Report CAL No.113 (Also Proc. 2nd Symposium on Hypervelocity Techniques, Denver, Colorado, U.S. (publ. Plenum Press, N.Y.))
- Mason, W.P. (1947) First and Second order equations for piezoelectric crystals expressed in tensor form, Bell. Sys. Tech. J. 26, p.80.
- Mason, W.P. (1950) Piezoelectric crystals and their application to ultrasonics, Van Nostrand.
- Mason, W.P., Forst, J.J. & Tornillo, L.M. (1962) Recent developments in semi-conductor strain transducers., Semiconductor & Conventional Strain gauges, Edit. by Dean & Douglas, Acad. Press.
- Mason, W.P. & Thurston, R.H. (1957) Use of piezoresistive materials in the measurement of displacement, force and torque, J. Acous. Soc. of Am. 29, p.1096.
- Miller, C.G. (1965) An experimental investigation of support interference on a blunt body of revolution at a Mach number of approximately 20, N.A.S.A. TN D-2742.
- Milne-Thomson, L.M. (1958) Theoretical Aerodynamics, Macmillan, (London & New York).
- Moffatt, W.G., Pearsall, G.W. & Wulff, J. (1964) The structure and properties of materials, Vol. I Structure, J. Wiley & Sons Ltd.
- Murray, W.M. & Stein, P.K. (1958) Strain gauge techniques, M.I.T. Press, Mass. U.S.
- McAlister, K.W., Stewart, D.A. & Peterson, V.L. (1971) Aerodynamic characteristics of a large-angle blunt cone with and without fence-type afterbodies, NASA TN D-6269.
- McDevitt, J.B., Harrison, D.R. & Lockman, W.K. (1966) Measurement of pressure and heat transfer by FM telemetry, IEEE Trans. on Aerospace & Elect. systems, AES-2(1) p.2-12., Also Proc. 1st ICIAF Paris, Sept. 1964.
- Neubert, H.K.P. (1963) Instrument Transducers, Oxford Univ. Press., London.
- Neubert, H.K.P. (1967) Strain Gauges, Macmillan.
- Nicolaidis, J.D. (1953) On the free-flight motion of missiles having slight configurational asymmetries, B.R.L. Rep. 858.
- Nisbett, J.S., Brennan, J.N. & Tarpley, H.I. (1960) High frequency strain gauge and accelerometer calibration, J.Ac.Soc.Am. 35, p.71.
- North, R.J. (1970) Spark Photography of models in free flight in a hypersonic shock-tunnel, Proc. 9th Int. Congr. on High speed photography, Denver.
- North, R.J. (1971) Possible applications of digital recording to the free-flight technique in short-duration facilities, ICIAF (Rhode-St-Genese).
- Nye, J.F. (1957) Physical properties of crystals, (Their representation by tensors and matrices)., Oxford Univ. Press.

- Oi, Koshiro (1965) Transient response of bonded strain-gauges, Proc. 2nd Int. Cong. on Exp. Mech., Washington, p.359-65., Publ. S.E.S.A.,(1966)
- Opatowski, T. (1966) Gun Tunnel Measurements of lift, drag and pitching moment on a 20° cone, a flat delta and a caret delta wing at a Mach number of 8.3., A.R.C., C.P.908.
- Opatowski, T. (1971) A three-component gun-tunnel balance designed for testing thin delta wings, A.R.C. R & M.3664.
- Pankhurst, R.C. & Holder, D.W. (1952) Wind tunnel techniques, Pitman & Sons Ltd.
- Pennelegion, L., Cash, R.F. & Bedder, D.F. (1967) Design and operating features of the NPL 6" shock tunnel, A.R.C. R & M.3449.
- Pennelegion, L., Cash, R.F. & Shilling, M.J. (1967) Free-flight tests in the N.P.L. 6 in (15 cm) shock-tunnel of model HB-2 using multiple spark recording, A.R.C. Current Paper CP.934.
- Perry, C.C. & Lissner, H.R. (1955) The strain-gauge primer, McGraw-Hill, N.Y. (see also: Strain-gauge instrumentation, Ch.17 of Shock & Vibration Handbook, Vol.I., Edit. by Harris & Crede, 1961, McGraw-Hill)
- Perry, R.W. (1964) The "longshot" type of high Reynolds number hypersonic tunnel, Proc. of 3rd Hypervelocity techniques symposium, Denver, Colorado.
- Perry, R.W. & MacDermott, W.N. (1958) Development of the spark-heated hypervelocity tunnel - hotshot, AEDC TN 58-6.
- Pfann, W.G. & Thurston, R.N. (1961) Semiconducting stress transducers utilising the transverse and shear piezoresistive effects, J. App. Phys. 32, p.2008.
- Pirrello, C.J., Hardin, R.D., Heckart, M.V. & Brown, K.R. (1971) An inventory of aeronautical ground research facilities, Vol.1. Wind tunnels. N.A.S.A. CR-1874, also ARC 33485 (1972).
- Poisson-Quinton, P. (1968) From wind-tunnel to flight, the role of the laboratory in aerospace design, J. Aircraft 5 (3), p.193-214.
- Prislin, R.H. (1966) Free-Flight and Free Oscillation Techniques for Wind-tunnel Dynamic-Stability Testing, NASA Jet Propulsion Laboratory Tech. Rep. No. 32-878.
- Rebuffel, P. (1956) Some strain-gauge balances used in French wind tunnels, AGARD Rep.6-T, 8th mtg. of W/T Panel, ONERA TN.No.31.
- Redwood, M. (1961a) Transient performance of a piezoelectric transducer, J.Ac.Soc.Am. 33, (4) p.527-36.
- Redwood, M. (1961b) Piezoelectric Generation of an electrical impulse, J.Ac.Soc.Am. 33, (10) p.1386-90.
- Reller, J.O. & Hamaker, F.M. (1955) An experimental investigation of the base pressure characteristics of non-lifting bodies of revolution at Mach numbers from 2.73 to 4.98, NACA TN 3393.
- Requardt, G. & Kabelitz, H.-P. (1971) Development of and Preliminary Investigations on a Free-Flight Testing System for a Gun Tunnel, Int. Congress on Instr. in Aero Sp. Fac., ICIASF Record.
- Requardt, G. & Kabelitz, H.-P. (1972) Development and tests of the prototype of a free-flight system for the Gun Tunnel, DFVLR Report DLR-FB 72-41.
- Requardt, G. & Myborny, W. (1973) An aerodynamic free-flight testing system for a gun tunnel, ICIASF Record 1973.
- Richards, B.E. & Clemens, P.L. (1971) Design of Freely-Oscillating cone-shaped models and Instrumentation limitations for measuring dynamic stability derivatives in intermittent facilities, (VKI Preprint 71-1), 4th ICIASF.
- Richards, B.E. & Enkenhus, K.R. (1970a) Hypersonic Testing in the VKI Longshot Free Piston Tunnel, AIAA J. 8, p.1020.
- Richards, B.E. & Enkenhus, K.R. (1970b) Dynamic stability measurements in the Longshot free piston tunnel, VKI Internal Note 36.
- Roark, R.J. (1954) Formulae for stress and strain, McGraw-Hill.
- Rohrbach, C. & Czaika, N. (1961) Materialpruefung 1, 121, R.A.E. translation No.821 (quoted by Higson, 1964)

- Sammonds, R.I. (1970) Spatial reference systems, Section 6.6 of AGARDograph 138 (Ballistic Range Technology, Ed. Canning, Ceiff & James).
- Sanchez, J.C. & Wright, W.V. (1962) Recent developments in flexible silicon strain gauges, in Semiconductor & Conventional Strain gauges, Edit. M. Dean, Acad. Press, N.Y.
- Schaguhn, W. (1970) Calibration of a balance for determining the aerodynamic forces in a shock-tunnel (in German), Diploma Thesis, Technischen Hochschule, Aachen.
- Schueler, C.J. (1960) An investigation of support interference on AGARD calibration model B, A.E.D.C. - TN-60-35.
- Schueler, C.J., Ward, L.K. & Hodapp, A.E. (1967) Techniques for Measurement of dynamic stability derivatives in ground test facilities, AGARDograph 121.
- Schultz, D.L. & Jones, T.V. (1973) Heat transfer measurements in short-duration hypersonic facilities, AGARDograph 165.
- Seiff, A. & Wilkins, M.E. (1961) Experimental Investigation of a hypersonic glider configuration at a Mach number of 6 and at full-scale Reynolds numbers, NASA TN D-341.
- Sheeran, W.J. & Duryea, G.R. (1969) The Application of the Accelerometer Force Balance in Short Duration Testing, AIAA 4th Aerodynamic Testing Conf. AIAA Paper No. 69-351, Cincinnati, Ohio.
- Sivier, K.R. & Bogdanoff, S.M. (1955) The effect of support interference on base pressure of a body of revolution at high Reynolds numbers, Princeton Univ. Rep. No. 332, (AFOSR TN 55-301).
- Smith, C.S. (1954) Piezoresistive effect in Silicon & Germanium, Phys.Rev.94, p.12.
- Spescha, von G.A. (1971) Piezoelectric multi-component force and moment measurement, Kistler Instruments AG. Reprint No. 20.065 e. English translation of 1970 German original.
- Spescha, von G.A. & Volle E. (1971) Piezoelectric measuring instruments, Kistler Instruments AG. Reprint No. 20.054(e). English translation of 1967 German original.
- Stollenwerk, E. (1966) Wire-release of free-flight models by use of electrical energy to sever wires at localised areas, Private communication to B. Dayman, referenced in AGARDograph 113.
- Thomson, W.T. (1966) Vibration theory and applications, George Allen & Unwin. (also Prentice-Hall (1965))
- Tracy, R.R. (1961) Wind-tunnel sting balances, Task Corpn. Rep. R-484. Presented at Western regional strain gauge committee Spring meeting, San Francisco, California.
- Vidal, R.J. (1956) Model instrumentation techniques for heat transfer and force measurements in a hypersonic shock tunnel, Cornell Aero. Lab. Rep. No. AD-917-A-1.
- Waterfall, A.P. (1972) A technique for the automatic, digital analysis of flight dynamic response data, A.R.C. R & M No.3699.
- Welsh, C.J., Ledford, R.L., Ward, L.K. & Rhudy, J.P. (1959) Dynamic stability tests in hypersonic tunnels at large model amplitudes, AEDC TR 59-24.
- Whitfield, J.D. (1959) Support interference at supersonic speeds, AGARD Report 300.
- Wilkins, M.E. (1970) Interpretation of the photographic record, AGARDograph 138, Chap.6, Section 9. (Edit. by Canning, Seiff & James)
- Wilkins, M.E. & Darsow, J.F. (1959) Finishing and Inspection of model surfaces for boundary-layer transition tests, NASA Memo 1-19-59A.
- Witliff, C.E. & Rudinger, G. (1958) Summary of Instrumentation development and aerodynamic research in a hypersonic shock-tunnel, Cornell Aero. Lab. Rep. AD-917-A-2.
- Wyborny, W. (1975) Private communication.
- Wyborny, W. & Requardt, G. (1974) A new aerodynamic free-flight testing system for six-component measurements in short duration wind-tunnels, AIAA Paper 74-613.

Some further references, not cited in the text

- Anderson, J.R. (1956) Strain gauge balances for wind tunnels - an outline of practice in the U.K. AGARD Rep.5. 8th mtg. of W/T panel.
- Bowman, J.E. (1965) Pitot pressure measurements in the wakes of unsupported models in a hypersonic gun tunnel, Royal Armament Research and Development Establishment Memorandum 54/65.
- Bowman, J.E. (1969) Measurement of centres of pressure of 9° spherically blunted cones in hypersonic flow by a free-flight method, 32nd S.T.A. Mtg. at F.F.A., Sweden.
- Cable, A.J. & Bowman, J.E. (1962) Hypersonic wind tunnel measurements of the normal forces and centres of pressure of three cone-cylinder-flare models, R.A.R.D.E. Memo (B) 19/62.
- Cash, R.F. & Shilling, M.J. (1965) Schlieren photography of free flight models in the N.P.L. 6 in. shock tunnel using a high-speed framing camera or a repetitive spark light source, NPL Aero Note 1031 - A.R.C.26 815.
- Darmon, J.M. & Devacht, A. (1967) The use of semi-conductor strain-gauges for measurement in hot-shot wind-tunnels, La Recherche Aerospaciale No.120.
- Davies, L., Cash, R.F., Catley, A. & Knight, S. (1968) Free-Flight tests in a shock-tunnel on 9° spherically-blunted cones with and without flats, at a Mach number of 8.6, NPL Aero.Rep.1280, A.R.C. 30 482, Hyp.708.
- Davies, L., Cash, R.F., Regan, J.D., Townsend, J.E.G. & Catley, A. (1971) Experiments on flat delta wings and waveriders up to angles of incidence and Mach numbers suitable for lifting reentry, Proc. of VIII Int. Shock-tube Symposium, London. (Ed. Stollery, Gaydon & Owen, publ. Chapman & Hall.)
- Fox, D.M. (1972) Speed of cinematographic films for high speed photography, R.A.E. T.R. No. 72087.
- Geiger, R.E. (1963) Some sphere drag measurements in low density shock tunnel flows, Gen. Elect. Co. Rep. R63 5D 23.
- Heyser, A., Wyborny, W., & Kabelitz, H.-P. (1966) Three-Component-Measurements on AGARD-Standard Models HB-1 and HB-2 in the DVL Gun Tunnel, Deutsche Luft- und Raumfahrt, Report 66-25.
- Hollander, L.E., Vick, G.L. & Diesel, T.J. (1960) The piezoresistive effect and its applications, Rev. Sci. Instr. 31, p.323.
- Horanoff, E.V. Design of a miniature, water-cooled, internal strain-gauge wind tunnel balance, NOL TR 64-136.
- Keyes, R.W. (1960) The Effects of Elastic deformation on the electrical conductivity of semiconductors, Solid State Physics 11, 149. Acad. Press.
- Kistler Instruments (1970) The piezoelectric measuring chain for internal ballistic pressure measurements, Kistler report No. 20.056, Kistler Instruments AG, Winterthur, Switzerland.
- Kussoy, M.I. & Horstman, C.C. (1970) Cone drag in rarefied hypersonic flow, AIAA J. 8 (2), p.315-20.
- Kussoy, M.I., Stewart, D.A. & Horstman, C.C. (1970) Sphere drag in near-free-molecule hypersonic flow, AIAA J. 8 (11) p.2104-5.
- Kussoy, M.I., Stewart, D.A. & Horstman, C.C. (1971) Sharp slender cones in near-free-molecule hypersonic flow, AIAA J. 9 (9), p.1879-81.
- Levin, G.M. (1969) The development of the free-flight technique for the determination of static and dynamic aerodynamic coefficients using Longshot, NASA Goddard Space Flight Centre, X-110-69-325.
- Lieu, B.H. & Horanoff, E.V. (1965) A miniature strain-gauge balance for hypersonic force measurements, AIAA J. 3, p.793.
- Moore, D.R., Stalmach, C.J., Pope, T.C. & Jenkins, J.E. (1967) Dynamic Stability Wind tunnel tests on a 10° cone with simulated ablation at M = 17, AIAA J. 5, p.1377.
- Moreau, R., Besson, J. & Hoarau, R. (1971) Electro-optical detectors for magnetic suspension and the study of the free motion of models, ONERA, T.P.No. 988, Presented at Symposium on Electromagnetic suspension, Southampton.
- McDevitt, J.B. & Larson, H.K. (1966) A technique for launching free-flying models in conventional wind-tunnels, AIAA Aerodynamic Testing Conf. AIAA Paper 66-773.

- Pennelegion, L., Smith, G.S. & Dolman, K. (1964) Millisecond measurements of Aerodynamic forces in a High pressure shock tunnel, Proc. of 1st ICIASF.
- Raghunath, B.J. & Parker, H.M. (1973) Evaluation of Aerodynamic derivatives from a magnetic balance system, AIAA J. 11 (7), p.897.
- Rosenman, L. (1968) Aerodynamic Force Measurements on a Slender Two Dimensional Wedge in the Hypersonic Viscous Interaction Regime, Aerospace Rep. No. TR-0158 (3240-10)-12, Air Force Rep. No. SAMS0 - TR-68-284.
- Whitfield, J.D. & Wolny, W. (1962) Hypersonic Static Stability of Blunt Slender Cones, AEDC TDR-62-166.
- Willmarth, W.W. (1971) Unsteady force and pressure measurements, Ann. Rev. of Fluid Mechanics, Vol.3, Annual Reviews Inc., Palo Alto, Calif. U.S.A.

### NOMENCLATURE

Note: Vectors, tensors and matrices are used freely throughout the text and some convention has had to be adopted to indicate such quantities while still using ordinary typescript. To some extent we have adopted the suffix notation, in particular when describing piezoelectricity and piezoresistivity in Chapter 3. Elsewhere we have, for conciseness adopted the following conventions:

cartesian vectors are underlined with the printers' symbol for bold-faced type; for example,  $\underline{x}$ ;  
 cartesian tensors are doubly underlined and enclosed in square brackets to emphasise the matrix operations which may be carried out on an array of the elements; for example,  $[\underline{S}]$ ;  
 square matrices are similarly denoted; for example,  $[\underline{M}]$ ;  
 column matrices (or column vectors) are denoted thus;  $\{\underline{x}\}$ .

a	width of ceramic beam; radius of cylindrical film used in optical telemetry system;	$C_m$	pitching moment coefficient (see $C_2$ );
$a_2, a_3$	distances defined in figure 4.10;	$C_n$	yawing moment coefficient (see $C_2$ );
$a_{ij}, a_{ij}$	flexibility coefficients defined by equations (2.144) & (2.145);	$C_{mq}$	typical aerodynamic derivative, $\equiv \frac{\partial C_m}{\partial \dot{q}}$
A	area; cross-sectional area;	$C_o$	static electrical capacitance of piezoelectric element;
$A_1, A_2, A_3$	defined by equations (2.76);	$C_s$	stray electrical capacitance;
$\underline{A}$	generalised aerodynamic force having components (X,Y,Z,L,M,N) in body-fixed frame;	$C_S$	side-force coefficient (side-force forms right-handed cartesian system with lift and drag);
AR	aspect ratio;	$C_W$	$\frac{2mg}{\rho V^2 S}$ ;
b	span;	d	arc diameter of circular arc flexure;
B	volume;	$d_{ijk}, d_{in}$	piezoelectric coefficients;
$B_1, B_2, B_3$	defined by equation (2.99);	D, $D_0$	drag, drag at zero lift;
c	viscous damping coefficient;	D	operator $\frac{d}{dt}$ ;
$\bar{c}$	representative length; mean chord;	$\underline{D}$	electric displacement vector
$[\underline{c}], c_{mn}$	elastic stiffness tensor, element thereof in reduced notation;	e	eccentricity, see figure 3.14;
$C_c$	electrical capacitance of cable	e	distance of centre of pressure aft of centre of mass;
$C_D, C_{D_0}$	drag coefficient, drag coefficient at zero lift; $\frac{\text{drag}}{\frac{1}{2}\rho V^2 S}$ ;	E	Young's modulus for an isotropic material;
$C_{D_2}$	coefficient defined by equation(2.94);	$\underline{E}$	electric field strength vector;
$C_{D_{eff}}$	effective drag coefficient defined by equation (2.96);	$f_d$	Doppler frequency;
$C_F$	force coefficient, $\frac{\text{force}}{\frac{1}{2}\rho V^2 S}$ ;	$f_0$	natural (cyclic) frequency;
$C_F$	feedback capacitance of charge amplifier;	$\{f\}$	column matrix of force-transducer outputs;
$C_i$	range-setting capacitance of voltage amplifier;	F(t)	time dependent force;
$C_L, C_{L_0}$	lift coefficient, lift coefficient at zero geometric incidence; $\frac{\text{lift}}{\frac{1}{2}\rho V^2 S}$ ;	$\underline{F}, F_i$	force vector, component thereof;
$C_2$	rolling moment coefficient; $\frac{\text{rolling moment}}{\frac{1}{2}\rho V^2 S b}$ for aeroplane-like shapes; for axially-symmetric shapes, $\bar{c}$ is used as the representative length for all moment coefficients;	$g, g_i$	specific gravitational force, components thereof;
		G, $G_1$	gauge factor = fractional resistance change/strain;
		$G_1'$	gauge factor resulting from changes in specific resistivity only $= \frac{\Delta \rho}{\rho_0 S_1}$ ;
		$G_2, G_3$	defined by equation (3.41);

$h, h_1, h_2$	lengths defined in figures 4.32 and 4.33;	$L_\alpha$	$\equiv \left( \frac{\partial L}{\partial \alpha} \right)_{\alpha=0}$	} typical aerodynamic derivatives;
$h, h_0$	specific enthalpy of test stream, stagnation specific enthalpy;	$L_{\dot{\alpha}}$	$\equiv \left( \frac{\partial L}{\partial \dot{\alpha}} \right)_{\dot{\alpha}=0}$	
$H$	distance between coplanar strips of flat strap flexure, figure 3.25;	$L_{\alpha\beta}$	$\equiv \left( \frac{\partial^2 L}{\partial \alpha \partial \beta} \right)_{\alpha=\beta=0}$	
$H_A$	moment of momentum vector about a point A;	$m$	mass;	
$i$	$\sqrt{-1}$ ;	$-m$	open-loop gain of amplifier;	
$\underline{i}, \underline{i}_j$	electric current vector, components thereof;	$m_\lambda$	longitudinal elastoresistance coefficient;	
$(\underline{i}, \underline{j}, \underline{k})$	unit vectors along body-fixed axes Cxyz;	$M$	Mach number;	
$(\underline{i}', \underline{j}', \underline{k}')$	unit vectors along fixed-plane, body axes Cx'y'z';	$M_i$	moment about axis $O_i$ ;	
$(\underline{i}'', \underline{j}'', \underline{k}'')$	unit vectors along laboratory-fixed axes $O\xi\eta\zeta$ ;	$\underline{M}'$	$M' + iN'$ ;	
$[\underline{I}]$	inertia tensor referred to the centre of mass C; referred to cartesian axes	$[\underline{M}], m_{ij}$	mass matrix; element thereof;	
	$[\underline{I}] \equiv \begin{bmatrix} I_{xx} & -I_{xy} & -I_{xz} \\ -I_{xy} & I_{yy} & -I_{yz} \\ -I_{xz} & -I_{yz} & I_{zz} \end{bmatrix}$	$[\underline{M}^*]$	diagonalised mass matrix;	
$I, I_{22}$	second moment of area of cross-section, about axis $O_2$ ;	$n$	number of oscillations during test period $\Delta t$ ;	
$\hat{I}_{ii}$	dimensionless moment of inertia, $\frac{2I_{ii}}{\rho S c b^2}$ ;	$n, N$	number of degrees of freedom;	
$k, k_i$	stiffness;	$N$	number of elements in crystal stack;	
$k_\theta$	rotational stiffness;	$p, p_t, p_0$	pressure, pitot pressure, isentropic stagnation pressure	
$k$	ratio of resistances in arms of Wheatstone bridge circuit;	$(p, q, r)$	angular rates about axes Cxyz;	
$k_{in}$	calibration coefficients defined by equation (3.56);	$(p', q', r')$	angular rates about axes Cx'y'z';	
$K$	$\frac{\rho S}{2m}$ ;	$(\hat{p}, \hat{q}, \hat{r})$	dimensionless forms of $p, q, r$ ; $\hat{p} = \frac{p c}{V}$ etc;	
$K$	calibration factor;	$q_i$	generalised coordinate;	
$[\underline{K}], k_{ij}$	stiffness matrix, element thereof;	$q_i^*$	principal coordinate;	
$[\underline{K}^*]$	diagonalised stiffness matrix;	$q_\infty$	dynamic pressure, $\frac{1}{2} \rho V^2$ ;	
$l$	length;	$Q$	apparent electric charge;	
$l_{ij}$	cosine of angle between $O_i$ and $O_j$ axes;	$\hat{Q}'$	$q' + ir'$ ;	
$L$	length;	$Q_F$	charge sensitivity to force, $Q/F$ ;	
$L$	lift;	$Q_i$	generalised force associated with coordinate $q_i$ ;	
$(L, M, N)$	components of aerodynamic moment about Cxyz;	$Q_p$	charge sensitivity to pressure, $Q/p$ ;	
$(L', M', N')$	components of aerodynamic moment about Cx'y'z';	$r_i$	fractional resistance change $\delta R_i/R_i$ ;	
$\underline{L}_A$	vector moment about a point A;	$\underline{r}$	position vector relative to centre of mass; $\underline{r} = x_i \underline{i} + y_j \underline{j} + z_k \underline{k}$ ;	
$[\underline{L}], [L_{ij}]$	matrix of direction cosines;	$R$	radial polar coordinate in laboratory-fixed frame, figure 2.2;	
		$R$	specific ideal-gas constant;	
		$R, R_0$	electrical resistance, electrical resistance at zero strain;	
		$R_F$	feedback resistance of charge amplifier;	
		$R_{in}$	input resistance;	
		$\underline{R}_A$	position vector of point A in inertial frame;	

$[R]$ , $r_{ij}$	linear transformation matrix; element thereof (see equation 2.131)	$(x_w, y_w, z_w)$	wind-axes;
$[R]^T$	transpose of $[R]$ ;	$(x', y', z)$	body-oriented, fixed plane axes;
$S_{ijkl}^E, S_{mn}^E$	elastic compliance tensor evaluated at constant field strength; the second form is in the reduced notation of Voigt (see, e.g. Mason, 1947) as follows $S_{1111} = S_{11}; S_{1122} = S_{12}; S_{1133} = S_{13}; S_{2222} = S_{22}$ etc., $S_{1212} = \frac{1}{2}S_{66}; S_{1112} = \frac{1}{2}S_{16}$ etc.; note the factor $\frac{1}{2}$ which appears because these terms occur twice;	$\{x\}$ , $x_i$	displacement (column) vector, component thereof ( $i = 1, 2 \dots n$ );
		$(x_1, x_2, x_3)$	general right-handed system of cartesian coordinates;
		$(X, Y, Z)$	components of aerodynamic force along Cxyz;
		$(X, Y, Z)$	crystallographic axes (see figure 3.2);
		$Y_1$	Young's modulus appropriate to uniaxial stress system applied to non-isotropic material, $(\sigma_1/S_1)$ ;
$S$	representative area, for example wing planform or body cross-sectional area;	$z, z_i$	distance along beam;
$S$	direct strain, used without a suffix where no ambiguity arises;	$z$	relative displacement, $(x - x)$ ;
$S_b$	direct strain due to bending only;	$\alpha$	angle of incidence
$[S]$ , $S_{ij}$ , $S_n$	strain tensor, element thereof, element thereof in reduced notation (see $[g]$ );	$\alpha_x$	angle of incidence of Cx axis (see equation (2.8));
$t, \hat{t}$	time, dimensionless time defined by equation (2.60);	$\alpha_R$	resultant incidence, $\arctan [\tan^2\alpha + \tan^2\beta]^{\frac{1}{2}}$ ; see also equation (2.59);
$t$	thickness;	$[a]$ , $a_{ij}$	matrix of coefficients defining linear relation between $\{A\}$ and $\{f\}$ ; $a_{ij} = \frac{\partial A_i}{\partial f_j}$ ;
$t_1$	duration of linear ramp rise;	$\beta$	angle of sideslip, see equation (2.9);
$t_p$	time at which peak amplitude occurs;	$\beta$	$\frac{m\omega_n^2}{(\pi L)^{\frac{1}{2}}}$ , see equation (2.143);
$T$	total kinetic energy of a system;	$[g]$ , $\beta_{ij}$	matrix of coefficients defining linear relation between $\{A\}$ and $\{y\}$ ; $\beta_{ij} = \frac{\partial A_i}{\partial y_j}$ ;
$T, T_0$	temperature, stagnation temperature;	$\gamma$	ratio of principal specific heat-capacities;
$(u, v, w)$	velocity components of body along Cxyz in inertial frame;	$\gamma_1, \gamma_2$	"trajectory" angles defining the direction of the relative wind, see equations (2.16) and (2.17);
$(u', v', w')$	velocity components of body along Cx'y'z' in inertial frame;	$\{y\}$	column matrix of accelerometer outputs;
$U$	Lagrangian potential energy function;	$\delta$	fractional damping during time $\Delta t$ ;
$(U_B, V_B, W_B)$	velocity components of body along O $\xi\eta\zeta$ in inertial frame;	$\epsilon$	flow "conicity", defined in figure 4.3;
$(U_\infty, V_\infty, W_\infty)$	velocity components of stream along O $\xi\eta\zeta$ in inertial frame;	$\epsilon_{ij}^\sigma$	dielectric permittivity at constant stress;
$v$	lateral deflection of beam;	$\epsilon_0$	dielectric permittivity of free space, 8.8542 pF/m;
$V$	magnitude of relative velocity between body and stream; $ \underline{V}_B - \underline{V}_\infty $ ;	$\zeta$	damping ratio, $c/(2\sqrt{km})$ ;
$V, \Delta V$	voltage, voltage change;	$(\xi, \eta, \zeta)$	laboratory-fixed coordinate frame, see figure 2.2;
$V_F$	voltage sensitivity to force, V/F;	$(\xi', \eta', \zeta)$	laboratory-fixed frame obtained by rotation of O $\xi\eta\zeta$ through $\pi$ about O $\zeta$ ;
$\underline{V}_B$	vector velocity of body in inertial frame;	$\theta$	angle of pitch;
$\underline{V}_\infty$	vector velocity of stream in inertial frame;	$\theta$	Celsius temperature;
$x, x_i$	displacement;		
$x_p$	peak displacement;		
$(x, y, z)$	body-fixed coordinate system; principal axes of body through centre of mass;		

$\kappa_{yy}$	radius of gyration about axis $Cy$ ;	$\tau$	time, pulse duration, time constant;
$\lambda$	angular polar coordinate, see figure 2.2;	$\tau_r$	rise time;
$\lambda$	wavelength of oscillatory motion; wavelength of light source;	$(\phi, \theta, \psi)$	Eulerian angles, angles of roll, pitch and yaw respectively, see figure 2.3;
$\mu$	dimensionless mass, $\frac{2m}{\rho S \bar{c}}$ ;	$(\phi_w, \theta_w, \psi_w)$	Eulerian angles defined in figure 2.6;
$\nu'$	Poisson's ratio	$\phi$	phase angle;
$\xi^*, \hat{\xi}^*$	relative displacements ( $U_\infty t - \xi$ ) and $\xi^*/\bar{c}$ respectively;	$\phi$	velocity potential of stream relative to laboratory;
$[\pi]_{\underline{\underline{z}}}, \pi_{ijk\ell}$	piezoresistivity tensor, element thereof;	$x, x_0$	displacement of base, amplitude thereof;
$\pi_{st}$	piezoresistivity tensor element in "reduced" notation/ $\rho_0$ ;	$\bar{\psi}$	$\theta + i\psi$ ;
$\pi_\ell$	longitudinal piezoresistance coefficient;	$\omega, \omega_i$	pulsatance (radian frequency);
$\rho$	density of test gas stream; density of material;	$\omega_n$	natural pulsatance of system with one degree of freedom, $\sqrt{k/m}$ ;
$[\rho]_{\underline{\underline{z}}}, \rho_{ij}$	specific resistivity tensor, element thereof;	$\omega_{n_i}$	natural pulsatance of $i^{\text{th}}$ mode;
$\rho_0$	specific resistivity of isotropic material including crystals of cubic structure in the unstrained state;	$\omega$	angular velocity of coordinate system;
$[\sigma]_{\underline{\underline{z}}}, \sigma_{ij}, \sigma_n$	stress tensor, element thereof, element in reduced notation; the suffix pairs are replaced as follows:	$(\omega_x, \omega_y, \omega_z)$	components of $\omega$ along $Cxyz$ ; identical with $(p, q, r)$ ;
		$\omega$	$ \omega $ ;
		$\Omega$	angular velocity of body;
		$[\Omega^2]_{\underline{\underline{z}}}, \omega_{n_i}^2$	eigenvalue matrix, element thereof;

$$\begin{bmatrix} \sigma_{11} & \sigma_{12} & \sigma_{13} \\ \sigma_{21} & \sigma_{22} & \sigma_{23} \\ \sigma_{31} & \sigma_{32} & \sigma_{33} \end{bmatrix} = \begin{bmatrix} \sigma_1 & \sigma_6 & \sigma_5 \\ \sigma_6 & \sigma_2 & \sigma_4 \\ \sigma_5 & \sigma_4 & \sigma_3 \end{bmatrix};$$

### SUFFICES

The majority of suffices are defined in the context in which they appear. The following conventions have been adopted:

- $i, j, k, \ell$  used with cartesian tensors take the values 1,2,3;
- $m, n, s, t$  used with the reduced notation of Voigt take the values 1,2,3, ..., 6; see  $[\sigma]$  for corresponding suffices;
- $o$  initial value; stagnation value;
- $C$  refers to centre of mass.

TABLE 3.1(a) Properties of Piezoelectric Materials

 $\alpha$  - quartz

$$\begin{bmatrix} s_{11} & s_{12} & s_{13} & s_{14} & 0 & 0 \\ s_{12} & s_{11} & s_{13} & -s_{14} & 0 & 0 \\ s_{13} & s_{13} & s_{33} & 0 & 0 & 0 \\ s_{14} & -s_{14} & 0 & s_{44} & 0 & 0 \\ 0 & 0 & 0 & 0 & s_{44} & 2s_{14} \\ 0 & 0 & 0 & 0 & 2s_{14} & 2(s_{11}-s_{12}) \end{bmatrix} \begin{bmatrix} \epsilon_{11} & 0 & 0 \\ 0 & \epsilon_{11} & 0 \\ 0 & 0 & \epsilon_{33} \end{bmatrix}$$

$$\begin{bmatrix} e_{11} & -e_{11} & 0 & e_{14} & 0 & 0 \\ 0 & 0 & 0 & 0 & -e_{14} & -e_{11} \\ 0 & 0 & 0 & 0 & 0 & 0 \end{bmatrix} \begin{bmatrix} d_{11} & -d_{11} & 0 & d_{14} & 0 & 0 \\ 0 & 0 & 0 & 0 & -d_{14} & -2d_{11} \\ 0 & 0 & 0 & 0 & 0 & 0 \end{bmatrix}$$

Rochelle Salt

$$\begin{bmatrix} s_{11} & s_{12} & s_{13} & 0 & 0 & 0 \\ s_{12} & s_{22} & s_{23} & 0 & 0 & 0 \\ s_{13} & s_{23} & s_{33} & 0 & 0 & 0 \\ 0 & 0 & 0 & s_{44} & 0 & 0 \\ 0 & 0 & 0 & 0 & s_{55} & 0 \\ 0 & 0 & 0 & 0 & 0 & s_{66} \end{bmatrix} \begin{bmatrix} \epsilon_{11} & 0 & 0 \\ 0 & \epsilon_{22} & 0 \\ 0 & 0 & \epsilon_{33} \end{bmatrix}$$

$$\begin{bmatrix} 0 & 0 & 0 & e_{14} & 0 & 0 \\ 0 & 0 & 0 & 0 & e_{25} & 0 \\ 0 & 0 & 0 & 0 & 0 & e_{36} \end{bmatrix} \begin{bmatrix} 0 & 0 & 0 & d_{14} & 0 & 0 \\ 0 & 0 & 0 & 0 & d_{25} & 0 \\ 0 & 0 & 0 & 0 & 0 & d_{36} \end{bmatrix}$$

Polarised ceramics

$$\begin{bmatrix} s_{11} & s_{12} & s_{13} & 0 & 0 & 0 \\ s_{12} & s_{11} & s_{13} & 0 & 0 & 0 \\ s_{13} & s_{13} & s_{33} & 0 & 0 & 0 \\ 0 & 0 & 0 & s_{44} & 0 & 0 \\ 0 & 0 & 0 & 0 & s_{44} & 0 \\ 0 & 0 & 0 & 0 & 0 & 2(s_{11}-s_{12}) \end{bmatrix} \begin{bmatrix} \epsilon_{11} & 0 & 0 \\ 0 & \epsilon_{11} & 0 \\ 0 & 0 & \epsilon_{33} \end{bmatrix}$$

$$\begin{bmatrix} 0 & 0 & 0 & 0 & e_{15} & 0 \\ 0 & 0 & 0 & e_{15} & 0 & 0 \\ e_{31} & e_{31} & e_{33} & 0 & 0 & 0 \end{bmatrix} \begin{bmatrix} 0 & 0 & 0 & 0 & d_{15} & 0 \\ 0 & 0 & 0 & d_{15} & 0 & 0 \\ d_{31} & d_{31} & d_{33} & 0 & 0 & 0 \end{bmatrix}$$

TABLE 3.1(b)

Quantity	Units	$\alpha$ -quartz	Rochelle Salt	BaTiO <sub>3</sub>	PZT-5A	PZT-5H	
$s_{11}^E$	$10^{-12} \text{m}^2/\text{N}$	12.77	51.8	8.6	16.4	16.5	
$s_{11}^D$		12.64		8.3	14.4	14.05	
$s_{12}^E$		-1.79	15.3	-2.6	-5.74	-4.78	
$s_{12}^D$		-1.66		-2.9	-7.71	-7.27	
$s_{13}^E$		-1.22	-21.1	-2.7	-7.22	-8.45	
$s_{13}^D$		-1.22		-1.9	-2.98	-3.05	
$s_{14}^E$		4.50		0	0	0	
$s_{14}^D$		4.46		0	0	0	
$s_{22}^E$		$s_{11}^E$	34.9	$s_{11}^E$	$s_{11}^E$	$s_{11}^E$	$s_{11}^E$
$s_{22}^D$		$s_{11}^D$		$s_{11}^D$	$s_{11}^D$	$s_{11}^D$	$s_{11}^D$
$s_{23}^E$		$s_{13}^E$	-10.3	$s_{13}^E$	$s_{13}^E$	$s_{13}^E$	$s_{13}^E$
$s_{23}^D$		$s_{13}^D$		$s_{13}^D$	$s_{13}^D$	$s_{13}^D$	$s_{13}^D$
$s_{33}^E$		9.60	33.4	9.1	18.8	20.7	
$s_{33}^D$		9.60		7.0	9.46	8.99	
$s_{44}^E$		20.04	79.8	32.2	47.5	43.5	
$s_{44}^D$		19.91		17.1	25.2	23.7	
$s_{55}^E$		$s_{44}^E$	328	$s_{44}^E$	$s_{44}^E$	$s_{44}^E$	$s_{44}^E$
$s_{55}^D$		$s_{44}^D$		$s_{44}^D$	$s_{44}^D$	$s_{44}^D$	$s_{44}^D$
$s_{66}^E$		29.12	101	$2(s_{11}^E - s_{12}^E)$	$2(s_{11}^E - s_{12}^E)$	$2(s_{11}^E - s_{12}^E)$	
$s_{66}^D$		28.58		$2(s_{11}^D - s_{12}^D)$	$2(s_{11}^D - s_{12}^D)$	$2(s_{11}^D - s_{12}^D)$	
$d_{11}$		$10^{-12} \text{m}/\text{V}$ or $\text{pC}/\text{N}$	2.31		0	0	0
$d_{14}$			0.727	100-300	0	0	0
$d_{15}$	0			242	584	741	
$d_{25}$	$-d_{14}$		-53	0	0	0	
$d_{31}$	0			-58	-171	-274	
$d_{33}$	0			149	374	593	
$d_{36}$	0		11.7	0	0	0	

TABLE 3.1(b) (Continued)

Quantity	Units	$\alpha$ -quartz	RocheUe Salt	BaTiO <sub>3</sub>	PZT-5A	PZT-5H
$\epsilon_{11}^T/\epsilon_0$		4.52		1300	1730	3130
$\epsilon_{11}^S/\epsilon_0$		4.43		1000	916	1700
$\epsilon_{22}^T/\epsilon_0$		$\epsilon_{11}^T/\epsilon_0$		$\epsilon_{11}^T/\epsilon_0$	$\epsilon_{11}^T/\epsilon_0$	$\epsilon_{11}^T/\epsilon_0$
$\epsilon_{22}^S/\epsilon_0$		$\epsilon_{11}^S/\epsilon_0$		$\epsilon_{11}^S/\epsilon_0$	$\epsilon_{11}^S/\epsilon_0$	$\epsilon_{11}^S/\epsilon_0$
$\epsilon_{33}^T/\epsilon_0$		4.64		1200	1700	3400
$\epsilon_{33}^S/\epsilon_0$		4.64		910	830	1470
Relative density		2.65	1.77	5.55	7.75	7.5
$\tau$ at 25°C	seconds			> 100	> 2000	> 2000
$\tau$ at 100°C				~ 0.3	~ 1800	> 2000
$\tau$ at 200°C				~ 0.002	~ 250	~ 1000
$\rho_{33}$ at 25°C	ohm cm	$\sim 10^{14}$		$> 10^{12}$	$> 10^{13}$	$> 10^{13}$
at 100°C		$\sim 10^{12}$		$> 10^9$	~ $10^{13}$	~ $10^{13}$
$\rho_{11}$ at 25°C		$\sim 10^{16}$	$10^{13}$	$> 10^{12}$	$> 10^{13}$	$> 10^{13}$
at 100°C			2000	$> 10^9$	~ $10^{13}$	~ $10^{13}$

TABLE 3.2(a) Performance Parameters for Various Modes

	$f_0$	$C_0$	$Q_p$	$V_p$	$Q_F$	$V_F$
Disc in Compression, Normal Mode	$\frac{1}{\sqrt{t} \sqrt{\rho S_{33}^D}}$	$\frac{\pi d^2}{4 t} \epsilon_{33}^T$	$d_{33} \frac{\pi d^2}{4}$	$\frac{d_{33}}{\epsilon_{33}^T} t$	$d_{33}$	$\frac{4 d_{33} t}{\pi \epsilon_{33}^T d^2}$
Plate, Transverse Mode	$\frac{1}{4h \sqrt{\rho S_{11}^E}}$	$\epsilon_{33}^T \frac{A}{t}$	$d_{31} A$	$\frac{d_{33}}{\epsilon_{33}^T} t$		
Shear Plate		$\epsilon_{11}^T \frac{A}{t}$			$d_{15}$	$\frac{d_{15} t}{\epsilon_{11}^T A}$
Shear Tube		$\epsilon_{11}^T \frac{\pi dh}{t}$			$d_{15}$	$\frac{d_{15} t}{\epsilon_{11}^T \pi dh}$
Cantilever Bimorph Beam, Series Connected.	$0.162 \frac{t}{\ell^2} \frac{1}{\sqrt{\rho S_{11}^E}}$	$\epsilon_{33}^T \frac{b \ell}{t}$			$\frac{3 \ell^2}{2 t^2} d_{31}$	$\frac{3}{2} \frac{d_{31} \ell}{\epsilon_{33}^T b t}$
Pinned End Bimorph Beam Series Connected	$0.454 \frac{t}{\ell^2} \frac{1}{\sqrt{\rho S_{11}^E}}$	$\epsilon_{33}^T \frac{b \ell}{t}$			$\frac{3 \ell^2}{8 t^2} d_{31}$	$\frac{3}{8} \frac{d_{31} \ell}{\epsilon_{33}^T b t}$
Pinned Edge Bimorph Disc, Series Connected	$0.988 \frac{t}{d^2} \frac{1}{\sqrt{\rho S_{11}^E}}$	$\frac{\pi}{4} \epsilon_{33}^T \frac{d^2}{t}$	$\frac{3 \pi}{64} d_{31} \frac{d^4}{t^2}$	$\frac{3}{16} \frac{d_{31} d^2}{\epsilon_{33}^T t}$	$\frac{3 d^2}{8 t^2} d_{31}$	$\frac{3}{2 \pi} \frac{d_{31} 1}{\epsilon_{33}^T t}$
Centrally Supported Disc, Series Connected	$0.732 \frac{t}{d^2} \frac{1}{\sqrt{\rho S_{11}^E}}$	$\frac{\pi}{4} \epsilon_{33}^T \frac{d^2}{t}$	$\frac{3 \pi}{64} d_{31} \frac{d^4}{t^2}$	$\frac{3}{16} \frac{d_{31} d^2}{\epsilon_{33}^T t}$		

TABLE 3.2(b) Performance parameters for various modes evaluated for PZT-5A

Note:- t, d,  $\ell$ , b, h, A are typically of order unity

t=mm; d, $\ell$ ,b,h=cm; A=cm <sup>2</sup>	$f_0$ (KHz)	$C_0$ (PF)	$Q_p$ (pC/torr)	$Q_F$ (pC/N)	$V_F$ (V/N)	$f_0 Q_F$ MHz pC/N
Normal Compression Disc	$\frac{923}{t}$	$1181 \frac{d^2}{t}$	$3.92 d^2$	374	$.316 \frac{t}{d^2}$	$\frac{345}{t}$
Plate-Transverse	$\frac{70.1}{h}$	$1505 \frac{A}{t}$	2.28 A			
Shear Plate		$1150 \frac{A}{t}$		584	$.382 \frac{t}{A}$	
Shear Tube		$3610 \frac{dh}{t}$		584	$.122 \frac{t}{dh}$	
Cantilever Beam, Series Connected	$4.54 \frac{t}{\ell^2}$	$1505 \frac{b \ell}{t}$		$25\ 600 \frac{\ell^2}{t^2}$		$\frac{116}{t}$
Cantilever Beam, Parallel Connected	$4.54 \frac{t}{\ell^2}$	$6020 \frac{b \ell}{t}$		$51\ 300 \frac{\ell^2}{t^2}$		$\frac{233}{t}$
Pinned End Beam, Series Connected	$12.70 \frac{t}{\ell^2}$	$1505 \frac{b \ell}{t}$		$6\ 410 \frac{\ell^2}{t^2}$		$\frac{68.7}{t}$
Pinned End Beam, Parallel Connected	$12.70 \frac{t}{\ell^2}$	$6020 \frac{b \ell}{t}$		$12\ 800 \frac{\ell^2}{t^2}$	$\frac{5.43}{t}$	$\frac{137}{t}$
Pinned Edge Disc Series Connected	$27.7 \frac{t}{d^2}$	$1181 \frac{d^2}{t}$	$33.55 \frac{d^4}{t^2}$	$6\ 410 \frac{d^2}{t^2}$		$\frac{177}{t}$
Pinned Edge Disc Parallel Connected	$27.7 \frac{t}{d^2}$	$4724 \frac{d^2}{t}$	$67.1 \frac{d^4}{t^2}$	$12\ 800 \frac{d^2}{t^2}$	$\frac{2.71}{t}$	$\frac{355}{t}$
Centrally Supported Disc, Series Connected	$20.5 \frac{t}{d^2}$	$1181 \frac{d^2}{t}$	$33.55 \frac{d^4}{t^2}$			
Centrally Supported Disc, Parallel Connected	$20.5 \frac{t}{d^2}$	$4724 \frac{d^2}{t}$	$67.1 \frac{d^4}{t^2}$			

TABLE 3.3 Piezoresistive properties of semiconductor materials used as strain gauges

Material	$\frac{\rho_0}{\text{ohm cm}}$	$\frac{\pi}{\text{m}^2/\text{N}} \times 10^{11}$				$G' = m_x$
		$\pi_{11}$	$\pi_{12}$	$\pi_{44}$	$\pi_x$	
Germanium, n	16.6	-5.2	-5.5	-138.7	-97.9	-15 <sub>z</sub>
Germanium, p	1.1	-3.7	+3.2	+96.7	+65.4	+101.5
Silicon, n	11.7	-102.2	+53.4	-13.6	-102	-133
Silicon, p	7.8	+6.6	-1.1	+138.1	+93.5	+175

These are typical values (after Smith, 1954) of the adiabatic piezoresistive coefficients at room temperature of Germanium and Silicon. The values of  $\pi_x$  and  $m_x$  are the largest numerical values. They occur along [111] crystal axes in each case except for n-type Silicon for which the minimum is along the [100] direction.

TABLE 4.1 Physical properties of some materials useful for making freely-flying models

Material	Relative density	Young's modulus	Ultimate strength	D.C. resistivity
		$\text{GN/m}^2$	$\text{MN/t}^2$	ohm cm
Foamed polyurethane	0.030	-	0.2 - 0.25	-
Polystyrene; foamed moulded	$\approx 0.13$ 1.05 - 1.08	2.5 - 4.0	35 - 65	$10^{17} - 10^{21}$
Polyvinyl chloride (PVC); rigid, unfoamed	1.36 - 1.41	1.5 - 4.5	35 - 60	$10^{12} - 10^{16}$
plasticised, unfoamed	1.15 - 1.65	-	15 - 20	$10^{11} - 10^{14}$
PTFE (Teflon)	2.1 - 2.3	0.23 - 0.45	10 - 45	$10^{19}$
Nylon	1.1	0.5 - 0.7	83	$10^{13} - 10^{14}$
Class, common flint	2.4 - 2.8 2.9 - 5.9			
Magnesium	1.74	40	100 - 200	
Beryllium	1.8	270		
Aluminium	2.58	72 - 75	60 - 250	
Duralumin	2.8	69	620	
Titanium alloy	4.5		1380	
Steel	7.8	200	500 - 2000	
Brass	8.4 - 8.7	85 - 105	450	
Silver	10.5	71 - 74	300 - 350	
Lead	11.3	$\approx 14$	13 - 21	
Mercury	13.6	-	-	
Tungsten, drawn	19.4	330	1520	
Platinum	21.37	150 - 170	240 - 340	

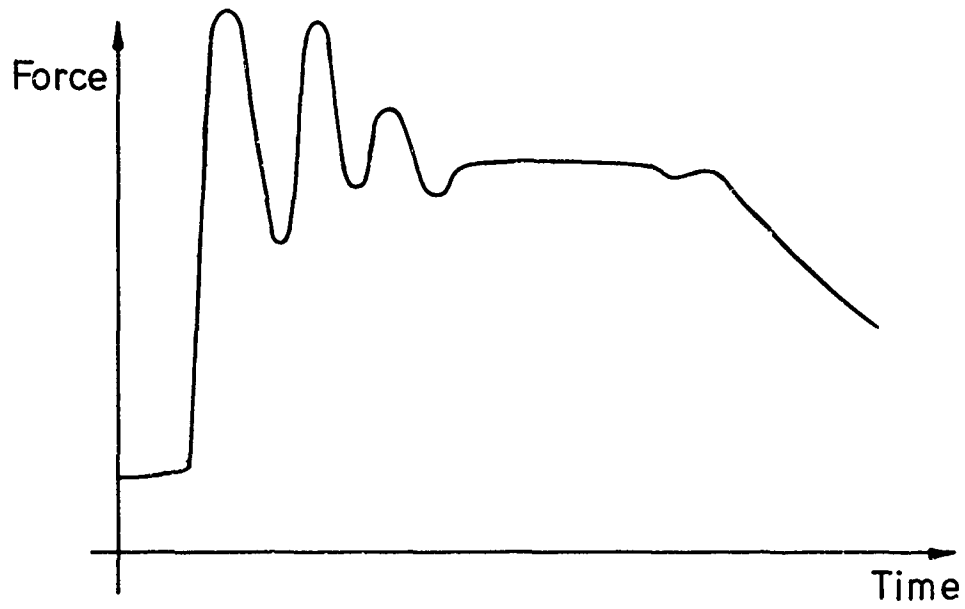


Figure 2.1. Representative sketch of the variation with time of a typical component of the force on a model in an impulse-tunnel.

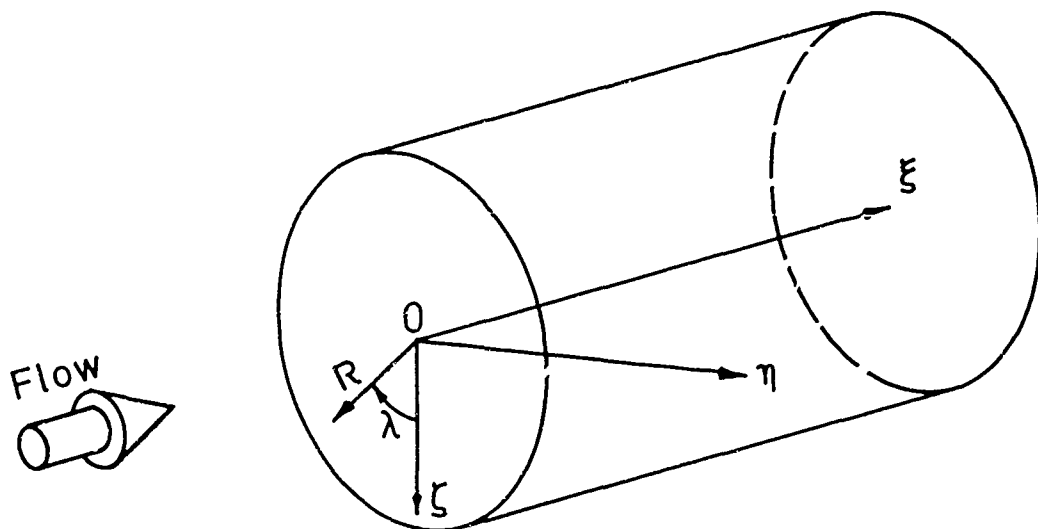
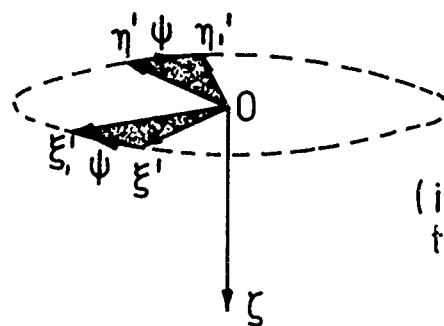
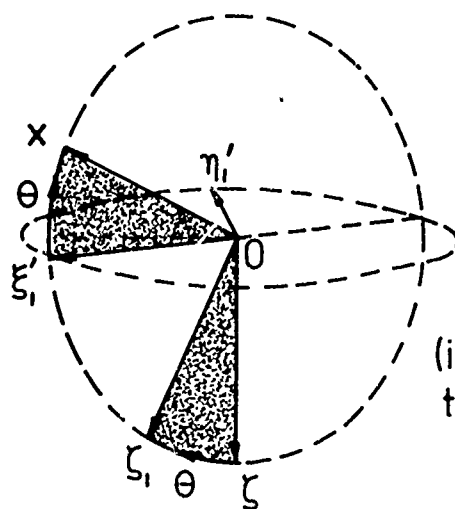


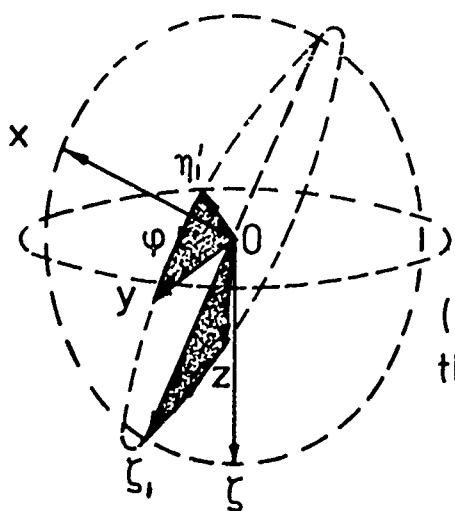
Figure 2.2. Laboratory-fixed coordinate frames.



(i) first rotation  
through  $\psi$  about  $Oz$



(ii) second rotation  
through  $\theta$  about  $O\eta_1'$



(iii) third rotation  
through  $\varphi$  about  $Ox$

Figure 2.3. Eulerian angles.

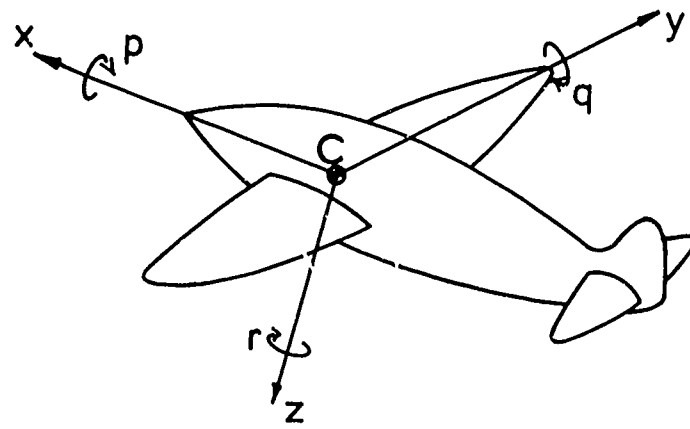


Figure 2.4. Body-fixed axes  $Cxyz$  and the angular velocity components  $(p,q,r)$ .

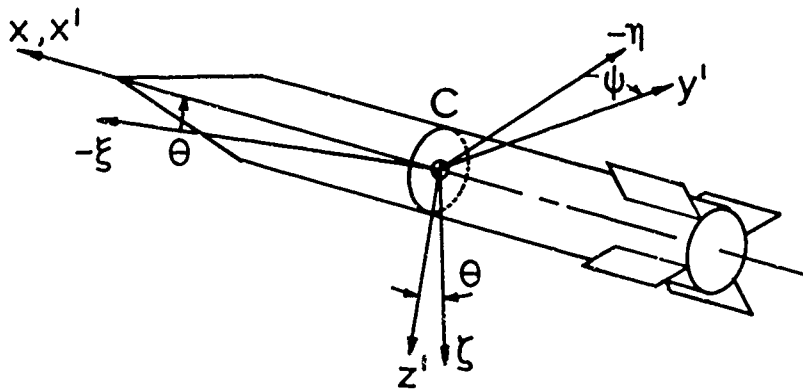


Figure 2.5. Body-oriented, fixed-plane axes  $Cx'y'z'$ . Such axes are useful for axially-symmetric shapes; the fixed-plane axes  $Cy'z'$  do not roll about  $Cx'$  though the body may do so.

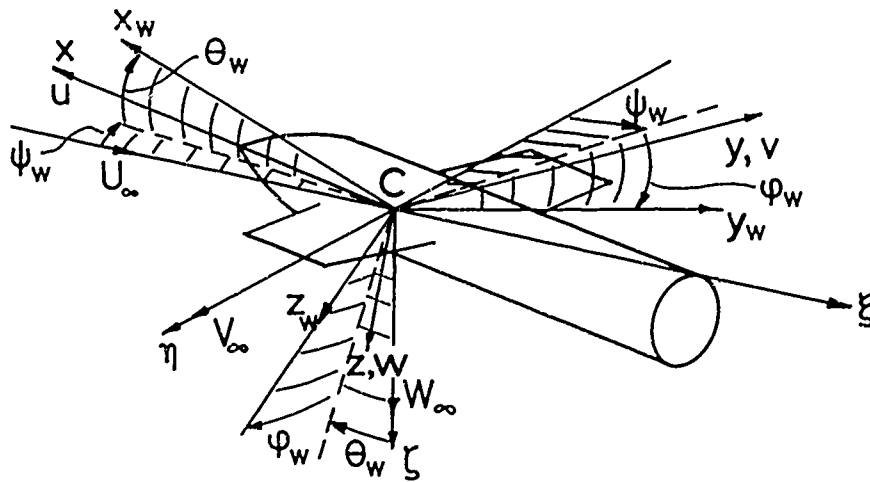


Figure 2.6. Wind axes  $Cx_w y_w z_w$ .

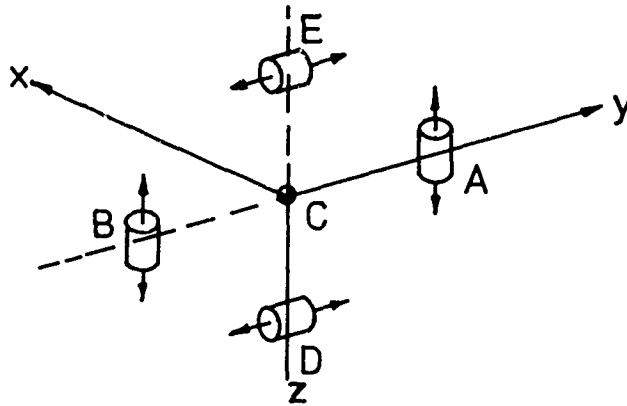


Figure 2.7. A commonly-used arrangement of linear accelerometers for measuring linear and angular accelerations.  $y_A + y_B = 0$ ;  $z_D + z_E = 0$ . Arrows indicate the axes of sensitivity.

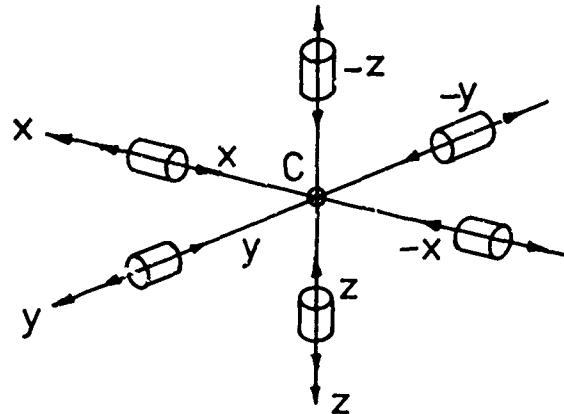


Figure 2.8. An "optimum arrangement" of linear accelerometers for determining  $\omega(t)$ . The accelerometers are placed symmetrically about the centre of mass C.

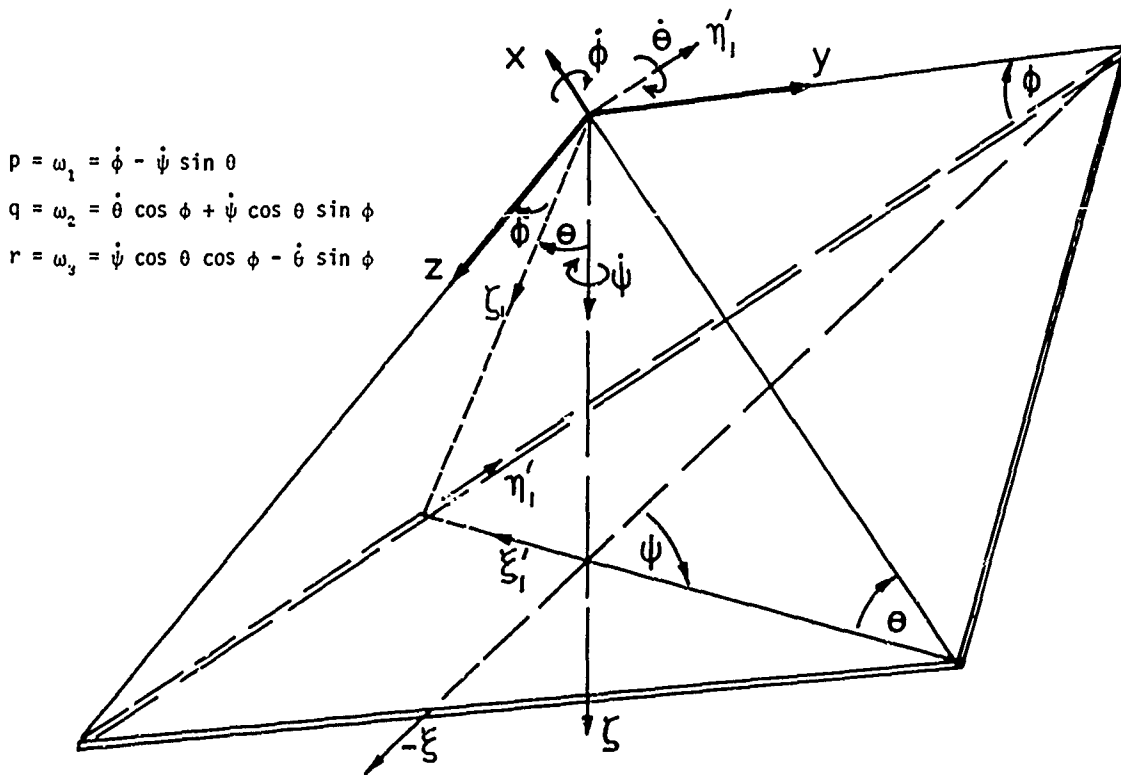


Figure 2.9. A "geometric derivation" of the relationship between the angular rates (p,q,r) in the body-fixed frame and the Eulerian angles ( $\psi, \theta, \phi$ ).

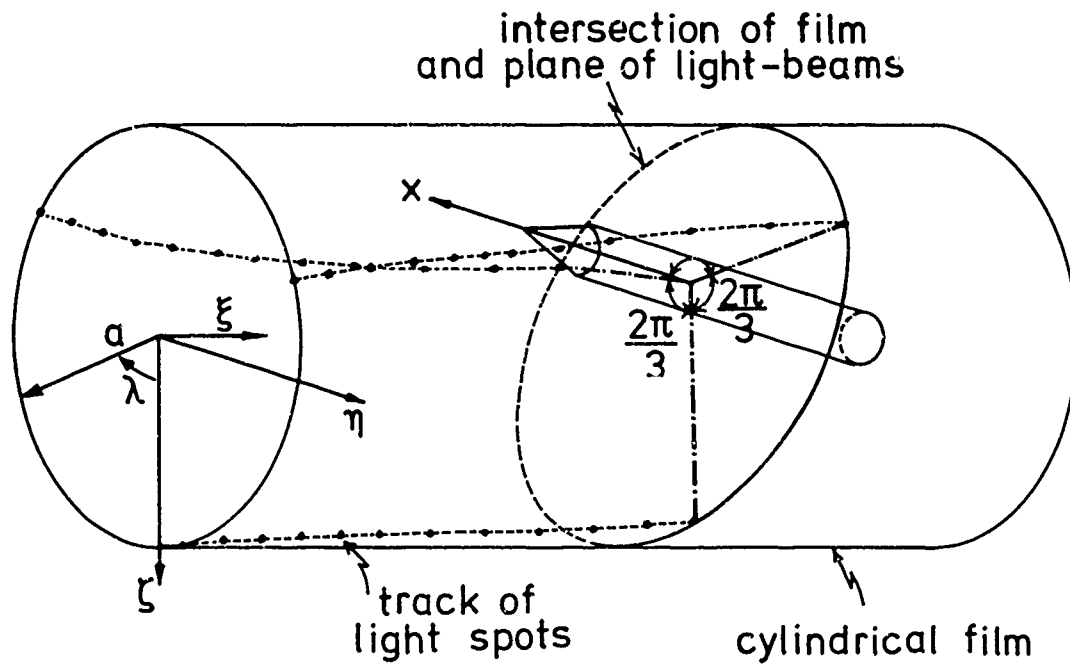


Figure 2.10. The principle of the D.F.V.L.R. (Porz Wahn) optical telemetry system. A flashing light within the model produces three beams 120° apart about the roll axis. A film, wrapped around the test-section records the three tracks of light spots.

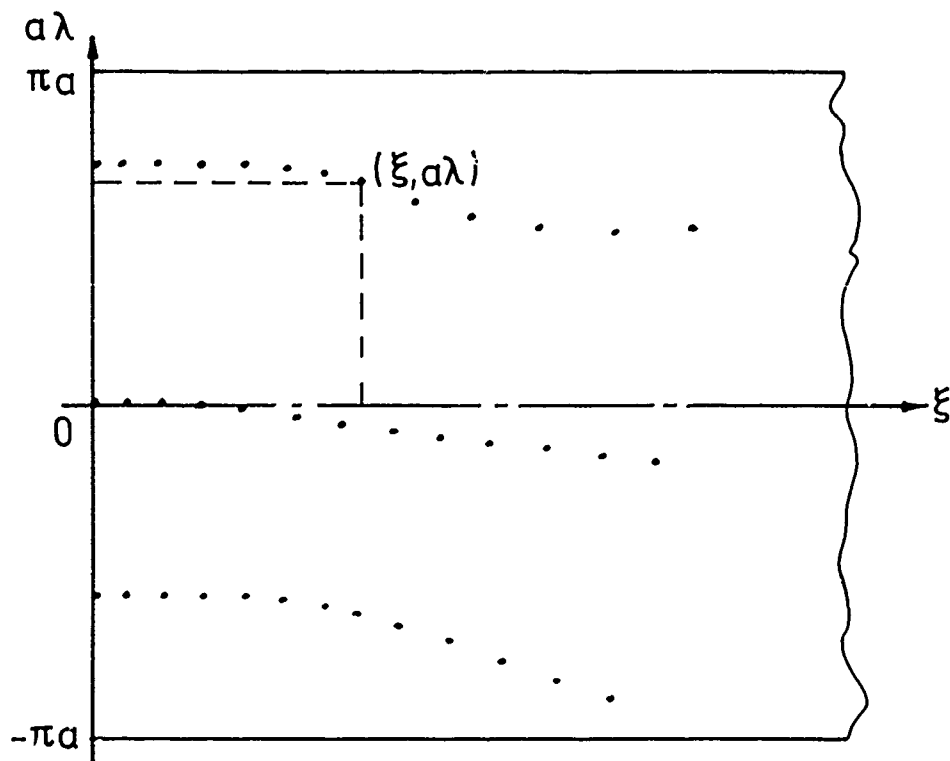


Figure 2.11. The unwrapped cylindrical film of figure 2.10 showing the relation between the coordinates in the laboratory-fixed frame  $(0\xi\eta\zeta)$  and measurements on the film.

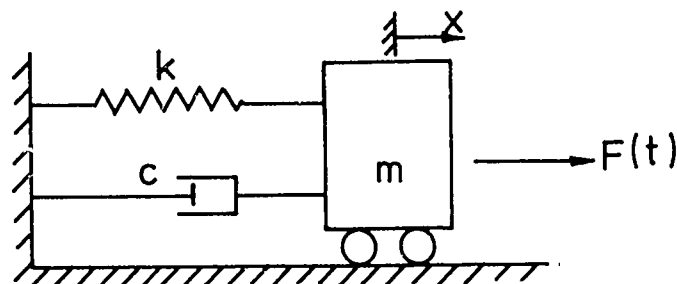
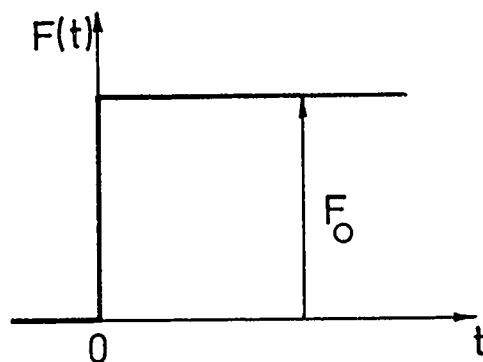
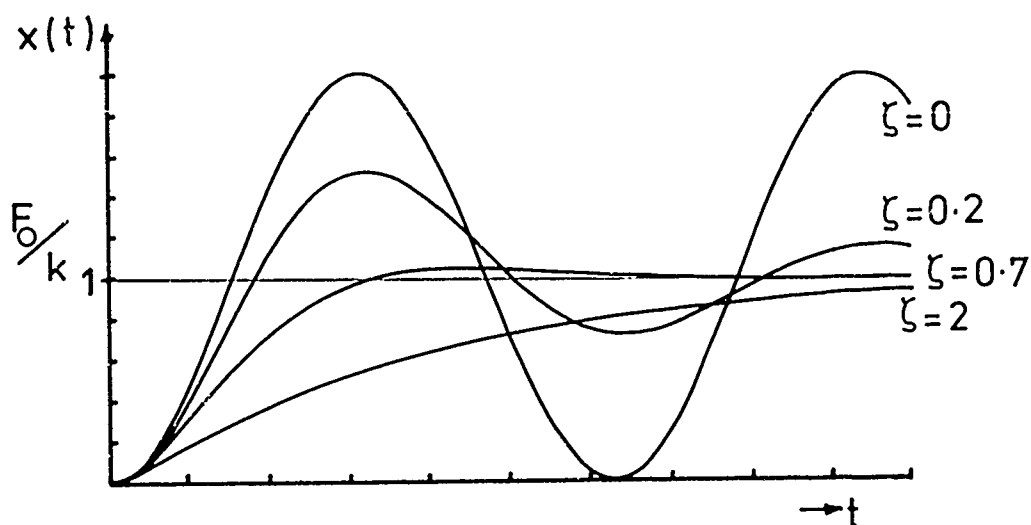


Figure 2.12. A simple, linear system having one degree of freedom. A force  $F(t)$  is applied to the body of mass  $m$ , the motion of which is restrained by a spring of stiffness  $k$  and a viscous damper of coefficient  $c$ .



a) step input,  
 $F = 0$  for  $t < 0$   
 $F = F_0$  for  $t > 0$



(b)

Figure 2.13. The response  $x(t)$ , of the system of figure 2.12, to a step input of force of magnitude  $F_0$ , for various values of the damping ratio  $\zeta = c/(2\sqrt{mk})$ .  
 (a) input force (b) responses.

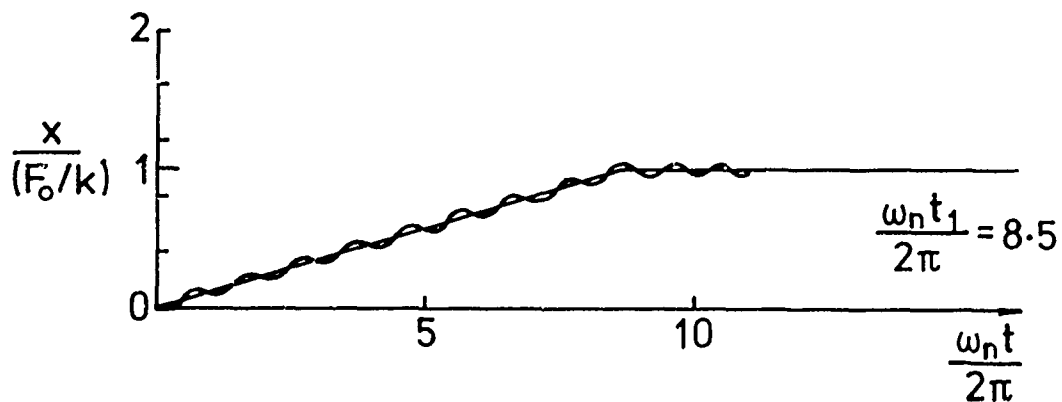
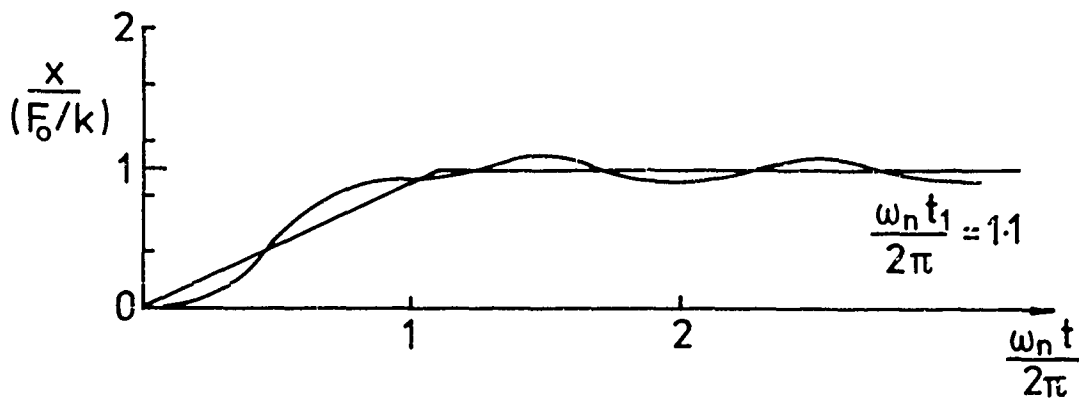
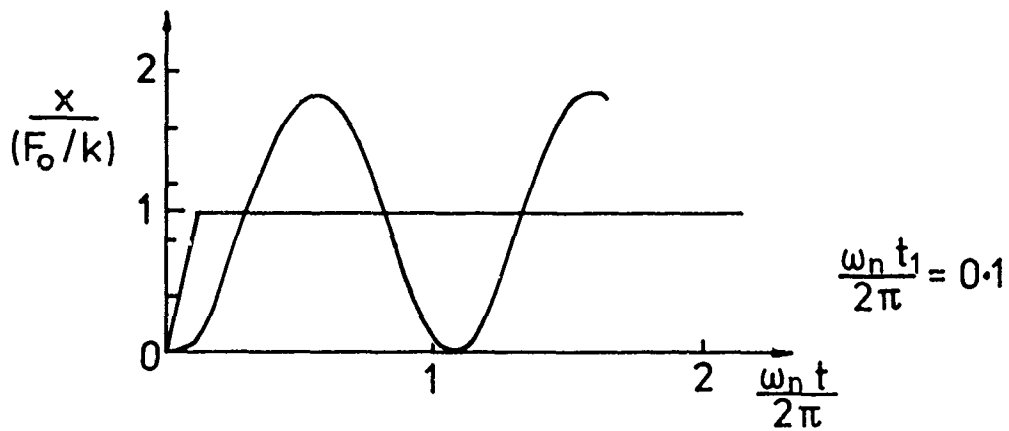
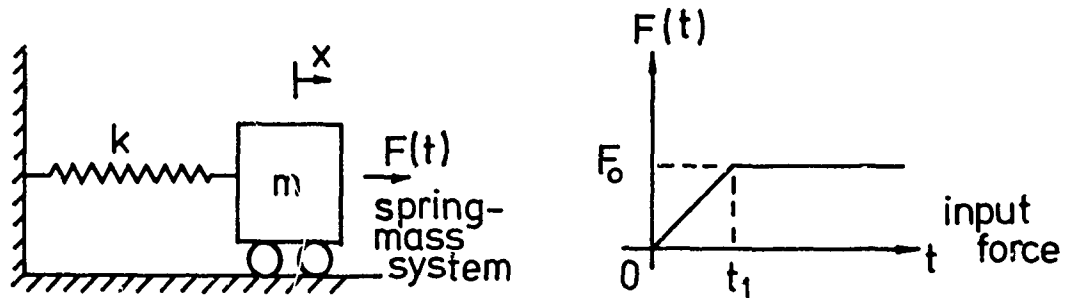


Figure 2.14. The response  $x(t)$  of an undamped linear system to a "ramp-step" force input for various values of the ratio of rise time  $t_1$  to characteristic period of the system  $2\pi/\omega_n$ .

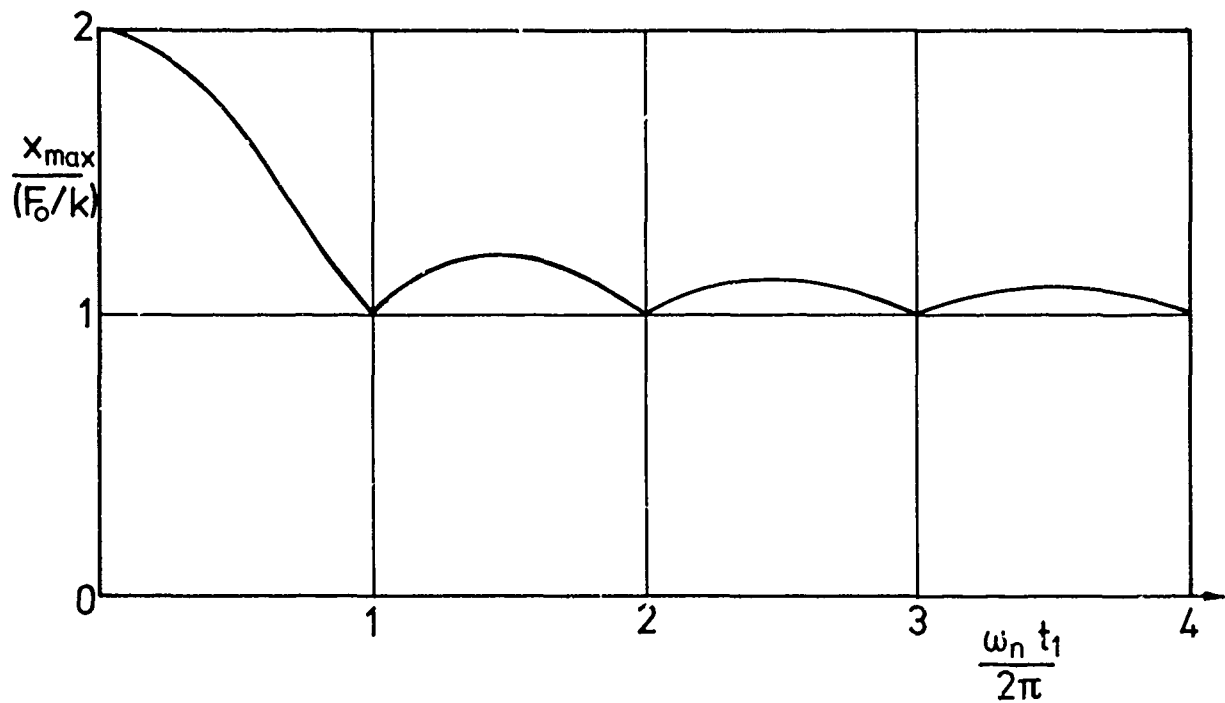


Figure 2.15. The "maximax" displacement spectra for the ramp-rise-step input.

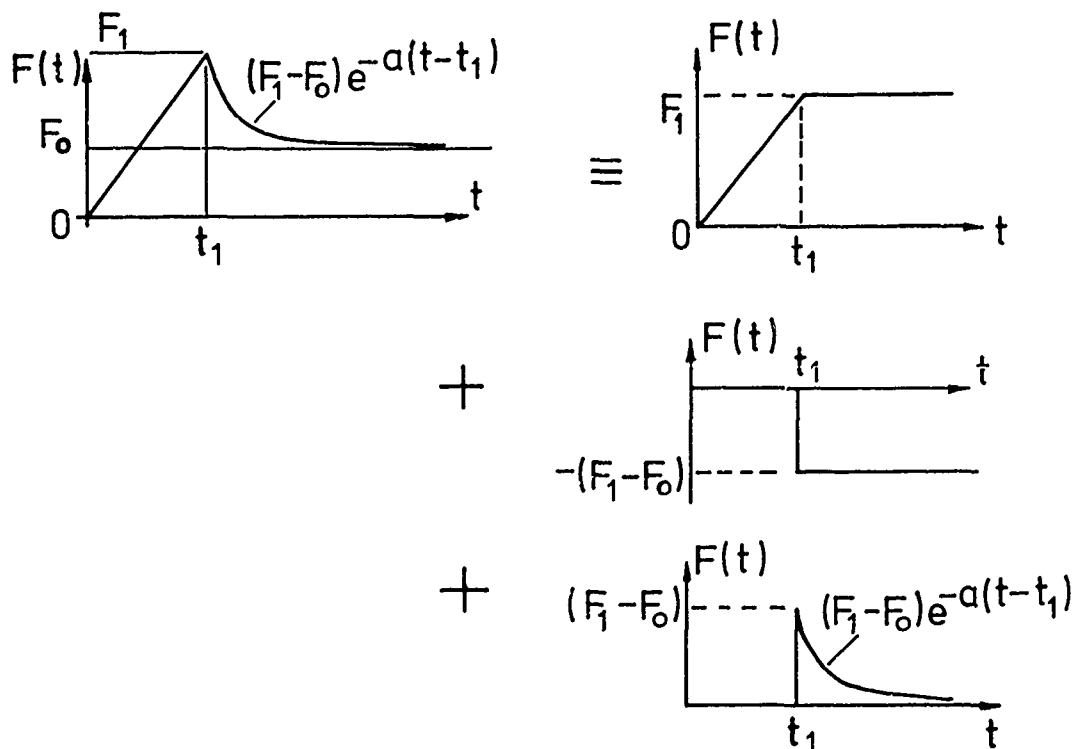


Figure 2.16. A simple idealisation of the input force which might be used to examine the effects of an "overshoot" in the input force function. For a linear system the response may be determined as the sum of the responses to the three simpler inputs from which the idealisation may be compounded.

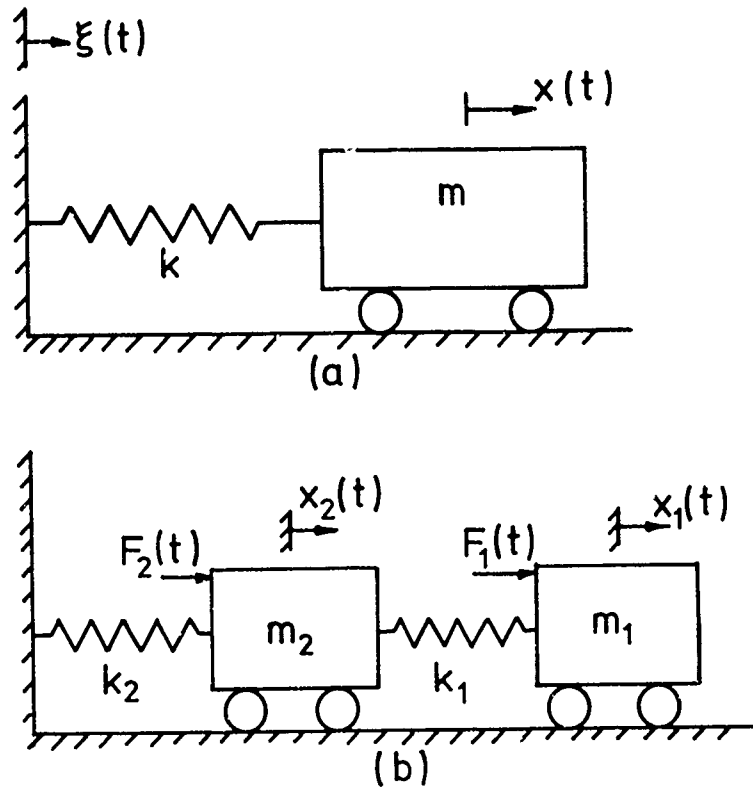


Figure 2.17. (a) An undamped system having one degree of freedom, undergoing base excitation. (b) An undamped system having two degrees of freedom.

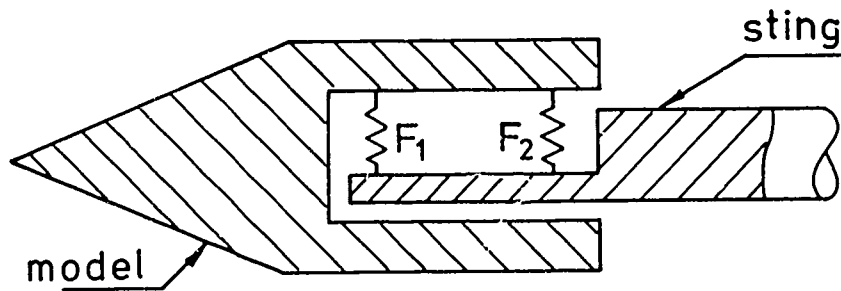


Figure 2.18. A frequently-used arrangement of force transducers for resolving normal-force and pitching moment. The transducers are represented by  $F_1$  and  $F_2$ .

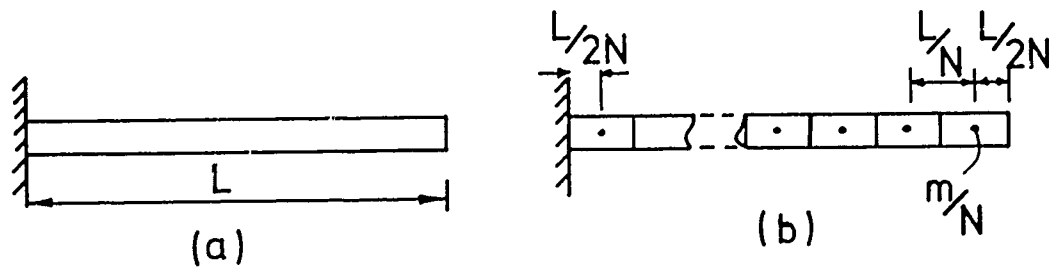


Figure 2.19. A lumped-parameter representation of a uniform cantilever.

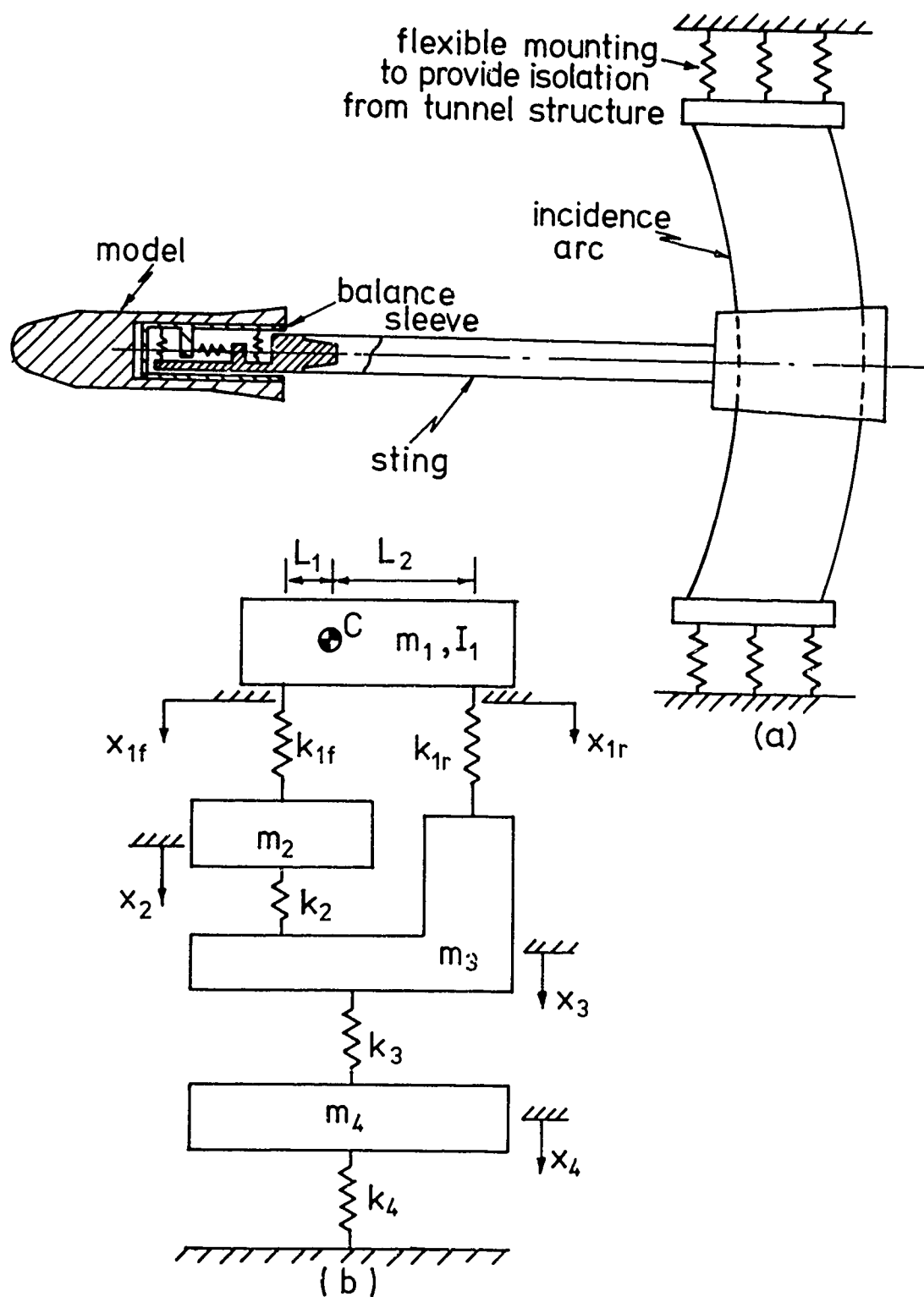


Figure 2.20. A lumped-parameter representation of the transverse motion in the pitch-plane of a three-component force balance; (a) schematic diagram of the model-balance-sting and arc-support assembly, (b) its representation. Representing the bending stiffness of the cantilever-sting by a single spring of stiffness  $k_3$  and an effective lumped mass  $m_3$  (at the position of the rear normal force transducer), means that only its fundamental mode is included. The balance body is often a thin shell, fairly flexible in bending; it is represented by  $k_2$  and  $m_2$ . Again only its fundamental mode is taken into account. The model is assumed to be a rigid body of mass  $m_1$  and moment of inertia  $I_1$  about axis  $Cy$ . The incidence-arc, slider and platform are represented by a body of mass  $m_4$  supported on soft springs of stiffness  $k_4$ .

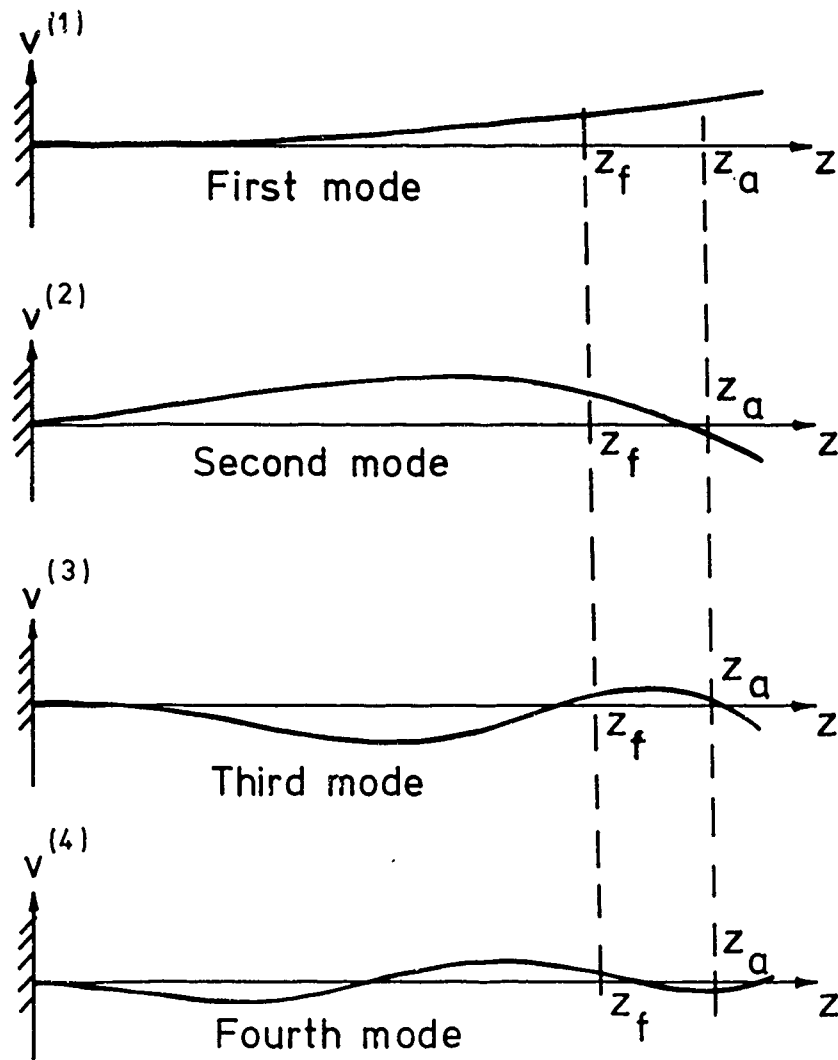


Figure 2.21. Schematic representation of the first four modal shapes of a uniform cantilever vibrating transversely.

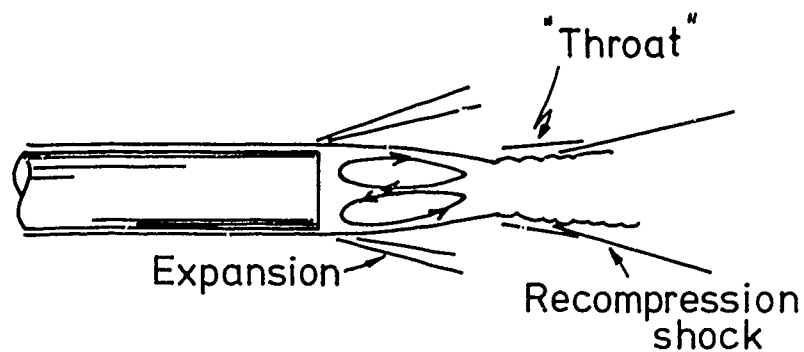


Figure 2.22. The undisturbed near-wake region of a slender, axially-symmetric body in a supersonic stream.

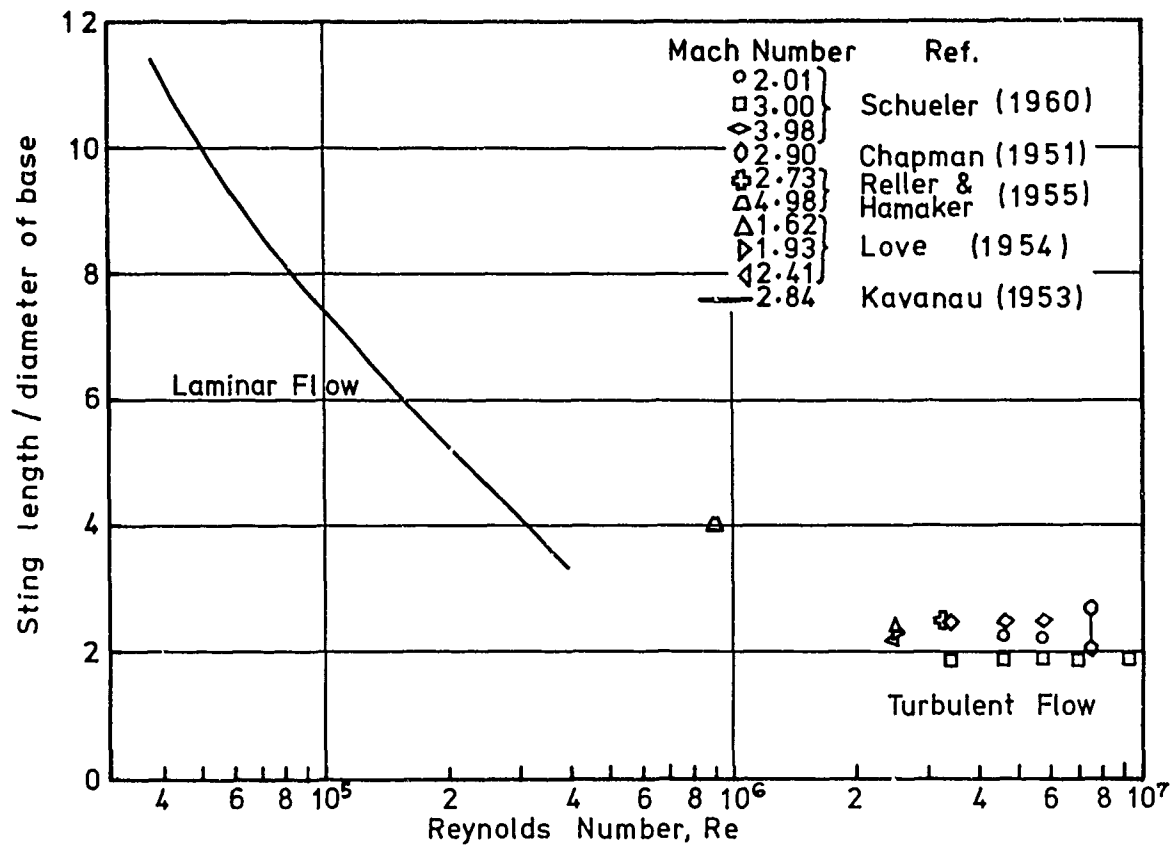


Figure 2.23. The effect of Reynolds number on critical sting length (after Schueler, 1960).

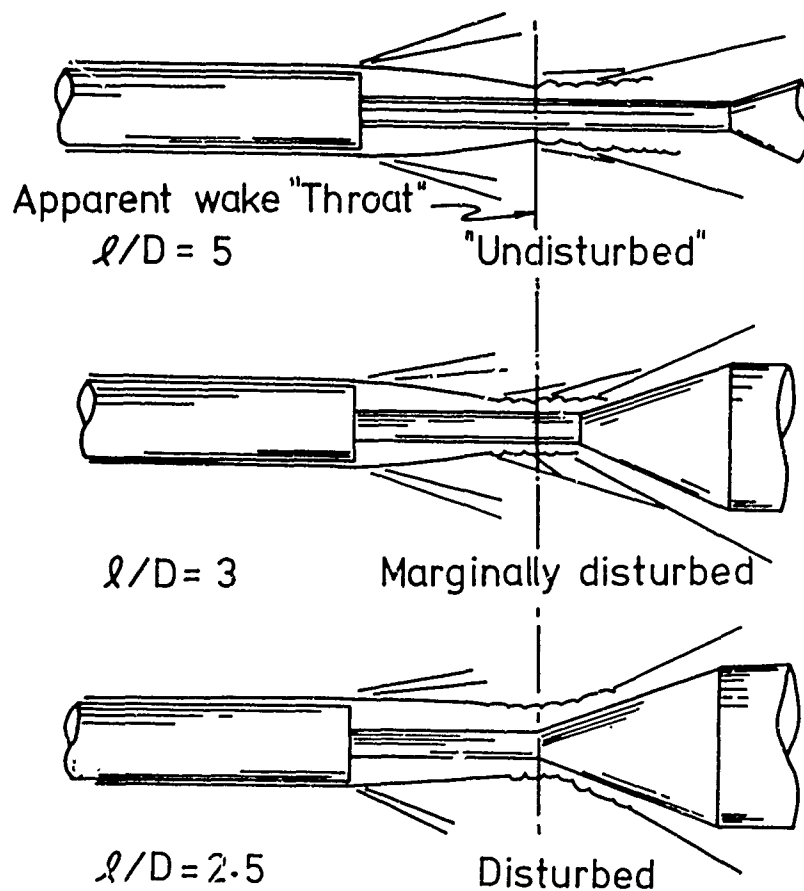


Figure 2.24. The effect of sting length on the "transitional wake" (after Whitfield, 1959).

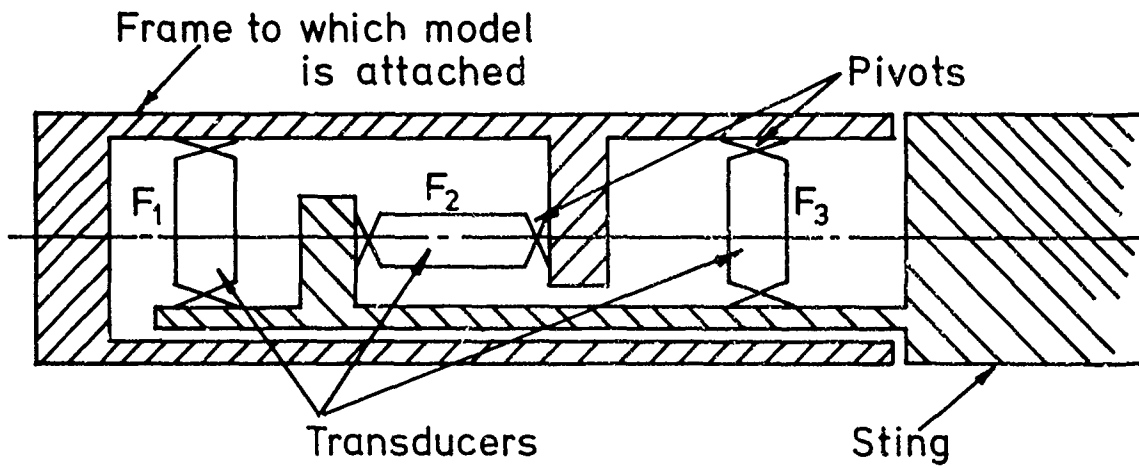


Figure 3.1. Schematic arrangement of force-transducers for a three-component balance.

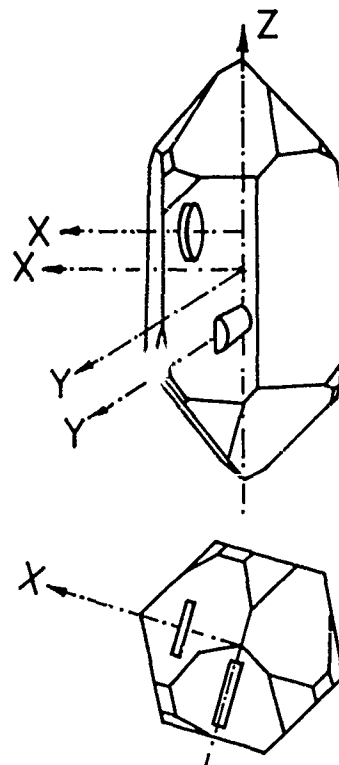
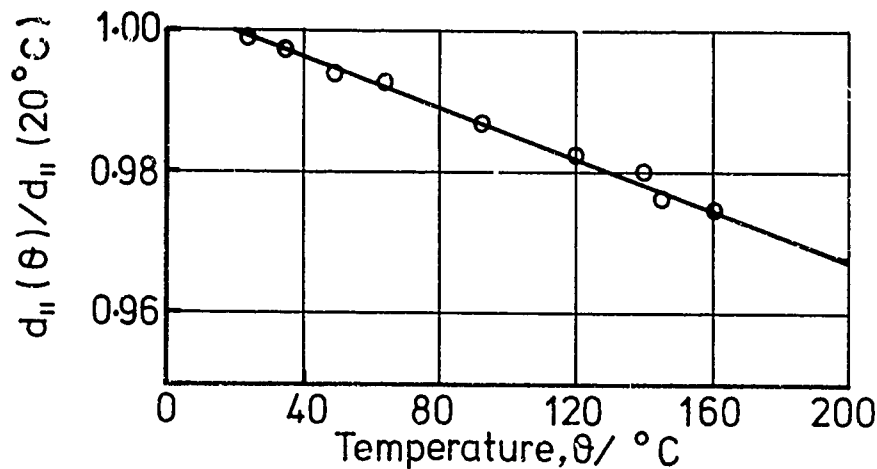
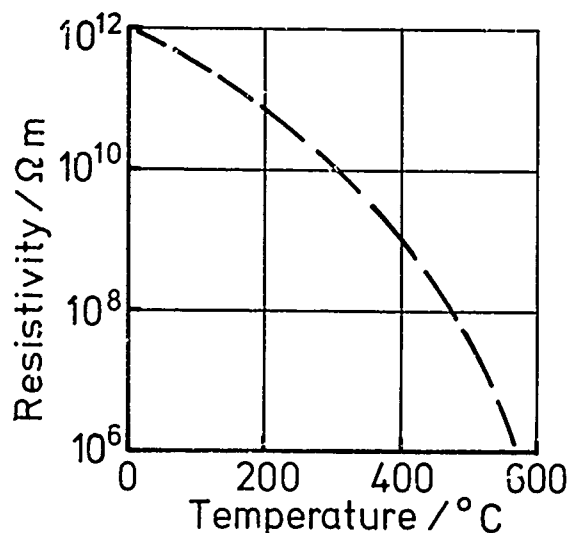


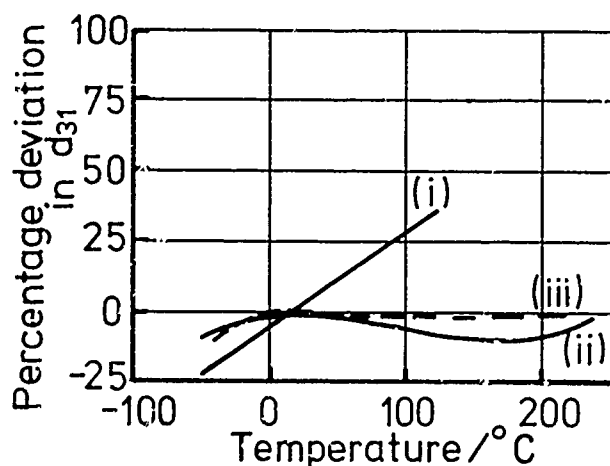
Figure 3.2. Quartz crystal "cuts" (after Kistler, 1970).



(a) Temperature dependence of piezoelectric coefficient  $d_{11}$  for quartz



(b) Variation of resistivity with temperature for quartz



(c) Temperature variation of  $d_{31}$  for some typical ceramics

i) High-sensitivity PZT-type material ~ G 1278

ii) BaTiO<sub>3</sub> ~ HD-11

iii) Moderate sensitivity, lead metaniobate ~ G-2000

Figure 3.3. Temperature dependence of some of the properties of some typical piezoelectric transducer materials. (G-1278, HD-11 and G-2000 are produced by Gulton Industries, Inc., Fullerton, California, U.S.A. under the trade name "Glennite".)

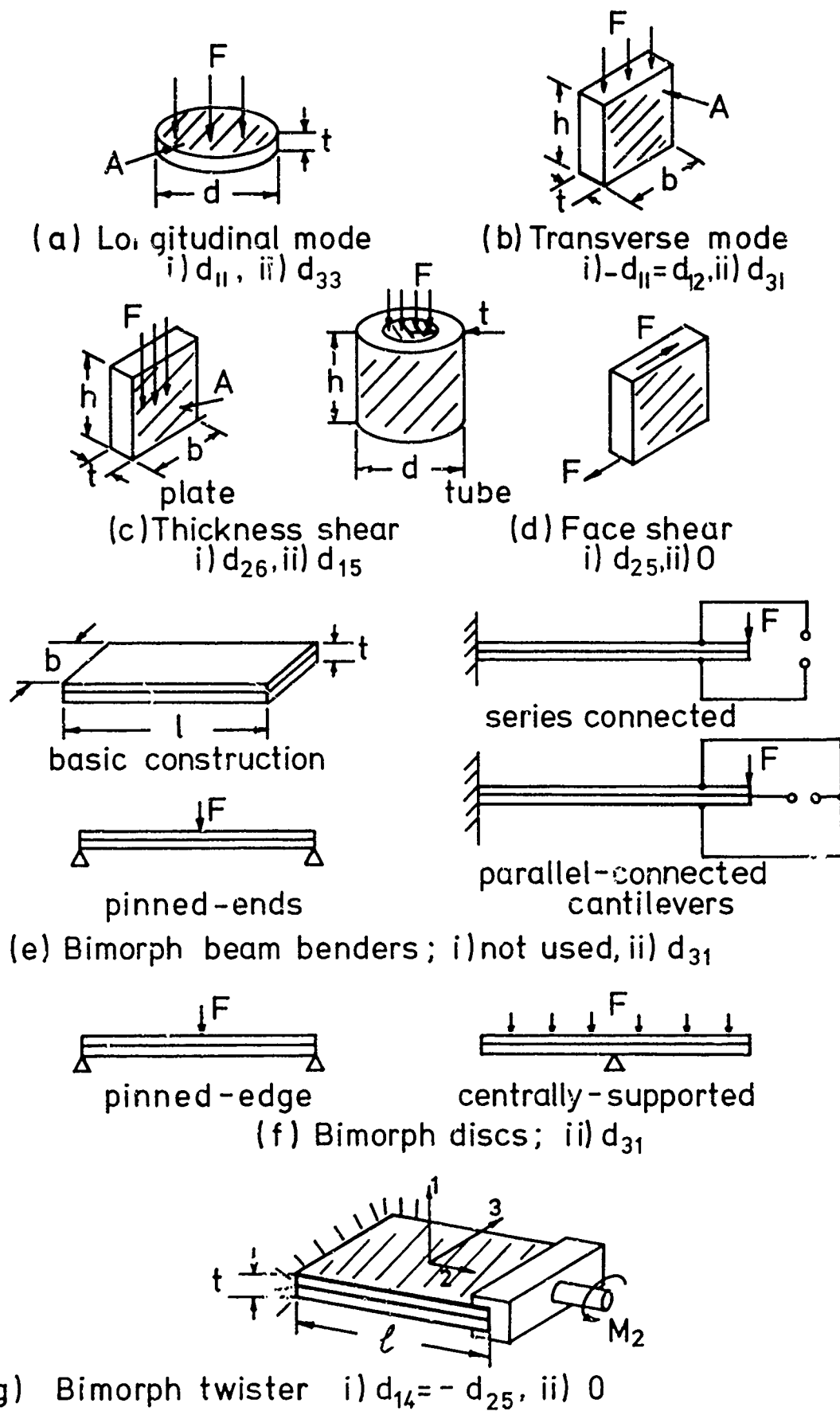


Figure 3.4. Some piezoelectric sensing element configurations. Relevant coefficients are shown for quartz (i) and ceramics (ii).

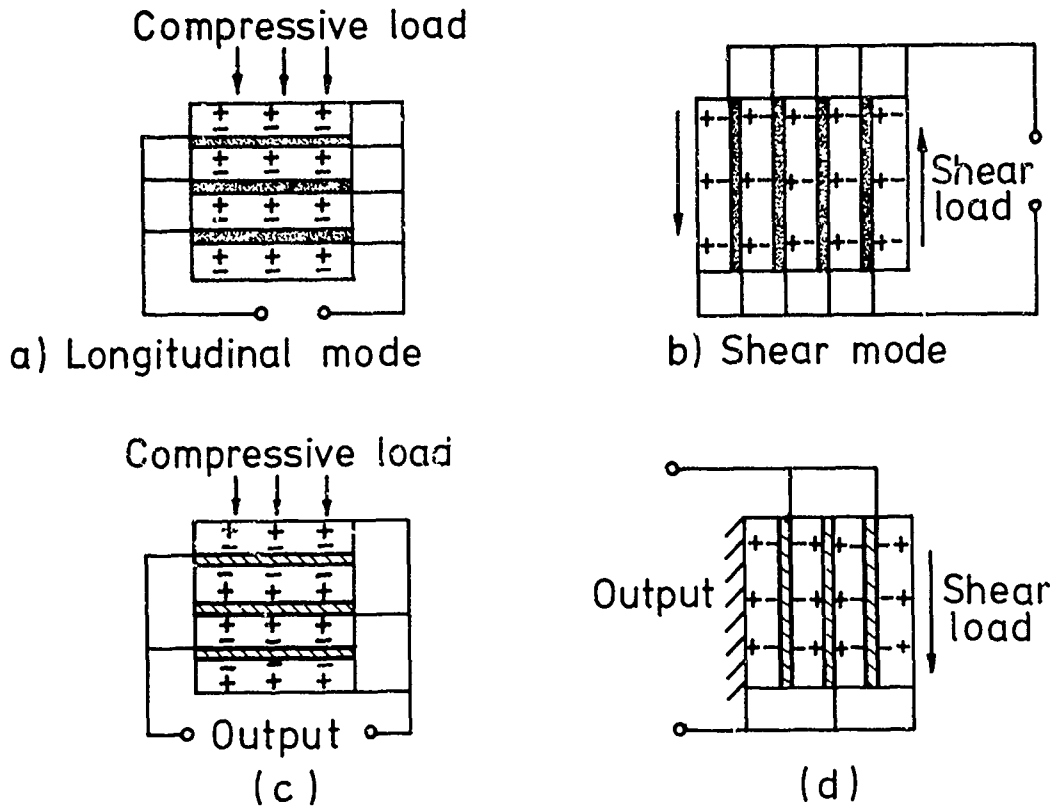


Figure 3.5. The "stacking" of piezoelectric elements to enhance the charge sensitivity to force. In (a) and (b) the elements have co-directional polarisation axes and insulating washers are necessary; in (c) and (d) adjacent elements are polarised in opposite direction.

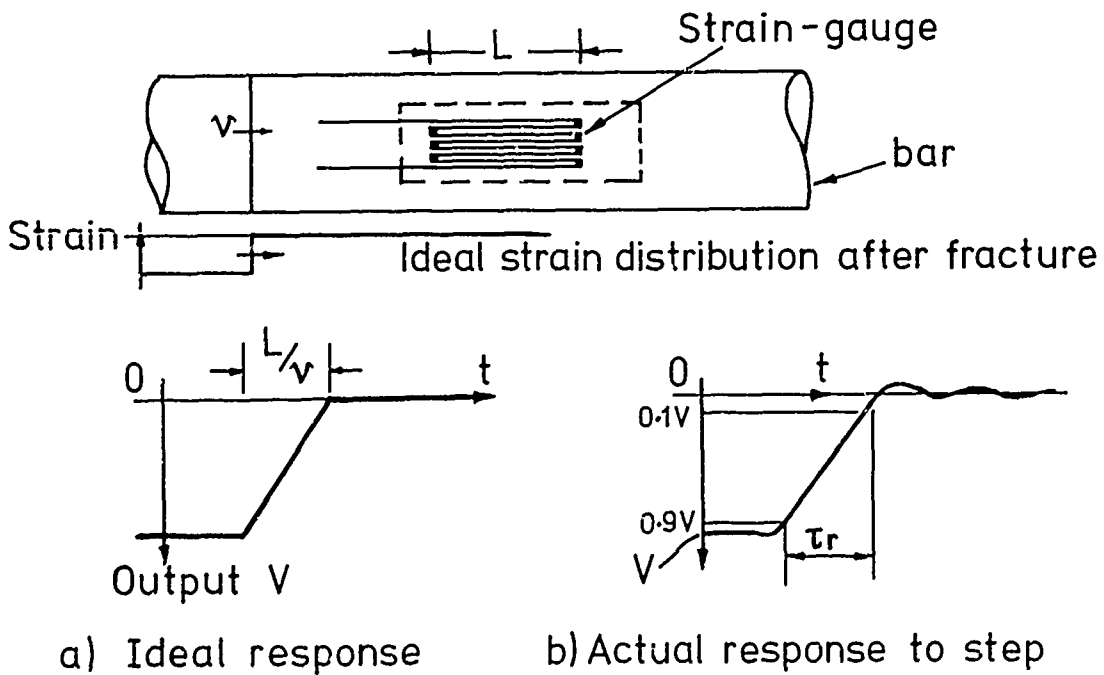


Figure 3.6. The dynamic response of piezoresistive strain gauges (after Koshiro Oi, 1965).

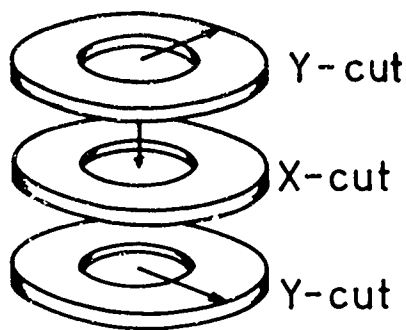


Figure 3.7. Quartz rings, X-cut for use in the longitudinal mode and Y-cut for use in the shear mode, as incorporated in load cells marketed by Kistler Instruments AG of Winterthur, Switzerland.

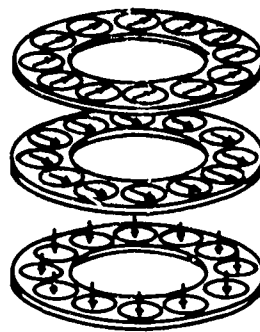


Figure 3.8. Rings containing suitably oriented quartz discs for incorporating in a load cell (after Kistler Instruments AG, Winterthur, Switzerland).

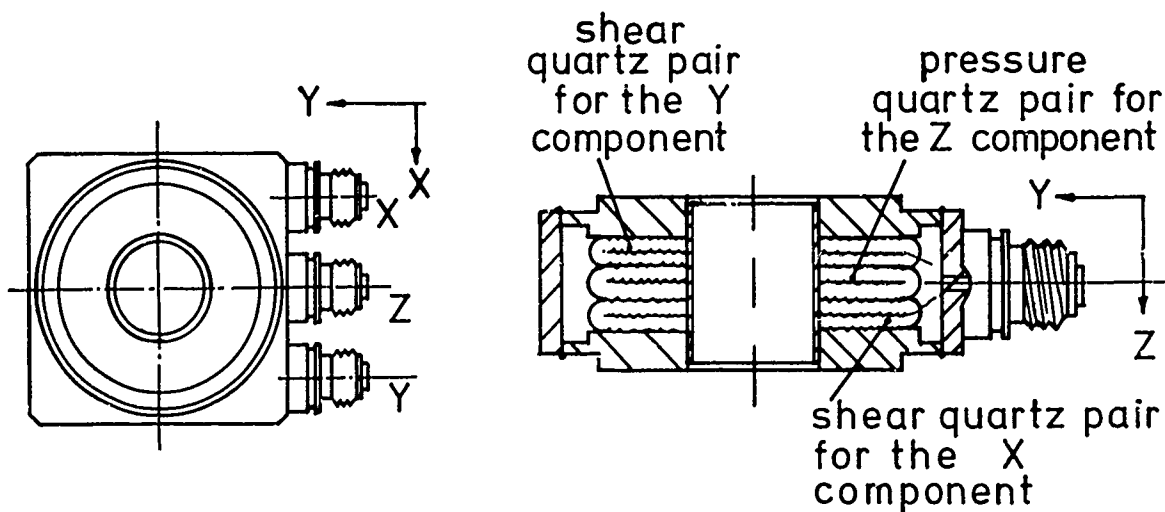


Figure 3.9. A three-component, quartz load-cell - type 9251, marketed by Kistler Instruments AG, Winterthur, Switzerland.

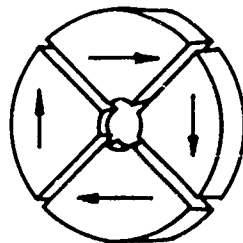


Figure 3.10. A sectored arrangement of shear sensitive elements for use as a torque transducer.

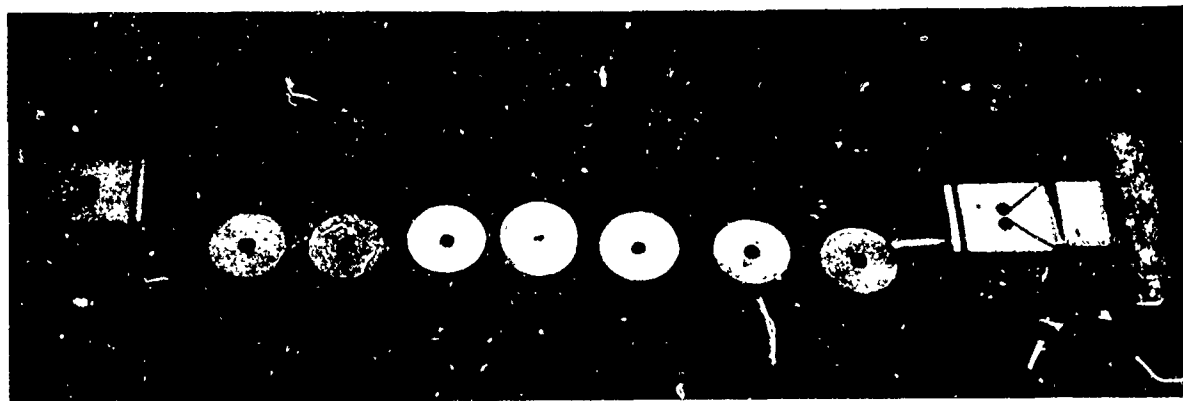


Figure 3.11. An "exploded view" of a force-transducer based on a PZT-disc used in the longitudinal mode. The ceramic is prestressed to about  $-10 \text{ MN/m}^2$  using a central (locked) screw, so that tensile loads can also be measured (after Cornell Aeronautical Laboratory).

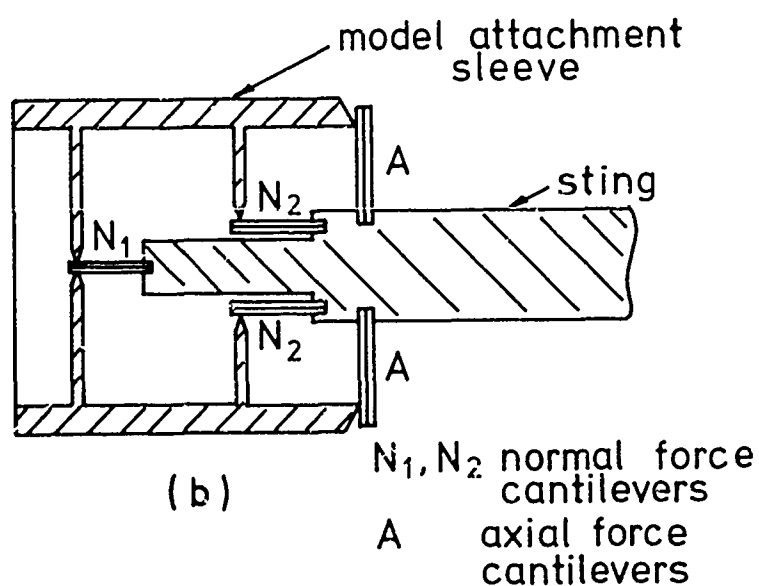
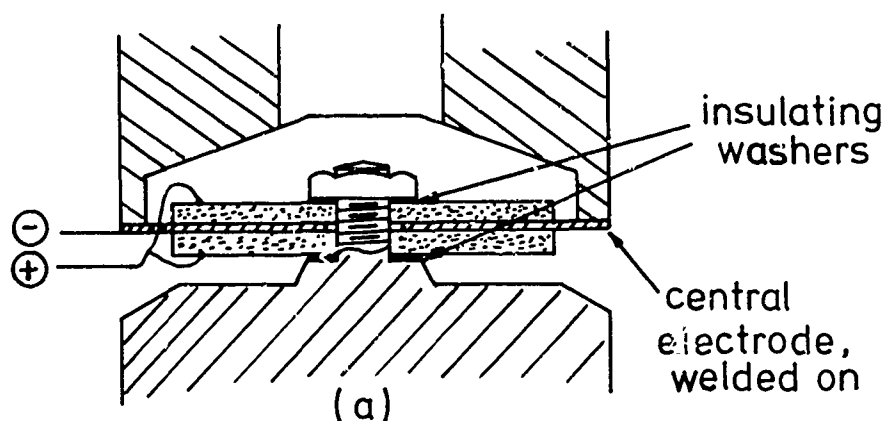


Figure 3.12. Schematic arrangements for very high sensitivity force transducers for use at low force levels;

(a) a single-component transducer based on a bimorph ceramic disc;

(b) a three-component transducer using bimorph ceramic beams.

Stops would need to be provided to limit the deflections.

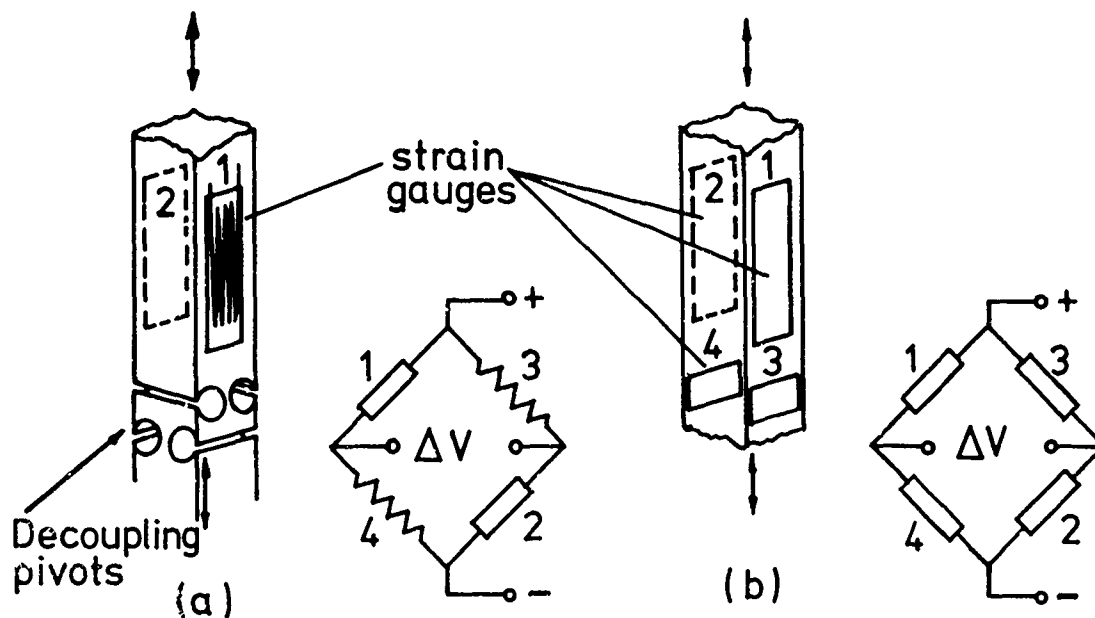


Figure 3.13. Simple prismatic load-link sensitive to tensile and compressive loads, (a) using a pair of resistance strain gauges connected in opposite arms of a Wheatstone bridge circuit to decouple bending loads, (b) using four gauges, one pair taking advantage of the "Poisson's ratio" effect to increase the sensitivity and provide temperature compensation.

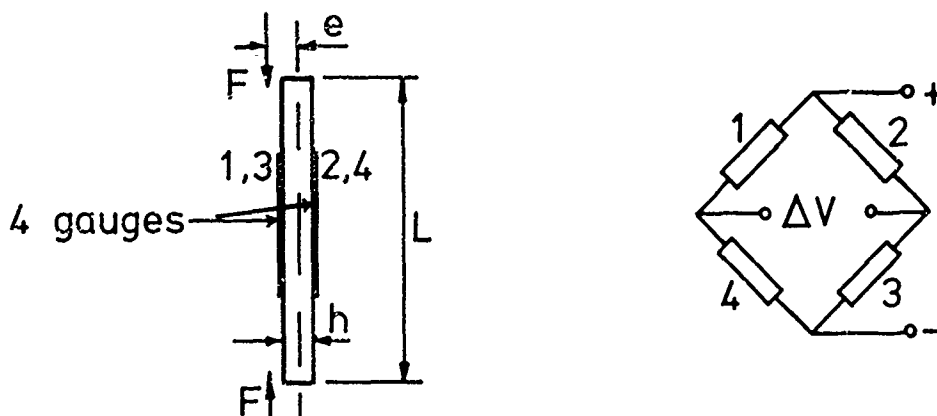


Figure 3.14. A force-link in the form of an eccentrically-loaded column. The strain gauges are connected so as to sense bending loads.

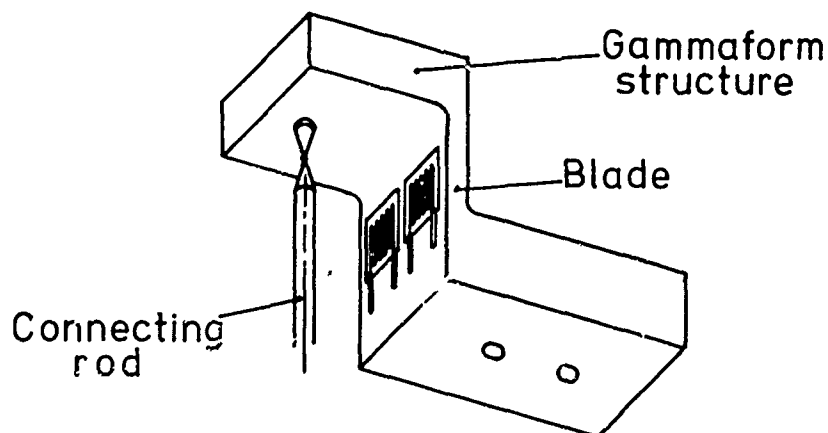
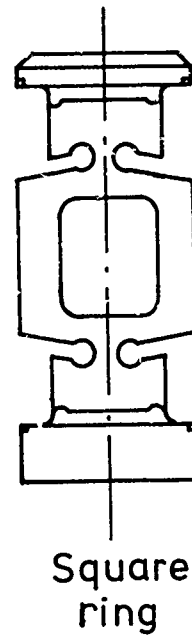
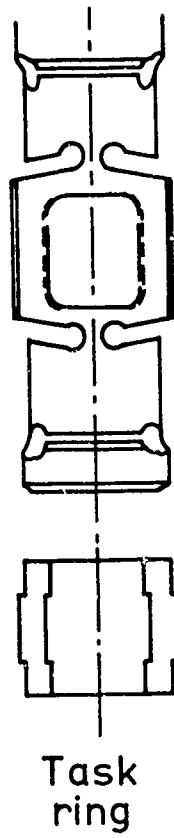
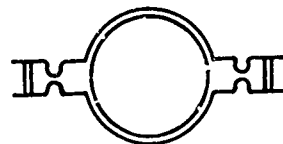
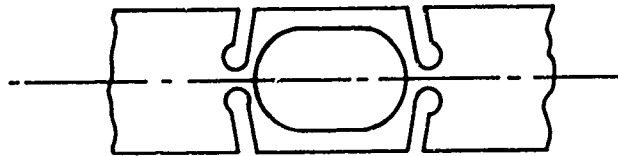


Figure 3.15. The "gammaform" load link; there is one pair of gauges on each side of the blade. (after Rebuffet, 1956).



Race track



Circular ring

Figure 3.16. Load-links in the form of rings. (The "Task ring" is reproduced by kind permission of Task Corporation, Anaheim, California, U.S.A.)

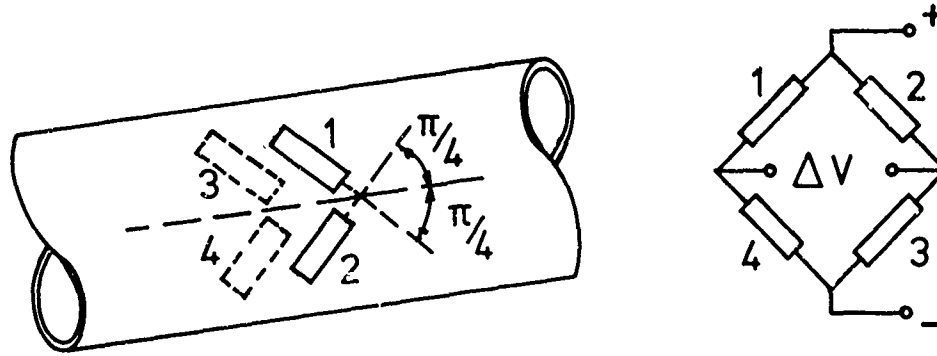


Figure 3.17. A torque-tube transducer for measuring rolling-moments - the output from the bridge is proportional to the shear strain in the thin wall.

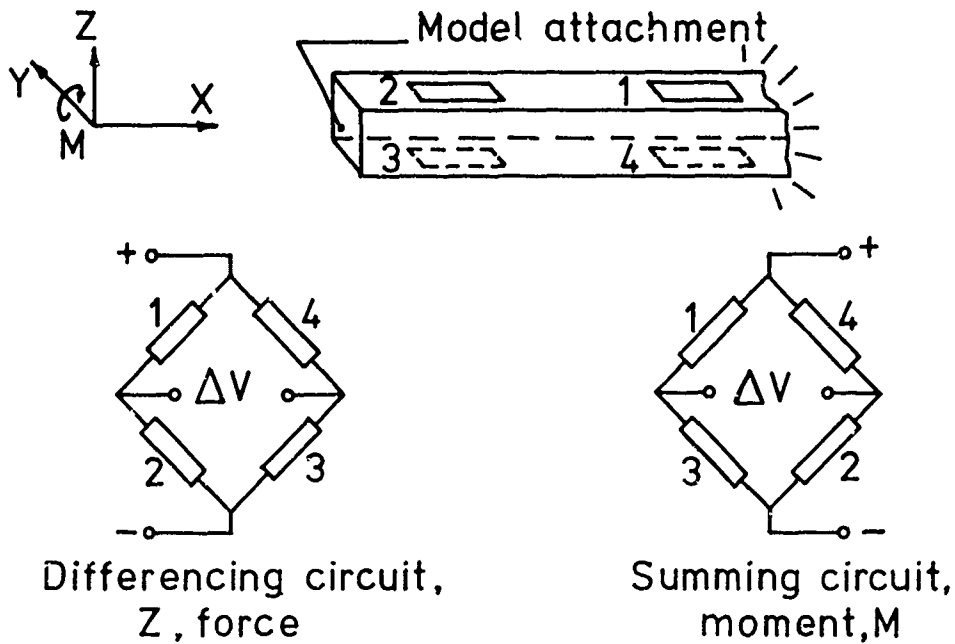


Figure 3.18. A simple cantilever, instrumented with strain-gauges for measuring the normal force or pitching moment.

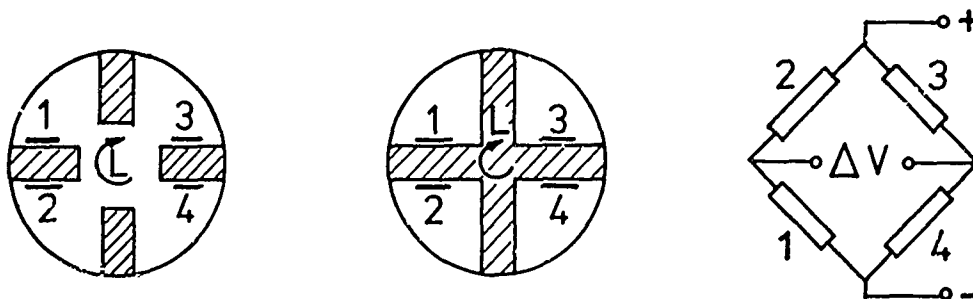


Figure 3.19. Specially-machined sections which are more sensitive to torque than a simple beam of the type shown in figure 3.18.

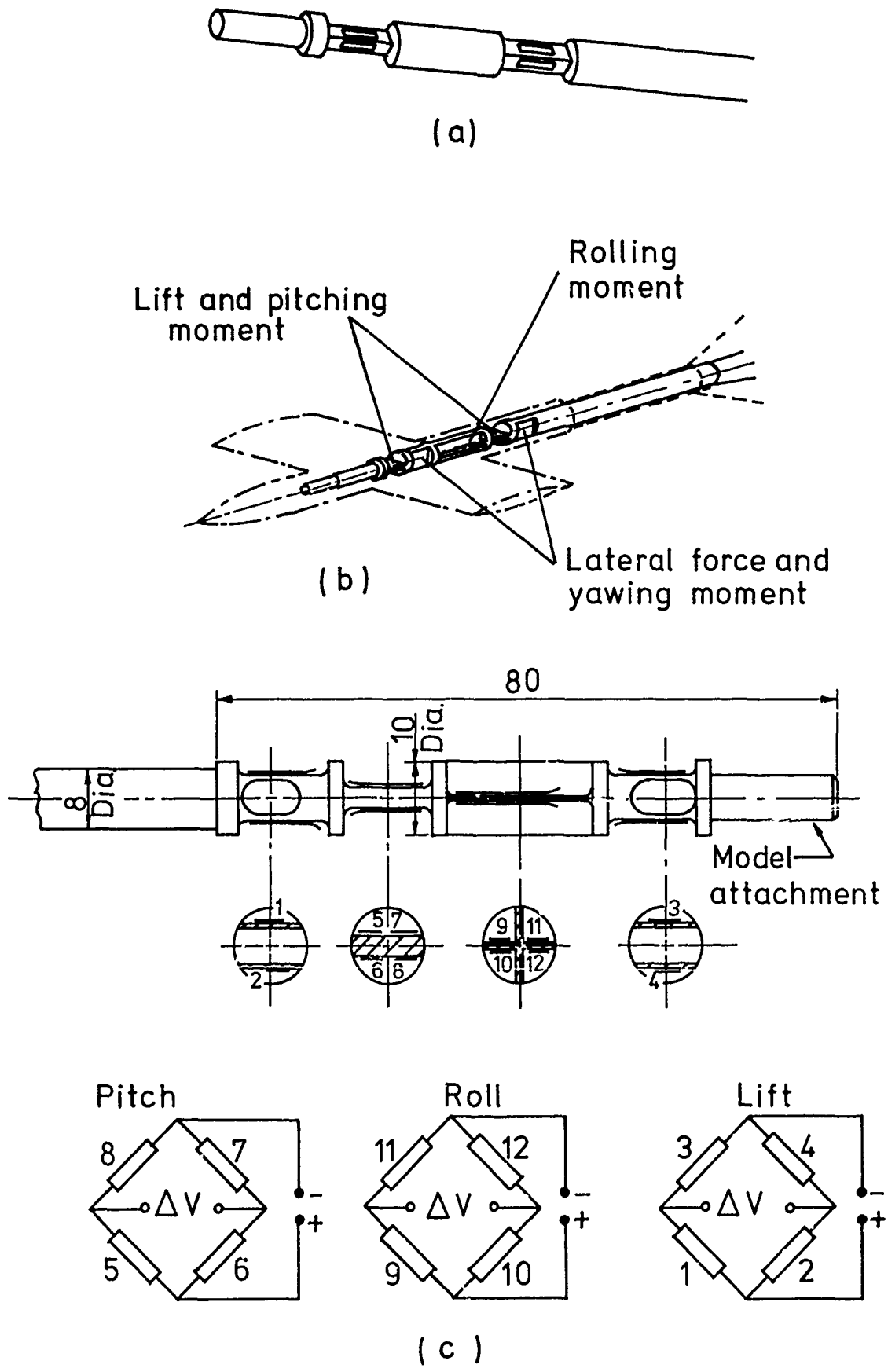


Figure 3.20. Some examples of instrumented, specially-machined cantilevers, or stings, for measuring five components of the load on a model in a conventional wind tunnel. The axial-load is not resolved by any of these arrangements (adapted from Rebuffet, 1956).

Reproduced from  
best available copy.

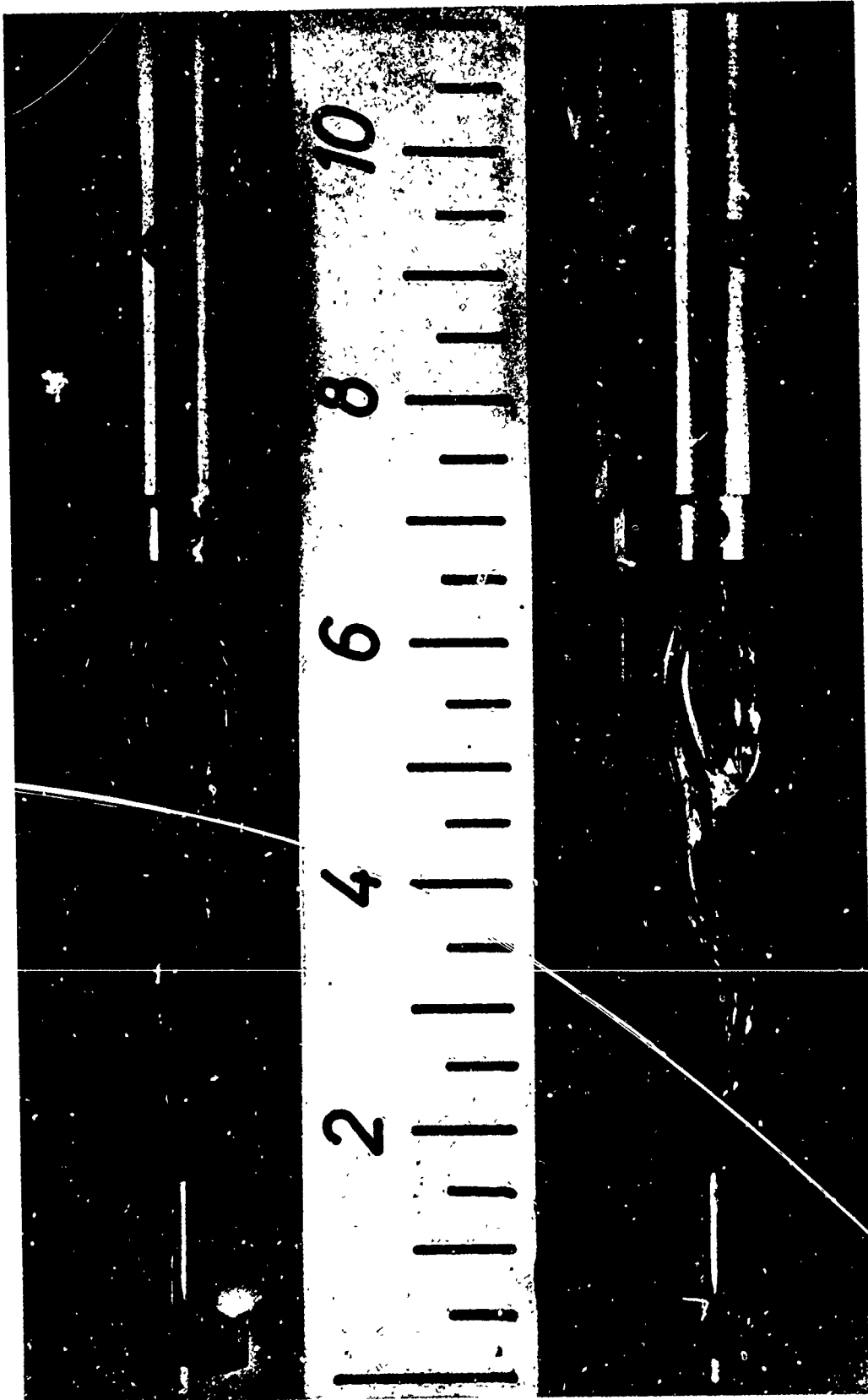


Figure 3.21. Strain-gauge balances designed for use in the gun-tunnel at the Institut für Stromungsmekaniik, Braunschweig. Conventional, metal-foil gauges were used.

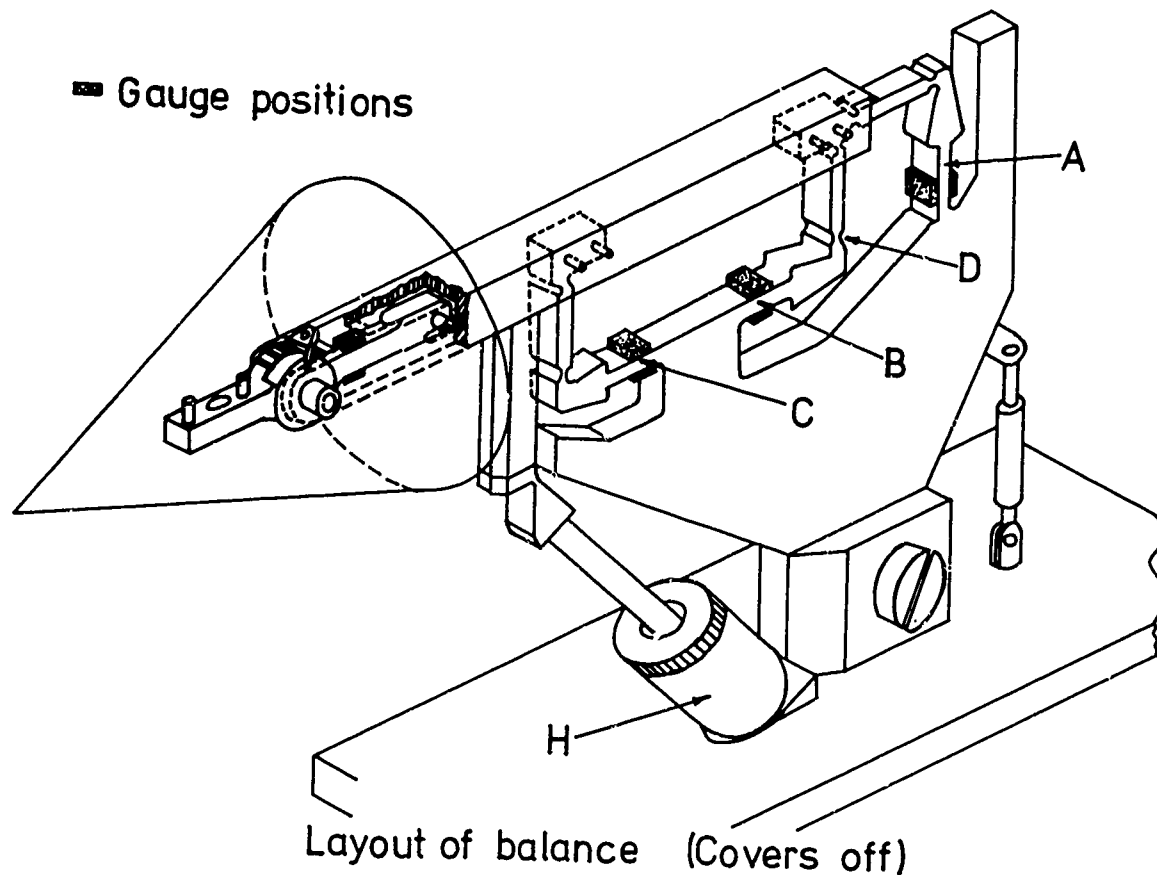


Figure 3.22. An "external" three-component, strain-gauge force balance, which incorporates an hydraulic damper H, designed for use in the gun-tunnel at Imperial College, London. The aft cantilever A measures drag, and cantilevers B and C measure lift. The latter pair were also intended to measure pitching moment but were not sensitive enough. Pitching moments were resolved by the gauges on the forward sub-beam. (Opatowski, 1966).

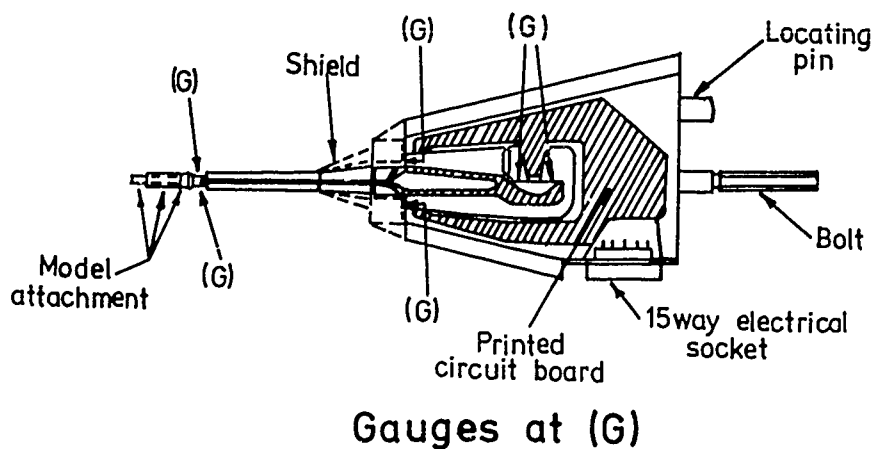


Figure 3.23. A more compact, three-component balance designed for use in the gun-tunnel at Imperial College, London. The foremost gauge pair measures the pitching moment. Four gauges at the rear, one either side of the two tension links, resolve the axial force, and a similar, "vertical" arrangement at the centre give the normal force. The lowest natural frequency, with no model attached was 350 Hz (Opatowski, 1971).

## Balance Body

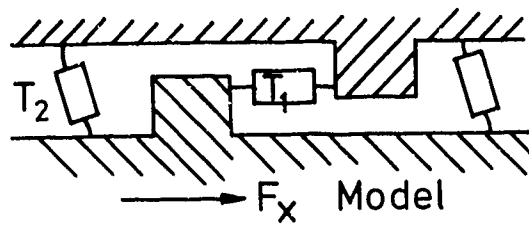


Figure 3.24. The angular displacements of the pivots of transducer  $T_2$  is governed largely by the axial displacement of transducer  $T_1$  at right angles to it. Provided these pivots are laterally very compliant,  $T_2$  does not respond significantly to a force  $F_1$  along the axis of  $T_1$ .

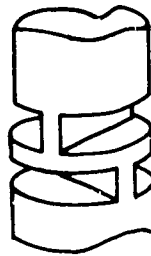
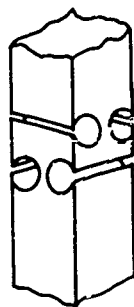
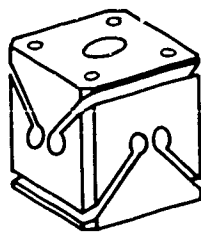


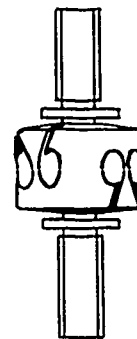
Figure 3.25. The basic principle of the elastic flexure - two thin flat strips at right angles to one another are positioned at each end of the force transducer.



(a)



(b)



(c)

Figure 3.26. Some practical examples of the more compact "circular-arc" flexures. Type (c) is marketed by Task Corporation, Anaheim, California, U.S.A.

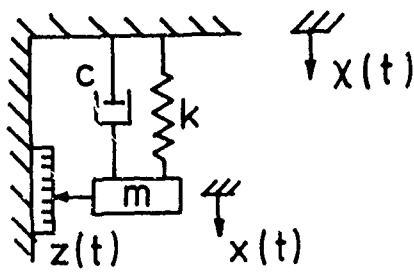


Figure 3.27. The principle of an accelerometer - the "absolute" motion  $x(t)$  of an inertial element is restrained by a spring of stiffness  $k$  and a viscous damper of coefficient  $c$ . The acceleration of the base  $\ddot{x}(t)$ , is inferred from the deflection  $z = (x - \chi)$  of the elastic element.

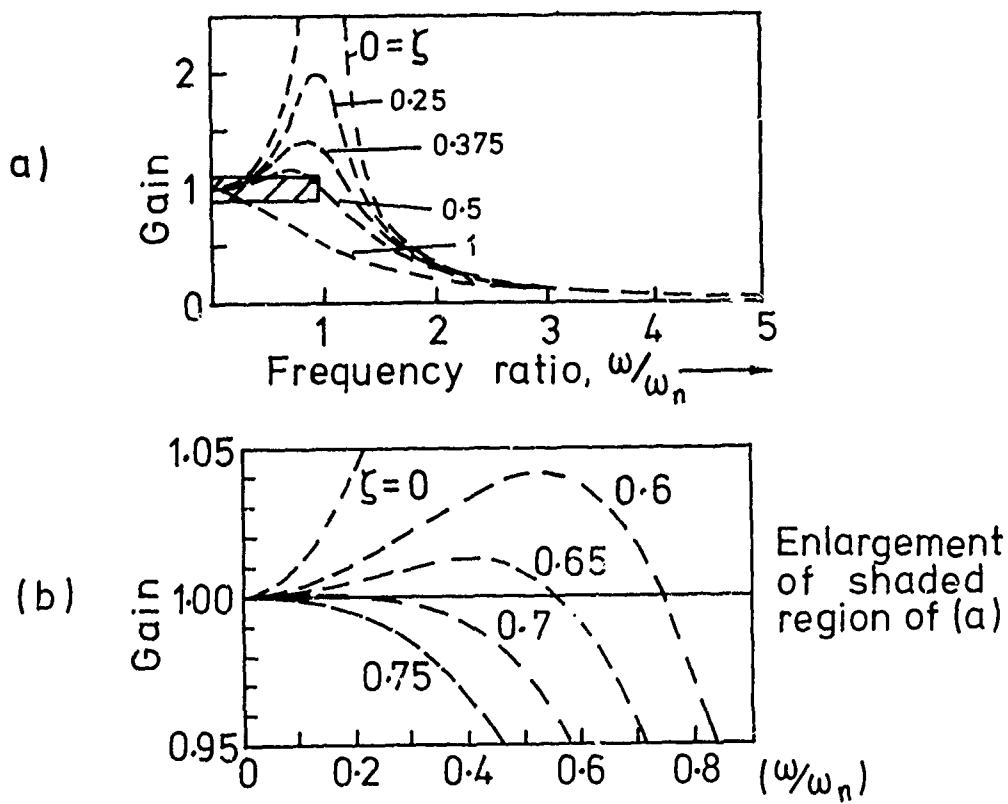


Figure 3.28. The gain factor  $\{[1 - (\frac{\omega}{\omega_n})^2]^2 + [2\zeta\frac{\omega}{\omega_n}]^2\}^{-\frac{1}{2}}$  as a function of frequency ratio  $\omega/\omega_n$  and damping ratio  $\zeta$ .

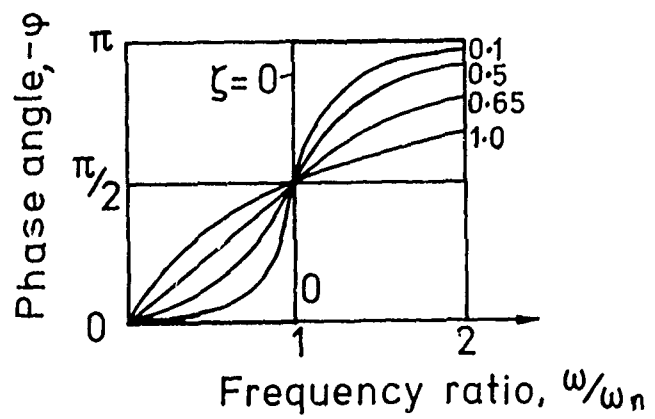


Figure 3.29. The phase difference  $\phi$ , between the response of an accelerometer and the acceleration of the object to which it is attached, as a function of frequency ratio and damping ratio  $\zeta$ . [Note that for  $\zeta = 0.65$ ,  $\phi/\omega \approx \text{constant} \approx \frac{1}{2}\pi/\omega_n$  for  $\omega < \omega_n$ ].

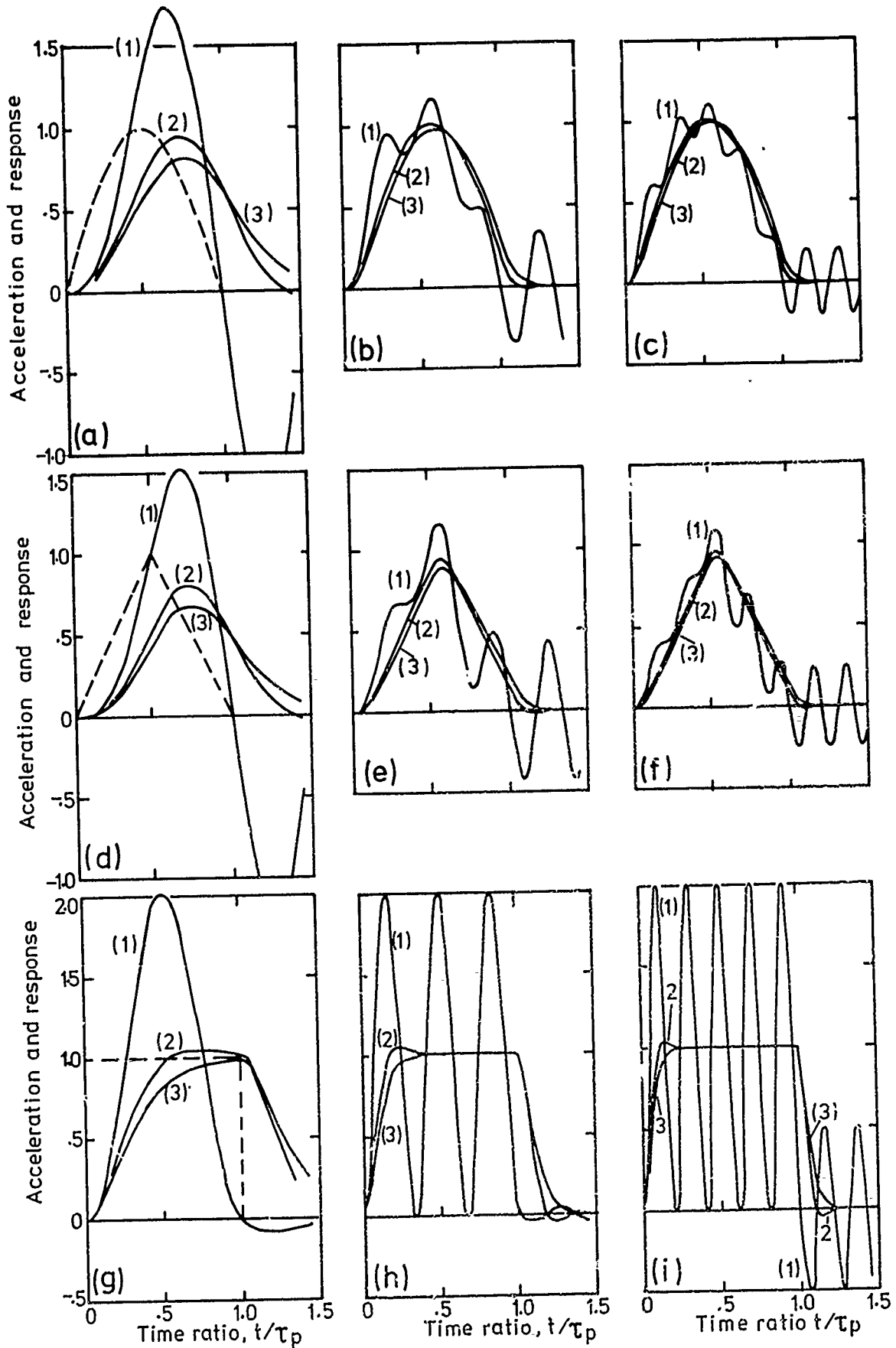


Figure 3.30. The transient response (full lines) of an accelerometer to various pulse inputs (dotted lines). The ratio of characteristic period ( $2\pi/\omega_n$ ), of the accelerometer to the pulse duration  $\tau$  is 1.014 for (a),(d),(g); 0.338 for (b),(e),(h) and 0.203 for (c),(f),(i).  $\zeta$  Curves labelled (1) are for  $\zeta = 0$ ; (2)  $\zeta = 0.7$  and (3)  $\zeta = 1$  (after Levy & Kroll, 1950).

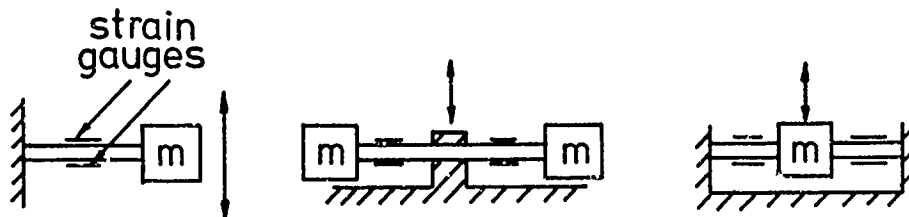


Figure 3.31. Schematic arrangements for accelerometers based upon strain-gauged beams carrying a seismic body. The sensitive direction is indicated by an arrow.

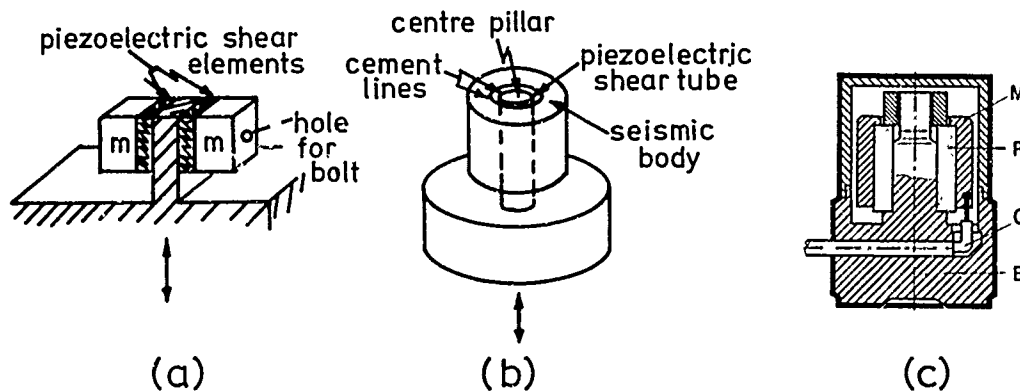


Figure 3.32. Schematic arrangements for piezoelectric, shear-element, accelerometers; (a) bolted construction using shear plates, (b) cemented construction using a shear tube, (c) a practical arrangement using a cemented shear tube (after Bruel & Kjaer, Naerum, Denmark).

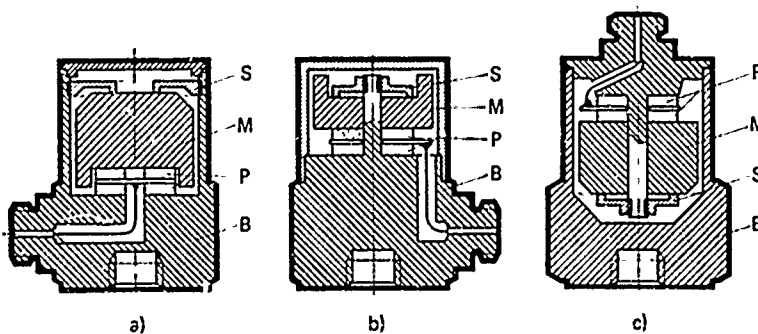


Figure 3.33. Schematic arrangements for piezoelectric compressive-mode accelerometers; (a) peripheral mounting, (b) centre-post mounting (c) centre-post inverted mounting (after Bruel & Kjaer, Naerum, Denmark). S = spring, M = seismic body, P = piezoelectric element, B = base.

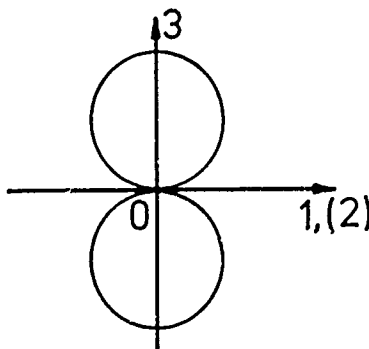


Figure 3.34. The idealised transverse sensitivity locus of an accelerometer; 03 is the axis of sensitivity.

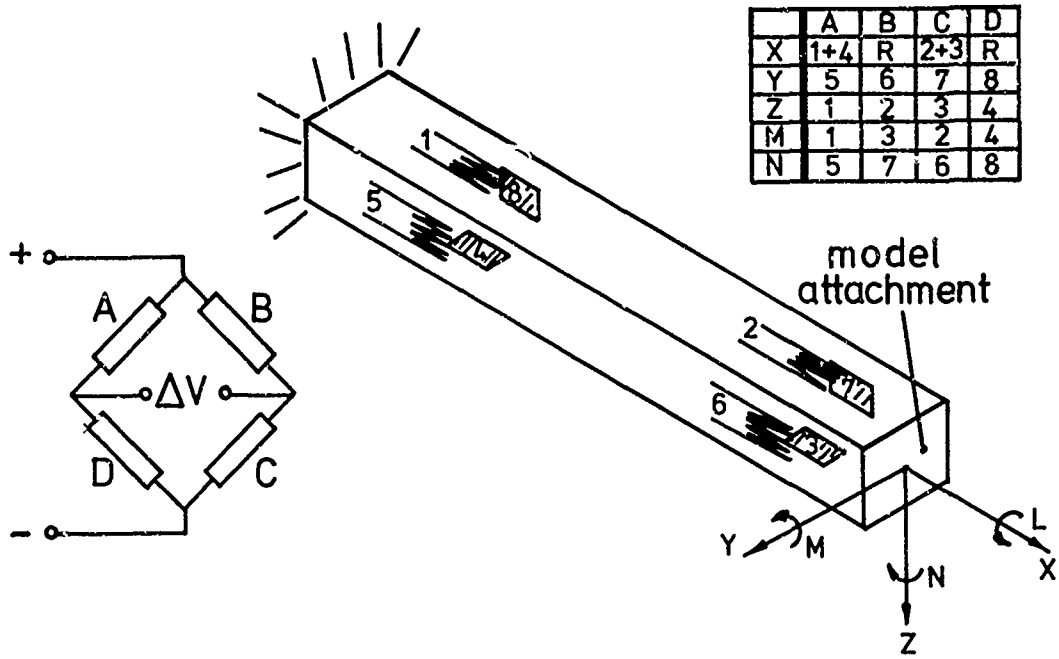
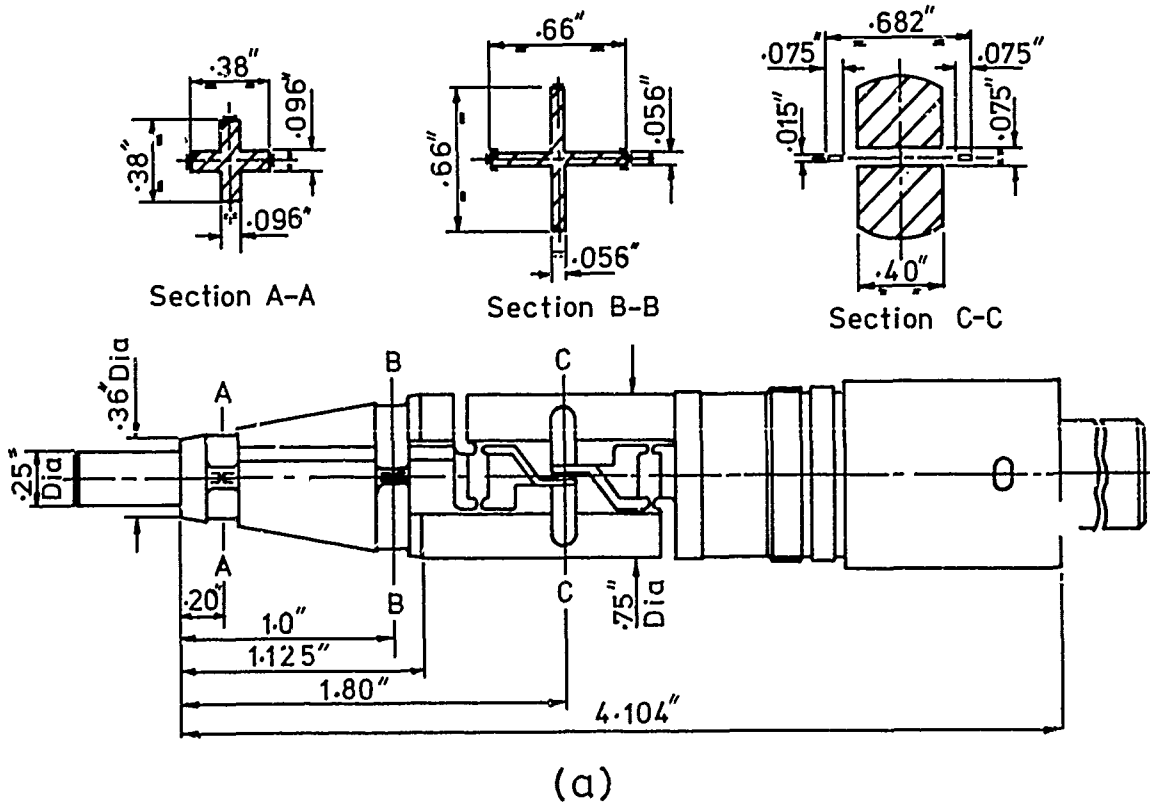
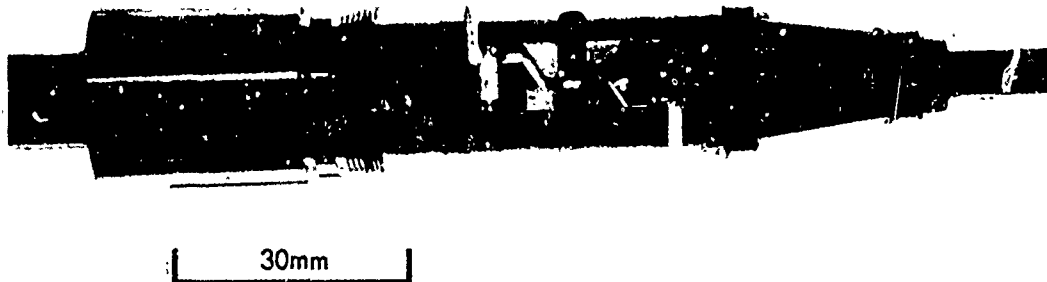


Figure 3.35. A simple cantilever of square cross-section, suitably strain-gauged to resolve all force components except the rolling moment L. (R is an external resistance.) Such an arrangement illustrates the principle of the single-piece balance, but in practice the sensitivity to several components would be inadequate.

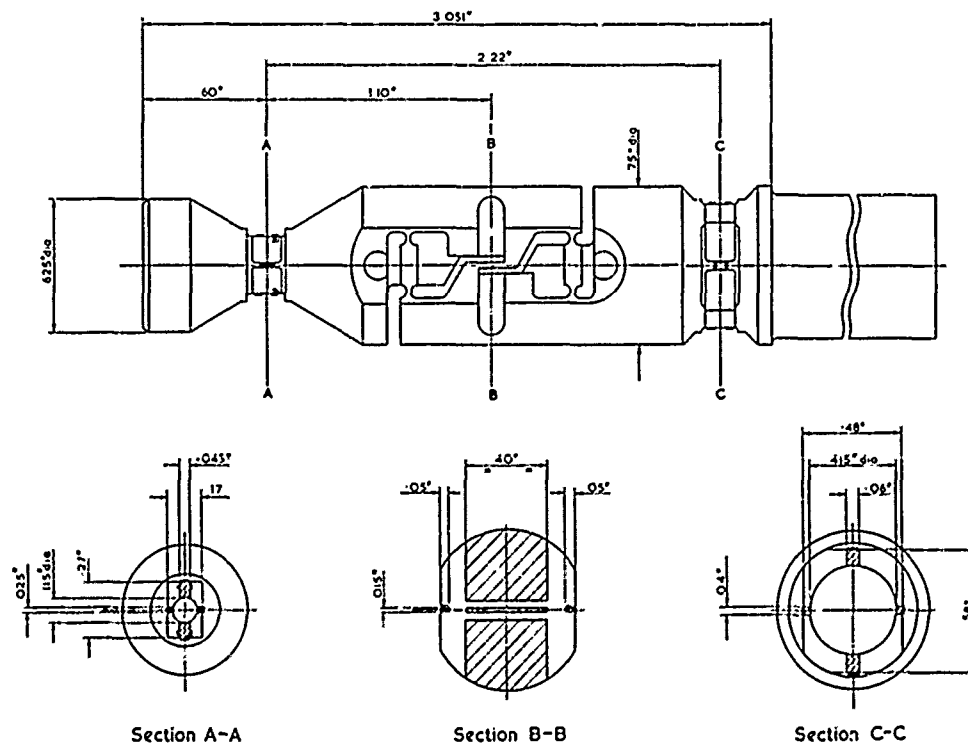


(a)

Figure 3.36. Single-piece strain-gauge balances cut from the solid using spark erosion machining. By removing only the minimum of material necessary to achieve adequate sensitivity and minimal cross-coupling, the highest possible frequency for the fundamental bending mode can be achieved.  
 (a) General layout of the R.A.E. Mark I balance (dimensions are in inches).



(b)



(c)

Figure 3.36. (Continued)

(b) Photograph of the R.A.E. Mark I balance.  
 (c) General layout of the R.A.E. Mark II balance (dimensions are in inches).  
 (Crown copyright; published by permission of H.M.S.O.)

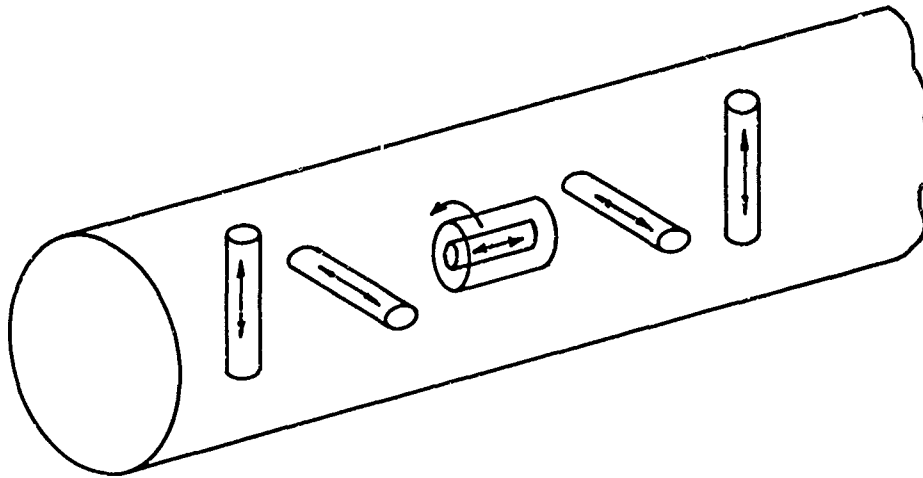


Figure 3.37. General idealised arrangement for the disposition of load-cells in a six-component balance. Such an arrangement fits neatly into a slender cylindrical package.

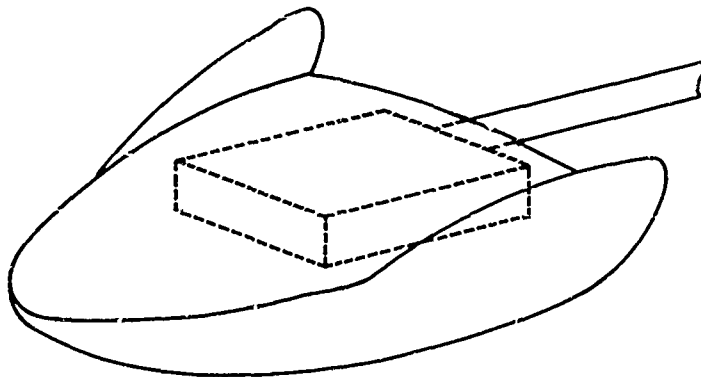


Figure 3.38. A balance-package shape suitable for a lifting-body configuration.

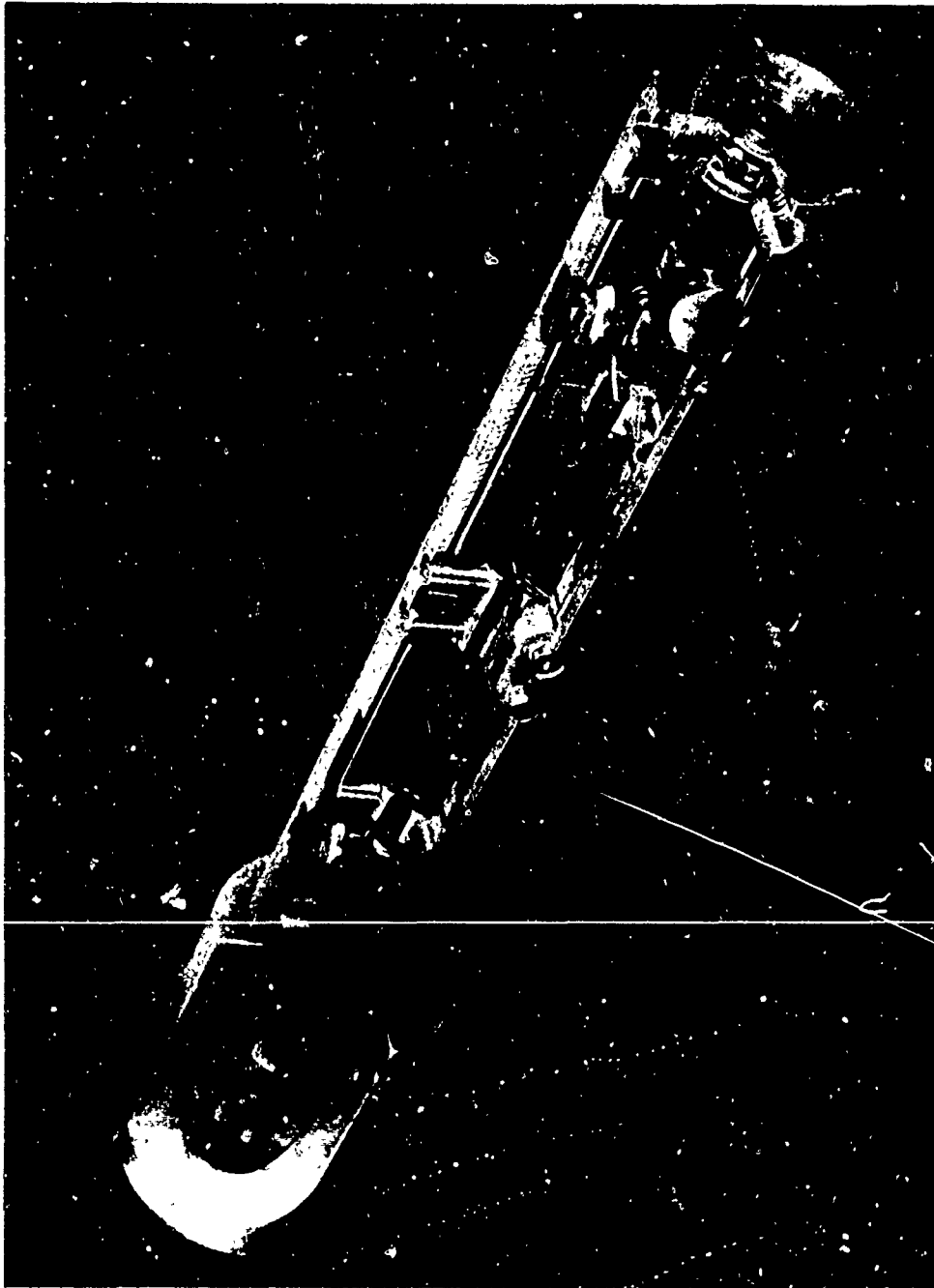


Figure 3.39. The "floating-frame" balance, marketed by Task Corporation, Anaheim, California, U.S.A., showing the dual element axial-force and rolling-moment transducers (reproduced with permission).

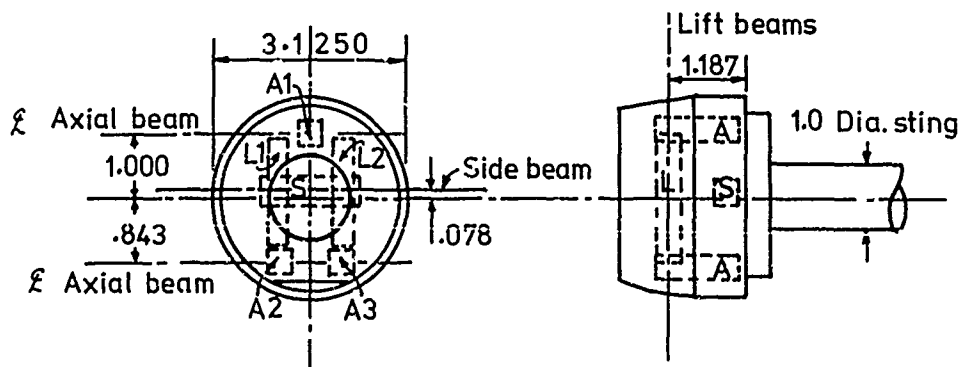


Figure 3.40. The Cornell Aeronautical Laboratory's six-component type H balance, designed for use with bluff bodies in a shock-tunnel. The dimensions are in inches. The axial elements  $A_1$ ,  $A_2$ , and  $A_3$  resolve the axial force, the pitching moment about an axis in the plane of  $L_1$  and  $L_2$ , and the yawing moment about an axis through the side force element  $S$ . The elements  $L_1$  and  $L_2$  resolve the vertical force and together with  $S$ , the rolling moment about the axis of the sting. The load capacities are approximately 400 N for  $A_1$ ,  $A_2$  and  $A_3$ , and 300 N for  $L_1$ ,  $L_2$  and  $S$ . (after Martin, Duryea & Stevenson, 1962). (A similar balance has been constructed at the Technischen Hochschule, Aachen (Schaguhn, 1970). The photograph is of the Aachen balance.)

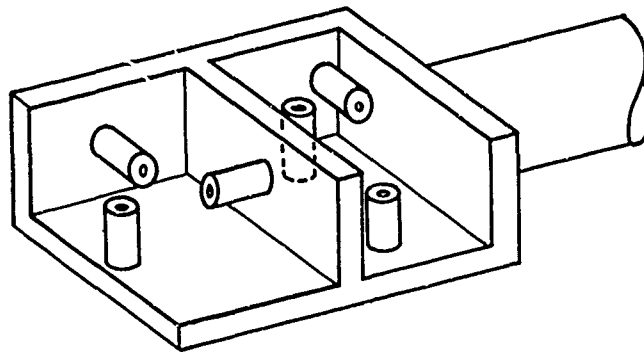


Figure 3.41. A possible force-resolution scheme which fits into a "rectangular package". An intermediate block might be used to provide a platform for attaching the model.

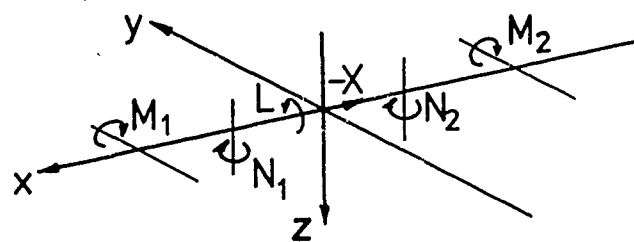


Figure 3.42. The "force-resolution system" appropriate to the strain-gauged cantilever.

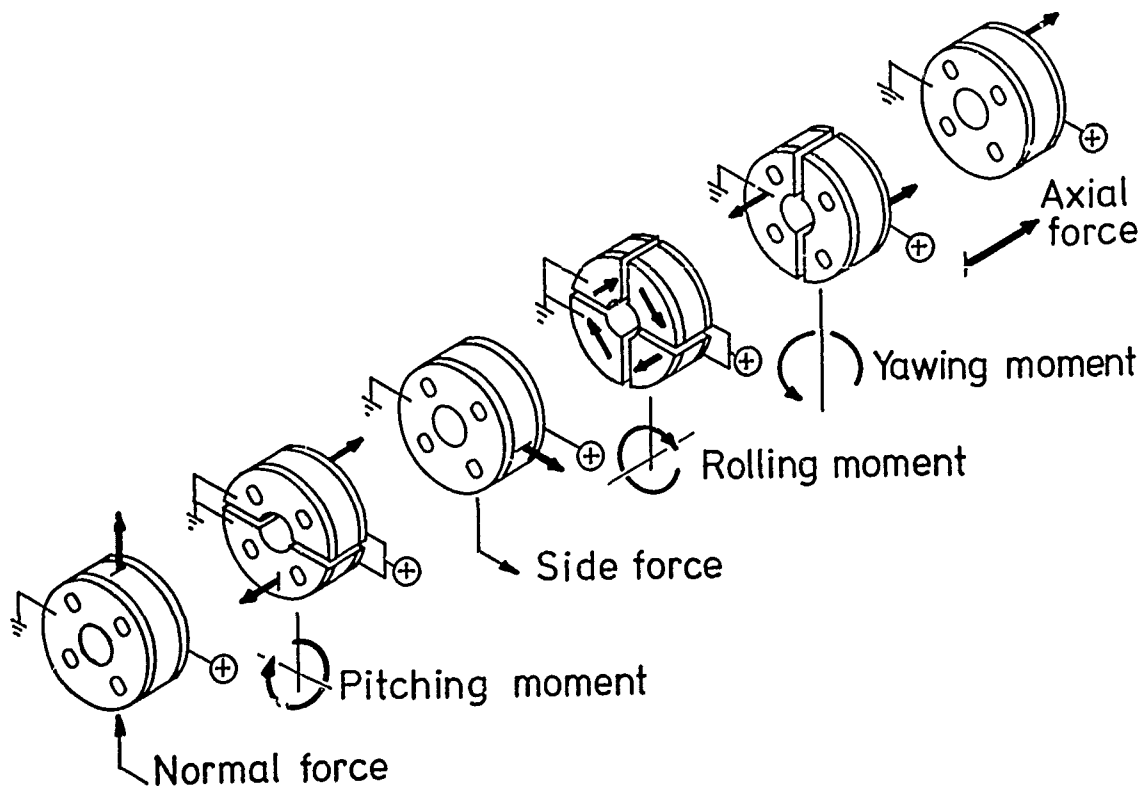


Figure 3.43. The Cornell Aeronautical Laboratory's six-component type K balance, designed for use with slender shapes in a shock-tunnel. Decoupling of the components is provided by the directional properties of the piezoelectric sensing elements (after Bogdan 1967).



Figure 3.44. Model support and incidence arc of the N.P.L. shock-tunnel (now at R.A.E., Farnborough). The arc is rigidly supported by a pillar mounted on the floor of the laboratory. It is "isolated" from the structure of the tunnel, by flexible metal bellows which also provide a pressure and vacuum seal. The upper support is identical, but has been removed for clarity. (after Pennelegion, Cash & Bedder, 1967; Crown copyright, published by permission of H.M.S.O).

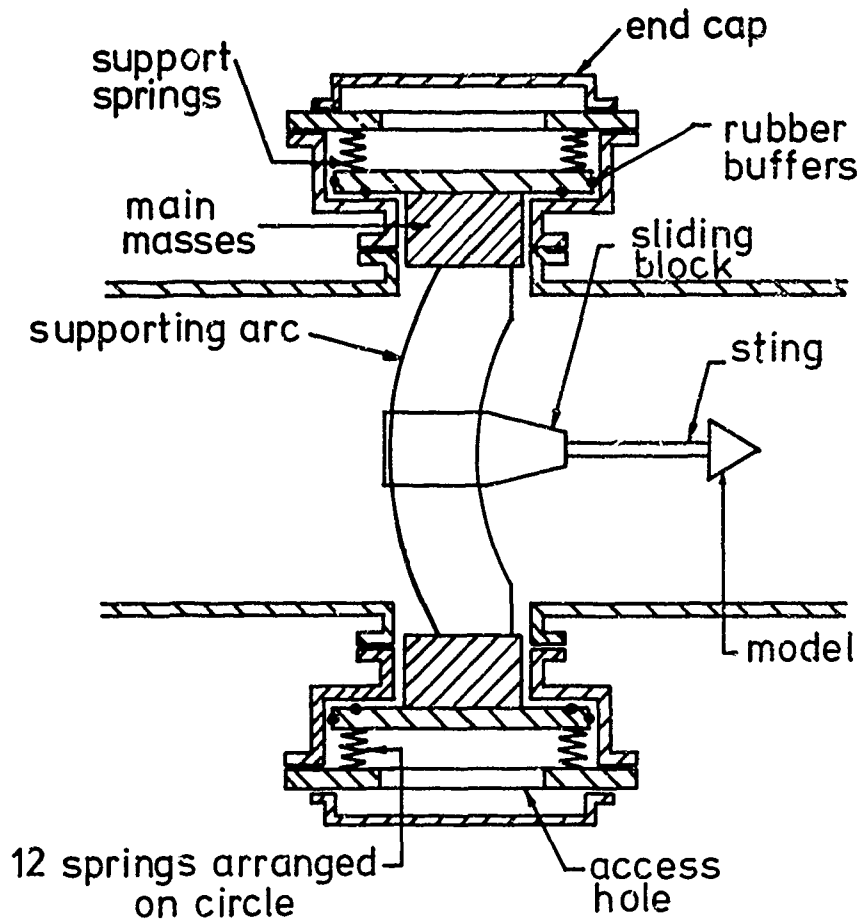


Figure 3.45. The "massive" support system used in the shock-tunnel at Queen Mary College, London. The total mass of approximately 39 kg is supported by 24 flexible springs each of stiffness about 0.1 N/m. The corresponding natural period of oscillation is very long compared with the test flow duration of order one millisecond (after Goodchild, 1968).

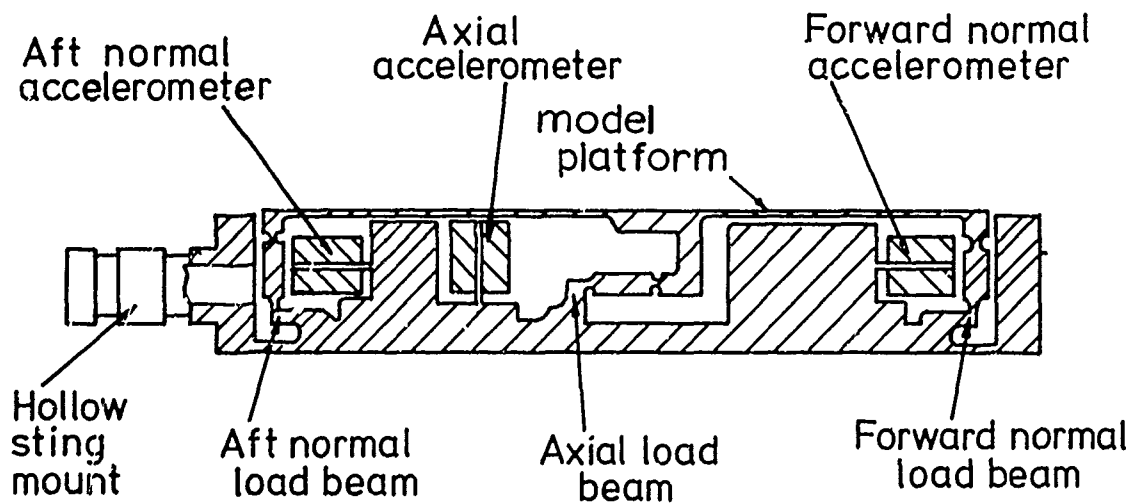


Figure 3.46. An acceleration-compensated, three-component balance (section drawn from a photograph published by Edenfield & Ledford, 1962).

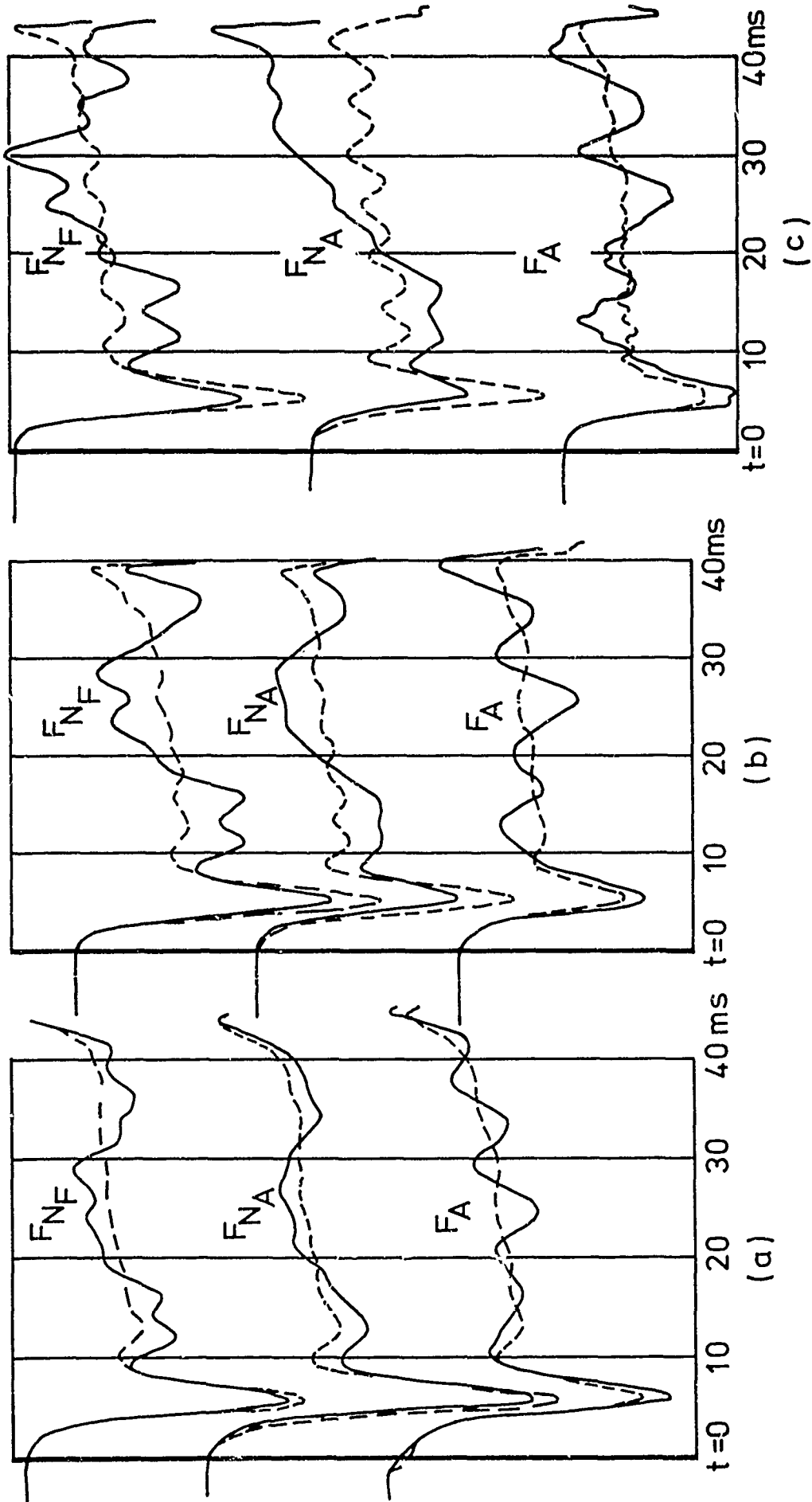


Figure 3.47. Oscillograph records obtained with the balance of figure 3.46 for models of different mass. The dashed lines are the compensated data, the full lines, uncompensated data.  
 (a) Model mass = 52 g,  $\alpha = 10^\circ$ ; (b) model mass = 144 g,  $\alpha = 15^\circ$ ; (c) model mass = 237 g,  $\alpha = 15^\circ$ .

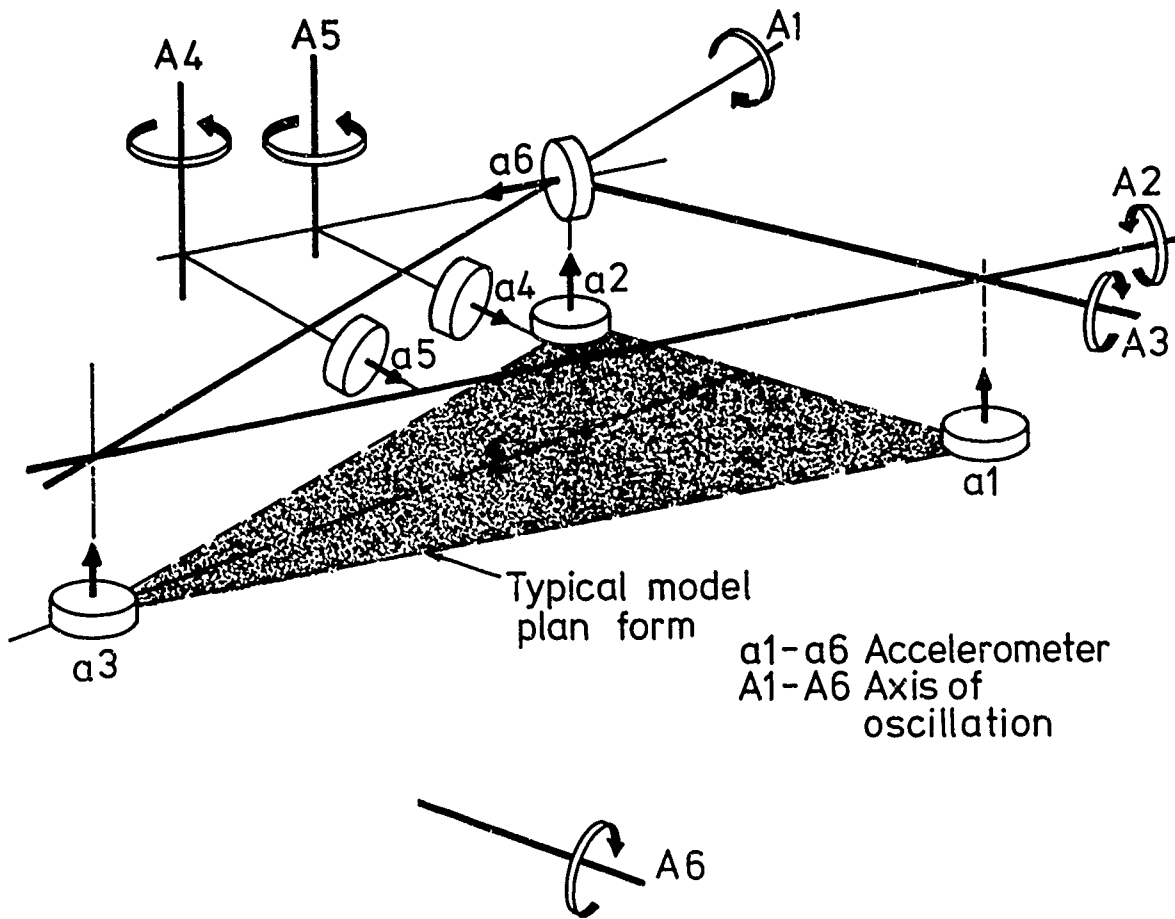


Figure 3.48. The disposition of accelerometers used in an acceleration-compensation scheme at Cornell Aeronautical Laboratory. Such an arrangement is only suitable when the angular velocities are small (after Martin, Duryea & Stevenson, 1962).

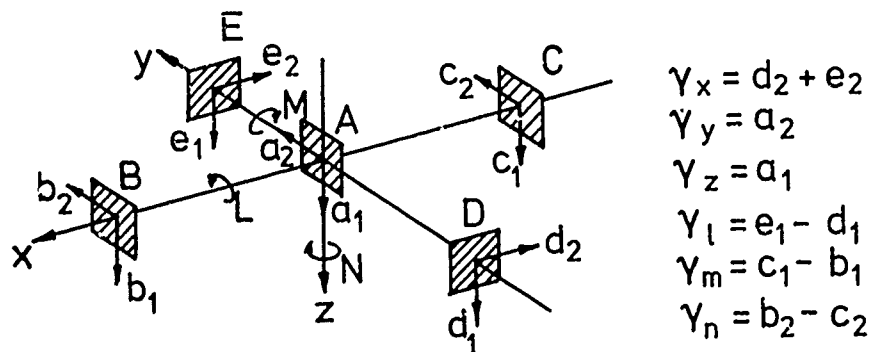


Figure 3.49. The arrangement of biaxial accelerometers used by Beaussier (1966).

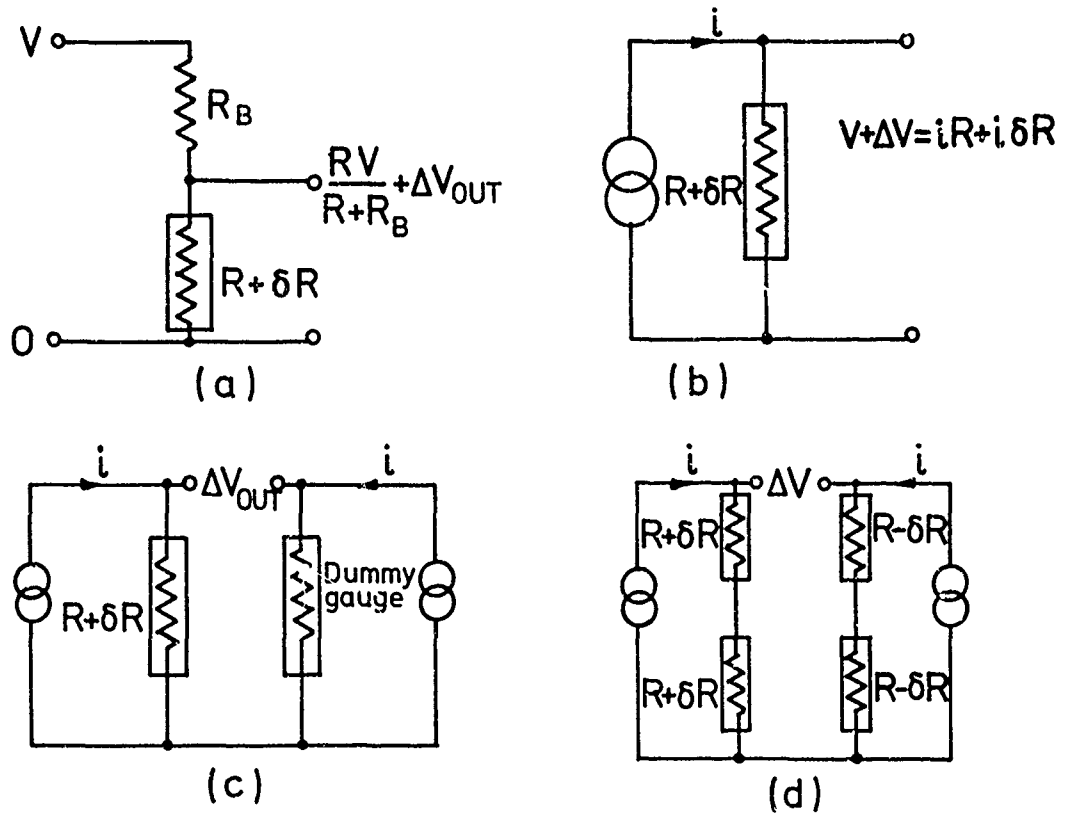


Figure 3.50. Circuit arrangements for energising resistance strain-gauges: (a) using a large value ballast resistor  $R_B$  to maintain constant current; (b) using a constant-current source; (c) using two constant-current sources to eliminate the d.c. level; (d) using four active gauges and two constant-current sources.

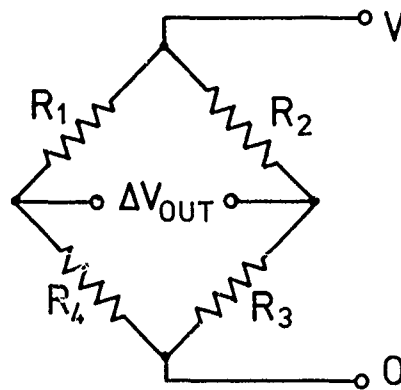


Figure 3.51. A simple Wheatstone bridge circuit operated by measuring the out-of-balance voltage,  $\Delta V$ .

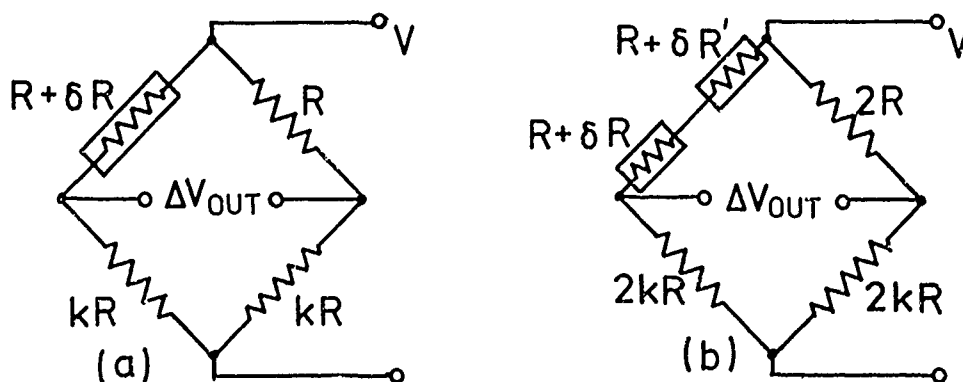


Figure 3.52(a) An unequal-arm bridge having one active gauge.  
 (b) An unequal-arm bridge having two active gauges in series in the same arm.

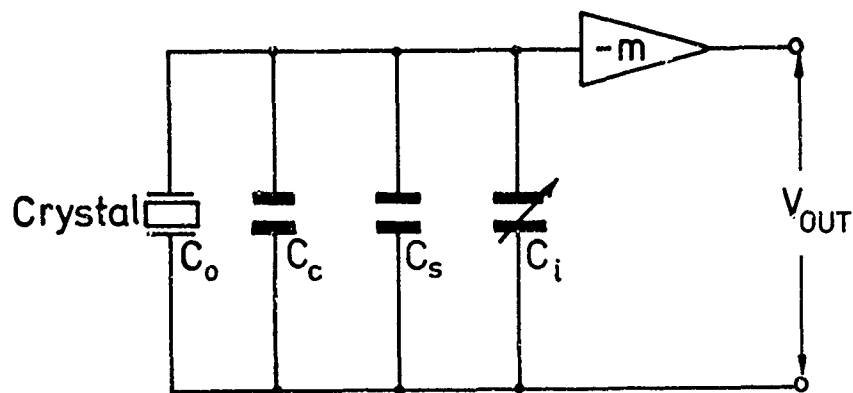


Figure 3.53. The simple voltage amplifier of open-loop gain  $-m$ .  $C_c$  represents the capacitance of the cable between the piezoelectric transducer of capacitance  $C_0$ , and the input where the stray capacitance is  $C_s$ .  $C_i$  is the range capacitance, used to adjust the overall sensitivity.

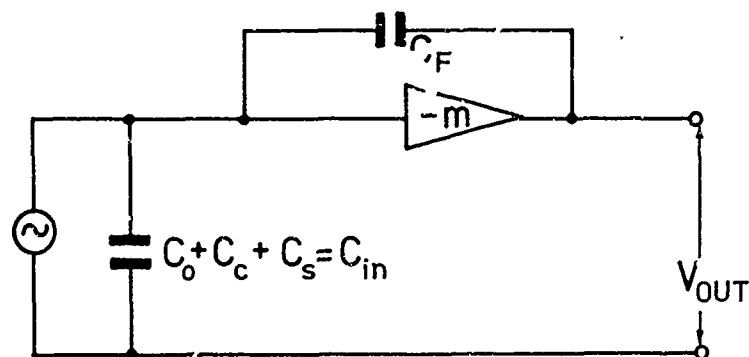


Figure 3.54. The charge amplifier - an operational amplifier having a very high input impedance and capacitive feedback.

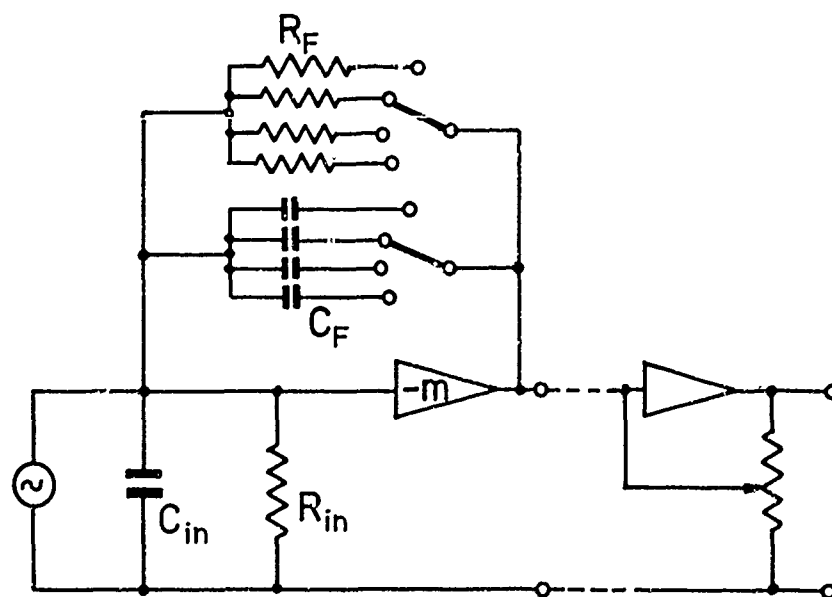


Figure 3.55. A charge amplifier in which both the sensitivity and the time constant are adjustable.

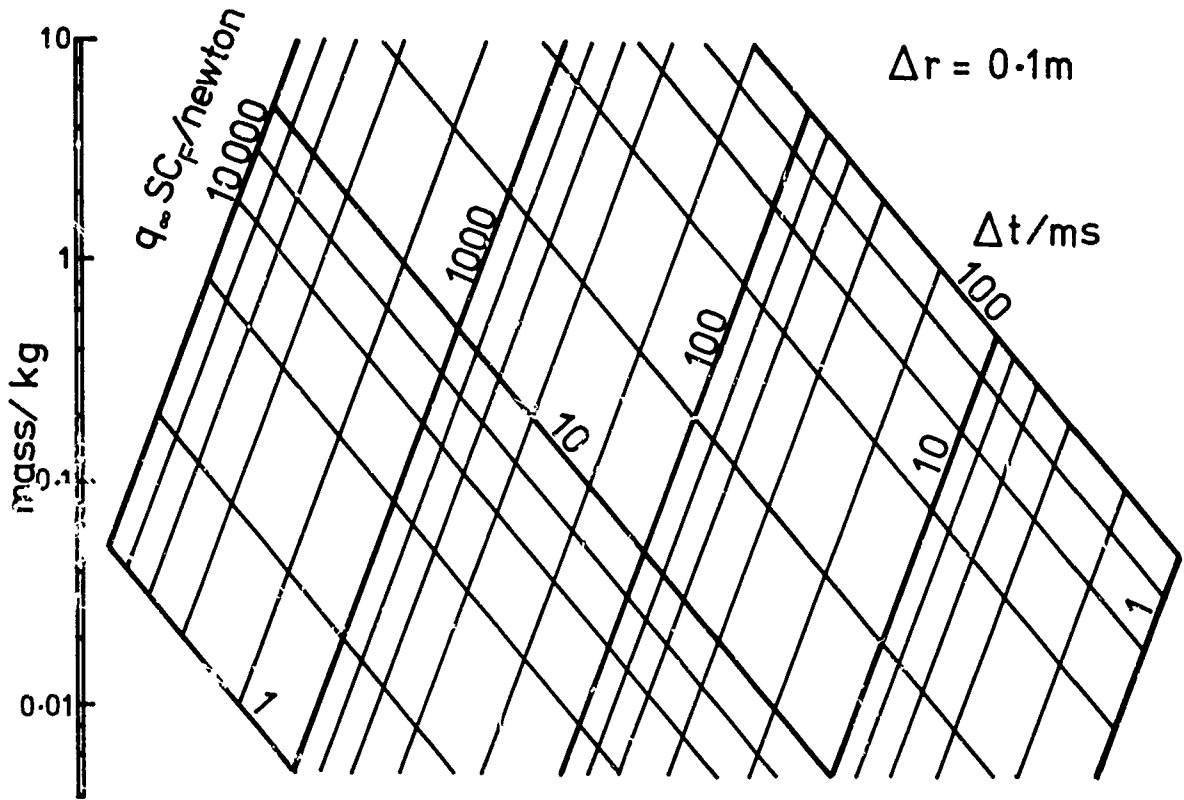


Figure 4.1. Mass of the model as a function of the test-duration  $\Delta t$  and the ballistic parameter ( $q_{\infty} SC_F$ ) for a fixed displacement of 10 cm.

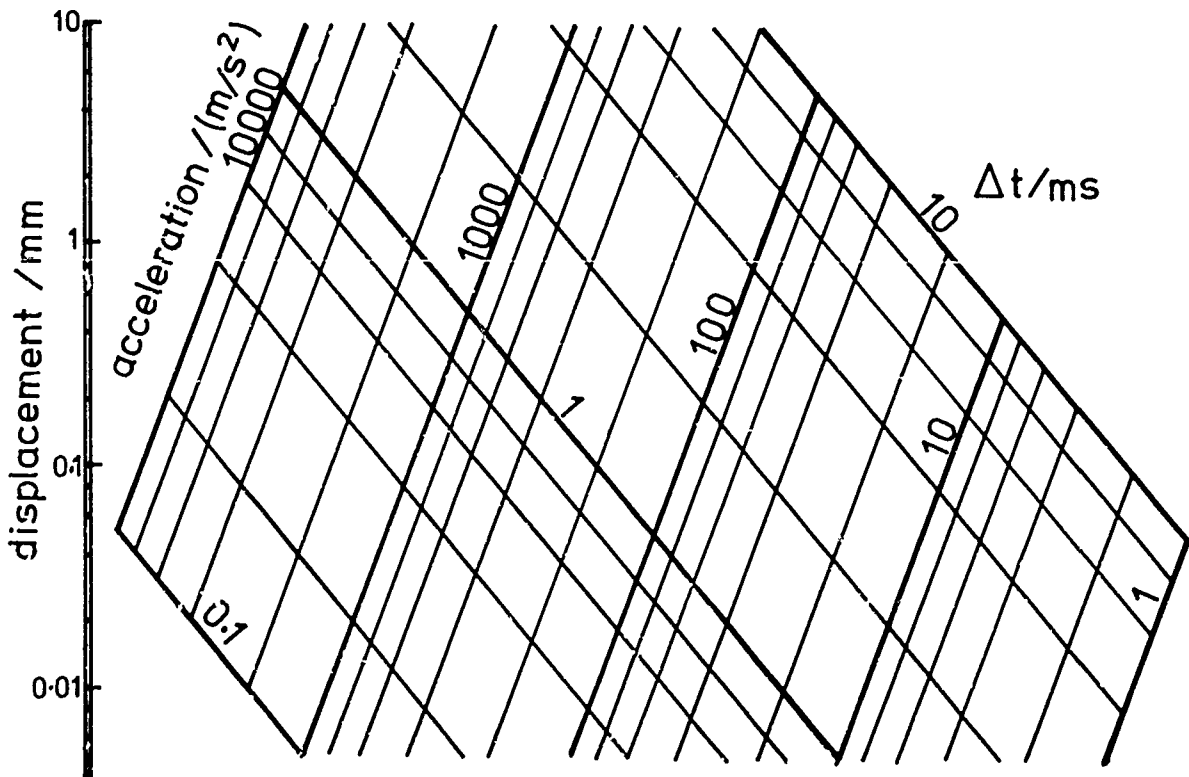


Figure 4.2. Displacement as a function of the test-duration  $\Delta t$  and the acceleration, assumed uniform.

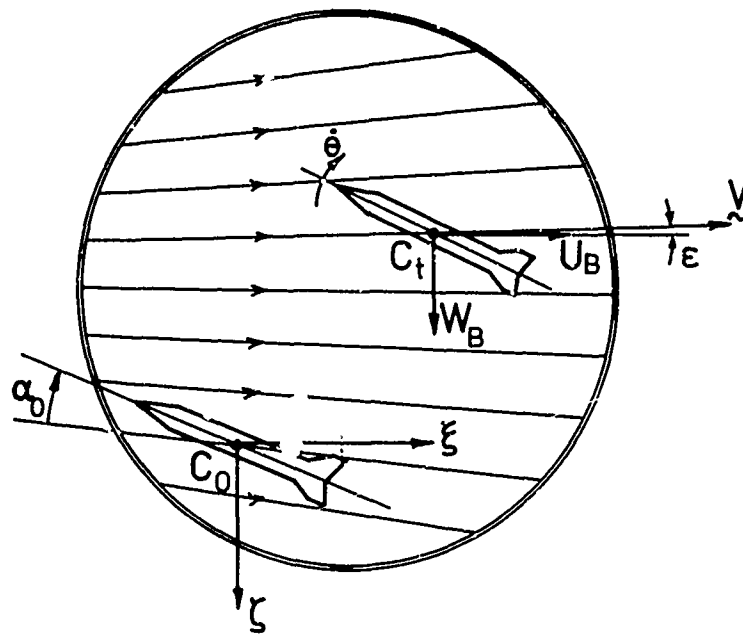


Figure 4.3. Model in planar free-flight showing the effects of conicity in the flow field.

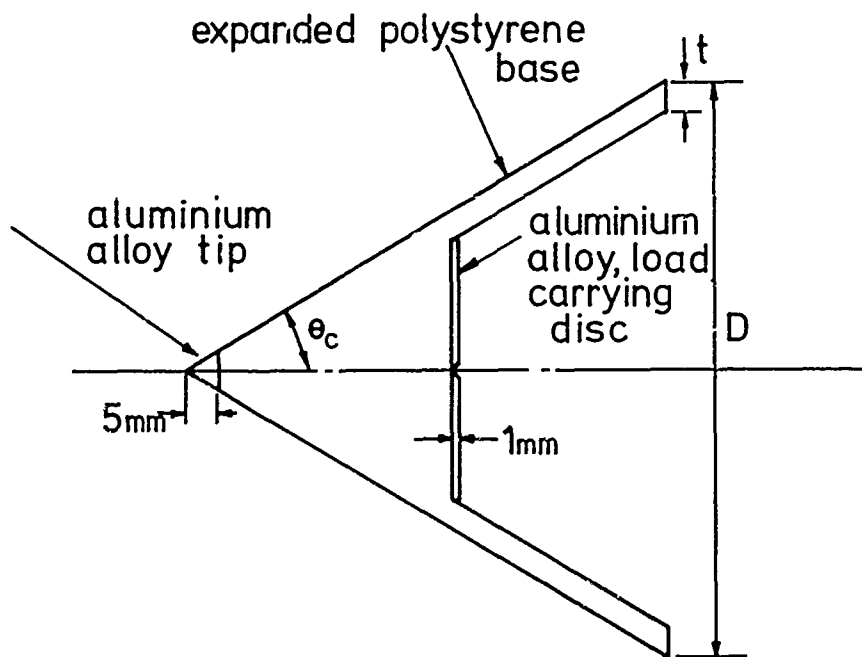


Figure 4.4. General features of the cones used by Richards & Clemens (1971) in their optimisation study for the design of pivoted models suitable for making measurements of pitching derivatives. Conditions assumed: relative density of aluminium alloy, 2.7; of expanded polystyrene, 0.13;  $(t/\text{mm}) = 1.5 + 0.0025 (D/\text{mm})$ .

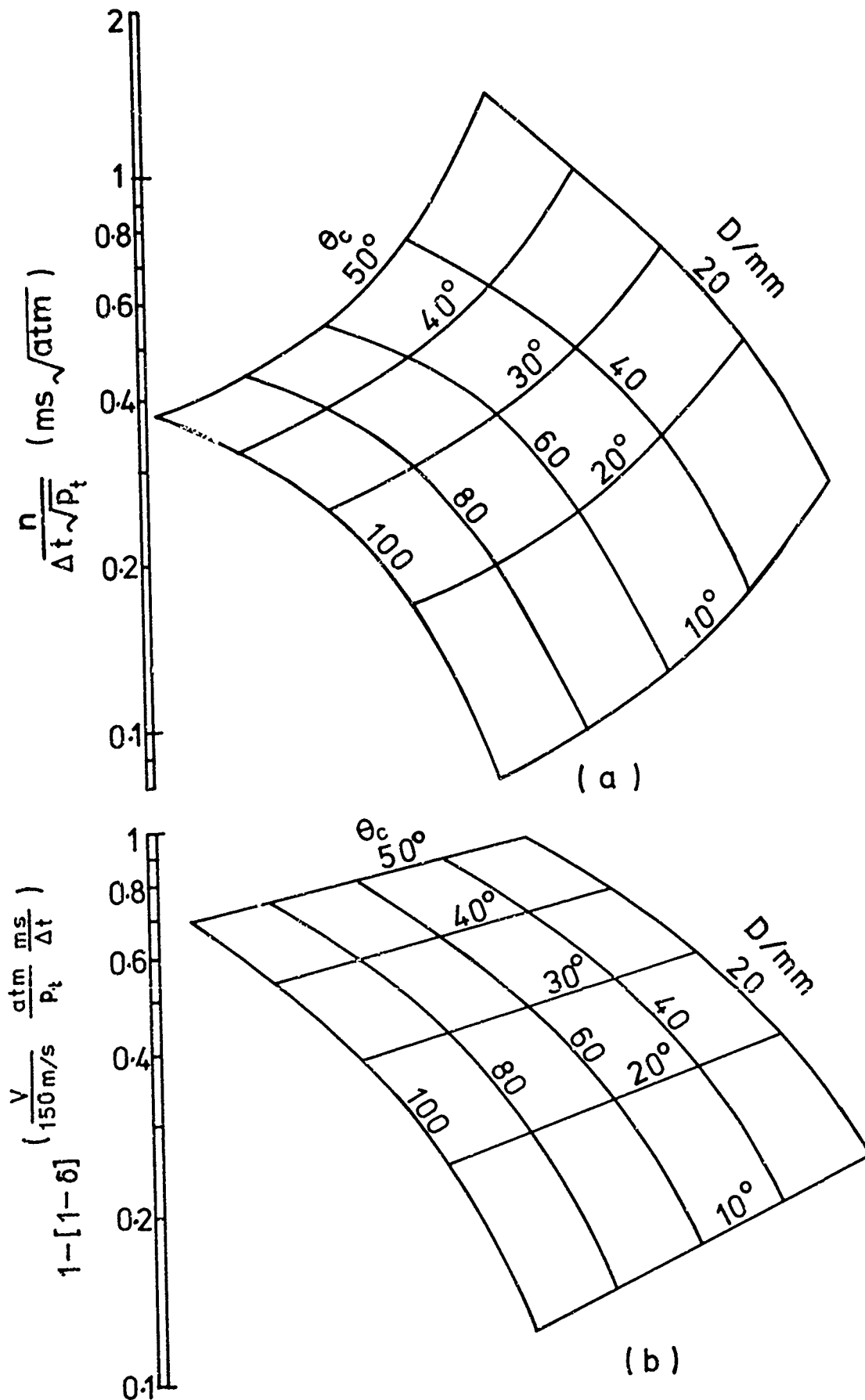


Figure 4.5. Results of the optimisation study of Richards & Clemens (1971): (a) number  $n$ , of oscillations, and (b) fractional decay  $\delta$ , which occurs during a test-time  $\Delta t$  in a stream of speed  $V$  and pitot pressure  $p_t$ . (The charts have been adapted from those of Richards & Clemens, and generalised according to a suggestion of theirs).

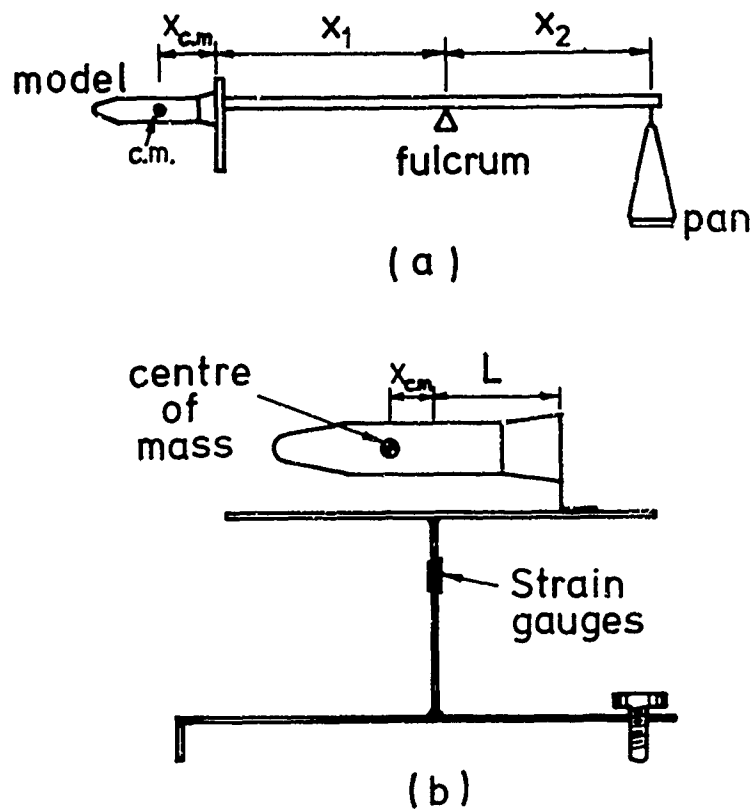
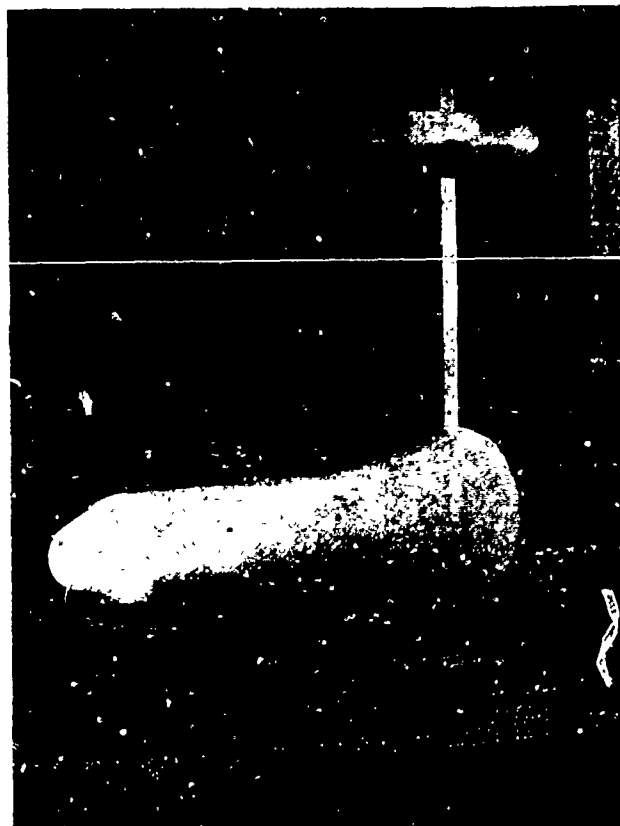


Figure 4.6. Apparatus for determining the position of the centre of mass of a model, (a) a modified analytical balance of the equal-arm type (after DeRose & Intrieri, 1970). (b) a special device based upon an eccentrically-loaded, slender column (after Grauer-Carstensen, 1971).



Reproduced from  
Best available copy.

Figure 4.7. A twin-thread suspension showing the lever mechanism used for fine adjustment of the incidence. (after Pennelegion, Cash & Shilling, 1967; Crown copyright, published by permission of H.M.S.O.)

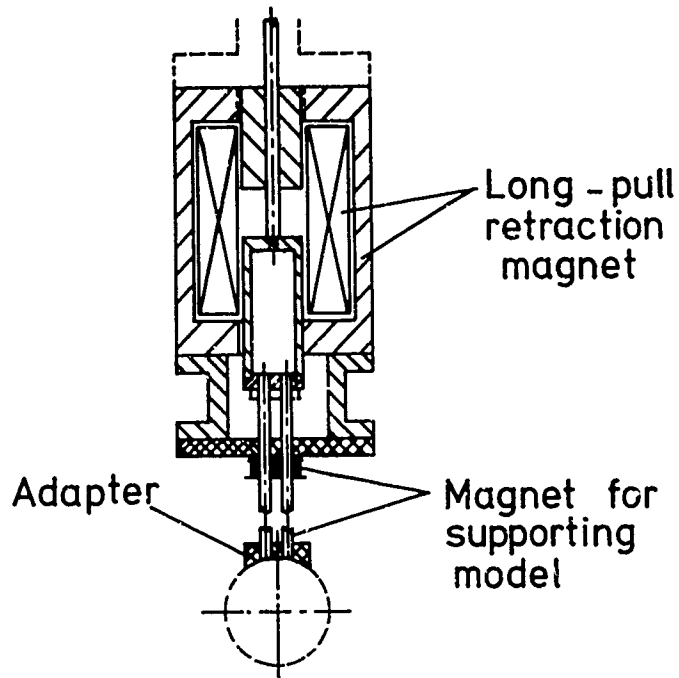


Figure 4.8. An electromagnetic suspension system. Upon release the support is retracted from the test section by the long-pull magnet (Requardt & Kabelitz, 1972).

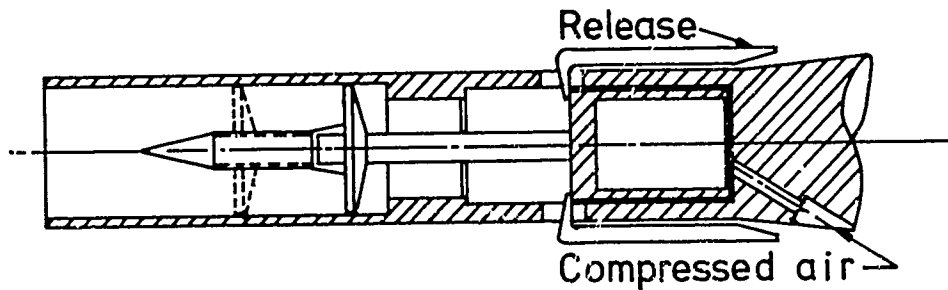
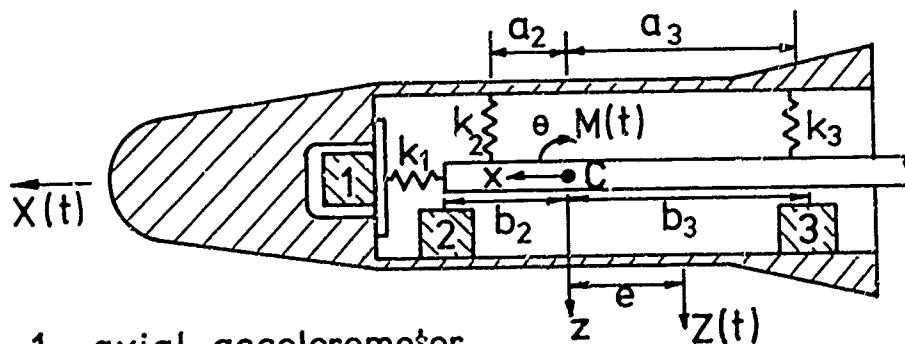


Figure 4.9. A compressed-air gun used to launch models upstream in the Ludwig-tube tunnels at D.F.V.L.R.-A.V.A., Göttingen (after Grauer-Carstensen, 1971).



1 axial accelerometer  
 2, 3 normal force and centre of pressure accelerometers

Figure 4.10. Schematic arrangement of a three-component accelerometer balance.

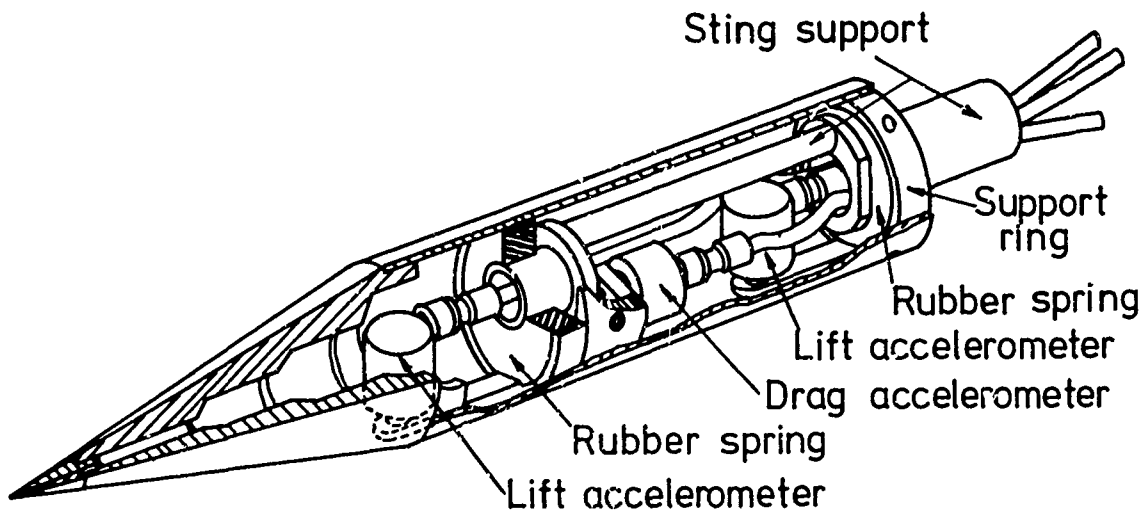


Figure 4.11. The first Cornell Aeronautical Laboratory accelerometer balance (after Vidal, 1956).

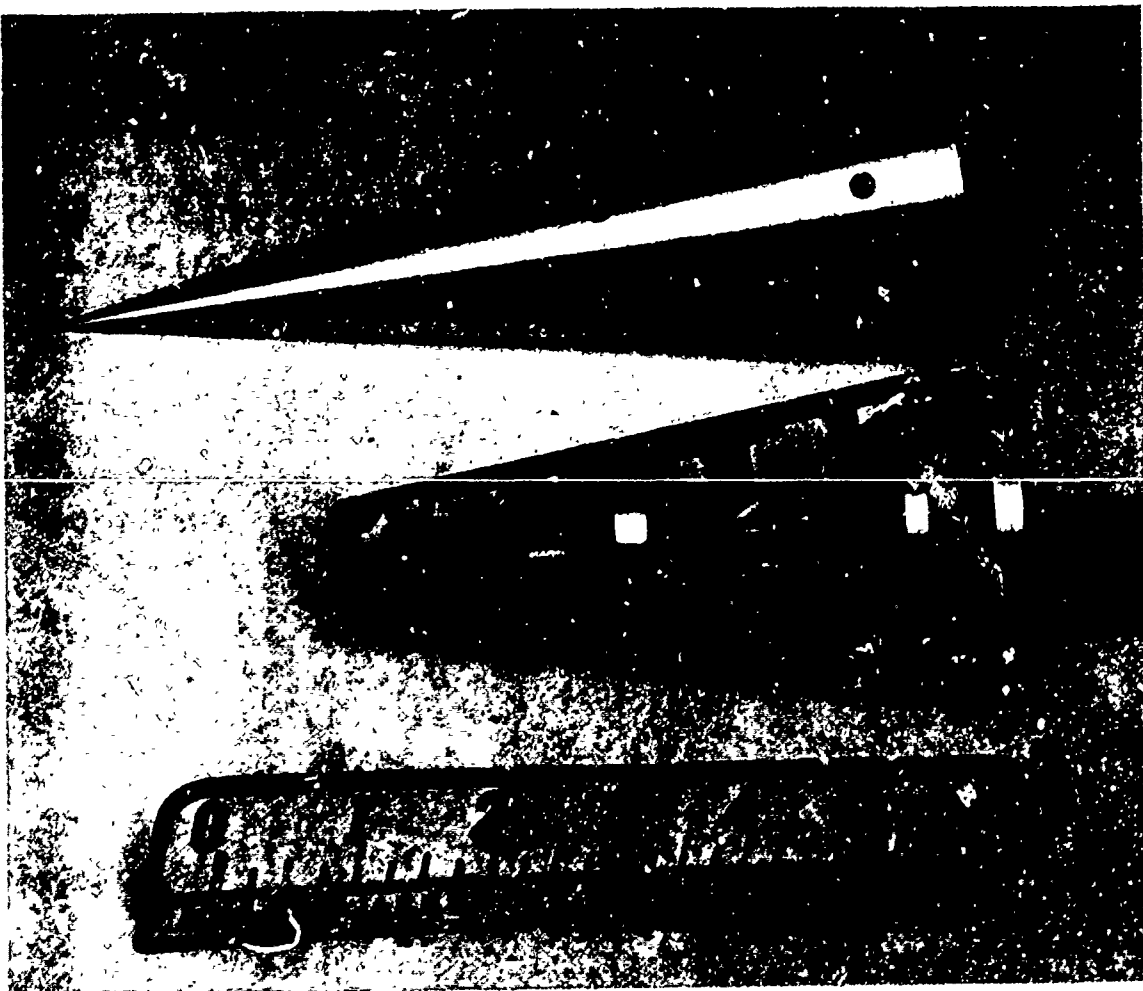


Figure 4.12. The second Cornell Aeronautical Laboratory accelerometer balance; the sponge rubber supports have been replaced by thin sheets of rubber, the rearmost of which also seals the base.

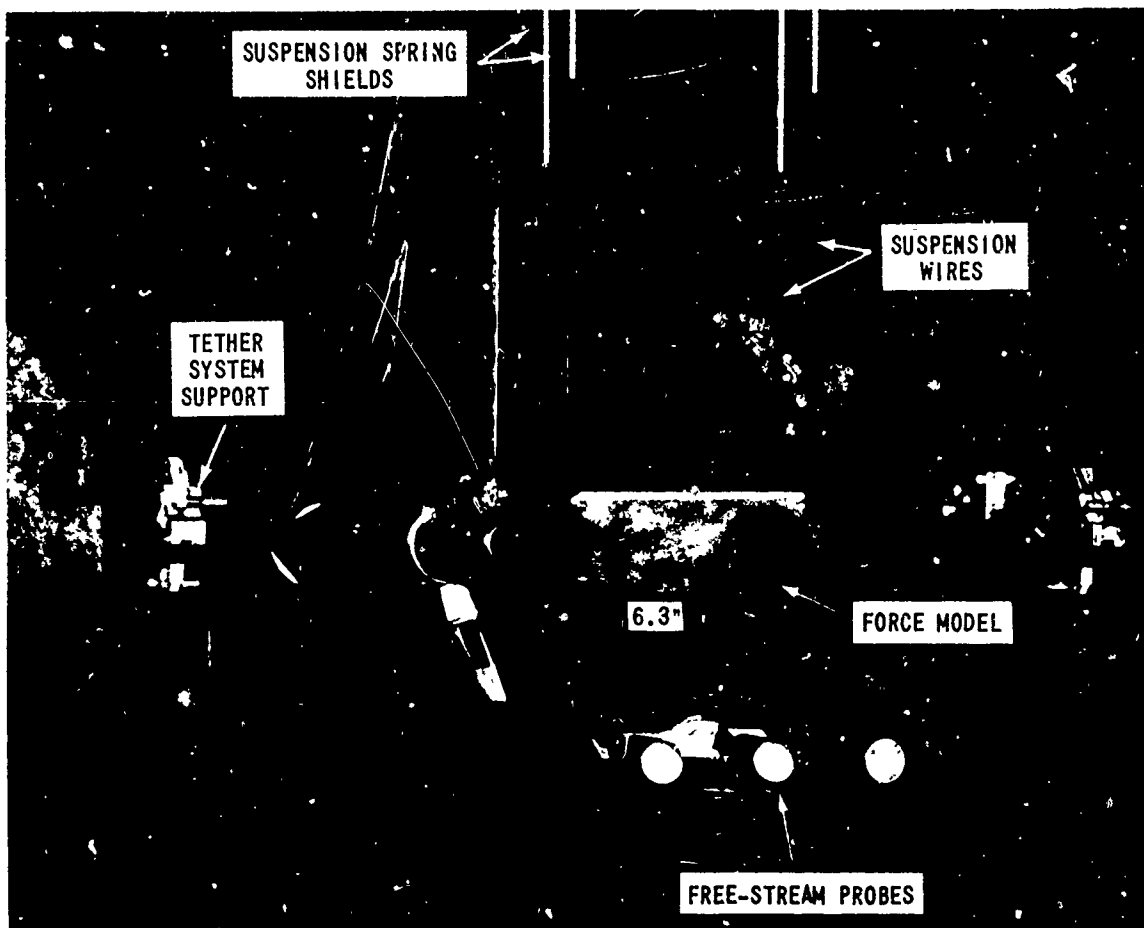


Figure 4.13. The wire suspension used by Sheeran & Duryea (1969).

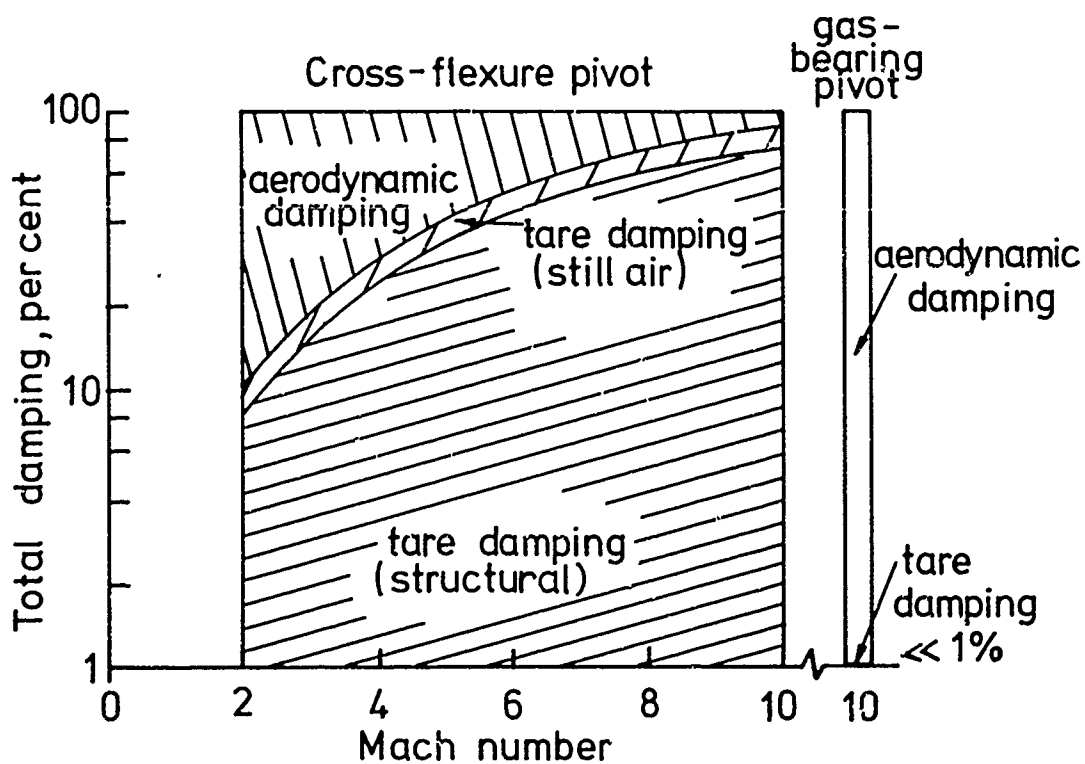
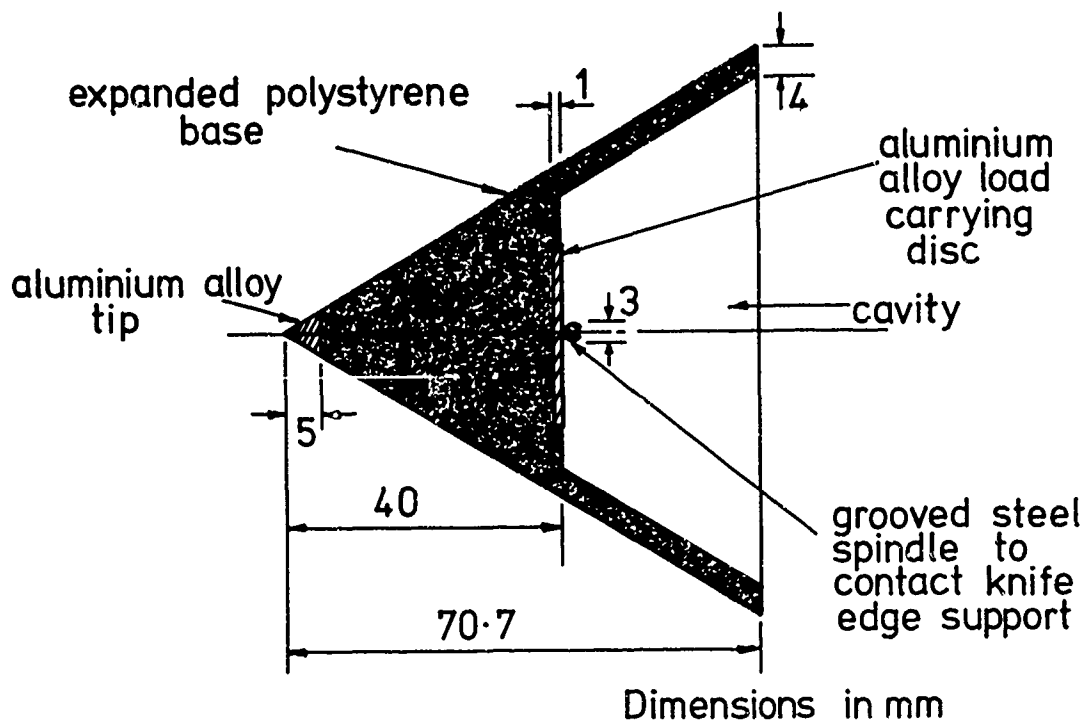
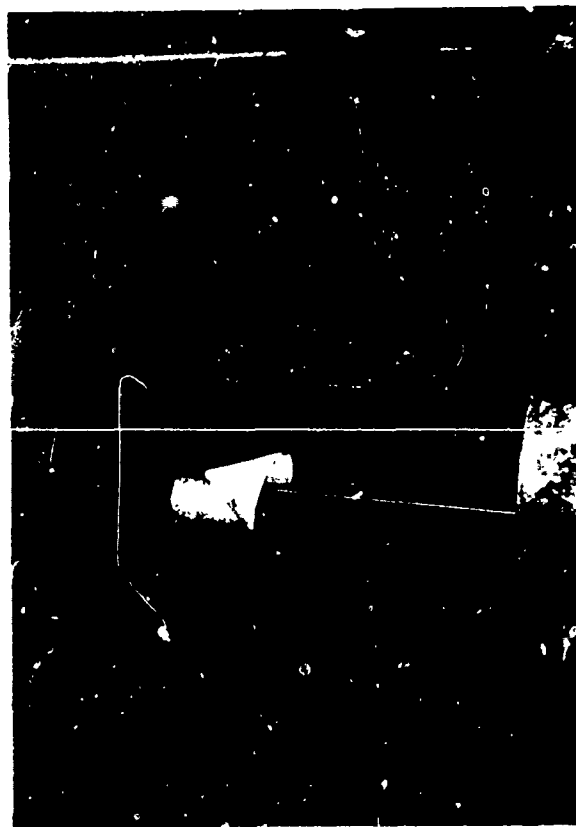


Figure 4.14. The relative damping of flexural pivot systems as a function of Mach number. The air damping is that for a spherically-blunted cone of semi-angle 15.5°. (reproduced from AGARDograph 121).



(a)



(b)

Figure 4.15. A knife-edge support used for oscillatory tests in the V.K.I. Longshot tunnel;  
 (a) a cross-section of the cone-model,  
 (b) the model supported in the test section, showing the thread used to set the initial incidence.

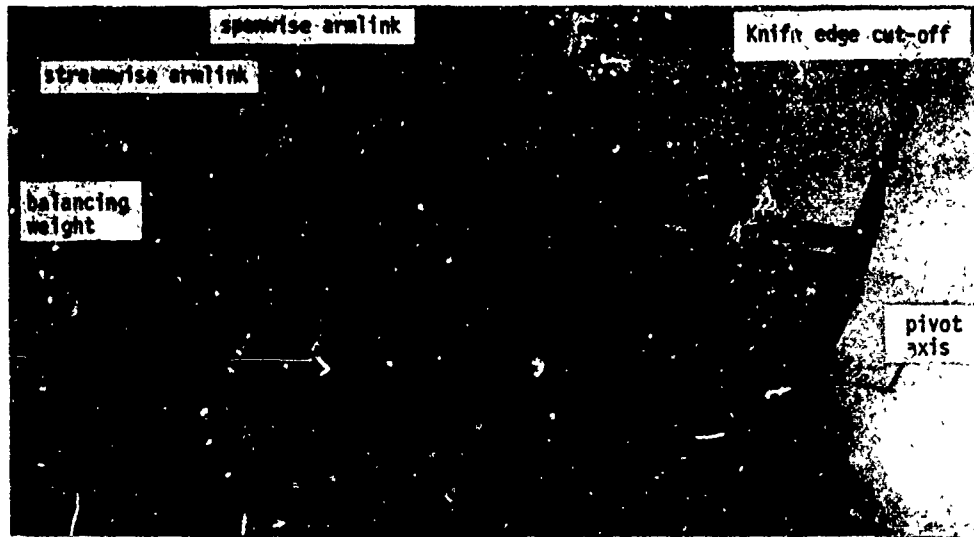


Figure 4.16. Double caret-delta model, with its supporting linkage (after Ghosh, 1973).

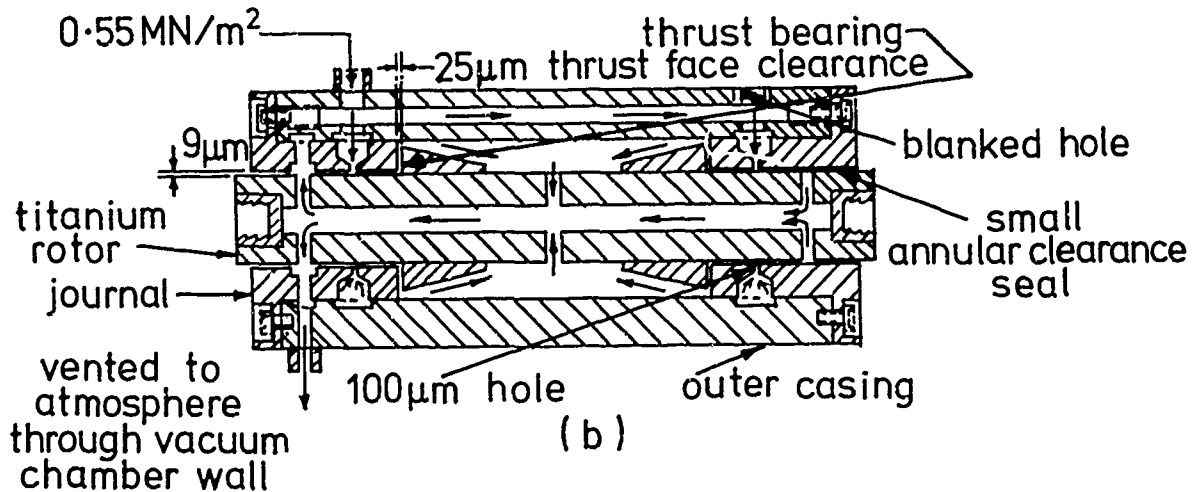
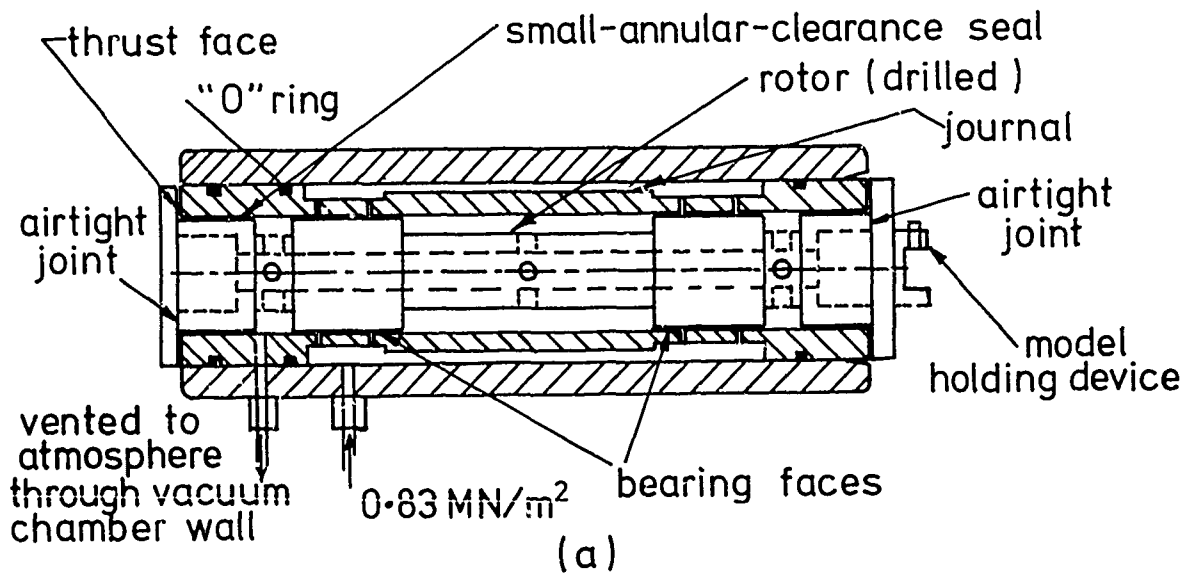
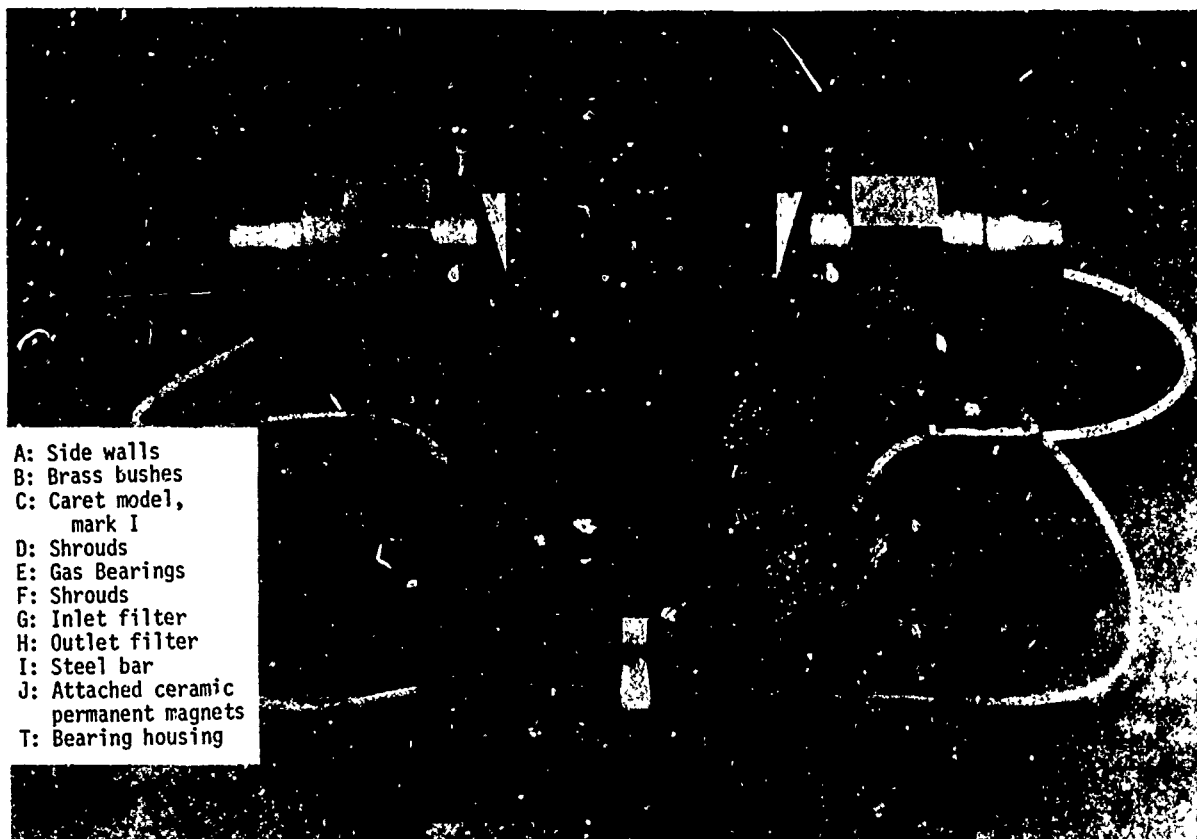
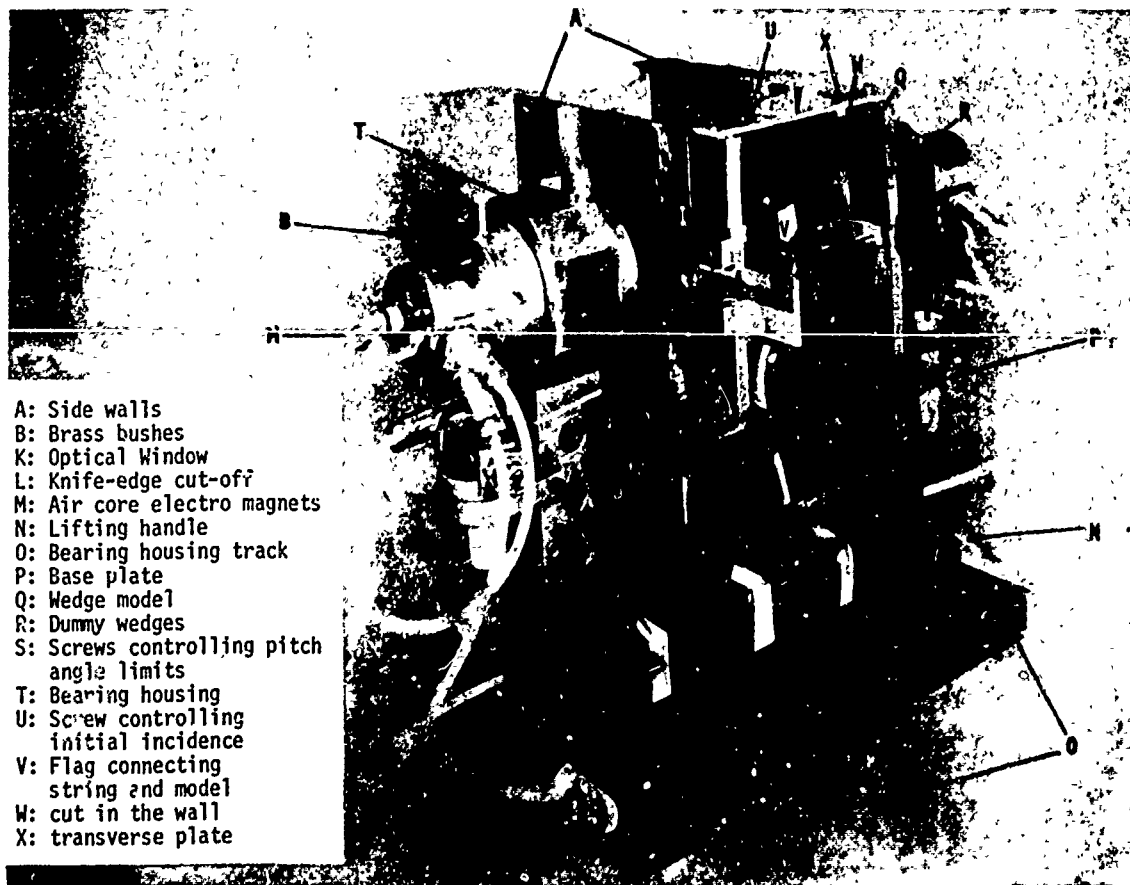


Figure 4.17. Gas-bearings used to support models for oscillatory tests in the gun-tunnel at the University of Southampton, (a) Mark I, (b) Mark II, (after Ghosh, 1973).



- A: Side walls
- B: Brass bushes
- C: Caret model,  
mark I
- D: Shrouds
- E: Gas Bearings
- F: Shrouds
- G: Inlet filter
- H: Outlet filter
- I: Steel bar
- J: Attached ceramic  
permanent magnets
- T: Bearing housing



- A: Side walls
- B: Brass bushes
- K: Optical Window
- L: Knife-edge cut-off
- M: Air core electro magnets
- N: Lifting handle
- O: Bearing housing track
- P: Base plate
- Q: Wedge model
- R: Dummy wedges
- S: Screws controlling pitch  
angle limits
- T: Bearing housing
- U: Screw controlling  
initial incidence
- V: Flag connecting  
string and model
- W: cut in the wall
- X: transverse plate

Figure 4.18. The complete gas-bearing pivot assembly, upper; front view, lower; viewed from the rear (after Ghosh, 1973).

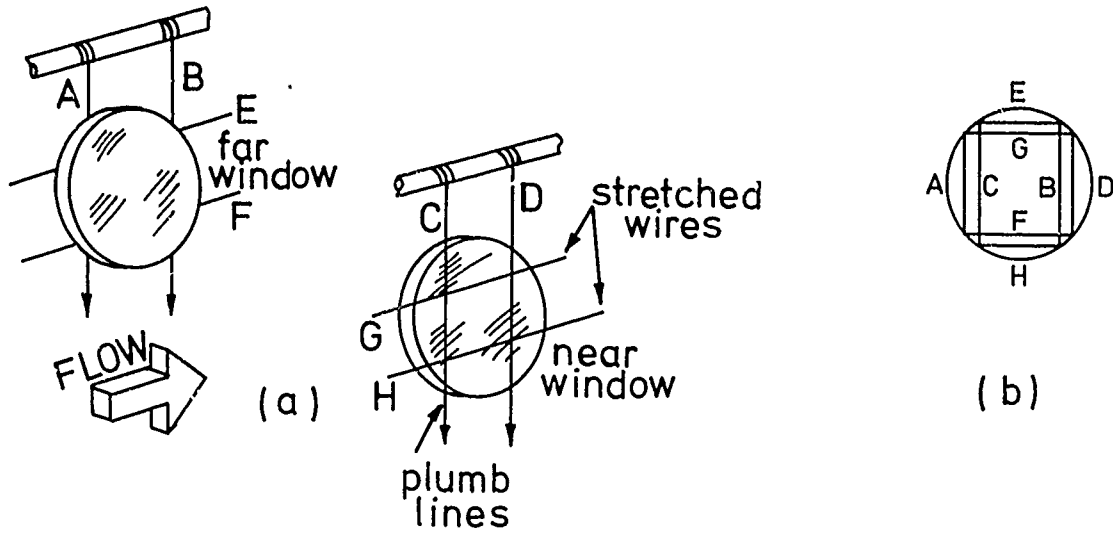


Figure 4.19. A spatial-reference system suitable for use with a shadowgraph optical system using a collimated light beam; (a) plumb lines define the vertical and stretched wires the horizontal directions; (b) images of the reference lines which are staggered to detect optical distortions.

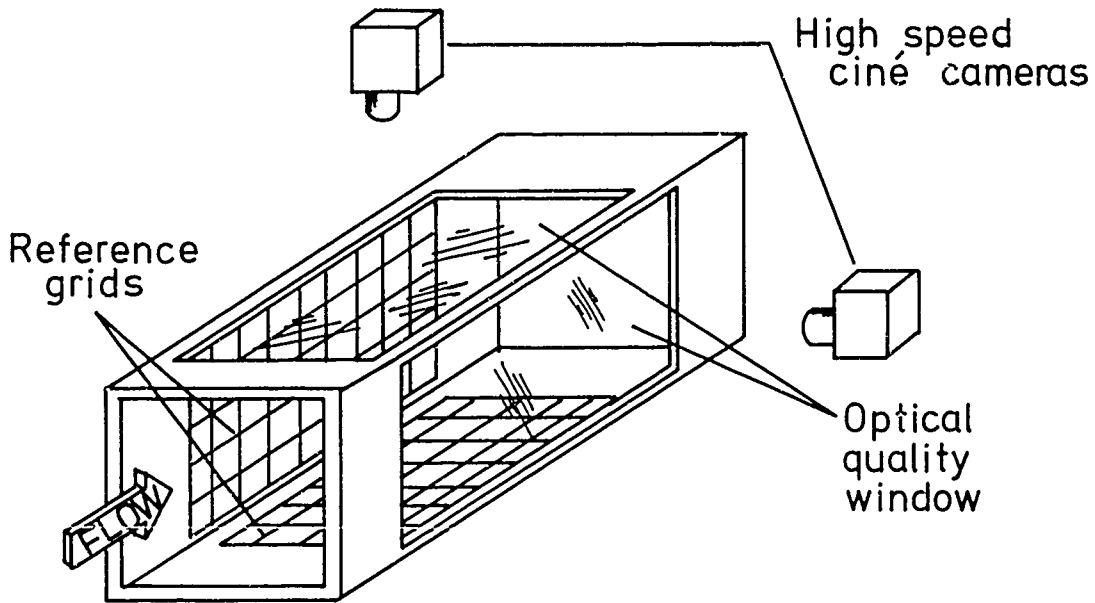


Figure 4.20. Reference-grids used with ciné cameras in the shock-tunnel at N.A.S.A.-Ames.

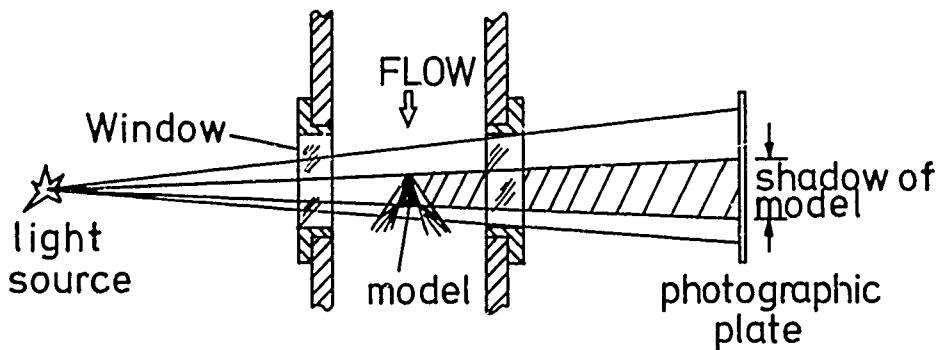


Figure 4.21. A point-source of light providing a conical beam.

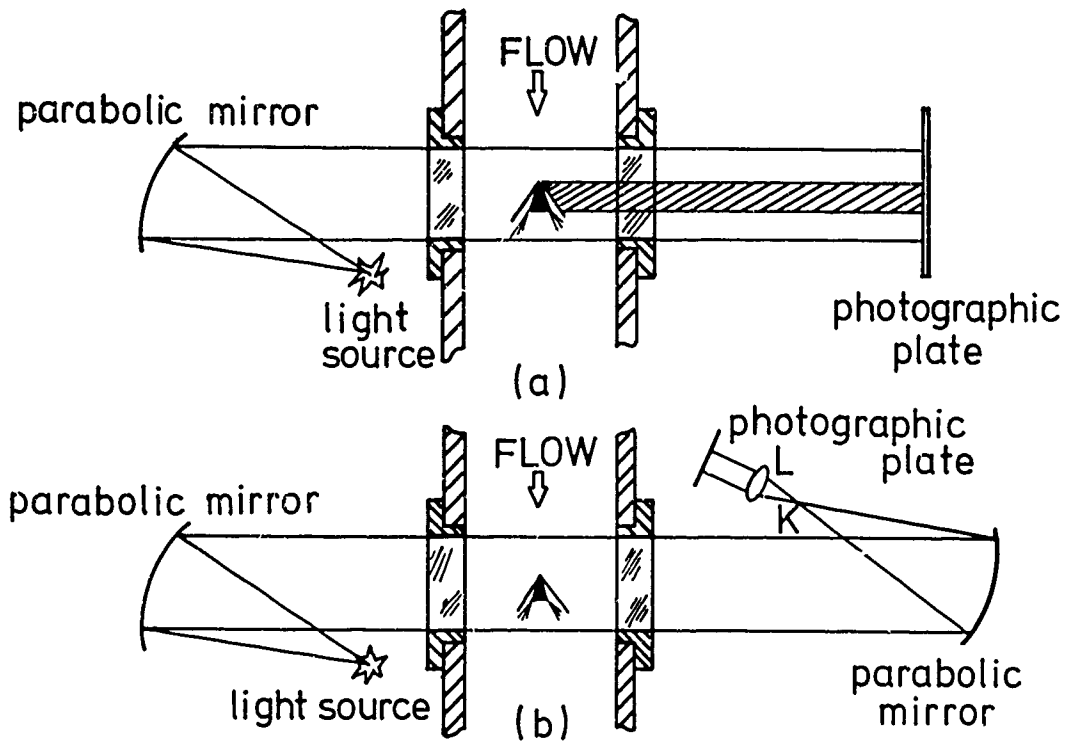


Figure 4.22. Optical systems for shadowgraph photography; (a) the direct-shadowgraph arrangement, (b) the focussed shadowgraph arrangement. The focal plane K is normally occupied by a knife-edge when the system is used for schlieren photography.

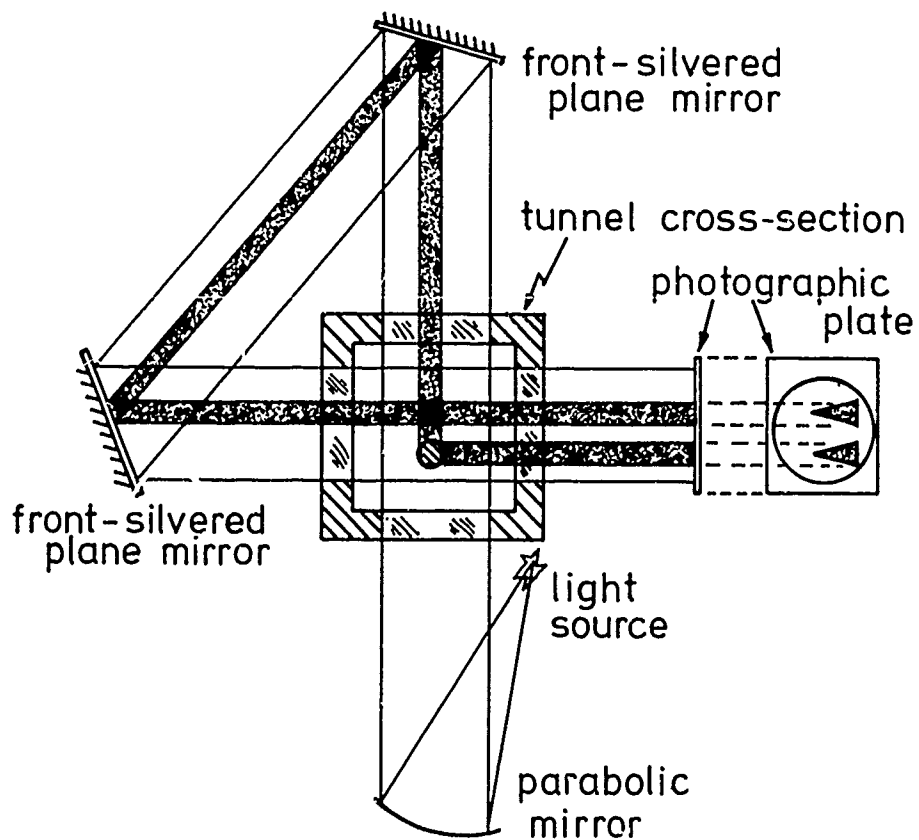
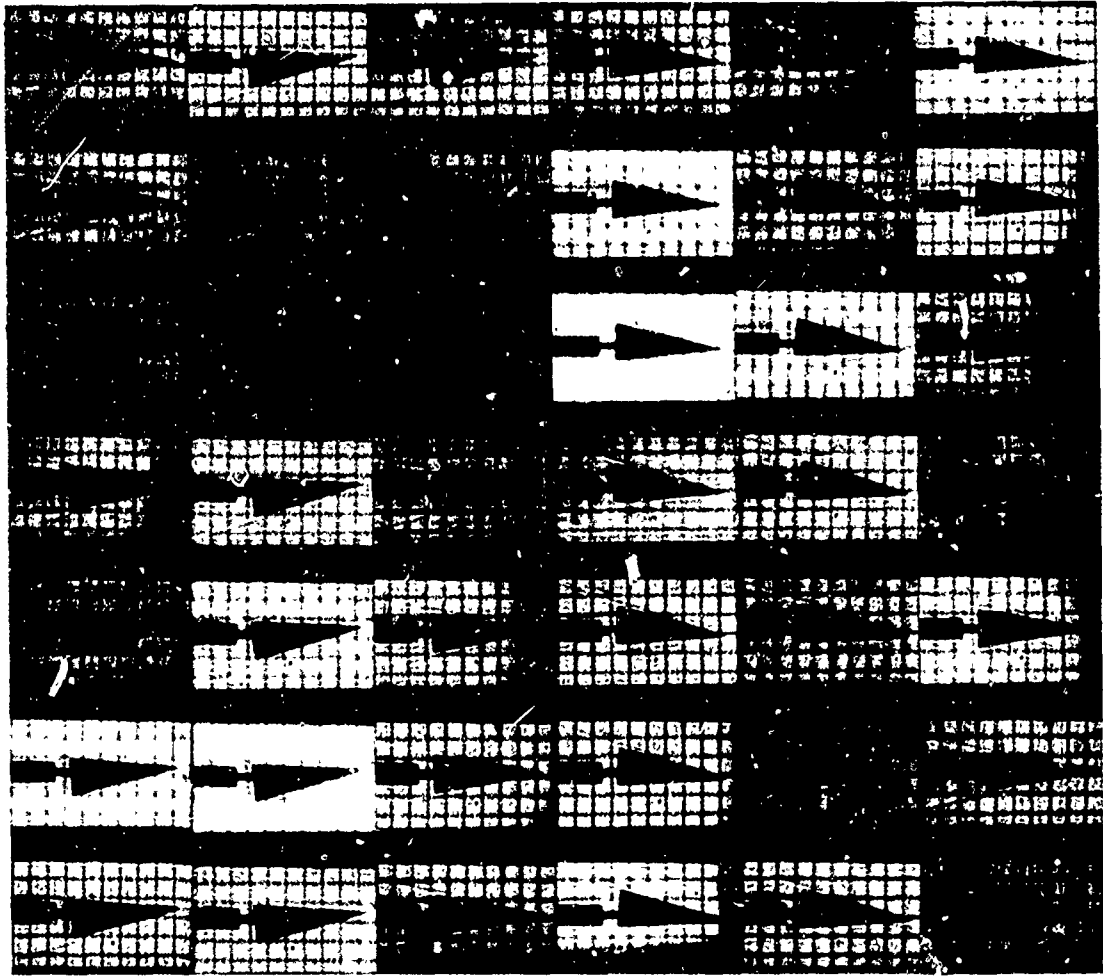


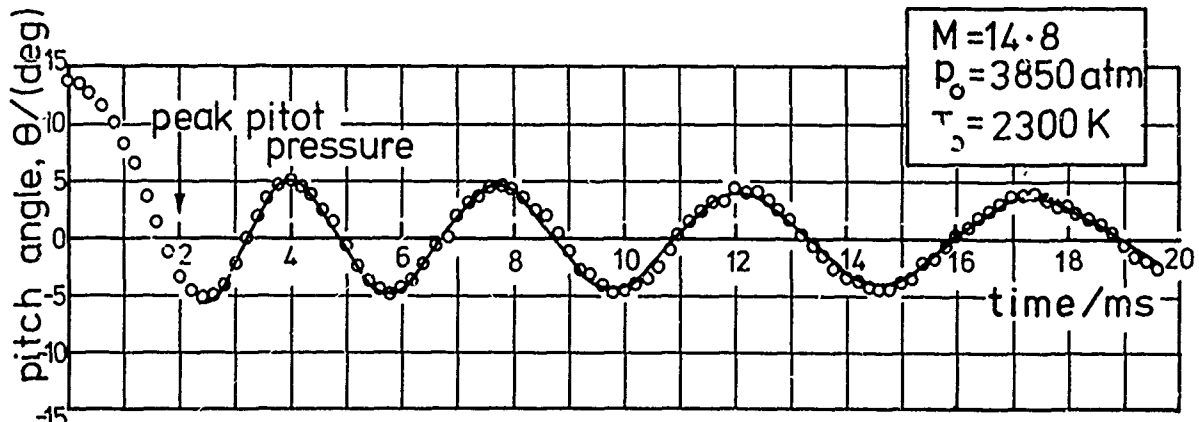
Figure 4.23. One example of a system which produces orthogonal views using a single light source.

1



42

Figure 4.24. A ciné-film record of a cone of 9° half-angle, about a knife-edge pivot in the V.K.I. Longshot tunnel (Richards & Clemens, 1971).



o experimental data      — theory using  $C_{m\alpha} = -0.339$  ;  
 $C_{m\dot{\alpha}} + C_{m\dot{q}} = -0.456$   
 (Newtonian values :  
 $C_{m\alpha} = -0.420$  ;  $C_{m\dot{\alpha}} + C_{m\dot{q}} = -0.228$  )

Figure 4.25. Pitch angle  $\theta$ , as a function of time  $t$ , from measurements of a ciné-film record such as that of figure 4.24. The cone semi-angle was 30°. (after Richards & Enkenhus, 1970 b).

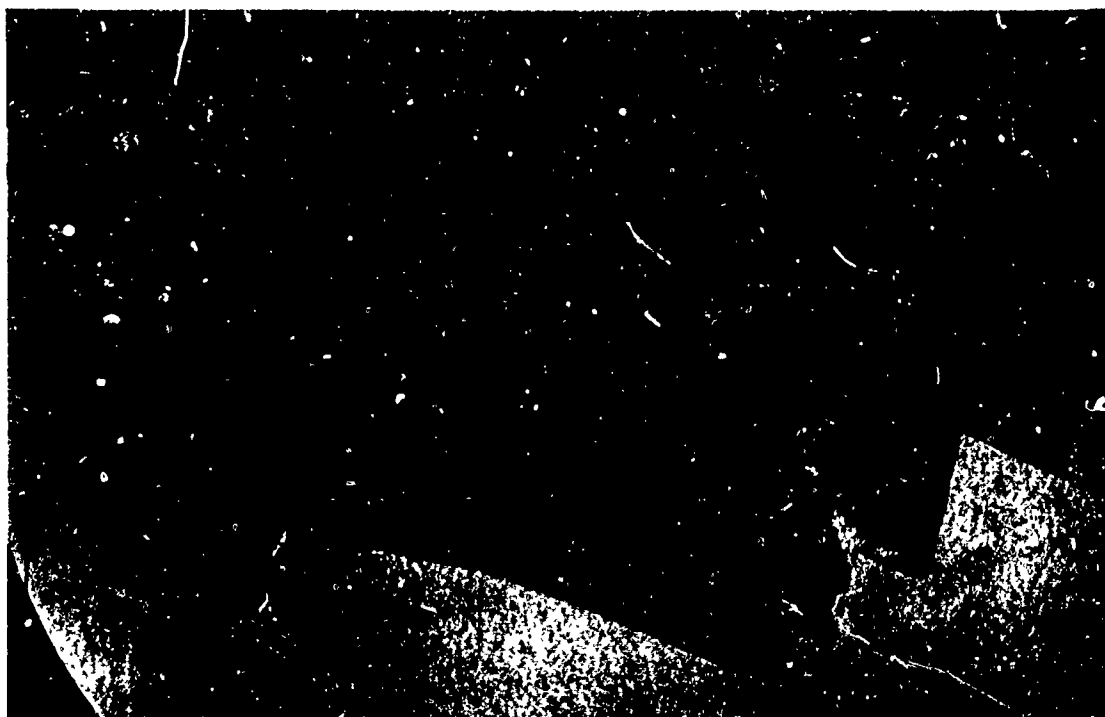


Figure 4.26. Multiply-exposed shadowgraph of a freely-flying model (after Pennelegion, Cash & Shilling, 1967; Crown copyright, published by permission of H.M.S.O.).

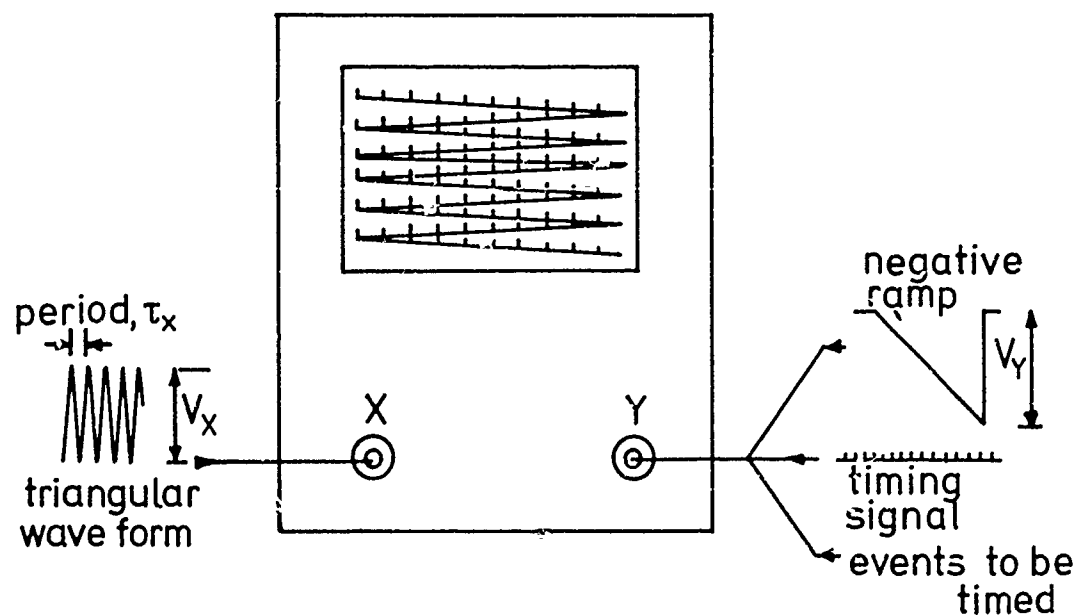


Figure 4.27. A raster time-base on an ordinary cathode ray oscilloscope. The voltages  $V_x$  and  $V_y$  are sufficient to provide full-scale deflection. The negative ramp on the Y-axis is conveniently of duration about  $5\tau_x$  ( $5.5\tau_x$  is shown on the diagram); the timing signal is of period  $0.05\tau_x$ . The events to be timed are shown as being put on the Y-axis; they may also be used to modulate the brightness.

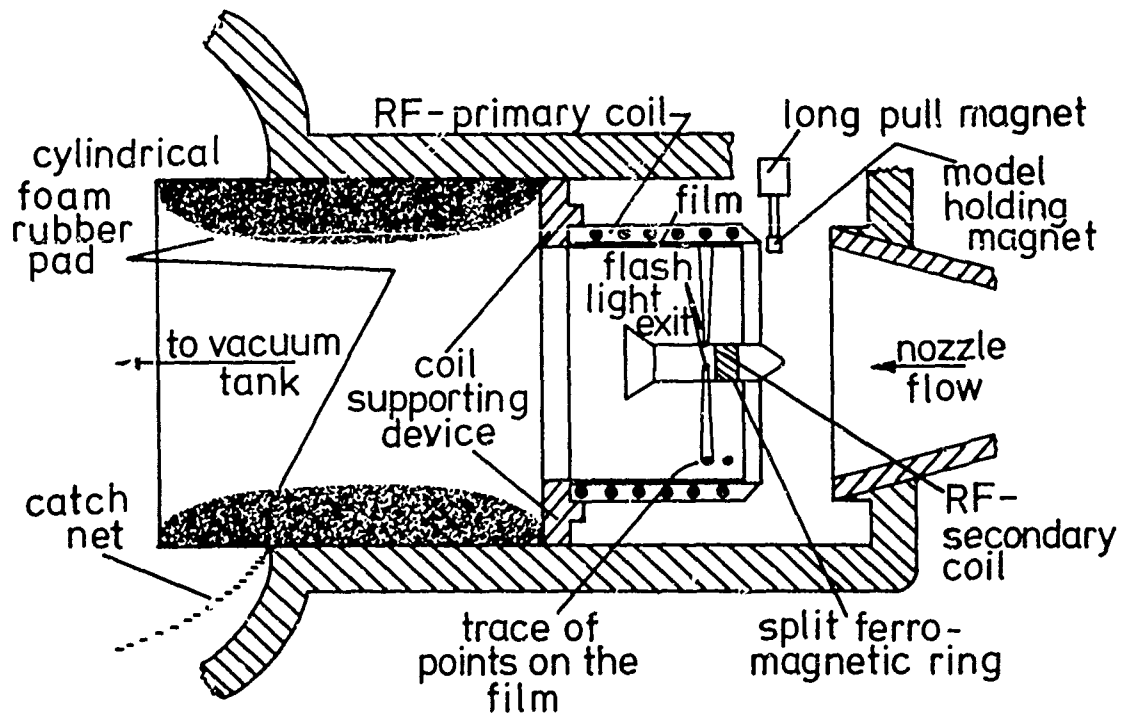
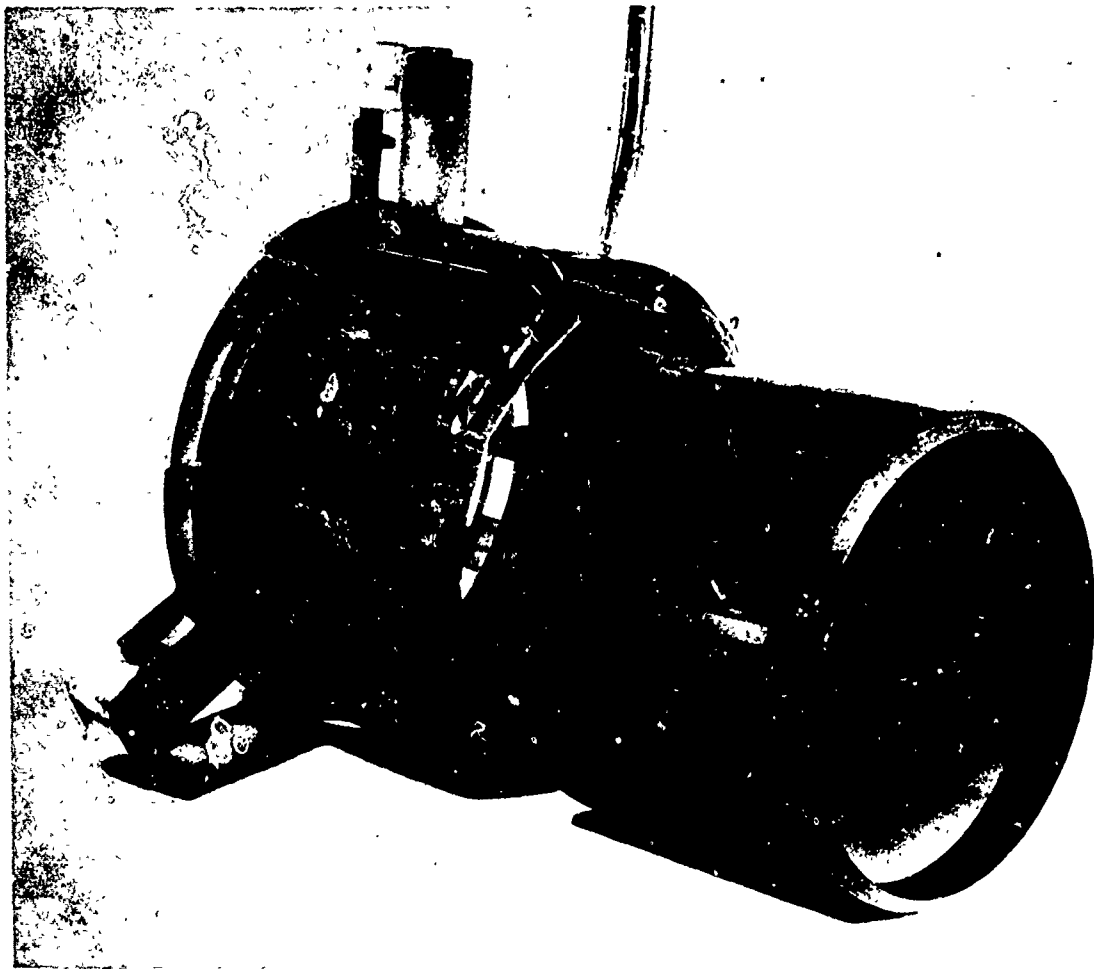


Figure 4.28. The optical telemetry system used in the gun tunnel at D.F.V.L.R. Porz-Wahn: upper, the filmholder and primary coil, lower; general layout. (after Requardt & Kabelitz, 1972).

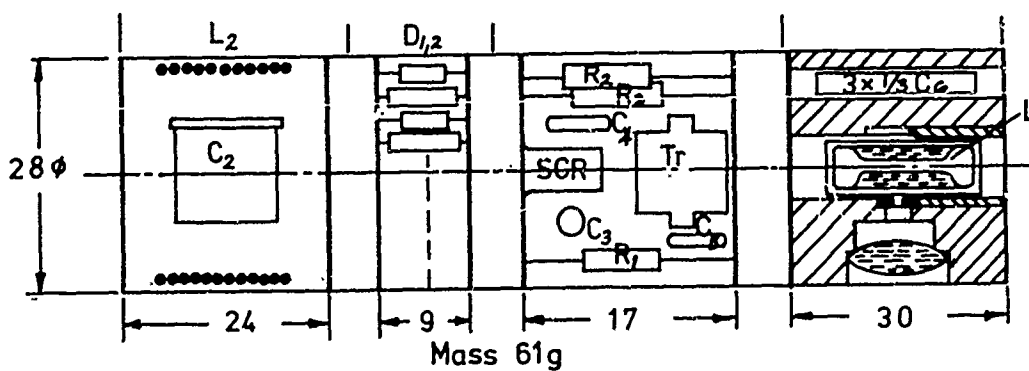
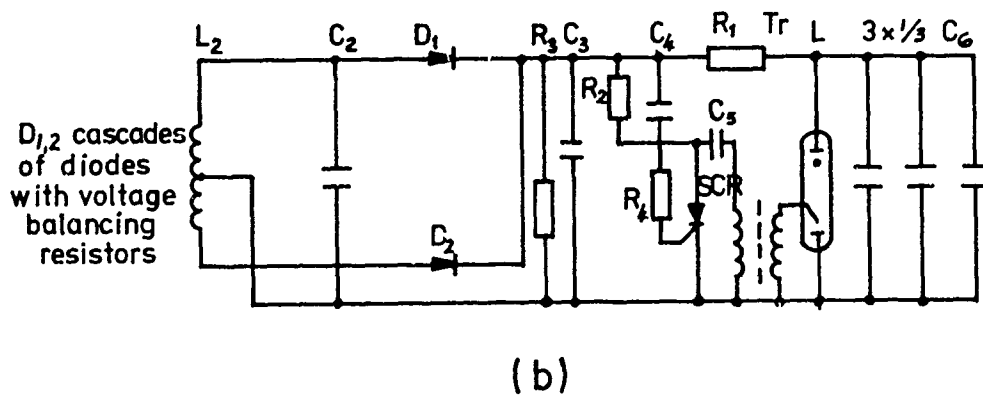
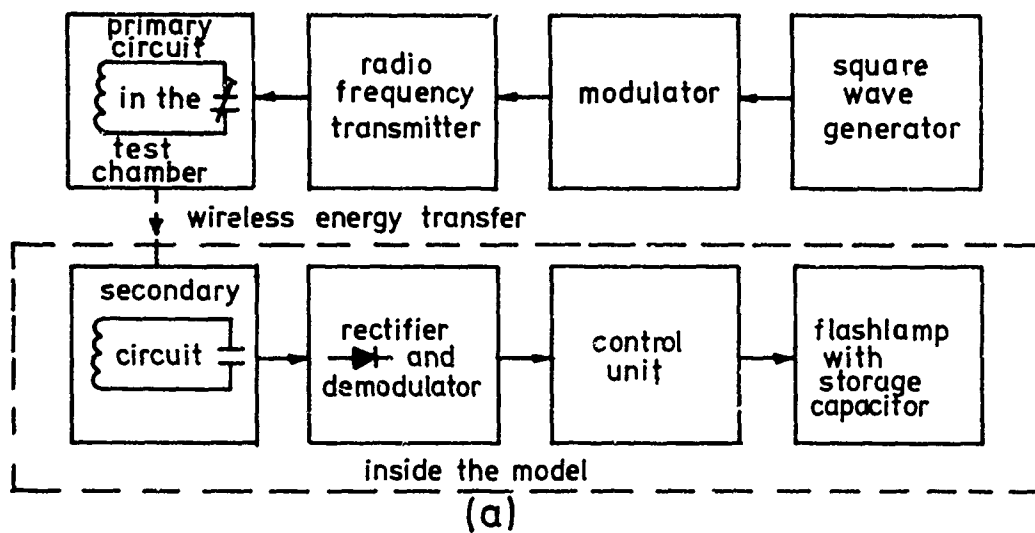


Figure 4.29. (a) A block diagram of the transmission system, (b) the circuit diagram and (c) the physical arrangement of the "package" carried aboard a model for the optical telemetry system (after Wyborny & Requardt, 1974).



Figure 4.30. The "potted" instrument package (after Wyborny & Requardt, 1974).

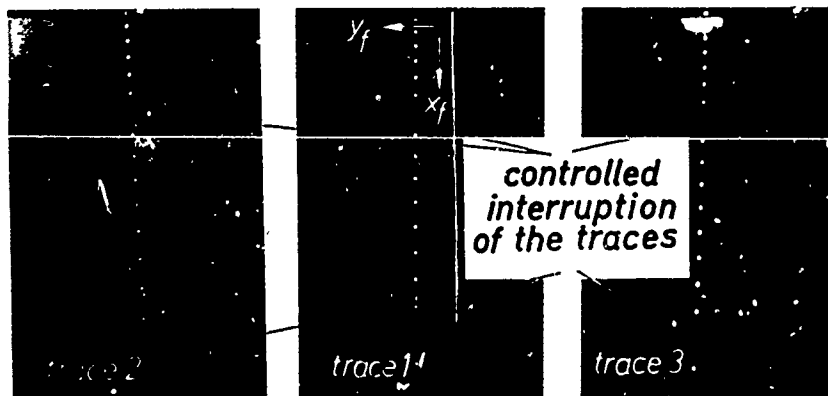


Figure 4.31. A typical record obtained using the optical telemetry system of D.F.V.L.R.-Porz-Wahn. The coordinates  $(x_f, y_f)$  correspond to  $(\xi, \lambda)$  of Chapter 2.

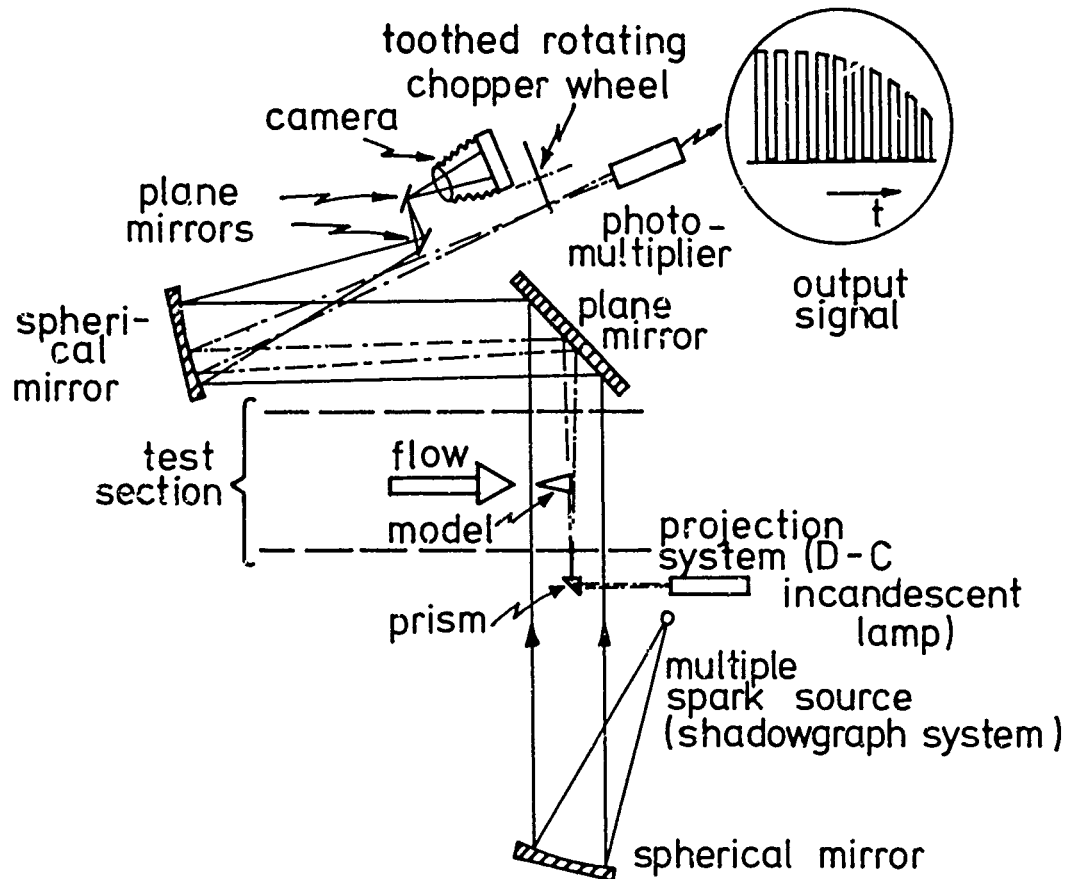


Figure 4.32. The light-occluding system proposed by Clemens (1971) for monitoring displacement vs. time. The system was tested in prototype form for models undergoing axial displacement only in the V.K.I. Longshot tunnel.

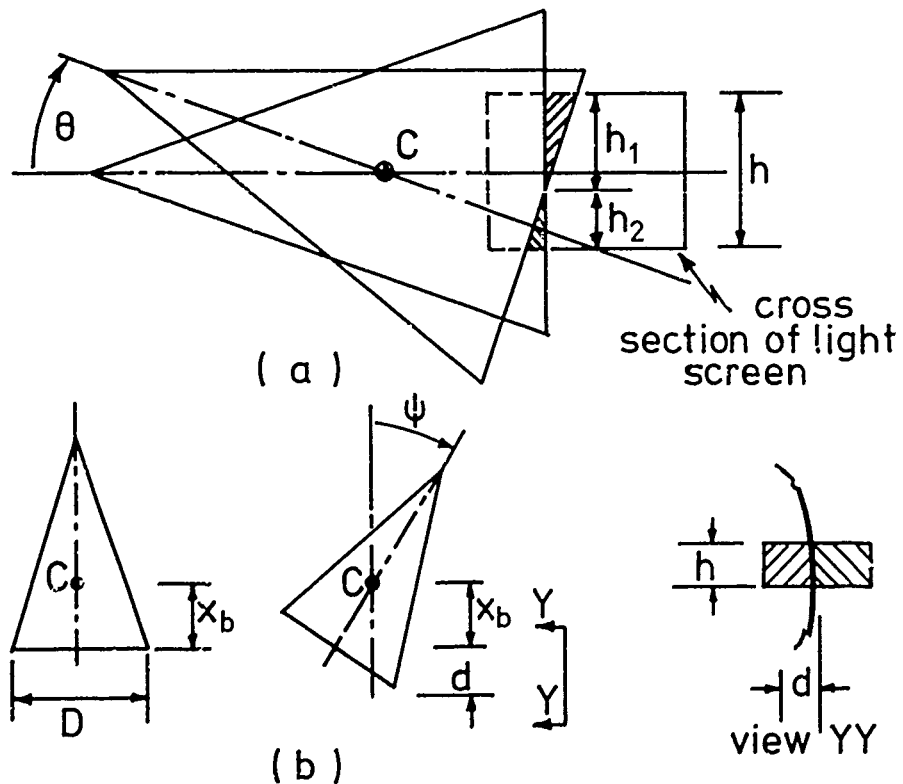


Figure 4.33. Interactions in the light-occluding system; (a) due to pitching motion, (b) due to yaw (after Clemens, 1971).

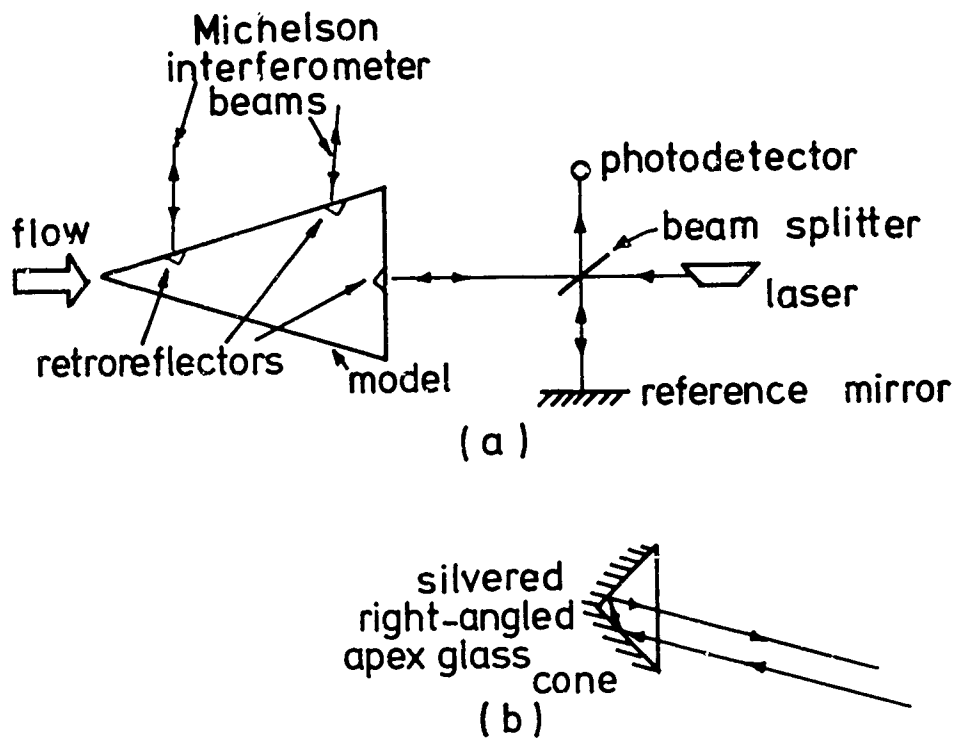


Figure 4.34. Interferometric methods; (a) application of the principle of the Michelson interferometer for measuring displacement, (after North, 1971), (b) a "retroreflector".

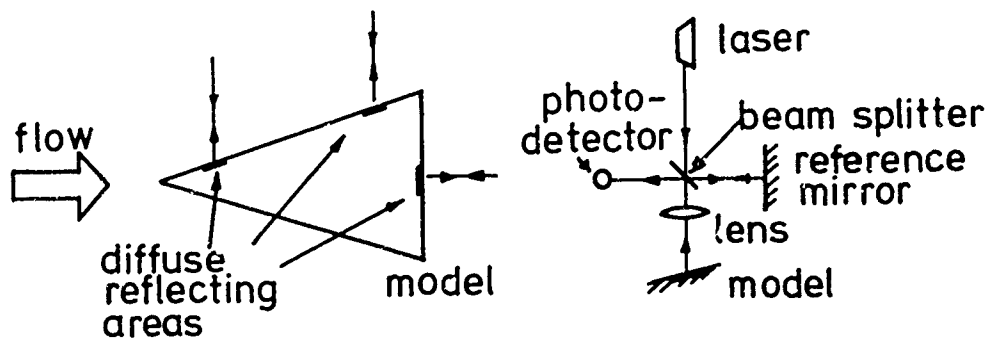


Figure 4.35. A "velocity-measuring" device using the Doppler frequency-shift (after North, 1971).

Reproduced from  
best available copy.

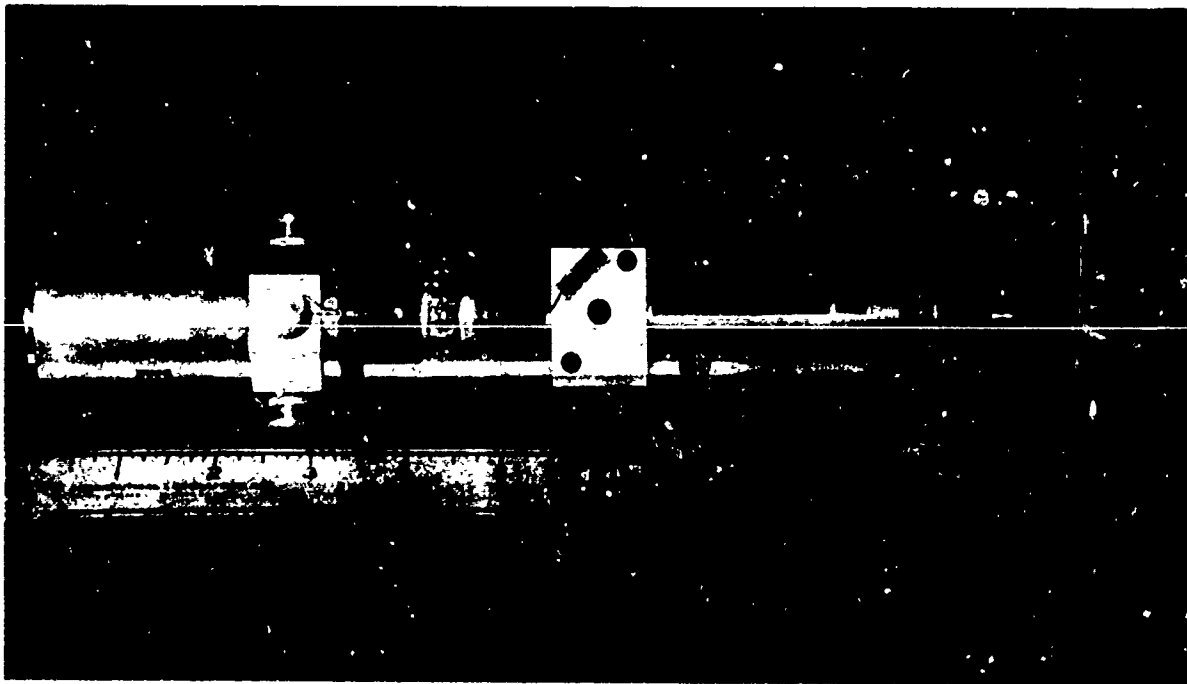
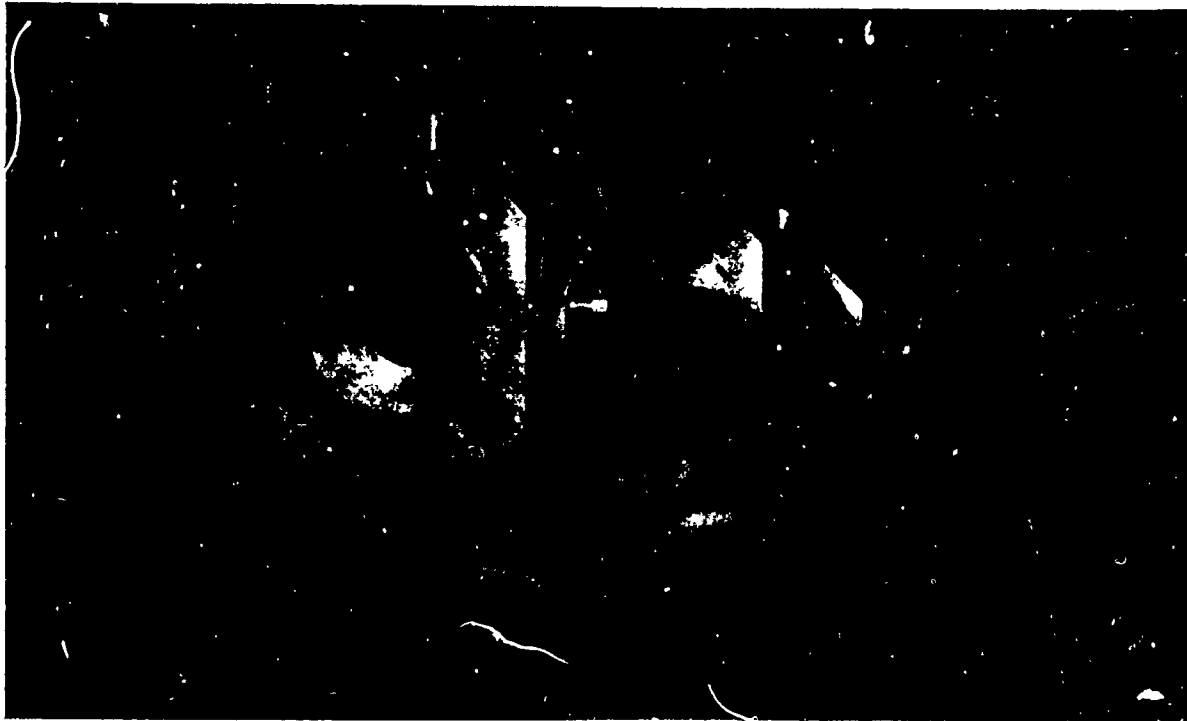


Figure 4.36. The five-component accelerometer balance of Duryea & Sheeran (1969).